# Stochastic Modeling Data Analysis & Statistical Applications

Lidia Filus,
Teresa Oliveira
Christos H Skiadas
*Editors*

ISAST 2015

# Stochastic Modeling, Data Analysis and Statistical Applications

*Edited by*

**Lidia Filus, Teresa Oliveira and Christos H Skiadas**

**ISAST 2015**

**Lidia Filus-Teresa Oliveira-Christos H Skiadas**
***Editors***

# Stochastic Modeling, Data Analysis and Statistical Applications



ISBN (print) : 978-618-5180-08-9

ISBN (e-book) : 978-618-5180-11-9

## Preface

This is the second book devoted to the 3rd Stochastic Modeling Techniques and Data Analysis (SMTDA) International Conference held in Lisbon, Portugal, June 11-14, 2014. Revised and expanded forms of papers from the conference presentations are included.

SMTDA main objective is to publish papers, both theoretical or practical, presenting new results having potential for solving real-life problems. Another important objective is to present new methods for solving these problems by analyzing the relevant data. Also, the use of recent advances in different fields is promoted such as for example, new optimization and statistical methods, data warehouse, data mining and knowledge systems, computing-aided decision supports and neural computing.

The first Chapter includes papers on Stochastic Modeling, First Passage Time and Copulas, whereas contributions on Statistics, Distributions, Bayesian Modeling are included in the second Chapter.
Papers on Model building and Modeling of particular cases are included in the third Chapter, and Data Analysis methods, techniques and applications are presented in the fourth Chapter.
Statistics in Health Sciences and Sports are presented in the fifth Chapter along with Statistical Modelling and Applications papers included in the sixth Chapter.
Chapter seven includes papers on Experimental Design and Related Topics, whereas Information Theory and Risk Analysis topics are analyzed in Chapter eight.
Time Series, Signals, Networks papers along with works on Statistical Quality Control are included in Chapters nine and ten.

Many thanks to the authors for their contribution and our sincere thanks to the referees for their hard work and dedication in providing an improved book form. We acknowledge the valuable support of the SMTDA committees and the secretariat. We are happy for editing another book of the SMTDA series.

*November 2015*

**Lidia Filus,** *Northeastern Illinois University, Chicago, Illinois, USA*

**Teresa Oliveira,** *Aberta University, Portugal*

**Christos H Skiadas**, *ManLab, Technical University of Crete, Chania, Greece*

# *Contents*

# 1 CHAPTER

## Stochastic Modeling, First Passage Time and Copulas

# An inverse First-passage Problem for One-dimensional Diffusions reflected between two boundaries

Mario Abundo

Dipartimento di Matematica
Università Tor Vergata, Roma, Italy
(E-mail: abundo@mat.uniroma2.it)

**Abstract.** We study an inverse first-passage problem for a one-dimensional, time-homogeneous diffusion $X(t)$ reflected between two boundaries $a$ and $b$, which starts from a random position $\eta$. Let $a \leq S \leq b$ be a given threshold, such that $P(\eta \in [a, S]) = 1$, and $F$ an assigned distribution function. The problem consists of finding the distribution of $\eta$ such that the first-passage time of $X$ trough $S$ has distribution $F$.
**Keywords:** First-passage-time,Inverse first-passage problem, Reflected diffusion.

## 1 Formulation of the problem and main results

Diffusion processes with reflecting boundaries appear in many applications in Economics and Finance (see e.g. Ball and Roma [7], Bertolla and Caballero [8], De Jong [11], Krugman [14], Svensson [26]), in Queueing (see e.g. Abate and Whitt [1], [2], Harrison [12], Srikant and Whitt [25], Ward and Glynn [28], [29]), and Mathematical Biology (see e.g. Ricciardi and Sacerdote [23]).

In all these, the knowledge of the distribution of the first-passage-time (FPT) of the reflected diffusion through an assigned barrier is very important. Although FPT problems have been studied mostly for ordinary diffusions, i.e. without reflecting (see e.g. Abundo [6], Darling and Siegert [10], Ricciardi and Sato [24], and references therein), more recently some results appeared about the FPT of a one-dimensional reflected diffusion, through a threshold $S$ (see e.g. Chuancun and Huiqing [9], Lijun *et al.* [17], Qin Hu *et al.* [22]).

In this paper, we focus on FPT problems for a one-dimensional, temporally homogeneous reflected diffusion process $X(t)$ with boundaries $a$ and $b$, which is the solution of the stochastic differential equation with reflecting boundaries (SDER):

*Stochastic Modeling, Data Analysis and Statistical Applications* (*pp.* 3-17 )
Lidia Filus - Teresa Oliveira - Christos H Skiadas (Eds)



$$\begin{cases} dX(t) = \mu(X(t))dt + \sigma(X(t))dB_t + dL_t - dU_t \\ X(0) = \eta \in [a,b] \end{cases} \tag{1}$$

where

$B_t$ is standard Brownian motion,

the initial position $\eta$ is a random variable, independent of $B_t$,

$L = \{L_t\}$ and $U = \{U_t\},\ t \geq 0$,

are the *regulators* of points $a$ and $b$, respectively, namely the local times of $X$ at $a$ and $b$.

The processes $L$ and $U$ are uniquely determined by the following properties (see e.g. Harrison [12]):

(i) both $L_t$ and $U_t$ are continuous nondecreasing processes with $L_0 = U_0 = 0$;

(ii) $X(t) \in [a,b]$ for every time $t \geq 0$;

(iii) $L$ and $U$ increase only when $X = a$ and $X = b$, respectively, that is, $\int_0^t \mathbf{1}_{\{X(s)=a\}} dL_s = L_t$ and $\int_0^t \mathbf{1}_{\{X(s)=b\}} dU_s = U_t$, for any $t \geq 0$.

We suppose that the coefficients $\mu(\cdot)$ and $\sigma(\cdot)$ are sufficiently regular (see e.g. Lions and Sznitman [21]), so that, for fixed initial value the SDER (1) has a unique strong solution $X(t)$, which remains in the interval $[a,b]$ for every time $t \geq 0$.

For this reason,

$X(t)$ is also called a *regulated diffusion* between $a$ and $b$.

If $S \in [a,b]$ is a threshold such that $P(a \leq \eta \leq S) = 1$, we consider the FPT of $X$ through $S$, namely $\tau_S = \inf\{t > 0 : X(t) = S\}$,

and we denote by

$\tau_S(x) = \inf\{t > 0 : X(t) = S | \eta = x\}$

the FPT of $X$ through $S$ with the condition that $\eta = x$.

We assume that $\tau_S(x)$ is finite with probability one $\forall x \in [a,S]$, and that it possesses a density $f(t|x)$.

The *inverse* FPT problem for diffusions generally focuses on determining the barrier $S$, when $f(t|x)$ is given (see e.g. Abundo [6], Zucca and Sacerdote [27]). Since we assume that the initial position $\eta$ is random, we consider a slight modification of the problem, that is the following inverse first-passage-time (IFPT) problem.

For a given distribution $F$, our aim is *to find the density $g$ of $\eta$ (if it exists) for which it results* $P(\tau_S \leq t) = F(t)$.

This IFPT problem has interesting applications in Mathematical Finance, in particular in credit risk modeling, where the FPT represents a default event of an obligor (see e.g. Jackson *et al.* [13]), in Biology, specially in the framework of diffusion models for neural activity (see e.g. Lansky and Smith [16]), and in

Queueing theory (see e.g. Abate and Whitt [1], [2], Harrison [12]). For ordinary diffusions, it was studied in Jackson *et al.* [13] in the case of Brownian motion, while some extensions to more general processes were obtained in Abundo [4], [5].

Let
$\mathcal{L}h(x) = \mu(x)h'(x) + \frac{1}{2}\sigma^2(x)h''(x),\ x \in (a,b)$,
the infinitesimal generator of $X(t)$,
acting on $C^2-$functions $h$ on $(a,b)$.
We recall the following result by Chuancun and Huiqing [9]:

**Theorem 1**

*Let $X$ be the solution of the SDER* (1) *with deterministic and fixed initial condition $X(0) = x$, and*
*let $S \in [a,b]$. For $x \in [a,S]$ and*
*$\theta \geq 0$, suppose that $u(x)$ satisfies the following equation:*

$$\begin{cases} \mathcal{L}u(x) = \theta u(x),\ x \in (a,S) \\ u'(a) = 0 \end{cases} . \tag{2}$$

*Then, if $u(S) \neq 0$ for $S \in [x,b]$,*
*the Laplace transform of $\tau_S(x)$ is explicitly given by:*

$$E\left(e^{-\theta\tau_S(x)}\right) = \frac{u(x)}{u(S)} . \tag{3}$$

□

By taking the $n-th$ derivative of $E\left(e^{-\theta\tau_S(x)}\right)$ with respect to $\theta$, and calculating it at
$\theta = 0$, we obtain (see Abundo [3]):

**Proposition 2**

*For $n = 1, 2, \ldots,$ the $n-th$ order moments of $\tau_S(x)$,*
*if they exist finite, are the solutions to the problems:*

$$\begin{cases} \mathcal{L}T_n(x) = -nT_{n-1}(x),\ x \in (a,S) \\ T_n(S) = 0,\ T_n'(a) = 0 \end{cases} , \tag{4}$$

*where $T_0(x) \equiv 1$.*

Now, we report the explicit solutions of problems (2) and (4) for the Laplace transform and the moments of $\tau_S(x)$, in the case of reflected Brownian motion with drift $\mu$. By solving (2) by quadratures and using (3), we get that the

Laplace transform of $\tau_S^{(\mu)}(x)$ is:

$$E\left(e^{-\theta\tau_S^{(\mu)}(x)}\right)$$
$$= e^{-(S-x)(\sqrt{\mu^2+2\theta}-\mu)} \cdot \frac{\theta e^{-2(x-a)\sqrt{\mu^2+2\theta}} + \mu^2 + \theta + \mu\sqrt{\mu^2+2\theta}}{\theta e^{-2(S-a)\sqrt{\mu^2+2\theta}} + \mu^2 + \theta + \mu\sqrt{\mu^2+2\theta}} \,. \quad (5)$$

For $a \to -\infty$ the right-hand member of (5) tends to
$e^{-(S-x)(\sqrt{\mu^2+2\theta}-\mu)}$, which is the well-known expression of the Laplace transform of the first-hitting time of ordinary Brownian motion with drift $\mu$ to $S$, when starting from $x < S$.

Taking the limit as $\mu$ goes to zero in (5), we obtain:

$$E\left(e^{-\theta\tau_S^{(0)}(x)}\right) = \frac{e^{-x\sqrt{2\theta}} + e^{-(2a-x)\sqrt{2\theta}}}{e^{-S\sqrt{2\theta}} + e^{-(2a-S)\sqrt{2\theta}}} \,. \quad (6)$$

In the special case $a = 0$, the expression above writes:

$$\frac{e^{-x\sqrt{2\theta}} + e^{x\sqrt{2\theta}}}{e^{-S\sqrt{2\theta}} + e^{S\sqrt{2\theta}}} = \frac{cosh(x\sqrt{2\theta})}{cosh(S\sqrt{2\theta})}, \; x \in [0, S]. \quad (7)$$

Then, Laplace transform inversion yields that, for $a = 0$ and $x \in [0, S]$ the density of $\tau_S^{(0)}(x)$ is, for $t \geq 0$ (cf. e.g. Darling and Siegert [10], Qin Hu *et al.* [22]):

$$f^{(0)}(t|x) = \frac{\pi}{S^2} \sum_{k=0}^{\infty} (-1)^k (k + \frac{1}{2}) \cos\left[(k + \frac{1}{2})\frac{\pi x}{S}\right] \exp\left[-(k + \frac{1}{2})^2 \frac{\pi^2 t}{2S^2}\right] \quad (8)$$

By solving (4) by quadratures, with $n = 1$ and $n = 2$, we obtain:

$$T_1^{(\mu)}(x) = \frac{1}{2\mu^2}\left[e^{2\mu(a-S)} - e^{2\mu(a-x)}\right] + \frac{S-x}{\mu}, \; x \in [a, S]. \quad (9)$$

$$T_2^{(\mu)}(x) = \frac{x^2}{\mu^2} - \frac{x}{\mu^3}\left(e^{2\mu(a-S)} + 1 + 2S\mu + e^{2\mu(a-x)}\right) + c_1 + c_2 e^{-2\mu x}, \quad (10)$$

where the constants $c_1$ and $c_2$ can be easily calculated.
Letting $\mu$ go to zero, we obtain:

$$T_1^{(0)}(x) = -x^2 + 2ax + S(S - 2a), \; x \in [a, S]. \quad (11)$$

and

$$T_2^{(0)}(x) = \frac{x^4}{3} - \frac{4}{3}ax^3 - 2S(S-2a)x^2 + Ax + B,\ x \in [a, S],$$

for certain constants $A$ and $B$. In particular, for $a = 0$, we get

$$T_1^{(0)}(x) = -x^2 + S^2,\ T_2^{(0)}(x) = \tfrac{x^4}{3} - 2S^2x^2 + \tfrac{5}{3}S^4$$

Explicit formulae for the Laplace transform of the first-hitting time to a barrier $S$ are known also for reflected OU process, reflected Bessel process and some other processes (see Chuancun and Huiqing [9], Lijun *et al.* [17]), but they involve special functions. An explicit spectral representation of the hitting time density was found in Qin Hu *et al.* [22] for reflected BM, and in Linetsky [19], [20] for Cox-Ingersoll-Ross (CIR) and OU processes.

### 1.1 The IFPT problem for reflected Brownian motion with drift

For a given barrier $S \in [a, b]$, and $X(0) = \eta \in [a, S]$, let us suppose that $\tau_S(x)$ is a.s. finite for every $x \in [a, S]$, and it possesses a density $f(t|x)$.

Moreover, we suppose that the initial position $\eta$ has a density $g(x)$ with support $(a, S)$; for $\theta \geq 0$ we denote by

$\widehat{f}(\theta|x) = \int_0^{+\infty} e^{-\theta x} f(t|x)dt$ the Laplace transform of $f(t|x)$

and by

$\widehat{g}(\theta) = \int_a^S e^{-\theta x} g(x)dx$ the (possibly bilateral) Laplace transform of $g$.

Then, the density of $\tau_S$ is obtained as $f(t) = \int_a^S f(t|x)g(x)dx$ and taking the Laplace transform on both sides we get $\widehat{f}(\theta) = \int_a^S \widehat{f}(\theta|x)g(x)dx$ .

Now, we go to solve the IFPT problem, in the case when $X = X^{(\mu)}$ is reflected BM with drift $\mu$, between the boundaries $a$ and $b$.

For a given FPT distribution function $F$ (or equivalently for a given FPT density $f = F'$)

our aim is to find the density $g$ of the random initial position $\eta$, if it exists, such that

$P(\tau_S \leq t) = F(t)$. The following result holds (see Abundo [3]):

**Theorem 3**

*For $S \in [a, b]$, let $X^{(\mu)}$ be BM with drift $\mu$, reflected between the boundaries $a$ and $b$ and starting from the random position $\eta \in [a, S]$; suppose that the FPT of $X^{(\mu)}$ through $S$ has an assigned probability density $f$ and denote by*

$\widehat{f}(\theta) = \int_0^{\infty} e^{-\theta t} f(t)dt,\ \theta \geq 0,$
*the Laplace transform of $f$.*

*Then, if there exists a solution $g$ to the IFPT problem for $X^{(\mu)}$, its Laplace transform $\widehat{g}(\theta)$, for $\theta \geq 0$, must satisfy the equation:*

$$\widehat{f}(\theta) =$$

$$[\theta e^{2a\sqrt{\mu^2+2\theta}}\widehat{g}(\sqrt{\mu^2+2\theta}+\mu) + (\mu^2+\theta+\mu\sqrt{\mu^2+2\theta}\ )\widehat{g}(\mu-\sqrt{\mu^2+2\theta}\ )]$$

$$\times\left\{\theta e^{-S(\sqrt{\mu^2+2\theta}-\mu)}e^{2a\sqrt{\mu^2+2\theta}} + (\mu^2+\theta+\mu\sqrt{\mu^2+2\theta}\ )e^{S(\sqrt{\mu^2+2\theta}+\mu)}\right\}^{-1} \quad (12)$$

*In particular, if* $\mu = 0$, *the above formula writes:*

$$\widehat{f}(\theta) = \frac{\widehat{g}(\sqrt{2\theta}) + \widehat{g}(-\sqrt{2\theta})e^{-2a\sqrt{2\theta}}}{e^{-S\sqrt{2\theta}} + e^{(S-2a)\sqrt{2\theta}}},\ \theta \geq 0. \quad (13)$$

*Furthermore, if* $\mu = 0$ *and we require that the density* $g$ *is symmetric with respect to* $(a+S)/2$,
*then:*

$$\widehat{g}(\theta) = \frac{e^{-S\theta} + e^{-(2a-S)\theta}}{1+e^{(S-a)\theta}}\ \widehat{f}\left(\frac{\theta^2}{2}\right),\ \theta \geq 0. \quad (14)$$

□

If $\widehat{f}(\theta)$ is analytic in a neighbor of $\theta = 0$, then the $k-$th order moments of $\tau_S$ exist finite and they are obtained in terms of $\widehat{f}(\theta)$ by
$E(\tau_S^k) = (-1)^k \frac{\partial^k}{\partial\theta^k}\widehat{f}(\theta)|_{\theta=0}$.

The same thing holds for the moments of $\eta$, if $\widehat{g}(\theta)$ is analytic.
Thus, we obtain:

$$E(\tau_S^{(\mu)}) = \frac{1}{\mu}E(S-\eta) - \frac{1}{2\mu^2}\ e^{2\mu a}E\left(e^{-2\mu\eta} - e^{-2\mu S}\right). \quad (15)$$

**Remark 4** Let $X(t)$ be regulated BM, and suppose that $\tau_S$ has Gamma distribution. Then, it can be shown that a solution $g$ to the IFPT problem, with $g$ symmetric with respect to $(a+S)/2$ does not exist (see Abundo [3]).

Now, we further investigate the question of the existence of solutions to the IFPT problem. Referring to regulated drifted BM, we will prove the existence of the density $g$ of the initial position $\eta \in [a, S]$ for a class of FPT densities $f$.

For the sake of simplicity, we limit ourselves to the case when $\mu = 0,\ a = 0,\ S = 1 < b$ and $g$ is required to be symmetric with respect to $1/2$; in fact, for $\mu \neq 0$ the calculations involved are far more complicated.
For any integer $k \geq 0$, set $I_k(\theta) = \int_{-1}^{1} e^{-\theta x}x^k dx$; as easily seen,

$I_0(\theta) = 2\sinh(\theta)/\theta$ and the recursive relation
$I_k(\theta) = \frac{(-1)^k e^{\theta} - e^{-\theta}}{\theta} + \frac{k}{\theta} I_{k-1}(\theta)$ allows to
calculate $I_k(\theta)$, for every $k$.
The following proposition holds (see Abundo [3]).

**Proposition 5**
*Let $X$ be regulated BM between the boundaries 0 and $b$, and let $S = 1 < b$; suppose that the Laplace transform of $f(t)$ has the form:*

$$\widehat{f}(\theta) = \widehat{f}_{2k}(\theta) := \frac{\cosh(\sqrt{\theta/2})}{\cosh(\sqrt{2\theta})} \left(1 + \frac{1}{2k}\right) \left[\sqrt{\frac{2}{\theta}} \sinh\left(\sqrt{\frac{\theta}{2}}\right) - I_{2k}\left(\sqrt{\frac{\theta}{2}}\right)\right], \tag{16}$$

*for some integer $k > 0$. Then, there exists the solution $g = g_{2k}$ of the IFPT problem for $X$, relative to the FPT density $f$, and it results:*

$$g_{2k}(x) = \left(1 + \frac{1}{2k}\right) \left(1 - (2x-1)^{2k}\right), \ x \in (0,1). \tag{17}$$

□

As an application of the results for regulated BM, we consider now the piecewise-continuous process $\xi(t)$, obtained by superimposing to BM a jump process, namely, for $\eta \in [a, S]$ and $t < T$, we set $\xi(t) = \eta + B_t$, where $T$ is an exponentially distributed time with parameter $\lambda > 0$; we suppose that for $t = T$ the process $\xi(t)$ makes an upward jump and it crosses the barrier $S$, irrespective of its state before the occurrence of the jump. This kind of behavior is observed e.g. in the presence of a so called *catastrophes*.

Next, let us consider the reflected diffusion $\overline{X}$ with boundaries $a$, $b$, associated to $\xi$. Then, for $\eta \in [a, S]$ the FPT of $\overline{X}$ over $S$ is $\overline{\tau}_S = \inf\{t > 0 : \overline{X}(t) \geq S\}$. Conditionally on $\eta = x$, we have:

$$P(\overline{\tau}_S(x) \leq t) = P(\overline{\tau}_S(x) \leq t | t < T) P(t < T) + 1 \cdot P(t \geq T)$$

$$= P(\tau_S(x) \leq t) e^{-\lambda t} + (1 - e^{-\lambda t}).$$

Taking the derivative, we obtain the FPT density of $\overline{X}$, conditional to the starting position $x$ :

$$\overline{f}(t|x) = e^{-\lambda t} f(t|x) + \lambda e^{-\lambda t} \int_t^{+\infty} f(s|x) ds.$$

By straightforward calculations, we obtain its Laplace transform:

$$\widehat{\overline{f}}(\theta|x) = \int_0^{\infty} e^{-\theta t} \overline{f}(t|x) dt = \frac{\theta}{\lambda + \theta} \widehat{f}(\lambda + \theta|x) + \frac{\lambda}{\lambda + \theta}, \ \theta \geq 0.$$

The following result holds (see Abundo [3]).

**Proposition 6** *For $a = 0 < S < b$, if there exists a function $\overline{g}$, symmetric with respect to $S/2$, which is the solution to the IFPT problem of $\overline{X}(t)$, relative to $S$ and the FPT density $\overline{f}$, then its Laplace transform is given by:*

$$\widehat{\overline{g}}(\theta) = \frac{2\cosh(S\theta)}{(\theta^2/2 - \lambda)(1 + e^{S\theta})} \left[ \frac{\theta^2}{2} \, \widehat{\overline{f}} \left( \frac{\theta^2}{2} - \lambda \right) - \lambda \right]. \tag{18}$$

□

**Remark 7** For $\lambda = 0$, namely when no jump occurs,
(18) reduces to (14) with $a = 0$.

### 1.2 Reduction of reflected diffusions to reflected Brownian motion

On the analogy of the definition holding for ordinary diffusions (see Abundo [5], [6]), we introduce the following:

**Definition**
*Let $X(t)$ be a diffusion with reflecting boundaries $a$ and $b$, which is driven by the SDER:*

$$dX(t) = \mu(X(t))dt + \sigma(X(t))dB_t + dL_t - dU_t, \;\; X(0) = x \in [a, b].$$

*We say that $X(t)$ is conjugated to regulated BM if there exists an increasing differentiable function $V(x)$, with $V(0) = 0$, such that, for any $t \geq 0$ it results $X(t) = V^{-1}\left(B_t + V(x) + \overline{L}_t - \overline{U}_t\right)$,*
*where $\overline{L}_t = V'(a)L_t$ and $\overline{U}_t = V'(b)U_t$ are regulators.*

A class of reflected diffusions which are conjugated to regulated BM is given by processes which are solutions of SDERs such as:

$$dX(t) = \frac{1}{2}\sigma(X(t))\sigma'(X(t))dt + \sigma(X(t))dB_t + L_t - U_t, \;\; X(0) = x \tag{19}$$

with $\sigma(\cdot) \geq 0$.
Indeed, if the integral
$V(x) := \int^x \frac{1}{\sigma(r)} dr$
is convergent,
by Itô's formula for
reflected diffusions (see e.g. Harrison [12]), one gets $V(X(t)) = B_t + V(x) + V'(a)L_t - V'(b)U_t$.

Let us consider a diffusion $X$ with reflecting boundaries $a$ and $b$, which is conjugated to regulated BM via the function $V$.

Then, the process $Y(t) := V(X(t))$ is regulated BM between the boundaries $V(a)$ and $V(b)$,

starting from $V(x)$, that is
$Y(t) = V(x) + B_t + \overline{L}_t - \overline{U}_t$ ,
where $\overline{L}_t = V'(a)L_t$ and $\overline{U}_t = V'(b)U_t$ are the regulators of $Y(t)$, which increase only when
$Y = V(a)$ and $Y = V(b)$, respectively.
Thus, for $x \in [a, S]$ :

$$\tau_S(x) = \inf\{t \geq 0 : X(t) = S | X(0) = x\} = \tau^Y_{S'}(V(x)),$$

where $S' = V(S)$ and the superscript refers to the process $Y$.

Therefore, the solution $g$ to the IFPT problem for $X$, relative to the FPT density $f$ and the barrier $S$, can be written in terms of the solution $\widetilde{g}$ to the IFPT problem for regulated BM $Y(t)$ relative to the FPT density $f$ and the barrier $V(S)$. If one seeks e.g. that $\widetilde{g}$ is symmetric with respect to $(V(a) + V(S))/2$, then (see (14)) the Laplace transform of $\widetilde{g}$ turns out to be:

$$\widehat{\widetilde{g}}(\theta) = \frac{e^{-V(S)\theta} + e^{-(2V(a)-V(S))\theta}}{1 + e^{(V(S)-V(a))\theta}} \ \widehat{f}\left(\frac{\theta^2}{2}\right), \ \theta \geq 0. \tag{20}$$

## 2 A few examples

**Example 1**

Let $X(t)$ be regulated BM with boundaries $a,\ b$ $(a < S < b)$, starting from $\eta \in [a, S]$ and consider the FPT density:

$$f(t) = \frac{1}{(S-a)^2} \sum_{k=0}^{\infty} \exp\left[-\frac{\left(k + \frac{1}{2}\right)^2 \pi^2 t}{2(S-a)^2}\right], \tag{21}$$

or the corresponding FPT Laplace transform:

$$\widehat{f}(\theta) = \frac{\tanh((S-a)\sqrt{2\theta})}{(S-a)\sqrt{2\theta}} \ . \tag{22}$$

Then, the solution $g$ to the IFPT problem for $X(t)$ is the uniform density in $(a, S)$.

In particular,
for $a = 0,\ S = 1$, (21) and (22) become:

$$f(t) = \sum_{k=0}^{\infty} \exp\left[-\frac{1}{2}\left(k + \frac{1}{2}\right)^2 \pi^2 t\right] \text{ and } \widehat{f}(\theta) = \frac{\tanh(\sqrt{2\theta})}{\sqrt{2\theta}} \tag{23}$$

and the solution $g$ to the IFPT problem is the uniform density in $(0, 1)$.

**Example 2**

For $a = 0 < S < b$, let $X(t)$ be regulated BM starting from $\eta \in [a, S]$, and consider the FPT density whose Laplace transform is:

$$\widehat{f}(\theta) = \frac{\pi^2}{2} \, \frac{1 + \cosh(S\sqrt{2\theta})}{\cosh(S\sqrt{2\theta})(2\theta S^2 + \pi^2)}$$

Then, the solution to the IFPT problem for $X$
is $g(x) = \frac{\pi}{2S} \sin\left(\frac{\pi x}{S}\right), \ x \in (0, S)$.

**Example 3**

Take $a = 0, \ S = 1$, and let $X(t)$ be regulated BM starting from $\eta \in [0, 1]$; consider the FPT density whose Laplace transform is:

$$\widehat{f}(\theta) = \frac{\left(1 + e^{\sqrt{2\theta}}\right)\left(e^{\sqrt{2\theta}} - 2e^{\sqrt{\theta/2}} + 1\right)}{\theta \cosh(\sqrt{2\theta}) e^{\sqrt{2\theta}}}$$

Then, the solution to the IFPT problem for $X$ is the triangular density in $[0, 1]$ :

$$g(x) = \begin{cases} 4x, & x \in [0, \frac{1}{2}] \\ 4x(1-x), & x \in (\frac{1}{2}, 1] \end{cases} \quad .$$

**Example 4**

Take $a = 0, \ S = 1$, and let $X(t)$ be regulated BM starting from $\eta \in [0, 1]$; consider the FPT density whose Laplace transform is:

$$\widehat{f}(\theta) = \frac{3\left(1 + e^{\sqrt{2\theta}}\right)\left(e^{-\sqrt{2\theta}}(\sqrt{2\theta} + 2) + \sqrt{2\theta} - 2\right)}{\theta\sqrt{2\theta}\left(e^{\sqrt{2\theta}} + e^{-\sqrt{2\theta}}\right)}$$

Then, the solution $g$ to the IFPT problem for $X$ is a Beta density in $[0, 1]$, i.e. $g(x) = 6x(1 - x)$.

Notice that $\widehat{f}$ and $g$ are obtained as special cases of $\widehat{f}_{2k}$ and $g_{2k}$ of Proposition 5, for $k = 1$.

**Example 5**

For $0 = a < S < b$ let $\overline{X}$ be the jump-process considered at the end of subsection 1.1, and
let:

$$\widehat{\overline{f}}(\theta) = \frac{1}{\lambda + \theta}\left[\frac{\theta \cdot \tanh(S\sqrt{2(\lambda + \theta)})}{S\sqrt{2(\lambda + \theta)}} + \lambda\right].$$

By Laplace inversion, one obtains:

$$\overline{f}(t) = e^{-\lambda t}\left[\sum_{k=0}^{\infty}\left(\frac{1}{S^2} + \frac{2\lambda S^2}{(k + \frac{1}{2})^2\pi^2}\right)\exp\left(-\frac{(k + 1/2)^2\pi^2 t}{2S^2}\right)\right],$$

which can be written as

$$\overline{f}(t) = e^{-\lambda t}\phi(t) + \lambda e^{-\lambda t}\int_t^\infty \phi(s)ds, \tag{24}$$

where $\phi(t)$ is the FPT density considered in Example 1 with $a = 0$, i.e.:

$$\phi(t) = \frac{1}{S^2}\sum_{k=0}^{\infty} \exp\left(-\frac{(k+1/2)^2\pi^2 t}{2S^2}\right). \tag{25}$$

Then, the solution $\overline{g}$ to the IFPT problem for $\overline{X}(t)$, relative to $S \in (0, b)$ and $\widehat{\overline{f}}$, which is symmetric with respect to $S/2$, is the uniform density in $(0, S)$.

**Example 6** (Reflected geometric Brownian motion)

Let $0 < a < S < b$, and $X(t)$ the solution of the SDER:

$$dX(t) = rX(t)dt + \sigma X(t)dB_t + dL_t - dU_t,\ X(0) = \eta \in [a, S],$$

where $r$ and $\sigma$ are positive constant.

The equation without reflecting is well-known in the framework of Mathematical Finance, since it describes the time evolution of a stock price.

As easily seen,

$$\ln X(t) = \ln \eta + \mu t + \sigma B_t + \bar{L}_t - \bar{U}_t,$$

where $\mu = r - \sigma^2/2$ and $\bar{L}_t, \bar{U}_t$ are regulators;
thus, $\ln X(t)/\sigma$ is regulated BM with drift $\mu/\sigma$,
between the boundaries $\frac{\ln a}{\sigma}$, $\frac{\ln b}{\sigma}$.

Then, the IFPT problem for $X(t)$ relative to $S$ and the FPT density $f$, is reduced to the IFPT problem for regulated drifted BM, starting from $\frac{\ln \eta}{\sigma}$, relative to $\frac{\ln S}{\sigma}$ and the same FPT density $f$.

**Example 7**

Let $X$ be a reflected diffusion in $[a, b]$, which is conjugated to regulated BM via the function $V$; then, examples of solutions to the IFPT problem for $X$ can be obtained from Examples 1-4 regarding regulated BM.

For instance, let us consider the FPT density

$$f(t) = \frac{1}{(V(S) - V(a))^2}\sum_{k=0}^{\infty} \exp\left[-\frac{\left(k+\frac{1}{2}\right)^2\pi^2 t}{2(V(S) - V(a))^2}\right], \tag{26}$$

Then, the solution to the IFPT problem for $X$ relative to the barrier $S$ ($a < S < b$) is

$$g(x) = \frac{V'(x)}{V(S) - V(a)} \cdot \mathbf{1}_{(a,S)}(x). \tag{27}$$

As explicit examples of reflected diffusions $X$ which are conjugated to regulated BM, we mention the following.

**(i)** The process driven by

$$\begin{cases} dX(t) = \frac{1}{3} X(t)^{1/3} dt + X(t)^{2/3}\, dB_t + dL_t - dU_t \\ X(0) = \eta \in [a,b] \end{cases}, \tag{28}$$

which is conjugated to regulated BM via the function
$V(x) = 3x^{1/3}$ i.e. $X(t) = \left(\eta^{1/3} + \frac{1}{3} B_t + \overline{L}_t - \overline{U}_t\right)^3$. Here, as well as in the next examples, $\overline{L}_t = V'(a) L_t$ and $\overline{U}_t = V'(b) U_t$ .

**(ii)** For $c > 0$, the process driven by

$$\begin{cases} dX(t) = \frac{3c^2}{8} (X(t))^{1/2} dt + c(X(t))^{3/4}\, dB_t + dL_t - dU_t \\ X(0) = \eta \in [a,b]\ (a \geq 0) \end{cases}, \tag{29}$$

which is conjugated to regulated BM via the function
$V(x) = \frac{4}{c} x^{1/4}$ i.e. $X(t) = \left(\eta^{1/4} + \frac{c}{4} B_t + \overline{L}_t - \overline{U}_t\right)^4$.

**(iii)** (Feller process or CIR model)
For $b > a \geq 0$, the process driven by

$$\begin{cases} dX(t) = \frac{1}{4} dt + \sqrt{X(t)}\, dB_t + dL_t - dU_t \\ X(0) = \eta \in [a,b] \end{cases}, \tag{30}$$

which is conjugated to regulated BM via the function

$V(x) = 2\sqrt{x}$ i.e. $X(t) = \frac{1}{4}(B_t + 2\sqrt{\eta} + \overline{L}_t - \overline{U}_t)^2$.
Notice that the process is always $\geq 0$.

**(iv)** (Wright & Fisher-like process)
For $0 \leq a < b \leq 1$, the process driven by:

$$\begin{cases} dX(t) = \left(\frac{1}{4} - \frac{1}{2} X(t)\right) dt + \sqrt{X(t)(1 - X(t))}\, dB_t + dL_t - dU_t \\ X(0) = \eta \in [a,b] \end{cases},$$

which is conjugated to regulated BM via the function

$V(x) = 2 \arcsin \sqrt{x}$.

This equation is used for instance in the Wright-Fisher model for population genetics and in certain diffusion models for neural activity (see e.g. Lanska *et al.* [15]); it results

$X(t) = \sin^2(B_t/2 + \arcsin\sqrt{\eta} + \overline{L}_t - \overline{U}_t)$ and so $X(t) \in [0,1]$ for all $t \geq 0$.

Notice that, if we take $a = 0$ and $b = 1$, both boundaries are attainable and there is no need for reflection in $a$ and $b$, because the process without reflecting cannot never exit the interval $[0,1]$ (see e.g. Abundo [5]).

If the FPT density is given by (26), from (27) we obtain that the solutions to the IFPT problems for the processes (i)–(iv) above, relative to the barrier $S$, are explicitly given by:

$$g(x) = \left[3x^{2/3}\left(S^{1/3} - a^{1/3}\right)\right]^{-1} \cdot \mathbf{1}_{(a,S)}(x) \ \textbf{(i)},$$
$$g(x) = \tfrac{1}{4}\left[x^{3/4}\left(S^{1/4} - a^{1/4}\right)\right]^{-1} \cdot \mathbf{1}_{(a,S)}(x) \ \textbf{(ii)},$$
$$g(x) = \tfrac{1}{2}\left[\sqrt{x}\left(\sqrt{S} - \sqrt{a}\right)\right]^{-1} \cdot \mathbf{1}_{(a,S)}(x) \ \textbf{(iii)}, \ \text{and}$$
$$g(x) = \tfrac{1}{2}\left[\left(\arcsin\sqrt{S} - \arcsin\sqrt{a}\right)\sqrt{x(1-x)}\ \right]^{-1} \cdot \mathbf{1}_{(a,S)}(x) \ \textbf{(iv)}.$$

## References


1. Abate, J. and Whitt, W., "Transient behavior of regulated Brownian motion. I. Starting at the origin". *Adv. Appl. Prob.*, 19: 560–598 (1987).

2. Abate, J. and Whitt, W., "Transient behavior of regulated Brownian motion. II. Nonzero initial conditions". *Adv. Appl. Prob.*, 19: 599–631 (1987).

3. Abundo, M., "One-dimensional reflected diffusions with two boundaries and an inverse first-hitting problem". *Preprint* (2014).

4. Abundo, M., "The double-barrier inverse first-passage problem for Wiener process with random starting point". *Statist. Probab. Lett.*, 83: 168–176 (2013).

5. Abundo, M., "An inverse first-passage problem for one-dimensional diffusions with random starting point". *Statist. Probab. Lett.*, 82 (1): 7–14 (2012).

6. Abundo, M., "Limit at zero of the first-passage time density and the inverse problem for one-dimensional diffusions". *Stochastic Anal. Appl.*, 24: 1119–1145 (2006).

7. Ball, C.A. and Roma, A., "Detecting mean reversions within reflecting barriers: applications to the European exchange rate mechanism". *Appl. Math. Finance*, 5: 1–15 (1998).

8. Bertolla, G. and Caballero, R.J., "Target zones and realignments". *Amer. Econom. Rev.*, 82: 520–536 (1992).

9. Chuancun, Y. and Huiqing, W., "The first passage time and the dividend value function for one-dimensional diffusion processes between two relecting barriers". *International Journal of Stochastic Analysis*, Article ID971212: 1–15 (2012); doi:10.1155/2012/971212.

10. Darling, D. A. and Siegert, A.J.F., "The first passage problem for a continuous Markov process". *Ann. Math. Statistics*, 24: 624–639 (1953).

11. De Jong, F., "A univariate analysis of European monetary system exchange rates using a target zone model". *J. Appl. Econometrics*, 9: 31–45 (1994).

12. Harrison, M., *Brownian motion and Stochastic Flow Systems.* John Wiley, New York (1985).

13. Jackson, K, Kreinin, A, and Zhang, W., "Randomization in the first hitting problem". *Statis. Probab. Lett.*, 79: 2422–2428 (2009).

14. Krugman, P.R. "Target zones and exchange rate dynamics". *Quart. J. Econom.*, 106: 669–682 (1991).

15. Lanska, V., Lansky, P. and Smiths, C.E., "Synaptic transmission in a diffusion model for neural activity". *J. Theor. Biol.*, 166: 393–406 (1994).

16. Lansky, P. and Smith, C.E., "The effect of a random initial value in neural first-passage-time models". *Math. Biosci.*, 93 (2): 191-215 (1989).

17. Lijun, B., Lidong, Z., Yongjin, W., "On the first passage times of reflected O-U processes with two-sided barriers". *Queueing Sys.*, 54: 313–316 (2006).

18. Linetsky, V., "On the transition densities for reflected diffusions". *Adv. Appl. Prob.*, 37: 435–460 (2005).

19. Linetsky, V., "Computing hitting time densities for CIR and OU diffusions: applications to mean-reverting models". *Journal of Computational Finance*, 7: 1–22 (2004).

20. Linetsky, V., "Lookback options and diffusion hitting times: a spectral expansion approach". *Finance and Stochastics*, 8(3): 373–398 (2004).

21. Lions, P.L. and Sznitman, A.S., "Stochastic differential equations with reflecting boundary conditions". *Comm. Pure Appl. Math.*, 37 (4): 511–537 (1984).

22. Qin Hu, Yong Jin Wang, Xuewei Yang, "The hitting time density for a reflected Brownian motion". *Comput Econ*, 40(1): 1–18 (2012).

23. Ricciardi, L.M. and Sacerdote, L., "On the probability densities of a Ornstein-Uhlenbeck process with a reflecting boundary". *J. Appl. Prob.*, 24: 355–369 (1987).

24. Ricciardi, L.M. and Sato, S., *Diffusion processes and first-passage-time problems*. In: Ricciardi L.M. (Ed.) Lectures in applied Mathematics and Informatics. Manchester University Press, Manchester (1990).

25. Srikant, R. and Whitt, W., "Simulation run lenghts to estimate blocking probabilities". *ACM Trans. Model. Comput. Simul.*, 6: 7–52 (1996).

26. Svensson, L.E.O., "The term structure of interest rate differentials in a target zone. Theory and Swedish data". *J. Monetary Econom.*, 28: 87–116 (1991).

27. Zucca, C. and Sacerdote, L., "On the inverse first-passage-time problem for a Wiener process". *Ann. Appl. Prob.*, 19 (4): 1319-1346 (2009).

28. Ward, A.R. and Glynn, P. W., "A diffusion approximation for a Markovian queue with reneging". *Queueing Sys.*, 43: 103-128 (2003).

29. Ward, A.R. and Glynn, P. W., "Properties of the reflected Ornstein-Uhlenbeck process". *Queueing Sys.*, 44: 109-123 (2003).

# Time Operator and Innovation. Applications to Financial Data

Ilias Gialampoukidis[1] and Ioannis Antoniou[2]

[1] Department of Mathematics, Aristotle University of Thessaloniki
Thessaloniki, 54124, Greece
(E-mail: iliasfg@math.auth.gr)
[2] Department of Mathematics, Aristotle University of Thessaloniki
Thessaloniki, 54124, Greece
(E-mail: iantonio@math.auth.gr)

**Abstract.** The theory of Time Operators has recently been applied into real life problems with the estimation of innovation probabilities. Based on the assumption that the asset values follow Geometric Brownian Motion with constant variance within each trading day, the internal Age of an asset turns out to be a new statistical index, assessing the average innovations. Moreover, the unpredictability of the $t$-th observation $X_t$ is estimated by the distribution of innovations of $X_t$. The innovation probabilities and internal Age are estimated using nonlinear stochastic variance models.
**Keywords:** Time Operator, Innovation, Financial Data, Stochastic Variance Models.

## 1 Introduction

The Time Operator of Dynamical Systems [1–3] has been extended to stochastic processes and has been related to the complexity of the stock price dynamics [4]. The application presented in [4] refers to a specific stock from the Athens stock market during the important Greek elections of June 2012, where the distribution of innovations within the eigenspaces of the Time Operator has been computed. In this work, we propose specific models from the literature for the prediction of the distribution of innovations of an asset, within a predefined trading period.

In section 2, we present the Time Operator associated with a stochastic process $X_t, t = 1, 2, \ldots$, through the construction of its eigenprojections, with eigenvalues the times $t = 1, 2, \ldots$. The average value of the Time Operator (Rayleigh quotient) defines the internal Age of the process (section 3). When the process is the evolution of an asset's price, it is shown [4] that the internal Age is a function of the variances of each trading day. The values Open $O_\tau$, High $H_\tau$, Low $L_\tau$ and Close $C_\tau$ are known for $\tau = 1, 2, \ldots, T$ so using the

*Stochastic Modeling, Data Analysis and Statistical Applications* (*pp.* 19-31)
Lidia Filus - Teresa Oliveira - Christos H Skiadas (Eds)



more efficient daily variance estimator we find, in section 4, the distribution of innovations and their mean, i.e. the internal Age.

The novelty of this work is the estimation of the innovation probabilities $p_\tau$ from future variances $\sigma_\tau^2$ where Open, High, Low, Close values are unknown. In section 5, we shall employ nonlinear stochastic variance models for the evolution of $\sigma_\tau^2$ and obtain an explicit innovation probability formula corresponding to each model.

In section 6, we present an application to a stock market index. The estimated variances $\sigma_\tau^2$ from stock market data are transformed using the Box-Cox transformation [5]. The nonlinear stochastic variance model is selected, among the existing ones, as the one with the best fit to the data.

## 2 Innovations and Time Operator of Stochastic Processes

Consider a stochastic process $X_1, X_2, \ldots$ with the correlation scalar product $< X, Y >= E[XY]$ and denote by $\mathfrak{S}$ the $\sigma$-algebra generated by the random variables $X_1, X_2, \ldots$. Assuming that $X_1, X_2, \ldots$ have finite mean and finite correlations, they live in the Hilbert space $L^2(\Omega, \mathfrak{S}, \mu)$, where $\Omega$ is their sample space.

The random variables $X_1, X_2, \ldots, X_t$ generate the $\sigma$-algebras $\mathfrak{S}_t, t = 1, 2, \ldots$ which define the natural filtration $\{\Omega, \emptyset\} = \mathfrak{S}_0 \subseteq \mathfrak{S}_1 \subseteq \mathfrak{S}_2 \subseteq \cdots \subseteq \mathfrak{S}$ of the stochastic process $X_1, X_2, \ldots$. From the natural filtration $\mathfrak{S}_t, t = 1, 2, \ldots$ of the stochastic process we construct the corresponding sequence of subspaces of $L^2(\Omega, \mathfrak{S}, \mu)$:

$$\mathcal{H}_0 = span\{1_\Omega\}, \quad \mathcal{H}_t = L^2(\Omega, \mathfrak{S}_t, \mu), \quad t = 1, 2, \ldots \tag{1}$$

where $\mathcal{H}_0$ is the Hilbert space of constant random variables. The orthocomplement of $\mathcal{H}_0$ is the Hilbert space $\mathcal{H}$ of fluctuations $\mathcal{H} = L^2(\Omega, \mathfrak{S}, \mu) \ominus \mathcal{H}_0$. Every random variable in $\mathcal{H}$ has the form:$X - E[X]1_\Omega, X \in L^2(\Omega, \mathfrak{S}, \mu)$. The family $\mathcal{H}_t, t = 1, 2, \ldots$ is a resolution of the identity of the Hilbert space $\mathcal{H}$, i.e. $\wedge_{t\in\mathbb{N}}\mathcal{H}_t = \emptyset, \vee_{t\in\mathbb{N}}\mathcal{H}_t = \mathcal{H}$ and $\mathcal{H}_t \subseteq \mathcal{H}_{t+1}, t \in \mathbb{N}$.

The projections: $E_t : \mathcal{H} \to \mathcal{H}_t, t = 0, 1, 2, \ldots$ onto the spaces $\mathcal{H}_t$ are the conditional expectations:

$$\mathbb{E}_t := E[.|\mathfrak{S}_t], t = 0, 1, 2, \ldots \tag{2}$$

and define the resolution of identity operator in $\mathcal{H} : \mathbb{E}_t, t = 0, 1, 2, \ldots$.

**Definition 1.** The self-adjoint operator with spectral projections the conditional expectations $\mathbb{E}_t$ (2) on the space of fluctuations $\mathcal{H}$ is called *the Time Operator of the stochastic process* $X_t, t = 1, 2, \ldots$:

$$\mathbb{T} = \sum_{t=1}^{\infty} t(\mathbb{E}_t \ominus \mathbb{E}_{t-1}) = \sum_{t=1}^{\infty} t\mathbb{P}_t \tag{3}$$

The eigenspaces of the Time Operator are the Hilbert spaces $\mathcal{N}_t := \mathcal{H}_t \ominus \mathcal{H}_{t-1}, t = 1, 2, \ldots$ and they are called *Innovation Spaces*. The projections $\mathbb{P}_t = \mathbb{E}_t \ominus \mathbb{E}_{t-1}$ onto the innovation spaces $\mathcal{N}_t, t = 1, 2, \ldots$ quantify the innovative part $\mathbb{P}_t Z$ of a random variable $Z$ at time step $t$.

For example, The Time Operator of Bernoulli Processes [3,4] is applied to the one-dimensional non-stationary random walk

$$X_0 = 0, \quad X_t = Z_1 + Z_2 + \cdots + Z_t, \quad t = 1, 2, \ldots \tag{4}$$

as follows [4]:

$$\mathbb{T}X_t = \sum_{\tau=1}^{\infty} \tau \mathbb{P}_\tau X_t = \sum_{\tau=1}^{\infty} \tau (Z_\tau - E[Z_\tau]) \tag{5}$$

where

$$Z_t = \begin{cases} 1 \text{ with probability } \pi_t \\ -1 \text{ with probability } 1 - \pi_t \end{cases}, \quad t = 1, 2, \ldots \tag{6}$$

## 3 The Internal Age of an Asset

The innovation probability of a random variable $A$ at time $t$, is defined as the probability to observe the random variable $A$ in the innovation space $\mathcal{N}_t$:

$$p_t(A) = prob\{A \in \mathcal{N}_t\} = \frac{\|\mathbb{P}_t A\|^2}{\|A - E[A]\|^2} = \frac{Var[\mathbb{P}_t A]}{Var[A]} \tag{7}$$

The Rayleigh quotient (expectation) of the Time Operator $\mathbb{T}$ for the random variable $A$ is called the internal Age of $A$ and is given by the formulas [4]:

$$Age(A) = \frac{< A - E[A], \mathbb{T}(A - E[A]) >}{\|A - E[A]\|^2} = \sum_{t=1}^{\infty} t p_t(A) \tag{8}$$

The internal Age is the average innovation time of the random variable $A$ and $p_t(A), t = 1, 2, \ldots$ is the distribution of innovations within the eigenspaces of $\mathbb{T}$.

When the Time Operator of Bernoulli Processes is applied to one-dimensional non-stationary random walk $X_t$ (4), the internal Age of $X_t$ is a function of the variance of the increments (6) [4, Theorem 5.2]:

$$Age(X_t) = \sum_{\tau=1}^{t} \tau \frac{\sigma_\tau^2}{\sum_{\nu=1}^{t} \sigma_\nu^2}, \quad t = 1, 2, \ldots. \tag{9}$$

where $\sigma_\tau^2 = Var[Z_\tau]$, and the innovation probabilities of the random walk $X_t$ are:

$$p_\tau = \frac{\sigma_\tau^2}{\sum_{\nu=1}^{t} \sigma_\nu^2}, \quad \tau = 1, 2, \ldots, t \tag{10}$$

Formulas (9) and (10) allow estimation of the innovation probabilities and internal Age through the estimation of the variances $\sigma_\tau^2$.

In order to estimate the internal Age and the innovation probabilities of an asset (stock, currency, etc.), we assume that the asset's prices $X_t, t = 1, 2, \ldots$ are a non-stationary random walk and the index set $X_t, t = 1, 2, \ldots$ of the random walk observations $X_t$ refers to trading days. Some hours of the day the market is open (trading period) and the rest of the day the market is closed. The values Open $O_\tau$, Close $C_\tau$, High $H_\tau$ and Low $L_\tau$ of the $\tau$-trading day are the available price information of each trading day. Moreover, we assume that the prices of an asset follow Geometric Brownian Motion within each trading day [6]. The variance $\sigma_t^2$ is assumed constant with each trading day, but variable from one trading day to another.

At time $t = T$ the observation $X_T$ corresponds to the present asset's price, at the end of today's trading period, so that the values Open $O_\tau$, Close $C_\tau$, High $H_\tau$ and Low $L_\tau$ are available. Hence, $t = T+1$ will stand for "tomorrow", i.e. the following trading day.

## 4 Innovation Probability Estimators from High, Low, Open and Closing Prices

In this section we discuss the estimation of the variance $\hat{\sigma}_\tau^2 = \hat{Var}[Z_\tau]$ of the increment $Z_\tau$ for each trading day $\tau$ for times $\tau \leq T$. In previous work [4], we have presented five popular unbiased estimators, namely the close-to-close estimator $\hat{\sigma}_{CC}^2$ [7], the high-low Parkinson estimator $\hat{\sigma}_P^2$ [7], the Garman-Klass estimator $\hat{\sigma}_{GK}^2$ [8], the Rogers-Satchell estimator $\hat{\sigma}_{RS}^2$ [9] and the Yang-Zhang estimator $\hat{\sigma}_{YZ}^2$ [10]. Among these known variance estimators:

- Parkinson's estimator $\hat{\sigma}_P^2$ [7] and the classic close-to-close estimator $\hat{\sigma}_{CC}^2$ [7] are less efficient than the Rogers-Satchell estimator $\hat{\sigma}_{RS}^2$ [9]
- The Yang-Zhang estimator $\hat{\sigma}_{YZ}^2$ [10] is not able to estimate the variance using data from only one trading day.
- The Garman-Klass estimator $\hat{\sigma}_{GK}^2$ [8] assumes that there is no upward or downward trend, while the Rogers-Satchell estimator $\hat{\sigma}_{RS}^2$ [9] does not.

Due to the above three reasons, the Rogers-Satchell estimator $\hat{\sigma}_{RS}^2$ [9] is the most efficient drift-independent variance estimator, allowing intraday estimations. Hence, the variance of the $\tau$-trading day is given as follows:

$$\hat{\sigma}_{RS(\tau)}^2 = u_\tau(u_\tau - c_\tau) + d_\tau(d_\tau - c_\tau) \tag{11}$$

where $u_\tau = \ln H_\tau - \ln O_\tau, \quad d_\tau = \ln L_\tau - \ln O_\tau, \quad c_\tau = \ln C_\tau - \ln O_\tau$.

**Corollary 1.** *The innovation probabilities of the asset's price at day $t$, $t = 1, 2, \ldots, T$ are estimated as follows:*

$$\hat{p}_\tau = \frac{u_\tau(u_\tau - c_\tau) + d_\tau(d_\tau - c_\tau)}{\sum_{\tau=1}^{t} u_\tau(u_\tau - c_\tau) + d_\tau(d_\tau - c_\tau)} \tag{12}$$

*The internal Age of the asset's price at day $t$ is given by:*

$$\hat{Age}(X_t) = \sum_{\tau=1}^{t} \tau \frac{u_\tau(u_\tau - c_\tau) + d_\tau(d_\tau - c_\tau)}{\sum_{\tau=1}^{t} u_\tau(u_\tau - c_\tau) + d_\tau(d_\tau - c_\tau)} \tag{13}$$

Corollary 1, may be used for the estimation of the internal Age and distribution of innovations of an asset's price at day $t$, when $t \leq T$. In the following section, we modify Eq. (12) and Eq. (13), using nonlinear stochastic variance models for estimations at day $t = T + 1$, i.e. the following trading day.

## 5 Innovation Probability Estimators from Nonlinear Stochastic Variance models

We shall estimate the distribution of innovations and the internal Age of the random variable $X_{T+1}$. The formula which gives the innovation probability of $X_{T+1}$ for the following trading day $(T + 1)$ is:

$$\hat{p}_{T+1} = \frac{\hat{\sigma}^2_{T+1}}{\hat{\sigma}^2_{T+1} + \sum_{\tau=1}^{T} \hat{\sigma}^2_{\tau}} \tag{14}$$

where $\hat{\sigma}^2_{T+1}$ is estimated from a stochastic variance evolution model and $\hat{\sigma}^2_{\tau}$ are estimated from Open, High, Low and Closing values $\tau = 1, 2, \ldots, T$. The values $O_{T+1}, C_{T+1}, H_{T+1}$ and $L_{T+1}$ have not been observed yet.

In [11] we find a classification of stochastic variance (volatility squared) models. They all assume that an asset's price, or stock market index, follows a Geometric Brownian Motion with variance $\sigma^2_{\tau}$ evolving according to its own stochastic process. We list the models and the corresponding innovation probability estimators $\hat{p}_{T+1}$, in Table 1.

| **Reference** | **Stochastic Variance Model** | **Innovation Probability** $\hat{p}_{T+1}$ |
|---|---|---|
| [12] | $\ln \sigma^2_{T+1} = \alpha + \beta\epsilon_T$ | $\frac{\exp(\alpha+\beta\epsilon_T)}{\exp(\alpha+\beta\epsilon_T)+\sum_{\tau=1}^{T}\sigma^2_{\tau}}$ |
| [13] | $\ln \sigma^2_{T+1} = \gamma(\ln \sigma^2_T - \alpha) + \alpha + \beta\epsilon_T$ | $\frac{\exp(\gamma(\ln \sigma^2_T-\alpha)+\alpha+\beta\epsilon_T)}{\exp(\gamma(\ln \sigma^2_T-\alpha)+\alpha+\beta\epsilon_T)+\sum_{\tau=1}^{T}\sigma^2_{\tau}}$ |
| [14,15] | $\ln \sigma^2_{T+1} = \ln \sigma^2_T + \alpha + \beta\epsilon_T$ | $\frac{\sigma^2_T \exp(\alpha+\beta\epsilon_T)}{\sigma^2_T \exp(\alpha+\beta\epsilon_T)+\sum_{\tau=1}^{T}\sigma^2_{\tau}}$ |
| [16–18] | $\sigma_{T+1} = \gamma(\sigma_T - \alpha) + \alpha + \beta\epsilon_T$ | $\frac{(\gamma(\sigma_T-\alpha)+\alpha+\beta\epsilon_T)^2}{(\gamma(\sigma_T-\alpha)+\alpha+\beta\epsilon_T)^2+\sum_{\tau=1}^{T}\sigma^2_{\tau}}$ |
| [19] | $\sigma^2_{T+1} = \gamma(\sigma^2_T - \alpha) + \alpha + \beta\epsilon_T$ | $\frac{\gamma(\sigma^2_T-\alpha)+\alpha+\beta\epsilon_T}{\gamma(\sigma^2_T-\alpha)+\alpha+\beta\epsilon_T+\sum_{\tau=1}^{T}\sigma^2_{\tau}}$ |
| [11] | $h(\sigma^2_{T+1}, \delta) = \alpha + \gamma(h(\sigma^2_T, \delta) - \alpha) + \beta\epsilon_T$ | $\frac{g(\alpha+\gamma(h(\sigma^2_T,\delta)-\alpha)+\beta\epsilon_T)}{g(\alpha+\gamma(h(\sigma^2_T,\delta)-\alpha)+\beta\epsilon_T)+\sum_{\tau=1}^{T}\sigma^2_{\tau}}$ |
| | $h(\sigma^2_{T+1}, \delta) = h(\sigma^2_T, \delta) + \alpha + \beta\epsilon_T$ | $\frac{g(h(\sigma^2_T,\delta)+\alpha+\beta\epsilon_T)}{g(h(\sigma^2_T,\delta)+\alpha+\beta\epsilon_T)+\sum_{\tau=1}^{T}\sigma^2_{\tau}}$ |

**Table 1.** Forecasting the innovation probability of the following trading day using stochastic variance models

In Yu *et al.* [11] the model involves the Box-Cox transformation of the variance $\sigma^2_{\tau}$:

$$h(\sigma^2_{\tau}, \delta) = \begin{cases} \frac{(\sigma^2_{\tau})^{\delta}-1}{\delta} & \text{if } \delta \neq 0 \\ \ln \sigma^2_{\tau} & \text{if } \delta = 0 \end{cases} \tag{15}$$

and the innovation probability $p_{T+1}$ the inverse Box-Cox transformation of the variance $\sigma_\tau^2$:

$$g(h(\sigma_\tau^2,\delta)) = \begin{cases} (1+\delta\cdot h(\sigma_\tau^2,\delta))^{\frac{1}{\delta}} & \text{if } \delta \neq 0 \\ \exp(h(\sigma_\tau^2,\delta)) & \text{if } \delta = 0 \end{cases} \tag{16}$$

The latest model of Yu *et al.* [11] is a generalization of the previous, most popular models:

- For $\delta = 0$, the model of Yu *et al.* [11] becomes the Wiggins model [13].
- For $\delta = 0.5$, the model of Yu *et al.* [11] becomes the Stein model [17].
- For $\delta = 1$, the model of Yu *et al.* [11] becomes the Andersen model [19].

Combining the most appropriate model (the one with the best fit to our data) with the Rogers-Satchell estimator:

$$\hat{Age}(X_{T+1}) = (T+1)\hat{p}_{T+1} + \sum_{\tau=1}^{T} \tau \frac{u_\tau(u_\tau - c_\tau) + d_\tau(d_\tau - c_\tau)}{\hat{\sigma}_{T+1}^2 + \sum_{\tau=1}^{T} u_\tau(u_\tau - c_\tau) + d_\tau(d_\tau - c_\tau)} \tag{17}$$

where $\hat{p}_{T+1}$ are given from Table 1 and $u_\tau, c_\tau, d_\tau$ are the quantities of Eq. (12).

In the case of the general model of Yu *et al.* [11] the transformed variances are assumed to follow an Ornstein-Uhlenbeck process [11], which is a mean-reverting process with parameters: $\alpha$ is the long-run variance, $\gamma$ is the rate at which the transformed variance $h(\sigma_\tau^2,\delta)$ reverts to $\alpha$, $\beta$ is the constant variance of the Gaussian increment:

$$h(\sigma_\tau^2,\delta) - \gamma(h(\sigma_{\tau-1}^2,\delta) - \alpha) - \alpha \tag{18}$$

In Zhang and King [20] we find Monte Carlo simulation techniques for the estimation of the parameters $\alpha, \beta, \gamma, \delta$. The process with the independent increments (18) assumes that the variances of an asset, or an index, revert to a constant value $\alpha$ in the long-run. This is an empirical assumption [6] and for statistically significant values of $\gamma$ estimated to be close to 1 (as in [20]) the model (19) can be simplified to assume that the variance increments

$$h(\sigma_\tau^2,\delta) - h(\sigma_{\tau-1}^2,\delta) \tag{19}$$

are normally distributed, with constant mean and variance. This is the case we examine in the following section. The most related work to this model in the literature is the NARCH model of Higgins and Bera [21,22] where the transformed errors of a time series follow an AR($p$) process, generalizing the ARCH and GARCH models of Engle [23] and Bollersev [24] respectively.

## 6 Application to Athens Stock Market General Index

We assume that the variance $\sigma_\tau^2$ within each trading day is constant and we use the Rogers-Satchell estimator (11) [9] which is more efficient than the classic close-to-close estimator.

| $\delta$ | **p-value** | **Decision** | $\delta$ | **p-value** | **Decision** |
|---|---|---|---|---|---|
| 0,20 | 0,019 | Reject | 0,33 | 0,106 | Accept |
| 0,21 | 0,029 | Reject | 0,34 | 0,112 | Accept |
| 0,23 | 0,06 | Accept | 0,36 | 0,092 | Accept |
| 0,24 | 0,069 | Accept | 0,37 | 0,086 | Accept |
| 0,25 | 0,092 | Accept | 0,38 | 0,076 | Accept |
| 0,26 | 0,112 | Accept | 0,39 | 0,061 | Accept |
| 0,27 | 0,122 | Accept | 0,40 | 0,061 | Accept |
| 0,28 | 0,148 | Accept | 0,41 | 0,051 | Accept |
| 0,29 | 0,143 | Accept | 0,42 | 0,043 | Reject |
| 0,30 | 0,164 | Accept | 0,43 | 0,036 | Reject |
| 0,31 | 0,14 | Accept | 0,44 | 0,025 | Reject |
| 0,32 | 0,106 | Accept | 0,45 | 0,02 | Reject |

**Table 2.** The normality of the increments is tested for several values of $\delta$ using the Kolmogorov-Smirnov test

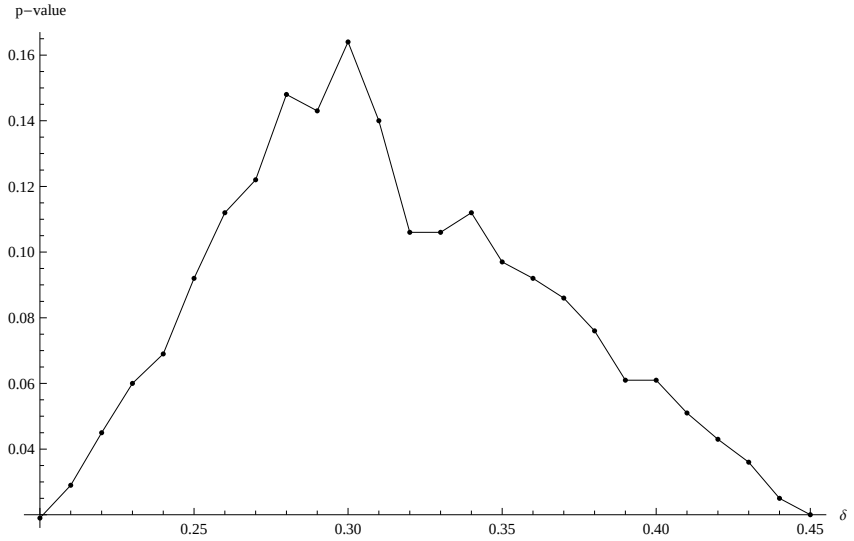


**Fig. 1.** The region $\delta \in [0.23, 0.41]$ involves transformed variances which are normally distributed (with significance level 0.05). The highest p-value (0.164) is attained at $\delta = 0.30$

We found evidence that the variances $\sigma_\tau^2$ the Athens General Stock Market Index from $18^{\text{th}}$ February 2009 to $17^{\text{th}}$ February 2014 are determined by the model:

$$h(\sigma_\tau^2, \delta) - h(\sigma_{\tau-1}^2, \delta) = \alpha + \beta \cdot \epsilon_\tau \tag{20}$$

where $\hat{a} = 0.0001, \hat{\beta} = 0.1016, \hat{\delta} = 0.30$ and $\epsilon_\tau$ are Gaussian zero centered, unit variance random variables.

We could not reject the hypothesis that the transformed variances $h(\sigma_\tau^2, \delta) - h(\sigma_{\tau-1}^2, \delta)$ of the Athens General Stock Market Index from $18^{\text{th}}$ February 2009 to $17^{\text{th}}$ February 2014 are normally distributed for $\delta \in [0.23, 0.41]$. The

Kolmogorov-Smirnov tests and their corresponding decision are shown in Table 2. Figure 1 shows the p-value of each Kolmogorov-Smirnov test corresponding to each selection of the power $\delta$. Data have been obtained from [25] and the computations have been done in SPSS Statistics 20.

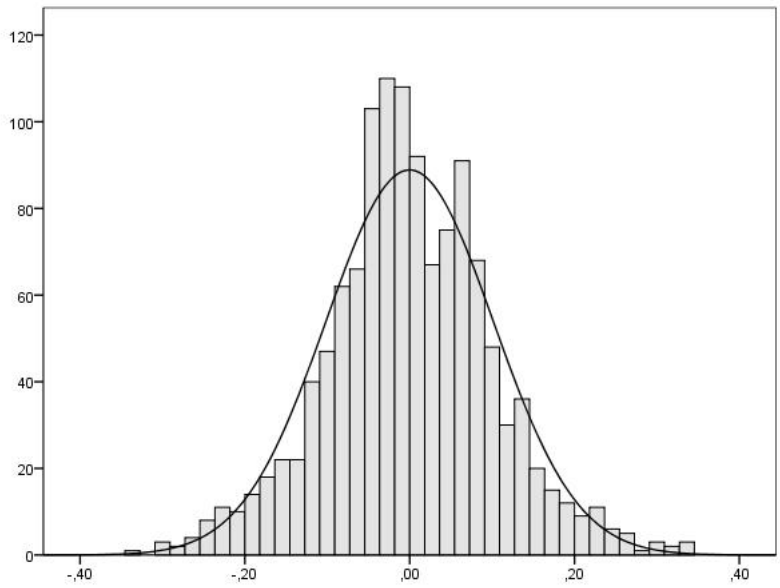


**Fig. 2.** Histogram of the transformed variances with the estimated normal curve, for $\delta = 0.30$

We report some of the statistics of the variable $h(\sigma_\tau^2, 0.30) - h(\sigma_{\tau-1}^2, 0.30)$. The sample has 1245 values having mean $-0.0001$, standard deviation 0.1016, skewness 0.077 and kurtosis 0.556. The spectrum of the sample is in the interval $[-0.3348, 0.3339]$.

**Corollary 2.** *The innovation probability $p_{T+1}$ for the Athens stock market general index is:*

$$p_{T+1} = \frac{\sigma_{T+1}^2}{\sigma_{T+1}^2 + \sum_{\tau=1}^{T} u_\tau(u_\tau - c_\tau) + d_\tau(d_\tau - c_\tau)} \tag{21}$$

*where* $\sigma_{T+1}^2 = \sqrt[0.30]{(u_T(u_T - c_T) + d_T(d_T - c_T))^{0.30} + 0.03\epsilon_T}$.

*Proof.* The highest p-value (0.164) is attained at $\delta = 0.30$, so the variance evolution model is:

$$\frac{(\sigma_\tau^2)^\delta - 1}{\delta} - \frac{(\sigma_{\tau-1}^2)^\delta - 1}{\delta} = \alpha + \beta\epsilon_\tau \tag{22}$$

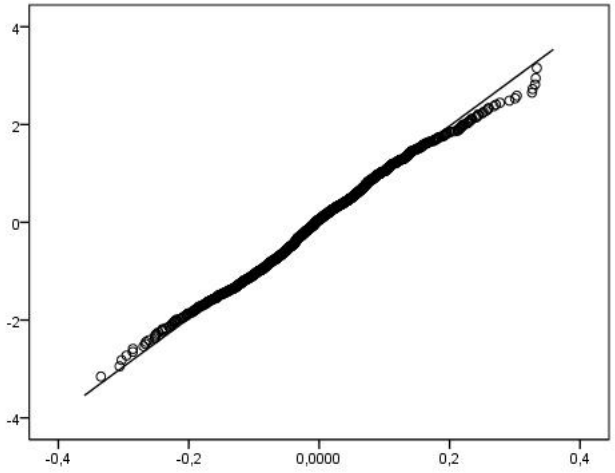


**Fig. 3.** Q-Q plot of the transformed variances for $\delta = 0.30$

where $\alpha = -0.0001, \beta = 0.1016, \epsilon_\tau$: zero mean, unit variance normally distributed random variable. Equivalently, $(\sigma_\tau^2)^\delta - (\sigma_{\tau-1}^2)^\delta = \delta\alpha + \delta\beta\epsilon_\tau$. Therefore, the variance is $\sigma_\tau^2 = \sqrt[\delta]{(\sigma_{\tau-1}^2)^\delta + \delta\alpha + \delta\beta\epsilon_\tau}$ and the innovation probability $p_{T+1}$ (21) is proved after substitution of the Rogers-Satchell estimator (11) to the variances $\sigma_\tau^2, \tau = 1, 2, \ldots, T$ and taking into account that $\delta\alpha = -0.00003 \cong 0$.

From the definition of the internal Age (8), formula (9) and Corollary 2, the internal Age computation is straightforward:

**Corollary 3.** *The internal Age of the following trading day is:*

$$\hat{Age}(X_{T+1}) = (T+1)\hat{p}_{T+1} + \sum_{\tau=1}^{T} \tau \frac{u_\tau(u_\tau - c_\tau) + d_\tau(d_\tau - c_\tau)}{\hat{\sigma}_{T+1}^2 + \sum_{\tau=1}^{T} u_\tau(u_\tau - c_\tau) + d_\tau(d_\tau - c_\tau)} \tag{23}$$

*where* $\sigma_{T+1}^2 = \sqrt[0.30]{(u_T(u_T - c_T) + d_T(d_T - c_T))^{0.30} + 0.03\epsilon_T}$ *and* $\hat{p}_{T+1}$ *is given by Corollary 2.*

The transformed variance increments $(\sigma_\tau^2)^\delta - (\sigma_{\tau-1}^2)^\delta$ are expected to be practically zero:

$$E[(\sigma_\tau^2)^\delta - (\sigma_{\tau-1}^2)^\delta] = E[\delta\alpha + \delta\beta\epsilon_\tau] = \delta\alpha + \delta\beta E[\epsilon_\tau] = \delta\alpha = -0.00003 \cong 0$$

Therefore, we may apply Corollaries 2 and 3 in any period of $T$ trading days for the estimation of the innovation probability based on Corollary 2 (expected innovation probability) and compare to the innovation probability estimations based on Open, High, Low and Close prices. Moreover, we may also estimate the internal Age, based on Corollary 3 (expected internal Age) and compare to the internal Age estimations based on Open, High, Low and Close prices.

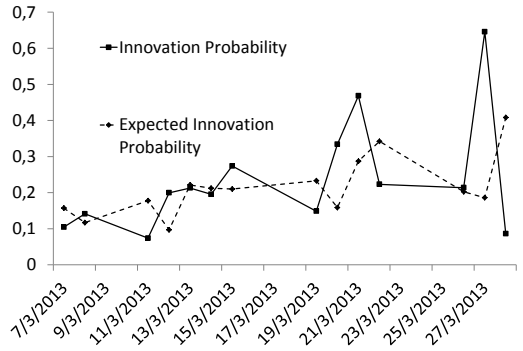


**Fig. 4.** The innovation probability of the following trading day based on Open, High, Low and Close prices (solid line). The expected innovation probability (dashed line) is based on Corollary 2.

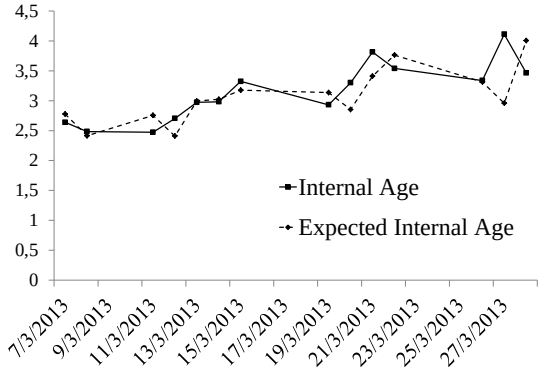


**Fig. 5.** The internal Age of the following trading day based on Open, High, Low and Close prices (solid line). The expected internal Age (dashed line) is based on Corollary 3.

We apply previous analysis on March 2013. This month has an extreme value related to the Cyprus bailout deal where large deposits were seized and the second-largest bank closed [26].

Based on the previous 3 trading days and the available information at the end of the present trading day ($T = 4$), we find the innovation probability and the internal Age of the following trading day. The values Open, Close, High, Low of the $5^{\text{th}}$ trading day are not known yet and the expected innovation probability and the expected internal Age are estimated from Corollaries 2 and 3 respectively. At the end of the $5^{\text{th}}$ trading day, we estimate the innovation probability and the internal Age using the Rogers-Satchell estimator (Corollary 1). The expected innovation probabilities (Corollary 2) are compared to the innovation probabilities (Corollary 1) in Figure 4. The expected internal Age (Corollary 3) is compared to the internal Age (Corollary 1) in Figure 5.

The internal Age of 5 successive trading days in March 2013 attains its maximum value at 27$^{\text{th}}$ March, i.e. one day after the announcement trading day date (26$^{\text{th}}$ March 2013). Greek firms with large deposits in Cypriot banks and projects running in Cyprus caused a strong impact on the Athens stock market index. This impact is quantified through the innovation probabilities and the internal Age of the corresponding dates demonstrating the high complexity of this trading period.

The estimations close to the 27$^{\text{th}}$ of March 2013 are not satisfactory, due to the external force that changed the dynamics of the stock value process. As long as the prices fluctuate according to its own innovations, the prediction of the innovation probabilities is satisfactory. The change in the dynamics was caused by a political decision, unpredictable so far for many scientists.

## 7 Concluding Remarks

We used the Rogers-Satchell estimator of the daily variance, which is more efficient than the classic close-to-close estimator and drift-independent. The most recent variance estimator of Yang and Zhang [10] uses data from more than one trading days.

From Corollary 3 we see that internal Age estimations are computed from past variances, using the Rogers-Satchell estimator, and future variances, using a model from Table 1. The most appropriate model is selected as the one with best fit to the corresponding data.

In case the independent increments $Z_\tau$ of Eq. (4) of the asset price dynamics are not Gaussian, Mandelbrot [27] proposed the Pareto distribution to model the changes in the logarithm of cotton prices. These distributions have infinite variance:

$$Var[Z_\tau] = \sigma_\tau^2 = \infty \tag{24}$$

In case Eq. (24) is true, i.e. the increments $Z_\tau$ of Eq. (4) have infinite variance, the innovation probability is always 100%:

$$\lim_{\sigma_{T+1}^2 \to \infty} p_{T+1} = \frac{\sigma_{T+1}^2}{\sigma_{T+1}^2 + \sum_{\tau=1}^{T} \sigma_\tau^2} = \frac{1}{1 + \frac{\sum_{\tau=1}^{T} \sigma_\tau^2}{\sigma_{T+1}^2}} \to 1 \tag{25}$$

The prediction in such a complex environment is not expected to be successful, no matter how many previous observations are used.

As shown in Figure 6, the survival function in logarithmic scale does not fit to a straight line. Therefore, the Pareto distribution does not fit to the differences of the logarithms of the closing prices.

In case the predicted variance $\hat{\sigma}_{T+1}$ of the following trading day is estimated from a constant known value $c$ (for example the 100-year average variance), Eq. (14) is of the form:

$$\hat{p}_{T+1} = \frac{\hat{\sigma}_{T+1}^2}{\hat{\sigma}_{T+1}^2 + \sum_{\tau=1}^{T} \hat{\sigma}_\tau^2} = \frac{c}{c + x} \tag{26}$$

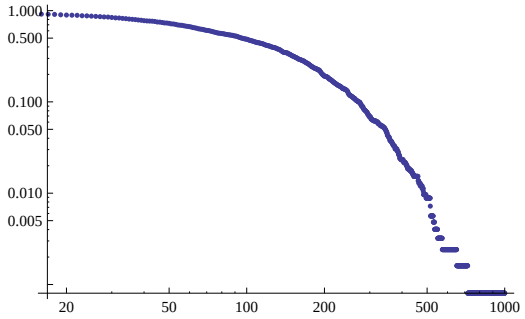


**Fig. 6.** LogLogPlot of the survival function $Prob[\ln C_t - \ln C_{t-1} > k]$ . Not power-law scaling.

Eq. (24) shows that periods of low uncertainty and variance ($x \to 0$) imply high innovation probability $\hat{p}_{T+1} \to 1$ the following trading day. Moreover, periods of high uncertainty and variance ($x \to \infty$) imply low innovation probability $\hat{p}_{T+1} \to 0$.

We estimated the innovation probabilities and the internal Age of the Athens general stock market index observations during March 2013. The significant event associated with this month is the recent bailout program of Cyprus, resulting to a severe local downward trend at the Athens General stock market index. The high complexity (measured here from the innovation probabilities and the internal Age) of specific trading dates is not affected by the sign of the local drift, i.e. it does not matter whether the local trend is upward or downward. We have recently illustrated the increasing distribution of innovations as we approach the important Greek elections of June 2012 [4], leading to an upward trend. The average innovation time is important for the risk assessment of specific trading days.

## Acknowledgements

We thank the Aristotle University of Thessaloniki and especially the Research Committee for supporting one of us (Ilias Gialampoukidis) by awarding him the Excellence Scholarship 2013. We also thank Karl Gustafson for useful discussions and comments.

## References

1. Misra B., Prigogine I. and M. Courbage. From deterministic dynamics to probabilistic descriptions. *Physica A*, 98, 1, 1–26, 1979
2. I. Prigogine. *From Being to Becoming*. Freeman, New York, 1980
3. M. Courbage and B. Misra. On the equivalence between Bernoulli dynamical systems and stochastic Markov processes. *Physica A*, 104, 3, 359–377, 1980
4. Gialampoukidis I., Gustafson K. and I. Antoniou. Financial Time Operator for Random Walk Markets. *Chaos, Solitons & Fractals* 57, 62–72, 2013

5. Box G.E.P, and D.R. Cox. An analysis of transformations. *Journal of the Royal Statistical Society* B, 211–252, 1964
6. J. Hull. *Options, Futures, and other Derivatives*, seventh ed., Pearson, New Jersey, 2009
7. M. Parkinson. The extreme value method for estimating the variance of the rate of return. *Journal of Business* 53, 61–65, 1980
8. M. Garman and M.J. Klass. On the Estimation of Security Price Volatilities from Historical Data. *Journal of Business* 53, 67–78, 1980
9. L. C. G. Rogers and S.E. Satchell. Estimating Variance from High, Low and Closing Prices. *Annals of Applied Probability* 1, 504–12, 1991
10. D. Yang and Q. Zhang. Drift Independent Volatility Estimation Based on High, Low, Open and Close Prices. *Journal of Business* 73, 477–491, 2000
11. Yu J., Yang Z. and X. Zhang. A class of nonlinear stochastic volatility models and its implications for pricing currency options. *Computational Statistics & Data Analysis* 51, 2218–2231, 2006
12. P. K. Clark. A subordinated stochastic process model with finite variance for speculative price. *Econometrica* 68, 135–155, 1973
13. J. B. Wiggins. Option values under stochastic volatility: Theory and empirical estimates. *Journal of financial economics* 19, 2, 351–372, 1987
14. Hull J. and A. White. The pricing of options on assets with stochastic volatilities. *The journal of finance* 42, 281–300, 1987
15. Johnson H. and D. Shanno. Option pricing when the variance is changing. *Journal of Financial and Quantitative Analysis* 22 ,143–152, 1987
16. L. O. Scott. Option pricing when the variance changes randomly: theory, estimation and an application. *Journal of Financial and Quantitative Analysis* 22, 419–439, 1987
17. Stein E. M. and J. C. Stein. Stock price distributions with stochastic volatility: an analytical approach. *Review of financial studies* 4, 727–752, 1991
18. S. L. Heston. A closed-form solution for options with stochastic volatility, with application to bond and currency options. *Review of financial studies* 6, 327–343, 1993
19. T. Andersen. Stochastic autoregressive volatility: a framework for volatility modeling. *Mathematical finance* 4, 75–102, 1994
20. Zhang X. and M. L. King. Box-Cox stochastic volatility models with heavy-tails and correlated errors. *Journal of Empirical Finance* 15, 3, 549–566, 2008
21. Higgins M. L. and A. K. Bera. A class of nonlinear ARCH models. Unpublished manuscript (Department of Economics, University of Illinois, Champaign, IL), 1989
22. Higgins M. L. and A. K. Bera. A class of nonlinear ARCH models. *International Economic Review* 137–158, 1992
23. R. F. Engle. Autoregressive conditional heteroscedasticity with estimates of the variance of United Kingdom inflation. *Econometrica: Journal of the Econometric Society*. 987–1007, 1982
24. T. Bollerslev. Generalized autoregressive conditional heteroskedasticity. *Journal of econometrics* 31.3, 307–327, 1986
25. http://www.naftemporiki.gr/finance/quote?id=GD.ATH
26. http://www.independent.co.uk/news/world/europe/cyprus-bailout-large-deposits-will-be-seized-and-secondlargest-bank-closed-in-10bn-eu-bailout-deal-8547104.html
27. B. Mandelbrot. The Variation of Certain Speculative Prices. *The Journal of Business* 36, 394–419, 1963

# Including Path Continuity Properties in Process Estimation

Lino Sant

Department of Statistics and Operations Research,
Faculty of Science, University of Malta, Msida, Malta
(e-mail: lino.sant@um.edu.mt)

**Abstract.** Estimation of parameters for processes with independent increments is many times effected exclusively through fitting an infinitely divisible distribution on increments obtained from finitely many readings. Ignoring path properties, which have been involved in data generation in the first place, must have negative effects. Much work has been done to improve the quality of simulated data from that generated through cumulative sums of independent random variates. Exact simulation tries to put in more realism about path properties. In this paper we study this situation within the simple context of Brownian motion, proposing two estimators which incorporate properties related to path continuity. Results obtained from simulations with data generated by various types of algorithms are compared and contrasted with ones obtained from the less sophisticated variance estimator.
**Keywords:** estimation from stationary and independent increments, simulated paths , continuity of paths.

## 1 Introduction

Parameter estimation, intended so as to help determine the type of stochastic process one should use for specific data generating mechanisms, is common in many applications of probability and statistical theory. Once the pioneers of random processes paved a highway towards deep structural results within the realm of the mathematically possible, effective use of stochastic models required a number of tasks. One important statistical task centres around devising reliable algorithms to estimate parameters and functionals of particular processes from a finite number of observations.

One widely used technique involved specifying a probability density function which captures the true distribution of the observations in a form which facilitates the estimation problem. The stationary, independent increments assumption, for example, simplifies many estimation tasks enormously by allowing standard methods like maximum likelihood to take over. However this type of assumption encapsulates much less than what would identify a particular process completely. Independent, stationary increments on their own are not sufficient to force a process to be Lévy. We need right continuity of paths

*Stochastic Modeling, Data Analysis and Statistical Applications* (*pp.* 33-43)
Lidia Filus - Teresa Oliveira - Christos H Skiadas (Eds)



besides stochastic continuity. There are many processes which could provide observations whose differences are effectively identically distributed, as well as independent, but nowhere close to being the process we want. For example, the class of all cumulative sums of centred normals with variance $\delta t$ cannot be identified with Wiener processes or with the class of all finite evaluations of a continuous path chosen in compliance with Wiener measure and sampled at discrete times. Similar considerations apply to Lévy processes.

## 2 Context

Rather than go for Lévy processes, we plan to take a step or two backwards and limit ourselves to Brownian motion, which in its simplicity offers a neater context to come to grips with the basics. We consider Brownian motion $B_t$, $t \in \mathbb{R}_+$, observed as a finite sequence of readings over equally spaced intervals of time at $0 = t_0 < t_1 < ... < t_n = t$. Random variables $B_{t_i}$ have increments $B_{t_{i+1}} - B_{t_i}$ which are independent, centred, normally distributed with variance $\sigma^2(t_{i+1} - t_i)$. The purely distributional properties of the increments might be what interests a statistician especially if he uses Brownian approximations to complex estimators via Donsker's theorem, or the Hungarian construction, to mention but just two much used approximations.

From the stochastic processes point of view the estimation of a process exclusively through increments loses a lot of information by ignoring the path properties of the parent process. Processes which jump at fixed times $t_i$ in normal increments are processes in their own right. Brownian motion is much more than that; including, as it does, the possibility of fleshing itself out on paths which are continuous with probability 1. We propose to study the differences between two scale estimators, which somehow recognize this property, with the classical one which ignores it.

The sequence of partial sums of centred iid normal random variables $S_n = \sum_{i=1}^{n} X_i$ is a discrete-parameter stochastic process, which interests statisticians for they come across it in many situations involving estimations of all sorts. Donsker's theorem tells us that this process can be ***approximated*** by Brownian motion. We zoom on the differences between these two processes. Elementary theory tells us that $\max_{0 \le s \le t} B_s$ is distributed as $|B_t|$. And this result utilizes continuity of the paths. The distribution of the maximum of $S_n$ above, suitably scaled, is different from that of $|B_t|$. Exact distributions of sum of independent, identically distributed random variables are hard to come by and very messy to establish. A number of published asymptotic results using Brownian approximations are available. The level of dissatisfaction with random walk approximations of this type as articulated in [1], has been brought to notice more than once. We displace this argument slightly by asking "What are we missing when we estimate Brownian motion solely through the independent increments assumption?"

We develop this idea further by exploiting differences between the exact distributions for the maximum of finite sums and the Brownian running maximum translated into statistics which depend on path continuity in the Brownian case. We quote some results and supply an accompanying graph:

$$\mathbb{E}[\max_{1\leq i\leq n} S_i] = \frac{\sigma}{\sqrt{2\pi}} \sum_{i=1}^{n-1} \frac{1}{\sqrt{i}} \tag{1}$$

$$\mathbb{E}[\max_{1\leq s\leq t} B_s] = \sqrt{\frac{2t}{\pi}} \tag{2}$$

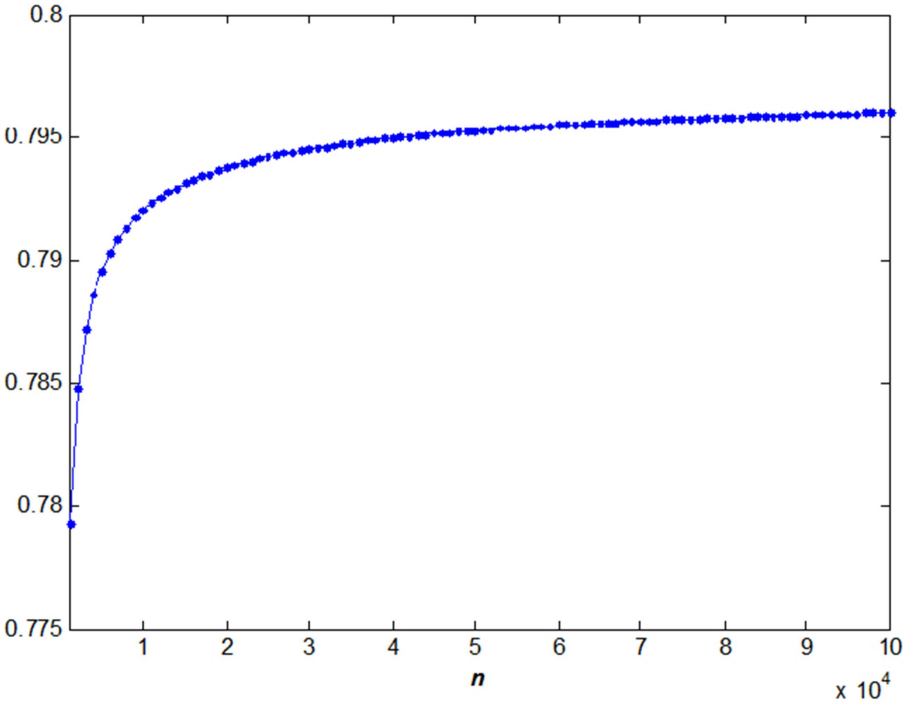


**Fig. 1.** Increase in Expected Maximum of Sums with no of terms $n$

The first equation is proved in [7]. We note that the expectation for the Brownian expression is always greater than for finite sums suitably scaled; $\sigma = \frac{1}{\sqrt{n}}$. We note how slow is the convergence of the finite sums to $\frac{1}{\sqrt{2\pi}} \approx 0.797884560802865$. At $n = 100000$ the sum equals $0.796040232112369$ . The emphasis on continuous paths for getting from one time instant to the next, enforced probabilistically by Wiener measure, lifts the expectation of the maximum value slightly higher than if we performed independent jumps at each time instant.

In a precise sense these problems have to be analysed in reverse within the context of simulation. Generating sample values, which are supposed to come from a Brownian process through independent normal increments, is very approximative. In some applications this just will not do.

## 3 Accurate Simulation of Brownian Paths

Simulated Brownian paths have many uses. Not only are they used in replicating physical and virtual phenomena which resemble Brownian motion, but they are used extensively in complex computations of various statistical functionals for which explicit analytical formulas are not known or not easily computable. High frequency financial data, for instance, needs to be collected and analyzed in a particular manner with a close watch on running maxima and local minima. This will enable modelling and pricing of barrier options products which constitute but one example as mentioned in [1]. In such cases the evaluation of functionals of Brownian paths needs to be carried out with high precision, not only in financial and actuarial applications but in others within the natural sciences.

The ability to replicate running maxima and minima credibly is therefore one feature which would be requested from simulations of Brownian motion. As we have noted the behaviour of these two extremes depend a lot on the continuity of paths. Reproducing faithfully maxima and minima has motivated a lot of work aimed at producing algorithms which are marketed as giving "exact" simulations. Much ingenuity has been displayed recently resulting in new developments this area. Actually most research has targeted more generally diffusion processes, with crucial input of techniques from importance and rejection sampling [3].

Our interest in simulation stems more from the fact that we would like to test our estimators using good simulated data. One cannot test accurately the quality of an estimator if the data on which the testing is effected is not exactly what it is supposed to be : random selections from a Brownian motion in our case. One of the arguments being pushed in this paper is that poorly representative simulated data may favour weaker algorithms, because certain important features, like properties inherited from continuity of paths, would be missing in the readings which will be used for calibration and evaluation purposes. So we settled for four methods, two which ignore continuity of paths, and two which have continuity inbuilt in their construction.

Furthermore we shall use data generated by four different algorithms:

- using cumulative sums of normal iid rv's [IID]
- using Brownian bridge interpolations [BB]
- using a Fourier series expansion of the sample paths [FS]
- using first passage times to construct an "exact algorithm" [EX]

The first algorithm needs no comment. The second consists of a random $N(0,1)$ end-point at $t = 1$ , with mid-points being generated as points of a

Brownian bridge in the manner of Lévy's construction. The third is implemented through the series expansion:

$$B_t = tZ_0 + \frac{\sqrt{2}}{\pi}\sum_{n=1}^{\infty}\frac{Z_n}{n}\sin n\pi t,\ 0 \le t \le 1$$

Continuity of paths is inbuilt through the series of functions, though continuity of the limit path would be assured only in the presence of uniform convergence. The fourth algorithm would be classified as an "exact" simulation. It uses a rejection algorithm as developed in [5] for the generation of a sequence of hitting times of Brownian motion as it crosses fixed boundaries starting from zero. The position of the path at intermediate time points $t_i$ are worked out using the distribution of Brownian bridge which is boxed in value between the values of the boundaries within which the path lives. The relevant distributional result is given further down in this paper.

## 4 The Wiener Measure

Sampling paths of a Wiener process randomly means that the probability of a given measurable set of paths being picked up is precisely the Wiener measure of that set. Individual paths have Wiener measure 0; let alone paths which pass through finitely many points at given corresponding instants of time. Being unable to go directly for Wiener measure, we have to hook on to it through particular properties of Brownian motion. Gaussianity of the finite-dimensional distributions of a process is a very important central property, but not sufficient to declare the process to be Wiener. So, as we have indicated, we shall somehow insist on continuity of the paths. Continuity of paths, when the readings are at finitely many points, obviously cannot be imposed directly. So we look for properties which continuity imposes on the behaviour over time on the process, and which are recoverable from, and reflected in, the running maxima and minima processes. Denoting these processes by $M_t = \max\limits_{0\le s\le t} B_s$ and $m_t = \min\limits_{0\le s\le t} B_s$, respectively, the technique for using, as well as enforcing, continuity properties on the paths is to box individual paths between these two processes and relate the three processes probabilistically. We shall need some important results relating to the above, which we now state. First we give two forms of the joint distributions of $(m_t, B_t, M_t)$ for $a \le x \le b$, and $a \le 0$, $b \ge 0$:

$$\mathbb{P}[m_t \le a, B_t \in dx, M_t \ge b] = \frac{dx}{\sigma\sqrt{2\pi t}} e^{\frac{-(x-2(M-m))^2}{2\sigma^2 t}} \tag{3}$$

$$\mathbb{P}[m_t > a, B_t \in dx, M_t < b] = \frac{dx}{\sigma\sqrt{2\pi t}}\sum_{k=-\infty}^{\infty} e^{\frac{-(x+2k(b-a)^2)}{(2\sigma^2 t)}} - e^{\frac{-(x-2a+2k(b-a))^2}{(2\sigma^2 t)}} \tag{4}$$

By marginalizing through $B_t$ we obtain the conditional distribution function for the running maximum and minimum:

$$\mathbb{P}[M_t \geq b, m_t \leq a | B_t = x] = exp\left(\frac{2(b-a)(x-2(b-a))}{\sigma^2 t}\right) \tag{5}$$

We obtain a formula for Wiener measure on $\mathcal{C}([0,1])$ suitably augmented by a set of probability 0, which we denote by $\mathbb{P}_{\mathbb{W}}$, by integrating out $x$ from $a$ to $b$ to obtain:

$$\begin{aligned}\mathbb{P}_{\mathbb{W}}[\{f \in \mathcal{C}([0,1] : a < f(s) < b, \forall s \text{ s.t. } 0 \leq s \leq t\}] = \\ \sum_{k=-\infty}^{\infty} \Phi\left(\frac{b+2k(b-a))}{\sigma\sqrt{2\pi t}}\right) - \Phi\left(\frac{a+2k(b-a))}{\sigma\sqrt{2\pi t}}\right) \\ + \sum_{k=-\infty}^{\infty} \Phi\left(\frac{b-2a+2k(b-a))}{\sigma\sqrt{2\pi t}}\right) - \Phi\left(\frac{a-2a+2k(b-a))}{\sigma\sqrt{2\pi t}}\right)\end{aligned} \tag{6}$$

These formulas will be found in various forms and variants in [2]. The last one is of particular interest to us. It has been known since the classical book by Feller on probability theory, not to mention Lévy's book on stochastic processes published in the 1940's. We shall denote the probability above in this formula by $\Psi_{\mathbb{W}}(a, b, t, \sigma)$. Though it involves a series, the formula it is derived from, namely (4), converges uniformly in $x \in [a, b]$ and does so very fast [6].

## 5 The Estimators

We propose now to take on an estimation problem for which the classical method, using exclusively distributional properties of independent increments, should be unbeatable. Not only does it exhibit unbiasedness but it achieves the Cramér-Rao minimum. We consider estimation of the variance $\sigma^2$ for which we devise two estimators which take continuity of paths into consideration. Such estimators should be more useful in estimation problems for linear and nonlinear diffusions. Generalizing this work to diffusions should be straightforward. It will not be attempted here, but left for future work because generalization will only make the notation and formulas so much more complicated as to hide the real issues. Since most results are asymptotic, sample size and discretization errors exert a strong influence. Largely we stay within the scope of maximum likelihood estimators. Such estimators are not unique in general. In some cases, more than one likelihood function can be used fruitfully. In our case we shall involve the running maximum and minimum in one estimator and the Wiener measure in the other, so as to factor in constraints which continuous paths satisfy.
Denoting increments by $X_i = B_{t_i} - B_{t_{i-1}}$ and letting $M_i = \max\limits_{0 \leq i \leq n} B_{t_i}$ , $m_i = \min\limits_{0 \leq i \leq n} B_{t_i}$ we write the joint density function using the usual iid assumption and multiply in the conditional distribution function from (5) :

$$\frac{1}{(\sqrt{2\pi}\sigma t)^n}\exp\left(\frac{-1}{2\sigma^2\delta t}\sum_{i=1}^{n}X_i^2\right)\exp\frac{2(M_n-m_n)(B_n-2(M_n-m_n))}{t\sigma^2}$$

We generate our first estimator as the maximizer of the log likelihood:

$$\widehat{\sigma^2}_1=\arg\min_{\boldsymbol{s^2}}\left[n\log(s)+\frac{1}{2\delta t s^2}\left(\sum_{i=1}^{n}X_i^2-\frac{4}{n}(M_n-m_n)(B_n-2(M_n-m_n))\right)\right] \tag{7}$$

For the second estimator we involve the Wiener measure by maximizing the probability that the path is included within the latest values of the maximum and minimum:

$$\widehat{\sigma^2}_2=\arg\min_{\boldsymbol{s^2}}\left[n\log(s)+\frac{1}{2\delta t s^2}\left(\sum_{i=1}^{n}X_i^2\right)-\log(\Psi(m_n,M_n,t,s))\right] \tag{8}$$

These two estimators introduce continuity of paths by stealth, as it were. They penalize parameter estimates which distributionally make current sample values of the running maximum and minimum less likely in two different senses. In this sense they can be considered as being of the maximum likelihood type. In fact the usual properties can be proved to be asymtotically true but we shall not indulge in this here.

## 6 Estimator Performance

We proceed to discuss how we shall test the performance of the estimators. It is customary to evaluate the qualities of estimators in terms of the usual, simple statistical properties like unbiasedness and efficiency. We shall indeed compute means and variances over large samples. Furthermore as benchmark performer we shall take the likelihood-based, common unsophisticated variance estimator :

$$\widehat{\sigma^2}_0=\frac{1}{n\delta t}\sum_{i=1}^{n}X_i^2 \tag{9}$$

Theoretically this is an unbiased, minimum variance estimator- but only relative to the information which we use in constructing it. This information excludes any reference to continuity of paths. Unexpected departures from its proven properties will make us uncomfortable about the quality of the data on which we are testing. So the usual statistical properties are worth checking. However, from a more pragmatic point of view, in many contexts there are other criteria in evaluating estimation procedures which would be more crucial.

Especially within financial modelling exercises, the more frequently closer to the true value, in absolute terms, the individual estimates are, the much better the estimators are to be considered. This observation leads us to formulate a criterion that estimators which have a higher probability of giving estimates closer to the true values than others are somehow to be preferred. Roughly speaking, we judge estimators which have higher rates of convergence in achieving consistency to be preferable. More precisely, given estimators $\hat{\boldsymbol{\theta}}_1, \hat{\boldsymbol{\theta}}_2$, if $\mathbb{P}[|\hat{\boldsymbol{\theta}}_1 - \boldsymbol{\theta}| > |\hat{\boldsymbol{\theta}}_2 - \boldsymbol{\theta}|] > 0.5$ then we declare $\hat{\boldsymbol{\theta}}_2$ to be preferable; more than 50 % of all samples should give $\hat{\boldsymbol{\theta}}_2$ estimates which are closer to the true value. We shall investigate how this probability changes as the number of observations over a time interval of the same length increases.

In our setting, again for the sake of transparency, we take $\sigma^2 = 1$ and the time interval is $[0, 1]$ with $n$ equally spaced instants at which we have the observations $B_i$. Four sets of data were generated by the corresponding four algorithms mentioned earlier. Each set consists of four collections of outputs from 1000 simulated "paths". The difference between the collections is the frequency at which the paths were measured. These frequencies correspond to the four values $n = 100, 200, 500$ and 1000 ( 128, 256, 512 and 1024 for DS2) giving equally spaced time instants $0, \frac{1}{n}, ...., \frac{n}{n}$ over the unit time interval. DS1 was generated using algorithm IID, DS2 using BB , DB3 using FS and DB4 using EX. Each sequence of $n$ readings, corresponding to one path was used to give estimates for $\sigma^2$ by each of the three methods described above.

## 7 Estimation Results from Simulations

Table 1 gives us the usual statistical measures for estimates from the benchmark estimator. As far as DS1 and DS2 are concerned, everything is as expected. Only the distributional properties of Brownian motion are taken into consideration by the simulating algorithms and $\widehat{\sigma^2}_0$ picks them up well enough. From DS3 and DS4, however, we see actually a deterioration of the estimate means as the sample size increases! The situation with the variance is also worse than for the other 2 algorithms. This evidence indicates that the closer the data generating mechanism follows the behaviour of selections from Brownian motion, the less faithfully are usual distributional properties observed because of discretization.

Tables 2 and 3 reveal that the behaviour of $\widehat{\sigma^2}_1$ is statistically very similar to that of $\widehat{\sigma^2}_2$. The second estimator is consistently more accurate and has less variability within its results for the datasets which represent Brownian motion worst. We also see that increasing sample size improved the quality of the estimates throughout. Compared to results for $\widehat{\sigma^2}_0$ we see that on DS3 and DS4 the two proposed estimators are indeed superior even though not by much. Considering that we are comparing performances on territory on which $\widehat{\sigma^2}_0$ should reign supreme, the two estimators have done well.

| | Estimator $\widehat{\sigma^2}_0$ | | | | | | | |
|---|---|---|---|---|---|---|---|---|
| No of obs | DS1 | | DS2(*) | | DS3 | | DS4 | |
| | Mean | Variance | Mean | Variance | Mean | Variance | Mean | Variance |
| 1000 | 0.99989 | 0.000498 | 0.99978 | 0.000504 | 0.97924 | 0.000921 | 0.98390 | 0.007510 |
| 500 | 0.99803 | 0.000985 | 0.99838 | 0.000993 | 0.98900 | 0.001048 | 0.99140 | 0.000981 |
| 200 | 1.00099 | 0.002279 | 0.99648 | 0.001991 | 0.99452 | 0.002518 | 0.99530 | 0.002300 |
| 100 | 0.99662 | 0.005442 | 0.99950 | 0.003980 | 0.99407 | 0.005551 | 0.99602 | 0.004811 |

**Table 1.** Means and Variances of $\widehat{\sigma^2}_0$ on All Datasets.

(*) sample sizes for DS2 were in fact 1024, 512 , 256 , 128

| | Estimator $\widehat{\sigma^2}_1$ | | | | | | | |
|---|---|---|---|---|---|---|---|---|
| No of obs | DS1 | | DS2(*) | | DS3 | | DS4 | |
| | Mean | Variance | Mean | Variance | Mean | Variance | Mean | Variance |
| 1000 | 1.00477 | 0.000550 | 1.00493 | 0.000558 | 0.98477 | 0.000770 | 0.98930 | 0.006344 |
| 500 | 1.00822 | 0.001190 | 1.00872 | 0.001201 | 0.99910 | 0.001054 | 1.00150 | 0.001113 |
| 200 | 1.02424 | 0.003561 | 1.01710 | 0.002761 | 1.01835 | 0.003410 | 1.01940 | 0.003400 |
| 100 | 1.04560 | 0.010754 | 1.03711 | 0.007026 | 1.03762 | 0.009348 | 1.04358 | 0.009627 |

**Table 2.** Means and Variances of $\widehat{\sigma^2}_1$ on All Datasets.

(*) sample sizes for DS2 were in fact 1024, 512 , 256 , 128

| | Estimator $\widehat{\sigma^2}_2$ | | | | | | | |
|---|---|---|---|---|---|---|---|---|
| No of obs | DS1 | | DS2(*) | | DS3 | | DS4 | |
| | Mean | Variance | Mean | Variance | Mean | Variance | Mean | Variance |
| 1000 | 1.00277 | 0.000507 | 1.00252 | 0.000507 | 0.98204 | 0.000824 | 0.98690 | 0.006660 |
| 500 | 1.00333 | 0.001001 | 1.00374 | 0.001056 | 0.99440 | 0.000961 | 0.99700 | 0.000986 |
| 200 | 1.01595 | 0.002589 | 1.00725 | 0.002130 | 1.00861 | 0.002625 | 1.00910 | 0.002400 |
| 100 | 1.02938 | 0.007224 | 1.02345 | 0.005010 | 1.02854 | 0.007669 | 1.03122 | 0.007269 |

**Table 3.** Means and Variances of $\widehat{\sigma^2}_2$ on All Datasets.

(*) sample sizes for DS2 were in fact 1024, 512 , 256 , 128

Finally we consider direct confrontation between our estimators and the benchmark. Table 4 gives very clear indications. For relatively low frequency data, the increase in information which is incorporated in $\widehat{\sigma^1}_2$ fails to beat the robust performance of the benchmark especially on the latter's home territory with data generated by IID and BB. For high frequency however the tables are turned with a remarkable increase in precision of $\widehat{\sigma^2}_1$. Over 70% of the estimates from $\widehat{\sigma^2}_1$ come closer to the true value than the benchmark.

Table 5 gives the same message as the previous one. It actually displays the excellent performance throughout of $\widehat{\sigma^2}_2$ which does better than $\widehat{\sigma^2}_1$. This in a sense was to be expected. Sampling from Brownian paths should reflect Wiener measure. And $\widehat{\sigma^2}_2$ tries to favoor parameter estimates which do exactly that directly.

| **Dataset DS1 using IID** | | | | |
|---|---|---|---|---|
| *No of obs* | 1000 | 500 | 200 | 100 |
| *Probability* | 0.452 | 0.461 | 0.408 | 0.406 |
| **Dataset DS2 using BB** | | | | |
| *No of obs* | 1024 | 512 | 256 | 128 |
| *Probability* | 0.461 | 0.467 | 0.451 | 0.391 |
| **Dataset DS3 using FS** | | | | |
| *No of obs* | 1000 | 500 | 200 | 100 |
| *Probability* | 0.787 | 0.574 | 0.464 | 0.409 |
| **Dataset DS4 using EX** | | | | |
| *No of obs* | 1000 | 500 | 200 | 100 |
| *Probability* | 0.719 | 0.569 | 0.434 | 0.401 |

**Table 4.** Estimated probs of Estimator $\widehat{\sigma^2}_1$ Giving Closer Estimates than $\widehat{\sigma^2}_0$

| **Dataset DS1 using IID** | | | | |
|---|---|---|---|---|
| *No of obs* | 1000 | 500 | 200 | 100 |
| *Probability* | 0.486 | 0.512 | 0.451 | 0.481 |
| **Dataset DS2 using BB** | | | | |
| *No of obs* | 1024 | 512 | 256 | 128 |
| *Probability* | 0.491 | 0.507 | 0.497 | 0.451 |
| **Dataset DS3 using FS** | | | | |
| *No of obs* | 1000 | 500 | 200 | 100 |
| *Probability* | 0.799 | 0.631 | 0.516 | 0.475 |
| **Dataset DS4 using EX** | | | | |
| *No of obs* | 1000 | 500 | 200 | 100 |
| *Probability* | 0.743 | 0.607 | 0.509 | 0.466 |

**Table 5.** Estimated probs of Estimator $\widehat{\sigma^2}_2$ Giving Closer Estimates than $\widehat{\sigma^2}_0$

## 8 Conclusion

The aim of this paper was to study ways in which incorporating path properties of a process, whose parameter is being estimated, improves estimator performance. This was implemented on a simple setting involving Brownian motion. Given the discrete structure of data available in many applications, knowledge of what happens between actual readings is missing. But that does not mean we do know what should happen probabilistically. The two estimators we proposed incorporates features which respond to path continuity features. And the results indicate that for high frequency data, the estimators are superior. When the time gap between readings is longer the effect of what should happen in between seems to relax. For empirical of analysis financial data this should have repercussions.

## References

1. Becker M., "Exact simulation of final, minimal and maximal values of Brownian motion and jump-diffusions with applications to option pricing", *Computational Management Science* 7, 1, 1-17 , (2010).
2. Borodin A.N. and Salminen P., "Handbook of Brownian Motion - Facts and Formulae", 2. Aufl. Probability and its Applications, Birkhäuser, Basel, 2002.
3. Beskos, A., Papaspiliopoulos O., Roberts, G. and Fearnhead P., "Exact and computationally efficient likelihood-based estimation for discretely observed diffusion processes", J. R. Stat. Soc. Ser. B Stat. Methodol. 68 333382 (2006).
4. Beskos, A., Peluchetti S. and Roberts G., "$\epsilon$-Strong simulation of the Brownian path", *Bernouilli* 18, 4, 1223-1248, (2012).
5. Burq Z.A. and Jones O.D., "Simulation of Brownian motion at first-passage times", *Mathematics and Computers in Simulation* 77, 64-71 , (2008).
6. Choi B.S. and Roh J.H., "On the trivariate joint distribution of Brownian motion and its maximum and minimum", *Statistical and Probability Letters*, 83, 1046-1053, (2013).
7. Tang Strait P., "On the Maximum and Minimum of Partial Sums of Random Variables" *Pacific Journal of Mathematics*, 53, 2 , 585-593 (1974).

# Estimation of Lévy Processes through Stochastic Programming

Lino Sant[1] and Mark Anthony Caruana[2]

[1] Department of Statistics and Operations Research,
Faculty of Science, University of Malta, Msida, Malta
(e-mail: lino.sant@um.edu.mt)
[2] Department of Statistics and Operations Research
Faculty of Science, University of Malta, Msida, Malta
(e-mail: mark.caruana@um.edu.mt)

**Abstract.** Estimation of Lévy processes with the use of the characteristic function has lately shifted much of its attention to nonparametric settings. However the parametric context still offers scope for study. The nature of neighbourhoods of the minima sought for by the integrated square error estimator (ISEE), and its variants, could be meaningfully related to a number of useful properties possessed by the estimator. Furthermore the numerical problems associated with the actual computation of parameter estimates have not been given exhaustive attention. In this paper through a slight reformulation of the ISEE formula, local geometric features of the optimal solution used in ISEE are studied. This formulation is subsequently proposed within a stochastic programming framework. The latter provides a powerful, productive methodology and an alternative theoretical framework which are entertained within this study. Results are presented and discussed.
**Keywords:** Lévy Processes, Characteristic Function, Stochastic Programming.

## 1 Introduction

In recent decades, there has been a sharp rise of interest in the study of Lévy processes. Evidence of this is given by the extensive amount of literature which has been focused not only on the application of Lévy processes in various fields − most prominently in finance − but also on parameter estimation problems. Some of the methods of estimation found in literature minimize some form of distance function that involves the characteristic function of a Lévy process and its empirical counterpart. As discussed in Sant and Caruana [9], the use of the empirical characteristic function in the parameter estimation problem causes a number of computational issues triggered by oscillatory integrands. Weight functions are usually used to control these oscillations thus reducing computational problems. However, there is no link between the choice of the weight function and the characteristic function. In response to this problem, the stochastic programming framework will allow the use of some properties

*Stochastic Modeling, Data Analysis and Statistical Applications* (*pp.* 45-52)
Lidia Filus - Teresa Oliveira - Christos H Skiadas (Eds)



of the characteristic function of continuous probability distributions to address the above mentioned computational issues. Throughout this paper we shall be using only continuous probability distributions.

## 2 Context

Given Lévy process $(Z_s)_{s\in\mathbb{R}_+}$, with independent and identically distributed increments which we denote by $X_j$, $j = 1\ldots,n$, we define the corresponding characteristic function $\rho(t,\boldsymbol{\theta}(s)) = \mathbb{E}[exp(itZ_s)]$, where for each $s$, $\boldsymbol{\theta}(s) \in \mathbb{R}^d$ is the vector of parameters which the process inherits from the infinitely divisible distribution corresponding to random variable $Z_s$. Usually, little time is spent to consider the shape that this vector of parameters can take. We note that $\rho(t,\boldsymbol{\theta}(ns/m)) = \mathbb{E}\left[exp(itZ_{ns/m})\right] = \rho(t,\boldsymbol{\theta}(s))^{n/m}$ from the infinite divisibility property forces $\rho(t,\boldsymbol{\theta}(s)) = \rho(t,\boldsymbol{\theta}(1))^s$.
This functional equation is of the Pixeder type and does not allow any type of parametrization. In fact, the Lévy-Khintcine and Lévy-Itô formulas propose their own parametrizations related to specific measure-theoretic and functional relationships. We address ourselves more to the parametrizations which are in common use and which in many cases have to obey certain structures before the corresponding family of distributions can be declared infinitely divisible (eg. the gamma distribution has to have its second parameter constant to achieve infinite divisibility). Using the polar representation we can write:

$$\rho(t,\boldsymbol{\theta}(s)) = R(t,\boldsymbol{\theta}(1))^s \exp[is\vartheta(t,\boldsymbol{\theta}(1))] = \rho_{\mathcal{R}}(t,\boldsymbol{\theta}(s)) + i\rho_{\mathcal{I}}(t,\boldsymbol{\theta}(s))$$

and we see that $R(t,\boldsymbol{\theta}(s)) = R(t,\boldsymbol{\theta}(1))^s$ and $s\vartheta(t,\boldsymbol{\theta}(s)) = s\vartheta(t,\boldsymbol{\theta}(1))$.
In fact inspecting the usual parametrizations for the common distributions, stable distributions, extreme value distributions and mixtures the relationships for the components of $\boldsymbol{\theta}$ are of the form: $\boldsymbol{\theta}_j(s) = as$ or $\boldsymbol{\theta}_j(s) = a$.
In what follows we shall work with $\rho(t,\boldsymbol{\theta}(\Delta s))$ where $\Delta s$ is a fixed time increment separating increments $X_j$ obtained from readings of a Lévy process with corresponding characteristic function which we shall denote from now onwards as $\rho(t,\boldsymbol{\theta})$. Furthermore it makes sense that as a minimal assumption we take continuity of $\rho$ with respect to $\boldsymbol{\theta}$ on some compact subset $\mathbf{K} \subseteq \mathbb{R}^d$ whereon $\boldsymbol{\theta}$ is allowed to vary. In effect estimations over unbounded subsets are in practice, not only hypothetical, but also impractical.
Next, we look at the problem of parameter estimation through the use of the characteristic function but with an unusual choice of objective function for minimization. In fact the corresponding problem can be reframed as a stochastic programming one.

## 3 Applying the Stochastic Programming Framework

A stochastic program can be written in the form

$$\arg\min_{\boldsymbol{\theta}}\{f(\boldsymbol{\theta}) = \mathbb{E}[F(\boldsymbol{\theta},X)]\}, \tag{1}$$

and we shall formulate the location of the true parameter $\boldsymbol{\theta}_0$ from $X_j$ in this way.
For $t \in \mathbb{R}$, $\boldsymbol{\theta} \in \mathbf{K}$ dropping the suffix for a general $X_j$ we have the random functions:

$$\begin{aligned} F(t,\boldsymbol{\theta},\omega) &= |e^{itX(\omega)} - \rho(t,\boldsymbol{\theta})|^2 - 1 \\ &= \rho_{\mathcal{R}}^2(t,\boldsymbol{\theta}) + \rho_{\mathcal{I}}^2(t,\boldsymbol{\theta}) - 2\cos(tX(\omega))\rho_{\mathcal{R}}(t,\boldsymbol{\theta}) - 2\sin(X(\omega))\rho_{\mathcal{I}}(t,\boldsymbol{\theta}) \end{aligned}$$

with corresponding bounded functional $f$ for bounded distribution functions $W$ over $\mathbb{R}_+$ defined as follows:

$$\begin{aligned} f(\boldsymbol{\theta}) &= \int_0^\infty \mathbb{E}[F(t,\theta)]dW(t) = \mathbb{E}\left[\int_0^\infty F(t,\boldsymbol{\theta})dW(t)\right] \\ &= \int_0^\infty \{\rho_{\mathcal{R}}^2(t,\boldsymbol{\theta}) + \rho_{\mathcal{I}}^2(t,\boldsymbol{\theta}) - 2\rho_{\mathcal{R}}(t,\boldsymbol{\theta}_0)\rho_{\mathcal{R}}(t,\boldsymbol{\theta}) - 2\rho_{\mathcal{I}}(t,\boldsymbol{\theta}_0)\rho_{\mathcal{I}}(t,\boldsymbol{\theta})\}dW(t) \end{aligned}$$

The above expectation can be approximated by making use of the set of previously defined increments $X_j$ , which give rise to the following sequence of random elements with values in $\mathcal{C}(\mathbf{K})$ :

$$F_n(\boldsymbol{\theta},\omega) = \frac{1}{n}\sum_{j=1}^n \int_0^\infty \left(\left|e^{itX_j(\omega)} - \rho(t,(\theta))\right|^2 - 1\right) dW(t) \tag{2}$$

$$= \frac{1}{n}\sum_{j=1}^n G_j(\omega,\boldsymbol{\theta}) \tag{3}$$

We assume that $\rho(t,\boldsymbol{\theta})$, and hence all functions $F$, $f$, $F_n$, are continuous with respect to $\boldsymbol{\theta}$ as it varies on a compact, metrizable set $\mathbf{K} \subseteq \mathbb{R}^d$. Hence, all functions can be considered as elements of $\mathcal{C}(\mathbf{K})$, the space of continuous functions on $\mathbf{K}$, which we recover as a separable Banach space under the supremum norm, which we denote by $\| \bullet \|$, where $\|F\| = \sup_{\boldsymbol{\theta}\in\mathbf{K}} |F(\boldsymbol{\theta})|$.
Next, we determine the asymptotic behavior of $F_n$ in the following theorem. Later we shall see that $F_n$ can be used to approximate the stochastic programming problem defined in (1).

**Theorem 1.** *The sequence of random elements $F_n(\boldsymbol{\theta},\omega)$ converges $\mathbb{P}$ a.s. and in $\mathbb{L}^p$ to $f(\boldsymbol{\theta})$. Furthermore under the condition that there exist constants $C_1$, $C_2$ such that for all $\boldsymbol{\theta}_1$ $\boldsymbol{\theta}_2 \in \mathbf{K}$:*

$$\begin{aligned} |\rho_{\mathcal{R}}(t,\boldsymbol{\theta}_2) - \rho_{\mathcal{R}}(t,\boldsymbol{\theta}_1)| &\le C_1\|\boldsymbol{\theta}_2 - \boldsymbol{\theta}_1)\| \\ |\rho_{\mathcal{I}}(t,\boldsymbol{\theta}_2) - \rho_{\mathcal{I}}(t,\boldsymbol{\theta}_1)| &\le C_2\|\boldsymbol{\theta}_2 - \boldsymbol{\theta}_1)\| \end{aligned}$$

*the sequence $F_n(\boldsymbol{\theta},\omega)$ obeys the CLT: $\sqrt{n}[F_n(\boldsymbol{\theta},\omega) - f(\boldsymbol{\theta})]$ converges in distribution to a Gaussian random element.*

*Proof.*
The inequality $\|G_j(\omega,\bullet)\| = \sup_{\boldsymbol{\theta}} \int_0^\infty \{|\exp(itX_j(\omega) - \rho(t,\boldsymbol{\theta}))|^2 - 1\}dW(t) \le \sup_{\boldsymbol{\theta}} \int_0^\infty 3dW(t) = 3$. This ensures that $\forall j$, $\mathbb{E}[\|G_j\|^p] < \infty$, $\forall p \ge 0$. By the

Strong Law of Large numbers for iid random variables with values in Banach spaces, the $\mathbb{P}$ a.s. limit of $F_n(\boldsymbol{\theta},\omega)$ is the expectation of each $G_j$ which is $f(\boldsymbol{\theta})$. Using the Dominated Convergence theorem we can deduce that convergence occurs also in $\mathbb{L}^p$ for $p \geq 1$ where we use results first obtained by Fortet and Mourier [1] and proved in detail in Ledoux and Talagrand [6], Corollary 7.10. We need distributional results and something about rates of convergence. These are usually supplied by the CLT. However, the CLT does not hold for Banach space-valued random elements with only the iid and finite variance assumptions. For $\mathcal{C}(\mathbf{K})$-valued random variables the CLT is assured under special conditions. Broadly speaking the condition that guarantees convergence of the CLT type is that the corresponding measures can be supported on a Hilbert subspace. We adapt them for our circumstances by using a Lipshcitz type condition which needs only concern the characteristic function under study.
The random function $\boldsymbol{\theta} \to \int_0^\infty F(t,\boldsymbol{\theta},\omega)dW(t)$ is bounded in $\mathbb{L}^2(\mathbf{K})$ and it is Lipschitz continuous:
$|F(t,\boldsymbol{\theta}_2,\omega) - F(t,\boldsymbol{\theta}_1,\omega) \leq 2|\rho_{\mathcal{R}}(t,\boldsymbol{\theta}_2) - \rho_{\mathcal{R}}(t,\boldsymbol{\theta}_1)| + 2|\rho_{\mathcal{I}}(t,\boldsymbol{\theta}_2) - \rho_{\mathcal{I}}(t,\boldsymbol{\theta}_1)| +$
$|\rho^2_{\mathcal{R}}(t,\boldsymbol{\theta}_2) - \rho^2_{\mathcal{R}}(t,\boldsymbol{\theta}_1)| + |\rho^2_{\mathcal{I}}(t,\boldsymbol{\theta}_2) - \rho^2_{\mathcal{I}}(t,\boldsymbol{\theta}_1)| \leq 4(C_1 + C_2)\|\boldsymbol{\theta}_2 - \boldsymbol{\theta}_1\|$.
The $G_j(\omega,\boldsymbol{\theta})$'s are independent copies of the random element above. Results for the CLT in Banach spaces as given in Jain and Marcus [3] allow us to conclude that suitably scaled and centered, the averaged random sequence of functions $\sqrt{n}\,[F_n(\boldsymbol{\theta}) - f(\boldsymbol{\theta})]$ converges in distribution to a random element of $\mathcal{C}(\mathbf{K})$. More precisely we have weak convergence to a Gaussian probability measure in the space of Borel probability measures on $\mathcal{C}(\mathbf{K})$. Furthermore the corresponding variance is

$$\mathbb{V}\mathrm{ar}\left[\int_0^\infty \left\{|\exp(itX) - \rho(t,\boldsymbol{\theta})|^2 - 1\right\} dW(t)\right].$$

□

Since $F_n(\boldsymbol{\theta},\omega)$ converges $\mathbb{P}$ almost surely to $f(\boldsymbol{\theta})$ then it makes sense to solve the following program:

$$\arg\min_{\boldsymbol{\theta}} \left( F_n(\boldsymbol{\theta},\omega) = \frac{1}{n}\sum_{j=1}^{n} \int_0^\infty \{|\exp(itx_j) - \rho(t,\boldsymbol{\theta})|^2 - 1\} dW(t) \right) \quad (4)$$

as an approximation to (1) and use corresponding methods to approach the required solution. The link is provided by the functional $\psi(g) = \inf_{\boldsymbol{\theta}\in\mathbf{K}} g(\boldsymbol{\theta})$. $\psi$ shares some geometrical properties with the norm, but clearly it is not linear. It is in fact the minimum of linear functionals, all of whom are elements of $\mathcal{M}(\mathbf{K})$, the dual of $\mathcal{C}(\mathbf{K})$, which is the space of all Radon measures on $\mathbf{K}$. Furthermore, $\psi$ is concave and hence is Hadamard differentiable at any $g \in \mathcal{C}(\mathbf{K})$.
Although we know that $F_n(\boldsymbol{\theta},\omega)$ converges $\mathbb{P}$ a.s. to $f(\boldsymbol{\theta})$, we still need to show that as the number of increments increases then $\hat{\boldsymbol{\theta}} = \arg\min_{\boldsymbol{\theta}}(F_n(\boldsymbol{\theta},\omega))$ will approach the true value $\boldsymbol{\theta}_0 = \arg\min_{\boldsymbol{\theta}}(f(\boldsymbol{\theta}))$. This result is proven in theorem 2.

**Theorem 2.** *The sequence of random variables* $\psi(F_n(\boldsymbol{\theta},\omega)) = \inf_{\boldsymbol{\theta}\in\mathbf{K}} F_n(\boldsymbol{\theta},\omega)$ *converges in probability to the constant* $f(\boldsymbol{\theta}_0) = \int_0^\infty |\rho(t,\boldsymbol{\theta}_0)|^2 dW(t)$.

*Furthermore* $\psi(F_n(\boldsymbol{\theta},\omega)) - f(\boldsymbol{\theta}_0) = o_{\mathbb{P}}(1)$ *and* $\lim_{n\to\infty} \arg\min_{\boldsymbol{\theta}} F_n((\theta),\omega) = \boldsymbol{\theta}_0$.

*Proof.*
For a fixed $\omega$, the function $F(t,\boldsymbol{\theta},\omega)$, being quadratic in $\rho_{\mathcal{R}}$ and $\rho_{\mathcal{I}}$, achieves its minimum value when $\rho_{\mathcal{R}} = cos(tX(\omega))$ and $\rho_{\mathcal{I}} = sin(tX(\omega))$ which in general may have no solution or more than one. On the other hand, $\mathbb{E}[F(t,\theta)]$ being quadratic in $\rho_{\mathcal{R}}$ and $\rho_{\mathcal{I}}$, achieves its minimum value when $\boldsymbol{\theta} = \boldsymbol{\theta}_0$. Unicity of characteristic functions assures uniqueness of this minimum $F(t,\boldsymbol{\theta}_0)$. It follows that for $f(\boldsymbol{\theta})$ we have:

$$\inf_{\boldsymbol{\theta}\in\mathbf{K}(F)} \int_0^\infty \mathbb{E}[F(t,\boldsymbol{\theta})]dW(t) = f(\boldsymbol{\theta}_0).$$

We are interested in the subdifferential $\partial\psi$ at our special function $f$. In effect for $g \in \mathcal{C}(\mathbf{K})$, $\partial\psi(g)$ is a set of elements of $\mathcal{M}(\mathbf{K})$, which following proposition 4.5.18 in Gasinski and Papageorgiou [2] we proceed to describe. It is the set of all positive Radon measures of total mass 1 concentrated on the points where $g$ attains its minima:
$\partial\psi(g) = \{\mu \in \mathcal{M}(\mathbf{K}) : \mu \geq 0 \;\&\; \langle\mu, 1\rangle = 1 \;\&\; \text{supp}(\mu) \subseteq \{\boldsymbol{\theta} \in \mathbf{K} : \psi(g) = g(\boldsymbol{\theta})\}\}$
Evaluated at our special function $f$, this subdifferential becomes: $\langle\partial\psi(f), h\rangle = \inf_{\boldsymbol{\theta}\in\mathbf{K}(f)} h(\boldsymbol{\theta})$.
Thus $\partial\psi(f)$, operating on $h$, returns the minimum of $h$ restricted to the points where $f$ achieves its minimum. In our case this happens at the single point $\boldsymbol{\theta}_0$. Using the Delta Method theorem for normed spaces, discussed in van der Vaart [10], with the Hadamard differentiable map $\psi$ operating on the convergent series of random elements $F_n(\boldsymbol{\theta},\omega)$ we get the convergence in probability results. The last limit follows from unicity of all minima involved.

□

This theorem assures us that, as the sample size increases, locating the value of $\boldsymbol{\theta}$ which minimizes the sample value $F_n(\boldsymbol{\theta},\omega)$ will get us closer to $\boldsymbol{\theta}_0 = \arg\min_{\boldsymbol{\theta}\in\mathbf{K}} f(\boldsymbol{\theta})$. This brings us securely to stochastic programming territory. In fact, the problem $\min_{\boldsymbol{\theta}} F_n(\boldsymbol{\theta},\omega)$ can be considered as a two-stage stochastic program.
In the following section we discuss a method by which this stochastic program can be solved.

## 4 Solving the Stochastic Program

A number of different methods can be used to solve two-stage or multi-stage stochastic programs. Shapiro [8] solves multi-sage stochastic programs with a linear objective function and linear constraints by making use of the Stochastic Dual Dynamic Programming Algorithm (SDDP) which in turn was introduced by Pinto and Pereira [7]. Shapiro argues that the backward step of the SDDP is the standard cutting plane algorithm and applied it to the problem he was studying. However Kelly's [5] cutting plane algorithm was designed on the

assumption that the objective function is convex over the feasible region. The objective function $F_n(\boldsymbol{\theta}, \omega)$ is not convex in general and hence Kelly's cutting plane algorithm cannot be used. The way forward is to replace the cutting plane algorithm with another method which can handle non-convex objective functions. The algorithm proposed by Karmitsa et. al. [4] still makes use of cutting planes and furthermore can be used for non-convex and non-smooth objective functions. The original minimization problem is first converted into a program with a linear objective function while the non-linearity and non-convexity of the original problem are moved to the constraint as shown below:

$$\arg\min_{\boldsymbol{\theta}, z}\{z | F_n(\boldsymbol{\theta}, \omega) - z \leq 0\} \tag{5}$$

Next, a sequence of auxiliary linear problems is built where the constraint in (5) is approximated by a number of cutting planes. During each iteration a search direction for the auxiliary problem is computed using the Feasible Direction Interior Point Method (FDIPM).
In the following section the performance of the method of estimation discussed in this paper is compared with that of other methods of estimation found in literature.

## 5 Simulation Results

Increments of three distinct Lévy processes were simulated using three different probability distributions. Using these increments, the parameters of the characteristic function of each distribution were estimated using not only the stochastic programming framework discussed above (which from now on we denote by SPM) but also other commonly used methods such as the method of maximum likelihood (MLE) and the Integrated squared error estimator (ISEE). When the integrand in (4), i.e. $\left\{\frac{1}{n}\sum_{j=1}^{n}\left|\exp(itx_j) - \rho(t, \boldsymbol{\theta})\right|^2 - 1\right\}$ is compared with the integrand in the ISEE, i.e. $\left|\frac{1}{n}\sum_{j=1}^{n}\left[\exp(itx_j)\right] - \rho(t, \boldsymbol{\theta})\right|^2$, one can easily show that for continuous distributions, the former goes to zero as $t \to \pm\infty$, while the latter does not and keeps on oscillating within a band as $t \to \pm\infty$. This indicates why our estimator behaves more smoothly.
The probability distributions chosen for these simulations are: the Stable distribution with parameters $(\alpha = 0.4, \beta = 0.5, \sigma = 1, \mu = 3)$, the gamma distribution with parameters $(\alpha = 2, \beta = 3)$ and an extreme value distribution: the Gumbel distribution with parameters $(\mu = 7, \beta = 0.05)$. The results obtained for the stable distribution using SPM were compared with the ISEE. Table 1 contains the simulation results of the parameter estimates for the stable distribution. The weight function which is necessary in ISEE was chosen to be $\exp(-t^2)$. The limits of integration in the SPM and ISEE are taken from 0 to some constant $T$. In particular, two different values of $T$ were chosen, namely, 10 and 20.
It is evident from table 1, that for both values of $T$, the estimates obtained from SPM have less bias and less variance than the estimates obtained from

| T | $\hat{\alpha}$ | $\hat{\beta}$ | $\hat{\sigma}$ | $\hat{\mu}$ | $\hat{\alpha}$ | $\hat{\beta}$ | $\hat{\sigma}$ | $\hat{\mu}$ |
|---|---|---|---|---|---|---|---|---|
| Estimates using SPM | | | | | Estimated Variance | | | |
| 10 | 0.41296 | 0.50995 | 0.96899 | 3.05113 | 6.589E-05 | 0.01278 | 0.00044 | 0.00100 |
| 20 | 0.40541 | 0.50131 | 1.00343 | 3.03293 | 2.640E-05 | 0.01284 | 0.00013 | 0.00023 |
| Estimates using ISEE | | | | | Estimated Variance | | | |
| 10 | 0.29874 | 0.49235 | 0.92826 | 3.14041 | 0.01793 | 0.00900 | 0.022675 | 0.02989 |
| 20 | 0.29923 | 0.49821 | 0.93229 | 3.13334 | 0.01630 | 0.01525 | 0.021106 | 0.02888 |

**Table 1.** Estimates for the Lévy Stable process.

ISEE.
Next we compare the results obtained for the Gumbel and Gamma distributions. In this case the estimates are compared with the simulations results obtained by using the method of maximum likelihood.

| | Gamma (2, 3) | | | | Gumbel (7, 0.5) | | | |
|---|---|---|---|---|---|---|---|---|
| SPM | Estimates | | Variance | | Estimates | | Variance | |
| 10 | 2.00259 | 2.99445 | 0.00044 | 0.001443 | 6.99779 | 0.04955 | 2.284E-07 | 9.05E-08 |
| 20 | 2.00052 | 2.99996 | 0.00035 | 0.001221 | 6.99924 | 0.04977 | 1.670E-07 | 8.63E-08 |
| | Estimates | | Variance | | Estimates | | Variance | |
| MLE | 2.00103 | 2.99498 | 0.00039 | 0.00142 | 6.99993 | 0.049926 | 1.455E-06 | 6.96E-07 |

**Table 2.** Estimates for the Gamma and Gumbel distribution.

It appears from table 2 that the results obtained from the method of maximum likelihood are comparable with the results obtained from the SPM method. In some cases, in particular when $T = 20$, the estimates obtained by the SPM for the Gamma distribution appear to be slightly better than the results obtained by the MLE. Furthermore the SPM estimates for the Gumbel distribution appear to have less variance.

## 6 Conclusion

The aim of this paper was to propose a method of parameter estimation that makes use of the stochastic programming framework as well as the properties of the real and imaginary parts of the characteristic function. These features reduce the computation problems triggered by the oscillatory nature of the empirical characteristic function. This enabled us to work with integrands whose behaviour was controlled nicely for numerical procedures to converge conformably. It was shown that as $n \to \infty$ the optimal solution of the proposed stochastic program approaches $\mathbb{P}$ a.s. the true vector of parameters. Furthermore, when compared with other methods of estimation, such as ISEE and MLE, the SPM was found to give better results when compared to former and gave comparable results to the latter. However, contrary to the MLE, the SPM is particularly useful when dealing with probability distributions, like

most infinitely divisible distributions or most stable distributions, whose density function is not known in closed form.

## References

1. Fortet R. and Mourier E., "Lois des grandes nombres pour des elements aleatoires prenant leurs valeurs dans un espace de Banach", *Comptes rendus hebdomadaires de l'Academeie des Sciences*, Paris, 237, 18-20, (1953).
2. Gasinski, L. and Papageorgiou N. S., *Nonlinear Analysis* , Chapman & Hall/CRC, Taylor & Francis Group, (2005).
3. Jain N. C, and Marcus M. B., "Central limit theorems for C(S)-valued random variables", *Journal of Functional Analysis* 19, 3, 216-231, (1975).
4. Karmitsa N., Tanaka M., Herskovits J., "Nonconvex Nonsmooth Minimisation via Cutting Planes and Feasible Direction Interior Point Method", *Turku Centre for Computer Science*, (2009).
5. Kelly J. E. Jr., "The Cutting-Plane Method for Solving Convex Programs", *Journal of the Society for Industrial and Applied Mathematics*, 8, 4, 703-712, (1960).
6. Ledoux M. and Talagrand M., *Probability in Banach Spaces*, Springer-Verlag Berlin Heidelberg, (1991, 2011).
7. Pereira M.V.F. and Pinto L.M.V.G., "Multi-stage stochastic optimization applied to energy planning", *Mathematical Programming*, 52, 359-375, (1991).
8. Shapiro A., "Analysis of stochastic dual dynamic programming method", *European Journal of Operational Research*, 209, 63-72, (2011).
9. Sant L. and Caruana M. A., "Products of Characteristic functions in Lévy Process Parameter Estimation" *Proceedings, 2nd Stochastic Modelling Techniques and Data Analysis International Conference*, 661 669, (2012).
10. van der Vaart A. W., *Asymptotic Statistics*, Cambridge University Press, pg 297, (2000).

# Tail dependence of enriched class of perturbed copulas with modelling applications

Jozef Komorník[1], Magda Komorníková[2], Jana Kalická[2], and Cuong Nguyen[3]

[1] Faculty of Managment, Comenius University, Odbojárov 10, P.O.Box 95, 820 05 Bratislava, Slovakia
(E-mail: Jozef.Komornik@fm.uniba.sk)
[2] Faculty of Civil Engineering, Slovak University of Technology, Radlinského 11, 813 68 Bratislava, Slovakia
(E-mail: Magda.Komornikova,Jana.Kalicka@stuba.sk)
[3] Faculty of Commerce, Lincoln University NZ, Canterbury, New Zealand
(E-mail: Cuong.Nguyen@lincoln.ac.n)

**Abstract.** In this paper, we extend our investigations of a special class of perturbations of copulas introduced in [6] as a partial generalization of Farlie – Gumbel – Morgenstern (FGM) class of copulas (for non–negative values of perturbation parameters). We construct an extension of such generalization for negative values of perturbation parameters and show that this kind of perturbations does not change the value of tail dependence of the original copulas. Subsequently we apply the studied class of perturbed copulas to modelling relations between returns of a investments in a selected important REIT indexes. We show that the optimal models for different pairs of indexes can be found in form of perturbations corresponding to both positive or negative values of perturbation parameters.
**Keywords:** Copula, Perturbation of copula, Tail dependence, Real Estate Investment Trust (REIT) index, Returns of REIT indexes.

## 1 Introduction

The notion of copula was first introduced by *Abe Sklar* (1959) [9] in a mathematical (statistical) sense. Sklar proved the theorem (*Sklar's theorem*) describing the copula function which build a multivariate distribution function from the marginal distribution functions. Since the introduction of copulas, they have gained a lot of popularity in several applied fields - like economy, finance, insurance, engineering, medicine, sociology.

Fitting of an appropriate copula to real data is one of major tasks in application of copulas. For this purpose, a large buffer of potential copulas has been designed (mainly parametric families) of copulas. Once we know approximately a copula $C$ appropriate to model the observed data, we look for a minor perturbation of $C$ which fit better then $C$ itself. This is, e.g., the case of Farlie–Gumbel–Morgenstern (FGM) class of copulas, all of them being a

*Stochastic Modeling, Data Analysis and Statistical Applications* (*pp.* 53-63)
Lidia Filus - Teresa Oliveira - Christos H Skiadas (Eds)



perturbation of the independence copula $\Pi$, $\Pi(u,v) = u\,v$. Recall that FGM family $\left(C_\alpha^{FGM}\right)_{\alpha\in[-1,1]}$ of copulas is given by

$$C_\alpha^{FGM}(u,v) = u\,v + \alpha\,u\,(1-u)\,v\,(1-v), \quad \alpha \in [-1,1].$$

We continued the attempt to generalize the FGM perturbations to any copula $C$ as described below by relations (7) – (9).

We have shown that for this class of perturbations, the values of the coefficients of tail dependence are the same as their values for the original copula $C$.

The paper is organized as follows. The second section is devoted to a brief overview of the theory of copulas. In the third section we discuss perturbations of bivariate copulas. The fourth section is bringing an overview of the tail dependence coefficients and contains the main theoretical result of this paper. In the fifth section we present the utilized methodology of copula fitting to two–dimensional time series. The sixth section contains application to real data modelling. Finally, some conclusions are presented.

## 2 Copulas

Copula represents a multivariate distribution that capture the dependence structure among random variables. It is a great tool for building flexible multivariate stochastic models. Copula offers the choice of an appropriate model for the dependence between random variables independently from the selection of marginal distributions. This concept was introduced in the early 50's and became popular in several fields beyond statistics and probability theory, such as finance, actuarial science, fuzzy set theory, hydrology, civil engineering, etc.

**Definition 1.** A function $C : [0,1]^2 \to [0,1]$ is called a (bivariate) copula whenever it is

**i)** 2–increasing, i.e.,

$$V_C\left([u_1,u_2]\times[v_1,v_2]\right) = C(u_1,v_1) + C(u_2,v_2) - C(u_1,v_2) - C(u_2,v_1) \geq 0$$

for all $0 \leq u_1 \leq u_2 \leq 1$, $0 \leq v_1 \leq v_2 \leq 1$ (recall that $V_C\left([u_1,u_2]\times[v_1,v_2]\right)$ is the $C$–volume of the rectangle $[u_1,u_2]\times[v_1,v_2]$);

**ii)** grounded, i.e., $C(u,0) = C(0,v) = 0$ for all $u,v \in [0,1]$;

**iii)** it has a neutral element $e = 1$, i.e., $C(u,1) = u$ and $C(1,v) = v$ for all $u,v \in [0,1]$.

For more details we recommend monographs Joe(1997) [4] and Nelsen(2006) [7]. The Table 1 provides a summary of some selected basic facts that are related to some classes of Archimedean copulas that we utilize in our analyses.

We follow the approach of Patton [8] and consider a so–called *survival copula* derived from a given copula $C(u,v)$ corresponding to the couple $(X,Y)$ by

$$\widehat{C}(u,v) = u + v - 1 + C(1-u,1-v) \tag{1}$$

which is the copula related to the couple $(-X,-Y)$ with the marginal distribution functions

$$F_{-X}(x) = 1 - F_X(-x^+) \text{ and } F_{-Y}(y) = 1 - F_Y(-y^+). \tag{2}$$

| Family of copulas | Parameter | Bivariate copula $C(u,v)$ |
|---|---|---|
| Gumbel | $\theta \geq 1$ | $e^{-[(-ln(u))^{\theta}+(-ln(v))^{\theta}]^{\frac{1}{\theta}}}$ |
| Clayton (strict) | $\theta > 0$ | $(u^{-\theta}+v^{-\theta}-1)^{-\frac{1}{\theta}}$ |
| Frank | $\theta \in \Re$ | $-\frac{1}{\theta}\ln(1+\frac{(e^{-\theta u}-1)\,(e^{-\theta v}-1)}{(e^{-\theta}-1)})$ |
| Joe | $\theta \in [1,\infty)$ | $1-\left((1-u)^{\theta}+(1-v)^{\theta}-(1-u)^{\theta}(1-v)^{\theta}\right)^{1/\theta}$ |
| Ali-Mikhail-Haq | $\theta \in [-1,1]$ | $\frac{uv}{1-\theta(1-u)(1-v)}$ |

**Table 1.** Some Archimedean copulas

## 3 Pertubation of bivariate copulas

Now, we will consider those bivariate copulas $C_H$ that can be expressed in the form

$$C_H(u,v) = C(u,v) + H(u,v) \tag{3}$$

where $C$ is a fixed copula and $H : [0,1]^2 \to [0,1]$ is a continuous function. Function $H$ is called *perturbation factor* and copula $C_H$ is called *perturbation* of $C$ by means of $H$. We recall, that for $f(u) = u\,(1-u)$, $g(v) = v\,(1-v)$, $H_\theta(u,v) = \theta\, f(u)g(v)$ is $FMG$ family of copulas based on perturbation of the copula $\Pi(u,v)$

$$C_\theta(u,v) = uv + H_\theta(u,v), \quad \theta \in [-1,1]\,. \tag{4}$$

Note that for $\theta \in [0,1]$ is $H_\theta(u,v) \geq 0$ and thus $C_\theta(u,v) \geq C(u,v)$ while for $\theta \in [-1,0]$ is $H_\theta(u,v) \leq 0$ and $C_\theta(u,v) \leq C(u,v)$ .

Another family of copulas based on perturbation was introduced in [1]:

$$C_{f,g}(u,v) = C(u,v) + f(u \vee v)g(u \wedge v), \tag{5}$$

where $f, g : [0,1] \to \Re$ are two non-zero continuous functions such that

$$\sup\{u \in [0,1] : f(u) \neq 0\} = 1 \text{ and } \inf\{u \in [0,1] : f(u) \neq 0\} = 0$$

(and similarly for g), with $u \vee v = \max(u,v)$ and $u \wedge v = \min(u,v)$. In other words, $C_{f,g}$ given by (5) is a perturbation of $C$ by means of $H(u,v) = f(u \vee v)g(u \wedge v)$.

In [6], the following a perturbation of bivariate copulas was introduced. It has the form

$$C_H(u,v) = max\,(0, C(u,v) + H(u,v))\,, \tag{6}$$

where the noise $H : [0,1]^2 \to \Re$, $H(u,0) \leq 0$ and $H(0,v) \leq 0$ for all $u, v \in [0,1]$. It is clearly that $e = 1$ is a neutral element of $C_H$ only if $H(u,1) = H(1,v) = 0$ for all $u, v \in [0,1]$.

In [6] the next perturbation method (valid for any copula $C$) was introduced.

**Theorem 1.** *Let $C : [0,1]^2 \to [0,1]$ be a copula and define $H_\alpha^C : [0,1]^2 \to [0,1], \alpha \in [0,1]$ by*

$$H_\alpha^C(u,v) = \alpha\,(u - C(u,v))\,(v - C(u,v)). \tag{7}$$

*Then* $C_{H_\alpha^C} : [0,1]^2 \to [0,1]$ *given by*

$$C_{H_\alpha^C} = C(u,v) + H_\alpha^C(u,v) \tag{8}$$

*is a copula for each* $\alpha \in [0,1]$ *and any copula* $C$.

Note again that $C_{H_\alpha^C} \geq C(u,v)$ for $\alpha \in [0,1]$.

Now we extend the definition $C_{H_\alpha^C}(u,v)$ for $\alpha \in [-1,0]$ such that $C_{H_\alpha^C}(u,v) \leq C(u,v)$.

**Theorem 2.** *Let* $C : [0,1]^2 \to [0,1]$ *be a copula and define* $H_\alpha^C[0,1]^2 \to [0,1], \alpha \in [-1,0]$ *by*

$$H_\alpha^C(u,v) = \alpha\, C(u,v)\ \left(C(u,v) - (u+v-1)\right). \tag{9}$$

*Then* $C_{H_\alpha^C} : [0,1]^2 \to [0,1]$ *given by (8) is a copula for each* $\alpha \in [-1,0]$ *and any copula* $C$.

The proof can be performed in a similar way as the proof of Theorem 1 in [6].

In the next section we will investigate tail dependencies for a given perturbed copulas.

## 4 Tail dependence of perturbed copulas

For a better specifications of the tail of a distributions, Joe [4] introduced the *lower and upper tail dependence coefficients* $\lambda_L$ and $\lambda_U$. The tail dependence coefficients are rank-invariant and they can be calculated from the copula $C$ of random variables $X, Y$.

**Definition 2.** Let $X$ and $Y$ be continuous random variables with distributions functions $F_X$ and $F_Y$ and with copula $C$, then the *lower tail dependence coefficient* is defined by

$$\lambda_L = lim_{u\to 0^+} P\left(Y \leq F_Y^{-1}(u) \mid X \leq F_X^{-1}(u)\right) = lim_{u\to 0^+} \frac{C(u,u)}{u}, \tag{10}$$

and the *upper tail dependence coefficient* by

$$\lambda_U = lim_{u\to 1^-} P\left(Y > F_Y^{-1}(u) \mid X > F_X^{-1}(u)\right) = lim_{u\to 1^-} \frac{1-2u+C(u,u)}{1-u}. \tag{11}$$

(provided that the above limits exist).

We can rewritten (11) in the form

$$\lambda_U = lim_{v\to 0^+} \frac{2v-1+C(1-v,1-v)}{v}. \tag{12}$$

It is well known (see [4,7]) that the Gumbel copula $C_\theta^G$, Clayton copula $C_\theta^{Cl}$, Joe copula $C_\theta^J$, Frank copula $C_\theta^F$ and Ali–Mikhail–Haq copula $C_\theta^{AMH}$ (see [5]) satisfy the relation

$$\lambda_L(C_\theta^G) = 2 - 2^{\frac{1}{\theta}}, \quad \lambda_U(C_\theta^G) = 0,$$

$$\lambda_L(C_\theta^{Cl}) = 0, \quad \lambda_U(C_\theta^{Cl}) = 2^{-\frac{1}{\theta}},$$

$$\lambda_L(C_\theta^{J}) = 2 - 2^{\frac{1}{\theta}}, \quad \lambda_U(C_\theta^{J}) = 0,$$

$$\lambda_L(C_\theta^{F}) = 0, \quad \lambda_U(C_\theta^{F}) = 0,$$

$$\lambda_L(C_\theta^{AMH}) = \begin{cases} 0.5 & \text{if } \theta = 1 \\ 0 & \text{if } -1 \leq \theta < 1 \end{cases}, \quad \lambda_U(C_\theta^{AMH}) = 0.$$

From (11) and (12) we directly obtain the following well known result.

**Proposition 1.** *The upper and lower tail dependence coefficients for a mixture of two copulas $C = \alpha C_1 + (1-\alpha)C_2$ are given in the next form*

$$\lambda_U(C) = \alpha\lambda_U(C_1) + (1-\alpha)\lambda_U(C_2)$$

*and*

$$\lambda_L(C) = \alpha\lambda_L(C_1) + (1-\alpha)\lambda_L(C_2).$$

Similarly, combining (11) and (12) with (1) we get the next familiar identity.

**Proposition 2.** *Let $\widehat{C}$ is survival copula of $C$. Then $\lambda_U(C) = \lambda_L(\widehat{C})$ and $\lambda_L(C) = \lambda_U(\widehat{C})$.*

$C$ is said to have lower (upper) tail dependence if and only if $\lambda_L \neq 0$ ($\lambda_U \neq 0$). As it can be seen from Definition 2, the tail dependence coefficients are connected with the *diagonal section* of the bivariate copula $C$, which is defined by the function

$$\delta_C : [0,1] \to [0,1], \delta_C(u) = C(u,u). \tag{13}$$

Combining (13) with (1) we obtain

$$\begin{aligned} \delta_{\widehat{C}}(u) &= 2u - 1 + \delta_C(1-u, 1-u) \\ \delta_C(u) &= 2u - 1 + \delta_{\widehat{C}}(1-u, 1-u) \end{aligned} \tag{14}$$

(because of $\widehat{\widehat{C}} = C$).

Coefficients of tail dependence can be expressed by means of formulas

$$\lambda_L(C) = \delta_C^{'}(0^+) \tag{15}$$

and (using (12))

$$\lambda_U(C) = 2 - \delta_C^{'}(1^-). \tag{16}$$

It was shown in [1] that for any copula of type (5), the upper and lower coefficients of tail dependence are given by the formulas

$$\lambda_U(C_{f,g}) = \lambda_U(C) - f^{'}(1^-)g(1),$$

and

$$\lambda_L(C_{f,g}) = \lambda_L(C) - f(0)g^{'}(0^+).$$

*Example 1.* We will consider *FGM* family of copulas given by (4). We have

$$\delta(u) = u^2\left[1+\theta\left(1-u\right)^2\right] \text{ for } \theta \in (-1,1).$$

Obviously, $\delta^{'}(0^+) = 0$ and $\delta^{'}(1^-) = 2$. Hence $\lambda_U(C_\theta) = \lambda_L(C_\theta) = 0$.

**Theorem 3.** *Let $C_{H_\alpha^C}$ be a copula given by (8) and (7). Then*

$$\lambda_L(C_{H_\alpha^C}) = \lambda_L(C) \tag{17}$$

*and*

$$\lambda_U(C_{H_\alpha^C}) = \lambda_U(C). \tag{18}$$

*Proof.* From (7) – (9) we get

$$|\delta_{C_{H_\alpha^C}} - \delta_C| \leq |\alpha| \cdot u^2,$$

thus

$$\lambda_L\left(C_{H_\alpha^C}\right) = \delta'_{C_{H_\alpha^C}}(0_+) = \delta'_C(0_+) = \lambda_L(C).$$

From (1), (7) – (9) we conclude that the survival copula to the perturbation $C_{H_\alpha^C}$ is identical to the perturbation of the survival copula $\widehat{C}$ (with the identical value of $\alpha$) and thus

$$\lambda_U\left(C_{H_\alpha^C}\right) = \lambda_L(\widehat{C}) = \lambda_U(C).$$

□

## 5 Fitting of copulas

In practical fitting of the data we have utilized the *maximum pseudolikelihood method* (MPL) of parameter estimation with initial parameters estimates received by the minimalization of the mean square distance to the empirical copula $C_n$ presented e.g. in Genest and Favre [3]

$$C_n(u,v) = \frac{1}{n}\sum_{i=1}^{n} \mathbf{1}\left(\frac{R_i}{n+1} \leq u, \frac{S_i}{n+1} \leq v\right)$$

where $n$ is the sample size, $R_i$ stands for the rank of $X_i$ among $X_1, \ldots, X_n$, $S_i$ stands for the rank of $Y_i$ among $Y_1, \ldots, Y_n$ and $\mathbf{1}(\Omega)$ denoting the indicator function of set $\Omega$. It requires that the copula $C_\theta(u,v)$ is absolutely continuous with density $c_\theta(u,v) = \frac{\partial^2}{\partial u\,\partial v} C_\theta(u,v)$. This method (described e.g. in Genest and Favre [3]) involves maximizing a rank-based log-likelihood of the form

$$L(\theta) = \sum_{i=1}^{n} \ln\left(c_\theta\left(\frac{R_i}{n+1}; \frac{S_i}{n+1}\right)\right),$$

where $\theta$ is vector of parameters in the model. Note that arguments $\frac{R_i}{n+1}$, $\frac{S_i}{n+1}$ equal to the corresponding values of the empirical marginal distributional functions of random variables $X$ and $Y$.

For selecting the optimal models we applied the Kolmogorov – Smirnov – Anderson – Darling (KSAD, for which we use the abbreviation $AD$) test statistic defined e.g. in Berg and Bakken [2]

$$AD(\theta) = \sqrt{n}\ \max|\frac{C_n\left(\frac{R_i}{n+1}, \frac{S_i}{n+1}\right) - C_\theta\left(\frac{R_i}{n+1}, \frac{S_i}{n+1}\right)}{C_\theta\left(\frac{R_i}{n+1}, \frac{S_i}{n+1}\right) * (1 - C_\theta\left(\frac{R_i}{n+1}, \frac{S_i}{n+1}\right))}| \tag{19}$$

for which we also constructed a GoF simulation based test, when comparing models with their submodels and different families of models.

## 6 Application to real data modeling

A REIT (**R**eal **E**state **I**nvestment **T**rust) is a company that mainly owns, and in most cases, operates income–producing real estate such as apartments, shopping centers, offices, hotels and warehouses. Some REITs also engage in financing real estate. The shares of many REITs are traded on major stock exchanges.

REIT Index Series is designed to present investors with a comprehensive family of REIT performance indexes that spans the commercial real estate space across the economy of the country. The index series provides investors with exposure to all investment and property sectors. In addition, the more narrowly focused property sector and sub–sector indexes provide the facility to concentrate commercial real estate exposure in more selected markets.

We have investigated the relations between 4 selected countries' (USA, Australia, Japan and UK) daily returns of the REIT (Real Estate Investment Trust) indexes (from the period January 2000 – August 2012) in different time periods, determined by the recent global financial markets crises (July 1, 2008 – April 30, 2009) that can be also clearly identified from next Figure 1, presenting the parallel development of the considered REIT indexes.

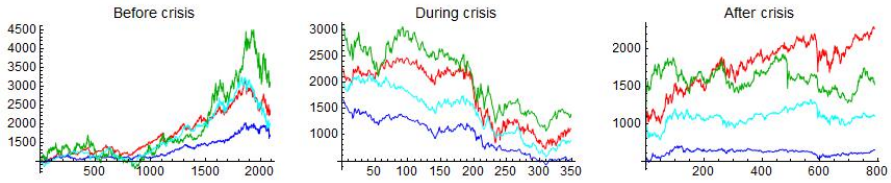


**Fig. 1.** Real Estate Investment Trust indexes in different time periods (USA = red, Australia = blue, Japan = green, UK = cyan)

We have performed filtering of the returns of all individual REIT indexes (in order to avoid a possible violation of the i.i.d. property) by ARMA–GARCH models (separately for the individual considered time sub-periods).

For all three time sub-periods and all couples of (filtered) returns of the REIT indexes we have performed the non–parametric correlation analyses based on the Kendall coefficients (see Table 2, 3 and 4). We have observed that the values of the correlation coefficients have dropped substantially between the first and the second considered time sub-periods and even more dramatically for the third sub-period.

| before crisis | USA | Australia | Japan | UK |
|---|---|---|---|---|
| USA | 1 | 0.994 | 0.731 | 0.737 |
| Australia | 0.994 | 1 | 0.727 | 0.738 |
| Japan | 0.731 | 0.727 | 1 | 0.609 |
| UK | 0.737 | 0.738 | 0.609 | 1 |

**Table 2.** The values of the Kendall's correlation coefficient $\tau$ for the pre–crisis period

| during crisis | USA | Australia | Japan | UK |
|---|---|---|---|---|
| USA | 1 | 0.301 | 0.267 | 0.306 |
| Australia | 0.301 | 1 | 0.535 | 0.397 |
| Japan | 0.267 | 0.535 | 1 | 0.378 |
| UK | 0.306 | 0.397 | 0.378 | 1 |

**Table 3.** The values of the Kendall's correlation coefficient $\tau$ for the crisis period

| after crisis | USA | Australia | Japan | UK |
|---|---|---|---|---|
| USA | 1 | 0.111 | 0.061 | 0.221 |
| Australia | 0.111 | 1 | 0.222 | 0.087 |
| Japan | 0.061 | 0.222 | 1 | 0.073 |
| UK | 0.221 | 0.087 | 0.073 | 1 |

**Table 4.** The values of the Kendall's correlation coefficient $\tau$ for the post–crisis period

We have applied the fitting by copulas to the residuals of ARMA–GARCH filters. We considered models from strict Archimedean copulas (Joe $C^J$, Frank $C^F$, Clayton $C^{Cl}$ and Gumbel $C^G$) families and their mixtures with corresponding survival copulas $\hat{C}$ as well as their perturbations given by (8). We also tried the Farlie–Gumbel–Morgenstern (FGM) and Ali–Mikhail–Haq (AMH) copulas, but these had the greatest values of the AD for all the pairs and time periods.

For estimation of parameters for each type of models we have used the maximum pseudo–likelihood method. For selecting the optimal models we have applied the Kolmogorov – Smirnov – Anderson – Darling (for which we have used the abbreviation $AD$) test statistic (19). For all of them, the simulation

based GoF test yielded p–value $> 0.1$. Overview of optimal types of copulas for all couples and all time sub–periods of the filtered returns of REIT indexes is in Table 5, Table 6 and Table 7 (where $\Delta AD$ represents the absolute value of the reduction of the $AD$ statistics for the optimal model for the considered couple of countries in comparison with the value of the $AD$ for the optimal non–perturbed model of the same type).

| Couple | Type of copula | $\alpha$ | $\Delta AD$ | $\theta$ | $\lambda_L$ | $\lambda_U$ |
|---|---|---|---|---|---|---|
| USA & Japan | $0.5 * (C^{Cl} + \widehat{C}^{Cl}) + H_\alpha^{0.5*(C^{Cl}+\widehat{C}^{Cl})}$ | 0.98 | 0.16 | 1.71 | 0.33 | 0.33 |
| USA & Australia | $0.5 * (C^{G} + \widehat{C}^{G}) + H_\alpha^{0.5*(C^{G}+\widehat{C}^{G})}$ | 0.97 | 0.11 | 6.64 | 0.44 | 0.44 |
| USA & U.K. | $0.5 * (C^{G} + \widehat{C}^{G}) + H_\alpha^{0.5*(C^{G}+\widehat{C}^{G})}$ | -0.09 | 0.04 | 2.70 | 0.32 | 0.32 |
| Japan & Australia | $0.5 * (C^{G} + \widehat{C}^{G}) + H_\alpha^{0.5*(C^{G}+\widehat{C}^{G})}$ | 0.89 | 0.23 | 1.91 | 0.28 | 0.28 |
| Japan & U.K. | $0.5 * (C^{G} + \widehat{C}^{G}) + H_\alpha^{0.5*(C^{G}+\widehat{C}^{G})}$ | -0.05 | 0.17 | 1.84 | 0.26 | 0.26 |
| U.K & Australia | $0.5 * (C^{G} + \widehat{C}^{G}) + H_\alpha^{0.5*(C^{G}+\widehat{C}^{G})}$ | -0.10 | 0.21 | 2.82 | 0.32 | 0.32 |

**Table 5.** The overview of best types of copulas for all couples of the (filtered) returns of REIT indexes before crisis

| Couple | Type of copula | $\alpha$ | $\Delta AD$ | $\theta$ | $\lambda_L$ | $\lambda_U$ |
|---|---|---|---|---|---|---|
| USA & Japan | $0.5 * (C^{G} + \widehat{C}^{G}) + H_\alpha^{0.5*(C^{G}+\widehat{C}^{G})}$ | -0.07 | 0.04 | 1.40 | 0.17 | 0.17 |
| USA & Australia | $0.5 * (C^{G} + \widehat{C}^{G}) + H_\alpha^{0.5*(C^{G}+\widehat{C}^{G})}$ | -0.31 | 0.20 | 1.95 | 0.20 | 0.20 |
| USA & U.K. | $C^{Cl} + H_\alpha^{C^{Cl}}$ | -0.26 | 0.03 | 1.43 | 0.45 | 0.00 |
| Japan & Australia | $0.5 * (C^{G} + \widehat{C}^{G}) + H_\alpha^{0.5*(C^{G}+\widehat{C}^{G})}$ | 0.44 | 0.03 | 2.01 | 0.29 | 0.29 |
| Japan & U.K. | $0.5 * (C^{G} + \widehat{C}^{G}) + H_\alpha^{0.5*(C^{G}+\widehat{C}^{G})}$ | 0.48 | 0.51 | 1.49 | 0.21 | 0.21 |
| U.K & Australia | $0.5 * (C^{G} + \widehat{C}^{G}) + H_\alpha^{0.5*(C^{G}+\widehat{C}^{G})}$ | 0.17 | 0.04 | 1.62 | 0.23 | 0.23 |

**Table 6.** The overview of best types of copulas for all couples of the (filtered) returns of REIT indexes during crisis

We can observe that most values of the coefficients of tail dependencies for the optimal copula models (with few exceptions) change between individual considered time periods in a similar way as the values of the Kendall correlation coefficients. They also have prevailingly dropped between the first and the second period and continued to fall between the second and the third period.

The most interesting observation is that the subclass of perturbations with negative values of $\alpha$ is strongly represented among the optimal models for all three periods (and prevailing in the third period).

| Couple | Type of copula | $\alpha$ | $\Delta AD$ | $\theta$ | $\lambda_L$ | $\lambda_U$ |
|---|---|---|---|---|---|---|
| USA & Japan | $C^{Cl} + H_\alpha^{C^{Cl}}$ | -0.22 | 0.69 | 0.29 | 0.07 | 0.00 |
| USA & Australia | $C^{Cl} + H_\alpha^{C^{Cl}}$ | -0.02 | 0.05 | 0.23 | 0.05 | 0.00 |
| USA & U.K. | $0.5 * (C^{Cl} + \widehat{C}^{Cl}) + H_\alpha^{0.5*(C^{Cl}+\widehat{C}^{Cl})}$ | -0.13 | 0.05 | 0.76 | 0.17 | 0.17 |
| Japan & Australia | $0.5 * (C^{J} + \widehat{C}^{J}) + H_\alpha^{0.5*(C^{J}+\widehat{C}^{J})}$ | -0.14 | 0.02 | 1.69 | 0.21 | 0.21 |
| Japan & U.K. | $0.5 * (C^{G} + \widehat{C}^{G}) + H_\alpha^{0.5*(C^{G}+\widehat{C}^{G})}$ | -0.57 | 0.43 | 1.42 | 0.08 | 0.08 |
| U.K & Australia | $C^{Cl} + H_\alpha^{C^{Cl}}$ | 0.24 | 0.58 | 0.08 | 0.009 | 0.00 |

**Table 7.** The overview of best types of copulas for all couples of the (filtered) returns of REIT indexes after crisis

## 7 Concluding remarks

In the theoretical part of the paper, we derived an important result for the special type of perturbed copulas, where the perturbations do not change the values of tail dependencies. In the practical part, we observed strongly decreasing trends (between the subsequent considered time periods) for the values of the Kendall correlation coefficients and similar trends for the values of tail dependence coefficients for the optimal copula models (for most considered couples of filtered returns of REIT indexes).

Despite the theoretical fact that the considered class of perturbations does not change the tail dependence coefficients of the considered copulas, their use yielded (often considerable) reductions of the values of $AD$ statistics.

The most interesting result of this paper is the demonstration of practical modeling applicability of newly introduced subclass of perturbations with negative perturbation parameters.

**Acknowledgement** The support of the grants APVV–0013–14 and VEGA 1/0420/15 is kindly announced.

## References

1. F. Durante, J.F. Sánchez, M.U. Flores: Bivariate copulas generated by perturbations. *Fuzzy Sets and System*, 228, 137–144, 2013.
2. D. Berg, H. Bakken: Copula Goodness-of-fit Tests: A Comparative Study. In: Working paper, University of Oslo and Norwegian Computing Center, 2006.
3. C. Genest, A.C. Favre: Everything you always wanted to know about copula modeling but were afraid to ask. *Journal of Hydrologic Engineering* **12**, 347–368 (2007)
4. H. Joe: Multivariate model and dependence concept. *Monographs on Statistics and Applied Probability*, 73, Chapman and Hall, 1997.
5. P. Kumar: Probability Distributions and Estimation of Ali–Mikhail–Haq Copula. *Applied Mathematical Sciences, Vol. **4**, No. 14, 657–666, 2010.*
6. *R. Mesiar, M. Komorníková, J. Komorník: Perturbation of bivariate copula.*Fuzzy Sets and System *Vol. **268**, 127–140, 2015.*

*7. R.B. Nelsen: An introduction to copulas. Second Edition.* Springer Series in Statistics*, Springer-Verlag, New York, 2007.*
*8. A.J. Patton: Modelling Asymmetric Exchange Rate Dependence.* International Economic Review *Vol.* ***47****, No. 2, 527–556, 2006.*
*9. A. Sklar: Fonctions de répartition à n dimensions et leurs margers.* Publ. Inst. Statist. Univ. Paris*, 8, 229–231, 1959.*

# Discrete semi Markov patient pathways through hospital care via Markov modelling

Aleka Papadopoulou[1], Sally McClean[2] and Lalit Garg[3]
[1]Department of Mathematics,
Aristotle University of Thessaloniki,
Thessaloniki 54124, Greece
(e-mail: apapado@math.auth.gr)
[2]School of Computing and Information Engineering,
University of Ulster,
Coleraine, Northern Ireland, UK, BT52 1SA
(e-mail: si.mcclean@ulster.ac.uk )
[3]Computer Information Systems
Faculty of Information & Communication Technology
University of Malta, Malta
(e-mail: lalit.garg@um.edu.mt )

## Abstract

In the present paper, we study the movement of patients through hospital care where each patient spends an amount of time in hospital, referred to as length of stay (LOS). In terms of semi-Markov modelling we can regard each patient pathway as a state of the semi-Markov model, therefore the holding time distribution of the *i*th state of the semi-Markov process is equivalent to the LOS distribution for the corresponding patient pathway. By assuming a closed system we envisage a situation where the hospital system is running at capacity, so any discharges are immediately replaced by new admissions to hospital. In the present paper a method is applied according to which we can describe first and second moments of numbers in each semi Markov patient pathway at any time via Markov modelling. Such values are useful for future capacity planning of patient demand on stretched hospital resources. The above results are illustrated numerically with healthcare data.

*Keywords*: Healthcare, Markov process, Semi Markov process, Population structure.

*Stochastic Modeling, Data Analysis and Statistical Applications* (pp. 65-72)
Lidia Filus - Teresa Oliveira - Christos H Skiadas (Eds)


## 1 The semi Markov system via Markov modelling

Semi Markov models (Iosifescu-Manu (1972), Howard (1971), McClean (1980, 1986), Janssen (1986), Mehlman(1979), Bartholomew *et al.*(1991), Vassiliou and Papadopoulou (1992) were introduced as stochastic tools, which can provide a general framework that can accommodate a great variety of applied probability models. A semi-Markov approach provides more generality than may be required to describe the complex semantics of the models. However, the complexity of analysis in semi Markov models discourages its application to real life problems and leads to the simpler choice of a Markov model which most of the time provides inaccurate results. In the present paper a method is applied according to which we can describe the expected population structure of an open semi Markov system in discrete time with fixed size via Markov modeling.

So, let us now consider a population which is stratified into a set of states according to various characteristics and $S$={1,2,...,k}. The expected population structure of the system at any given time is described by the vector $\mathbf{N}(t)=[N_1(t), N_2(t),..., N_k(t)]'$ where $N_i(t)$ is the expected population in state $i$ at time $t$. Also we assume that the individual transitions between the states occur according to a homogeneous semi Markov chain. In this respect let us denote by $\mathbf{P}$ the transition probability matrix of the embedded Markov chain and $\mathbf{H}(m)$ the matrix of holding time probabilities.

Let us now suppose that when an individual is in state $i$ at time $t$ and entered state $i$ at time $t$-$d$ (i.e. at its last transition) then the individual is in duration state ($i$,$d$) at time $t$. The transition probabilities between the duration states are of two types: the actual transitions (i.e. transitions from state ($i$,$d$) to ( $j$,0) for every $i$ and $j$) and the virtual transitions (i.e. transitions from state ($i$,$d$) to ($i$,$d$+1) for every $i$). The definition of the duration states and the calculation of the transition probabilities between them provides the tool to form an equivalent Markov model containing all the information from the semi Markov system (Papadopoulou and Vassiliou (2011)). Thus the new state space is S*={(1,0), (1,1),…(1,$b_1$-1),… ($i$,$d$),…,($k$,0), ($k$,1),…($k$,$b_k$-1)}, where $b_i$ is the maximum possible duration in the original state $i$ and the corresponding transition probability matrix is of the form

$$\mathbf{M}_{(b\,x\,b)} = \begin{bmatrix} \mathbf{S}_{11} & \mathbf{T}_{12} & \mathbf{T}_{13} & \dots & \dots & \mathbf{T}_{1k} \\ \mathbf{T}_{21} & \mathbf{S}_{22} & \mathbf{T}_{23} & \dots & \dots & \mathbf{T}_{2k} \\ \dots & \dots & \dots & \dots & \dots & \dots \\ \dots & \dots & \dots & \dots & \dots & \dots \\ \dots & \dots & \dots & \dots & \dots & \dots \\ \dots & \dots & \dots & \dots & \dots & \dots \\ \mathbf{T}_{k-1,1} & \mathbf{T}_{k-1,2} & \mathbf{T}_{k-1,3} & \dots & \dots & \mathbf{T}_{k-1,k} \\ \mathbf{T}_{k1} & \mathbf{T}_{k2} & \mathbf{T}_{k3} & \dots & \dots & \mathbf{S}_{kk} \end{bmatrix}$$

where $b = \sum b_i$ while the $\mathbf{S}_{i,i}$ diagonal matrices have as super-diagonal elements the transition probabilities for the virtual transitions and as first column elements the probability of re-entry to that state and $\mathbf{T}_{i,j}$ matrices have as first column elements the transition probabilities for the actual transitions between states. We therefore define:

$$\mathbf{S}_{i,i} = \begin{bmatrix} \pi_i(1-\alpha_1^{(i)}) & \alpha_1^{(i)} & 0 & 0 & \dots & 0 \\ \pi_i(1-\alpha_2^{(i)}) & 0 & \alpha_2^{(i)} & 0 & \dots & 0 \\ \pi_i(1-\alpha_3^{(i)}) & 0 & 0 & \alpha_3^{(i)} & \dots & 0 \\ \dots & \dots & \dots & \dots & \dots & 0 \\ \dots & 0 & 0 & 0 & \dots & 0 \\ \dots & \dots & \dots & \dots & \dots & \dots \\ \pi_i(1-\alpha_{b_i-1}^{(i)}) & 0 & 0 & 0 & \dots & \alpha_{b_i-1}^{(i)} \\ \pi_i & 0 & 0 & 0 & \dots & 0 \end{bmatrix}$$

while

$$\mathbf{T}_{i,j} = \begin{bmatrix} \pi_j(1-\alpha_1^{(i)}) & 0 & 0 & 0 & \dots & 0 \\ \pi_j(1-\alpha_2^{(i)}) & 0 & 0 & 0 & \dots & 0 \\ \pi_j(1-\alpha_3^{(i)}) & 0 & 0 & 0 & \dots & 0 \\ \dots & \dots & \dots & \dots & \dots & 0 \\ \dots & 0 & 0 & 0 & \dots & 0 \\ \dots & \dots & \dots & \dots & \dots & \dots \\ \pi_j(1-\alpha_{b_i-1}^{(i)}) & 0 & 0 & 0 & \dots & 0 \\ \pi_j & 0 & 0 & 0 & \dots & 0 \end{bmatrix}$$

where the first column of $\mathbf{S}_{i,\,i}$ represents probability of re-entry to state $i$ having left one of the duration states of $i$, for $i$=1, …$d_i$, and the first column of $\mathbf{T}_{i,\,j}$ represents probability of re-entry to state $j$ having left one of the duration states of $i$, for $j$=1,…$k$ and $i$=1, …$d_i$. The super-diagonal elements of $\mathbf{S}_{i,\,i}$ represents probability of transition from (new) state ($i$,$d$) to ($i$,$d$+1) for every $i$. $\pi_i$ is the probability of entry to (old) state $i$ and $a_x^{(i)}$ is the probability of remaining in pathway i for at least one more unit of time given that the current holding time is $x$. Hence, $1\text{-}a_x^{(i)}$ is the probability of discharge from pathway i given that the current holding time is $x$.

All of the above matrices are defined as functions of the basic parameters of the semi Markov system. So, now we can define the expected population structure for the new model. Let

$$\mathbf{N}^*(t) = \left\lfloor E(n_{1,0}(t)), E(n_{1,1}(t)),..., E(n_{1,b_1-1}(t)),..., E(n_{i,d}(t)),..., E(n_{k,0}(t)),..., E(n_{k,b_k-1}(t)) \right\rfloor$$

where $n_{i,d}(t)$ is the population in state $(i,d)$ at time $t$. It is obvious that $n_i(t)=\sum_{d=0}^{b_i-1} n_{i,d}(t)$ for every $i$=1,2,..,$k$. Hence, the expected population structure of the old (semi Markov) system can be described as follows:

$$\mathbf{N}(t)=\left[\sum_{d=0}^{b_1-1}E(n_{1,d}(t)),\ \sum_{d=0}^{b_2-1}E(n_{2,d}(t)),...,\ \sum_{d=0}^{b_i-1}E(n_{i,d}(t)),...,\ \sum_{d=0}^{b_k-1}E(n_{k,d}(t))\right] \quad (1)$$

where

$E(n_{j,d}(t))=\sum_{i=1}^{k}\sum_{x=0}^{b_i-1} n_{i,x}(0)M^{(t)}_{(i,x)(j,d)}$ and $M^{(t)}_{(i,x)(j,d)}$ is the element of $\mathbf{M}^t$ in the position: $\left(x+1+\sum_{z=1}^{i-1}b_z(\text{row}),\ d+1+\sum_{z=1}^{j-1}b_z(\text{column})\right)$.

By applying well known properties of variances and covariances we get that

$$Cov(n_i(t),n_j(t))=Cov\left(\sum_{d=0}^{b_i-1}n_{i,d}(t),\sum_{d=0}^{b_j-1}n_{j,d}(t)\right)=\sum_{d_1=0}^{b_i-1}\sum_{d_2=0}^{b_j-1}Cov(n_{i,d_1}(t),n_{j,d_2}(t)) \quad (2)$$

It is known from (Bartholomew, 1982) that the variances and covariances of $n_z(t)$, $n_r(t)$ of a Markov system are described by

$$Cov(n_z(t),n_r(t))=\sum_{x=1}^{k}\sum_{s=1}^{k}p_{xz}p_{sr}Cov(n_x(t-1),n_s(t-1))+\sum_{x=1}^{k}(\delta_{zr}p_{xz}-p_{xz}p_{xr})E(n_x(t-1)) \quad (3)$$

with initial conditions $Cov(n_z(0),n_r(0))=0$.

Hence, from (2),(3) we get that the variances and covariances of $n_i(t)$, $n_j(t)$ of the old (semi Markov) system can be described as follows:

$$Cov(n_i(t),n_j(t))=\sum_{d_1=0}^{b_i-1}\sum_{d_2=0}^{b_j-1}Cov(n_{i,d_1}(t),n_{j,d_2}(t))=$$

$$=\sum_{d_1=0}^{b_i-1}\sum_{d_2=0}^{b_j-1}\sum_{(m,d_3)}\sum_{(q,d_4)}M_{(m,d_3)(i,d_1)}M_{(q,d_4)(j,d_2)}Cov(n_{(m,d_3)}(t-1)n_{(q,d_4)}(t-1))+$$

$$+\sum_{d_1=0}^{b_i-1}\sum_{d_2=0}^{b_j-1}\sum_{(m,d_3)}\left(\delta_{(i,d_1)(j,d_2)}M_{(m,d_3)(i,d_1)}-M_{(m,d_3)(i,d_1)}M_{(m,d_3)(j,d_2)}\right)E(n_{(m,d_3)}(t-1))$$

, (4)

where in the sums $\sum_{(m,d_3)} \sum_{(q,d_4)}$ , $\sum_{(m,d_3)}$ the counters $(m,d_3), (q,d_4)$ take all the possible values for every m=1,2,…,k and $d_3$=0,1,..., $b_m - 1$, q=1,2,…,k and $d_4$=0,1,…, $b_q - 1$.

The initial conditions are $Cov(n_{(m,d)}(0), n_{(r,q)}(0)) = 0$.

From (4) and for i=j we get the variance of $n_i(t)$.

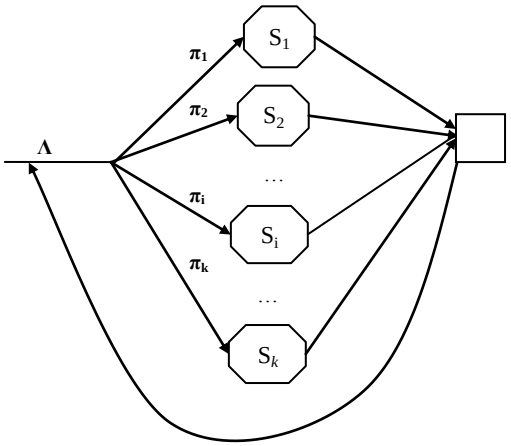


*Figure 1*

In Figure 1, we present the original semi Markov system while Figure 2 shows the same system transformed into a Markov system, as described above.

## 2. The Healthcare Application

As an example of the use of this approach in a healthcare environment, we consider the movement of patients through hospital care where each patient spends an amount of time in hospital, referred to as length of stay (LOS). In particular, we consider stroke patients where we regard stroke as a good paradigm example, affecting large numbers of patients with a resulting heavy burden on society.

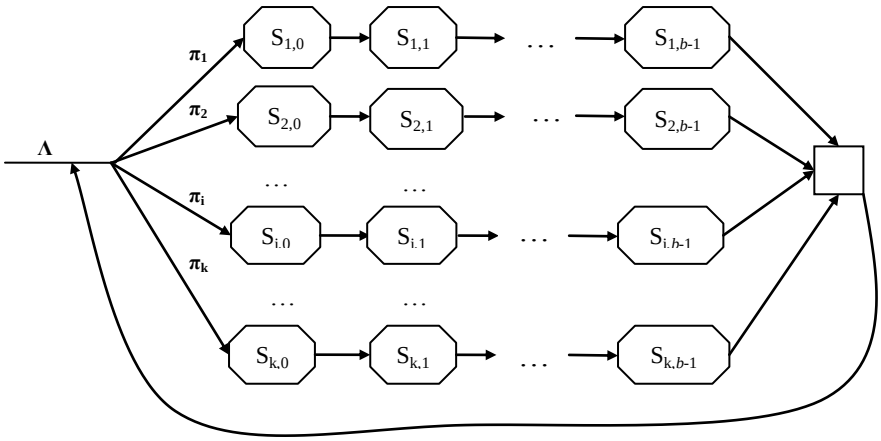


*Figure 2*

For example, in the UK it is estimated that Stroke disease costs over £7 billion a year, including community and social services, and costs to the labour force, as well as direct costs for hospital care.

We have previously defined stroke patient pathways (McClean et al., 2011) through hospital care, on the basis of diagnosis, gender, age and outcome, using log-rank tests to assess equality of survival distributions of LOS in hospital. Cox proportional hazards models were also employed to assess the effect of relevant covariates. On the basis of these tests we have defined 27 groups, each relating to a different patient pathway with respect to their LOS distribution. So patients in different pathways have different LOS distributions. Such pathways are characterised by the available covariates. Thus in the case of Stroke disease, examples of pathways are female, older patients, diagnosed with a haemorrhagic stroke and discharged to a

private nursing home or male, younger patients with a transitory ischaemic attack, who were discharged to their own home. We note that, although we have discussed this framework specifically with respect to Stroke disease and the corresponding data available in our previous study, the concept is easily generalisable to other diseases and conditions, with different possible covariates.

In terms of the semi-Markov model discussed in the previous section, we regard each patient pathway as a state of the semi-Markov model, where pathway $i$ is follow with probability $\pi_i$ for $i$-1,…,$k$. The holding time distribution of the $i$th state of the semi-Markov process is therefore

equivalent to the LOS distribution for the corresponding patient pathway.

By assuming a fixed size system we envisage a situation where the hospital system is running at capacity, so any discharges are immediately replaced by new admissions to the hospital.

Thus we can use the theory of the previous section to determine the distribution of population structure, in particular first and second moments of numbers in each patient pathway at any time. Such values are useful for future capacity planning of patient demand on stretched hospital resources.

Finally we discuss how to obtain the parameter estimates of our Markov representation of the original semi-Markov model. For each state of the Markov model $(i, j)$ we define $\alpha_{ij}$ as the probability of transition into state $S_{i,\,j+1}$ given that the individual has already been in pathway $i$ for duration $t_j$, for $i$=1,…,$k$ and $j$=1,…$b_i$-1. Then $\beta_{ij}$ = 1-$\alpha_{ij}$ is the probability of discharge from state $S_{i,j}$ given that the individual has already been in pathway $i$ for duration $t_j$, for $i$=1,…,$k$ and $j$=1,… $b_i$-1.

As estimators for $\alpha_{ij}$ and $\beta_{ij}$, we employ Kaplan-Maier type non-parametric maximum likelihood estimators (NPLMEs) (Bartholomew et al., 1991), as follows:

$\hat{\alpha}_{ij}$ = the number of pathway $i$ patients who progress to another day in hospital divided by the number of patients that have stayed in hospital for $t_j$ days. Also,

$\hat{\beta}_{ij}$ = 1-$\hat{\alpha}_{ij}$ , for $i$=1,…,$k$ and $j$=1,… $b$-1.

**References**


1. Bartholomew, D. J., Forbes, A. F., and McClean, S. I., Statistical Techniques for Manpower Planning, Wiley, Chichester (1991).
2. Howard, R.A., Dynamic Probabilistic systems, Wiley, Chichester (1971).
3. Iosifescu-Manu A., Non homogeneous semi-Markov processes, Stud. Lere. Mat. **24**, 529-533 (1972).
4. Janssen, J. (Ed.), Semi-Markov Models: Theory and Applications, Plenum Press, New York. (1986).
5. McClean, S. I., A semi-Markovian model for a multigrade population, J. Appl. Probab. **17,** 846-852 (1980).
6. McClean, S. I., Semi-Markov models for manpower planning, in Semi-Markov Models: Theory and Applications (J. Janssen, Ed.), Plenum, New York. (1986).

7. McClean, S.I., Barton, M, Garg, L. and Fullerton, K., A Modeling Framework that combines Markov Models and Discrete Event Simulation for Stroke Patient Care, ACM Transactions on Modeling and Computer Simulation 21(4) (2011).
8. Mehlmann, A., Semi-Markovian manpower models in continuous time, J. Appl. Probab. **16**, 416-422 (1979)
9. Papadopoulou A.A and P-CG Vassiliou, On the variances and covariances of the duration state sizes of semi Markov systems MSMPRF2011 Conference 19-23/9, Chalkidiki, Greece (2011).
10. Vassiliou P-CG and Papadopoulou A.A., Non homogeneous semi-Markov systems and maintainability of the state sizes. J Appl Prob **27**, 756–76 (1992).

# 2 CHAPTER

## Statistics, Distributions, Bayesian Modeling

# On the effect of Bayesian prior assumptions in the solution of geophysical inverse problems

Robert G Aykroyd[1], Hugo Hidalgo-Silva[2], and Enrique Gómez-Treviño[3]

[1] Department of Statistics, University of Leeds, Leeds, LS2 9JT, UK
(e-mail: r.g.aykroyd@leeds.ac.uk)
[2] Departamento de Ciencias de la Computación, Centro de Investigación Cientfica y Educación Superior de Ensenada, México, (e-mail: hugo@cicese.mx)
[3] Departamento de Geofsica Aplicada, Centro de Investigación Cientfica y Educación Superior de Ensenada, México, (e-mail: egomez@cicese.mx)

**Abstract.** The Bayesian modelling approach provides a natural framework to use for the solution of ill-posed inverse problems. In this paper the focus is on the reconstruction of the subsurface electrical conductivity distribution from surface voltage measurements — a commonly used geophysical technique which allows the earth's internal structure to be investigated indirectly. The key components of the Bayesian framework are the prior distribution and the likelihood which jointly quantify knowledge of the process being described. These components play equal roles in the posterior distribution — which is the basis for estimation. The likelihood is usually well defined from physical considerations, but the choice of prior distribution is more subjective. This paper compares different prior model descriptions using posterior estimation using a Markov chain Monte Carlo algorithm.
**Keywords:** Bayesian modelling, Inverse problems, MCMC, Posterior estimation, Regularization.

## 1 Introduction

Geophysical surveys are used to investigate the earth's subsurface structure from a few metres below the surface to as deep as several hundreds of kilometres. Surface data can be collected using many geophysical techniques, such as electromagnetic, gravimetric or seismic, and provide a cheap, safe and fast approach, but give indirect information about the subsurface. Here, the subsurface electrical conductivity distribution is estimated from surface electrical voltage measurements — see Hidalgo-Silva and Gómez-Treviño (2013b).

In this paper a Bayesian modelling approach is adopted which defines the error model as a likelihood and regularization in terms of prior distributions with the resulting posterior distribution being the focus for estimation — see for example Besag et al. (1995) and Gilks et al. (1995) — this is in contrast to the use of deterministic algorithms as in Hidalgo-Silva and Gómez-Treviño (2013a). Estimation of unknowns is performed using a Markov chain Monte

*Stochastic Modeling, Data Analysis and Statistical Applications* (*pp.* 75-86)
Lidia Filus - Teresa Oliveira - Christos H Skiadas (Eds)



Carlo (MCMC) algorithm which also allows uncertainties to be quantified, as well as conductivity distributions to be estimated. Section 2 discusses modelling, Section 3 describes MCMC estimation and Section 4 shows numerical results. Finally, some discussion and conclusions are given in Section 5.

## 2 Bayesian modeling

### 2.1 General

The aim of a generic inverse problem is to estimate an unknown function, $\mathbf{x}(\mathbf{s}), \mathbf{s} \in \Omega$, within some region, from a finite set of measurements $\mathbf{y} = \{y_i : i = 1, \ldots, n\}$ taken outside the region. In many examples the region will be partitioned into pixels and the function correspondingly discretized to give unknowns $\mathbf{x} = \{x_j : j = 1, \ldots, m\}$. The data, $\mathbf{y}$, depend on $\mathbf{x}$ though a deterministic relationship, and noise. Often the relationship is linear and the noise is well modelled by a Gaussian distribution leading to the likelihood

$$f(\mathbf{y}|\mathbf{x}) = \frac{1}{(2\pi\sigma^2)^{n/2}} \exp\left\{-\frac{1}{2\sigma^2}||\mathbf{y} - G\,\mathbf{x}||^2\right\}, \qquad \sigma > 0.$$

In the geosounding application considered here, although the exact relationship is nonlinear, it will be assumed that a linear approximation is adequate – the calculation of the corresponding kernel matrix $G$ is described in Hidalgo-Silva and Gómez-Treviño (2013b) and references therein.

For estimation, evidence from the data and from prior beliefs are brought together by combining the likelihood and a prior distribution, denoted $p(\mathbf{x})$, using Bayes theorem, to form the posterior distribution, defined as

$$p(\mathbf{x}|\mathbf{y}) = f(\mathbf{y}|\mathbf{x})p(\mathbf{x})/f(\mathbf{y}).$$

The denominator can be dropped, as it contains no information about the unknown $\mathbf{x}$ and hence is not needed for estimation, leading to the key equation

$$p(\mathbf{x}|\mathbf{y}) \propto f(\mathbf{y}|\mathbf{x})p(\mathbf{x}).$$

This highlights the equal importance of the likelihood and prior distribution. In classical statistics the likelihood alone would be the basis for estimation and a point estimate found using maximum likelihood. In the Bayesian approach the equivalent is to calculate a point estimate using the value maximizing the posterior distribution, $\hat{\mathbf{x}}_{MAP} = \text{argmax}_{\mathbf{x}}\, p(\mathbf{x}|\mathbf{y})$, which is called the maximum a posteriori (MAP) estimate. An example of a Bayesian analysis of archaeological survey data can be found in Aykroyd et al. (2001).

### 2.2 Pixel-based prior models

The prior distribution describes detailed expert knowledge or general beliefs about the unknown function by quantifying the relative plausibility of different values of $\mathbf{x}$. Two common families of prior distribution are

$$p_1(\mathbf{x}) = \frac{\kappa(q)}{\lambda^m} \exp\left( -\sum_{j=1}^{m} \left| \frac{x_j}{\lambda} \right|^q \right), \qquad q \geq 0, \lambda > 0, \tag{1}$$

which gives higher probability to values close to zero, and

$$p_2(\mathbf{x}) = \frac{\kappa(q)}{\lambda^m} \exp\left( -\sum_{j=1}^{m} \left| \frac{x_j - \bar{x}_{N(j)}}{\lambda} \right|^q \right), \qquad q \geq 0, \lambda > 0, \tag{2}$$

which gives higher probability to smoother spatial patterns. In each the sum is over all pixels, the parameter $\lambda$ controls the variability in the pixel values, and $\bar{x}_{N(j)}$ is the mean of the neighbours of pixel $j$. It is important to note that Equation (2) is an improper density, in that it has an infinite integral. This can easily be seen by realising that any constant added to all the $x$ values will yield an identical density value. However, the posterior density will be proper as the data provides ample information about the mean value, hence posterior estimation is well defined.

When used as a prior distribution, Equation (1) will shrink values towards zero and Equation (2) will shrink *differences* towards zero. Although using $0 \leq q \leq 1$ will lead to small values being thresholded to zero, for $0 \leq q < 1$ the distribution is non-differentiable at zero which can cause problems for estimation algorithms. The $q = 1$ case gives the Laplace distribution whereas $q = 2$ gives the Gaussian distribution. It is interesting to note links with other approaches. The first prior distribution, with $q = 2$, has Tikhonov regularization as a special case and the second, with $q = 1$, has total variation as a special case.

### 2.3 Extensions to the standard prior models

Now suppose that the local variability is allowed to vary with an individual prior parameter, $\lambda_j$, for each pixel. This converts homogeneous models into inhomogeneous models. Rather than allowing these to change in an uncontrolled manner, knowledge of the spatial structure will be used. In particular, it will be assumed that the prior parameter changes with depth and the form

$$\lambda_j = \lambda \times e^{\kappa d_j}$$

will be considered where $d_j$ is the depth of pixel $j$ below the surface. The parameter $\kappa$ controls the direction and rate of change of variability as the depth changes. If $\kappa < 0$ then the variability decreases with depth, if $\kappa > 0$, (the case considered later) then it increases with depth, and when $\kappa = 0$ the variability is independent of depth (the standard homogeneous case). The inhomogeneous prior model corresponding to the homogeneous smoothing prior of Equation (2) can then be defined as

$$p_3(\mathbf{x}) = \frac{\kappa(q,\alpha)}{\lambda^m} \exp\left\{ -\sum_{j=1}^{m} e^{-\kappa d_j} \left| \frac{x_j - \bar{x}_{N(j)}}{\lambda} \right|^q \right\}, \qquad q \geq 0, \lambda > 0. \tag{3}$$

As before the parameter $\lambda$ controls the amount of local variation. This is another example of an improper prior.

Now consider another situation, this time where there is a dictionary of likely pixel values, $\boldsymbol{\mu} = (\mu_1, \ldots)$, then consider the prior

$$p_4(\mathbf{x}) = \frac{\kappa(q)}{\lambda^m} \exp\left\{ -\sum_{j=1}^{m} \min_k \left\{ \left| \frac{x_j - \mu_k}{\lambda} \right|^q \right\} \right\}, \qquad q \geq 0, \lambda > 0. \tag{4}$$

This prior gives higher probability to values close to any of the dictionary values, with $\lambda$ controlling the variation around these values. Note that if $\boldsymbol{\mu} \equiv (0)$, then this reduces to Equation (1).

### 2.4 Hybrid prior models

The prior distributions defined in Equations (1)-(3) lead to methods which are equivalent to approaches used in regression. A good review is given in Hastie et al. (2009), who also go on to discuss generalizations. Two such generalizations, which are interesting for use as prior distributions in image reconstruction, are the *elastic net* which corresponds to the distribution

$$p_5(\mathbf{x}) = \frac{\kappa(\alpha)}{\lambda^m} \exp\left\{ -\alpha \sum_{j=1}^{m} \left| \frac{x_j}{\lambda} \right| - (1-\alpha) \sum_{j=1}^{m} \left( \frac{x_j}{\lambda} \right)^2 \right\}, \qquad \begin{array}{l} \lambda > 0, \\ 0 \leq \alpha \leq 1, \end{array} \tag{5}$$

which shrinks values in a similar way to Equation (1) with $q \leq 1$, but it is differentiable at zero, and the *fused lasso* with corresponding distribution

$$p_6(\mathbf{x}) = \frac{\kappa(\alpha)}{\lambda^m} \exp\left\{ -\alpha \sum_{j=1}^{m} \left| \frac{x_j}{\lambda} \right| - (1-\alpha) \sum_{j=1}^{m} \left| \frac{x_j - \bar{x}_{N(j)}}{\lambda} \right| \right\}, \quad \begin{array}{l} \lambda > 0, \\ 0 \leq \alpha \leq 1, \end{array} \tag{6}$$

which is capable of both shrinkage towards zero and spatial smoothing. In particular, there is a tendency to shrink blocks of neighbouring values.

## 3 Estimation and the MCMC algorithm

The aim of the analysis is to estimate the value of the unknown parameters, $\mathbf{x}$, from the data using the posterior distribution. It is common in such reconstruction problems for the unknown parameter vector to be high dimensional and the posterior distribution to be complex making analytic solution impossible and even numerical algorithms require careful design and must be implemented efficiently. Here the Markov chain Monte Carlo (MCMC) method is used to produce a correlated sample from the target posterior distribution – for theoretical details see Gamerman and Lopes (2006) and Brooks et al. (2011), and for practical examples see Gilks et al. (1995).

Set an initial value for $\mathbf{x}$, call this $\mathbf{x}^0$
Repeat the following steps for $k = 1, \ldots, K$
  Repeat the following steps for $i = 1, \ldots, m$
    Generate $\epsilon$ from a Gaussian distribution $N(0, \tau^2)$
    Generate a proposed new value $x_i^* = x_i^k + \epsilon$
    Evaluate

$$\alpha = \min\left\{1, \frac{p(x_1^k, \ldots, x_{i-1}^k, x_i^*, \ x_{i+1}^{k-1}, \ldots, x_m^{k-1}|\mathbf{y})}{p(x_1^k, \ldots, x_{i-1}^k, x_i^{k-1} x_{i+1}^{k-1}, \ldots, x_m^{k-1}|\mathbf{y})}\right\}$$

    Generate $u$ from a uniform distribution, $U(0, 1)$
    If $\alpha > u$ then accept the proposal and set $x_i^k = x_i^*$, otherwise $x_i^k = x_i^{k-1}$
  End repeat
End repeat
Discard initial values and use remainder to make inference.

**Fig. 1.** A simple random walk Metropolis-Hastings algorithm.

One of the simplest schemes is the random walk Metropolis-Hastings algorithm – details of the algorithm are shown in Figure 1. From an arbitrary starting point, $\boldsymbol{x}^0$, the sample path of a discrete time Markov process is simulated to produce values $\boldsymbol{x}^1, \ldots, \boldsymbol{x}^K$. In particular, at each step only a single variable is proposed and further the proposal is a Gaussian perturbation of the previous value. To have the required posterior distribution as its equilibrium distribution then detailed balance must hold requiring each proposal to be accepted with a carefully specified probability. Initial values will depend on the starting point but the remaining sample will have the same statistical properties as a sample obtained directly from the posterior distribution and hence are used for estimation. Once the sample has been generated from the posterior distribution, a number of possible estimators are available, but the most usually calculated are the posterior mean and the posterior variance which are given by the mean and variance of the posterior sample.

Clearly, key issues are how many iterations to discard, how big a sample to collect and the value of the proposal variance, $\tau^2$. When choosing a value for the proposal variance, it is important to realise that both low and high values lead to long transient periods and highly correlated samples and hence unreliable estimation. A reasonable proposal variance can be chosen adaptively during the early burn-in period, and it has been proven theoretically that for a wide variety of high dimensional problems an acceptance rate of 23.4% (Roberts et al., 1997) is optimal. It is wise to also check Markov chain paths and to calculate sample autocorrelation functions. For good estimation the paths should look "random" and autocorrelation functions be close to zero for all except small lags. A variety of more formal convergence diagnostics are available, see for example Raftery and Banfield (1991) and Cowles and Carlin (1996).

This procedure can easily be converted into a simulated annealing algorithm (Geman and Geman, 1984), to allow the maximum a posteriori (MAP) estimate to be found, by changing the acceptance probability to $\alpha^{1/T_k}$ where

a temperature, $T_k$, is included which decreases as the iterations progress, with $T_k = 2\log(1+k)$ being one choice of annealing schedule. The MAP estimate is taken as the final iteration. This approach should not get caught in local optima and requires only function evaluations.

# 4 Results

## 4.1 General

In this section a range of posterior summaries are presented using a synthetic data example motivated by field data from Las Auras, a potential water reservoir site near the city of Tecate, México (Hidalgo-Silva and Gómez-Treviño, 2013b). Figure 2 shows the true conductivity distribution used to generate synthetic data where each pixel represents a 40m×40m area. The study region contains two high conducting regions within a low conducting background. In

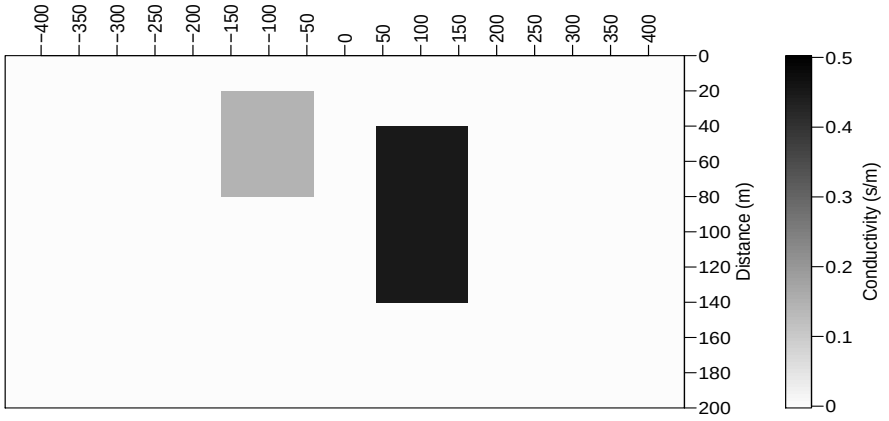


**Fig. 2.** Conductivity distribution used to generate synthetic data.

practice, to collect real measurements, an alternating current in a transmitter coil is generated, creating an alternating magnetic field in the surrounding area which, in turn, produces an electromotive force in receiver coils spread across the study site. Importantly, the measured voltages depend on the exact subsurface conductivity distribution. Although the relationship between the subsurface conductivity and the surface measurements is nonlinear, it can be well approximated by a linear model (Pérez-Flores et al., 2001) as mentioned in Section 2. Here 5 sets of measurements are used incorporating low-level Gaussian noise, based on different configurations, and for each 34 measurements are taken at equal intervals between -170m and 160m from a central reference point mid-way between the high conductivity regions.

## 4.2 Pixel-based prior models

Figure 3 shows the MAP estimate using a Laplace prior distribution with $\lambda = 0.5$, that is using Equation (1) with $q = 1$. As can be seen from the figure, both

high conductivity regions are clearly visible. In particular, the top edges and sides are well defined and correctly positioned. The bottom edges, however, are poorly resolved which means that the vertical extent would be judged to be too small. The expected shrinkage towards zero can be seen clearly in the background, but also it has occurred in the high conductivity regions where the estimated conductivity is lower than the true value. Although the contrast against the background is good, the piecewise constant conductivity is not evident.

This reconstruction highlights the non-uniform sensitivity which is typical of such limited access data collection problems. That is, the surface measurements contain little information about the deeper locations which leaves the prior model to have greater influence. In this case, without data information, the prior is more likely to shrink values at deeper locations to zero.

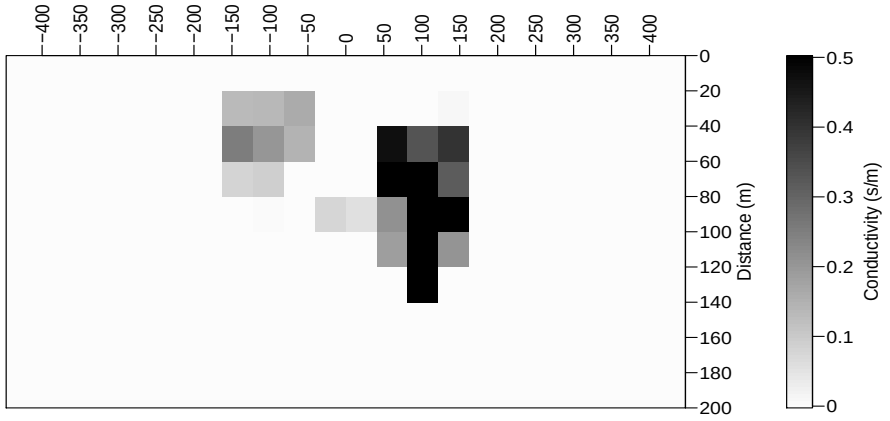


**Fig. 3.** Reconstruction using $L_1$ shrinkage prior where $\lambda = 0.5$.

The MAP estimate using a Gaussian smoothing prior with $\lambda = 0.2$, that is Equation (2) with $q = 2$, is shown in Figure 4. Again, the top edge and upper parts of the sides are well defined, there is improved uniformity within the regions and the estimated conductivity is closer to the true value. However, again the prior is allowed to dominate at greater depths due the lack of relevant information from the data. This prior distribution should have the effect of shrinking the differences towards zero, that is smoothing. This effect is clearly seen at the bottom edge of the regions where excessive smoothing has extended the estimated regions well below the true boundaries. This gives extremely biased estimates of vertical extent and hence is unacceptable.

### 4.3 Extensions to the standard prior models

To reduce the effect of the dominance of the prior at greater depth, the inhomogeneous prior, Equation (3), is proposed. The resulting reconstruction is shown in Figure 5 where $q = 2$, $\lambda = 0.2$ and $\kappa = 0.5$. Note that the values for $q$ and $\lambda$ have been fixed at the values corresponding to the Gaussian smoothing

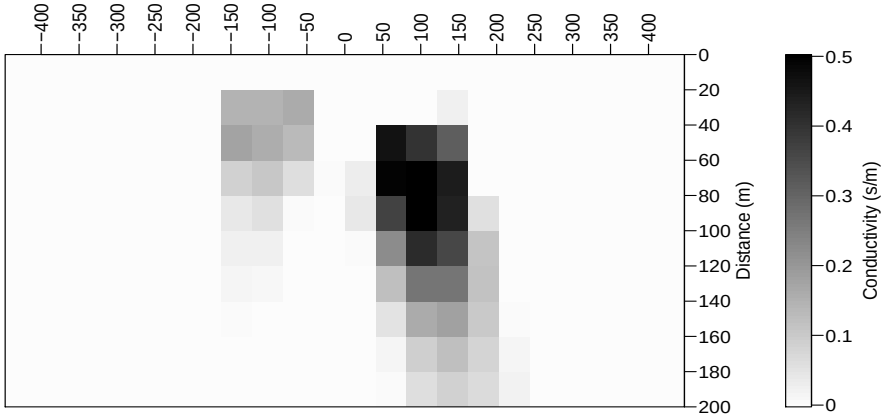


**Fig. 4.** Reconstruction using $L_2$ smoothing prior where $\lambda = 0.2$.

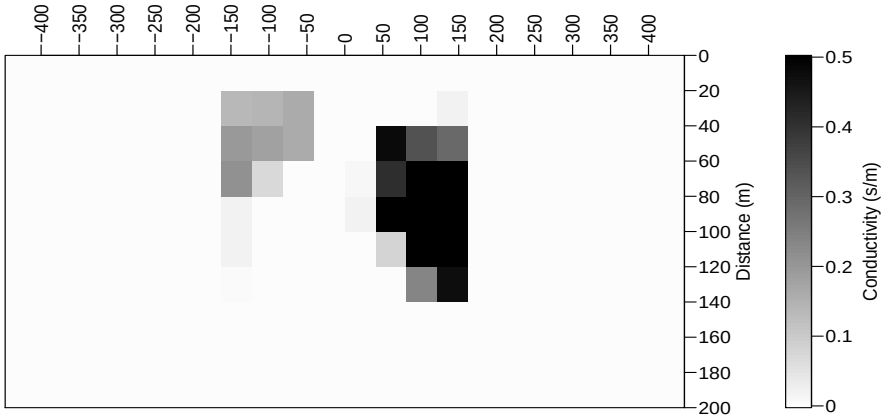


**Fig. 5.** Reconstruction using $L_2$ smoothing prior with depth-related adjustment where $\lambda = 0.2$ and $\kappa = 0.5$.

prior. Hence Figure 5 can be compared directly with Figure 4 — which can be considered as the case $\kappa = 0$. There is a clear improvement over the standard Gaussian smoothing prior. There are now reasonably well-defined lower edges allowing the extents to be well estimated. The resolution of the sides of the right-hand feature is also much improved. This reconstruction would be considered acceptable in contrast to the unacceptable appearance of the homogeneous Gaussian reconstruction in Figure 4.

Next consider the reconstruction in Figure 6. This uses dictionary values $\boldsymbol{\mu} = (0, 0.15, 0.45)$ and $\lambda = 0.05$. This prior distribution should have the effect of shrinking the estimates towards one of the dictionary values. Indeed the estimates are closer to the true values with well defined extents and reasonable piecewise constant value. Note that the prior parameter value has been chosen much smaller than used to produce Figure 3 where such a small value would have caused the estimates to be unacceptably shrunk towards zero. Clearly,

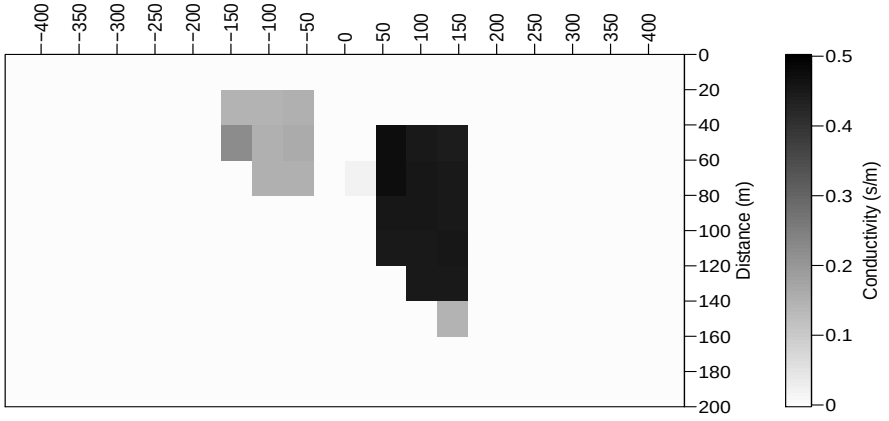


**Fig. 6.** Reconstruction using clustering prior with $\lambda = 0.05$ and $\boldsymbol{\mu} = (0, 0.15, 0.45)$.

accurately specified dictionary values are not always available and hence such accuracy may not be reproducible in practice. Instead some automatic procedure would be needed to estimate these values. It is worth noting, however, that in a reconstruction (not shown here) using a reduced dictionary without the center value, that is with $\boldsymbol{\mu} = (0, 0.45)$ and keeping $\lambda = 0.02$, the left-hand feature is still reasonably reconstructed. This means there is substantial robustness to miss-specification.

### 4.4 Hybrid prior models

Figure 7 shows the MAP estimate using a hybrid prior, Equation (5), with shrinking Laplace prior and smoothing Gaussian prior with $\lambda = 0.1$ and $\alpha = 0.48$. This choice of parameters has given the two types of shrinkage prior almost equal weight. For the Laplace shrinkage component the effective variability parameter $\lambda/\alpha \approx 0.2$ which is lower than when used on its own, and for the Gaussian shrinkage component, $\lambda/(1-\alpha) \approx 0.2$. From Figure 7 the constant regions are smoother than in Figure 3, and there is slightly better resolution of the bottom edges, hence in combination there is a useful improvement in accuracy. There has been no attempt to optimise the accuracy of estimation in the choice of these parameters, only to produce an illustrative example, and hence there is substantial scope for developing a procedure to automatically select suitable parameter values.

Figure 8 shows the MAP estimate (top) and the posterior standard deviation (bottom) for the hybrid prior, Equation (6), with parameters $\lambda = 0.1$ and $\alpha = 0.05$. This value of $\alpha$ means that almost all the contribution is from the Laplace smoothing component with effective variability parameter $\lambda/(1-\alpha) \approx 10$ and very little on the Laplace shrinkage with $\lambda/\alpha \approx 0.5$.

From Figure 8(a) there is good contrast between the high conductivity regions and the background and better uniform conductivity within the regions, but again in each the vertical extent is not reproduced well. Again, no attempt has been made to optimise the choice of parameters and hence it may well

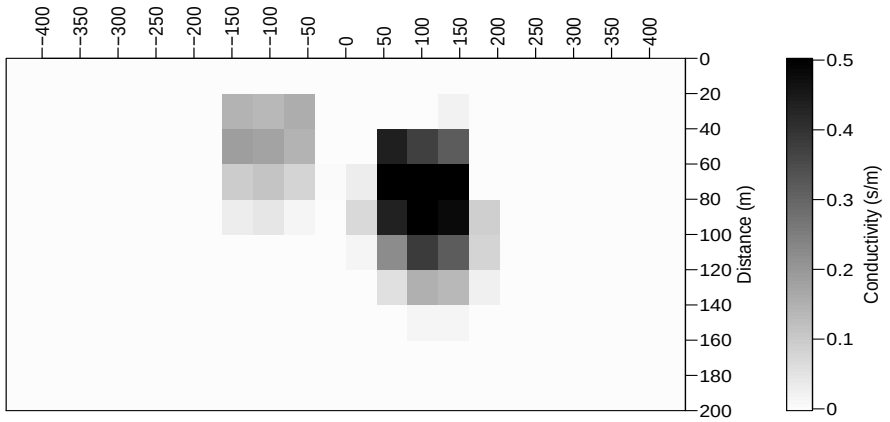


**Fig. 7.** Reconstruction using the elastic net prior distribution with hybrid $L_1$ shrinking and $L_2$ shrinkage using $\lambda = 0.1$ and $\alpha = 0.48$.

be possible to produce further improvement. The variability as measured by the posterior standard deviation, Figure 8(b), is lower near the surface and increases with depth. This reinforces the difficulty of estimation far from the surface — a characteristic of problems such as geosounding.

## 5 Discussion

This paper describes the Bayesian approach to image reconstruction and the MCMC estimation algorithm, and applies them to the problem of reconstructing the subsurface conductivity from surface data. This approach makes explicit use of statistical descriptions and probability models and encourages natural description and intuitive interpretation without any need to follow a mathematically or computationally convenient path.

The standard regularized least-squared approach has a straightforward interpretation within a probabilistic setting, and the widely used Tikhanov and total variation regularization are special cases of broad classes of prior distributions. This interpretation of regularization as a probability function immediately allows the option of using other probability functions. The examples considered here are only a start and there is a need to fully investigate the benefits of each type of model. A key part of such an investigation will be objective and automatic choice of the model parameters, $q$, $\lambda$ and $\alpha$.

There is also substantial scope to extend the modelling, for example by including data from multiple sources – Aykroyd and Al-Gezeri (2014) consider combining surface and borehole data. Also, other styles of modelling can be considered, for example Hidalgo et al. (1998) consider the use of piecewise constant functions. A great benefit of the statistical approach when linked with MCMC estimation is the great flexibility over the choice of prior distributions and output summaries. The resulting statistical analysis is based around a probability distribution and so a wide range of possible summaries are available which are far beyond a single point estimate.

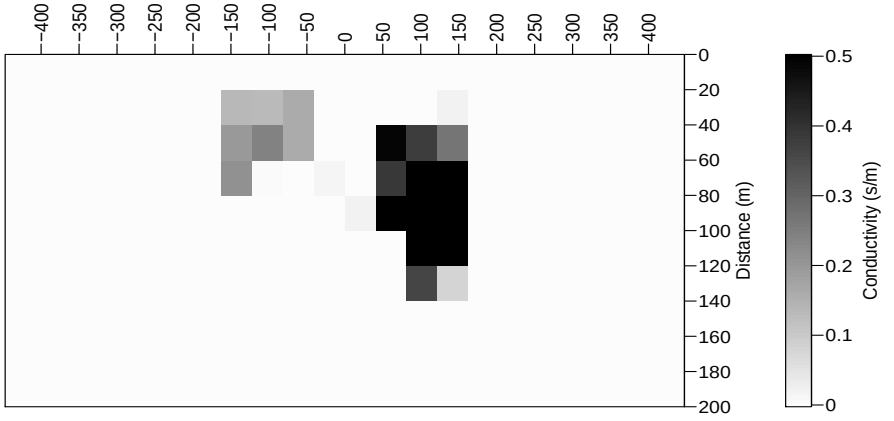


(a) MAP estimate.

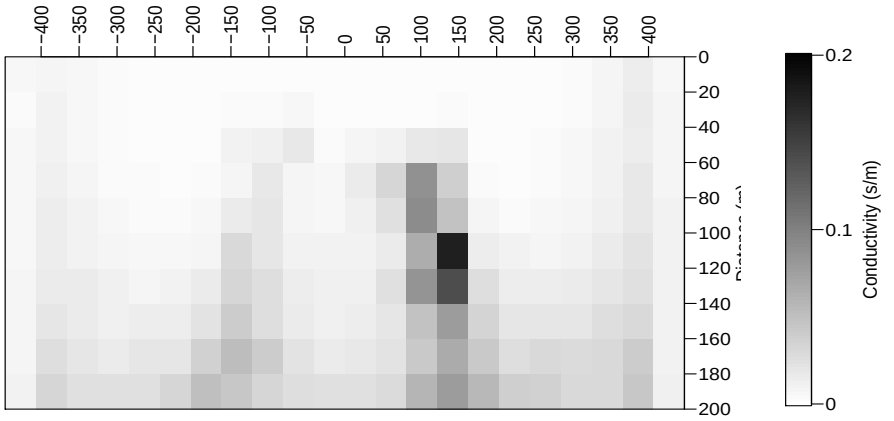


(b) Posterior standard deviation.

**Fig. 8.** Reconstruction using the fused lasso prior distribution with hybrid $L_1$ shrinkage and $L_1$ smoothing where $\lambda = 0.1$ and $\alpha = 0.05$.

# Bibliography


Aykroyd, R. G. and Al-Gezeri, S. M. (2014). 3D modelling and depth estimation in archaeological geophysics, *Chilean Journal of Statistics* **5**: 19–35.

Aykroyd, R. G., Haigh, J. G. B. and Allum, G. T. (2001). Bayesian methods applied to survey data from archaeological magnetometry, *Journal of the American Statistical Association* **96**: 64–76.

Besag, J., Green, P. J., Higdon, D. and Mengersen, K. (1995). Bayesian computation and stochastic systems, *Statistical Science* **10**: 1–41.

Brooks, S., Gelman, A., Jones, G. and Meng, X.-L. (2011). *Handbook of Markov Chain Monte Carlo*, Chapman & Hall/CRC.

Cowles, M. K. and Carlin, B. P. (1996). Markov chain Monte Carlo convergence diagnostics:A comparative review, *J. Am. Stat. Soc.* **91**: 883–904.

Gamerman, D. and Lopes, H. F. (2006). *Markov Chain Monte Carlo: Stochastic Simulation for Bayesian Inference*, 2nd edn, Chapman & Hall/CRC Texts in Statistical Science.

Geman, S. and Geman, D. (1984). Stochastic relaxation, Gibbs distributions and the Bayesian restoration of images, *IEEE Trans. PAMI.* **6**: 721–741.

Gilks, W., Richardson, S. and Spiegelhalter, D. (1995). *Markov Chain Monte Carlo in Practice*, Chapman & Hall/CRC.

Hastie, T., Tibshirani, R. and Friedman, J. (2009). *The Elements of Statistical Learning: Data Mining, Inference, and Prediction*, second edn, Springer Series in Statistics.

Hidalgo, H., Marroquín, J. L. and Gómez-Treviño, E. (1998). Piecewise smooth models for electromagnetic inverse problems, *IEEE Transactions on Geoscience and Remote Sensing,* **36**: 556–561.

Hidalgo-Silva, H. and Gómez-Treviño, E. (2013a). Inversion of electromagnetic geosoundings using coordinate descent optimization, *Inverse Problems in Science and Engineering* **21**: 1183–1198.

Hidalgo-Silva, H. and Gómez-Treviño, E. (2013b). Iterative algorithms for 2D geosounding inversion, *4th Inverse Problems, Design and Optimization Symposium, Albi, France, June 26-28, 2013.*

Pérez-Flores, M. A., Méndez-Delgado, S. and Gómez-Treviño, E. (2001). Imaging low-frequency and dc electromagnetic fields using a simple linear approximation, *Geophysics* **66**: 1067–1081.

Raftery, A. E. and Banfield, J. D. (1991). Stopping the Gibbs sampler, the use of morphology, and other issues in spatial statistics, *Ann. Inst. Statist. Math.* **43**: 32–43.

Roberts, G., Gelman, A. and Gilks, W. (1997). Weak convergence and optimal scaling of random walk Metropolis algorithms, *Ann. Appl. Prob.* **7**: 110–120.

# Monitoring the covariance matrix of a multivariate skew normal distribution

Adelaide M. Figueiredo[1] and Fernanda O. Figueiredo[2]

[1] Faculdade de Economia da Universidade do Porto and LIAAD-INESC Porto
(E-mail: adelaide@fep.up.pt)
[2] Faculdade de Economia da Universidade do Porto and Centro de Estatística e Aplicações, Universidade de Lisboa
(E-mail: otilia@fep.up.pt)

**Abstract.** The multivariate skew normal distribution is very useful for modeling asymmetric data in many practical applications, and in particular in Statistical Quality Control for monitoring several quality characteristics. In this study in order to monitor the covariance matrix of a multivariate skew normal process, we consider a control chart based on the Statis methodology. More precisely, the chart is based on a similarity measure between two data tables, the $RV$ coefficient. The performance of this chart is evaluated for several skew-normal processes.

**Keywords:** Control chart, Monte Carlo simulation, Multivariate skew normal distribution, Process monitoring, $RV$ coefficient, STATIS, Statistical Quality Control.

## 1 Introduction

In Statistical Quality Control it is crucial to monitor simultaneously several quality characteristics. Often these characteristics are correlated and thus, multivariate techniques of quality control are more appropriate than univariate methods for monitoring the individual characteristics. Many multivariate techniques of quality control have been proposed in the literature, in particular many control charts have appeared for monitoring processes.
Control charts are the tools most used for process monitoring in Statistical Quality Control (SQC) and were introduced by Shewhart at Bell Laboratories in 1924. Control charts help us to decide if the process that is being monitored is in-control or out-of-control. When a control chart triggers an out-of-control signal, which may be eventually a false alarm, it is important to investigate what are the causes responsible for the emission of such signal, so that appropriate actions may be taken.

Several multivariate schemes have been proposed for monitoring the mean vector or the covariance matrix of a multivariate process. In particular, control charts based on the Hotelling $T^2$ statistic, among others, have been implemented for monitoring the mean vector, and control charts based on the generalised variance (Alt, 1985) and based on the maximum of the sample variances

*Stochastic Modeling, Data Analysis and Statistical Applications* (*pp.* 87-94)
Lidia Filus - Teresa Oliveira - Christos H Skiadas (Eds)



or on the maximum of the ranges (Costa and Machado, 2008a, 2008b), among other charts have been proposed for monitoring the covariance matrix.
Additionally, several control schemes have appeared in the literature to monitor simultaneously the mean vector and the covariance matrix of a process (Chen et al., 2005, Zhang and Chang, 2008, etc).

Figueiredo and Figueiredo (2014) proposed a control scheme for controlling the variability of a multivariate process based on Statis methodology. More precisely, this scheme is based on a similarity measure between two positive semi-definite matrices, the $RV$ coefficient proposed by Escoufier (1973).
In this study we consider the previous control scheme for monitoring the covariance matrix of a multivariate skew normal process.

The STATIS (Structuration des Tableaux a Trois Indices de la Statistique) methodology was introduced by L′Hermier des Plantes (1976) and later developed by Lavit (1988) and Lavit et al. (1994). This methodology enables us to analyse simultaneously several data tables measured on the same individuals or variables for different circumstances or time instants.
We'll use this methodology for comparing several data tables. More precisely, we'll compare the relations between the variables along the data tables through the covariance matrices and we'll determine the compromise covariance matrix. Statis methodology has been applied in Statistical Quality Control to monitor batch processes (see for instance, Scepi, 2002, Gourvénec et al., 2005 and Niang et al., 2009).

The multivariate skew normal distribution was proposed by Azzalini and Dalla Valle (1996), and further discussed by Azzalini and Capitanio (1999) and others. This distribution is an extension of the univariate skew normal distribution, such that the marginal densities are scalar skew-normal. It also extends the multivariate normal distribution, by the addition of a shape parameter.

In Section 2 we briefly refer the multivariate skew normal distribution, in Section 3 we describe the control chart based on $RV$ coefficient between the compromise covariance matrix obtained from a set of reference samples and the covariance matrix of a new sample. In Section 4 we evaluate the performance of the chart for monitoring the covariance matrix of a multivariate skew normal process.

## 2 The multivariate skew normal distribution

A $k$-dimensional random variable $\mathbf{Z}$ is said to have a multivariate skew normal distribution if it has density function

$$f(\mathbf{z}) = 2\ \phi_k(\mathbf{z}\ ;\Omega_{\mathbf{z}})\ \Phi\left(\boldsymbol{\alpha}'\mathbf{z}\right), \quad \mathbf{z} \in \mathbb{R}^k, \tag{1}$$

where $\phi_k(\mathbf{z};\Omega_{\mathbf{z}})$ is $k$-dimensional normal density with zero mean and correlation matrix $\Omega_{\mathbf{z}}$, $\Phi\left(.\right)$ is the $N(0,1)$ distribution function and $\boldsymbol{\alpha}$ is a $k$-dimensional vector.

When $\boldsymbol{\alpha} = \mathbf{0}$, density (1) reduces to the multivariate normal distribution $N_k(\mathbf{0},\Omega_{\mathbf{z}})$ density. The parameter $\boldsymbol{\alpha}$ is then referred as a shape parameter.

Next, we introduce location and scale parameters, which are not allowed in density (1). Let

$$\mathbf{Y} = \boldsymbol{\xi} + \omega\ \mathbf{z},$$

where $\boldsymbol{\xi} = (\xi_1, ..., \xi_k)'$ and $\omega = diag\,(w_1, ..., w_k)$ are location and scale parameters respectively, being $w_i > 0, i = 1, ..., k$. The density function of $\mathbf{Y}$ is

$$g(\mathbf{y}) = 2\ \phi_k(\mathbf{y} - \boldsymbol{\xi};\ \Omega)\ \Phi\left(\boldsymbol{\alpha}'\omega^{-1}\,(\mathbf{y} - \boldsymbol{\xi})\right), \quad \mathbf{y} \in \mathbb{R}^k, \tag{2}$$

where $\Omega = \omega\ \Omega_{\mathbf{z}}\ \omega$ is a covariance matrix. We will use the notation $\mathbf{Y} \sim SN_k\,(\boldsymbol{\xi}, \Omega, \boldsymbol{\alpha})$ to indicate that $\mathbf{Y}$ has density function (2).
For more details about this distribution, see Azzalini and Dalla Valle (1996) and Azzalini and Capitanio (1999).

## 3 Control chart for monitoring the covariance matrix

We consider $K$ reference samples of size $n$ measured on $p$ variables taken in $K$ different time instants, when the process is in the in-control state, and we represent these matrices by their covariance matrices $V_k$ 's. See the following scheme.

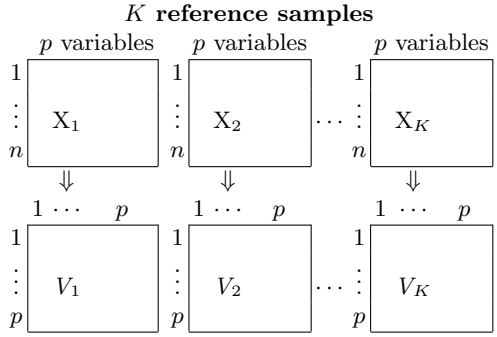


We determine the compromise covariance matrix, $V$, as defined in the Statis methodology, a weighted mean of the $K$ covariance matrices $V_k$ 's:

$$V = \sum_{k=1}^{K} \alpha_k V_k,$$

where the weights $\alpha_k$ represent the agreement between the $K$ tables and the compromise, and are obtained from the $RV$ coefficients.
The $RV$ coefficient (Escoufier, 1973) between $V_k$ and $V_{k'}$ is defined by

$$RV(V_k, V_{k'}) = \frac{Tr(V_k Q V_{k'} Q)}{\sqrt{Tr\,(V_k Q)^2\, Tr\,(V_{k'} Q)^2}},$$

where $Tr$ denotes the trace operator of a matrix and $Q$ is the metric in the individuals space, defined by the identity matrix or by a diagonal matrix whose main elements are equal to the reciprocal of the variances of the variables. The

$RV$ coefficient varies between 0 and 1. The closer the $RV$ coefficient is to 1, the more similar the two covariance matrices $V_k$ and $V_{k'}$ are.
More precisely, the weights $\alpha_k$ are the elements of the eigenvector associated with the largest eigenvalue of the following matrix $Z$ containing the $RV$ coefficients between the $V_k$ 's:

$$Z = \begin{pmatrix} 1 & RV(V_1, V_2) & \cdots & RV(V_1, V_K) \\ RV(V_2, V_1) & 1 & \cdots & RV(V_2, V_K) \\ \vdots & \vdots & \ddots & \vdots \\ RV(V_K, V_1) & RV(V_K, V_2) & \cdots & 1 \end{pmatrix}$$

The control chart, which we denote $RV$-chart, is implemented as follows. For a new time instant $k+1$, we compare its covariance matrix $V_{k+1}$ with the compromise covariance matrix $V$ through the $RV$ coefficient. Denoting CL the control limit of the chart, we consider the following decision criterion:

- If $RV(V, V_{k+1}) \geq$ CL we consider that the process is in-control.
- Otherwise, we decide that the process is out-of-control. In this case it is important to identify which variables are responsible for this situation.

The exact distribution of the $RV$ coefficient is unknown, and thus we fix CL at an empirical percentile of the sampling distribution of the $RV$ coefficient.

## 4 Performance of the control chart for a skew normal process

For evaluating the efficiency of the $RV$-chart, we computed by simulation the Average Run Length (ARL), the most commonly used measure of performance of control charts.
We generated multivariate skew normal processes $SN_p(\boldsymbol{\xi}, \Omega, \boldsymbol{\alpha})$, for $p$=2,3 assuming different structures for the covariance matrices when the process is in-control and out-of-control and different shape parameters. In each case, we obtained the compromise covariance matrix based on 4 reference samples generated when the process is in-control. For a false alarm rate $\alpha$=0.005, we determined the control limit of the chart, i.e., the percentile 0.5% of the distribution of the $RV$ coefficient, obtained through a Monte Carlo simulation experiment of size 100000 and we calculated the in-control and out-of-control ARL values through 10000 replicates for different shape parameters and structures of the covariance matrix.
More precisely, we generated samples from a bivariate skew normal distribution $SN_2(\boldsymbol{\xi}, \Omega, \boldsymbol{\alpha})$ with location vector $\boldsymbol{\xi} = (0,0)'$, covariance matrix $\Omega = \begin{pmatrix} 1 & \sigma_{12} \\ \sigma_{12} & 1 \end{pmatrix}$ and shape parameter $\boldsymbol{\alpha}$. Note that we could consider another location vector because we will work with centered data. The unit variances in $\Omega$ imply that the covariance is equal to the linear correlation coefficient. Some

obtained results are presented in Tables 1, 2 and 3. We also generated samples from a multivariate skew normal distribution $SN_3(\boldsymbol{\xi}, \Omega, \boldsymbol{\alpha})$ with location vector $\boldsymbol{\xi} = (0,0,0)'$, covariance matrix $\Omega = \begin{pmatrix} 1 & \sigma_{12} & \sigma_{13} \\ \sigma_{12} & 1 & \sigma_{23} \\ \sigma_{13} & \sigma_{23} & 1 \end{pmatrix}$ and shape parameter $\boldsymbol{\alpha}$. As previously we could use another location vector and the unit variances imply covariances equal to the correlation coefficients. Some obtained results are indicated in Tables 4 and 5.

| | | | | | | | | | | |
|---|---|---|---|---|---|---|---|---|---|---|
| | $\sigma_{12}$= 0 in-control | | | | | | | | | |
| $\boldsymbol{\alpha}'$ | (0,0) | (2,2) | (6,6) | (-2,-2) | (-6,-6) | (0,0) | (2,2) | (6,6) | (-2,-2) | (-6,-6) |
| n | | | 5 | | | | | 15 | | |
| CL | 0.359 | 0.331 | 0.324 | 0.333 | 0.323 | 0.696 | 0.704 | 0.707 | 0.698 | 0.708 |
| $\sigma_{12}$ | | | ARL | | | | | ARL | | |
| **0** | **198.1** | **206.2** | **201.8** | **193.4** | **203.3** | **196.3** | **186.2** | **204.1** | **209.3** | **197.4** |
| 0.4 | 89.0 | 60.4 | 54.1 | 58.3 | 54.5 | 39.5 | 12.3 | 11.3 | 13.0 | 10.9 |
| 0.75 | 69.8 | 15.2 | 12.9 | 15.0 | 13.0 | 6.2 | 1.7 | 1.6 | 1.8 | 1.6 |
| 0.95 | 32.1 | 4.3 | 3.5 | 4.3 | 3.5 | 2.5 | 1.0 | 1.0 | 1.0 | 1.0 |

**Table 1.** Control limit and ARL for several shape parameters $\boldsymbol{\alpha}$ and $n$=5,15, being $\sigma_{12}$= 0 when the process is in-control. The in-control ARL values are in bold.

| | | | | | | | | | | |
|---|---|---|---|---|---|---|---|---|---|---|
| | $\sigma_{12}$= 0 in-control | | | | | | | | | |
| $\boldsymbol{\alpha}'$ | (0,0) | (-2,6) | (2,-6) | (0,2) | (0,-2) | (0,0) | (-2,6) | (2,-6) | (0,2) | (0,-2) |
| n | | | 5 | | | | | 15 | | |
| CL | 0.359 | 0.325 | 0.323 | 0.337 | 0.340 | 0.696 | 0.705 | 0.705 | 0.698 | 0.696 |
| $\sigma_{12}$ | | | ARL | | | | | ARL | | |
| **0** | **198.1** | **198.4** | **205.6** | **205.2** | **196.3** | **196.3** | **201.9** | **204.1** | **193.1** | **201.5** |
| -0.4 | **143.7** | 84.7 | **88.8** | **181.1** | **170.7** | 40.2 | 22.7 | 23.1 | 7.9 | 82.0 |
| -0.75 | 69.1 | 29.7 | 29.6 | 114.9 | 109.4 | 6.1 | 2.7 | 2.7 | 11.2 | 11.5 |
| -0.95 | 32.3 | 9.3 | 9.5 | 57.2 | 53.7 | 2.5 | 1.1 | 1.1 | 2.3 | 2.3 |

**Table 2.** Control limit and ARL for several shape parameters $\boldsymbol{\alpha}$ and $n$=5,15, being $\sigma_{12}$= 0 when the process is in-control. The in-control ARL values are in bold.

The control limit and the ARL depend on the sample size (see Tables 1-3) and in general, depend on the shape parameter and on the structure of covariance of covariance matrix. See Tables 1-5.

From these tables, we observe that the in-control ARL is large and approximately equal to the expected value 200. When the process is out-of-control, the ARL quickly decreases as the sample size increases.

For a bivariate process with correlation matrix equal to the identity matrix, the chart detects easily a positive correlation when both components of the shape vector are null or have the same sign (positive or negative). Moreover, the detection is as fast as larger is the value of the correlation. See Table 1.

| $\sigma_{12}$= 0.9 in-control | | | | | | | | | | |
|---|---|---|---|---|---|---|---|---|---|---|
| $\boldsymbol{\alpha}'$ | (0,0) | (2,2) | (6,6) | (-2,-2) | (-6,-6) | (0,0) | (2,2) | (6,6) | (-2,-2) | (-6,-6) |
| n | | | 5 | | | | | 15 | | |
| CL | 0.596 | 0.357 | 0.328 | 0.368 | 0.336 | 0.949 | 0.855 | 0.836 | 0.855 | 0.835 |
| $\sigma_{12}$ | | | ARL | | | | | ARL | | |
| **0.9** | **191.6** | **202.6** | **208.5** | **184.1** | **189.2** | **204.2** | **201.9** | **190.6** | **201.0** | **197.9** |
| 0.75 | 32.0 | 36.3 | 37.9 | 32.7 | 35.2 | 9.6 | 7.6 | 7.3 | 7.4 | 7.5 |
| 0.5 | 8.5 | 10.2 | 10.8 | 8 | 10.5 | 1.9 | 1.7 | 1.7 | 1.7 | 1.7 |
| 0 | 2.4 | 3.1 | 3.3 | 2.9 | 3.1 | 1.0 | 1.0 | 1.0 | 1.0 | 1.0 |
| -0.9 | 1.0 | 1.1 | 1.1 | 1.1 | 1.1 | 1.0 | 1.0 | 1.0 | 1.0 | 1.0 |

**Table 3.** Control limit and ARL for several shape parameters $\boldsymbol{\alpha}$ and $n$=5,15, being $\sigma_{12}$= 0.9 when the process is in-control. The in-control ARL values are in bold.

| $\sigma_{ij}= 0, i \neq j$, in-control | | | | | |
|---|---|---|---|---|---|
| $\boldsymbol{\alpha}'$ | (0,0,0) | (2,2,2) | (6,6,6) | (-2,-2,-2) | (-6,-6,-6) |
| CL | 0.671 | 0.676 | 0.678 | 0.676 | 0.678 |
| $\sigma_{12}, \sigma_{13}, \sigma_{23}$ | | | ARL | | |
| **0,0,0** | **201.4** | **201.2** | **195.8** | **195.8** | **194.1** |
| 0.4,0.4,0.4 | 13.9 | 10.4 | 10.1 | 10.6 | 9.8 |
| 0.75,0.75,0.75 | 1.9 | 1.3 | 1.3 | 1.3 | 1.3 |
| 0.95,0.95,0.95 | 1.2 | 1.0 | 1.0 | 1.0 | 1.0 |
| 0.5,0.2,0.9 | 3.5 | 1.8 | 1.7 | 1.8 | 1.7 |
| 0.9,0.75,0.9 | 1.4 | 1.0 | 1.0 | 1.0 | 1.0 |

**Table 4.** Control limit and ARL for several shape parameters $\boldsymbol{\alpha}$ and $n$=15, being $\sigma_{ij}= 0, i \neq j$ when the process is in-control. The in-control ARL values are in bold.

| $\sigma_{ij}= 0.9, i \neq j$, in-control | | | | | |
|---|---|---|---|---|---|
| $\boldsymbol{\alpha}'$ | (0,0,0) | (2,2,2) | (6,6,6) | (-2,-2,-2) | (-6,-6,-6) |
| CL | 0.951 | 0.845 | 0.833 | 0.844 | 0.834 |
| $\sigma_{12}, \sigma_{13}, \sigma_{23}$ | | | ARL | | |
| **0.9,0.9,0.9** | **200.0** | **201.1** | **202.4** | **202.7** | **196.6** |
| 0.75,0.75,0.75 | 6.7 | 5.8 | 5.9 | 6.0 | 5.9 |
| 0.5,0.5,0.5 | 1.4 | 1.3 | 1.3 | 1.3 | 1.3 |
| 0,0,0 | 1.0 | 1.0 | 1.0 | 1.0 | 1.0 |
| 0.9,0.5,0.1 | 1.2 | 1.2 | 1.2 | 1.2 | 1.2 |
| 0.1,0.5,0.3 | 1.0 | 1.0 | 1.0 | 1.0 | 1.0 |

**Table 5.** Control limit and ARL for several shape parameters $\boldsymbol{\alpha}$ and $n$=15, being $\sigma_{ij}= 0.9, i \neq j$ when the process is in-control. The in-control ARL values are in bold.

If the process is normal ($\boldsymbol{\alpha} = \mathbf{0}$) or when one component of the shape vector is positive and the other is negative, the chart easily detects a negative correlation, being more sensitive to large negative correlations. See Table 2.
In a 3-dimensional framework with data from a normal or a skew normal process with a shape parameter, having all components positive or negative and when the correlation matrix is equal to the identity matrix or has all off-diagonal elements equal to 0.9, the chart detects changes in the correlations as fast as we move away from the in-control correlation structure. See Tables 4 and 5.

To conclude, the analysed cases suggest that the $RV$-control chart enables us to detect easily changes in the correlations between variables when the process has a normal or a skew normal multivariate distribution, being therefore a very useful monitoring tool in a large variety of industrial applications.

## Acknowledgement

This work is financed by the ERDF – European Regional Development Fund through the COMPETE Programme (Operational Programme for Competitiveness) and by National Funds through the FCT – Fundação para a Ciência e Tecnologia (Portuguese Foundation for Science and Technology) within the project FCOMP-01-0124-FEDER-037281 and the project PEst-OE/MAT/UI0 006/2014 (CEA/UL).

## References

1. F. B. Alt. Multivariate quality control. In *Encyclopedia of Statistical Sciences, S. Kotz and N. L. Johnson (eds)*, Wiley, New York, 1985.
2. A. Azzalini and A. Capitanio. Statistical applications of the multivariate skew normal distribution. *J. R. Statist. Soc. B*, 61, part 3, pp. 579-602, 1999.
3. A. Azzalini and A. Dalla Valle. The multivariate skew-normal distribution. *Biometrica*, 83, no.4, pp. 715-726, 1996.
4. G. Chen, S. W. Cheng and H. Xie. A new multivariate control chart for monitoring both location and dispersion. *Communications in Statistics: Simulation and Computation*, 34, 203–217, 2005.
5. A. F. B. Costa and M. A. G. Machado. A new chart based on sample variances for monitoring the covariance matrix of multivariate processes. *The International Journal of Advanced Manufacturing Technology*, 41, 770–779, 2008a.
6. A. F. B. Costa and M. A. G. Machado. A new multivariate control chart for monitoring the covariance matrix of bivariate processes. *Communications in Statistics: Simulation and Computation*, 37, 1453–1465, 2008b.
7. Y. Escoufier. Le traitement des variables vectorielles.*Biometrics*, 29, 751–760, 1973.
8. A. Figueiredo and F. Figueiredo. Monitoring the variability of a multivariate normal process using STATIS. In *Proceedings of COMPSTAT 2014*, 2014.
9. S. Gourvénec, I. Stanimirova and O.A. Saby. Monitoring batch process with the STATIS approach. *Journal of Chemometrics*, 19, 288–300, 2005.
10. D. M. Hawkins and E. M. Maboudou-Tchao. Multivariate exponentially weighted moving covariance matrix. *Technometrics*, 50, 155–166, 2008.
11. H. Hotelling. Multivariate quality control, illustrated by the air testing of sample bombsights. *Techniques of Statistical Analysis, McGraw Hill*, New York, pp. 111-184, 1947.
12. C. Lavit. *Analyse Conjointe de Tableaux Quantitatives.* Collection Méthodes+Programmes, Masson, 1988.
13. C. Lavit, Y. Escoufier, R. Sabatier and P. Traissac. The ACT (Statis method). *Computational Statistics and Data Analysis*, 18, 97–119, 1994.
14. H. L′Hermier Des Plantes. *Structuration des Tableaux a Trois Indices de la Statistique.* Thèse de 3 ème cycle. Université de Montpellier II, 1976.

15. N. Niang, F.S. Fogliatto and G. Saporta. *Batch Process Monitoring by three-way data analysis approach.* The XIII International Conference Applied Stochastic Models and Data Analysis (ASMDA 2009), June 30-July 3, Vilnius, Lithuania, 2009.
16. G. Scepi. *Parametric and non parametric multivariate quality control charts.* IN Lauro, C. et al. (Eds) Multivariate Total Quality Control, 163–189. Heidelberg: Physica-Verlag, 2002.
17. G. Zhang and S. I. Chang. Multivariate EWMA control charts using individual observations for process mean and variance monitoring and diagnosis. *International Journal of Production Research*, 46, pp. 6855-6881, 2008.

# An approach to estimate the exact distribution of the Local Whittle estimator

Josu Arteche[1] and Jesus Orbe[1]

[1] Dept. of Econometrics and Statistics, University of the Basque Country UPV/EHU, Bilbao, Spain
(E-mail: josu.arteche@ehu.es)
[2] Dept. of Econometrics and Statistics, University of the Basque Country UPV/EHU, Bilbao, Spain
(E-mail: jesus.orbe@ehu.es)

**Abstract.** The asymptotic distribution of the LW estimator may be a poor approximation of the exact one in small sample sizes or even with larger samples when the memory parameter is larger than 0.75. In other situations the asymptotic distribution is unknown, as for example in a noninvertible context or in some nonlinear transformations of long memory processes, where only consistency has been obtained. For all these cases a bootstrap strategy based on resampling the standardized periodogram is proposed.

**Keywords:** Bootstrap, Long memory, Local Whittle.

## 1 Introduction

Long memory is a common feature of many time series. It means that observations which are far apart maintain a significant relationship such that the autocorrelations are not summable. This implies that the spectral density function $f(\lambda)$ diverges at the origin. In fact, the most common definition of long memory is established by the behaviour of the spectral density function around the origin such that it satisfies

$$f(\lambda) \sim C\lambda^{-2d} \quad \text{as } \lambda \to 0 \tag{1}$$

for a finite positive constant $C$, where $a \sim b$ means that $a/b \to 1$. The memory parameter $d$ governs the persistence of the series. If $d = 0$ the series has short memory, whereas a value of $d > 0$ implies long memory or strong dependence such that $f(\lambda)$ diverges at $\lambda = 0$. Finally the antipersistent case $d < 0$ entails a zero in the spectral density function at the origin, usually caused by overdifferencing.

Parametric estimation methods such as (quasi) maximum likelihood or the Whittle approximation entail a risk of inconsistency if the model is misspecified. In order to avoid that risk, semiparametric or local techniques have been

*Stochastic Modeling, Data Analysis and Statistical Applications* (*pp.* 95-107)
Lidia Filus - Teresa Oliveira - Christos H Skiadas (Eds)



proposed to estimate $d$, which only restrict the behaviour of the spectral density around the pole as in (1). One of the most popular is the Local Whittle estimation (LW), which is the estimator with which we are concerned in this paper. It was first proposed by Künsch[16] but it was not until Robinson[21] that its nice asymptotic properties were proved in the stationary and invertible case $-1/2 < d < 1/2$. In particular Robinson showed consistency, pivotal asymptotic normal distribution and higher efficiency than other rival techniques (such as the log periodogram regression) under very mild conditions, allowing for non Gaussian series. Velasco[26], Phillips and Shimotsu[19] and Shao and Wu[22] extended the asymptotic properties of the LW estimator to the nonstationary case, obtaining consistency for $d \leq 1$ and asymptotic normality for $d < 3/4$. For larger values of $d$ the asymptotic distribution is non normal and the estimator is inconsistent for $d > 1$.

The standard asymptotic distribution of the LW estimator and its pivotal characteristic (at least for $d < 3/4$) makes it very simple to implement asymptotic inference. However the asymptotic approximation may not be satisfactory in moderate samples or even in large samples if $d \in (0.75, 1]$(see Phillips and Shimotsu[19]). In other situations the LW is known to be consistent but the asymptotic distribution is not known, as for example in noninvertible fractionally integrated processes where the LW estimator may even be inconsistent if the bandwidth is too large (Shimotsu and Phillips[24]), and in some nonlinear transformations of long memory series (Dalla et al.[5]). In all these cases the bootstrap can be useful to get reliable approximations of the exact distribution of the LW estimator.

The bootstrap was originally designed for samples of independent observations, but some refinements have been proposed to deal with dependent data. In this context there are basically two approaches. One is based on describing the dependence through a parametric model with independent disturbances. The sieve bootstrap follows this spirit but instead of identifying the correct model, an AR model of sufficiently high order is estimated to capture the relevant dependence of the series such that the residuals are close to being independent. The second approach does not rely on any model but attempts to retain the structure of dependence by resampling overlapping or nonoverlapping blocks of observations. This is the block bootstrap designed to maintain the dependence inside the block while assuming independence between blocks.

The applicability of these methods to long memory series is influenced by the strong persistence of the series. However, in order to get bootstrap approximations to the distribution of the Local Whittle estimator there is no need to obtain bootstrap samples of the original series: only resampling of the periodogram is necessary. This means that the problems originated by the strong dependence of the data are partially avoided, since the transformation that leads to the periodogram implies a significant modification in the structure of dependence. For example, the periodogram ordinates of weak dependent series are asymptotically independent. But periodogram ordinates of long memory series are not asymptotically independent around the spectral pole and they show a marked structure that should be replicated by the bootstrap samples.

Paparoditis and Politis[18] adapt a local bootstrap suggestion introduced by Shi[23] and set out to resample near periodogram ordinates locally, thus retaining the global structure of the periodogram. Thus, a local strategy seems to be more adequate under long memory where the periodogram shows a marked structure. But this structure compels the use of a very narrow interval around the frequency of interest, which affects the performance of the bootstrap. In fact, Silva et al.[25] propose resampling within a neighbourhood of only one or two frequencies. Franke and Härdle[8] and Dahlhaus and Janas[6], dealing with weak dependent series, propose instead resampling Studentized periodogram ordinates obtained by dividing the periodogram by an estimate of the spectral density function. In this context, the main challenge with long memory series is to obtain an estimator of the spectral density that is consistent over the whole band of frequencies used in the resampling scheme. Traditional estimators (based on kernels) have been shown to be inconsistent at frequencies close to the spectral pole (Velasco[27]) and some other option seems necessary to Studentize the periodogram. Taking into account these considerations we propose two different bootstrap strategies:

- Use the spectral density estimator proposed by Hidalgo and Yajima[9] to standardize the periodogram. Then apply a global Efron's bootstrap to the Studentized periodogram.
- Estimating the spectral density can be avoided by resampling a locally standardized periodogram where the pole is damped by scaling with a function that is proportional to the spectral density around the origin, namely $\lambda_j^{-2\hat{d}}$ for $\hat{d}$ a consistent estimator of $d$ (e.g. the local Whittle estimator). Global resampling does not succeed to retain the remaining structure of the periodogram , so the local bootstrap is used instead to obtain bootstrap samples of the locally standardized periodogram.

## 2 Estimation method

In what follows we consider long memory series $x_t$ with a spectral density function satisfying

$$f(\lambda) = |\lambda|^{-2d} g(\lambda) \quad \lambda \in [-\pi, \pi] \tag{2}$$

where $d$ is the memory parameter and $g(\lambda)$ controls the weak dependence of the series and is assumed to be positive and bounded over all the frequencies $\lambda \in [-\pi, \pi]$.

The LW estimator is obtained by minimizing a local version of the Whittle function around the origin, which is the region where the specification of the spectral density function in (2) plays its part. For a series of $n$ observations $x_t$, $t = 1, 2, ..., n$, with spectral density satisfying (2), the LW estimate $\hat{d}$ is obtained by minimizing

$$R(d) = \log\left(\frac{1}{m}\sum_{j=1}^{m} \lambda_j^{2d} I_j\right) - \frac{2d}{m}\sum_{j=1}^{m} \log \lambda_j \tag{3}$$

where $I_j$ is the periodogram of $x_t$, $t = 1, 2, ..., n$, at Fourier frequency $\lambda_j = 2\pi j/n$ defined as

$$I_j = I(\lambda_j) = \frac{1}{2\pi n}\left|\sum_{t=1}^{n} x_t \exp(-i\lambda_j t)\right|^2$$

and $m$ is the bandwidth that represents the number of frequencies used in the estimation. Robinson[21] analyzes the LW estimator in a stationary and invertible context implying $|d| < 1/2$ and shows its consistency and asymptotic distribution

$$\sqrt{m}(\hat{d} - d) \xrightarrow{d} N\left(0, \frac{1}{4}\right). \tag{4}$$

However the distribution in (4) can be a bad approximation of the exact one in finite samples. One source of inaccuracy lies in the fact that the finite sample variance tends to exceed the asymptotic variance in (4). To palliate this problem Hurvich and Chen[10] and Arteche[2] proposed that instead of the asymptotic variance $1/4m$ a Hessian based approximation should be used, defined as

$$\widehat{var}(\hat{d}) = \left(4\sum_{j=1}^{m}\left(\log\lambda_j - \frac{1}{m}\sum_{k=1}^{m}\log\lambda_k\right)^2\right)^{-1}, \tag{5}$$

which gives much better results in terms of coverage of confidence intervals.

Velasco[26] and Phillips and Shimotsu[19] extended the asymptotic properties of the LW estimator to the nonstationary case, allowing for $d \geq 1/2$. Switching from a stationary to a nonstationary context brings about the problem of initial values. Both papers use alternative definitions of nonstationary long memory, which differ in the assumptions imposed in the initialization of the process. Phillips and Shimotsu[19] consider the so called type II long memory process. In this context Phillips and Shimotsu[19] proved that $\hat{d} \xrightarrow{p} d$ as $n \to \infty$ for $d \in (1/2, 1]$ but $\hat{d} \xrightarrow{p} 1$ for $d > 1$. With respect to the asymptotic distribution, (4) remains valid for $d \in (1/2, 3/4)$. However the asymptotic distribution changes for larger values of $d$ as follows:

$$\begin{aligned}
\sqrt{m}(\hat{d} - d) &\xrightarrow{d} \frac{1}{2}U_1 + J(d)U_2^2 \quad \text{if } d = \frac{3}{4}, \\
m^{2-2d}(\hat{d} - d) &\xrightarrow{d} J(d)U_2^2 \quad \text{if } d \in (3/4, 1), \\
\sqrt{m}(\hat{d} - d) &\xrightarrow{d} \frac{-U_1 + \sqrt{2}U_2U_3}{2(1 + U_3^2)}, \quad \text{if } d = 1
\end{aligned} \tag{6}$$

where $U_i$, $i = 1, 2, 3$ are mutually independent standard normal random variables and $J(d) = (2\pi)^{2d-2}\Gamma(d)^{-2}(2d-1)^{-3}(1-d)$.

Velasco[26] proposes instead what is known as a type I long memory process. In this context Velasco[26] shows the consistency of the LW estimator for values of $d < 1$ and the asymptotic normality in (4) for $d < 3/4$. Shao and Wu[22] extend the analysis for larger values of $d$ obtaining the same asymptotic results as in Phillips and Shimotsu[19] for type II long memory with the only change

of a different function $J(d)$ in (6). Special mention must be made of the case $d \in (3/4, 1)$. The asymptotic distribution of the LW estimator implies a positive bias and skewness, which are not evident in finite samples as noted in the simulations by Phillips and Shimotsu[19] for sample sizes as large as 500. As a consequence, inference based on the asymptotic distribution might lead to unreliable conclusions and some refinement seems necessary.

In other situations the LW estimator is known to be consistent but the asymptotic distribution is unknown. This is the case in a noninvertible antipersistent situation with $d < -1/2$. A similar situation arises for nonlinear transformations of long memory processes. One common transformation is taking squares, which are often used as approximations to the volatility of the series. Consistency of the LW estimator in nonlinear time series has been shown by Dalla et al.[5] but the asymptotic distribution remains unknown and the central limit theorem leading to (4) might no longer hold.

## 3 Bootstrap proposals

The bootstrap was originally proposed for i.i.d. series, but its applicability has been extended to time series where the data obey a dependence structure. Generating bootstrap samples that replicate the strong persistence of the series is not a simple task, and a blind use of traditional bootstrap techniques may lead to distorting results. In general, model based bootstraps have been proposed for that purpose such that finally resampling is executed among residuals that are close to being independent (see Poskitt[20], Kapetanios and Papailias[12], Kreiss et al.[15]). These procedures depend heavily on a prior estimation of the model that must be correctly specified. Model free bootstrap strategies, such as the block bootstrap, avoid this problem but their application to get bootstrap samples replicating the structure of dependence of the original long memory series is not trouble free (see Lahiri[17], or Kim and Nordman[13]).

However, in order to approximate the distribution of the LW estimator there is no need to obtain bootstrap replications of the original data: only the behaviour of the periodogram needs to be mimicked. For that purpose, frequency domain bootstrap strategies are valuable tools because they are designed to resample the periodogram and, although they may not have the ability to produce bootstrap replicates of the time series, they have the additional advantage of not requiring parametric assumptions. Among the initial proposals, Franke and Härdle[8] and Dahlhaus and Janas[6] apply Efron's bootstrap method to the periodogram Studentized by an estimate of the spectral density function, showing its validity for kernel spectral density estimates and ratio statistics. Its applicability has been proven valid for weakly dependent series but no results are available for long memory series where the asymptotic independence of periodogram ordinates does not hold at frequencies close to the spectral pole. Moreover, Studentizing the periodogram requires an estimator of the spectral density function that has to be uniformly consistent over the frequency band $(0, \pi]$ and the kernel estimator proposed by the authors has been shown to be consistent only at frequencies far from the spectral pole (Velasco[27]), which

limits its applicability in long memory series characterized by a concentration of spectral power around the origin.

A different alternative for mimicking the structure of the periodogram, the local bootstrap, was proposed by Paparoditis and Politis[18] and applied in long memory series by Silva et al.[25] and Arteche and Orbe[4]. However, the marked structure of the periodogram around the origin forces the use of a very narrow neighbourhood around the frequency of interest, which affects the performance of the bootstrap. This limitation can be avoided by adapting the idea of Franke and Härdle[8] and Dahlhaus and Janas[6] of resampling standardized periodograms with a less marked structure than the original one.

With all these considerations we propose two different bootstrap approaches based on different strategies to standardize the periodogram:

- Use a consistent estimator of the spectral density function to Studentize the periodogram. This is a natural extension of the proposal by Franke and Härdle[8] and Dahlhaus and Janas[6], but, as pointed out by Kim and Nordman[14], the problem of obtaining a nonparametric estimator of the spectral density uniformly consistent over the whole band of Fourier frequencies arises in long memory series. It is only very recently that Arteche[3] has proved the consistency of the proposal by Hidalgo and Yajima[9], improving on other more traditional techniques that lack consistency at frequencies close to the spectral pole. This estimator is defined as

$$\hat{f}_j = \hat{f}(\lambda_j) = \frac{|\lambda_j|^{-2\hat{d}}}{2m^* + \mathbf{1}_{j>m^*}} \sum_{k=-m^*,\neq -j}^{m^*} |\lambda_j + \lambda_k|^{2\hat{d}} I(\lambda_j + \lambda_k) \qquad (7)$$

  for $j = 1, ..., [n/2]$ where $\hat{d}$ is the LW estimator and $m^*$ is a bandwidth number. The *Studentized periodogram*, defined as $\hat{v}_j^{(0)} = I_j/\hat{f}_j$, is then resampled over the whole band of Fourier frequencies in a global bootstrap strategy.
- Use a local standardization of the periodogram by dividing the periodogram ordinates by an expression that is proportional to the spectral density function around the origin as defined in (1). This avoids estimating the spectral density and gets the *locally standardized periodogram* defined as $\hat{v}_j^{(1)} = I_j \lambda_j^{2\hat{d}}$ for $j = 1, ..., [n/2]$. To replicate the remaining structure in the locally standardized periodogram, a global resampling such as that proposed for $\hat{v}_j^{(0)}$ is not adequate. We therefore propose instead to apply a local bootstrap to $\hat{v}_j^{(1)}$.

Thus, the bootstrap strategies that we propose for the LW estimator consist of the following steps:

**1.** Obtain $\hat{v}_j^{(i)}$, $i = 0, 1$, for $j = 1, ..., [n/2]$ with a bandwidth $m$ for the LW estimate $\hat{d}$, and $m^*$ for $\hat{f}_j$ (only needed for $\hat{v}_j^{(0)}$).

**2.** Let $k_n = [n/2]$ for $\hat{v}_j^{(0)}$ and select a resampling width $k_n \in \mathcal{N}$, $k_n \leq [n/2]$ if $\hat{v}_j^{(1)}$ is used.

**3.** Define i.i.d. discrete random variables $S_1, ..., S_m$ taking values in the set $\{0, \pm 1, , ..., \pm k_n\}$ with equal probability $1/(2k_n + 1)$.
**4.** Generate $B$ bootstrap series $\hat{v}_{bj}^{*(i)} = \hat{v}_{|j+S_j|}^{(i)}$ if $|j + S_j| > 0$, $\hat{v}_{bj}^{*(i)} = \hat{v}_1^{(i)}$ if $j + S_j = 0$ for $b = 1, 2, ..., B$ and $j = 1, ..., m$.
**5.** Generate $B$ bootstrap samples for the periodogram $I_{bj}^{*(1)} = \lambda_j^{-2\hat{d}} \hat{v}_{bj}^{*(1)}$, $I_{bj}^{*(0)} = \hat{f}_j \hat{v}_{bj}^{*(0)}$ for $b = 1, 2, ..., B$ and $j = 1, ..., m$.
**6.** Obtain the $B$ bootstrap LW estimates $\hat{d}_b^{*(i)}$, $b = 1, ..., B$ by minimizing $R(d)$ in (3) with the periodogram $I_j$ replaced by $I_{bj}^{*(i)}$.

*Remark 1:* The bandwidth for Local Whittle estimation $m$ remains fixed during the entire procedure.

*Remark 2:* Even though $m$ is kept fixed, the procedure is not fully automatic because it requires the intervention of the user in the selection of $k_n$ for the local bootstrap or $m^*$ for the estimation of the spectral density function in the global bootstrap strategy. But both quantities can be chosen on a data driven basis. The resampling width $k_n$ can be selected based on the form of $\hat{v}_j^{(1)}$, the higher the structure the lower $k_n$ should be chosen to keep the global structure of $\hat{v}_j^{(1)}$ in the bootstrap samples $\hat{v}_{bj}^{*(1)}$. The bandwidth $m^*$ can be chosen similarly because $\hat{f}_j$ is based on a moving average of neighbour $\hat{v}_k^{(1)}$s and thus it can be selected using the same criteria.

## 4 Simulation study

In this section the performance of our proposals is compared with the asymptotic distribution (when an analytical expression exists).

### 4.1 Stationary and invertible case $-1/2 < d < 1/2$

The asymptotic distribution of the LW estimator in (4) is very convenient for asymptotic inference thanks to its standard distribution with fully specified asymptotic variance. However, the asymptotic distribution may not be a good approximation of the exact one. For example, the variance in the asymptotic distribution in (4) has been shown to be a poor approximation of the true variance in finite samples. Hurvich and Chen[10] and Arteche[2] propose instead the Hessian based approximation of the variance described in (5) and find that it leads to much better results than the asymptotic variance in terms of coverage frequencies of confidence intervals. We compare all these proposals with the bootstrap strategies defined in the previous section. The comparison is based first on confidence intervals, analysing the coverage of the intervals obtained with the following strategies:

**Option 1.** The asymptotic distribution in (4), that is

$$CI_{1-\alpha}^1 = \left( \hat{d} - 0.5m^{-1/2} z_{1-\frac{\alpha}{2}}; \quad \hat{d} - 0.5m^{-1/2} z_{\frac{\alpha}{2}} \right)$$

where $z_\alpha$ indicates the $100 \cdot \alpha$th percentile of the asymptotic distribution ($N(0, 1)$ in the stationary and invertible case).

**Option 2.** As in Option 1 but using the Hessian based approximation of the variance in (5)

$$CI^2_{1-\alpha} = \left( \hat{d} - \sqrt{\hat{var}(\hat{d})} z_{1-\frac{\alpha}{2}}; \quad \hat{d} - \sqrt{\hat{var}(\hat{d})} z_{\frac{\alpha}{2}} \right).$$

**Option 3($m^*$).** Using the global bootstrap strategy based on the Studentized periodogram $\hat{v}_j^{(0)}$ for different bandwidths $m^*$. In this case the confidence intervals are as follows:

$$CI^3_{1-\alpha}(m^*) = \left( \hat{d}^{*(0)}_{\left((B+1)(\frac{\alpha}{2})\right)} \quad ; \quad \hat{d}^{*(0)}_{\left((B+1)(1-\frac{\alpha}{2})\right)} \right),$$

where the $\hat{d}^{*(0)}_{(j)}$ denotes the $j$th ordered value of the bootstrap estimates of $d$. The $\alpha/2$ percentile is thus estimated by the $(B+1)(\frac{\alpha}{2})$ ordered value of $\hat{d}^{*(0)}$. We choose a B value such that $(B+1)(\frac{\alpha}{2})$ is an integer.

**Option 4($k_n$).** $CI^4_{1-\alpha}(k_n)$ is calculated similarly but using the local bootstrap strategy based on the locally standardized periodogram $\hat{v}_j^{(1)}$ for different resampling widths $k_n$. The confidence intervals are obtained as in Option 4 but with $\hat{d}^{*(1)}_{(j)}$.

The performance of all these options is analysed in ARFIMA models defined as

$$(1-\phi L)(1-L)^d X_t = \epsilon_t, \quad t = 1, 2, ..., n,$$

for $n = 128$ and $\epsilon_t \sim NID(0,1)$. Two values of $d$ are considered, $d = 0$ and 0.4, corresponding to short memory and stationary long memory. Two values of $\phi$ are also examined, $\phi = 0.3$ and 0.8, the latter inducing a significant bias in the estimation of $d$ if a large $m$ is used. In this Monte Carlo analysis the values $m = 5, 10, 20$ are used. 1000 replications of these models are generated to compare the performance of the previous strategies for constructing confidence intervals. For options 3 and 4 the number of bootstrap samples is $B = 999$. Instead of choosing a single $m^*$ ($k_n$) the sensitivity of the bootstrap proposals is assessed by considering different values $m^* = 3, 5, 7$ and $k_n = 2, 5, 10, 20$. The set of values considered for $m^*$ are chosen in a sensible region taking into account the form of the spectral density of the $AR(1)$ weak dependent component. Larger values would lead to an estimate of $f(\lambda)$ that is too smooth around frequency zero. The values of $k_n$ are selected similarly based on the form of the locally standardized periodogram $\hat{v}_j^{(1)}$, where larger values of $k_n$ lead to worse results.

Tables 1 and 2 show the coverage frequencies in percentages (top number in each cell) and the average length (bottom number) of confidence intervals for a 95% nominal confidence level over 1000 Monte Carlo replications. The following conclusions can be drawn:

- The variance correction in $CI^2_{1-\alpha}$ results in a significant improvement in coverage frequencies, with an unavoidable enlargement of the length of the intervals, though they still tend to undercover.

- Both bootstrap strategies in options 3 and 4 tend to lead to coverage closer to nominal, even with narrower intervals in some cases.
- The global bootstrap based on the Studentized periodogram is less sensitive to changes in $m^*$ than the local bootstrap based on the local standardized periodogram is to the choice of $k_n$. Large values of $k_n$ tend to lead to overcoverage with too wide intervals. Large values of $m^*$ also tend to lead to an increase in coverage but overcoverage is less evident.
- The choice of $m$ has a significant impact on the performance of all the techniques, especially when $\phi = 0.8$. In that case a large $m$ induces a high bias in the estimation of $d$ that significantly affects the coverage of all the CIs, but in every case the bootstrap strategies proposed here outperform the other techniques.

**Table 1.** Coverage for $ARFIMA(1, d, 0)$ with $\phi = 0.3$ ($n = 128$)

| | d=0 | | | d=0.4 | | |
|---|---|---|---|---|---|---|
| | m=5 | m=10 | m=20 | m=5 | m=10 | m=20 |
| $CI^1_{0.95}$ | 0.662 | 0.811 | 0.823 | 0.678 | 0.795 | 0.815 |
| | 0.877 | 0.620 | 0.438 | 0.877 | 0.620 | 0.438 |
| $CI^2_{0.95}$ | 0.894 | 0.925 | 0.912 | 0.887 | 0.917 | 0.905 |
| | 1.542 | 0.891 | 0.553 | 1.542 | 0.891 | 0.553 |
| $CI^3_{0.95}(m^* = 3)$ | 0.940 | 0.936 | 0.932 | 0.942 | 0.917 | 0.926 |
| | 1.713 | 0.935 | 0.549 | 1.750 | 0.929 | 0.546 |
| $CI^3_{0.95}(m^* = 5)$ | 0.967 | 0.950 | 0.937 | 0.960 | 0.948 | 0.943 |
| | 1.771 | 0.963 | 0.564 | 1.800 | 0.958 | 0.561 |
| $CI^3_{0.95}(m^* = 7)$ | 0.962 | 0.969 | 0.953 | 0.957 | 0.965 | 0.948 |
| | 1.787 | 0.977 | 0.574 | 1.817 | 0.970 | 0.570 |
| $CI^4_{0.95}(k_n = 2)$ | 0.847 | 0.873 | 0.852 | 0.846 | 0.841 | 0.836 |
| | 1.316 | 0.804 | 0.501 | 1.327 | 0.802 | 0.501 |
| $CI^4_{0.95}(k_n = 5)$ | 0.946 | 0.924 | 0.904 | 0.947 | 0.929 | 0.899 |
| | 1.543 | 0.891 | 0.546 | 1.564 | 0.894 | 0.546 |
| $CI^4_{0.95}(k_n = 10)$ | 0.982 | 0.964 | 0.941 | 0.977 | 0.956 | 0.934 |
| | 1.775 | 0.929 | 0.562 | 1.807 | 0.934 | 0.562 |
| $CI^4_{0.95}(k_n = 20)$ | 1.000 | 0.975 | 0.957 | 1.000 | 0.966 | 0.958 |
| | 1.958 | 1.013 | 0.573 | 2.001 | 1.013 | 0.575 |

The top number in each cell is the coverage frequency. The bottom number is the length of the CI.

In practice, $m^*$ ($k_n$) needs to be selected prior to the application of the bootstrap. This choice can be based on the smoothness of $\hat{v}_j^{(1)}$ as explained in Remark 2 above. The lack of significant structure in $\hat{v}_j^{(1)}$ indicates that a large $m^*$ and $k_n$ should be used.

### 4.2 Nonstationary case $1/2 \leq d \leq 1$

In a nonstationary context the situation varies with the value of $d$ according to the intervals where the asymptotic distribution in (6) is defined. When $d < 3/4$

**Table 2.** Coverage for $ARFIMA(1,d,0)$ with $\phi = 0.8$ ($n = 128$)

| | d=0 | | | d=0.4 | | |
|---|---|---|---|---|---|---|
| | m=5 | m=10 | m=20 | m=5 | m=10 | m=20 |
| $CI^1_{0.95}$ | 0.627 | 0.402 | 0.022 | 0.606 | 0.419 | 0.021 |
| | 0.877 | 0.620 | 0.438 | 0.876 | 0.620 | 0.438 |
| $CI^2_{0.95}$ | 0.900 | 0.623 | 0.043 | 0.873 | 0.641 | 0.057 |
| | 1.542 | 0.891 | 0.553 | 1.542 | 0.891 | 0.553 |
| $CI^3_{0.95}(m^*=3)$ | 0.977 | 0.764 | 0.068 | 0.965 | 0.775 | 0.076 |
| | 1.751 | 0.935 | 0.557 | 1.722 | 0.912 | 0.543 |
| $CI^3_{0.95}(m^*=5)$ | 0.981 | 0.772 | 0.058 | 0.979 | 0.775 | 0.072 |
| | 1.809 | 0.965 | 0.572 | 1.766 | 0.940 | 0.556 |
| $CI^3_{0.95}(m^*=7)$ | 0.975 | 0.762 | 0.051 | 0.968 | 0.757 | 0.065 |
| | 1.828 | 0.978 | 0.580 | 1.785 | 0.953 | 0.564 |
| $CI^4_{0.95}(k_n=2)$ | 0.788 | 0.557 | 0.067 | 0.797 | 0.550 | 0.091 |
| | 1.323 | 0.835 | 0.545 | 1.321 | 0.827 | 0.536 |
| $CI^4_{0.95}(k_n=5)$ | 0.906 | 0.646 | 0.081 | 0.903 | 0.628 | 0.100 |
| | 1.581 | 0.927 | 0.591 | 1.574 | 0.915 | 0.580 |
| $CI^4_{0.95}(k_n=10)$ | 0.951 | 0.666 | 0.053 | 0.953 | 0.671 | 0.069 |
| | 1.876 | 0.972 | 0.592 | 1.863 | 0.957 | 0.581 |
| $CI^4_{0.95}(k_n=20)$ | 0.977 | 0.749 | 0.046 | 0.981 | 0.746 | 0.056 |
| | 2.193 | 1.088 | 0.602 | 2.163 | 1.063 | 0.590 |

The top number in each cell is the coverage frequency. The bottom number is the length of the CI.

all the results are similar to those discussed in the stationary case. For other values of $d$ the asymptotic distribution changes, which affects the way in which it approximates the exact distribution.

We focus here on the interval $3/4 < d < 1$, where, as noted by Phillips and Shimotsu[19] the discrepancies between the asymptotic distribution and the finite sample distribution are most apparent. In this case no refinements to improve the approximation of the distribution have been proposed. As a result, we compare the asymptotic expression in Option 1 (with the corresponding asymptotic distribution) with the bootstrap strategies in Options 3($m^*$) and 4($k_n$).

1000 replications of a type II long memory process as defined in Philips and Shimotsu[19] are generated with $x_0 = 0$, $d = 0.8$ and $u_t$ standard normal for $n = 512$. A larger sample size is chosen here to show that even in that case the asymptotic distribution is a poor approximation of the real one, whereas the bootstrap approximation gives much more reliable results. The values of $m$, $m^*$ and $k_n$ analysed here are $m = 20, 40, 70$, $m^* = 5, 10, 20$ and $k_n = 5, 20, 40, 70$. Table 3 shows coverage frequencies and the lengths of the confidence intervals for a 95% nominal confidence. $CI^1_{0.95}$ clearly undercovers evidencing that the asymptotic distribution is far from the exact one. All the intervals based on the bootstrap strategies proposed in this paper offer much better coverage even with shorter intervals.

**Table 3.** CI coverage in $ARFIMA(0, 0.8, 0)$

| | m=20 | m=40 | m=70 |
|---|---|---|---|
| $CI^1_{0.95}$ | 0.549 | 0.577 | 0.557 |
| | 0.496 | 0.376 | 0.300 |
| $CI^3_{0.95}(m^* = 5)$ | 0.929 | 0.907 | 0.907 |
| | 0.560 | 0.353 | 0.251 |
| $CI^3_{0.95}(m^* = 10)$ | 0.954 | 0.921 | 0.921 |
| | 0.575 | 0.361 | 0.257 |
| $CI^3_{0.95}(m^* = 20)$ | 0.974 | 0.952 | 0.924 |
| | 0.584 | 0.367 | 0.261 |
| $CI^4_{0.95}(k_n = 5)$ | 0.902 | 0.892 | 0.888 |
| | 0.523 | 0.335 | 0.240 |
| $CI^4_{0.95}(k_n = 20)$ | 0.962 | 0.931 | 0.916 |
| | 0.558 | 0.356 | 0.254 |
| $CI^4_{0.95}(k_n = 40)$ | 0.958 | 0.960 | 0.942 |
| | 0.589 | 0.361 | 0.259 |
| $CI^4_{0.95}(k_n = 70)$ | 0.968 | 0.951 | 0.954 |
| | 0.604 | 0.370 | 0.260 |

The top number in each cell is the coverage frequency. The bottom number is the length of the CI.

### 4.3 Unknown asymptotic distribution

In this subsection we analyse the performance of the techniques proposed in two situations where the LW estimator is consistent but its asymptotic distribution is unknown: noninvertible ARFIMA and nonlinear transformations of long memory series. In particular we generate 1000 replications of series generated as:

- $ARFIMA(0, -0.7, 0)$, $(1 - L)^{-0.7} X_t = \epsilon_t$ for $\epsilon_t$ standard normal.
- $X_t = Y_t^2$ for $(1 - 0.3L)(1 - L)^{0.4} X_t = \epsilon_t$ and $\epsilon_t$ standard normal.

The sample size and bandwidth parameters are those considered in Section 4.1. Note that the second model is just the squares of one the stationary $ARFIMA$ models analysed previously.

Table 4 shows the coverage frequencies for both cases. The noninvertible case shows no significant differences with respect to the invertible case, with good coverage close to the exact ones. The results for the squared transformation are also satisfactory, but a comparison with the results obtained for the untransformed $ARFIMA$ shows that a lower bandwidth $m$ seems to be necessary here to get better results.

## 5 Conclusion

We propose two bootstrap strategies for estimating the exact distribution of the LW estimator that significantly outperform the approximation offered by the asymptotic distribution in a wide range of situations. The proposals are

**Table 4.** Coverage for $ARFIMA(0,-0.7,0)$ and squared $ARFIMA(1,0.4,0)$ ($n = 128$)

| | $ARFIMA\ (0,-0.7,0)$ | | | squared $ARFIMA\ (1,0.4,0)$ | | |
|---|---|---|---|---|---|---|
| | m=5 | m=10 | m=20 | m=5 | m=10 | m=20 |
| $CI^3_{0.95}(m^*=3)$ | 0.972 | 0.947 | 0.916 | 0.925 | 0.844 | 0.789 |
| | 1.409 | 0.883 | 0.538 | 1.697 | 0.892 | 0.525 |
| $CI^3_{0.95}(m^*=5)$ | 0.995 | 0.959 | 0.929 | 0.952 | 0.892 | 0.812 |
| | 1.487 | 0.917 | 0.555 | 1.751 | 0.923 | 0.542 |
| $CI^3_{0.95}(m^*=7)$ | 0.992 | 0.964 | 0.937 | 0.954 | 0.918 | 0.838 |
| | 1.514 | 0.934 | 0.564 | 1.775 | 0.939 | 0.551 |
| $CI^4_{0.95}(k_n=2)$ | 0.806 | 0.820 | 0.782 | 0.845 | 0.770 | 0.716 |
| | 1.163 | 0.748 | 0.476 | 1.221 | 0.739 | 0.462 |
| $CI^4_{0.95}(k_n=5)$ | 0.948 | 0.909 | 0.853 | 0.932 | 0.853 | 0.773 |
| | 1.341 | 0.841 | 0.524 | 1.455 | 0.833 | 0.511 |
| $CI^4_{0.95}(k_n=10)$ | 0.988 | 0.955 | 0.901 | 0.972 | 0.910 | 0.823 |
| | 1.535 | 0.886 | 0.548 | 1.722 | 0.877 | 0.532 |
| $CI^4_{0.95}(k_n=20)$ | 1.000 | 0.970 | 0.936 | 0.998 | 0.930 | 0.870 |
| | 1.685 | 0.959 | 0.563 | 1.931 | 0.975 | 0.548 |

The top number in each cell is the coverage frequency. The bottom number is the length of the CI.

based on resampling two different standardized periodograms in order to obtain bootstrap replicates of the original periodogram. As a result the potential applications of these techniques are far more general than shown here: they can be used to obtain bootstrap replicates of the periodogram in similar estimation strategies based on a Whittle criterion, as for example the modified LW estimator of Hurvich et al.[11] and the local polynomial Whittle estimators of Andrews and Sun[1] and Frederiksen et al.[7].

## References

1. Andrews, D.W.K., Sun, Y., 2004. Adaptive Local Polynomial Whittle Estimation of Long-Range Dependence. Econom. 72, 569-614.
2. Arteche, J., 2006. Semiparametric estimation in perturbed long memory series. Comput. Statist. Data Anal. 51, 2118-2141.
3. Arteche, J., 2014. Signal extraction in Long Memory Stochastic Volatility. Preprint.
4. Arteche, J., Orbe, J., 2009. Using the bootstrap for finite sample confidence intervals of the log periodogram regression. Comput. Statist. Data Anal. 53, 1940-1953.
5. Dalla, V., Giraitis, L., Hidalgo, J., 2005. Consistent estimation of the memory parameter for nonlinear time series. J. Time Ser. Anal. 27, 211-251.
6. Dahlhaus, R., Janas, D., 1996. A frequency domain bootstrap for ratio statistics in time series analysis. Ann. Statist. 24, 1934-1963.
7. Frederiksen, P., Nielsen, F.S., Nielsen, M.O., 2012. Local polynomial Whittle estimation of perturbed fractional processes. J. Econom. 167, 42617447.
8. Franke, J., Härdle, W., 1992. On bootstrapping kernel spectral estimates. Ann. Statist. 20, 121-145.

9. Hidalgo, J., Yajima, Y., 2002. Prediction and signal extraction of strongly dependent processes in the frequency domain. Econom. Theor. 18, 584-624.
10. Hurvich, C.M., Chen, W.W., 2000. An efficient taper for potentially overdifferenced long-memory time series. J. Time Ser. Anal. 21, 155-180.
11. Hurvich, C.M., Moulines, E., Soulier, P., 2005. Estimating long memory in volatility. Econom. 73, 1283-1328.
12. Kapetanios, G., Papailias, F. 2011. Block bootstrap and long memory. Working paper 679, School of Economics and Finance, Queen Mary, University of London.
13. Kim, Y.M., Nordman, D.J., 2011. Properties of a block bootstrap under long-range dependence. Sankhya Ser A 73, 7917109.
14. Kim, Y.M., Nordman, D.J., 2013. A frequency domain bootstrap for Whittle estimation under long-range dependence. J. Multivariate Anal. 115, 405-420.
15. Kreiss, J.P., Paparoditis, E., Politis, D.N., 2011. On the range of validity of the autoregressive sieve bootstrap. Ann. Statist. 39, 2103-2130.
16. Kunsch, H., 1987. Statistical aspects of self-similar processes. In Yu.A. Prohorov & V.V. Sazonov (eds), Proceedings of the 1st World Congress of the Bernoulli Society, vol. 1, 671774. Science Press.
17. Lahiri, S.N., 1993. On the moving block bootstrap under long range dependence. Stat. Probabil. Lett. 18, 405-413.
18. Paparoditis, E., Politis, D., 1999. The local bootstrap for periodogram statistics. J. Time Ser. Anal. 20, 193-222.
19. Phillips, P.C.B., Shimotsu, K., 2004. Local Whittle estimation in nonstationary and unit root cases. Ann. Statist. 32, 656-692.
20. Poskitt, D.S., 2007. Properties of the sieve bootstrap for fractionally integrated and non-invertible processes. J. Time Ser. Anal. 29, 224-250.
21. Robinson, P.M., 1995. Gaussian semiparametric estimation of long-range dependence. Ann. Statist. 23, 1630-1661.
22. Shao, X., Wu, W.B., 2007. Local Whittle estimation of fractional integration for nonlinear processes. Econom. Theor. 23, 899-929.
23. Shi, S. G., 1991. Local bootstrap. Ann. Inst. Stat. Math. 43, 667-676.
24. Shimotsu, K., Phillips. P.C.B., 2006. Local Whittle estimation of fractional integration and some of its variants. J. Econom. 130, 209-233.
25. Silva, E.M., Franco, G.C., Reisen, V.A., Cruz, F.R.B., 2006. Local bootstrap approaches for fractional differential parameter estimation in ARFIMA models. Comput. Statist. Data Anal. 51, 1002-1011.
26. Velasco, C., 1999. Gaussian semiparametric estimation of non-stationary time series, Journal Time Ser. Anal. 20, 87-127.
27. Velasco, C., 2003. Nonparametric frequency domain analysis of nonstationary multivariate time series. J. Stat. Plan. Infer. 116, 209-247.

# Modeling of multivariate skewness measure distribution

Margus Pihlak

Tallinn University of Technology (e-mail: margus.pihlak@ttu.ee)

**Abstract.** In this paper the distribution of random variables skewness measure is modeled. Firstly we present some results of matrix algebra useful in multivariate statistical analyses. Then we apply the central limit theorem on modeling of multivariate skewness measure distribution. That skewness measure is introduced in [6].
**Keywords:** Central limit theorem, Multivariate skewness measure, Skewness measure distribution.

## 1 Introduction and basic notations

In the firs section we introduce some notations used in the paper. The $k$-dimensional zero vector is denoted as $\mathbf{0}_k$. The transposed matrix $\mathbf{A}$ is denoted as $\mathbf{A}'$.

Let us have random vectors $\mathbf{X}_i = (\mathbf{X}_{i1}, \mathbf{X}_{i2}, \ldots, \mathbf{X}_{ik})'$ where index $i = 1, 2, ..., n$ is for observations and $k$ denotes number of variables. These random vectors are independent and identically distributed copies (each copy for one observations) of a random $k$-vector $\mathbf{X}$. Let

$$\overline{\mathbf{x}} = \frac{1}{n}\sum_{i=1}^{n}\mathbf{X}_i$$

and

$$\mathbf{S} = \frac{1}{n-1}\sum_{i=1}^{n}(\mathbf{X}_i - \overline{\mathbf{x}})(\mathbf{X}_i - \overline{\mathbf{x}})'$$

be the estimators of the sample mean $E(\mathbf{X}) = \mu$ and the covariance matrix $D(\mathbf{X}) = \mathbf{\Sigma}$ respectively.

Now we present matrix operations used in this paper. One of the widely used matrix operation in multivariate statistics is Kronecker product (or tensor product) $\mathbf{A} \otimes \mathbf{B}$ of matrices $\mathbf{A} : m \times n$ and $\mathbf{B} : p \times q$ which is defined as a partitioned matrix

$$\mathbf{A} \otimes \mathbf{B} = [a_{ij}\mathbf{B}], i = 1, 2, \ldots, m; j = 1, 2, \ldots, n.$$

*Stochastic Modeling, Data Analysis and Statistical Applications* (*pp.* 109-113)
Lidia Filus - Teresa Oliveira - Christos H Skiadas (Eds)



By means of Kronecker product we can present the third and the fourth order moments of vector $\mathbf{X}$ :

$$m_3(\mathbf{X}) = E(\mathbf{X} \otimes \mathbf{X}' \otimes \mathbf{X})$$

and

$$m_4(\mathbf{X}) = E(\mathbf{X} \otimes \mathbf{X}' \otimes \mathbf{X} \otimes \mathbf{X}').$$

The corresponding central moments

$$\overline{m_3}(\mathbf{X}) = E\{(\mathbf{X} - \mu) \otimes (\mathbf{X} - \mu)' \otimes (\mathbf{X} - \mu)\}$$

and

$$\overline{m_4}(\mathbf{X}) = E\{(\mathbf{X} - \mu) \otimes (\mathbf{X} - \mu)' \otimes (\mathbf{X} - \mu) \otimes (\mathbf{X} - \mu)'\}.$$

The third order moment of random vector $\mathbf{X}$ is $k^2 \times k$-matrix and its fourth order moment is $k^2 \times k^2$-matrix.

The operation vec($\mathbf{X}$) denotes a $mn$-vector obtained from $m \times n$-matrix by stacking its columns one under another in natural order. For the properties of Kronecker product and vec-operator the interested reader is referred to [2] or [4]. In the next section skewness measure will be defined be means of the star-product of the matrices. The star-product was introduced in [7] where some basic properties of the operation were presented and proved.

**Definition 1.** *Let us have matrix* $\mathbf{A} : m \times n$ *and a partitioned matrix* $\mathbf{B} : \times ns$ *consisting of* $r \times s$*-blocks* $\mathbf{B}_{ij}, i = 1, 2, \dots m; j = 1, 2, \dots n$. *Then the star-product* $\mathbf{A} * \mathbf{B}$ *is a* $r \times s$*-matrix*

$$\mathbf{A} * \mathbf{B} = \sum_{i=1}^{n} \sum_{j=1}^{m} a_{ij} \mathbf{B}_{ij}.$$

The star product is inverse operation of Kronecker product in sense of increasing and decreasing of matrix dimensions. One of the star-product applications is presented in the paper [12]. Let us give an example how the star product works.

**Example.** Let us have matrices $A : 2 \times 2$ and partitioned matrix $B : 4 \times 4$ with $2 \times 2$-blocks $B_{11}, ..., B_{22}$. Then

$$A * B = \begin{pmatrix} a_{11} & a_{12} \\ a_{21} & a_{22} \end{pmatrix} * \begin{pmatrix} B_{11} & B_{12} \\ B_{21} & B_{22} \end{pmatrix} =$$

$$= a_{11}B_{11} + ... + a_{22}B_{22}.$$

We also use the matrix derivative defined following H. Neudecker in [10].

**Definition 2.** *Let the elements of the matrix* $\mathbf{Y} : r \times s$ *be functions of matrix* $\mathbf{X} : p \times q$. *Assume that for all* $i = 1, 2, \dots p$; $j = 1, 2, \dots q$; $k = 1, 2, \dots r$ *and* $l = 1, 2, \dots s$ *partial derivatives* $\dfrac{\partial y_{kl}}{\partial x_{ij}}$ *exist and are continuous in an open set A. Then the matrix* $\dfrac{d\mathbf{Y}}{d\mathbf{X}}$ *is called matrix derivative of matrix* $\mathbf{Y} : r \times r$ *by matrix* $\mathbf{X} : p \times q$ *in a set A, if*

$$\frac{d\mathbf{Y}}{d\mathbf{X}} = \frac{d}{dvec'(\mathbf{X})} \otimes vec(\mathbf{Y})$$

*where*

$$\frac{d}{d\mathrm{vec}'(\mathbf{X})} = \left( \frac{\partial}{\partial x_{11}} \quad \cdots \quad \frac{\partial}{\partial x_{p1}} \quad \cdots \quad \frac{\partial}{\partial x_{1q}} \quad \cdots \quad \frac{\partial}{\partial x_{pq}} \right).$$

Matrix derivative defined by Definition 2 is called *Neudecker* matrix derivative. This matrix derivative has been in last 40 years a useful tool in multivariate statistics.

## 2 Multivariate measures of skewness

In this section we present multivariate skewness measure by means of matrix operation described above. A skewness measure in multivariate case was introduced in Mardia [8]. Mori et al [9] have introduced a skewness measure as a vector. B. Klar in [3] has given thorough overview of the skewness problem. In this paper is also examined asymptotic distribution of different skewness characteristics. In Kollo [6] a skewness measure vector is introduced and applied in Independent Component Analyses (ICA).

The skewness measure in multivariate case is presented through the the third order moments as

$$\mathbf{s}(\mathbf{X}) = E(\mathbf{Y} \otimes \mathbf{Y}' \otimes \mathbf{Y}) \tag{1}$$

where

$$\mathbf{Y} = \mathbf{\Sigma}^{-1/2}(\mathbf{X} - \mu).$$

In Kollo [6] a skewness measure based on (1) is introduced by means of the star product:

$$\mathbf{b}(\mathbf{X}) = \mathbf{1}_{k\times k} * \mathbf{s}(\mathbf{X}) \tag{2}$$

where

$$\mathbf{1}_{k\times k} = \begin{pmatrix} 1 & \cdots & 1 \\ \vdots & \ddots & \vdots \\ 1 & \cdots & 1 \end{pmatrix}.$$

In [5] the Mardia's skewness measure is presented as through the third order moment:

$$\beta = \mathrm{tr}(m_3'(\mathbf{Y} m_3(\mathbf{Y})$$

where operation tr denotes the trace of matrix. A sample estimate $\widehat{\mathbf{b}(\mathbf{X})}$ of the skewness vector (2) we can present in the form:

$$\widehat{\mathbf{b}(\mathbf{X})} = \mathbf{1}_{k\times k} * \sum_{i=1}^{n} (\mathbf{y}_i \otimes \mathbf{y}_i' \otimes \mathbf{y}_i) \tag{3}$$

where

$$\mathbf{y}_i = \mathbf{S}^{-1/2}(\mathbf{x}_i - \overline{\mathbf{x}})$$

$\overline{\mathbf{x}}$ and $\mathbf{S}$ are the sample mean vector and the sample covariance matrix of the initial sample $(\mathbf{x}_1, \mathbf{x}_2, \ldots, \mathbf{x}_n)$. The estimator $\widehat{\mathbf{b}(\mathbf{X})}$ is random $k$-vector.

## 3 Modeling the multivariate skewness measure distribution

In this section we model the distribution of the random variable $\widehat{\mathbf{b}(\mathbf{X})}$ defined by equality (3). From this equality concludes that $\widehat{\mathbf{b}(\mathbf{X})}$ is $k$-vector. Let us have a sequence of independent and identically distributed random vectors $\{\mathbf{X}_n\}_{n=1}^{\infty}$. Let $E(\mathbf{X}_n) = \mu$ and $D(\mathbf{X}_n) = \mathbf{\Sigma}$. Then according to the central limit theorem the distribution of the random vector $\sqrt{n}(\mathbf{X}_n - \mu)$ converges to the normal distribution $N(\mathbf{0}_k, \mathbf{\Sigma})$ where $\mathbf{0}_k$ denotes $k$-dimensional zero vector.

Let us introduce $k^2 + k$-vector

$$\mathbf{Z}_n = \begin{pmatrix} \overline{\mathbf{x}} \\ \mathrm{vec}(\mathbf{S}) \end{pmatrix}.$$

Applying the central limit this random vector we get the following convergence in distribution

$$\sqrt{n}(\mathbf{Z}_n - E(\mathbf{Z}_n)) \mapsto N(\mathbf{0}_{k^2+k}, \mathbf{\Pi})$$

where $(k^2 + k) \times (k^2 + k)$-dimensional partitioned matrix

$$\mathbf{\Pi} = \begin{pmatrix} \mathbf{\Sigma} & \overline{m_3}'(\mathbf{X}) \\ \overline{m_3}(\mathbf{X}) & \mathbf{\Pi}_4 \end{pmatrix}.$$

The $k^2 \times k^2-$block $\mathbf{\Pi}_4 = \overline{m_4}(\mathbf{X}) - \mathrm{vec}(\mathbf{\Sigma})\mathrm{vec}'(\mathbf{\Sigma})$ ([11]). This convergence can be generalized by means of the following theorem.

**Theorem 1.** *Let $\{\mathbf{Z}_n\}_{n=1}^{\infty}$ be a sequence of $k^2 + k$-component random vectors and $\nu$ be a fixed vector such that $\sqrt{n}(\mathbf{Z}_n - \nu)$ has the limiting distribution $N(\mathbf{0}_{k^2+k}, \mathbf{\Pi})$ as $n \to \infty$. Let the function $g : R^{k^2+k} \to R^k$ have continuous partial derivatives at $\mathbf{z}_n = \nu$. Then the distribution of random vector $\sqrt{n}(g(\mathbf{Z}_n) - g(\nu))$ converges to the normal distribution $N(\mathbf{0}_{k^2+k}, g'_{\mathbf{z}_n}\mathbf{\Pi}g_{\mathbf{z}_n})$ where $(k^2 + k) \times k$-matrix*

$$g_{\mathbf{z}_n} = \left.\frac{dg(\mathbf{z}_n)}{d\mathbf{z}_n}\right|_{\mathbf{z}_n=\nu}$$

*is Neudecker matrix derivative at $\mathbf{z}_n = \nu$.* The proof of Theorem 1 can be found in the book of T. W. Andreson ([1], page 132).

In our case the function

$$g(\mathbf{z}_n) = g\begin{pmatrix} \overline{\mathbf{x}} \\ \mathrm{vec}(\mathbf{S}) \end{pmatrix} = \widehat{\mathbf{b}(\mathbf{X})}.$$

Applying Theorem 1 we get the following convergence in distribution:

$$\sqrt{n}(\widehat{\mathbf{b}(\mathbf{X})} - \mathbf{b}(\mathbf{X})) \mapsto N(\mathbf{0}_k, \mathbf{\Sigma}_{\mathbf{b}}).$$

Here the $k \times k$-matrix

$$\mathbf{\Sigma}_{\mathbf{b}} = g'_{\mathbf{z}_n}\mathbf{\Pi}g_{\mathbf{z}_n}\Big|_{\mathbf{z}_n=(\,\mu \quad \mathrm{vec}'(\mathbf{\Sigma})\,)'} =$$

$$= \left( \frac{d\widehat{\mathbf{b}(\mathbf{X})}}{d\overline{\mathbf{x}}} \quad \frac{d\widehat{\mathbf{b}(\mathbf{X})}}{d\mathbf{S}} \right) \begin{pmatrix} \mathbf{\Sigma} & \overline{m_3}'(\mathbf{X}) \\ \overline{m_3}(\mathbf{X}) & \mathbf{\Pi}_4 \end{pmatrix} \begin{pmatrix} \frac{d\widehat{\mathbf{b}(\mathbf{X})}}{d\overline{\mathbf{x}}} \\ \frac{d\widehat{\mathbf{b}(\mathbf{X})}}{d\mathbf{S}} \end{pmatrix} \Bigg|_{\overline{\mathbf{x}}=\mu,\mathbf{S}=\mathbf{\Sigma}} =$$

$$= \frac{d\widehat{\mathbf{b}(\mathbf{X})}}{d\overline{\mathbf{x}}} \mathbf{\Sigma} \frac{d\widehat{\mathbf{b}(\mathbf{X})}}{d\overline{\mathbf{x}}}' \Bigg|_{\overline{\mathbf{x}}=\mu,\mathbf{S}=\mathbf{\Sigma}} + \frac{d\widehat{\mathbf{b}(\mathbf{X})}}{d\mathbf{S}} \overline{m_3}(\mathbf{X}) \frac{d\widehat{\mathbf{b}(\mathbf{X})}}{d\overline{\mathbf{x}}}' \Bigg|_{\overline{\mathbf{x}}=\mu,\mathbf{S}=\mathbf{\Sigma}} +$$

$$+ \frac{d\widehat{\mathbf{b}(\mathbf{X})}}{d\overline{\mathbf{x}}} \overline{m_3}(\mathbf{X})' \frac{d\widehat{\mathbf{b}(\mathbf{X})}}{d\mathbf{S}}' \Bigg|_{\overline{\mathbf{x}}=\mu,\mathbf{S}=\mathbf{\Sigma}} + \frac{d\widehat{\mathbf{b}(\mathbf{X})}}{d\mathbf{S}} \mathbf{\Pi} \frac{d\widehat{\mathbf{b}(\mathbf{X})}}{d\mathbf{S}}' \Bigg|_{\overline{\mathbf{x}}=\mu,\mathbf{S}=\mathbf{\Sigma}}.$$

Here $\frac{d\widehat{\mathbf{b}(\mathbf{X})}}{d\overline{\mathbf{x}}}$ and $\frac{d\widehat{\mathbf{b}(\mathbf{X})}}{d\mathbf{S}}$ are $k \times k$- and $k \times k^2$-dimensional *Neudecker* matrix derivatives respectively.

Knowing the skewness measure distribution enables to estimate asymmetry of $k$-dimensional data. We can find for $\alpha$-confidence interval for skewness vector $\mathbf{b}(\mathbf{X})$. The problem of asymmetry is actual on environmental data for example.

## Acknowledgement

This paper is supported by Estonian Ministry of Education and Science target financed theme Nr. SF0140011s09.

## References

1. Anderson, T. W. (2003) *An Introduction to Multivariate Statistical Analysis*. Wiley, New York.
2. Harville, A. (1997) *Matrix Algebra from a Statistican's Perspective*. Springer, New York.
3. Klar, B. (2002) A Treatment of Multivariate Skewness, Kurtosis, and Related Statistics. *Journal of Multivariate Analysis*, **83**, 141-165.
4. Kollo, T., von Rosen, D. (2005) *Advanced Multivariate Statistics with Matrices*. Springer, Dordrecht.
5. Kollo T., Srivastava M. S. (2004) Estimation and testing of parameters in multivariate Laplace distribution. *Comm. Statist.*, **33**, 2363-2687.
6. Kollo, T. (2008) Multivariate skewness and kurtosis measures with an application in ICA. *Journal of Multivariate Analyses*, **99**, 2328-2338.
7. MacRae, E. C. (1974) Matrix derivatives with an applications to an adaptive linear decision problem. *The Annals of Statistics*, **7**, 381-394
8. Mardia, K. V. (1970) Measures of multivariate skewness and kurtosis measures with applications. *Biometrika*, **57**, 519-530.
9. Mori, T. F., Rohatgi, V. K., Szkely. (1993) On multivariate skewness and kurtosis. *Theory Probab. Appl*, **38**, 547-551.
10. Neudecker, H. (1969) Some theorems on matrix differentiations with special reference to Kronecker matrix products. *J. Amer. Stat. Assoc.*, **64**, 953-963.
11. Parring, A-M. (1979) Estimation asymptotic characteristic function of sample (in Russian). *Acta et Commetationes Universitatis Tartuensis de Mathematica*, **492**, 86-90.
12. Pihlak, M. (2004) Matrix integral. *Linear Algebra and Its Applications*, **388**, 315-325

# A Stochastic Modelling of The Extraction Process : Response Surface Methodology

**Selin SAHIN**[1] and **Ruya SAMLI**[2]

[1]Department of Chemical Engineering, Istanbul University, Istanbul, Turkey
Email: selins@istanbul.edu.tr
[2]Department of Computer Engineering, Istanbul University, Istanbul, Turkey
Email: ruyasamli@istanbul.edu.tr

**Abstract:** In this study, polyphenolic material amount in olive tree (*Olea europaea*) leaves extracted by ultrasound-assisted extraction (UAE) were investigated. The effect of three parameters such as temperature (25–35–45 ℃), time (60–90–120 min) and pH (3–7–11) were determined by both experimental and Response Surface Methodology (RSM) techniques. While applying RSM to the experimental results, a computer simulation was written in MATLAB simulation program to see the responses for each parameter scenario. The experimental results were compared with those of calculated from RSM. The differences between experimental and calculated results were expressed as percentage (% Dif). RSM was found to be an appropriate method for the UAE of olive leaves, owing to its high accuracy.

**Keywords:** Simulation; Process parameters; Response Surface Methodology; Modelling; Olive tree (*Olea europaea*) leaves; Ultrasound-assisted extraction.

## 1 Introduction

Experimental studies are the first chosen study type in many different science fields. Chemistry, chemical engineering, environmental engineering, textile engineering, mettalurgical and materials engineering, civil engineering, medicine, biology are some of these fields. The problem of determining the material behaviours according to various factors (temperature, concentration ratio, time, mixing amount, pH, purity, pressure) is an ancient problem that is tried to be solved by experimental studies. Although experimental studies can give realistic results, they are limited by the properties of materials used. Also, experimental studies require long periods of time, high cost and laboratory facilities. Because of these disadvantages of experiments, modelling the experimental studies in a simulation environment is an alternative study type. Alternatively, a structural element that is desired to be examined can be modelled in a computer environment without the aforementioned limitations. It must not be forgotten however that the accuracy of the computer model is related to material assumptions and experimental conditions on a large scale.

*Stochastic Modeling, Data Analysis and Statistical Applications* (pp. 115-119)
Lidia Filus - Teresa Oliveira - Christos H Skiadas (Eds)



Computer softwares, while they do not replace experimental work yet, can offer ease and guide the design phase. Within this scope, in recent years, experimental studies have been simulated by different methods such as optimisation method, regression analysis, neural networks etc. In this paper, it is aimed to simulate the chemical extraction processes and optimize them as done in many studies by using a stochastic modelling method, response surface methodology.

In this study, olive tree (*Olea europaea*) leaves were used as the research material in order to investigate the ultrasound-assisted extraction (UAE) parameters such as time, temperature and pH, and to observe the total phenolic content with different combinations of these parameters. Response Surface Methodolgy (RSM), a kind of mathematical modelling was applied to the experiments made to find the polyphenolic content in olive leaf extracts. This modelling operation can be seperated into three parts. First of all RSM was applied in the mathematical direction. Secondly, a computer simulation with MATLAB simulation program was constituted for the datas.

## 2 Extraction Process

An important process of chemical engineering is revealing the phenolic content of natural plant extracts. The more phenolic material in a plant extract, the more industrial value. There are many parameters that can affect the extraction process. Plant material, extraction method, preliminary preparations, solvent type, solid to solvent ratio, extraction temperature and pressure, extraction time and pH are some of these. A lot of researchers study the effects of these parameters on the extract. That's why, experiments with two, three, four or more parameters and different conditions were made.

In this study, as an agricultural and industrial waste of olive oil and table oil productions, olive tree (Olea europaea) leaves were used as the material. The purpose of the study is to investigate the extraction parameters such as time (20, 40, 60 min), temperature (25, 35, 45 ℃) and pH (3, 7, 11) and to observe the total phenolic content with different combinations of these parameters. Totaly, 27 experiments whose results are shown in Table 1 were performed.

## 3 Response Surface Methodology (RSM)

Response Surface Method (RSM) is an experimental optimization procedure based on physical experiments or computer experiments (simulations) and experimented observations (Box et al., 1978). In most of the experimental investigations, there are many parameters affecting each other besides the results. However, the effects of parameters to each other are ignored in many methods. The effects of distinct parameter to the results are solely calculated. In fact, parameters usually affect each other especially in physical experiments. For example, if the parameters are accepted as density and temperature,

handling only the distinct effect cannot be enough, since temperature can also affect the density. RSM is a method that aims to eliminate this lack.

In RSM, a function is a must to be obtained for prediction. This function's general formula is

$$Y = \beta_0 + \sum_{i=1}^{k} \beta_i X_i + \sum_{i<j}^{k} \beta_i X_i X_j + \sum_{i=i}^{k} \beta_{ii} X_i^2 + \cdots \quad \text{Eq. 1.}$$

where Y represents the result (or with the name in RSM – response), $\beta_i, \forall i$ are regression coefficients, $X_i, \forall i$ are the independent parameters.

It is very important to fomulate the effects of parameters to the result by the experiments, and to calculate the conditions that renders the maximum phenolic content in extraction processes. In this study, three independent parameters were used. Those were $X_1$ (time, min), $X_2$ (temperature, ℃) and $X_3$ (pH). The result named response in this method is Y (mg GAE/g dried leaf). Thus, the function of this study containing three independent variables is expressed with equation below:

$$Y = \beta_0 + \beta_1 X_1 + \beta_2 X_2 + \beta_3 X_3 + \beta_{11} X_1^2 + \beta_{22} X_2^2 + \beta_{33} X_3^2 + \beta_{12} X_1 X_2 + \beta_{13} X_1 X_3 + \beta_{23} X_2 X_3$$

When RSM is applied to the experimental values with the help of MATLAB simulation program, the coefficients of this equation are calculated as below :

$$Y = 66.1766 + (-0.0757\, x_1) + (-1.7392\, x_2) + (-3.0641 x_3) + 0.0012 x_1^2 + 0.0251\, x_2^2 + (-0.0333 x_3^2) + (-0.0022\, x_1 x_2) + 0.0019\, x_1 x_3 + 0.0368 x_2 x_3.$$

The results obtained by experiments and these RSM equations are summarized as in the table below (Table 1).

## 3 Conclusions

As an agricultural and industrial waste, olive leaves are a potential cheap, renewable and abundant source of polyphenols. These valuable compounds in olive leaf powders and leaf extracts are responsible for many health benefits, and therefore there is a growing interest to utilize olive leaf powders or extracts in various industrial applications such as food supplements, cosmetic and pharmaceutical industries. In this study olive leaves are chosen as a research material. The phenolic content in the leaf extracts was acquired by ultrasound-assisted extraction through different time, temperature and pH conditions. Therefore, 27 experiments with different combinations of 3 time, 3 temperature

and 3 pH values were carried out. After chemical experimental studies were completed, a simulation in MATLAB program was coded for applying RSM method to these results. Each parameter effect was formulated. When we look at the result table, it can be seen that the difference percent between experimental results and RSM results are consistent to each other and so it can be said that RSM is an appropriate method for modelling chemical extraction process.

Table 1 : The parameters, experimental and RSM results

| Experiment No | Time(min) | T(°C) | pH | Experimental Result | RSM Result |
|---|---|---|---|---|---|
| 1 | 60 | 25 | 3 | 28.37525361 | 28.4721 |
| 2 | 90 | 25 | 3 | 30.85166135 | 30.1221 |
| 3 | 120 | 25 | 3 | 33.42621939 | 33.9321 |
| 4 | 60 | 25 | 7 | 20.22347134 | 19.0197 |
| 5 | 90 | 25 | 7 | 23.09649878 | 20.8977 |
| 6 | 120 | 25 | 7 | 24.44219842 | 24.9357 |
| 7 | 60 | 25 | 11 | 8.686059414 | 8.5017 |
| 8 | 90 | 25 | 11 | 10.36635493 | 10.6077 |
| 9 | 120 | 25 | 11 | 12.07093217 | 12.8437 |
| 10 | 60 | 35 | 3 | 25.84592294 | 25.9241 |
| 11 | 90 | 35 | 3 | 27.0173689 | 26.9141 |
| 12 | 120 | 35 | 3 | 29.48776513 | 30.0641 |
| 13 | 60 | 35 | 7 | 18.22195617 | 17.9437 |
| 14 | 90 | 35 | 7 | 18.94426521 | 19.1617 |
| 15 | 120 | 35 | 7 | 22.11482171 | 22.5397 |
| 16 | 60 | 35 | 11 | 9.615632406 | 9.5247 |
| 17 | 90 | 35 | 11 | 10.13668612 | 10.3437 |
| 18 | 120 | 35 | 11 | 11.78750117 | 10.7467 |
| 19 | 60 | 45 | 3 | 27.22277895 | 28.3961 |
| 20 | 90 | 45 | 3 | 28.52836874 | 28.7261 |
| 21 | 120 | 45 | 3 | 30.80288682 | 31.2161 |
| 22 | 60 | 45 | 7 | 20.09370254 | 20.4157 |
| 23 | 90 | 45 | 7 | 22.09506734 | 22.4457 |
| 24 | 120 | 45 | 7 | 23.09952589 | 23.9637 |
| 25 | 60 | 45 | 11 | 14.26655863 | 14.3137 |
| 26 | 90 | 45 | 11 | 15.67107964 | 15.0997 |
| 27 | 120 | 45 | 11 | 17.23937872 | 18.0457 |

## References

1. Guinda, A., Use of solid residue from the olive industry. Grasas Y. Aceites, **57**, 107–115, (2006).
2. Martinez, J. L., Supercritical Fluid Extraction of Nutraceuticals and Bioactive Compounds. CRC Press, Taylor and Francis Group, (2007).
3. Grigonis, D., Venskutonis, P. R., Sivik, B., Sandahl, M., Eskilsson, C. S., Comparison of different extraction techniques for isolation of antioxidants from sweet grass (Hierochloë odorata). Journal of Supercritical Fluids, **33**, 223–233, (2005).
4. Carley, K.M., Kamneva, N.Y., Reminga J., Response Surface Methodology, CASOS Technical Report, (2004).
5. Bradley, N., The Response Surface Methodology, Master Thesis, Department of Mathematical Sciences, Indiana University of South Bend, (2007).
6. Box, G. E. P., and Wilson, K.B., On the Experimental Attainment of Optimum Conditions (with discussion). Journal of the Royal Statistical Society Series **B13(1):** 1–45, (1951).

# 3 CHAPTER

## Models and Modeling

# The Portuguese Stable Equivalent Population: A model and trends

Renato Fernandes[1,2] and Pedro Campos[1,3]

[1] LIAAD /INESC TEC
Porto, Portugal
[2] University of Porto, Faculty of Sciences
Porto, Portugal
(e-mail: renato.fernandes@fc.up.pt)
[3] University of Porto, Faculty of Economics
Porto, Portugal
(e-mail: pcampos@fep.up.pt)

**Abstract.** Stable population theory provides a broadly useful mathematical framework for studying population's age structure and growth that are mainly determined by rates of fertility, mortality and migration. This work uses an Agent-Based model to simulate the behavior of the Portuguese population under the Stable model, and provides scenarios for the sustainability of the social security system.
**Keywords:** Stable Population Model, Agent-Based simulation, Social Security System.

## Acknowledgments

"This work is financed by the ERDF European Regional Development Fund through the COMPETE Programme (operational programme for competitiveness) and by National Funds through the FCT Fundação para a Ciência e a Tecnologia (Portuguese Foundation for Science and Technology) within project FCOMP-01-0124-FEDER-037281".

## 1 Introduction

The future and sustainability of social security systems is a matter of concern in modern economies. Generally, there are two main different funding streams for insurance within the security systems: the contributive regime relies on wage contributions and the subsidized regime receives financing from other sources, generally the governments. As with all social insurance programs, the provision of old age pensions involves the actual and future population that contributes to (and earns from) the system. Therefore, some background knowledge about population dynamics and demography are needed in order to project the future and the sustainability of the social security systems. Mainstream theories of

*Stochastic Modeling, Data Analysis and Statistical Applications* (*pp.* 119-135)
Lidia Filus - Teresa Oliveira - Christos H Skiadas (Eds)



population projections are more focused on econometrical links rather than on the complexity underlying the variable of the problem.

Agent-based models Wooldridge[17] Ferber [5], constitute an alternative to mainstream techniques, such as econometrical models, since they deal with the complex interactions between the individuals in the system. In addition, stable population theory provides a broadly useful mathematical framework for studying population's age structure and growth that are mainly determined by rates of fertility, mortality and migration. A stable population is a limit population to which actual populations tend when their mortality and fertility rates remain constant. In this work, we create an Agent-Based model to simulate the behavior of the Portuguese population under the Stable model and provide clues for the sustainability of the social security system.

Our work is organized as follows: in section 2 we provide an introduction to the stable population model; in section 3, we describe the model of the Portuguese Stable Equivalent Population and the details of the social security System. Results and Conclusions are in sections 4 and 5, respectively.

## 2 The Stable population model

The long-term implications of the maintenance of constant demographic patterns over a long period in a population may have important consequences in the population´s structure. All individuals being linearly independent, they tend toward a structure that is independent of the conditions of the past, LeBras[8]. A stable population emerges when some characteristics persist over the long term: (i) age-specific fertility rates are constant; (ii) age-specific death rates are constant; and (iii) age-specific net migration rates are zero. The Stable model, in its simplest continuous form is a one sex model and can be defined by the Lotka equation - Le Bras[8] Amegandjin[1] Keyfitz[7] Pressat[11] Tapinos[14] Schryock, Siegel et al[12] among others):

$$\int_{\alpha}^{\beta} e^{-rx} p(x)\phi(x)dx = 1. \tag{1}$$

Where $\phi(x)dx$ represents the number of female births in age interval $(x, x+dx)$, $p(x)$ is the probability of female survival until age $x$, and $(\alpha, \beta)$ is the female fertility interval. The solution of this equation is given by $r$, the intrinsic growth rate, which an approximation can be given by $ln(R_0/K_1)$, where $R_0$ is the net reproduction rate and $K_1$ is the average fertility age.

After finding the value of $r$ (the intrinsic growth rate), we can compute the equivalent stable population for a given population at time $t$. The equivalent stable population of the actual population is regarded as a transitional state. The reverse is, however, impossible: a stable state can be reached by starting from many actual populations There are also other theoretical concepts related to stable populations that are not explored in this work: semi-stable population, which is a theoretical concept, and the study of their properties being a problem of pure mathematics; and the concept of a quasi-stable population,

which, on the other hand, is based on experience. The properties of quasistable populations are based on empirical data, which may be revised as a result of further experiments [15]. In the following sections we create synthetic populations, based on simple methods of Agent-Based simulations, and compute the stable equivalent of the population for a 30 year period.

## 3 Portuguese Population Base Model

In this model, each agent (a.k.a. person) is created with one gender (male or female), and different death and birth rates.

Then, at each step (year) the population is updated by eliminating some agents, giving birth to new ones and computing the new global death and birth rates.

- Let $l_1$ be the starting year for the simulation and let $a_{i,j,k,l}$ represent the agent of age $i \in \{0, 1, \ldots, 99\}$, sex $j \in \{M, F\}$, personal index $k \in \mathbb{N}$ and year $l \in \mathbb{N} \backslash \{1, 2, \ldots, l_1 - 1\}$; $a_{i,j,k,l} = 1$ if the agent is alive by year $l$ and $a_{i,j,k,l} = 0$ if the agent is dead by the year $l$ (if $a_{i,j,k,l_n} = 0$ then $a_{i,j,k,l_m} = 0$ for all $l_m > l_n$)
- Let $p_{i,j,l}$ be the number of alive agents by the end of the year $l$ with age $i$ and sex $j$

$$p_{i,j,l} = \sum_k a_{i,j,k,l}; \tag{2}$$

- Let $mr_l$ be the male proportion in the year $l$

$$mr_l = \frac{\sum_i p_{i,M,l}}{\sum_{i,j} p_{i,j,l}} \tag{3}$$

- Let $d_{i,j,l}$ be the number of deaths that occurred in the year $l$ of agents with age $i$ and sex $j$

$$d_{i,j,l} = \#\{a_{i,j,k,l} = 0 \wedge a_{i-1,j,k,l-1} = 1\}, i \neq 0, \tag{4}$$

$$d_{0,j,l} = \sum_{i_n} b_{i_n,j,l} - p_{0,j,l}; \tag{5}$$

- Let $b_{i,l}$ be the number of births of agents in the year $l$, given birth by females of age $i$.

Then it is set:

- $dr_{i,j,l+1} = \frac{d_{i,j,l}}{d_{i,j,l} + p_{i,j,l}}$ as the death rates the year $l+1$ of agents of age $i$ and sex $j$;
- $br_{i,l+1} = \frac{b_{i,l}}{d_{i,F,l} + p_{i,F,l}}$ as the birth rates used for the year $l+1$ of female agents of age $i$.

And the following variables are created:

- $X_{i,j,l+1}$ a random variable refering to $dr_{i,j,l+1}$ with $\sigma d_{i,j,l+1} = min\{0.02, \frac{dr_{i,j,l+1}}{3}, \frac{1-dr_{i,j,l+1}}{3}\}$ such that

$$X_{i,j,l+1} \sim N(0, \sigma d_{i,j,l+1}); \tag{6}$$

- $Y_{i,l+1}$ a random variable refering to $br_{i,l+1}$ with $\sigma b_{i,l+1} = min\{0.02, \frac{br_{i,l+1}}{3}, \frac{1-br_{i,l+1}}{3}\}$ such that

$$Y_{i,l+1} \sim N(0, \sigma b_{i,j,l+1}). \tag{7}$$

With these distributions each agent is given:

- $ad_{i+1,j,k,l+1}$ which is the death probability of the agent $k$ of age $i+1$ and sex $j$ for the year $l+1$ and it is given by

$$ad_{i+1,j,k,l+1} = dr_{i+1,j,l+1} + x_{i+1,j,l+1}, x_{i+1,j,l+1} \in X_{i+1,j,l+1} \tag{8}$$

- $ab_{i+1,F,k,l+1}$ which is the giving birth probability of the female agent $k$ of age $i+1$ for the year $l+1$ and it is given by

$$ab_{i+1,F,k,l+1} = br_{i+1,l+1} + y_{i+1,l+1}, y_{i+1,l+1} \in Y_{i+1,l+1} \tag{9}$$

As for the evolution process there is a cycle of updates:

**Step 1.** Increase the simulation year
**Step 2.** Age every living agents
**Step 3.** Give birth to new agents according to the birth rates of females, i.e., it is generated $U_1, U_2 \sim U(0,1)$ and if $U_1 < ab_{i,F,k,l}$ then a new agent is born. If $U_2 < mr_l$ then the new agent is male, else it is female.
**Step 4.** Randomly "kill" agents, i.e., according to $U_3 \sim U(0,1)$ and if $U_3 < ad_{i,j,k,l}$ then is set $a_{i,j,k,l} = 0$.
**Step 5.** Compute the next year birth, death and male proportion rates $br_{i,l+1}, dr_{i,j,l+1}, mr_l$.
**Step 6.** Define each agent's birth and death rates $abi, F, k, l, adi, j, k, l$ for the following year.

### 3.1 Model Validation

After computing several simulations for the previously presented model using the Portuguese census information from 1981, 1991 and 2001 as starting data [6], we gathered a very vast amount of data. Means and standard deviations were computed for each year, age and gender for different variables. These results were then compared with the real census data of 1991, 2001 and 2011.

Data comparison is made in the following way: relative diferences between simulated data and real data are computed, in order to find the relative and absolute errors.

The relative diferences are defined as $(simulated - real)/real$ and the absolute diferences are defined as $simulated - real$.


Fig. 1: Relative diferences between simulated population and real population

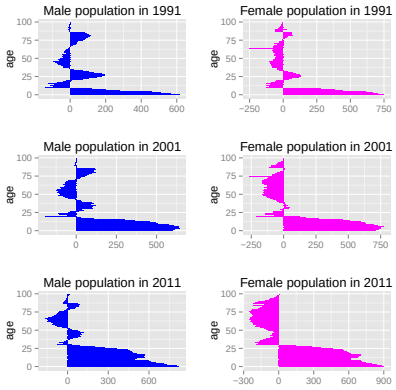


Fig. 2: Absolute diferences between simulated population and real population

Figures 1, 2 show the relative errors for the simulations started in the year 1981. Negative errors refer to situations where simulated population is lower in number than the real population (positive values for the opposite situation). The greatest relative errors are found mostly in the elderly ages, with errors being close to $-100\%$ in the first 10 years and in following years shifting to 100% or higher. The other high density relative errors are found in the younger ages rounding a 50% relative error, meaning that the simulated population is 50% larger than the real one in younger ages. The latter errors can be easily explained due to the fact that birth rates are decreasing in those years. Despite the stochasticity of this model, it maintains the same average birth rate in the first year through all over the simulation period. We can state that errors in the older ages are not very high, since they refer to a very small amount of the population,in absolute terms.

As for the midle age population, both relative and absolute errors are very small, which shows that the model sounds to be suitable for those age classes, during that period.

### 3.2 Population Projection

Aimimg at enhancing the model, we studied the errors in order to build confidence intervals for the projections, by adapting and computing the error implementation of Michael Stoto [13]. In [13], gaps are computed for the differences between the several periods of the simulation.

- Let $\Delta r_{j,k}$ be the average error between all simulations for each stating year $j \in \{1981, 1991, 2001\}$ and for jump gap $k \in \{10, 20, 30\}$;
- Let $b_j$ be mean of the errors for all jump gaps $k$ for each starting year $j$;
- Let $e_{j,k}$ be

$$\Delta r_{j,k} - b_j; \tag{10}$$

- Then the variance for $\Delta r_{j,k}$ is given by

$$var(\Delta r_{j,k}) = var(b_j) + var(e_{j,k}) \tag{11}$$

- and $\sigma$ will be called the standard deviation of $\Delta r_{j,k}$.
- To incorporate the errors in our projections, we added and subtracted $2\sigma$ to the means of all projections.

From figure 6 to 11 it can be seen that there is a tendency for the population to reduce, even considering the error confidence interval, so most likely that is what will happen in the future. The amount of decrease is yet unknown as there is a very large variation in the possible scenarios.

As for each age, in the lowest and highest ages there is a tendency for the population to decrease right from the start (young ages). For midle ages, it seems that there will be an increase of population for some years, before it starts to decrease like in every other age. In addition, this decrease appears to be more intense in female population.

### 3.3 Stable Equivalent Population

As it was previously introduced in section 2, the Stable Equivalent Population is a model of population dynamics appropriate for particular situations, such as the actual Portuguese population, of nearly constant natality and mortality rates and nearly null migration rate.

We have computed the Stable Equivalent Population based on the projected population for each year from 2011 to 2041 and then we have computed the relative diferences between the projected population and its Stable Equivalente as $(projected - stable)/stable$

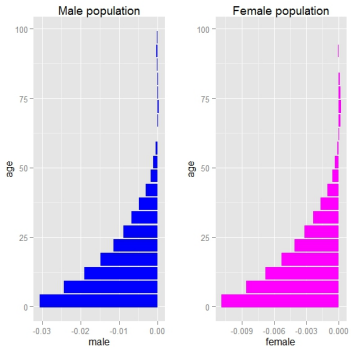


Fig. 3: Relative diferences for 2021

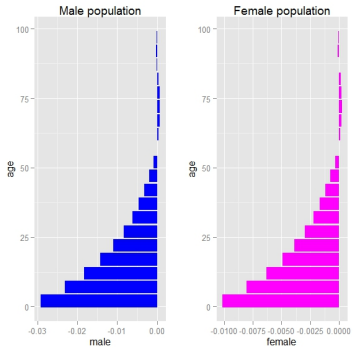


Fig. 4: Relative diferences for 2031

From figures 3,4,5 we can state that in the age of 50 and higher, the realtive error in 2021 is always very close to 0 and in the previous ages it increases in

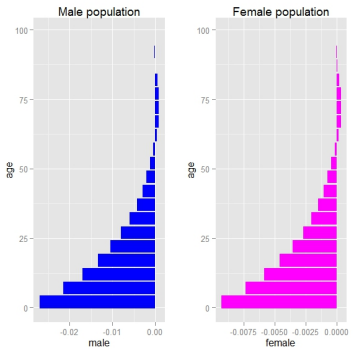


Fig. 5: Relative diferences for 2041

inverse proportion to the age till 0.03% for the male population and 0.01% for the female population. This tendency remains the same in the years of 2031 and 2041 with the only diference being that for each year, the relative diference is facing a small reduction.

It is possible to deduce that Portuguese population is tending to its Stable Equivalent, based on actual slow fertility, mortality and migration trends.

## 4 Social Security Model

The Social Security Model is an expansion of the previously presented Population Model. We use the Population Model for an evolutive overview and include the Social Security parameters in the model: activity, employment, retirement, schooling, job qualification, and remuneration.

- Let $ac_{i,j,k,l}$ be the parameter for economic activity of the agent $k$ of age $i$ of sex $j$ in the year $l$; $ac_{i,j,k,l} = 1$ means that the agent is active and $ac_{i,j,k,l} = 0$ means that the agent is inactive (retired, pensionist, student, etc.). Obviously death agents are inactive;
- Let $cr_{i,j,l}$ be the activity rates of agents of age $i$ and sex $j$ in the year $l$ and they are computed as

$$cr_{i,j,l} = \frac{\sum_k ac_{i,j,k,l}}{\sum_k a_{i,j,k,l}} \tag{12}$$

- Let $c_{i,j}$ be the proportion of the population of age $i$ and sex $j$ that is active. This proportions are given to the model based on 2011 Portuguese rates [6];
- Let $\epsilon$ be threshold parameter with $\epsilon \in [0, 1]$;
- Let $ae_{i,j,k,l}$ be the parameter for employment status of the agent $k$ of age $i$ of sex $j$ in the year $l$; $ae_{i,j,k,l} = 1$ means that the agent is employed and $ae_{i,j,k,l} = 0$ means that the agent is unemployed. Obviously, inactive agents are unemployed;

- Let $er_{i,j,l}$ be the employment rates of agents of age $i$ and sex $j$ in the year $l$ and they are computed as

$$er_{i,j,l} = \frac{\sum_k ae_{i,j,k,l}}{\sum_k ac_{i,j,k,l}} \tag{13}$$

- Let $e_{i,j}$ be the proportion of the population of age $i$ and sex $j$ that is employed. This proportions are given to the model based on 2011 Portuguese rates [6];
- Let $ar_{i,j,k,l}$ be the parameter for retirement status of the agent $k$ of age $i$ of sex $j$ in the year $l$; $ar_{i,j,k,l} = 1$ means that the agent is retired and $ar_{i,j,k,l} = 0$ means that the agent is not retired. If $i_r$ is defined as the minimum age for retirement, then $i < i_r \Rightarrow ar_{i,j,k,l} = 0$ and $i > i_r + 10 \Rightarrow ar_{i,j,k,l} = 1$. If the agent gets retired at some point, that status can never be changed back. Obviously, if an agent is retired then it is also inactive.
- Let $rr_{i,j,l}$ be the retirement rates of agents of age $i$ and sex $j$ in the year $l$ and they are computed as

$$rr_{i,j,l} = \frac{\sum_k ar_{i,j,k,l}}{\sum_k a_{i,j,k,l}} \tag{14}$$

- Let $r_{i,j}$ be the proportion of the population of age $i$ and sex $j$ that is retired. These proportions are given to the model based on 2011 Portuguese rates [6];
- Let $as_{i,j,k,l}$ be the schooling level of the agent $k$ in the year $l$. $as_{i,j,k,l} \in \{1, 2, 3, 4, 5, 6\}$ where 1 refers to a schooling level under 4th grade, 2 refers to 4th grade, 3 refers to 6th grade, 4 refers to 9th grade, 5 refers to high school and 6 refers to superior education;
- Let $s_{i,j}$ be the schooling level rates of persons of age $i$ and sex $j$ of the Portuguese population in 2011 [6];
- Let $aq_{i,j,k,l}$ be the job qualification of the agent $k$ in the year $l$. $as_{i,j,k,l} \in \{1, 2, 3, 4, 5, 6\}$ where 1 refers to a qualification of not qualified professional, 2 refers to semi-qualified professional, 3 refers to qualified professional, 4 refers to highly qualified professional, 5 refers to team leader and 6 refers to member of administration board;
- Let $q_{i,j}$ be the job qualification rates of agents of age $i$ and sex $j$ of the Portuguese population in 2011 [10];
- Let $aw_{i,j,k,l,s,q}$ be the wage of the agent $k$ in the year $l$ with schooling level $s$ and work qualification $q$.
- Let $w_{j,s,q}$ be the wage of persons of sex $j$, schooling leve $s$ and work qualification $q$ based on data from Portugal in 2011 [6],[10].

Now we can explain how these parameters are updated. As with population parameters, these are updated every year, depending on previous year.

**Step 1.** Update the activity of the agents in the current year $l_c$. If $|cr_{i,j,l_c} - c_{i,j}| > \epsilon$ then we generate $U_4 \sim U(0, 1)$ for each agent of age $i$ and sex $j$ and if $U_4 < ac_{i,j,k,l}$ then agent $k$ is set as active else it is set as inactive;

**Step 2.** Update the employment status of the agents. We generate $U_5 \sim U(0,1)$ and if $U_5 < ae_{i,j,k,l}$ then agent $k$ is set as employed else it is set as unemployed;

**Step 3.** Update retirement status of the agents. If $i_r \leq i \leq i_r + 10$ and $ac_{i,j,k,l} = 0$ then it is generated $U_6 \sim U(0,1)$ and if $U_6 < ar_{i,j,k,l}$ then agent $k$ is set as retired. When an agent gets retired, its retirement pension is defined and it remains the same till agent's death. Let $ap_{i,j,k,l}$ be the retirement pension of agent $k$ and $y$ its total working years then

$$ap_{i,j,k,l} = y * 0.002 * \sum_{\substack{last\,5 \\ working\,years}} \frac{aw_{i,j,k,l,s,q} * 14}{5} \tag{15}$$

The multiplication by 14 refers to the fact that in Portugal a employee earns 12+2=14 salaries per year.

**Step 4.** Update schooling and work qualification. When an agent gets employed for the first time these parameters are defined. They are decided randomly using the Inversion Method [3] of $U_7, U_8 \sim U(0,1)$ using the rates of the schooling/work qualification for the age of the agent. On the following years these parameters are updated using the same mecanism with a small exception: they are always increasing.

**Step 5.** Update wages. The wage of an employed agent is defined as $aw_{i,j,k,l,s,q} = W_{j,s,q}$.

**Step 6.** Pay taxes. Every agent contributes to the Social Security capital with a determined contribution tax $C$ of its wage. As We will be modeling the Social Security system itself and not the tax payers, We will assume that $C$ is the joint contribution from both the employee and employer. Let $TC_l$ be the total contribution on the year $l$ then

$$TC_l = C * \sum aw_{i,j,k,l,s,q} * a_{i,j,k,l} \tag{16}$$

**Step 7.** Pay retirement pensions. Every living retired agent receives its retirement pension which is subtracted from the Social Security capital, $Tp_l$, i.e. the total retirement pensions paid that year,

$$Tp_l = \sum ap_{i,j,k,l} * a_{i,j,k,l} \tag{17}$$

**Step 8.** Update the Social Security capital $SS_l$. The Social Security capital for the year l is set as

$$SS_l = SS_{l-1} + TC_l - Tp_l \tag{18}$$

### 4.1 Results

Taking the average of simulations and including a confidence interval based on two standard deviations, figures 12, 13, 14 were produced for the cases of minimun retirement age $55, 65, 75$ and to contribution tax $32.7\%, 40\%, 45\%$

It is fairly easy to uderstand that both increasing contribution tax or increasing the minimum age for retirement leads to an increase in the Social Security capital and a decrease in the tendency to reach a point of decrease of the capital. In Portugal, the current minimum age of retirement is 66, so with this model one should expect an eventual decrease on the Social Security capital in the following years, according to these simulations.

In addition, one can see that the increase of the minimum age of retirement influences much more the increase of the Social Security capital than an increase in the contribution tax. So evaluating the current tendency one could say that delaying the retirement age is one of the best course of action.

So, considering these results, we can see that Social Security is currently unsustainable but with some increases in the parameters of the model, this outcome may change.

It is worth to note that this model is simplified as it only takes into account the revenues from the contributions of tax payers and the expenses from the retirement pensions. However, there are also other expenses like the maintenace of public schools and hospitals, subsidies for the unemployed and many other types of pensions.

## References

1. Amegandjin, J., *Dmographie Mathematique*, Economica, Paris (1989).
2. Borella, M., "Social Security Systems and the Distribution of Income: An Application to the Italian case" Wp cerp n 8/01 (2001).
3. Devroye, Luc, *Non-Uniform Random Variate Generation* 1 Edition, Springer (1986).
4. Diebold, Francis X. , *The Past, Present, Future of Macroeconomic Forecastin*, Journal of Economic Perspectives, Vol. 12, No. 2 (1998).
5. Ferber, J. *Multi-Agent Systems - An Introduction to Distributed Artificial Intelligence*, Addison-Wesley Longman, Harlow (1999).
6. INE, Instituto Nacional de Estatstica, Portugal, web portal, data of census 2011, available at: www.ine.pt/en/ (2012).
7. Keyfitz, N., *Applied Mathematical Demography*, John Wiley and Sons, New York (1977).
8. Le Bras. H., *The Nature of Demography*, Princeton (2008).
9. Mazzaferro, C. and Morciano, M., *A Dynamic Microsimulation Model for the Italian Social Security System*, Cappaper n. 48 (2012).
10. Office for strategy and studies. Www.gee.min-ecoomia.pt/en/ (2012).
11. Pressat, R., *L´analyse Démographique*, 4e. Édition, Presses Universitaires de France, Paris (1983).
12. Schryock, Henry S., Siegel, Jacob S. et al , *The Methods and Materials Of Demography*, Ed. Stockwell, Edward G., Academic Press Inc., San Diego, California (1976).
13. Stoto, Michael A. , *Accuracy of Population Projections*, Journal of the American Statistical Association, Vol. 78, No. 381 (1983).
14. Tapinos, G., *Éléments De Dmographie*, Armand Colin, Paris (1985).
15. United Nations , *The Concept of a Stable Population - Application To The Study Of Populations of Countries with Incomplete Demographic Statistics*, United Nations Publications, Sales No. E.65.xiii.3 (1968).

16. Wilensky, U., Netlogo, Http://ccl.northwestern.edu/netlogo/ (1999).
17. Wooldridge, M. , *An Introduction to MultiAgent Systems*, John Wiley and Sons, Sussex (2002).

## Annex

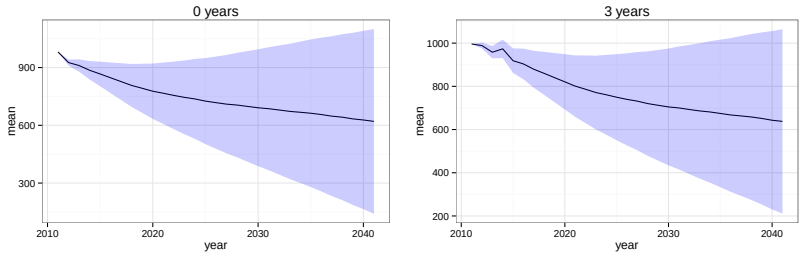


Fig. 6: Projection of the male population of age 0 to 9 for 30 years

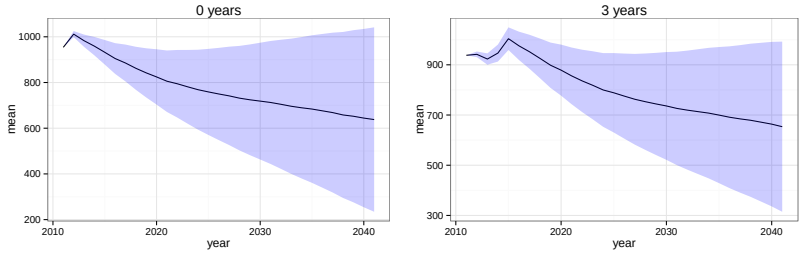


Fig. 7: Projection of the female population of age 0 to 9 for 30 years

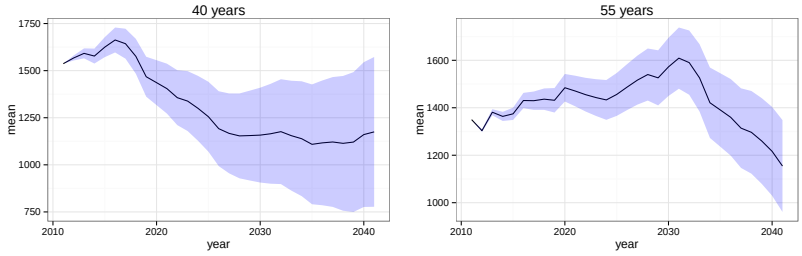


Fig. 8: Projection of the male population of age 40 to 49 for 30 years

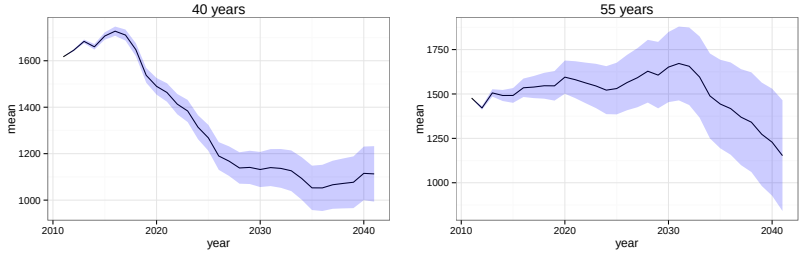


Fig. 9: Projection of the female population of age 40 to 49 for 30 years

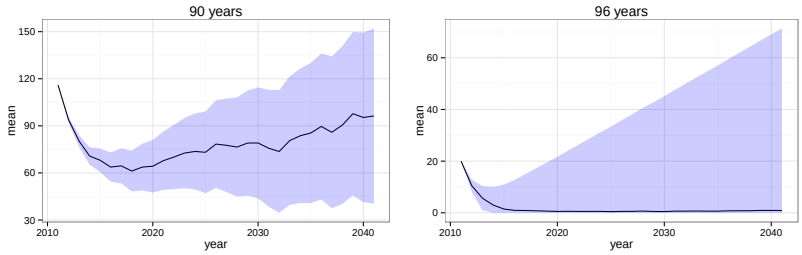


Fig. 10: Projection of the male population of age 90 to 99 for 30 years

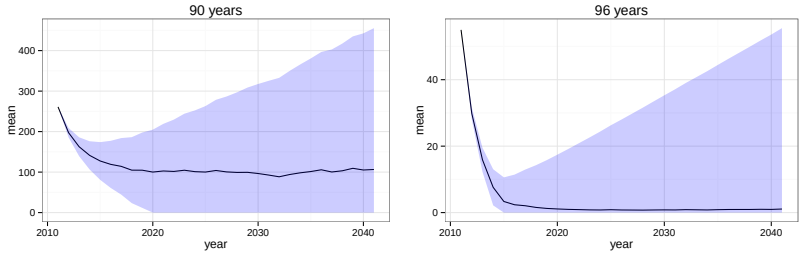


Fig. 11: Projection of the female population of age 90 to 99 for 30 years

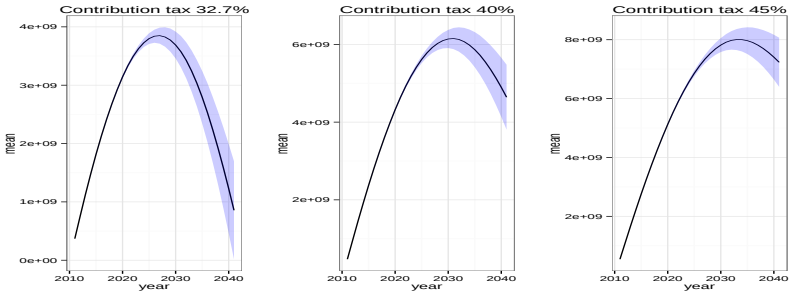


Fig. 12: Projection of the Social Security capital with minimum retirement age 55 for 30 years

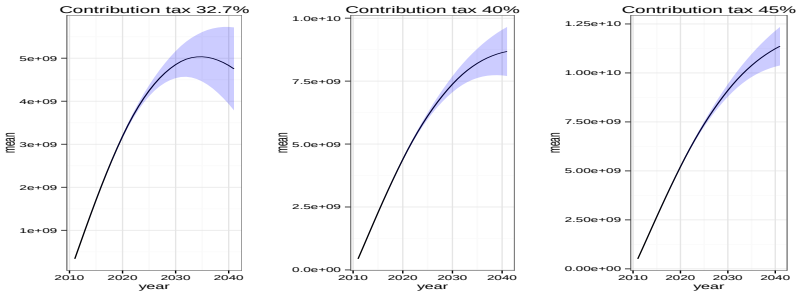


Fig. 13: Projection of the Social Security capital with minimum retirement age 65 for 30 years

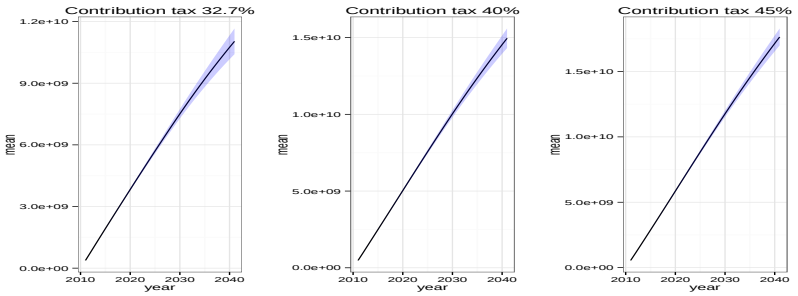


Fig. 14: Projection of the Social Security capital with minimum retirement age 75 for 30 years

# Two-Stage Kalman Filtering for Discrete Systems Using Nonparametric Algorithms[1]

**Gennady M. Koshkin and Valery I. Smagin**

Tomsk State University, Tomsk, Russia
Email: kgm@mail.tsu.ru
Email: vsm@mail.tsu.ru

**Abstract:** The paper addressed the filtering problem with using nonparametric algorithms for discrete stochastic systems with unknown input. The two-stage algorithm on the base of the Kalman filtering and nonparametric estimator for systems with unknown input is designed and explored. Examples are given to illustrate the usefulness of the proposed results in comparison with the known algorithms.
**Keywords:** Kalman filter, Unknown input, Two-stage filtering algorithm, Nonparametric estimator.

## 1 Introduction

An important issue of the Kalman filtering [1] is construction of algorithms for the class of systems with unknown additive perturbations. Such systems are used as the models of real physical systems, as the models of objects with unknown errors, and in control problems for economic systems. The known methods to calculate estimates of a state vector are based on the algorithms of estimation of an unknown perturbation [2-9].

In this paper, for discrete systems with unknown perturbations the two-stage optimal filtering with use of nonparametric estimators for unknown input are proposed. Examples are given to illustrate the properties of the proposed procedures in comparison with the known algorithms.

## 2 The problem statement

Consider the mathematical model of the linear discrete-time stochastic system with unknown input in the form:

$$x(k+1) = Ax(k) + Br(k) + q(k),\ \ x(0) = x_0, \qquad (1)$$

[1]Supported by Russian Foundation for Basic Research, projects 13-08-00744, 13-08-01015A, Tomsk State University Competitiveness Improvement Program, and the project "Goszadanie Minobrrnauki Rossii"

*Stochastic Modeling, Data Analysis and Statistical Applications* (pp. 137-143)
Lidia Filus - Teresa Oliveira - Christos H Skiadas (Eds)



$$y(k) = Hx(k) + v(k)\,, \tag{2}$$

where $x(k)$ is the state of the object, $r(k)$ is an unknown input, $y(k)$ is the measurement, $A$, $B$, and $H$ are matrices of the appropriate dimensions. It is assumed random perturbations $q(k)$ and the noise measurements $v(k)$ are not correlated between themselves and are subject to the Gaussian distribution with zero mean and the corresponding covariance: $\mathrm{E}[q(k)q(k)^{\mathrm{T}}] = Q\delta(k,t)$, $\mathrm{E}[v(k)v(k)^{\mathrm{T}}] = V\delta(k,t)$, where $\delta(k,t)$ is the Kronecker symbol, i.e., $\delta(k,t) = 1$ if $k = t$, and $\delta(k,t) = 0$ when $k \neq t$. It is also proposed that the vector of initial conditions is uncorrelated with values $q(k)$ and $v(k)$. This vector is defined by the following characteristics:

$$\mathrm{E}[x(0)] = \bar{x}_0\,,\ \mathrm{E}[(x(0) - \bar{x}_0)(x(0) - \bar{x}_0)^{\mathrm{T}}] = P_0\,.$$

## 3 The estimation algorithm of an unknown input and state space vector

In this paper, the optimal filter is defined by the following full-order Kalman filter. Filter equations have the form:

$$\hat{x}(k+1) = A\hat{x}(k) + B\hat{r}(k) + K(k)[y(k+1) - H(A\hat{x}(k) + B\hat{r}(k))]\,,\ \hat{x}(0) = \bar{x}_0\,, \tag{3}$$

$$P(k+1/k) = AP(k)A^{\mathrm{T}} + Q\,, \tag{4}$$

$$K(k) = P(k+1/k)H^{\mathrm{T}}[HP(k)H^{\mathrm{T}} + V]^{-1}\,, \tag{5}$$

$$P(k+1) = (I - K(k)H)P(k+1/k)\,,\ P(0) = P_0\,, \tag{6}$$

where $\hat{x}(k)$ and $\hat{r}(k)$ are estimators, $P(k) = \mathrm{E}[(x(k) - \hat{x}(k))(x(k) - \hat{x}(k))^{\mathrm{T}}]$.

However, formulas (3)–(6) can not be applied immediately because $\hat{r}(k)$ is unknown. Obtain estimator $\hat{r}(k)$ by making use of the following criteria:

$$J(r(k-1)) = \mathrm{E}\left[\sum_{i=1}^{k} \|u(i)\|_C^2 + \|r(i-1)\|_D^2\right], \tag{7}$$

where $u(i) = y(i) - H\hat{x}(i)$ is the innovation process, $\|\cdot\|_C^2$ is the Euclidian norm, $C$ and $D$ are symmetric positive definite weight matrices.

Optimal estimator of the unknown input at moment $k = 1$ is found by minimization of the criteria:

$$J(r(0)) = \min_{r(0)} \mathrm{E}\left[\|y(1) - H\hat{x}(1)\|_C^2 + \|r(0)\|_D^2\right]. \tag{8}$$

Substituting $\hat{x}(1) = A\hat{x}(0) + Br(0)$ into (8), we have

$$J(r(0)) = \min_{r(0)} \mathrm{E}\left[ \left\| y(1) - HA\hat{x}(0) - HBr(0) \right\|_C^2 + \left\| r(0) \right\|_D^2 \right]. \quad (9)$$

Transform the norms in (9) and obtain

$$J(r(1)) = \min_{r(0)} \mathrm{E}\left[ \alpha_0 - 2r(0)^{\mathrm{T}} B^{\mathrm{T}} H^{\mathrm{T}} V (y(1) - HA\hat{x}(0)) + \left\| r(0) \right\|_{B^{\mathrm{T}} H^{\mathrm{T}} CHB + D}^2 \right]. \quad (10)$$

Here, the parameter $\alpha_0$ does not depend on $r(0)$. First, differentiate (10) w.r.t. $r(0)$, and then find the optimal estimator of the unknown input from the equation

$$\frac{dJ(r(0))}{dr(0)} = 2(B^{\mathrm{T}} H^{\mathrm{T}} CHB + D) r(0) - 2B^{\mathrm{T}} H^{\mathrm{T}} C \, \mathrm{E}[y(1) - HA\hat{x}(0)] = 0. \quad (11)$$

So, at the moment $k = 1$, we obtain the optimal estimator of the unknown input:

$$\hat{r}(0) = S\mathrm{E}[y(1) - HA\hat{x}(0)], \quad (12)$$

where

$$S = (B^{\mathrm{T}} H^{\mathrm{T}} CHB + D)^{-1} B^{\mathrm{T}} H^{\mathrm{T}} C. \quad (13)$$

Analogously, at the moment $k = 2$, the optimal estimator of the unknown input is found from the following criteria:

$$J(r(1)) = \min_{r(1)} \mathrm{E}\left[ \left\| y(2) - H\hat{x}(2) \right\|_C^2 + \left\| r(1) \right\|_D^2 \right] + J(\hat{r}(0)). \quad (14)$$

Taking into account (14) and the expression $\hat{x}(2) = A\hat{x}(1) + Br(1)$ at the moment $k = 2$, we have

$$J(r(1)) = \min_{r(1)} \mathrm{E}\left[ \left\| y(2) - HA\hat{x}(1) - HBr(1) \right\|_C^2 + \left\| r(1) \right\|_D^2 \right] + J(\hat{r}(0)).$$

As in the case of (10)

$$J(r(1)) = \min_{r(1)} \mathrm{E}\left[ \alpha_1 - 2r(1)^{\mathrm{T}} B^{\mathrm{T}} H^{\mathrm{T}} C (y(2) - HA\hat{x}(1)) + \left\| r(1) \right\|_{B^{\mathrm{T}} H^{\mathrm{T}} CHB + D}^2 \right], \quad (15)$$

where the value $\alpha_1$ does not depend on $r(1)$. Differentiating (15) w.r.t. $r(1)$, as in the first step, we obtain the optimal estimator:

$$\hat{r}(1) = S\mathrm{E}[y(2) - HA\hat{x}(1)]. \quad (16)$$

Using the mathematical induction, for the next steps

$$\hat{r}(k) = S\mathrm{E}[w(k)]. \quad (17)$$

Here, the matrix $S$ is given by the formula (13), and $w(k) = y(k) - HA\hat{x}(k-1)$.

Now, let us calculate value E[$w(k)$] using nonparametric estimators [10]. Applying the well known kernel estimates, we obtain

$$\hat{r}(k) = S\hat{w}_{np}(k)\,, \tag{18}$$

where the $j$ component of the vector takes the form:

$$\hat{w}_{np,\,j}(k) = \frac{\sum\limits_{i=1}^{k} w_j(i) K_j\left(\dfrac{k-i+1}{h_{i,\,j}}\right)}{\sum\limits_{i=1}^{k} K_j\left(\dfrac{k-i+1}{h_{i,\,j}}\right)}\,. \tag{19}$$

In formula (19), $K_j(\cdot)$ is a kernel function, $h_{i,\,j}$ is a bandwidth parameter. We use the Gaussian kernels, and the bandwidths calculated by the cross-validation method [11].

## 4. Simulations

Apply the filtering algorithm using nonparametric estimates, i.e., (3)–(6) and (18), to the model of the second order (1) and to the observations (2) with the parameters:

$$A = \begin{pmatrix} 0 & 1 \\ 0.05 & 0.9 \end{pmatrix},\ B = \begin{pmatrix} 1.0 & 0 \\ 0 & 1.0 \end{pmatrix},\ r = \begin{pmatrix} 5 \\ 2 \end{pmatrix},\ Q = \begin{pmatrix} 0.01 & 0 \\ 0 & 0.02 \end{pmatrix},$$

$$V = \begin{pmatrix} 0.8 & 0 \\ 0 & 1.2 \end{pmatrix},\ H = \begin{pmatrix} 1.0 & 0 \\ 0 & 1.0 \end{pmatrix},\ P_0 = \begin{pmatrix} 1.0 & 0 \\ 0 & 1.0 \end{pmatrix},$$

$$C = \begin{pmatrix} 1.0 & 0 \\ 0 & 1.0 \end{pmatrix},\ D = \begin{pmatrix} 0 & 0 \\ 0 & 0 \end{pmatrix},\ \bar{x}_0 = \begin{pmatrix} 5 \\ 2 \end{pmatrix}.$$

By the simulations, the proposed algorithms are compared with the algorithms using the LSM estimates from [3, 4]. These comparisons are given in Figures 1–4:

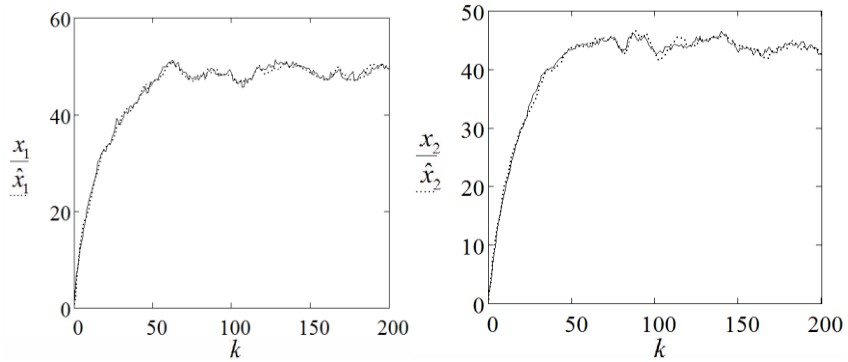

Fig. 1. The dependence on the components of state vectors and the nonparametric estimates of these components (3)–(6), (18)

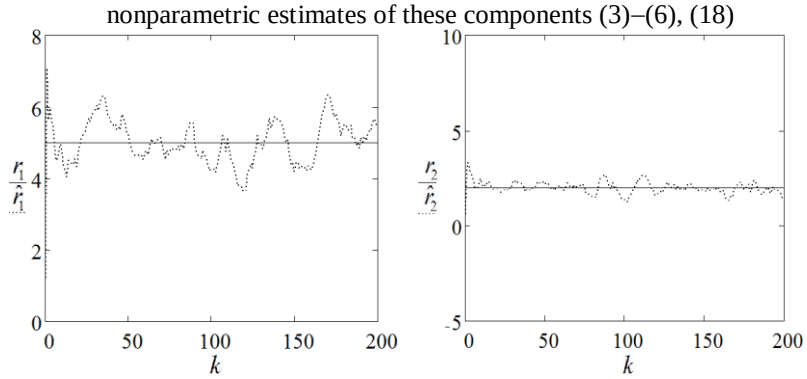


Fig. 2. The estimation of the unknown inputs by nonparametric algorithms (3)–(6), (18)

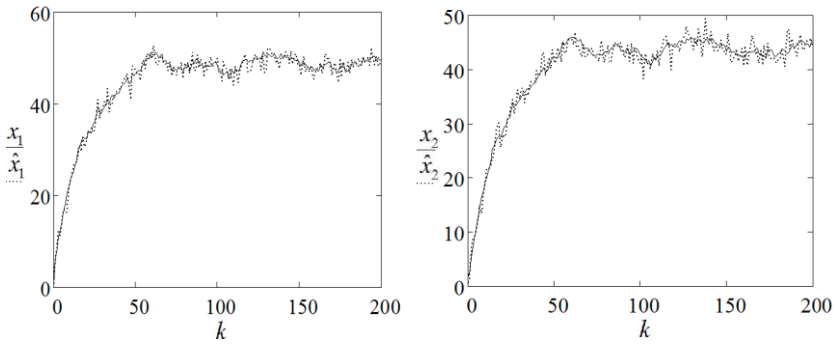


Fig. 3. The dependence on the components of state vectors and the LSM estimates of these components from the papers [3, 4]

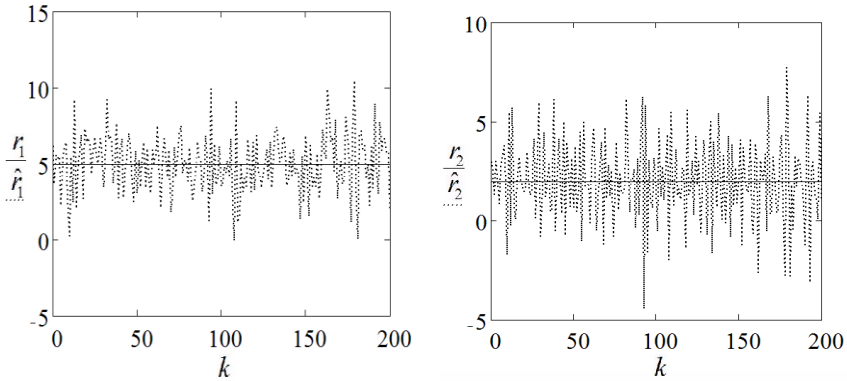


Fig. 4. The estimation of the unknown inputs by the LSM estimates from the papers [3, 4]

In Tables 1 and 2, the standard errors of estimation

$$\sigma_{x,i} = \frac{\sqrt{\sum_{k=1}^{N} (x_i(k) - \hat{x}_i(k))^2}}{N-1},$$

$$\sigma_{r,i} = \frac{\sqrt{\sum_{k=1}^{N} (r_i(k) - \hat{r}_i(k))^2}}{N-1}, \; i = \overline{1,2},$$

are given for two filtering algorithms ($N = 200$) by averaging 50 realizations.

Table 1. Standart Errors for Filtering Algorithm with Using Nonparametric Estimates

| $\sigma_{x,1}$ | $\sigma_{x,2}$ | $\sigma_{r,1}$ | $\sigma_{r,2}$ |
|---|---|---|---|
| 0.885 | 0.945 | 0.751 | 0.449 |

Table 2. Standart Errors for Filtering Algorithms with Using the LSM-estimates

| $\sigma_{x,1}$ | $\sigma_{x,2}$ | $\sigma_{r,1}$ | $\sigma_{r,2}$ |
|---|---|---|---|
| 1.348 | 1.514 | 2.014 | 2.082 |

## 5 Conclusion

In this paper, we deal with two-step algorithm of the Kalman filtering for systems with unknown input. The proposed method has been verified by the simulations study. Figures show that the filtering procedures, using nonparametric estimates, have the advantages in the accuracy in comparison with the known algorithms using LSM-estimates (cf. Fig. 1 and 3, Fig. 2 and 4, Table 1 and 2).

## References

1. Kalman, R.E. and Busy, R. A new results in linear filtering and prediction theory. *Trans. ASME J. Basic Engr.* 83, 95–108 (1961)
2. Astrom, K. and Eykhoff, P. System identification – A survey. *Automatica*. **7**, 123-162 (1971)

3. Janczak, D. and Grishin, Y. State Estimation of Linear Dynamic System with Unknown Input and Uncertain Observation Using Dynamic Programming. *Control and Cibernetics*. **35**, 4, 851–862 (2006)
4. Gillijns, S. and Moor, B. Unbiased minimum-variance input and state estimation for linear discrete-time systems. *Automatica*. **43**, 111–116 (2007)
5. Hsien, C.-S. On the Optimal of Two-Stage Kalman Filter for Systems whis Unknown Input. *Asian Journal of Control*, **12**, 4, 510–523 (2010)
6. Darouach, M., Zasadzinski, M. and Xu S. J. Full-order observers for linear systems with unknown inputs. *IEEE Trans. on Automat. Contr*. **39**, 606–609 (1994)
7. Hou, M., Patton, R. Optimal filtering for systems with unknown inputs. *IEEE Trans. on Automat. Contr*. **43**, 445–449 (1998)
8. Smagin, S.V. Filtering in linear discrete systems with unknown perturbartion. *Optoelectronic, Instrumentation and Data Processing*. **45**, 6, 513–519 (2009)
9. Witczak, M. Fault diagnosis and fault-tolerant control strategies for non-linear systems. Chapter 2. Unknown input observers and filters. *Lecture Notes in Electrical Engineering. Springer International Publishing, Switzerland*, 9-56 (2014)
10. Dobrovidov, A., Koshkin, G., and Vasiliev, V. Non-Parametric State Space Models. *Heber, UT 84032, USA. Kendrick Press, Inc.* (2012)
11. Leung, D. Cross-validation in nonparametric regression with outliers. *Annals of Statistics.* **33,** 2291–2310 (2005)

# Estimating Multi-Factor Discretely Observed Vasicek Term Structure Models with non-Gaussian Innovations

Takayuki Shiohama

Department of Management Science, Faculty of Engineering, Tokyo University of Science, Tokyo, Japan
(E-mail: shiohama@ms.kagu.tus.ac.jp)

**Abstract.** In this paper, we propose a multi-factor model in which discretely observed short-term interest rates follow a non-Gaussian and dependent process. The state-space formulation has the advantage of taking into account the cross-sectional as well as time-series restrictions on data and measurement errors in the observed yield curve. We clarify the non-Gaussian and dependent processes of short-term interest rate dynamics and show that these features are important to capture the dynamics of the observed yield curve.
**Keywords:** Asymptotic expansion, state-space model, term structure model, Vasicek model.

## 1 Introduction

The term structure of interest rates describes the relationship between the yield on a zero-coupon bond and its maturity. Understanding the dynamics of bond yields plays a critical role in monetary policy, derivative pricing and forecasting, and risk-management analysis. We need to accurately understand the term structure of interest rates to evaluate the prices of interest rate derivatives. A number of theoretical term structure models have been proposed in the literature. The early models that are still widely used include the ones proposed by Vasicek[10] and Cox *et al.*[4].

Although single-factor Vasicek models have been widely used in the theoretical literature, empirical research has shown that they fail to appropriately capture the behavior of short-term interest rates. The aim of this paper is to develop a closed-form valuation for pricing the zero-coupon bonds of multi-factor Vasicek term structure models wherein innovations of the underlying short-term interest rates follow non-Gaussian and dependent processes. Honda *et al.*[7] and Shiohama and Tamaki[9] consider the higher-order asymptotic valuation and European call options for zero-coupon bonds by using single-factor discretely observed Vasicek models with a non-Gaussian and dependent error

*Stochastic Modeling, Data Analysis and Statistical Applications* (*pp.* 145-154)
Lidia Filus - Teresa Oliveira - Christos H Skiadas (Eds)



structure. Miura *et al.*[8] develop a closed-form valuation for pricing defaultable bonds incorporating a stochastic risk-free interest rate and defaultable intensity having non-Gaussian and dependent processes.

This paper is organized as follows: Section 2 describes the multi-factor term structure model based on the discretely sampled Vasicek model with non-Gaussian innovation and presents the analytic expression for the approximate zero-coupon bond prices. Section 3 discusses the state-space formulation of the model and the estimation procedures. Section 4 presents the data used and illustrates the empirical results of the proposed models. Finally, some conclusions are offered in Section 5.

## 2 Multi-Factor Models

The model used for analysis is the discretely sampled short-term interest rates model with interval $\Delta$. We assume that the spot interest rate is the sum of $K$ state variables $X_{j,t}$,

$$r_t = \sum_{j=1}^{K} X_{j,t},$$

and that the state variables are driven by non-Gaussian and dependent innovations. Such models are considered in Honda *et al.*[7], Shiohama and Tamaki [9], and Miura *et al.*[8]. Each factor $X_{j,t}$ is of the form

$$X_{j,t} - X_{j,t-1} = \kappa_j(\mu_j - X_{j,t-1})\Delta + \Delta^{1/2} Z_{j,t}, \quad j = 1, \ldots, K, \tag{1}$$

where $Z_{j,t}$ is independent such that $E[Z_{i,t}Z_{j,t}] = 0$ for $i \neq j$, $\mu_j$ is the long-term mean of $X_{j,t}$, and $\kappa_j$ represents the mean of reversion parameters. The innovations $\{Z_{j,t}\}$ are fourth-order stationary in the following sense.

**Assumption 1** *For $j \in \{1, 2, \ldots, K\}$, the process $\{\boldsymbol{Z} = (Z_{1,t}, \ldots, Z_{K,t})'\}$ is fourth-order stationary in the sense that*

1. $E[Z_{j,t}] = 0$,
2. $cum(Z_{j,t}, Z_{j,t+u}) = c_{Z_j}(u)$,
3. $cum(Z_{j,t}, Z_{j,t+u_1}, Z_{j,t+u_2}) = c_{Z_j}(u_1, u_2)$,
4. $cum(Z_{j,t}, Z_{j,t+u_1}, Z_{j,t+u_2}, Z_{j,t+u_3}) = c_{Z_j}(u_1, u_2, u_3)$.

**Assumption 2** *The $k$-th order cumulants $c_{Z_j}(u_1, \ldots, u_{k-1})$ of $Z_{j,t}$, $j = 1, \ldots, K$, for $k = 2, 3, 4$ satisfy*

$$\sum_{u_1, \cdots, u_{k-1} = -\infty}^{\infty} |c_{Z_j}(u_1, \ldots, u_{k-1})| < \infty.$$

Assumptions 1 and 2 are satisfied by a wide class of time-series models containing univariate autoregressive-moving-average (ARMA) and generalized autoregressive conditional heteroskedastic (GARCH) processes.

Hereafter, we assume that the current time is set at $t = 0$ and that the initial factors $X_{j,0}$ are observable and fixed. Then, $r_t$ is discretely sampled at times $0, \Delta, 2\Delta, \ldots, n\Delta(\equiv T)$ over $[0, T]$. For notational convenience, we use the following notation. Assume that

$$A_{j,u} = \mu_j(u\Delta - B_{j,u}), \qquad B_{j,u} = \frac{1}{2\kappa_j}(1+\upsilon_j)(1-\upsilon_j^u),$$
$$a_{j,u} = \frac{2}{\kappa_j \Delta}\left\{1 - \frac{1}{2}\upsilon_j^{u-1}(1+\upsilon_j)\right\},$$

where $\upsilon_j = 1 - \kappa_j\Delta$ for $j = 1, \ldots, K$ and $u = 1, \ldots, n$. Then, from Honda *et al.*[7], it follows that

$$P(0,T) = E_0^Q\left[\exp\left(-\int_0^T r_t dt\right)\right] = E_0^Q\left[\exp\left(-\sum_{j=1}^K \int_0^T X_{j,t} dt\right)\right]$$
$$= \prod_{j=1}^K E_t^Q\left[\exp\left(\int_0^T X_{j,t} dt\right)\right] \approx \prod_{j=1}^K E_0^{\tilde{Q}}\left[\exp\left\{-\Delta\left(\frac{1}{2}r_0 + \sum_{u=1}^{n-1} r_u + \frac{1}{2}r_n\right)\right\}\right]$$
$$= \prod_{j=1}^K \exp(-A_{j,n} - B_{j,n} r_0) AF_{j,n}$$

where $E_0^{\tilde{Q}}$ represents the expectation under an asymptotic risk-neutral measure, which is discussed in Miura *et al.*[8], and

$$AF_{j,n} = E_0^{\tilde{Q}}\left[\exp\left(-\frac{\Delta^{3/2}}{2}\sum_{u=1}^n a_{j,u} Z_{j,n-u+1}\right)\right]. \tag{2}$$

Assume further that

$$Y_{j,n} = \Delta^{1/2}\sum_{u=1}^n b_{j,u} Z_{j,n-u+1} \quad \text{and} \quad b_{j,u} = \frac{\Delta}{2}a_{i,j} = \frac{1}{\kappa_j}\left\{1 - \frac{1}{2}\upsilon_j^{u-1}(1+\upsilon_j)\right\}. \tag{3}$$

From process $\{Y_{j,n}\}$, we express the product of the $AF_{j,n}$ terms as

$$\prod_{j=1}^K AF_{j,n} = E_0^{\tilde{Q}}\left[\exp\left(-\sum_{j=1}^K Y_{j,n}\right)\right].$$

We give an analytic approximation of the zero-coupon bond prices for multi-factor discretely observed Vasicek term structure models with non-Gaussian and dependent innovations by the Edgeworth expansion of the joint density function of $\boldsymbol{Y}_n = (Y_{1,n}, \ldots, Y_{K,n})'$. It is clear that the processes $\{Y_{j,n}\}$, $j = 1, \ldots, K$ are fourth-order stationary with $\mathrm{Var}(Y_{j,n}) = \sigma_{j,n}^2$; the third- and fourth-order cumulants are denoted respectively as

$$\mathrm{cum}(Y_{j,n}, Y_{j,n}, Y_{j,n}) = n^{-1/2} C_{Y_j}^{(3)} \quad \text{and} \quad \mathrm{cum}(Y_{j,n}, Y_{j,n}, Y_{j,n}, Y_{j,n}) = n^{-1} C_{Y_j}^{(4)}.$$

Now, we have the following assumption.

**Assumption 3** *The $J$-th order ($J \geq 5$) cumulants of $\{Y_{j,n}\}$, $j = 1, \ldots, K$ are of the order $O(n^{-J/2+1})$.*

Since this model is calibrated to the market interest rates, we need to include the risk premium before pricing the zero-coupon bonds. We assume that the $j$-th factor's market price of risk $\lambda_j$ is constant, and we and define $\bar{\mu}_j = \mu_j - \lambda_i \sigma_{X_j}/\kappa_j$.

From the asymptotic expansion of the defaultable bond price of Miura *et al.*[8], we derive the following formula for the nominal price of a pure discount bond with face value 1 maturing at time $T$.

**Theorem 1** *From Assumptions 1–3, we express the current bond price of the $K$-factor discretely observed Vasicek term structure model as*

$$P(0,T) = \exp\left(A(T) - \sum_{j=1}^{K} B_{j,n} X_{j,0}\right) D(T) \tag{4}$$

*where*

$$A(T) = \sum_{j=1}^{K} A_{j,n} = \sum_{j=1}^{K} \left[-\bar{\mu}_j (n\Delta - B_{j,n}) + \frac{1}{2}\sigma_{j,n}^2\right],$$

$$D(T) = \prod_{j=1}^{K} \exp\left(-\frac{1}{6\sqrt{n}} C_{Y_j}^{(3)} + \frac{1}{24n} C_{Y_j}^{(4)}\right),$$

$$B_{j,n} = \frac{1}{2\kappa_j}(2 - \kappa_j\Delta)(1 - (1 - \kappa_j\Delta)^n).$$

We omit the proof of Theorem 1 since it is analogous to the results obtained in Honda *et al.*[7] and Miura *et al.*[8].

The analytic expressions given in Theorem 1 for the bond price and yield are based on the discrete time models with non-Gaussian and dependent innovations. From these expressions, the linkage between continuous and discrete schemes for short-term interest rate models is apparent. If $Z_{j,t}$s have a standard normal distribution, since $\Delta \to 0$, the bond price tends toward standard multi-factor Vasicek term structures.

## 3 State-Space Representation and Estimation

The application of Kalman filtering methods in the estimation of term structure models using cross-sectional and time-series data has been investigated by Duan and Simonate[5], Chen and Schott[3], and Babbs and Nowman[1,2].

We estimate the model by using the state-space representation of term structure models with non-Gaussian innovations. Our proposed model is a discrete scheme with non-Gaussian innovations and hence the corresponding state-space model is also non-Gaussian, although Kalman filtering can still be applied to obtain the approximate moments of the model and the resulting filter is quasi-optimal.

Let $R_t(\tau)$ denote a continuously compounded yield on a zero-coupon bond of maturity $\tau$ with corresponding discrete sample size $\tau/\Delta = n$. The state-space formulation of the model consists of measurement and transition equations. To construct a measurement equation, we need $N$ zero-coupon rates and use the following relationship between zero-coupon yield and the price of zero-coupon bonds:

$$R_t(\tau) = -\frac{\ln P(0,\tau)}{\tau} = -\frac{1}{\tau}\left((A(\tau) + \ln D(\tau)) - \sum_{i=1}^{K} B_{j,n} X_{j,n}\right).$$

Then, the measurement equation has the following form with $K = 3$

$$\begin{bmatrix} R_t(\tau_1) \\ R_t(\tau_2) \\ \vdots \\ R_t(\tau_N) \end{bmatrix} = \begin{bmatrix} -\frac{A(\tau_1)-\ln D(\tau_1)}{\tau_1} \\ -\frac{A(\tau_2)-\ln D(\tau_2)}{\tau_2} \\ \vdots \\ -\frac{A(\tau_N)-\ln D(\tau_N)}{\tau_N} \end{bmatrix} + \begin{bmatrix} \frac{B_{1,n_1}}{\tau_1} & \frac{B_{2,n_1}}{\tau_1} & \frac{B_{3,n_1}}{\tau_1} \\ \frac{B_{1,n_2}}{\tau_2} & \frac{B_{2,n_2}}{\tau_2} & \frac{B_{3,n_2}}{\tau_2} \\ \vdots & \vdots & \vdots \\ \frac{B_{1,n_N}}{\tau_N} & \frac{B_{2,n_N}}{\tau_N} & \frac{B_{3,n_N}}{\tau_N} \end{bmatrix} \begin{bmatrix} X_{1,t} \\ X_{2,t} \\ X_{3,t} \end{bmatrix} + \begin{bmatrix} \varepsilon_{t,1} \\ \varepsilon_{t,2} \\ \vdots \\ \varepsilon_{t,N} \end{bmatrix},$$

or

$$\boldsymbol{R}_t = \boldsymbol{A}(\boldsymbol{\Psi}) + \boldsymbol{H}(\boldsymbol{\Psi})\boldsymbol{X}_t + \boldsymbol{\varepsilon}_t,$$

where $\boldsymbol{\Psi}$ denotes the unknown parameter vectors to be estimated and $\boldsymbol{\varepsilon}_t \sim N(\boldsymbol{0}, \boldsymbol{V}_\varepsilon)$ with $\boldsymbol{V}_\varepsilon = \mathrm{diag}(h_1^2, \ldots, h_N^2)$.

To obtain the transition equation for the state-space model, we need the conditional mean and variance of the state variable process. From the recursive substitution in (1) and because $v_j = 1 - \kappa_j \Delta$, $X_{j,n}$ can be represented as

$$X_{j,n} = (1 - v_j^n)\bar{\mu}_j + v_j^n X_{j,0} + \Delta^{1/2} \sum_{u=1}^{n} v_j^{u-1} Z_{j,n-u+1}.$$

For simplicity, we assume that sequence $\{Z_{j,n}\}$ is i.i.d. with zero mean and finite variance $\sigma_{Z_j}^2$. Then, the variance of $X_{j,n}$ becomes

$$\sigma_{X_j}^2 = \sigma_{Z_j}^2 \left[\frac{1 - v_j^{2(n-1)}}{2\kappa_j - \kappa_j^2 \Delta}\right]. \tag{5}$$

The exact discrete-time model is a VAR(1), and the transition system is as follows:

$$\begin{bmatrix} X_{1,t} \\ X_{2,t} \\ X_{3,t} \end{bmatrix} = \begin{bmatrix} \bar{\mu}_1\kappa_1\Delta \\ \bar{\mu}_2\kappa_2\Delta \\ \bar{\mu}_3\kappa_3\Delta \end{bmatrix} + \begin{bmatrix} 1-\kappa_1\Delta & 0 & 0 \\ 0 & 1-\kappa_2\Delta & 0 \\ 0 & 0 & 1-\kappa_3\Delta \end{bmatrix} \begin{bmatrix} X_{1,t-1} \\ X_{2,t-1} \\ X_{3,t-1} \end{bmatrix} + \begin{bmatrix} \eta_{t,1} \\ \eta_{t,2} \\ \eta_{t,3} \end{bmatrix},$$

or

$$\boldsymbol{X}_t = \boldsymbol{C}(\boldsymbol{\Psi}) + \boldsymbol{F}(\boldsymbol{\Psi})X_{t-1} + \boldsymbol{\eta}_t(\boldsymbol{\Psi})$$

where $\eta_t \sim N(\boldsymbol{0}, \boldsymbol{V}_\eta)$ with $\boldsymbol{V}_\eta = \mathrm{diag}(\sigma_{X_1}^2, \sigma_{X_2}^2, \sigma_{X_3}^2)$.

Since our models are in state-space form, we can construct Kalman filtering for the three-factor model in which we want to minimize the mean squared error between $R_t(\tau_i)$ and $\widehat{R_t}(\tau_i)$.

**Example** Assume that $\{Z_{j,t}\}$ follows a GARCH(1,1) process

$$Z_{j,t} = h_{t,j}^{1/2}\varepsilon_{j,t}, \quad h_{j,t} = \omega_j + \alpha_j Z_{j,t-1}^2 + \beta_j h_{j,t-1},$$

where $\{\varepsilon_{t,j}\}$ follows a sequence of i.i.d. standard normal random variables. The parameter values must satisfy $\omega_j > 0$, $\alpha_j, \beta_j \geq 0$, $\alpha_j + \beta_j < 1$, and $1 - 2\alpha_j^2 - (\alpha_j + \beta_j)^2 > 0$. Thus, $\sigma_{X_j}^2$ in (5) would become

$$\sigma_{X_j}^2 = \frac{\omega_j}{1 - \alpha_j - \beta_j}\left[\frac{1 - v_j^{2(n-1)}}{2\kappa_j - \kappa_j^2\Delta}\right].$$

Furthermore, $C_{Y_j}^{(3)}$ and $C_{Y_j}^{(4)}$ in the definition of $D(T)$ in Theorem 1 would become

$$C_{Y_j}^{(3)} = 0,$$
$$C_{Y_j}^{(4)} = \frac{3}{n}\int_{-\pi}^{\pi} |B_{j,2}(\lambda)^2| f_{Z_j^2}(\lambda)\mathrm{d}\lambda - 2\frac{3\{(1-(\alpha_j+\beta_j)^2)\}}{1-(\alpha_j+\beta_j)^2-2\alpha_j^2}\frac{1}{n}\sum_{u=1}^{n} b_{j,u}^4,$$

where $B_2(\lambda) = \sum_{u=1}^{n} b_{j,u}^2 e^{\boldsymbol{i}j\lambda}$ and

$$f_{Z_j^2}(\lambda) = \frac{\sigma_{\nu_j}^2}{2\pi}\frac{1 + \beta_j^2 - 2\beta_j\cos\lambda}{1 + (\alpha_j+\beta_j)^2 - 2(\alpha_j+\beta_j)\cos\lambda}$$

with

$$\sigma_{\nu_j}^2 = \frac{2\omega_j^2(1+\alpha_j+\beta_j)}{\{1-(\alpha_j+\beta_j)\}\{1-2\alpha_j^2-(\alpha_j+\beta_j)^2\}}.$$

From this parametrization in state-space representation, we can explicitly estimate the GARCH(1,1)-driven multi-factor term structure models.

## 4 Data Analysis

The data used in this study consist of zero-coupon adjusted Japanese Government Bond (JGB) yields obtained from Bloomberg. We use weekly sampled data that are set $\Delta = 1/52$. The data cover the period October 1, 1999, to December 27, 2013, with a total of $T = 744$ observations. The maturities included are 1/4, 1/2, 1,2,3,4,5,6,7,8,9,10,15,20, and 30 years, that is, a total of $N = 15$ different maturities. We discuss the application of Kalman filtering to one-, two-, and three-factor models with discretely observed non-Gaussian innovations. For a fair comparison, we also estimate the corresponding multi-factor Vasicek term structure models.

| | Vasicek model (a) | | | non-Gaussian model (b) | | | Difference(%) (b)/(a)-1 | | |
|---|---|---|---|---|---|---|---|---|---|
| | $K=1$ | $K=2$ | $K=3$ | $K=1$ | $K=2$ | $K=3$ | $K=1$ | $K=2$ | $K=3$ |
| 3 Month | 31.84 | 2.94 | 1.88 | 28.83 | 4.11 | 1.67 | -9.43 | 39.81 | -11.03 |
| 6 Month | 27.61 | 0.93 | 0.63 | 28.20 | 1.78 | 0.57 | 2.12 | 90.58 | -9.76 |
| 1 Year | 22.57 | 1.29 | 1.23 | 23.16 | 1.20 | 1.23 | 2.64 | -6.45 | -0.31 |
| 2 Year | 15.35 | 5.25 | 3.48 | 13.67 | 3.37 | 3.10 | -10.97 | -35.77 | -10.94 |
| 3 Year | 12.13 | 7.48 | 3.59 | 9.34 | 4.71 | 3.40 | -23.05 | -37.10 | -5.38 |
| 4 Year | 10.49 | 7.87 | 3.33 | 8.35 | 5.72 | 3.21 | -20.41 | -27.34 | -3.73 |
| 5 Year | 11.03 | 7.64 | 3.15 | 9.74 | 6.25 | 3.10 | -11.66 | -18.28 | -1.44 |
| 6 Year | 13.34 | 7.87 | 3.77 | 12.73 | 6.12 | 3.65 | -4.58 | -22.21 | -3.26 |
| 7 Year | 15.17 | 7.56 | 4.79 | 15.22 | 6.06 | 4.66 | 0.29 | -19.80 | -2.82 |
| 8 Year | 19.59 | 9.09 | 6.71 | 19.76 | 7.14 | 6.57 | 0.89 | -21.39 | -2.17 |
| 9 Year | 19.47 | 7.56 | 5.94 | 19.37 | 6.39 | 5.89 | -0.52 | -15.39 | -0.77 |
| 10 Year | 18.29 | 6.78 | 5.36 | 17.84 | 6.34 | 5.39 | -2.43 | -6.43 | 0.52 |
| 15 Year | 13.02 | 10.73 | 10.73 | 14.84 | 13.44 | 11.04 | 14.03 | 25.22 | 2.95 |
| 20 Year | 20.34 | 12.61 | 6.03 | 20.88 | 14.54 | 6.12 | 2.70 | 15.33 | 1.57 |
| 30 Year | 33.38 | 27.95 | 6.88 | 33.51 | 22.86 | 7.15 | 0.41 | -18.22 | 4.05 |
| Total | 283.61 | 123.54 | 67.50 | 275.45 | 110.03 | 66.75 | -2.88 | -10.93 | -1.11 |

**Table 1.** Sum of squared errors with different maturities and models

Table 1 gives the sum of the squared errors for the estimated models with various maturities. For the bond yield with maturity $\tau_i$, the entry in the cell is

$$SSE(\tau_i) = \sum_{t=1}^{T} (R_t(\tau_i)^{(obs)} - \widehat{R}_t(\tau_i)^{(model)})^2,$$

and the total mean squared error is calculated as

$$Total\ SSE = \sum_{i=1}^{N} \sum_{t=1}^{T} (R_t(\tau_i)^{(obs)} - \widehat{R}_t(\tau_i)^{(model)})^2.$$

From Table 1, it is clear that the sum of the squared errors is small for non-Gaussian models compared with those corresponding to one-, two-, and three-factor Vasicek models. As the number of factors increase, the calibration errors get smaller. We also observe that non-Gaussian models perform better for maturities not longer than 10 years whereas for longer maturities the Vasicek term structure models perform better. This is because the distribution of $\{Y_{j,n}\}$ tends be normal as the sample size $n$ increases by the Central Limit Theorem. Hence, non-Gaussian modeling is much better for short maturities of bond yields, where the underlying short-term interest rates exhibit highly non-Gaussian behavior.

Table 2 gives the parameter estimation results. As for the sum of long-run mean levels, Vasicek models tend to have quite high levels, with 6.1% for two-factor and 6.3% for three-factor models, whereas those with non-Gaussian models have levels of -2% and 2.6% for two- and three-factor models, respectively. We see that the three-factor models with non-Gaussian innovations can

| Parameter | Vasicek model | | | non-Gaussian model | | |
|---|---|---|---|---|---|---|
| | 1-factor | 2-factor | 3-factor | 1-factor | 2-factor | 3-factor |
| $\mu_1$ | -0.290 | 0.140 | 7.330 | 0.189 | -0.873 | -0.802 |
| $\mu_2$ | | 6.030 | -4.370 | | -1.210 | 2.200 |
| $\mu_3$ | | | 3.350 | | | 1.280 |
| $\lambda_1$ | 2.380 | -2.040 | -0.039 | 2.430 | -12.000 | 8.120 |
| $\lambda_2$ | | 0.909 | 3.010 | | 3.720 | -10.000 |
| $\lambda_3$ | | | 1.800 | | | -0.507 |
| $\kappa_1$ | 0.009 | 0.560 | 0.251 | 0.003 | 0.325 | 0.212 |
| $\kappa_2$ | | 0.094 | 0.396 | | 0.093 | 0.415 |
| $\kappa_3$ | | | 0.009 | | | 0.023 |
| $\sigma_1$ | 0.012 | 0.114 | 0.001 | 0.015 | 0.003 | 0.019 |
| $\sigma_2$ | | 0.085 | 0.003 | | 0.183 | 0.019 |
| $\sigma_3$ | | | 4.27E-04 | | | 0.002 |
| $C_1^{(3)}$ | | | | 0.709 | 2.020 | -0.622 |
| $C_1^{(4)}$ | | | | -0.636 | 7.320 | -0.103 |
| $C_2^{(3)}$ | | | | | -1.480 | -0.451 |
| $C_2^{(4)}$ | | | | | 0.487 | 3.110 |
| $C_3^{(3)}$ | | | | | | 0.999 |
| $C_3^{(4)}$ | | | | | | 2.460 |

**Table 2.** Estimates of one-, two- , and three- factor Vasicek models and non-Gaussian models

appropriately capture the long-run interest rate levels. Most of the estimates for the sum of risk premia are negative. This is because the risk in a bond associate with the spot rate is generally proportional to the sensitivity of bond prices; that is, $\partial P(0,T)/\partial X_{j,0} < 0$.

The effects of skewness on zero-coupon yields can be seen as the parameter values of $C_j^{(3)}$; these values vary from -1.5 to 2.0 for the one-, two-, and three-factor models. From these values, we find that the effect of skewness of the underlying innovation process is small. On the other hand, the effect of kurtosis on zero-coupon yields is apparent for some factors in two- and three-factor models.

The observed term structure of the JGB yield estimated with fitted yield curve and various models are shown in Figure 1. We choose the JGB yield of December 20, 2013, as our example. The figure shows a typical shape for JGB yields under quantitative and qualitative easing policies with low interest rate levels for short maturities. From these two figures, we find the fitting performances of non-Gaussian models superior to those of the Vasicek term structure models.

## 5 Summary and Conclusions

In this paper, we introduced multi-factor discretely observed Vasicek term structure models and presented a method to estimate these models by using the Kalman filter. The advantage of incorporating non-Gaussian effects

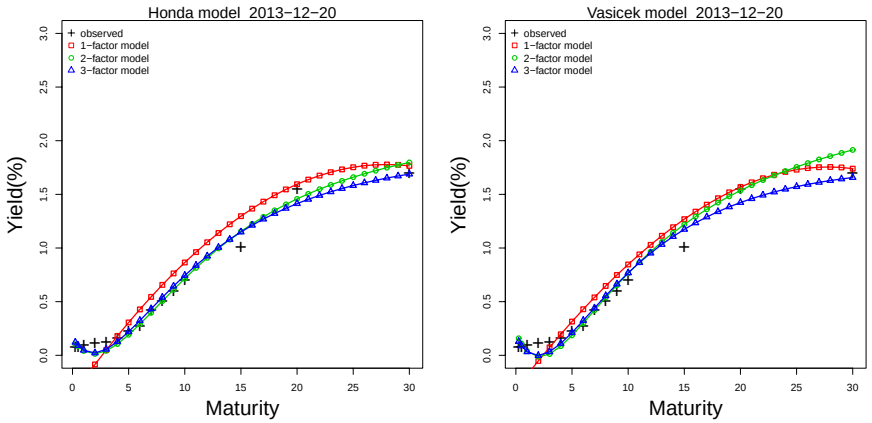


**Fig. 1.** Estimated and observed term structures of Japanese Government bond yields for the non-Gaussian state-space model (left) and the Vasicek model (right) for the one-, two-, and three-facrors.

for short-term interest rate processes becomes clear when we investigate the JGB yield calibration. The following are possible research topics. A particle filtering method may be used to compute the estimates of model parameters as well as state variables. The various interest rate derivatives evaluated using the proposed model may be investigated.

## Acknowledgements

This study was supported by Grant-in-Aid for Scientific Research (C) (40361844) and the Norinchukin Bank and Nochu Information System Endowed Chair of Financial Engineering in the Department of Management Science, Tokyo University of Science.

## References

1. S. H. Babbs and K. B. Nowman. An application of generalized Vasicek term structure models to the UK gilt-edged market: a Kalman filtering analysis. *Applied Financial Economics*, **8**, 637–644, 1998.
2. S. H. Babbs and K. B. Nowman. Kalman filtering of generalized Vasicek term structure models. *Journal of Financial and Quantitative Analysis*, **34**, 115–130, 1999.
3. R. -R. Chen and L. Scott. Maximum likelihood estimation for a multifactor equilibrium model of the term structure of interest rates. *Journal of Fixed Income*. **3**, 14–31, 1993.
4. C. Cox, J. Ingersoll and S. A. Ross. A theory of the term structure of interest rates. *Econometrica*, **53**, 385–407, 1985.

5. J. C. Duan and J.-D. Simonate. Estimating and testing exponential-affine term structure models by Kalman filter. Discussion paper, Centre universitaire de recherche et analyze des organizations (CIRANO), 1995.
6. J. D. Duffie and R. Kan. A yield-factor model of interest rates. *Mathematical Finance*, **6**, 379–406, 1996.
7. T. Honda, K. Tamaki and T. Shiohama. Higher order asymptotic bond price valuation for interest rates with non-Gaussian dependent innovations. *Finance Research Letters*, **7**, 60–69, 2010.
8. M. Miura, K. Tamaki and T. Shiohama. Asymptotic expansion for term structures of defaultable bonds with non-Gaussian dependent innovations. *Asia-Pacific Financial Markets*, **20**, 311–344, 2013.
9. T. Shiohama and K. Tamaki. Asymptotic expansion for interest rates with non-Gaussian dependent innovations. In Nishiyama, Y. (Ed.), *Interest rates: Term structure models, monetary policy, and prediction*. New York: Nova Science Publishers, 19–61, 2012.
10. O. Vasicek. An equilibrium characterization of the term structure. *Journal of Financial Economics*, **5**, 177–188, 1977.

# 4 CHAPTER

## Data Analysis

# The Study of Correlation Dimension of the EEG Signals in a State of Meditation by means of Empirical Mode Decomposition

Ludmila A. Dmitrieva[1,2], Igor E. Kanunikov[2,3], Maria N. Krivoshapova[4], Yuri A. Kuperin[1,2], Nikolai M. Smetanin[1], Maria A. Shaptiley[4]

[1] Department of Physics, Saint-Petersburg State University, Ulyanovskaya Str., 3, 198504, Saint-Petersburg, Russia
(E-mails: madam.mila-dmitrieva@yandex.ru, yuri.kuperin@gmail.com, smt0@bk.ru)

[2] Department of Liberal Arts and Sciences, Saint-Petersburg State University, Galernaya Str., 58-60, 199000, Saint-Petersburg, Russia
(E-mails: madam.mila-dmitrieva@yandex.ru, yuri.kuperin@gmail.com, smt0@bk.ru)

[3] Department of Biology, Saint-Petersburg State University, University Embankment, 7/9, 199034, Saint-Petersburg, Russia
(E-mail: igorkan@mail.ru)

[4] Scientific Research Center of Health "Exyclub", Saint-Petersburg, Russia
(E-mails: krivmn@gmail.com, shaptileym@gmail.com)

**Abstract.** The aim of this work was to develop an indicator for finding differences in the multichannel EEG of experienced and inexperienced subjects in the states of meditation and rest. As such an indicator, we have chosen the difference between the correlation dimensions of the EEG channels reconstructed attractors and the corresponding EMD-filtered correlation dimensions (we denote this difference as DifD2). Under the EMD- filtered EEG correlation dimension here we understand the correlation dimension calculated from EEG signal, in which the first two modes of empirical decomposition (EMD) are dropped. The authors previously showed that the sum of the first two EMD-modes of EEG are stochastic components (both physical and physiological noise). Thus, the smaller the difference DifD2, the less noise in the EEG signals. Calculations were performed for 5 experienced and 5 inexperienced subjects in the states of meditation and rest. Unfiltered correlation dimensions were calculated in the embedding dimension equal to 5. EMD-filtered correlation dimensions are calculated in the embedding dimension equal to 4. Then obtained results of calculations were processed by standard statistical method "Repeated ANOVA". It turned out that DifD2 in a state of meditation for experienced subjects was significantly lower than that of the inexperienced subjects. This distinction is achieved mainly due to the frontal and parietal channels. For experienced subjects the difference DifD2 in the meditation state turned out to be significantly lower than that in the rest state. This difference is achieved by the parietal and occipital channels. Neurophysiologic explanations of the obtained results will be presented in this paper.

**Keywords:** correlation dimension, empirical mode decomposition (EMD), EMD-filtered correlation dimensions, meditation, indicator DifD2.

*Stochastic Modeling, Data Analysis and Statistical Applications* (*pp*. 157-169)
Lidia Filus - Teresa Oliveira - Christos H Skiadas (Eds)



## 1 Introduction

In this paper we investigate the multichannel electroencephalograms (EEG) in an altered state of consciousness of subjects, namely, in meditation. Description of this state of consciousness is presented below. The main objective of the work is the following. Based on nonlinear dynamics methods to find sustainable quantitative characteristics that distinguishes the EEG in meditation and the normal state of the human brain (in the rest). To achieve this goal we applied multifractal analysis and study of the reconstructed attractors properties corresponding to the time series of multi-channel EEG. In particular we assessed and analyzed the correlation dimensions of the reconstructed attractors depending on the embedding dimension in the lag space. The basis of our method is based on calculation of the difference between the usual correlation dimension and the so-called filtered correlation dimension. This difference was considered as a quantitative indicator which allows to discriminate between different states of consciousness (meditation and rest). The main hypothesis of the study is that this indicator is robust and sensitive to the different states of consciousness and different experience of meditation practice of subjects. It should be noted that over the past 50 years, various meditative states are in the interests of physiologists, psychologists and clinicians. There is a considerable amount of work devoted to the study of meditation using EEG (see for example Cahn and Polich [1]). At the same time, in most studies the main method for studying EEG in meditation is the Fourier spectral analysis, which, is known to be the linear method. However, it is well known that the EEG time series are nonlinear. Therefore, the linear method of Fourier analysis is not able to extract from the EEG records some complex nonlinear properties. There are only few amount of studies of states of meditation with the use of nonlinear dynamics, as the author knows, though recently such methods become increasingly popular in the study of EEG, for example for people suffering from epilepsy. Examples of works in which the nonlinear dynamics methods were used to study meditation are Aftanas and Golocheikine [2], Natarajan *at al.*[3], Goshvarpour [4]. The most interesting work is Goshvarpour [4], where the correlation dimensions of the EEG series were calculated. However, unlike the present work, the resulting estimates are not explicitly compared for various conditions and subjects, and only fed to the input of a variety of classifiers.

If we consider the classification given in Lutz *at al*. [10], where there are two main directions in meditation techniques - meditation with the focus of attention (focused attention, FA-meditation) and meditation free perception (open monitoring, OM-meditation). Technique that was used to create a database of EEG in the present paper can be attributed to OM-meditation.

## 2 Description of the multifractal methods

This section provides a brief overview of the theory of methods of nonlinear dynamics used in this paper. More information about the theoretical foundations

can be found in the books Mandelbrot [5], Bozhokin and Parshin [6], Shuster [7].

First, we give the definition of a fractal and multifractal. As fractals one call geometric objects: line, surface, spatial body with highly rugged shape and have the property of self-similarity under scaling transformation. In a broader sense, fractals can be understood as a set of points in Euclidean space with fractional Hausdorff dimension which is strictly less than the topological dimension of the embedding space for fractal (Mandelbrot [5]). Multifractal is a heterogeneous fractal that can be determined not by a single construction algorithm but by several successive algorithms. Each of them generates a pattern with its own fractal dimension.

For discrete time series the concept of the reconstructed attractor (Shuster [7]) is introduced. Namely, suppose we have a time series $\{x_t\}_{t=1}^{N}$, which appears as observed realization of one of the variables describing the dynamic system. We construct a set of vectors, $z_m(t) = \left( x_t, \quad x_{t-\tau}, \quad ..., \quad x_{t-\tau(m-1)} \right)$, where the parameter $\tau$ is called the lag, and $m$ is embedding dimension. The resulting set of vectors will define a certain set of points in $m$-dimensional space, which is called the lag space. If the points are concentrated near some hypersurface of codimension 1, 2, , m-1 then this hypersurface is called reconstructed attractor.

An important fact in the study of the reconstructed attractor is the Takens theorem (Shuster [7]) which states that the real attractor in d - dimensional phase space of the dynamical system and the reconstructed attractor in m - dimensional lag space are related by reversible differentiable mapping. Thus both attractors are topologically equivalent and, in particular, have identical fractal characteristics. The Takens theorem thus allows us to study the properties of attractors of dynamical system even in the case where a dynamic system that produced the analyzed time series is unknown.

To describe the multifractal quantitatively one usually calculates the multifractal spectrum (Legendre spectrum), which includes a number of fractal dimensions which are inherent elements of any multifractal (Bozhokin and Parshin [6]). To determine the correlation dimension of the multifractal reconstructed attractor we define coverage of studied set by m-dimensional cubes with edges of size $\varepsilon$. Then, for each cube of coverage, we calculate the probability $p_i(\varepsilon)$ of falling multifractal points in the cube with the number $i$. Further, for any integer $q$ one can define the generalized Renyi dimensions by the following relation:

$$D_q = \lim_{\varepsilon \to 0} \frac{1}{q-1} \frac{\ln \sum_{i=1}^{N(\varepsilon)} p_i^q}{\ln \varepsilon} \tag{1}$$

Obviously, certain defined Renyi dimensions $D_q(\tau, m)$ depend not only on $q$, but also on the reconstruction parameters $\tau$ and $m$. Dimension $D_2$ is called correlation dimension, since it is determined by the correlation between points in one cell of the partition. From (1) we obtain an expression for the correlation dimension:

$$D_2(\tau, m) = \lim_{\varepsilon \to 0} \frac{\ln \sum_{i=1}^{N(\varepsilon)} p_i^2}{\ln \varepsilon} \tag{2}$$

There are various algorithms to select the optimal lag $\tau$. The simplest is the construction of the autocorrelation function for the time series $\{x_t\}_{t=1}^N$. Then, according to Shuster [7] the optimal value for $\tau$ is the smallest lag corresponding to the first zero of the autocorrelation function. Thus, we can fix one parameter $\tau$ and consider the dependence of $D_2(m)$ for the reconstructed attractor of the time series $\{x_t\}_{t=1}^N$. One of the methods for determining $D_2(m)$ is calculation of the so-called correlation integral (sum) (Shuster [7]):

$$C(\varepsilon) = \lim_{N \to \infty} \frac{1}{N^2} \sum_{i,j} \theta\left(\varepsilon - \left\| x_i - x_j \right\|\right) \tag{3}$$

where $\theta(\bullet)$ is the Heaviside theta function.

For the correlation integral we have the following power-law behavior,

$$C(\varepsilon) \approx \varepsilon^{D_2} \tag{4}$$

which allows practically calculate $D_2(m)$. Thus, we can construct dependence of $D_2(m)$ on the embedding dimension $m$ for a particular reconstructed attractor. It turns out (Shuster [7]) that for a random time series and time series generated by a deterministic dynamical system the behavior of $D_2(m)$ is significantly different. For a random series one has relation $D_2(m) \approx m$ (for example for white noise see Fig. 1b). For the time series of deterministic dynamical system the correlation dimension $D_2(m)$ starting from a certain value of $m$ saturates, i.e. $D_2(m) \approx const$ (example for the harmonic oscillator and its solutions see on Fig. 1a)

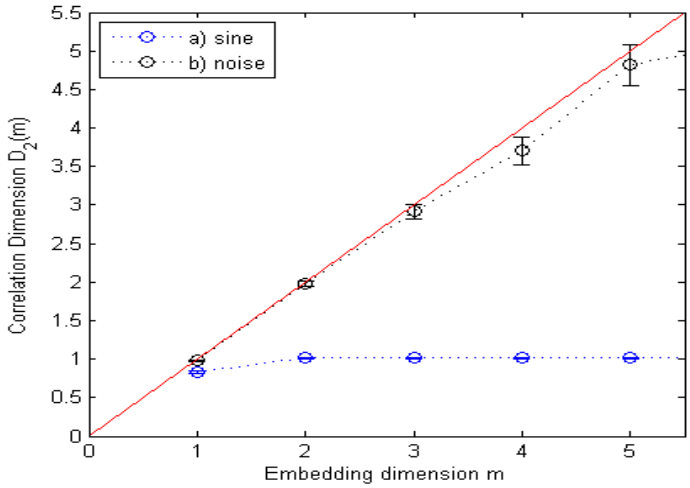


Fig. 1. Examples of dependencies. The abscissa value is the embedding dimension, the vertical axis value is the value of the correlation dimension. Red color marked line is $D_2(m) = m$. Black color dash line (b) shows dependence $D_2(m)$ for white noise, blue color dash line (a) shows dependence $D_2(m)$ for the harmonic oscillator and its solutions.

## 3 Algorithm of Empirical Mode Decomposition (EMD)

The EMD method is an iterative computational procedure in which the original data (continuous or discrete signal) is decomposed into empirical modes or internal vibrations (intrinsic mode functions, IMF). Decomposition into empirical modes allows to analyze local phenomena, so this method can be used effectively in the processing the non-stationary time series (Huang *at al.*[8]).
Let $X(t)$ is the analyzed signal. The essence of the EMD method lies in the sequential calculation and empirical modes $c_j$ and residues $r_j = r_{j-1} - c_j$ where j = 1,2,3, ..., n and $r_0 = X(t)$. As a result, we obtain an expansion of the signal below

$$X(t) = \sum_{j=1}^{n} c_j + r_n \qquad (5)$$

Here n is number of empirical modes, which are obtained during the calculations (Huang *at al.*[8]). Empirical mode $c_j$ is a function that has the following properties:

- Number of extremes of the function (maxima and minima) and the number of zero crossings must not differ by more than one;
- At any point, the mean value of the envelope function defined by the local maxima and local minima must be zero.

EMD algorithm method can be realized as follows:

1. Find the signal extremes. They should be located between every two successive sign changes of the time series.

2. Construct two signal envelopes: lower (ν) and upper (μ). It is possible to use splines (e.g., cubic).

3. Calculate the average value $m_1$ and the difference $h_1$ between the signal and its average value:

$$X(t) - m_1 = h_1 \tag{6}$$

If the difference obtained satisfies the definition of an empirical mode, the process stops. In this case, the obtained average value is an empirical fashion.

4. Otherwise, repeat the previous steps already for this difference $h_1$ (search extremes, building envelope, calculation of the mean and its subtraction):

$$h_1 - m_{11} = h_{11} \tag{7}$$

5. As a result of performing a sequence of iterations of the form

$$h_{1(k-1)} - m_{1k} = h_{1k} \tag{8}$$

it is necessary to obtain the function

$$c_1 = h_{1k} \tag{9}$$

which satisfies the definition of an empirical mode. Once an empirical mode, denoted as $c_1$ extracted, iterations are terminated (Huang *at al.*[8]).

6. Residue $r_1 = X - c_1$ is calculated and the whole algorithm is repeated again, but for the function $r_1$. Getting residues occurs as long as newly computed residue will be a monotonic function for which will be impossible to allocate empirical mode.

As noted above for the EEG signals sum of the first two EMD modes is the noise (physical and physiological). The EMD method allows to remove the sum of the first two modes of the original signal:

$$X^f(t) = \sum_{j=3}^{n} c_j + r_n \tag{10}$$

and get a filtered from the noise signal $X^f(t)$.

## 4 Description of the electroencephalograms database

In the present study we investigated the database of 19-channel EEG (arrangement of electrodes see on Fig. 2), which was provided by the Research

Centre "Exyclub" and includes 2 records for 10 subjects. First record (hereinafter -rest) corresponds to the usual state test with eyes closed, and no movements. Second record (hereinafter - meditation) was preceded by 2-minute "instruction-guided", whose meaning lies in the fact that the subject was asked to minimize "wandering mind", and is not involved in the usual automatic cascade of semantic associations.

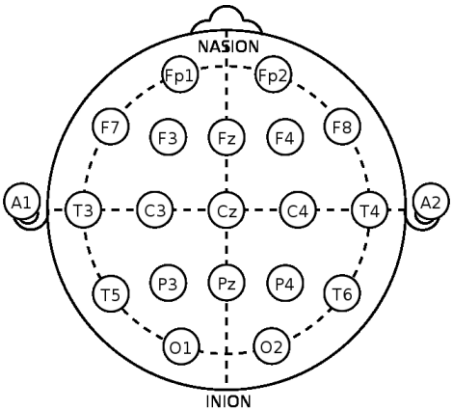

Fig. 2. The channels arrangement

We call the subject as “experienced meditator” if he practiced meditation in the past at least 500 hours. The subjects who was exposed to meditation training 100 hours or less will be referred as "inexperienced meditators". Below are given some parameters EEG recordings:
1. The sampling frequency is 500Hz;
2. Length for a single record is 120 ÷ 140 sec (60,000 ÷ 70,000 samples);
3. Maximum amplitude is up to 60 mV.

## 5 Analysis of the correlation dimension

Below we investigate the multifractal properties of the reconstructed attractor, namely dependence $D_2(m)$. The main instrument we used (the program d2 ) was developed by the authors on the basis of package TISEAN (Hegger *at al.* [9]). The d2 program designed to calculate the approximate correlation sum, correlation dimension and correlation entropy for a set of multi-dimensional data. The program d2 allows to pass from the value $D_2(\varepsilon, m)$ to $\tilde{D}_2(m)$, which depends only on the embedding dimension. Such a transition is performed by averaging over $\varepsilon$ in the range from the value specified by “Left epsilon” to the value specified by “Right epsilon”. That is, values $D_2(\varepsilon, m)$ and $\tilde{D}_2(m)$ are related as follows:

$$\tilde{D}_2\left(m\right) = \left\langle D_2\left(\varepsilon, m\right)\right\rangle \Big|_{\substack{\varepsilon > \varepsilon_{Left} \\ \varepsilon < \varepsilon_{Right}}} \tag{11}$$

Here, the angle brackets denotes averaging over the specified interval. Accuracy of $\tilde{D}_2\left(m\right)$ is defined as the standard deviation of the sample of $D_2\left(\varepsilon, m\right)$ values with $\varepsilon$ values taken from the interval $\varepsilon_{Left} < \varepsilon < \varepsilon_{Right}$ .

Further analysis for dependencies $\tilde{D}_2\left(m\right)$ was carried out for all EEG time series in both states of brain (rest and meditation). Empirically the range E for averaging over $\varepsilon$ , namely $\mathrm{E} = \left[0.6,\ \ 3\right]$, has been established.

In this paper, we monitor not only the dependencies $\tilde{D}_2\left(m\right)$ of the original series, but also for the analogous dependences $\tilde{D}_2^f\left(m\right)$ for EMD-filtered EEG time series. This difference is denoted as follows:

$$DifD_2 = \tilde{D}_2 - \tilde{D}_2^f \tag{12}$$

Under the EMD-filtered EEG correlation dimension we understand the correlation dimension calculated from EEG channels from which we have dropped the first two modes of EMD-decomposition (see Eq.(10)). Thus, the smaller this difference $DifD_2$, the less "noise" contains in the EEG signal. Calculations were performed by 5 experienced and 5 inexperienced subjects in a state of meditation and rest. For each subject the evaluation of these differences was carried out on the 10 fragments of each EEG channel. Each fragment consisted from 10,000 samples (record to last 20 seconds). Unfiltered correlation dimensions have been calculated at the embedding dimension m=5. After dropping the first two modes, EMD-filtered correlation dimensions have been calculated at the embedding dimension m=4. Such choice of embedding dimensions m in both cases was determined by points on the axis of abscissa, at which the correlation dimensions began to saturate.

## 6 Statistical analysis

The main hypotheses, which statistically will be checked in the present section are the following. The difference between the usual and EMD-filtered correlation dimensions is less in the state of meditation than in the rest state. One can anticipate that for experienced subjects the meditation and rest states according to above introduced indicator $DifD_2$ differes statistically significant. At the same time for inexperienced subjects the above distinction between states could be not significant. We would also check if there is any distinction in our

indicator $DifD_2$ for the left and the right hemisphere in the meditation and rest states. Remind that smaller the difference $DifD_2$, the less "noise" contains in the EEG signal.

Standard method of multifactor analysis of variance with repeated measures (Repeated ANOVA) and *t*-test for means for dependent samples were chosen as methods of analysis and test of suggested hypotheses (the program STATISTICA has been used).

The Figure 3 below gives the grafical and statistical results of Repeated ANOVA for the factors “Type” (experienced (Exper) or inexperienced (Inexp) subjects) and “STATE” (meditation (Dif_med) or rest (Dif_fon)).

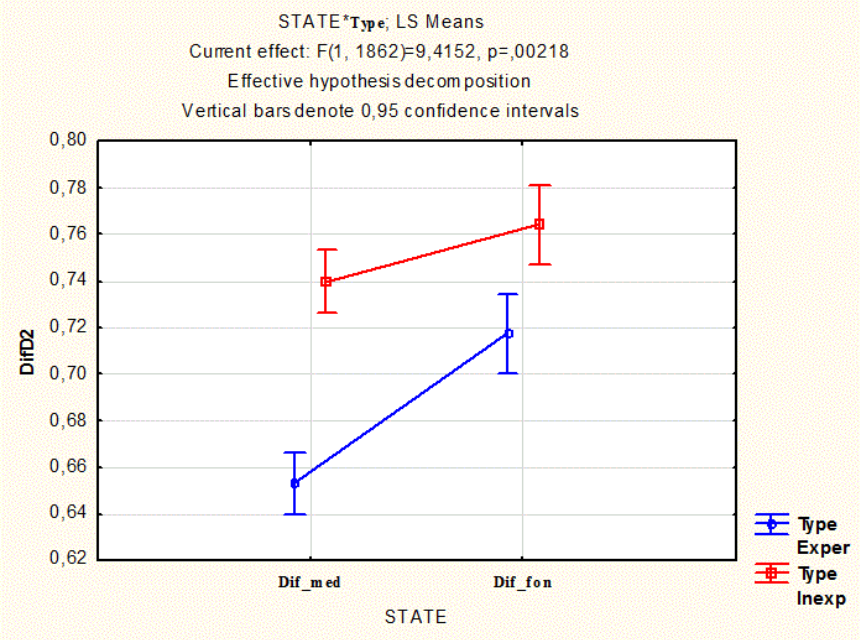


Fig. 3.Comparison of the average values of DifD2

The Fig. 3 above leads to the following conclusion. Interaction between factor "Type" and the factor "STATE" is significant ($p<0.01$). That is DifD2 for experienced subjects in meditation is lower than that in the rest. For inexperienced subjects the tendency is the same but distinction between states is smaller. The following table reveals, whether these differences are significant.

| Cell No. | Scheffe test; variable DV_1 (Cordim_1тип)<br>Probabilities for Post Hoc Tests<br>Error: Between; Within; Pooled MS = ,05871, df = 3375,3 | | | | | |
|---|---|---|---|---|---|---|
| | **Type** | **STATE** | **1<br>0,65299** | **2<br>0,71733** | **3<br>0,73952** | **4<br>0,76412** |
| 1 | **Exper** | **Dif_med** | | 0,000000 | 0,000000 | 0,000000 |
| 2 | **Exper** | **Dif_fon** | 0,00000 | | 0,263439 | 0,000515 |
| 3 | **Inexp** | **Dif_med** | 0,00000 | 0,263439 | | 0,065693 |
| 4 | **Inexp** | **Dif_fon** | 0,00000 | 0,000515 | 0,065693 | |

Table. 1.Probabilities for Post Hoc Tests

In the Table 1 the results of post hoc test for pairewise comparison are given for 4 pairs: experienced subjects in meditation, experienced subjects in rest, inexperienced subjects in meditation, inexperienced subjects in rest In the table cells one can find the corresponding "pairwise" p-levels. The values of p-levels greater than 0.05 means that distinction between averaged values of idicator DifD2 in the corresponding pair is not statisticslly significant. Thus, accoding to indiator DifD2 for experienced subjects meditation state differes from rest state on very high level of significance. For inexperienced subjects this is not true. In meditation state the distinction between experienced and ineperienced subjects is also highly significant. So meditation is characterized by significantly less noise in EEG only for experienced subjects but not for inexperienced. Another effect is that experienced subjects “manage to significantly reduce the noise in brain” during meditation in comparison with rest state. Inexperienced subjects do not posess such ability. One more interesting fact is that the average value of the difference of correlation dimensions (DifD2) over all channels in the rest state for experienced meditators is significantly lower than that of inexperienced meditators. The physiological explanation of this fact is offered in conclusions.

The Figure 4 below grafically allows to see that for experienced subjects the distinction between meditation and rest states is achieved mainly due to the parietal and occipital channels.
The Figure 5 below grafically allows to see that in meditation state the difference DifD2 for experienced and inexperienced subjects is achieved mainly due to the frontal and parietal channels

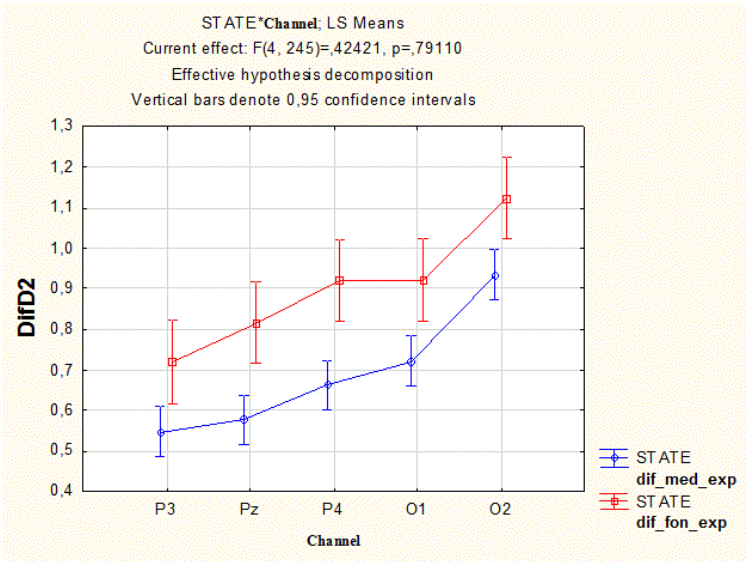


Fig. 4. The difference DifD2 for experienced subjects in the parietal and occipital channels

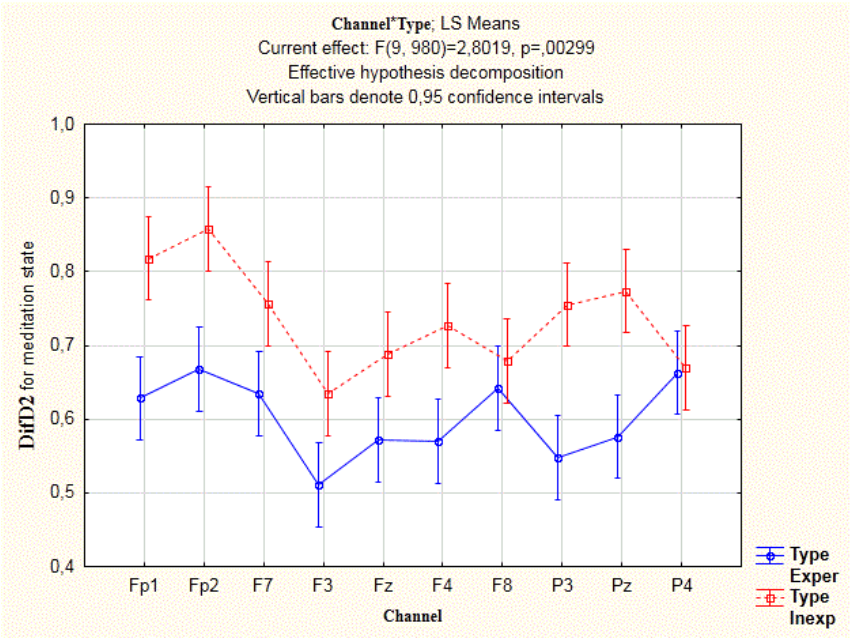


Fig. 5. The difference DifD2 in meditation state in the frontal and parietal channels

Finally, we have checked if there is any distinction in our indicator DifD2 for the left and the right hemisphere in the meditation and rest states. It turned out that the experienced meditators average difference of correlation dimension (DifD2) in the left hemisphere is significantly smaller than for the right one. Here we have applied one-tailed *t*-test for means for dependent samples. It gave $p < 0.001$ as the significance level. At the same time for inexperienced subjects the difference is statistically insignificant **(***p* = 0.33). The physiological explanation of this fact is offered in conclusions.

## Conclusions

In this paper we developed a new method for discriminating between rest and meditation, as well as between experienced and inexperienced subjects. Constructed method is based on multifractal analysis and EMD decomposition of multichannel EEG. More specifically, in the framework of these approaches to the analysis of EEG, a new indicator DifD2 has been constructed. With this indicator main results were obtained as listed below.

1. It turned out that the DifD2 in a state of meditation for experienced subjects is significantly lower than that of the inexperienced subjects. It should be noted that this distinction is achieved mainly due to the frontal and parietal channels.
2. For experienced subjects the difference DifD2 in the meditation state turned out to be significantly lower than that in the rest state. It should be noted that this difference is achieved mainly by the parietal and occipital channels.
3. It turned out that the experienced meditators average difference of correlation dimension (DifD2) in the left hemisphere is significantly smaller than for the right one. At the same time for inexperienced subjects the difference is statistically insignificant. This allows us to associate this fact with the presence of positive emotions in the left hemisphere during meditation.
4. The average value of the difference of correlation dimension (DifD2) over all channels in the rest state for experienced meditators was significantly lower than that of inexperienced meditators. This could be explained by the presence of the neuroplastic brain reorganization for experienced meditators.

In addition it should be noted that for the above studies has been developed and used specialized software in the MATLAB environment. It can be used in further studies, for example, to identify individual differences in groups of subjects, both experienced and inexperienced.

## References

1. Cahn B.R, Polich J. Meditation states and traits: EEG, ERP, and neuroimaging studies. Psychological Bulletin; 132, 2, 180{211, 2006.
2. Aftanas L.I, Golocheikine S.A. Non-linear dynamic complexity of the human EEG during meditation. Neurosci Lett., 330, 2:143{146, 2002.
3. Natarajan K., Acharya U R., Alias F., Tiboleng T., Puthusserypady, S.K. Nonlinear analysis of EEG signals at different mental states. BioMedical Engineering Online 3, 2004.

4. Goshvarpour A. Clafssification of Electroencephalographic Changes in Meditation and Rest: using Correlation Dimension and Wavelet Coefficients. I.J. Information Technology and Computer Sciences 3, 24{30, 2012.
5. Mandelbrot B. The Fractal Geometry of Nature, W.H. Freeman and Company, New York, 2002.
6. Bozhokin S.V., Parshin D.A.. Fractals and Multifractals, NIC "Regular and Chaotic Dynamics", Izhevsk, 2001. (in Russian).
7. Shuster G. Deterministic chaos, Mir, Moscow, 1988 (in Russian).
8. Huang N. E., Shen Z., Long S. R., Wu M. C., Shih H. H., Zheng Q., Yen N.-C., Tung C. C., and Liu H. H. The empirical mode decomposition and the Hilbert spectrum for nonlinear and non-stationary time series analysis. Proceedings of R. Soc. London, Ser. A, 454, 903{995, 1998.
9. Hegger R., Kantz H., Schreiber T.. TISEAN. Nonlinear Time Series Analysis [Official website]. URL: http://www.mpipks-dresden.mpg.de/~tisean/ (date accessed: 05/18/2014).
10. Lutz A., Slagter H.A., Dunne J.D., Davidson R.J. Attention regulation and monitoring in meditation. Trends in Cognitive Sciences. 12(4):163{169. 2008.

# Ranking charity applications

**Cong Xu and James M Freeman**

Manchester Business School, The University of Manchester, Booth Street East, Manchester, M15 6PB, UK

**Abstract.** How can a charity ensure that only its most worthy causes are supported? One approach that has proven effective in the past is AHP (Analytic Hierarchy Process). Now a new method – based on a hybrid AHP / Evidential Reasoning (ER) adaptation - has become available, claiming distinct advantages over straight AHP. By contrasting the two procedures for a real-life dataset – we demonstrate AHP/ER's superiority in both theoretical and practical respects.

**Keywords:** Analytic Hierarchy Process, Dummy variables, Evidential Reasoning, Intelligent Decision Software, Utility

## 1 Introduction

Buxton and District Lions Club (http://www.buxtonlions.com/index.html) belongs to the International Association of Lions Clubs. As such, each year, the Club runs a variety of fund-raising events (see for example Fig.1), the income from which is then used to resource good causes - primarily within the local area.

*Stochastic Modeling, Data Analysis and Statistical Applications* (pp. 171-181)
Lidia Filus - Teresa Oliveira - Christos H Skiadas (Eds)

Fig. 1. Participants in the BDLC's Ladies' Ruff Stuff Challenge

On average, BDLC raises £5,000 - £6,000 in donations annually. From experience this is never sufficient to meet the charitable demands upon the Club - hence the need for applications to be systematically evaluated (by the body's charity committee) to determine which, if any of them, should be earmarked for BDLC support.

In an effort to make the committee's screening process more objective and scientific, AHP [2] [3] was tested by Pang [1] on the thirteen grant applications received by BDLC in 1999. Seven criteria were considered in the application - four of them, quantitative and three, qualitative (binary) – as described in Table 1.

QUANTITATIVE ATTRIBUTES
"How long will the benefit last" (**Duration**)
"Numbers of people who benefit" (**Numbers**)
"How well resourced" (**Resource**)
"Impact of funding" (**Impact**)

QUALITATIVE ATTRIBUTES
"Any possibility of alternative funding" (**Alternative funding**)
"Direct or indirect applications" (**Direct**)
"Help with daily living" (**Living**)

Table 1. Decision criteria

Because of theoretical limitations with AHP at the time, only the quantitative criteria could be used in the resultant (EXCEL-based) analysis - final rankings from which are summarised in Table 2. However, providing strong vindication for the procedure, these were found to significantly correlate with actual funding decisions made by the Club.

| Alternatives | Priority | Overall Ranking |
|---|---|---|
| **Buxton Mountain Rescue Team** | **0.190** | **1** |
| **Buxton Opportunity club** | **0.177** | **2** |
| Heartbeat | 0.144 | 3 |
| **Burbage Football Club** | **0.119** | **4** |
| **Bereaved lady** | **0.061** | **6** |
| Buxton Samaritans | 0.095 | 5 |
| Disabled man | 0.039 | 8 |
| **Disabled riders** | **0.040** | **7** |
| Holidays for disabled | 0.037 | 9 |
| PC for disadvantage school pupil | 0.032 | 10 |
| Wheelchair applicant | 0.027 | 11 |
| Chapel band | 0.022 | 12 |
| Nepal travel | 0.017 | 13 |

Bold entries in the table correspond with applications that were finally funded by BDLC.
Table 2. Original AHP Summary

Building on this promising start, the data have now been re-analysed using a combined AHP/ER approach with the advantage that both quantitative and qualitative data (see Table 3) can be taken into account in the computations. Relevant results are detailed in the next section of the paper. Beforehand, background is provided on ER and the Intelligent Decision System (IDS) software[4] used to operationalise the analysis.

| | Any possibility of alternative funding? | direct or indirect applications? | Help with daily living? |
|---|---|---|---|
| Buxton Mountain Rescue Team | 1 | 1 | 0 |
| Buxton Opportunity club | 1 | 0 | 0 |
| Heartbeat | 1 | 1 | 0 |
| Burbage Football Club | 1 | 1 | 0 |
| Bereaved lady | 0 | 1 | 1 |
| Buxton Samaritans | 1 | 1 | 0 |
| Disabled man | 0 | 1 | 1 |
| Disabled riders | 1 | 1 | 1 |
| Holidays for disabled | 1 | 0 | 0 |
| PC for disadvantage school pupil | 1 | 1 | 0 |
| Wheelchair applicant | 1 | 1 | 1 |
| Chapel band | 1 | 1 | 0 |
| Nepal travel | 1 | 1 | 0 |

YYes is scored ‘1’ and No is scored ‘0’ here.
Table 3. Qualitative data details

## 2 Evidential reasoning and IDS

ER significantly extends the application of multiple criteria decision analysis (MCDA) methods by allowing formal belief structures to be incorporated into the modelling under conditions of uncertainty.
The approach itself is very flexible enabling uncertainty to be accommodated in many different guises e.g. as single numerical values, probability distributions, subjective judgments with degrees of belief … leading to greater realism and reliability in the overall assessment.
The re-analysis of the BDLC data was performed using the IDS software. As

well providing a systematic interface for the model formulation, IDS offers a range of powerful facilities – not least its ability to incorporate different risk outlooks into the analysis as well as an exhaustive sensitivity testing provision.

Typically, four distinct stages are involved in an IDS modelling application: for the BDLC data these can be illustrated as follows:

1. **"Define the alternatives"** (See Table 2)
2. **"Define the attributes"** (see Table 1)
3. **"Assign attributes weights"** For this stage of the project the **Eigenvector (AHP)** IDS option was selected over the **Geometric mean,** and **Mixed approach** alternatives - see the values obtained in Table 4 which compare very closely with those based on the traditional method set out in the Appendix**)**
4.

| | Weight |
|---|---|
| Duration | 0.424 |
| Number | 0.201 |
| Resource | 0.161 |
| Impact | 0.08 |
| Living | 0.066 |
| Alternative Funding | 0.034 |
| Direct | 0.033 |

Table 4. Attribute weights generated by IDS for the 7-Criteria Model

5. **"Convert grades"**.

As there are two levels of attributes for the BDLC data, grades from lower level attributes (*applications*) have to be converted and aggregated into the higher-level attributes (*criteria*). However, the process for handling qualitative data and quantitative data is different. IDS provides two different ways of aggregating them. One way is by **rule based transformation** and the other – the one used for the project - is **utility based transformation**[5]

In the latter case, IDS offers two sub-options for determining managers' utility types: **Visual Scoring**, and **Direct Assignment**. Visual scoring, the choice used here, involves computer graphical manipulation whereas Direct Assignment allows managers' utilities to be represented by specific utility values.

Following on, utility scores - assuming a risk neutral attitude to risk - were obtained from IDS as follows:

| Alternatives | IDS Utility score | Ranking |
|---|---|---|
| Buxton Mountain Rescue Team | 0.907 | 1 |
| Buxton Opportunity club | 0.776 | 2 |
| Heartbeat | 0.683 | 3 |
| Burbage Football Club | 0.505 | 4 |
| Bereaved lady | 0.281 | 6 |
| Buxton Samaritans | 0.463 | 5 |
| Disabled man | 0.189 | 7 |
| Disabled riders | 0.156 | 8 |
| Holidays for disabled | 0.072 | 11 |
| PC for disadvantage school pupil | 0.078 | 10 |
| Wheelchair applicant | 0.087 | 9 |
| Chapel band | 0.038 | 12 |
| Nepal travel | 0.016 | 13 |

Table 5. IDS Rankings (7 criteria model) Risk neutral attitude

Corresponding graphical output is shown in Figure 2.

Equivalent graphs for risk averse and risk welcoming attitudes are shown in Figures 3 and 4 respectively:

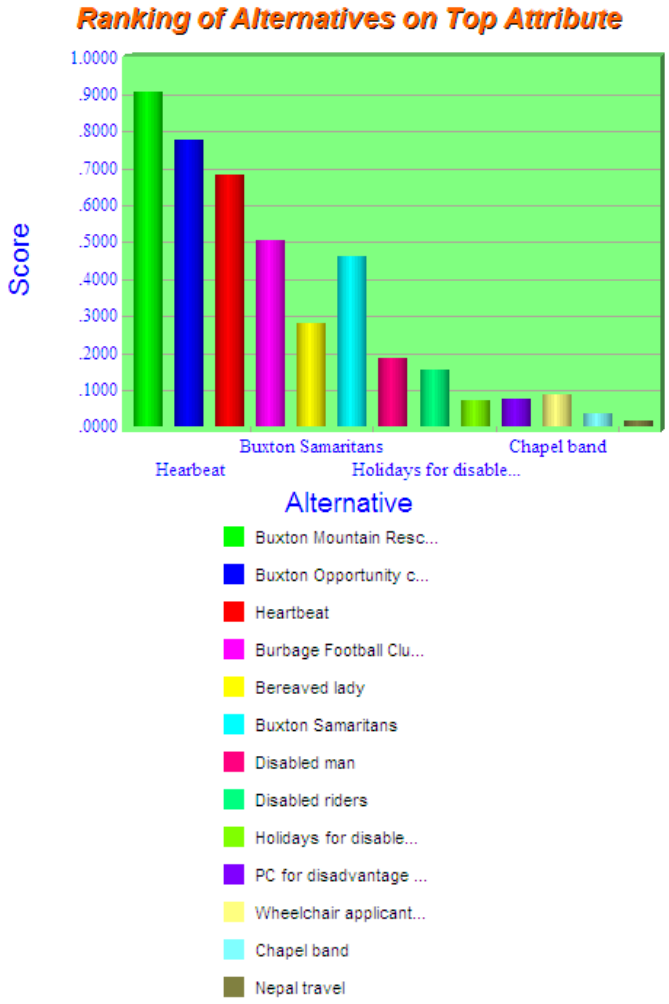


Fig. 2. Utility scores by alternative. Risk neutral attitude

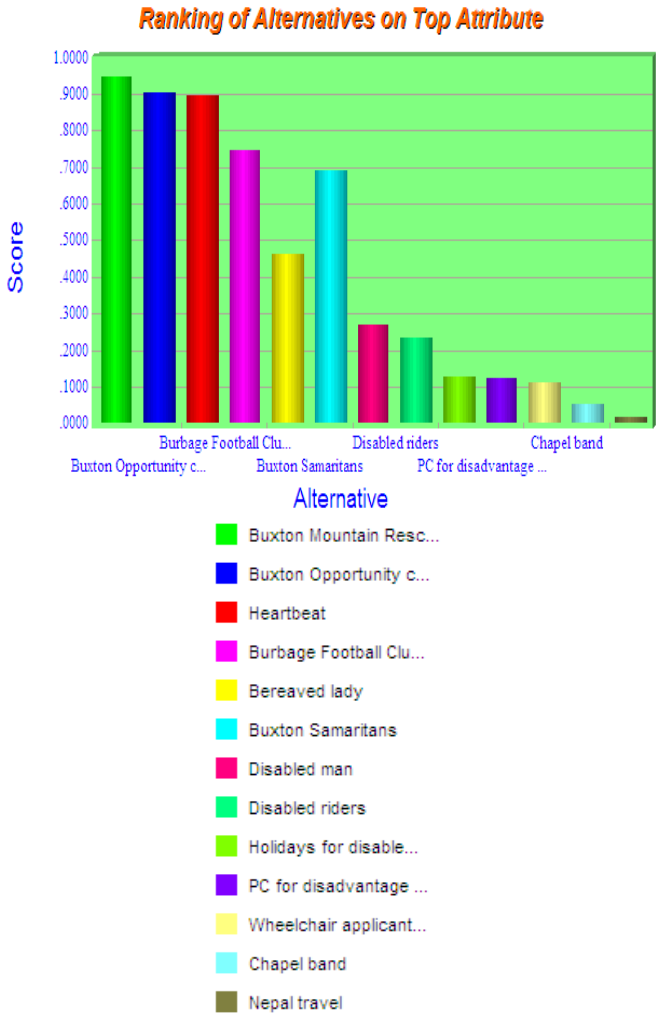


Fig. 3. Utility scores by alternative. Risk averse attitude

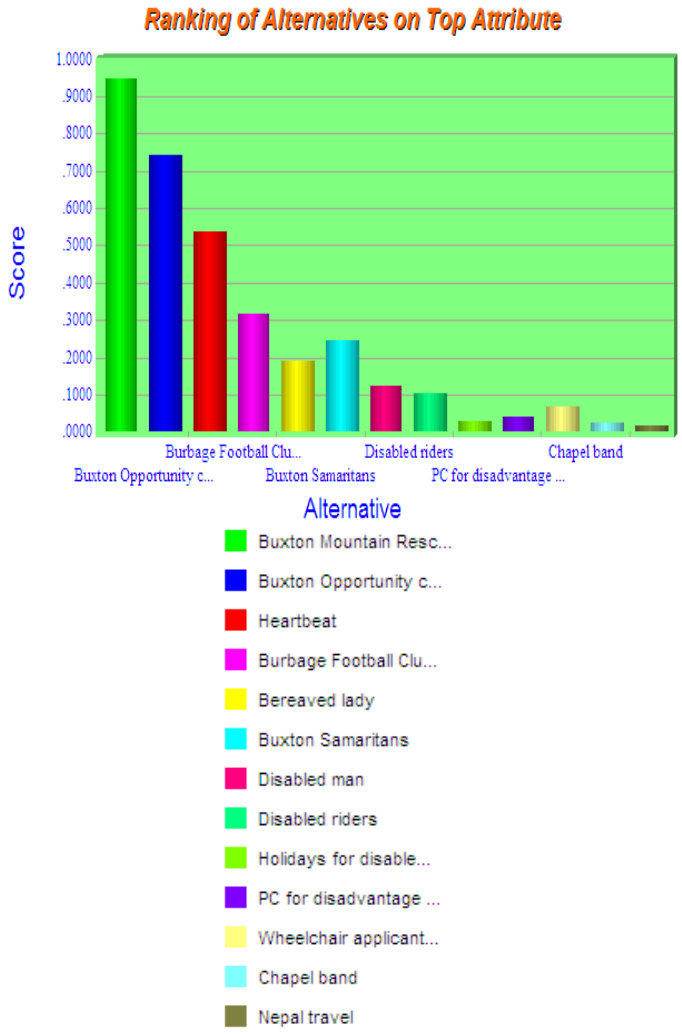


Fig. 4. Utility scores by alternative. Risk welcoming attitude

Of interest, all three rankings here can be shown to be significantly correlated. This overall consistency backed up by selected sensitivity results – see e.g. Figure 5 – suggest the ER/AHP rankings obtained for this particular dataset are remarkably robust.

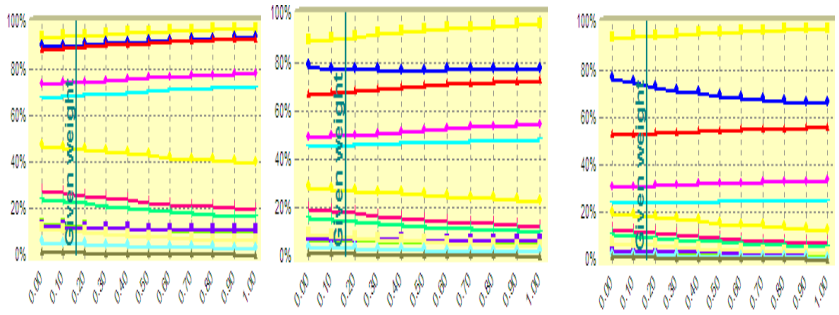


**(7-Criteria model Risk averse)** **(7-Criteria model Risk neutral)** **(7-Criteria model Risk taking)**

Fig. 5. Sensitivity analysis re changes in weight value for "How well resourced"

## 4 Conclusions

Results from an AHP/ER analysis of a historical dataset on charity applications contrast markedly with those from a longstanding analysis based on set-piece AHP. More to the point, the new approach was found to outperform its predecessor in virtually every respect:

1. Whereas AHP was able to only handle quantitative criteria in the modeling, AHP/ER was able to deal with both quantitative and qualitative criteria.
2. IDS – the system used for the AHP/ER modeling here –substantially outclassed the open-ended EXCEL-based code generated for the AHP in scope and user-friendliness.
3. Utility stereotypes can be automatically taken into account in an IDS analysis enabling decision-makers' preferences to be directly incorporated into the results.
4. Similarly, IDS's sensitivity analysis capability is impressively comprehensive: not only does the system highlight the specific points where changes in data inputs cause overall rankings to change but it routinely maps out feasible regions associated with a given solution.

Irrespective of the utility type considered, the rankings for the first 8 of the BDLC alternatives remained the same: 1-Buxton Mountain Rescue Team, 2-Buxton Opportunity club, 3-Heartbeat, 4-Burbage Football Club, 5- Buxton Samaritans, 6- Bereaved lady, 7-Disabled man, 8-Disabled riders. Similarly, the rankings for the last 2 alternatives were also found to be unchanged: 12- Chapel band, 13- Nepal travel. Not surprisingly, this translated into significant agreement between all three of the seven criteria rankings obtained and indeed between them and the old AHP-based ranking.

## References

1. J. Freeman and H.C. Pang. Separating the Haves from Have-nots – how the Analytic Hierarchy Process was used to Priorities applications for charitable funding. OR Insight 13, 4, 14{20, 2000.

2. T.L. Saaty. What is the analytic hierarchy process? Springer Berlin Heidelberg. 109{121, 1988.

3. T.L. Saaty. How to make a decision: the analytic hierarchy process. Interfaces, 24, 6, 19{43, 1994.

4. D. L Xu and J. B Yang. Intelligent Decision System for self-assessment. Journal of Multi-criteria Decision Analysis, 12, 1, 43{60, 2003.

5. J. B. Yang. Rule and utility based evidential reasoning approach for multi-attribute decision analysis under uncertainties. European Journal of Operational Research. 131, 1, 31{61, 2001.

## Appendix

The basis of the application comparisons that follow is the fundamental scale:

| Verbal judgement or preference | Numerical rating |
|---|---|
| Extremely preferred | 9 |
| Very strongly to extremely | 8 |
| Very strongly preferred | 7 |
| Strongly to very strongly | 6 |
| Strongly preferred | 5 |
| Moderately to strongly | 4 |
| Moderately preferred | 3 |
| Equally to moderately | 2 |
| Equally preferred | 1 |

*Step 1: Calculate the sum of each column.*

| | Duration | Number | Resource | Impact | Living | Alternative funding | Direct |
|---|---|---|---|---|---|---|---|
| Duration | 1 | 4 | 4 | 5 | 5 | 8 | 8 |
| Number | 0.25 | 1 | 2 | 4 | 3 | 5 | 5 |
| Resource | 0.25 | 0.5 | 1 | 4 | 3 | 4 | 5 |
| Impact | 0.2 | 0.25 | 0.25 | 1 | 1 | 4 | 4 |
| Living | 0.2 | 0.33 | 0.33 | 1 | 1 | 2 | 2 |
| Alternative Funding | 0.125 | 0.2 | 0.25 | 0.25 | 0.5 | 1 | 1 |
| Direct | 0.125 | 0.2 | 0.2 | 0.25 | 0.5 | 1 | 1 |
| **Total** | **2.15** | **6.48** | **8.03** | **15.5** | **14** | **25** | **26** |

*Step 2: Normalization*

| | Duration | Number | Resource | Impact | Living | Alternative funding | Direct |
|---|---|---|---|---|---|---|---|
| Duration | 0.465 | 0.617 | 0.498 | 0.323 | 0.357 | 0.320 | 0.308 |
| Number | 0.116 | 0.154 | 0.249 | 0.258 | 0.214 | 0.200 | 0.192 |
| Resource | 0.116 | 0.077 | 0.124 | 0.258 | 0.214 | 0.160 | 0.192 |
| Impact | 0.093 | 0.039 | 0.031 | 0.065 | 0.071 | 0.160 | 0.154 |
| Living | 0.093 | 0.051 | 0.041 | 0.065 | 0.071 | 0.080 | 0.077 |
| Alternative Funding | 0.058 | 0.031 | 0.031 | 0.016 | 0.036 | 0.040 | 0.038 |
| Direct | 0.058 | 0.031 | 0.025 | 0.016 | 0.036 | 0.040 | 0.038 |
| Total | 1 | 1 | 1 | 1 | 1 | 1 | 1 |

*Step 3: Calculate Row average*

| | Duration | Number | Resource | Impact | Living | Alternative funding | Direct | **Row average** |
|---|---|---|---|---|---|---|---|---|
| Duration | 0.465 | 0.617 | 0.498 | 0.323 | 0.357 | 0.320 | 0.308 | **0.412** |
| Number | 0.116 | 0.154 | 0.249 | 0.258 | 0.214 | 0.200 | 0.192 | **0.198** |
| Resource | 0.116 | 0.077 | 0.124 | 0.258 | 0.214 | 0.160 | 0.192 | **0.163** |
| Impact | 0.093 | 0.039 | 0.031 | 0.065 | 0.071 | 0.160 | 0.154 | **0.087** |
| Living | 0.093 | 0.051 | 0.041 | 0.065 | 0.071 | 0.080 | 0.077 | **0.068** |
| Alternative Funding | 0.058 | 0.031 | 0.031 | 0.016 | 0.036 | 0.040 | 0.038 | **0.036** |
| Direct | 0.058 | 0.031 | 0.025 | 0.016 | 0.036 | 0.040 | 0.038 | **0.035** |

The row averages in the last table correspond with those summarised in Table 4 using IDS. The consistency index (Saaty, 1980) for the latter can be shown to be zero signifying the weights from this analysis are perfectly consistent.

# Evolution of electoral behavior by principal axes methods

Margarita Marín[1] and Campo Elías Pardo[2]

[1] Universidad Nacional de Colombia
Bogotá, Colombia
(e-mail: mmarinj@unal.edu.cu)
[2] Universidad Nacional de Colombia
Bogotá, Colombia
(e-mail: cepardot@unal.edu.co)

**Abstract.** This paper study the common voting patterns in Colombian presidential elections between 1986 to 2010. Contingency tables are building with sub-partitions on rows and columns, where the rows correspond to the Colombian municipalities, according to their population size and the columns correspond to the votes for candidates in each electoral period. Weighted Intra Blocks Correspondence Analysis (WIBCA) with cluster analysis is develop to study voting patterns, eliminating the variability induced by population differences and election periods. It is possible to conclude that there is an electoral pattern, mainly in the municipalities with population under 20.000, which is more clear before the 2002 election period.
**Keywords:** WIBCA, Contingency Tables, Cluster Analysis.

## 1 Introduction

In 1990 Bautista and Pachecho[1] made an study of Colombian presidential election in the period of 1972 to 1990, by the implementation of Principal Component Analysis (PCA) of a dataset that contains the results for all the departments in every period for the Liberal, Conservador and left candidates. They found that the Liberal and Conservador parties have a negative correlated behavior, and that the poll for the left candidates is independent of the results of the others candidates. This work was development before the proclamation of the 1991 new Colombian Political Constitution and the electoral reform in the 90's which laid the groundwork for more flexible rules that allows the entry and exit of new political parties in Colombian. Also, before 1986 the electoral results were reported at the departmental level and the law 136 (CNC[2]) changed the political division of Colombia by created new departments and municipalities.

With this changes in mind, if one considerate this methodology for study the current Colombian presidential election, is possible to find results that do not reflect the reality, since this method does not discount the variation introduce by the change in time caused by the entry and exit the of the new candidate

*Stochastic Modeling, Data Analysis and Statistical Applications* (*pp.* 183-193)
Lidia Filus - Teresa Oliveira - Christos H Skiadas (Eds)



and political parties and the differences in the electoral behaivor of the small municipalities and the big cities.

This work study the Colombian presidential election between 1986 and 2010, excluding the variation introduce by the change of political actors in time and the differences of population size. For this, this paper is divided in five parts including this introduction. In the second part the methodology is explained, then the data and the results are displayed and finally the conclusions are presented.

## 2 Methodology

### 2.1 Principal Components Analysis

The Principal Components Analysis (PCA) is a methodology to describe large data sets by the generation of orthogonal variables (known as axes) to the original variables which keeps the most variance (inertia)(UST[3]). This representation allows the study of the relation between rows according to their values of the columns, the relation between the columns and the reduction of dimensionality (Pardo and Cabreras[4]).

Then, from the standardized matrix $\mathbf{X}$ of data, with $n$ rows y $p$ columns is possible to find the row and column geometrical representation of this matrix which correspond to the distance (or metric) $\mathbf{M}$ and $\mathbf{D}$ respectively. This combination of data matrix and metric matrices can be written as $\mathbf{ACP}(\mathbf{X}, \mathbf{M}, \mathbf{D})$ (Escofier and Pagès [5]).

It is possible to demonstrate that the orthogonal axes that maximize the projected inertia corresponds to the eigenvectors associate to the higher eigenvalue of the correlation matrix (Lebart *et al.*[6]).

Then, the rows of the data can be represent as the union of pairs of axes, known as factorial planes, where the plane of the first and second axes (associate whit the first and second eigenvalues and eigenvector) constitute the best projection. In these planes, nearby points indicate similarity between the individuals and distant points indicate dissimilarity. In the case of the columns the representation obtained by crossing pairs of axes allows to get a plane where the points are represented as vectors and the angles formed between the pairs of them indicate the correlation of the columns (Lebart *et al.*[6]).

### 2.2 Correspondence Analysis with respect to a model

The CA methodology can be used to find the best representation for contingency tables (where the rows and columns represent different variables set) [Benzécri [7], Lebart *et al.*[6]], and can be seen as a Weightes Principal Component Analysis (Pardo *et al.* [8]), denoted as $ACP(\mathbf{X}, \mathbf{M}, \mathbf{D})$.

Escofier[9] generalized the CA to consider it as the relation with a model, which is a matrix that have a relation with $\mathbf{F}$. The best know example of a model is the independence model that arises by multiplying the marginals of the matrix of frequencies $\mathbf{F}$.

For example, one can consider the $\mathbf{F}$ as the frequency table an $\mathbf{H}$ as the independence model matrix with general term $h_{ik}^{lj} = f_{i.}^{l.} f_{.k}^{.j}$. Then, in the Simple Correspondence Analysis (SCA) which is an $ACP(\mathbf{X}, \mathbf{M}, \mathbf{D})$ where $\mathbf{X}$ has general term $x_{ik}^{lj} = \frac{f_{ik}^{lj} - f_{i.}^{l.} f_{.k}^{.j}}{f_{i.}^{l.} f_{.k}^{.j}}$, $\mathbf{M} = diag(f_{.k}^{.j})$ and $\mathbf{D} = diag(f_{i.}^{l.})$, can also be seen as a $AC(\mathbf{F}, \mathbf{H})$ with respect to the independence model.

### 2.3 Weighted Intra Blocks Correspondence Analysis

Intra Blocks Correspondence Analysis (IBCA) is a methodology use to represent contingency tables with sub-partitions in rows and columns. In order to facilitate the explanation of the IBCA, the Colombian presidential elections data is presented in the Table 1. In this case, *Ele* represent the year of the election, *Can* the candidate, *Cat* a group of municipalities according to their population size and *Mun* the municipality. One can see that the groups creates to new structures known as band and block.

Table 1: Contingency table with sub-partitions in rows and columns for the presidencial municipality elections

| | | **Ele86** | ... | **Ele10** |
|---|---|---|---|---|
| | | **Can1 Can2** ... | ... ... ... ... | ... **Can26 Can27** |
| **Cat1** | **Mun1** | | | |
| | **Mun2** | | | |
| | ... | | | |
| ... | ... | | | |
| | ... | | | |
| | ... | | | |
| | ... | | | |
| **Cat7** | **Mun960** | | | |
| | **Mun961** | | | |

A band is the partition of the table, created by a group of variables in the rows (row bands) or in the columns (column bands). In the case of the Table 1 an example of row band is the vote for all candidates in all elections for municipalities in category 1, and an example of column band is the voting in all the municipalities and all the categories for 1986 election. A block is create by the intersection of a row band with a column band so, in the Table 1, an example of block is the voting for all the candidates in the 1986 election in all the municipalities in category 1.

Then, the IBCA allows to study the relationship between the municipalities and the candidates, excluding the variation introduce by the size of the populations and the year of elections. This is possible, because this methodology preforms an CA with respect to independence model between the row and columns bands, which subtract the inertia generate by the bands leaving only the inertia of the variables within the blocks (Pardo[10]).

This implies that the IBCA can be seen as a $PCA(\mathbf{X}, \mathbf{D}, \mathbf{M})$ or an $CA(\mathbf{F}, \mathbf{B})$, where the general term of each matrix is presented in the Table 2 [Pardo[10], Pardo[8]].

Table 2: General terms in the IBCA matrix

| **Method** | **Matrix** X | **Matrix D** | **Matrix M** | **Modelo** |
|---|---|---|---|---|
| **IBCA** | $x_{ik}^{lj} = \frac{f_{ik}^{lj} - \frac{f_{i.}^{lj} f_{.k}^{lj}}{f_{..}^{lj}}}{f_{i.}^{l.} f_{.k}^{.j}}$ | $diag(f_{i.}^{l.})$ | $diag(f_{.k}^{.j})$ | $b_{ik}^{lj} = \frac{f_{i.}^{lj} f_{.k}^{lj}}{f_{..}^{lj}}$ |

However, the IBCA great limitation is that can be influenced by oversized bands (bands whit a lot of variables or weight). Taking this into account, Pardo[10] propose the Weighted Intra Blocks Correspondence Analysis (WIBCA) (as an extension of the Multiple Factorial Analysis for Contingency Table (MFACT) presented by Bécue-Bartaut and Pagès[11] in which is possible to introduce simultaneously weights to **M** y **D**, in order to eliminate the effect of the oversized bands. Pardo[10] demonstrate that this weighted matrix are $\mathbf{M} = diag(\alpha_j f_{.j}^{.k})$ and $\mathbf{D} = diag(\beta_l f_{l.}^{i.})$, where $\alpha_j$ y $\beta_l$ are the weights, which have to be estimated by iterative process.

### 2.4 Clustering strategy

In addition to the previous methodology, this papers implements clustering strategies for the interpretation of the results at the municipality level. This is necessary since the amount of municipalities complicates the individual analysis for the rows.

Having this in mind, in this work the mix algorithm for the classification of the individuals is used. This algorithm implement the Ward algorithm, for hierarchical classification, in order to choose the number of clusters, the gravity centres and an initial classification. Then, the results are optimized by the $K$-means algorithm (Lebart *et al.* [6]).

## 3 The data

This paper study the relations between Colombian municipalities and votes for the principals presidential candidates en each election from 1986 to 2010, according with the configuration present in the Table 1.

In Colombia the presidential term has a duration of 4 year, that means that in the period of interest seven presidential election took place. Also, this paper only considers the 27 candidates who obtained a total number of votes greater than the blank vote. The Table 3 shows the candidates included in the analysis and the year of participation.

Also, this work only takes into account the 961 municipalities, and not the 1120 municipalities that currently exist, with voting between 1986 and 2010. The absence of voting in the other 159 municipalities can respond to various reasons such as lack of the municipality, inability to install polling stations because of armed conflict, among other reasons.

Table 3: Presidential candidates and year of participation

| Election year | Candidate Name | Candidate-year code |
|---|---|---|
| 1986 | Virgilio Barco | Bar86 |
| | Alvaro Gomez | Gom86 |
| | Jaime Pardo | Par86 |
| 1990 | Cesar Gaviria | Gav90 |
| | Alvaro Gomez | Gom90 |
| | Rodrigo Lloreda | Llo90 |
| | Antonio Navarro | Nav90 |
| 1994 | Antonio Navarro | Nav94 |
| | Andres Pastrana | Pas94 |
| | Ernesto Samper | Sam94 |
| 1998 | Harold Bedoya | Bed98 |
| | Andres Pastrana | Pas98 |
| | Noemi Sanin | San98 |
| | Horacio Serpa | Ser98 |
| 2002 | Luis Garzon | Gar2 |
| | Noemi Sanin | San2 |
| | Horacio Serpa | Ser2 |
| | Alvaro Uribe | Uri2 |
| 2006 | Carlos Gaviria | Gav6 |
| | Horacio Serpa | Ser6 |
| | Alvaro Uribe | Uri6 |
| 2010 | German Vargas Lleras | Lle10 |
| | Antanas Mockus | Moc10 |
| | Rafael Pardo | Par10 |
| | Gustavo Petro | Pet10 |
| | Noemi Sanin | San10 |
| | Juan Manuel Santos | Sant10 |

Table 4: Classification of Colombian municipality according to population size

| Category | Minimum | Maximum | Number of municipalities |
|---|---|---|---|
| **Cat1** | 500.001 | - | 9 |
| **Cat2** | 100.001 | 500.000 | 51 |
| **Cat3** | 50.001 | 10.0000 | 60 |
| **Cat4** | 30.001 | 50.000 | 107 |
| **Cat5** | 20.001 | 30.000 | 134 |
| **Cat6** | 10.001 | 20.000 | 317 |
| **Cat7** | 0 | 10.000 | 441 |

The municipality classification, for the creation of the bands, is made according to the parameters established in the law 136 (CNC[2]) which is presented in the Table 4.

## 4 Application

This section present the principal results for the application of the WIBCA in the Colombian presidential elections data. For the implementation of the WIBCA the R-package *pamctd* is used (Pardo[13]) and for the cluster classification the R-package FactoClass (Pardo and Del Campo[12])are employed. In some cases was necessary to modify the functions to make them compatible.

The inertia analysis and the Figure 1 (which represent the first two axes and the centres of the cluster analysis) shows the candidates with the higher percent of votes. The first and second axes explain the 51% of the inertia

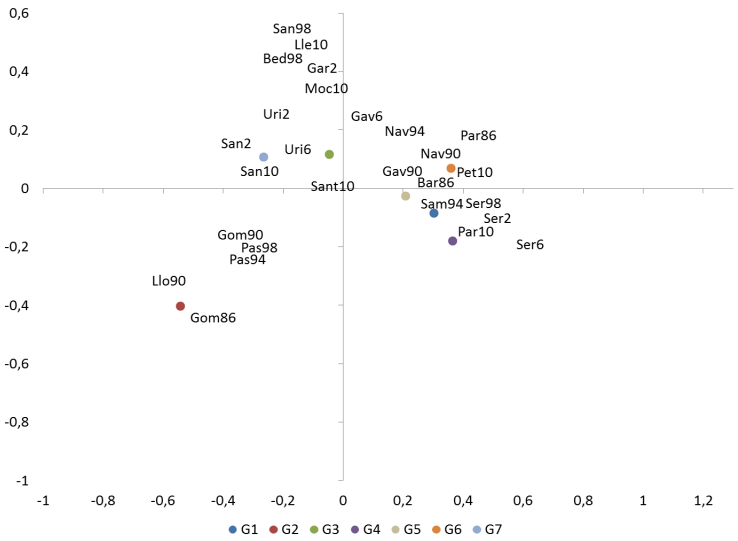


Fig. 1: WIBCA for municipalities presidential elections between 1986 and 2010

(31% and 20% respectively) and identify the candidates of the Liberal and Conservador parties like Serpa, Pastrana, Samper and Barco. The second axis is also associate with candidates who do not belong to traditional Colombian parties like Lleras, Uribe in 2002 and Mockus.

Leftist candidates like Petro, Gaviria, Jaime Pardo and Navarro are characterized by the third and fourth axes (11% and 9% of the inertia respectively) which means that this candidates do not have as many percentage of votes as the previous ones but they receive voting from a different set of municipalities that the previous candidates.

Finally, candidates like Santos and Uribe in 2006 are represented by all the axes. This could mean that this candidates get votes from all the municipalities and not only an specific category of municipality.

The Tables 5 and 6 has the cluster characterization of the WIBCA that is also presented in the Figure 1 and represented in the Figures 2, 3 and 4. In the first group the candidates Barco, Jaime Pardo, Cesar Gaviria, Samper, Serpa, Rafael Pardo and Santos present a higher percentage of voting, comparing with their national result. Except for Jaime Pardo and Santos, these candidates are affiliate with the Liberal party. This cluster has 10% of the voting, 232 municipalities and around the 75% of this municipalities (Figure 2) belong to categories 6 and 7.

In the second group the candidates Gomez, Lloreda, Pastrana, Sanin, Uribe and Santos have a higher percentage of voting, comparing with their national percentage. Except for Uribe and Santos, these candidate represent the Conservador party. This cluster has 8% of the voting, 212 municipalities and around the 80% of this municipalities (Figure 4) belong to categories 6 and 7.

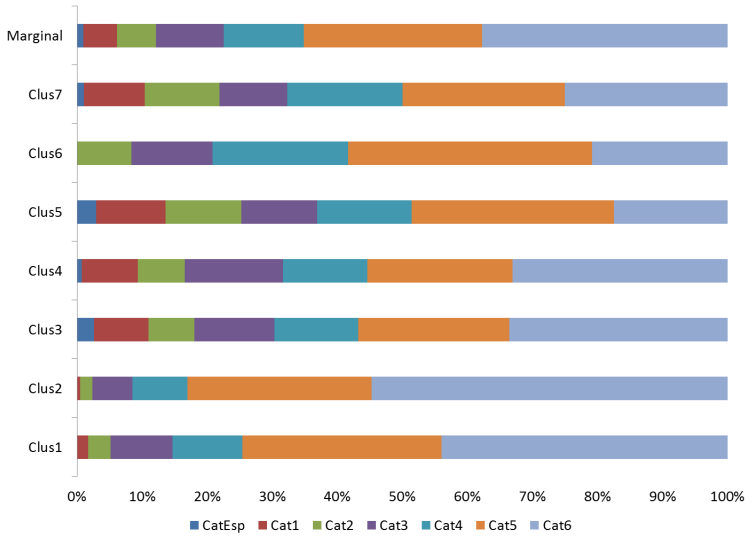


Fig. 2: Relationship between clusters and categories of municipalities

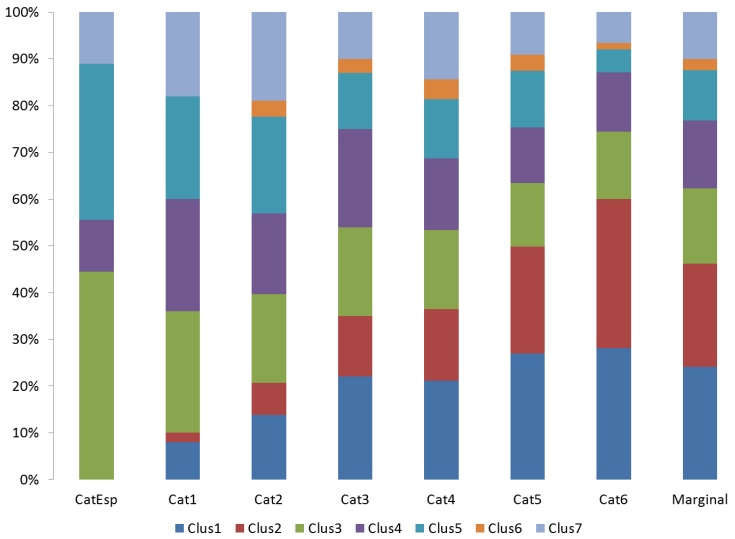


Fig. 3: Relationship between categories and cluster of municipalities

The third group presents the most similar percentage of the vote compare with the national level. This cluster has 40% of the voting, 155 municipalities and and has not a dominant category.

In the fourth group the candidates Barco, Cesar Gaviria, Samper, Serpa, Rafael Pardo and Petro show a higher percentage of voting, comparing with their national result. Except for Petro, these candidates are affiliate with the

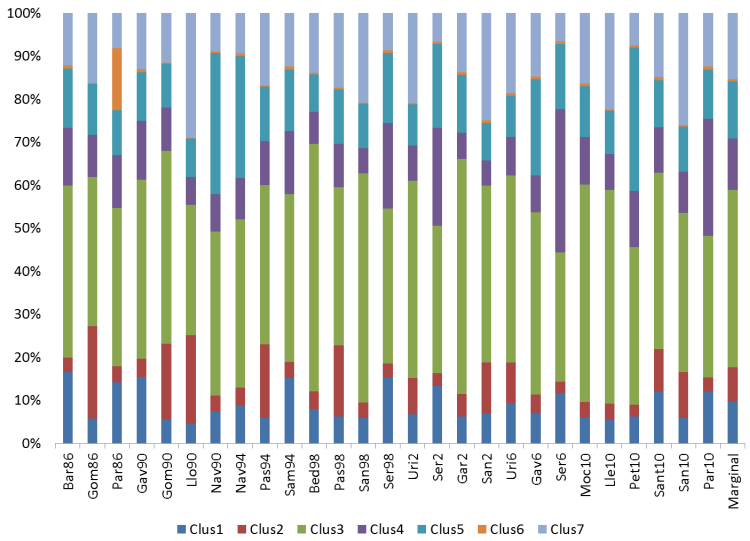


Fig. 4: Relationship between clusters and candidats

Liberal party. This cluster has 12% of the voting, 139 municipalities and has not a dominant category.

In the fifth group the candidates Barco, Navarro, Samper, Serpa, Carlos Gaviria and Petro have a higher percentage of voting, comparing with their national result. This candidates can be associate with leftist politics. This cluster has 13% of the voting, 103 municipalities and has not a dominant category.

In the sixth group the candidates Barco, Jaime Pardo, Cesar Gaviria, Samper, Gaviria, Pardo and Santos present a higher percentage of voting, comparing with their national result. Except for Santos, this candidates are associate whit softer leftist politics that the ones in the fifth group. This cluster has 1% of the voting, 24 municipalities and and has not a dominant category.

In the seven group the candidate Gomez, Lloreda, Pastrana, Sanin, Uribe, Lleras and Mockus show a higher percentage of voting, comparing with their national result. The majority of this candidates are associate whit right policies. This cluster has 15% of the voting, 96 municipalities and and has not a dominant category.

Table 5: Cluster characterization for the presidential elections between 1986 and 2010: groups one to four

| Candidate | Group 1 | | Group 2 | | Group 3 | | Group 4 | | Mean |
|---|---|---|---|---|---|---|---|---|---|
| | Clas/Cat | Cat/Clas | Clas/Cat | Cat/Clas | Clas/Cat | Cat/Clas | Clas/Cat | Cat/Clas | |
| **Bar86** | 16,5 | 11,2 | 3,4 | 2,8 | 40 | 6,4 | 13,4 | 7,4 | 6,6 |
| **Gom86** | 5,8 | 2,4 | 21,4 | 10,9 | 34,7 | 3,4 | 9,8 | 3,3 | 4 |
| **Par86** | 14,2 | 0,7 | 3,6 | 0,2 | 36,8 | 0,4 | 12,3 | 0,5 | 0,5 |
| **Gav90** | 15,4 | 7,1 | 4,2 | 2,4 | 41,7 | 4,5 | 13,7 | 5,1 | 4,5 |
| **Gom90** | 5,6 | 1,3 | 17,5 | 4,9 | 44,8 | 2,4 | 10,1 | 1,9 | 2,2 |
| **Llo90** | 4,6 | 0,5 | 20,5 | 2,9 | 30,3 | 0,8 | 6,5 | 0,6 | 1,1 |
| **Nav90** | 7,5 | 0,9 | 3,6 | 0,5 | 38,2 | 1,1 | 8,7 | 0,9 | 1,2 |
| **Nav94** | 8,8 | 0,3 | 4,1 | 0,2 | 39,2 | 0,3 | 9,5 | 0,3 | 0,3 |
| **Pas94** | 5,9 | 2,4 | 17,1 | 8,7 | 36,9 | 3,6 | 10,3 | 3,5 | 4 |
| **Sam94** | 15,1 | 6,3 | 3,7 | 1,9 | 39 | 3,8 | 14,7 | 5 | 4,1 |
| **Bed98** | 8 | 0,2 | 4,1 | 0,2 | 57,5 | 0,4 | 7,4 | 0,2 | 0,3 |
| **Pas98** | 6,2 | 3,6 | 16,6 | 11,7 | 36,8 | 5 | 10,1 | 4,7 | 5,6 |
| **San98** | 5,9 | 2,7 | 3,6 | 2 | 53,3 | 5,8 | 5,8 | 2,1 | 4,4 |
| **Ser98** | 15,3 | 9 | 3,1 | 2,2 | 36,1 | 5 | 19,8 | 9,4 | 5,7 |
| **Gar2** | 6,2 | 0,7 | 5,2 | 0,7 | 54,6 | 1,4 | 6,1 | 0,5 | 1,1 |
| **San2** | 7 | 0,7 | 11,8 | 1,5 | | | 5,9 | 0,5 | 1 |
| **Ser2** | 13,3 | 7,3 | 3 | 2 | 34,4 | 4,5 | 22,7 | 10,2 | 5,4 |
| **Uri2** | 6,7 | 6,1 | 8,5 | 9,5 | 45,9 | 9,9 | 8,2 | 6,1 | 8,9 |
| **Gav6** | 7,1 | 2,9 | 4,3 | 2,1 | 42,3 | 4,1 | 8,7 | 2,9 | 4 |
| **Ser6** | 11,7 | 2,6 | 2,7 | 0,7 | 30,1 | 1,6 | 33,3 | 5,9 | 2,1 |
| **Uri6** | 9,4 | 10,8 | 9,4 | 13,2 | 43,5 | 11,8 | 9 | 8,4 | 11,2 |
| **Lle10** | 5,5 | 1,3 | 3,7 | 1,1 | 49,7 | 2,8 | 8,3 | 1,6 | 2,3 |
| **Moc10** | 5,9 | 2,9 | 3,6 | 2,2 | 50,6 | 5,9 | 11,1 | 4,5 | 4,8 |
| **Par10** | 12 | 1,2 | 3,3 | 0,4 | 32,9 | 0,8 | 27,2 | 2,2 | 1 |
| **Pet10** | 6,3 | 1,3 | 2,7 | 0,7 | 36,7 | 1,8 | 13 | 2,2 | 2 |
| **San10** | 5,8 | 0,8 | 10,7 | 1,9 | 37 | 1,2 | 9,7 | 1,1 | 1,4 |
| **Sant10** | 12 | 12,6 | 9,9 | 12,6 | 40,9 | 10,1 | 10,6 | 9 | 10,1 |

## 5 Conclusions

This paper analyse the relation between municipalities and the results of presidential elections between 1986 and 2010, excluding the variation introduce by the size of the populations and the year of elections. For this a Weighted Intra Blocks Correspondence Analysis (WIBCA) and a mix algorithm of classification is used.

The first plan and inertia analysis show that the candidates with the higher percent of votes are the best represented in this two axes, specially the candidates Serpa, Pastrana, Samper, Barco, Lleras, Uribe in 2002 and Mockus. In the other hand, leftist candidates like Petro, Gaviria, Jaime Pardo and Navarro are characterized by the third and fourth axes, which means that this candidates do not have as many percentage of votes which means that they receive voting from a different set of municipalities as the previous candidates. Finally, candidates like Santos and Uribe in 2006 are represented by all the axes, because this candidates get votes from all the municipalities and not only an specific type.

The cluster analysis of this results shows the existence of a electoral patron in the small population size municipalities. One group of this municipalities vote for candidates which can be associate with the Liberal party and the other group vote for candidates close to the Conservador party. However, in the 2006

Table 6: Cluster characterization for the presidential elections between 1986 and 2010: groups five to seven

| Candidate | Group 5 | | Group 6 | | Group 7 | | Mean |
|---|---|---|---|---|---|---|---|
| | Clas/Cat | Cat/Clas | Clas/Cat | Cat/Clas | Clas/Cat | Cat/Clas | |
| **Bar86** | 13,9 | 6,9 | 0,7 | 7,7 | 12,2 | 5,2 | 6,6 |
| **Gom86** | 11,9 | 3,6 | 0,2 | 1,5 | 16,2 | 4,3 | 4 |
| **Par86** | 10,5 | 0,4 | 14,4 | 12,5 | 8,2 | 0,3 | 0,5 |
| **Gav90** | 11,3 | 3,8 | 0,7 | 5,6 | 13 | 3,8 | 4,5 |
| **Gom90** | 10,1 | 1,7 | 0,3 | 1,3 | 11,5 | 1,7 | 2,2 |
| **Llo90** | 8,9 | 0,8 | 0,2 | 0,4 | 29 | 2,2 | 1,1 |
| **Nav90** | 32,8 | 2,9 | 0,3 | 0,6 | 9 | 0,7 | 1,2 |
| **Nav94** | 28,4 | 0,7 | | | 9,5 | 0,2 | 0,3 |
| **Pas94** | 12,6 | 3,8 | 0,3 | 2,2 | 16,8 | 4,4 | 4 |
| **Sam94** | 14,3 | 4,4 | 0,7 | 5 | 12,4 | 3,3 | 4,1 |
| **Bed98** | 8,7 | 0,2 | 0,3 | 0,2 | 13,9 | 0,3 | 0,3 |
| **Pas98** | 12,7 | 5,4 | 0,3 | 2,8 | 17,4 | 6,4 | 5,6 |
| **San98** | 10,4 | 3,5 | 0,3 | 2 | 20,8 | 6 | 4,4 |
| **Ser98** | 16,4 | 7 | 0,5 | 5,2 | 8,7 | 3,2 | 5,7 |
| **Gar2** | 13,5 | 1,1 | | | 13,8 | 0,9 | 1,1 |
| **San2** | 8,7 | 0,7 | 0,5 | 0,9 | 25 | 1,6 | 1 |
| **Ser2** | 19,5 | 7,9 | 0,5 | 4,3 | 6,7 | 2,3 | 5,4 |
| **Uri2** | 9,5 | 6,4 | 0,3 | 4,4 | 21 | 12,2 | 8,9 |
| **Gav6** | 22,3 | 6,7 | 0,7 | 5,1 | 14,7 | 3,9 | 4 |
| **Ser6** | 15,2 | 2,4 | 0,5 | 2 | 6,6 | 0,9 | 2,1 |
| **Uri6** | 9,6 | 8,1 | 0,6 | 10,9 | 18,7 | 13,6 | 11,2 |
| **Lle10** | 10,2 | 1,8 | 0,2 | 0,8 | 22,4 | 3,4 | 2,3 |
| **Moc10** | 11,8 | 4,3 | 0,5 | 4,6 | 16,4 | 5,1 | 4,8 |
| **Par10** | 11,4 | 0,8 | 0,7 | 1,2 | 12,4 | 0,8 | 1 |
| **Pet10** | 33,3 | 5,1 | 0,5 | 1,9 | 7,5 | 1 | 2 |
| **San10** | 10,4 | 1,1 | 0,4 | 1 | 26,1 | 2,3 | 1,4 |
| **Sant10** | 10,9 | 8,3 | 0,8 | 14,4 | 14,8 | 9,8 | 10,1 |

election, this patron is less clear, because of the tendency of Santos and Uribe to get votes from all the municipalities.

## References


1. L. Bautista and P. Pacheco, Análisis de la evolución del comportamiento electoral departamental en los últimos años: aplicación de los métodos factoriales al estudio de series temporales cortas. *Revista Colombiana de Estadística*, vol. 19, pp. 94-112, 1989.
2. CNC, *Ley 136*. Congreso Nacional de Colombia, 1994
3. USTA-OCHA.,Índice de riesgo en situación humanitaria, *Universidad Santo Tomás (USTA) y Oficina para la coordinación de Asuntos Humanitarios (OCHA)*, Bogotá, 2009.
4. C. Pardo and G. Cabarcas, Métodos estadísticos multivariados en investigación social, *Simposio de Estadística. Universidad Nacional de Colombia*, Santa Marta, 2001.
5. B. Escofier and J. Pagès, Análisis factoriales simples y múltiples: objetivos, métodos e interpretaciones. *Servicio Editorial Universidad del País Vasco*, 1992.
6. L. Lebart, M. Piron, and A. Morineau, Statisitique exploratoire multidimensionnelle. Visualisation et inférence en fouilles de données. *Dunod*, Paris, 2006.
7. J. Benzécri, Statistical analysis as a tool to make patterns emerge from the data in methodologies of pattern recognition. *Academic Press*, 1969.

8. C. E. Pardo, M. Bécue-Bertaut, and J. Ortiz, Análisis de correspondencias de tablas de contingencias con subparticiones en filas y columnas, *Revista Colombiana de Estadística*, vol. 36, pp. 115-144, 2013.
9. B. Escofier, Analyse factorielle en reference a un modele. application a l'analyse de tableaux d'echanges, *Revue de Statistique Appliquée*, vol. 32, no. 4, pp. 25-36, 1984.
10. C. E. Pardo, Métodos en ejes principales para tablas de contingencia con estructuras de partición en filas y columnas. *PhD thesis, Universidad Nacional de Colombia. Facultad de Ciencias*, Bogotá, 2011.
11. M. Bécue-Bertaut and J. Pagès, A principal axes method for comparing contingency tables: MFACT, *Computational Statistics and Data Analysis*, vol. 45, pp. 481-503, Apr. 2004.
12. C. Pardo and P. DelCampo, Combinación de métodos factoriales y de análisis de conglomerados en R: el paquete FactoClass, *Revista Colombiana de Estadística*, vol. 30, no. 2, pp. 231-245, 2007.
13. C. Pardo, pamctdp: Principal Axes Methods for Contingency Tables with Partition Structures on Rows and Columns. R, 2013.

# Hierarchical Cluster Analysis of Groups of Individuals: Application to Business Data

**Áurea Sousa [1], Helena Bacelar-Nicolau[2], and Osvaldo Silva[3]**

[1] Dep. of Math., CEEAplA, University of Azores, Ponta Delgada, Azores, Portugal (Email: aurea@uac.pt)
[2] Faculty of Psychology, LEAD; ISAMB, CEA; University of Lisbon, Lisboa, Portugal (Email: hbacelar@fp.ul.pt)
[3] Dep. of Math., CES-UA, University of Azores, Ponta Delgada, Azores, Portugal (Email: osilva@uac.pt)

**Abstract:** We present one example, in which the data are issued from a questionnaire in order to find satisfaction typologies (with the services provided by an automobile company) of independent groups of individuals. The Agglomerative Hierarchical Cluster Analysis (*AHCA*) was based on two approaches: one based on a particular case of the generalized weighted affinity coefficient, which deals with classical data, and the other one on the weighted generalized affinity coefficient for the case of symbolic/complex data. Both measures of comparison between elements were combined with classical and probabilistic aggregation criteria. We used the global statistics of levels (*STAT)* to evaluate the quality of the obtained partitions.

**Keywords:** Hierarchical cluster analysis, Affinity coefficient, Independent groups of individuals, *VL* Methodology, Classical data, Symbolic data.

## 1 Introduction

Recent computational advances allow us to summarize very large datasets in terms of their underlying concepts, which can only be described by symbolic or complex data. Each entry of a symbolic data table can contain one or several values such as subsets of categories, intervals of the real dataset $\mathcal{R}$, or frequency distributions (e. g., Bacelar-Nicolau, 2000; Bock and Diday, 2000; Bacelar-Nicolau et al., 2009, 2010). A symbolic variable Y with domain (or range or observation space) $\mathcal{Y}$ is a mapping $E \longrightarrow B$ defined on a set $E$ of statistical entities (individuals, classes, objects,…). Depending of the specification of $B$ in terms of $\mathcal{Y}$, symbolic variables can be classified as: classical single-valued, set-valued, interval, multi-valued (categorical or quantitative), and modal (probabilistic) variables. A variable $Y$ is modal with observation space $\mathcal{Y}$ if, for each $a \in E, Y(a) = \pi_a$ is a non-negative measure on $\mathcal{Y}$, such as a frequency distribution, a probability distribution or a weighting (Bock and Diday, 2000).

*Stochastic Modeling, Data Analysis and Statistical Applications* (pp. 195-203)
Lidia Filus - Teresa Oliveira - Christos H Skiadas (Eds)



Here, in the case of symbolic data we will focus on Ascendant Hierarchical Cluster Analysis (*AHCA*) of data units described by modal variables. The *VL* methodology (*V* for Validity, *L* for Linkage) is a probabilistic approach for clustering methods, based on the cumulative distribution function of basic similarity coefficients, and the probabilistic aggregation criteria under this methodology resort essentially to probabilistic notions for the definition of the comparative functions (e.g. Lerman 1970, 1981; Nicolau, 1983; Bacelar-Nicolau, 1985, 1987, 1988; Nicolau and Bacelar-Nicolau, 1998). In this work, two classical aggregation criteria, Single Linkage (*SL*) and Complete Linkage (*CL*), as well as three probabilistic aggregation criteria - in the scope of the *VL* methodology- *AVL*, *AV1*, and *AVB*, are used to look for satisfaction typologies of independent groups of individuals in two contexts: classical data and symbolic/complex data. The measures of comparison between elements are based on the affinity coefficient.
Two different approaches of *AHCA* of independent groups of individuals are described in Section 2. In the first one the data units (independent groups of individuals) are described by classical single-valued variables defined on an ordinal scale and a particular case of the generalized weighted affinity coefficient was used. The second one is based on the weighted generalized affinity coefficient for the case of symbolic data. In Section 3 we refer some experimental results from Business area. Section 4 contains some concluding remarks about this work and its results.

## 2 AHCA of independent groups of subjects

From the affinity coefficient between two discrete probability distributions proposed by Matusita (1951) as the basic similarity measure for comparing two probability laws of the same type, Bacelar-Nicolau (1980, 1988) introduced the affinity coefficient, as a basic similarity coefficient between pairs of variables or of subjects in cluster analysis context (corresponding to pairs of columns or rows of a data matrix). Later on she extended that coefficient to different types of data, including complex or symbolic data and variables of mixed types (heterogeneous data), possibly with different weights (Bacelar-Nicolau, 2000, 2002; Bacelar-Nicolau et al., 2009, 2010). The extension of the affinity coefficient for the case of symbolic data is called weighted generalized affinity coefficient. In the present work, we use two different approaches of *AHCA* of independent groups of individuals based on two different generalized approaches for the affinity coefficient.

**Approach 1: particular case of the weighted generalized affinity coefficient**
In this approach, the data are initially represented in *G* tables (one table for each one of the independent groups of individuals), containing, respectively, $N_1$, $N_2$,…, $N_G$, individuals described by *p* identical variables defined on an ordinal scale. Later, *G* new tables, each one containing the same number $n = min\{N_1, N_2, \ldots, N_G\}$ of individuals (selected from a stratified random sampling) have to be obtained from the initial corresponding tables. Each new table corresponds to a

(*n*×p) data table, and $x_{ihj}$ (*i*=1,…, *n*, *h=1,..., G, j=1,..., p)* is the value of the individual *i*, belonging to the table $T_h$ (abbreviated, *h*), in the *j-th* variable (see Table 1). Then, the total scores of each independent group of individuals in each variable are computed as follows, where $x_{\bullet hj} = \sum_{i=1}^{n} x_{ihj}$ (*i*=1,…, *n*, *h=1,..., G, j=1,..., p)* is the total score of the group *h* in the variable *j* (sum in the column *j* of $T_h$*):*

Table 1. *G* new tables (same number *n*= *min*{$N_1$, $N_2$, …, $N_G$} of subjects)

| | $T_1$ *(Group 1)* | | | | $T_G$ *(Group G)* |
|---|---|---|---|---|---|
| *Ind. i* | $V_1$ ⋯ $V_p$ | | | *Ind. i* | $V_1$ ⋯ $V_P$ |
| *1* | $x_{111} \cdots x_{11p}$ | | ... | 1 | $x_{1G1} \cdots x_{1Gp}$ |
| *2* | $x_{211} \cdots x_{21p}$ | | ... | 2 | $x_{2G1} \cdots x_{2Gp}$ |
| ⋮ | ⋮ | | ... | ⋮ | ⋮ |
| *n* | $x_{n11} \cdots x_{n1p}$ | | ... | *n* | $x_{nG1} \cdots x_{nGp}$ |
| *Total* | $x_{\bullet 11} \cdots x_{\bullet 1p}$ | | | *Total* | $x_{\bullet G1} \cdots x_{\bullet Gp}$ |

The computation of the affinity coefficient between the groups *h* and *h'*, with *h*, *h'*=1, …, *G*, and *h*≠*h*', is based on the following data matrix (Table 2), and in the formula (1):

Table 2. Classical data matrix (approach 1)

| | $V_1$ ⋯ $V_p$ |
|---|---|
| *Group 1* | $x_{\bullet 11} \cdots x_{\bullet 1p}$ |
| *Group 2* | $x_{\bullet 21} \cdots x_{\bullet 2p}$ |
| ⋮ | ⋮ |
| *Group G* | $x_{\bullet G1} \cdots x_{\bullet Gp}$ |

$$a(h,h') = \frac{1}{p}\sum_{j=1}^{p} \sqrt{\frac{x_{\bullet hj}}{x_{\bullet h\bullet}} \cdot \frac{x_{\bullet h'j}}{x_{\bullet h'\bullet}}}\,, \qquad (1)$$

where $x_{\bullet h\bullet} = \sum_{j=1}^{p} x_{\bullet hj}$ (respectively, $x_{\bullet h'\bullet} = \sum_{j=1}^{p} x_{\bullet h'j}$) is the total score of the group *h,* in the *p* variables [sum in the row *h* (respectively, *h*') of Table 2]*:*

**Approach 2: weighted generalized affinity coefficient (case of modal data)**
Given a set of *N* data units (typically groups of individuals: symbolic data units) described by *p* modal variables, $Y_1$,...,$Y_p$ (each variable may have a different number of "modalities"), the weighted generalized affinity coefficient between the data units *k* and *k'* is given by:

$$a(k,k') = \sum_{j=1}^{p} \pi_j \, aff(k,k';j) = \sum_{j=1}^{p} \pi_j \sum_{\ell=1}^{m_j} \sqrt{\frac{x_{kj\ell}}{x_{kj\bullet}} \cdot \frac{x_{k'j\ell}}{x_{k'j\bullet}}} \qquad (2)$$

where: $aff(k,k';j)$ is the generalized local affinity between $k$ and $k'$ over the *j-th* variable, $m_j$ is the number of modalities of the *j-th* variable; $x_{kj\ell}$ is the number of individuals (in the unit $k$) which share the category $\ell$ of $Y_j$; $x_{kj\bullet} = \sum_{\ell=1}^{m_j} x_{kj\ell}$ , $x_{k'j\bullet} = \sum_{\ell=1}^{m_j} x_{k'j\ell}$ , and the weights, $\pi_j$, verify the condition : $\pi_j \geq 0$ *and* $\sum \pi_j = 1$ (see Table 3).

Either the local affinities or the whole weighted generalized affinity coefficient, take values in the interval [0,1] and satisfy a set of proprieties which characterize affinity measurement as a robust similarity coefficient (e.g., Bacelar-Nicolau, 2002; Bacelar-Nicolau et al., 2009). The coefficient associated to the first approach is a particular case of the coefficient associated to this second approach.

Table 3. Symbolic data matrix $\underline{X}$ with integer frequency distributions

| | ⋯ | $Y_j$ | ⋯ | $Y_{j'}$ | ⋯ |
|---|---|---|---|---|---|
| ⋮ | ⋯ | ⋯ | ⋯ | ⋯ | ⋯ |
| $k$ | ⋯ | $\left(x_{kj1},\cdots,x_{kjm_j}\right)$ | ⋯ | $\left(x_{kj'1},\cdots,x_{kj'm_{j'}}\right)$ | ⋯ |
| ⋮ | ⋯ | ⋯ | ⋯ | ⋯ | ⋯ |
| $k'$ | ⋯ | $\left(x_{k'j1},\cdots,x_{k'jm_j}\right)$ | ⋯ | $\left(x_{k'j'1},\cdots,x_{k'j'm_{j'}}\right)$ | ⋯ |
| ⋮ | ⋯ | ⋯ | ⋯ | ⋯ | ⋯ |

This approach is appropriated when we deal with large datasets.

## 3 Experimental results based on business data

Data were collected using a questionnaire applied to 450 customers in order to evaluate the satisfaction (latent variable) with the services provided by an automobile company, based on 18 component variables, which are described in Sousa et al. (2014). The variables (items) are measured in a scale with ordered modalities (1- *very dissatisfied (VD)*, 2- *generally dissatisfied (GD)*, 3- *neither satisfied nor dissatisfied (NSND)*, 4- *generally satisfied (GS)* and 5- *very satisfied (VS)*). The respondents are distributed by 11 professional occupations (O1- *Doctors, architects and engineers*; O2- *Teachers*; O3-*Businessmen*; O4-*Salesmen*; O5-*Employees of banks and insurance companies*; O6-*Military and police*; O7-*Administrative and similar*; O8- *Employees of the civil construction*; O9- *Employees of the commerce and industry*; O10- *Employees of hotels and restaurants*; O11- *Employees of other services*. The numbers of individuals in each modality of the variable "*Professional occupation*", with 11 modalities, are respectively 45, 40, 79, 42, 38, 40, 35, 34, 51, 24, 22.

The clustering of the 11 professional occupations was based on two approaches (see Section 2). The measures of comparison between elements were combined

with two classical aggregation criteria, *Single Linkage* (*SL*) and *Complete Linkage* (*CL*), and three probabilistic aggregation criteria, *AVL*, *AV1*, and *AVB*. In the present work, the validation of the results is based on the global statistics of levels (*STAT*), as proposed by Lerman (1970, 1981) and Bacelar-Nicolau (1980, 1985), in both paradigms (classical and symbolic data).

In the first approach the data were initially represented in *11* tables (one table for each professional occupation), containing, respectively, 45, 40, 79, 42, 38, 40, 35, 34, 51, 24 and 22 subjects, described by *18* identical variables. Then, *11* new tables, composed by $n$=22 ($n = min\{45, 40, 79, 42, 38, 40, 35, 34, 51, 24, 22\}$) rows (selected from a stratified random sampling) were obtained from the initial corresponding tables (see Table 1). The *AHCA* of the professional occupations was based on a classical data matrix, as Table 2, composed by 11 rows and 18 variables ($V_1$ to $V_{18}$). The entry corresponding to the intersection between the *h-th* row and the *j-th* column of this data matrix contains the total scores of the group *h* (*h*=1,…,11) in the variable *j* (*j=1,…,18*). In this approach, the value of the affinity coefficient between the professional occupations *h* ($O_h$) and *h'* ($O_{h'}$) is given by formula (1).

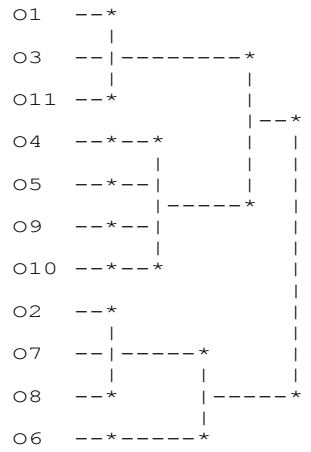


Fig. 1. Dendrogram obtained with *CL*, *AVL*, *AV1* and *AVB* (Approach 1)

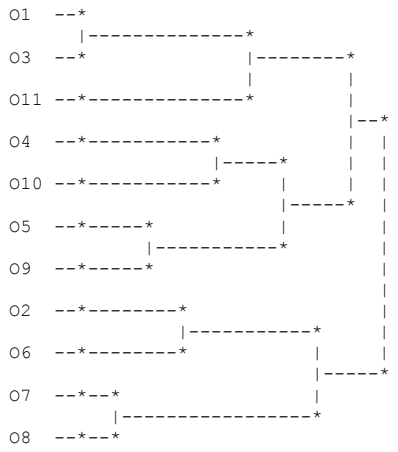


Fig. 2. Dendrogram obtained with *AVL* and *AV1* methods (Approach 2)

The selected partition is the partition into two clusters (*STAT*=5.5222), which was obtained at level 9 by all aggregation criteria (see Figure 1).

In the second approach (case of a symbolic data table for modal variables), from the initial data table (450 × 18), the subjects were distributed into 11 groups according to their professional occupation. The data units, O1 to O11, contain, respectively, 45, 40, 79, 42, 38, 40, 35, 34, 51, 24 and 22 individuals and each entry of the new data table contains a frequency distribution. In fact, the *11*

professional occupations correspond to symbolic data units (rows of a symbolic data table as Table 3) described by *18* modal variables ($V_1$ to $V_{18}$) .
Figure 2 shows the dendrogram associated with the *AVL* and *AV1* methods. The best partition is the partition into three clusters (*STAT*=5.5372), which was obtained at level 8 by all aggregation criteria.
The clustering results provided by both approaches were compared. Note that at levels 7 and 8 both approaches provide the same partitions (respectively, into two and into three clusters).

Table 4. Responses given by the subjects belonging to each cluster (%)

| | | | **V1** | | | | | **V2** | | | | | **V3** | | |
|---|---|---|---|---|---|---|---|---|---|---|---|---|---|---|---|
| | **1** | **2** | **3** | **4** | **5** | **1** | **2** | **3** | **4** | **5** | **1** | **2** | **3** | **4** | **5** |
| **C1** | 0% | 0% | 63% | 25% | 12% | 0% | 8% | 14% | 79% | 0% | 0% | 0% | 0% | 4% | 96% |
| **C2** | 0% | 0% | 30% | 65% | 5% | 0% | 6% | 55% | 35% | 3% | 0% | 0% | 3% | 45% | 52% |
| **C3** | 0% | 0% | 3% | 96% | 1% | 0% | 5% | 81% | 7% | 8% | 0% | 0% | 3% | 82% | 15% |
| | | | **V4** | | | | | **V5** | | | | | **V6** | | |
| | **1** | **2** | **3** | **4** | **5** | **1** | **2** | **3** | **4** | **5** | **1** | **2** | **3** | **4** | **5** |
| **C1** | 0% | 0% | 76% | 20% | 4% | 8% | 13% | 55% | 23% | 2% | 0% | 8% | 9% | 79% | 5% |
| **C2** | 0% | 0% | 41% | 57% | 2% | 4% | 16% | 69% | 11% | 0% | 0% | 6% | 48% | 41% | 5% |
| **C3** | 0% | 0% | 9% | 91% | 0% | 1% | 13% | 80% | 7% | 0% | 0% | 5% | 80% | 7% | 9% |
| | | | | **V7** | | | | **V8** | | | | | **V9** | | |
| | **1** | **2** | **3** | **4** | **5** | **1** | **2** | **3** | **4** | **5** | **1** | **2** | **3** | **4** | **5** |
| **C1** | 0% | 5% | 8% | 86% | 0% | 0% | 0% | 4% | 92% | 4% | 0% | 0% | 0% | 4% | 96% |
| **C2** | 0% | 4% | 45% | 48% | 4% | 0% | 0% | 37% | 56% | 7% | 0% | 0% | 8% | 40% | 52% |
| **C3** | 0% | 3% | 79% | 11% | 8% | 0% | 0% | 66% | 21% | 13% | 0% | 0% | 10% | 75% | 15% |
| | | | **V10** | | | | | **V11** | | | | | **V12** | | |
| | **1** | **2** | **3** | **4** | **5** | **1** | **2** | **3** | **4** | **5** | **1** | **2** | **3** | **4** | **5** |
| **C1** | 0% | 0% | 4% | 51% | 45% | 0% | 0% | 3% | 27% | 69% | 0% | 0% | 0% | 17% | 83% |
| **C2** | 0% | 3% | 15% | 59% | 23% | 0% | 3% | 14% | 54% | 29% | 0% | 0% | 12% | 41% | 47% |
| **C3** | 0% | 3% | 22% | 70% | 4% | 0% | 3% | 18% | 74% | 5% | 0% | 0% | 17% | 68% | 15% |
| | | | **V13** | | | | | **V14** | | | | **V15** | | | |
| | **1** | **2** | **3** | **4** | **5** | **1** | **2** | **3** | **4** | **5** | **1** | **2** | **3** | **4** | **5** |
| **C1** | 4% | 16% | 47% | 27% | 5% | 0% | 0% | 14% | 86% | 0% | 0% | 0% | 0% | 15% | 85% |
| **C2** | 4% | 16% | 62% | 15% | 3% | 0% | 3% | 45% | 45% | 6% | 0% | 0% | 12% | 43% | 45% |
| **C3** | 4% | 9% | 73% | 11% | 2% | 0% | 3% | 79% | 7% | 11% | 0% | 0% | 17% | 73% | 9% |
| | | | **V16** | | | | | **V17** | | | | | **V18** | | |
| | **1** | **2** | **3** | **4** | **5** | **1** | **2** | **3** | **4** | **5** | **1** | **2** | **3** | **4** | **5** |

| | | | | | | | | | | | | | | | |
|---|---|---|---|---|---|---|---|---|---|---|---|---|---|---|---|
| ***C1*** | *0%* | *0%* | *75%* | *16%* | *9%* | *0%* | *0%* | *75%* | *12%* | *13%* | *3%* | *17%* | *51%* | *23%* | *5%* |
| ***C2*** | *0%* | *0%* | *39%* | *59%* | *3%* | *0%* | *0%* | *39%* | *57%* | *5%* | *2%* | *18%* | *69%* | *9%* | *2%* |
| ***C3*** | *0%* | *0%* | *7%* | *93%* | *1%* | *0%* | *0%* | *7%* | *93%* | *1%* | *0%* | *13%* | *77%* | *10%* | *0%* |

The differences between the clustering results appear to be due, in part, to the sampling process associated to the first approach and to the fact that in this approach we work only with the total scores of each independent group of individuals in each variable. Thus, in the remainder text, we will only refer to the best partition provided by the second approach: ***Cluster 1:*** {O1, O3, O11}; ***Cluster 2:*** **{**O4, O5, O9, O10}; ***Cluster 3:*** **{**O2, O6, O7, O8}. From the observation of Table 4, it can be seen some of the main differences between the profiles associated to these three clusters.

In a 2D Zoom Star, axes are linked by a line that connects most frequent categorical values of each variable, so it allows us to identify the main characteristics of the objects. Figure 3 shows the 2D Zoom Stars associated to the clusters of the second approach. We observe that, for instance, most respondents included into cluster 3 are: generally satisfied with the aspects associated to variables V1, V3, V4, V9, V10, V11, V12, V15, V16 and V17; and neither satisfied nor dissatisfied with the aspects associated to variables V2, V5, V6, V7, V8, V13, V14 and V18 (see Figure 3 and Table 4).

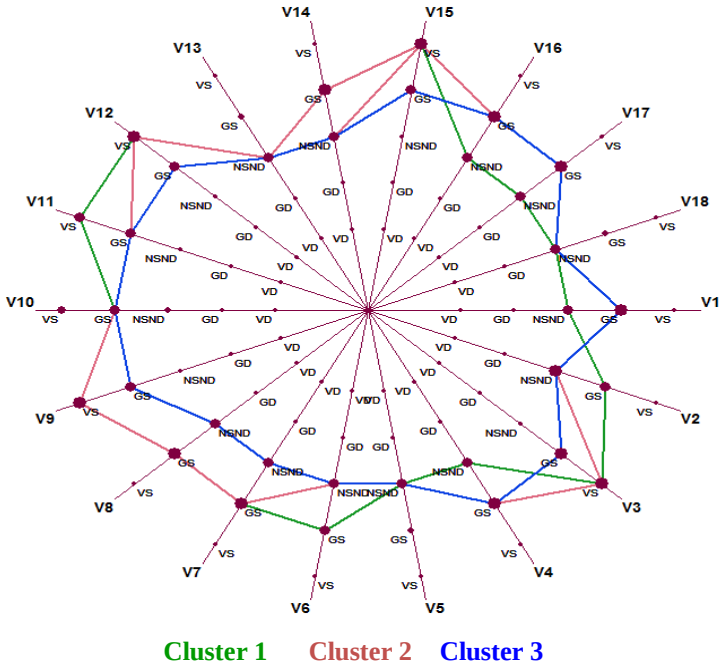


Fig. 3. 2D *Zoom Stars representation for the clusters- Approach 2*

## 4 Conclusions

The knowledge about the satisfaction profiles is useful, because customers respond better to the Market segmentation strategies which address their specific needs.
In the case of the first approach we loss information because we can´t work with the entire sample but only with a stratified random subsample, and this approach works only with the total scores of each independent group of individuals in each variable (that is, we also loss information about the scores of the groups in the modalities of the variables). Contrary, using the second approach (weighted generalized affinity coefficient, for complex or symbolic objects) it is possible to work with the entire dataset, and with the frequency distributions associated to the scores of each independent group of individuals in the modalities of each variable.
The differences between the clustering results (satisfaction typologies) provided by the two approaches of *AHCA* of independent groups of individuals were due, in part, to the smaller number of individuals of each group when we apply the first approach as a consequence of the sampling process. Nevertheless, we might have opted by inquiring a larger number of individuals in each group, during the planning of the investigation.

## References

1. Bacelar-Nicolau, H., Contributions to the Study of Comparison Coefficients in Cluster Analysis, PhD Thesis (in Portuguese), Universidade de Lisboa (1980).
2. Bacelar-Nicolau, H., The affinity coefficient in cluster analysis, Methods of Operations Research, vol. 53, Martin J. Bekmann et al (ed.), Verlag Anton Hain, Munchen, pp. 507-512 (1985).
3. Bacelar-Nicolau, H., On the distribution equivalence in cluster analysis, In Proceedings of the NATO ASI on Pattern Recognition Theory and Applications, Springer - Verlag, New York, pp. 73-79 (1987).
4. Bacelar-Nicolau, H., Two Probabilistic Models for Classification of Variables in Frequency Tables, In: Bock, H.-H. (Eds.), Classification and Related Methods of Data Analysis, North Holland, pp. 181-186 (1988)
5. Bacelar-Nicolau, H., The Affinity Coefficient, In: Analysis of Symbolic Data: Exploratory Methods for Extracting Statistical Information from Complex Data, H.-H. Bock and E. Diday (Eds.), Series: Studies in Classification, Data Analysis, and Knowledge Organization, Springer-Verlag, Berlin, pp. 160-165 (2000).
6. Bacelar-Nicolau, H., On the Generalised Affinity Coefficient for Complex Data, *Biocybernetics and Biomedical Engineering*, vol. 22, no. 1, pp. 31-42, (2002).
7. Bacelar-Nicolau, H.; Nicolau, F.C.; Sousa, Á.; Bacelar-Nicolau, L., Measuring Similarity of Complex and Heterogeneous Data in Clustering of Large Data Sets, *Biocybernetics and Biomedical Engineering*, vol. 29, no. 2, pp. 9-18 (2009).
8. Bacelar-Nicolau, H.; Nicolau, F.C.; Sousa, Á.; Bacelar-Nicolau, L., Clustering Complex Heterogeneous Data Using a Probabilistic Approach, In *Proceedings of Stochastic Modeling Techniques and Data Analysis International Conference* (SMTDA2010), pp. 85-93 (2010) (electronic publication).

9. Bock, H.-H. and Diday, E., Analysis of Symbolic Data: Exploratory Methods for Extracting Statistical Information from Complex Data, Series: Studies in Classification, Data Analysis, and Knowledge Organization, Springer-Verlag, Berlin (2000).
10. Lerman, I. C., Sur l`Analyse des Données Préalable à une Classification Automatique (Proposition d'une Nouvelle Mesure de Similarité), Rev. Mathématiques et Sciences Humaines, vol. 32, no. 8, pp. 5-15 (1970).
11. Lerman, I. C., Classification et Analyse Ordinale des Données, Dunod, Paris (1981).
12. Matusita, K., On the Theory of Statistical Decision Functions, Ann. Instit. Stat. Math, vol. III, pp. 1-30 (1951).
13. Nicolau, F.C., Cluster Analysis and Distribution Function, Methods of Operations Research, vol. 45, pp. 431-433 (1983).
14. Nicolau, F.C. and Bacelar-Nicolau, H., Some Trends in the Classification of Variables, In: Hayashi, C., Ohsumi, N., Yajima, K., Tanaka, Y., Bock, H.-H., Baba, Y. (Eds.), Data Science, Classification, and Related Methods. Springer-Verlag, pp. 89-98 (1998).
15. Sousa, Á., Bacelar-Nicolau, H., Silva, O., Cluster Analysis of Business Data. *Asian Journal of Business and Management*, 2(1) 18-26 (2014).

# Monte-Carlo Reliability Evaluation of the Ring Detector based on Heavily Masked Normalized Correlation

**Samuel Kosolapov**

Signal and Image Processing Laboratory, ORT Braude Academic College of Engineering, Karmiel, Israel
Email: ksamuel@braude.ac.il

**Abstract:** A number of general-purpose ring and circle detectors are known. In most cases, template matching and Hough transform are used to detect rings inside the image. However, ring detectors described in the literature were found impractical for the real-life implementation of the camera-based Instant Feedback System (IFS). Goal of the IFS is to collect answers of the students to the multiple-choice questions during the lecture. In the frames of the camera-based IFS, students answer to the specific multiple-choice question by presenting to the camera a specially designed IFS cards. Image of the class contains plurality of IFS cards in the different orientations and of different sizes, which makes recognition non-trivial. To simplify recognition, preferred design of IFS card contains bounding black ring and some other IFS specific elements positioned inside the bounding ring. IFS cards in the periphery of the real-life image are geometrically distorted, making standard template match approach too slow and non-reliable. To cope with this problem, standard Normalized Correlation template-matching algorithm was modified by adding the mask hiding the IFS elements inside the ring. In this case the number of templates needed to isolate IFS card is significantly smaller. In order to evaluate reliability of the proposed algorithm, special software Monte-Carlo simulator was created. Monte-Carlo simulation results show that in case of non-overlapped cards recognition error is less than 1%, which can be considered as adequate for the real-life camera-based IFS. Developed approach can be used to speed-up recognition in the other practically interesting cases, for example, for the traffic signs recognition.

**Keywords:** Image Processing, Ring Detector, Normalized Correlation, IFS, Monte-Carlo simulation

## 1. Introduction

In many practically important application there is a need to find rings (or circles) in the image. A number of general-purpose ring and circle detectors are known. In most cases modifications of template maching algorithms and Hough

*Stochastic Modeling, Data Analysis and Statistical Applications* (pp. 205-212)
Lidia Filus - Teresa Oliveira - Christos H Skiadas (Eds)



Transform algorithms are used. Those approches are implemented in a number of popular libraries and software packages. For example, MATLAB contains *"imfindcircles"* function to automatically detect circles or circular objects in an image. This function requres a radius range in pixels to search for the circles and a number of "sensitivity" parameters. This function implements two different methods. Using "two-stage method" enables to detects parts of the circles, so that overlapping circular objects can be detected. Additional option in MAPTLAB is to use *"CircularHough_Grd"* based on "Circular Hough Transform" [1]. As in the previous case, a range of radii and other "sensitivity" parameters must be specified. In case ellipse must be found, modifications of the "Randomized Hough Transform" [2] based on original algorithm [3] can be used. Popular "OpenCV" library contains function *"HoughCircles"* [4]. This library can be used to create PC, Android and iPhone real-time application.

However, ring detectors described in the above examples were found impractical for the real-life implementation of the camera-based Instant Feedback System (IFS). Goal of the IFS is to collect answers of the students to the multiple-choice questions during the lecture. In the frames of the camera-based IFS, students answer to the specific multiple-choice question by presenting to the camera a specially designed IFS cards [5]. Photo of the class contains plurality of IFS cards images in the different orientations and of different sizes, which makes recognition and analysis non-trivial.

## 2. IFS Card Design

To simplify recognition and analysis of the IFS cards, preferred design of IFS card contains bounding black ring and some other IFS specific elements.

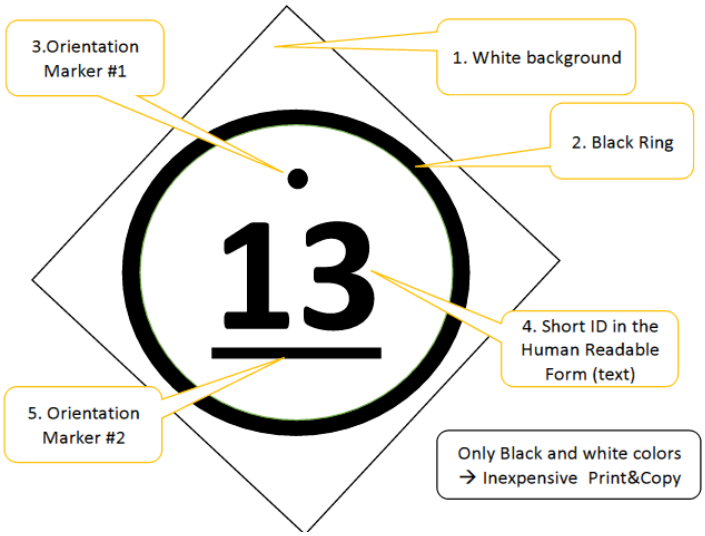


**Fig. 1.** IFS Card Design

Figure 1 presents IFS card design described in this work. IFS Card is printed on the thick white paper by using any available black and white printer. Background of the card is white (1). The card has a black ring (2), orientation markers (3 and 5) and two-digit number in the human-readable form (4). This number designates short ID of the specific student (for example, number of the student in the class list). Orientation of the IFS card specifies number of the selected answer. Orientation markers (3 and 5) prevents orientation ambiguity for the numbers like 66-99. Described design does not contains color element, so that set of cards can be copied using standard copy-machine.

## 3. Steps in the IFS Card recognition and analysis

Human observer analyzing the image of the class easily recognizes bounding black ring and the number inside the ring for any possible orientation. For the computer the problem of recognition of the plurality of the IFS cards is not trivial, because orientation and sizes of the bounding rings and digits are different. Direct template-matching approach is possible, but time consuming, because a very big number of templates (having different digits in the different sizes and in the different orientations) must be used. For this specific IFS design, the search can be executed faster. On the first step, only bounding rings (of different sizes) are to be found. Then sub images inside the bounding rings are to be scaled to the "standard size". On the second step markers inside sub-images are to be used to evaluate specific IFS card orientation and rotate its digits to the "standard position". On the third step OCR or direct template match algorithm can be used to recognize two digits of the "standard size" and in the "standard orientation".

## 4. Ring Detector based on Heavily Masked Normalized Correlation

Very popular and practical template matching algorithm widely used in the Image Processing is "2D Normalized Correlation":

$$R[row,col] = \frac{\sum_{y=0}^{m-1}\{\sum_{x=0}^{n-1}(T[row,col]-\bar{T})(I[row+y,col+x]-\bar{I})\}}{\sqrt{\sum_{y=0}^{m-1}\{\sum_{x=0}^{n-1}(T[row,col]-\bar{T})^2(I[row+y,col+x]-\bar{I})^2\}}}$$

High value of the R (close to 1.0) means that template T is found inside the image I starting from [row, col]. Normalization is needed to make recognition invariant to the brightness variations. Unfortunately, direct implementation of this algorithm in our case is not practical, because of markers and digits inside the bounding ring. To cope with this problem, standard Normalized Correlation

template-matching algorithm was modified by adding the mask hiding the markers and digits inside the ring.


**Fig. 2**. Mask used to find the ring

Figure 2 presents green region that is to be used to find bounding black ring. Pixels outside the green ring are to be excluded from the sums in the Normalized Correlation equation. Number of pixels to be used for the calculation of the sums is significantly smaller.

Despite idea of masking looks simple and nearly obvious, exact analog was not found in the literature.

## 5. Monte-Carlo Simulator

In order to evaluate reliability of the proposed algorithm, special software Monte-Carlo simulator was created as Windows Forms Desktop C# .NET application.

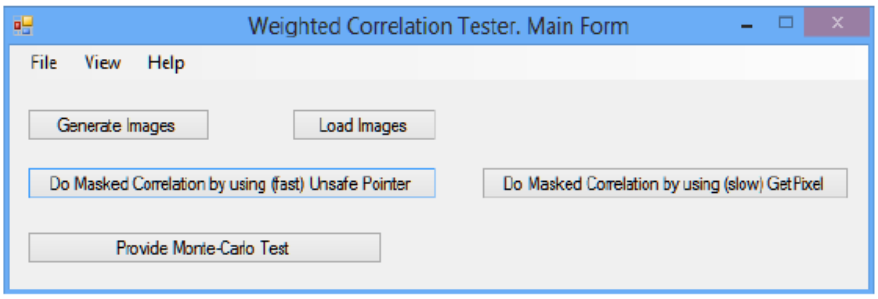


**Fig. 3.** Appearance of the Monte-Carlo software simulator

Figure 3 presents appearance of the simulator. Pressing the button "Generate Images" call "Pattern Generator Form" (see Figure 4). Operator can specify a background image (for example, image of the real class), number of IFS cards to place on this background image in the pseudo-random sizes, positions and orientations. Additional geometrical parameters of the IFS cards, noise level and some others (like level of geometrical distortions, level of cards overlap) can be specified.

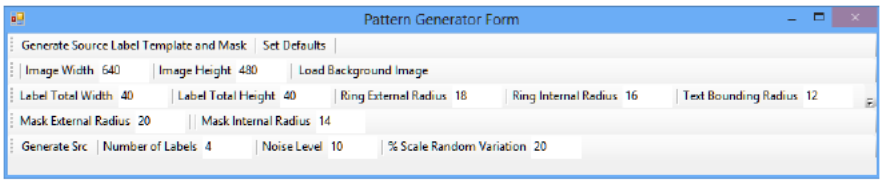


**Fig. 4.** Pattern Generator Form

Pressing button "Generate Src" creates a number of images: "Label", "Template", "Mask" (see Figure 5) and resulted synthetic image (see Figure 6)

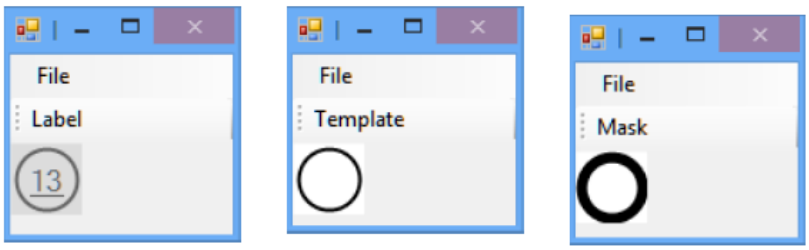


**Fig. 5.** Label, Template, Mask.

Label, Template and Mask can be stored to files and loaded from files.

Second part of the Monte-Carlo simulator attempts to recognize IFS cards in the image in test. Currently, two implementations of the Heavily Masked Normalized Correlations are supported: by using unsafe pointer and by using GetPixel function. Obviously, implementation with unsafe pointer is nearly 100 times faster: VGA size image was processed during 5 seconds. Typical results of the processing are presented in the Figure 7. Current utility deals with ring recognition only because other recognitions steps are trivial. Button "Provide Monte-Carlo Tests" provides long series of tests {create image – process

image} while collecting recognition success rate.


**Fig. 6.** Resulted synthetic image


**Fig. 7.** Results of Heavily Masked Normalized Correlation algorithm: Region of the Higest Correlation value (~ 0.99) marked by red cross (Label #10).

## Conclusions

Monte-Carlo simulation results provided on synthetic images show that in case of non-overlapped cards circles detection success is close to 99%, which can be considered as adequate for the real-life camera-based IFS, because, practically, processed image of the class, with recognized cards marked as "green", must be presented to the lecturer for the final approval. By visually inspecting image of the class, human observer (lecturer) will easily reveal non-recognized (and/or cards recognized in the wrong way) cards, and manually correct the final grades list. Despite the need of this manual inspection, time to get the final grades list still is fast enough (number of seconds) to consider all the process as Instant Feedback System. High detection rate can be achieved only in case that cards are not overlapped and in case that camera resolution is high enough to properly resolve elements of the IFS cards. Practically, for the camera with 16 Mpixel resolution, reliable IFS cards recognition is limited to the class of 20-30 students. In case of bigger class, a number of images must be obtained, which may be considered as not convenient or even not practical for the selected camera-based concept.

## Future R&D and Applications

Current implementation was limited to the rings detection on synthetic images only. Next R&D will include evaluation of the IFS card orientation and OCR of the number (short ID) inside the ring as for the synthetic as for real class images. It can be expected, that Heavily Masked Normalized Correlation may be instrumental for the fast markers search inside the external ring. More, considering that practical number of short IDs is limited to 30, OCR algorithm can analyze only unique parts of the IDs by using properly selected masks. According to our preliminary evaluations, in this case, OCR speed can be increased at least by factor 3. Developed ring detection algorithm uses no third party libraries and thus can be ported to any platform (PC, Android, and iPhone) by using any modern programming language (C, C++, C#, Java, Python, etc.) Additionally, this algorithm can easily be implemented as web service or web/cloud application. In case of cloud implementation of the camera-cased IFS multiple-choice exam lecturer will grab the image of the class by using simple cloud application for the standard smartphone. Grabbed image (or images) will be immediately send to the cloud server for the proper image processing. Cloud image processing time may be very short. Additional advantage of the cloud approach is that no software installation is needed. Additionally, developed Heavily Masked Normalized Correlation approach can be used to speed-up recognition in the other practically interesting cases, for example, for the traffic signs recognition.

## References

[1] Tao Peng. Detect circles with various radii in grayscale image via Hough Transform. . MATLAB Central, 2005

[2] McLaughlin and Robert. Randomized Hough Transform. Improved Ellipse Detection with Comparison. Technical Report JP98-01, 1998.

[3] Lei XU, Erkki OJA, Pekka Kultanena. A new curve detection method: Randomized Hough Transform. Pattern Recognition Letters, 11 331-338, 1990

[4] OpenCV Library http://opencv.org/

[5] S. Kosolapov, E. Gershikov and N. Sabag, "Feasibility of Camera-Based Instant Feedback System", *Think Mind*, Content 2013 Proceedings, 23-29, 2013

# 5 CHAPTER

## Statistics in Health Sciences and Sports

# Body composition and food intake in athletes and non athletes portuguese male adolescents

Domingos J. Lopes da Silva[1], Teresa A. Oliveira[2], and Amílcar Oliveira[3]

[1] Corresponding author. Escola Superior de Educação de Fafe and Escola Secundária3 de Barcelinhos, Portugal
(E-mail: domingosjlsilva@gmail.com)
[2] Universidade Aberta and CEAUL, Portugal
(E-mail: teresa.oliveira@uab.pt)
[3] Universidade Aberta and CEAUL, Portugal
(E-mail: amilcar.oliveira@uab.pt)

**Abstract.** The aim of the present study was to establish comparisons between male adolescent athletes and non-athletes, aged between 15 and 16, belonging to two schools of Barcelos (a city in the North of Portugal), and regarding the following components: 1) body composition, and 2) food intake. The sample was constituted by 118 subjects, of which 40 were athletes and 78 non-athletes. Weight and height were measured. The feeding pattern was obtained with the application of a semi-quantitative food frequency questionnaire; the data was treated using "The Food Processor Plus, 7.0" program. The assessment of body composition was determined through measurement of 4 skinfolds: tricipital, bicipital, sub-scapular and supra-iliac. The statistical procedures used were the mean, the standard-deviation, the minimum and the maximum, and the Student's independent samples t-test. The data were normally distributed, and the variances were homogeneous. The accepted statistical significance level was of 5%. The main results and conclusions were the following: 1) athletes had higher energy intakes than non-athletes, confirmed by the consumption of larger amounts of carbohydrates, lipids and proteins; 2) in this age stratum, differences in body composition between athletes and non-athletes were not evident.
**Keywords:** Exploratory data analysis, body composition estimation, levene test, t-test.

## 1 Introduction

Concerns about food hygiene date back to ancient Greece, when famous athletes like Lampis of Lacone or Milo of Cretonne, already recognized the importance and the merit of adopting certain eating habits, in search of better athletic performances.
At the present time, the anthropometric measures, by skinfolds (SKF) method, and nutrition assessment, by the recourse to food frequency questionnaires (FFQ) are some field practices more used in body composition estimation as

*Stochastic Modeling, Data Analysis and Statistical Applications* (*pp.* 215 - 224)
Lidia Filus - Teresa Oliveira - Christos H Skiadas (Eds)



well as in nutritional intake, respectively, particularly in detection of psychosomatic and chronic imbalances in relation to energy intake to expenditure ratio (Gibson[18], Willett[51], Silva and Rodrigues[45], Silva *et. al.*[47]).
When we compare athletes with non-athletes, regarding food intake and energy expenditure, we know that the first are subjected to a more intense physical work volume, therefore, they have an increased need of food intake, as a way to compensate for the imbalance due to regular physical activity Pendergast *et. al.*[37]. However, the comparison of body composition between male adolescents, athletes and non-athletes, do not assume evident differences Silva *et. al.*[46].
The sports diet, according to (Craplet *et. al.*[9], Rodrigues[41], Hamm[19], Jeukendrup and Cronin[24], Silva *et. al.*[47]) is assumed as a variable of capital importance in the search to obtain high competitive performances, that is, the physical ability is strictly dependent upon the feeding process.
On the other hand, systematic and regular training, as well as competition and the adoption of appropriate eating habits, have remarkable effects on the body structure (particularly, the development of muscle mass), the typology of fibers, capillarization and metabolism Hertogh *et. al.*[21]. Therefore, the establishment of comparisons and eventual relationships with the nutritional profiles and body composition between athletes and non-athletes adolescent males is stated as the main reason for this study.

## 2 Methods

**Subjects**. The sample was composed by 118 volunteer males, according to ACSM[1], of which 40 were athletes (ATHL) [we considered athlete, a subject who has been undergoing for at least 6 months a regular sports activity, organized and oriented by a coach, with a minimum of 2 sessions and 4 hours of practice per week, apart from the curricular lessons of physical education with 2 sessions and 3 hours per week. The sports practice were: football (n=27), basketball (n=6), rolling skate (n=3), karate (n=2), sprint run (n=1) and table tennis (n=1)], and 78 non-athletes (NATH) [we considered non-athlete a subject whose only physical activity is the school lessons of physical education, 2 sessions and 3 hours per week], aged between 15 and 16 years (ATHL: 15.6 $\pm$ 0.50 years; NATHL: 15.3 $\pm$ 0.47 years). All the subjects participated in all the proposed tests.
**Food habits assessment**. The estimation of the food intake was accomplished through the use of a semi-quantitative FFQ, referring to preceding year to interview, aided by the illustration of a photographic coloured manual containing all the food items used in the questionnaire, serving not only as a visual means for the subject, but also allowing the choice of multiples and submultiples of average amounts (Lopes *et. al.*[29], Barros *et. al.*[2], Rebelo *et. al.*[39], Rodrigues *et. al.*[42]). Food Processor Plus, version 7.0, was then used to convert the data collected by the FFQ into nutrient intakes ESHA Research[15].
**Anthropometric measurements**. According to the proposals and the protocol defined by Harrison *et. al.*[20], the following anthropometrics measures were undertaken: height and body weight, bicipital, tricipital, sub-scapular and

supra-iliac SKF. A "Slim-Guide" caliper was used for the SKF Donoghue[11].
**Body composition estimation**. We used the indirect method based on anthropometrical measurements, diving the body mass into two compartments, taking into account the proposals of Durnin and Womersley[13], to estimate body density (BD); percentage of body fat mass (%FM) was obtained using to the equation by Siri[48] and the amount of fat-free body mass (FFM) was determined by direct calculation, by subtraction.
**Statistical procedures**. All the variables were statistically treated. We used the most important descriptive measures: mean ($\bar{x}$) and standard-deviation (s). The minimum (Min) and the maximum (Max), was used to show the external deviations. The Kolmogorov-Smirnov test was used, and indicated that the data distribution was normal. The Levene statistics showed that the variances were homogeneous. The Student's independent samples t-test (p) was used to determine the differences between the two groups of subjects. The statistical significance level was of 5% ($\alpha = 0.05$). The SPSS 19.0 was the statistical program used to carry out the analysis.

## 3 Results

All results will be presented as mean ± standard-deviation, minimum, maximum, as well as the t-test p value (p). Table 1 allows us to verify the differences between the two groups concerning the amount of daily calories intake. Athletes subjects ingested significantly higher amount of energy than non-athletes subjects ($p = 0.021$). Both groups presented a moderate coefficient of variation (ATHL: 24.98; NATH: 22.58).

**Table 1.** Daily dietary energy (kcal) intake by both groups.

| | ATHLETES | | | NON-ATHLETES | | | |
|---|---|---|---|---|---|---|---|
| | $\bar{x}$ | s | Min-Máx | $\bar{x}$ | s | Min-Máx | p |
| Energy (kcal) | 3203 | 800.04 | 1947-4932 | 2897 | 654.09 | 1875-4825 | 0.021 |

**Macronutrients**
With statistically significant evidence, adolescent athletes consumed higher amounts of carbohydrates (complex and total), and proteins; the cholesterol intake is significantly higher in the athletes sample. The sugars, as well as the saturated, monounsaturated, and polyunsaturated fat present a marginal statistical evidence ($0.05 < p < 0.10$), in all cases due to higher mean values of athletes subjects.

**Table 2.** Macronutrients intake results.

| | ATHLETES | | | NON-ATHLETES | | | |
|---|---|---|---|---|---|---|---|
| Macronutrients | $\bar{x}$ | s | Min-Máx | $\bar{x}$ | s | Min-Máx | p |
| **Carbohydrates (CHO):** | | | | | | | |
| Sugars (g) | 162 | 50.61 | 88-302 | 146 | 48.20 | 42-261 | 0.091 (ns) |
| Complex CHO (g) | 161 | 57.10 | 78-182 | 141 | 47.33 | 57-265 | 0.047 |
| Total CHO (g) | 398 | 119.09 | 239-663 | 357 | 98.69 | 177-647 | 0.050 |
| **Lipids:** | | | | | | | |
| Saturated Fat (g) | 39 | 10.98 | 23-65 | 35 | 9.04 | 13-55 | 0.062 (ns) |
| Monounsaturated Fat (g) | 46 | 12.65 | 26-88 | 41 | 10.49 | 18-73 | 0.060 (ns) |
| Polyunsaturated Fat (g) | 21 | 5.37 | 11-36 | 19 | 5.26 | 8-33 | 0.206 (ns) |
| Cholesterol (mg) | 591 | 173.31 | 337-1062 | 494 | 144.08 | 231-833 | 0.002 |
| Total Fat (g) | 115 | 30.06 | 67-199 | 105 | 25.11 | 49-162 | 0.055 (ns) |
| Proteins (g) | 144 | 37.57 | 75-256 | 131 | 29.84 | 82-229 | 0.044 |

ns – not significant ($p > 0.05$)

### Body Composition

The results show a great homogeneity of the two studied samples, that is, in spite of athletes register higher mean values of height and body weight, the differences between both groups are not statistically significant ($p > 0.05$). In the same way, at the level of internal body structure, comparatively to non-athletes, the athletes present, in average, less skinfold thickness, higher body density, and higher lean body mass, what is important in the context of sports competitive practice, however, no statistically significant differences exist between both groups ($p > 0.05$). The fat-free mass, present a marginal statistical difference, due to higher mean value of athletes ($p < 0.10$).

**Table 3.** Body composition results.

| | ATHLETES | | | NON-ATHLETES | | | |
|---|---|---|---|---|---|---|---|
| Variables | $\bar{x}$ | s | Min-Máx | $\bar{x}$ | s | Min-Máx | p |
| Body mass (k) | 62.5 | 9.34 | 42.5-89 | 60.1 | 9.85 | 42-83.5 | 0.193 (ns) |
| Height (cm) | 173.8 | 6.18 | 162-190 | 172.5 | 6.66 | 158-189 | 0.335 (ns) |
| $\sum 4SKF$ (mm) | 30.9 | 11.40 | 15.5-79.6 | 32.6 | 12.65 | 16.5-70.5 | 0.466 (ns) |
| BD (g/cc) | 1.0704 | 0.01 | 1.04-1.09 | 1.0692 | 0.01 | 1.05-1.09 | 0.497 (ns) |
| FM (%) | 12.5 | 3.82 | 5.0-24.6 | 13.0 | 4.15 | 5.7-23.1 | 0.494 (ns) |
| FFM (k) | 54.5 | 6.67 | 40.3-67.0 | 51.9 | 6.95 | 37.9-67.3 | 0.062 (ns) |

ns – not significant ($p > 0.05$)
$\sum 4SKF$ – sum of four SKF

## DISCUSSION

**Food Intake**. Physical activity can be assessed by determining the energy intake (Saris[43], Silva *et. al.*[46], Rodrigues *et. al.*[42], Silva *et. al.*[47]). Several methods are used and expressed in the literature to calculate the needs and the daily energy expenditures Dwyer[14]. In the present study we used a semi-quantitative FFQ. So far, few studies have been published on food intake, body composition and physical activity in the adolescent Portuguese population. The accomplishment of FFQ results is a dificult task, more so when they are applied to adolescent populations (Marble[31], Fidler *et. al.*[16]). Therefore, such FFQ should not be very constraining, but fast and precise in the application, so that they can be acceptable and valid. Such characteristics have been largely aimed at the questionnaire type, approach and consequent treatment of data (Gibson[18], Willett[51], Lopes *et. al.*[29], Lopes[28], Moreira *et. al.*[33]).

**Energy Requeriments**. The energy intake values of athletes (3203kcal) are

in accordance with the interval recommended by Creff and Bérard[10] (3000 to 3500kcal/day) or Leleuch[26] (2800 to 3500kcal/day), while for non-athletes (2897kcal) is slightly higher than that recommended by COMA (1991), that is to say, 2775kcal/day, but near to 2900kcal DRI (2002) recommendation. Among sportsmen, the present sample show higher values of energy intake than the wrestlers, and balanced with the footballers and athletics of Rybeire *et. al.*[40], and lower values than the swimmers of Berning *et. al.*[5] study.

**Macronutrients**. In this study, the values for carbohydrate intake, the most important nutrient within sports practice, expressed as percentage of total energy intake (ATHL: 1750%; NATH: 1749%) were below the interval defined by Brouns[6], between 60-70% for athletes and 55-65% for non-athletes adolescents. The daily values for total fat intake, recommended by Brouns[6] for sportsmen are between 20-30%. The athlete's sample exceeded this recommendation by about 2%. For non-athletes, Brouns[6] suggests intakes between 20 and 35%. The values in the present study (33%) are actually in accordance with the suggested interval. Higher serum cholesterol levels currently represent one of the most serious risk factors in the premature appearance of cardiovascular disease. According to the National Education Programs Working Group on the Management of Patients with Hypertension and High Blood Cholesterol (1991), the "wanted or convenient" levels of serum cholesterol most lie below 240mg/day. An analysis of the results (Table 2) allows us to verify that both groups ingested amounts considerably above the recommended requirements (ATHL: 591.0 mg; NATH: 494.1 mg).

Heyward[22] recommends a balanced intake of fat intake, with 10% of total daily fat intake supplied equally by saturated, monounsaturated and polyunsaturated fat. If we compare these values with those obtained in this study, we conclude that the athletes and non-athletes ingest relatively large amounts of these nutritients (Table 4). The suitable daily percentage of proteins proposed by Heyward[22] for non-sportsmen is approximately 12%, while Wilmore and Costil[52] increase the interval to 12-15%. For sportsmen, Creff and Bérard[10] suggest around 15%. From the analysis of our results we verify that both groups ingest larger amounts to those prescribed in the literature (ATHL and NATH $\approx$18%).

In short, when we compared the results between athletes and non-athletes (Table 4), we verify a similarity between the percentages of macronutrients ingested by each group. However, the data presented in Table 2 shows the significant differences ($p < 0.05$) between these groups in some macronutrients. On the other hand, data emerging from the literature (Hamm[19], Pendergast *et. al.*[37]) confirms a high intake of fats, sugar and cholesterol, a balanced intake of protein, but an insufficient one of complex carbohydrates between the actual intake of macronutrients and the recommended doses, in sportive or sedentary population, which confirms the data from the present study.

**Body Composition** The determination of the FFM and FM in young people is a hard task, because, it is very difficult to know, if the slight fluctuations verified in body composition, are due to the growth process or to the regular physical activity and food intake, or both (Malina[30], Bellisle *et. al.*[3]). Despite the athletes presented thinner SKF and smaller percentage

**Table 4.** Nutrient intakes as percentage of total energy intake (TEI) in both groups.

| | ATHLETES | NON-ATHLETES |
|---|---|---|
| Nutrients | TEI - % | TEI - % |
| CHO total | 49.7 | 49.3 |
| Proteins total | 18.0 | 18.1 |
| Total Fat | 32.3 | 32.6 |
| Saturated Fat | 11.0 | 10.9 |
| Monounsaturated Fat | 12.9 | 12.7 |
| Polyunsaturated Fat | 5.9 | 5.9 |

of body fat, the present study results, show no statistically significant differences ($p > 0.05$) between both groups, what is demonstrative of homogeneity. However, the increased amount of exercise is accompanied by a decrease in the %FM and increase of FFM and bone mineral density in sports populations (Cisar *et. al.*[7], Bergman and Boyungs[4], Penteado *et. al.*[38]). Due to the diversity of sports practice, there are several researchers who refer to the ≪ideal values≫ of FM in accordance with the type of physical activity practiced and its demands (Wilmore[53], Ward *et. al.*[50], Lohman[27], Högström *et. al.*[23], Silva *et. al.*[47]). The athletes presented different body composition values from those observed in the sedentary population [23], which corroborates the opinion of some early researches (Parizkova[35], Forbes[17]), these differences are due to regular physical load to which the sportsmen are subject. However, the analysis of Table 3, does not prove this data. Similarly, some of the studies accomplished with male Portuguese adolescents, are not unanimous in relation to the values found for FFM and FM (Sobral[49], Silva[44]). The height and the body weight show no statistical significant difference when both groups are compared (Table 3). In fact, in what concerns growth development, the revision of literature is practically unanimous in admitting the inexistence of significant differences induced by the regular practice of physical activities in children and adolescents (Sobral[49], Montecinos[32], Landry and Driscoll[25]). In short, despite a great number of studies aimed to prove physical exercise to be an important contribution to the maintenance of body weight and the modification of body composition in children and adolescents (*Pate et. al.*[36], Malina[30]), such data are not clear or objective according to the results obtained in the present study.

## 4 Conclusions

With regards to the nutritional profile, compared with the non-athletes, the athletes showed higher intakes of all the macronutrients. Such data sustains the thesis that larger energy expenditures are matched by larger caloric intakes. This procedure seems to be consistent with the training loads. As the differences in body composition between both groups have not shown statistical meaning, we conclude that the physical activity among subjects of the same age, sex, height and body composition, seems to be the determinant factor in the variation of macronutrients intake and energy expenditure. Lastly, in terms of distribution of macronutrients, this study indicates the existence of a certain imbalance between the caloric intake and the level of physical activity, which influences the maintenance of a well balanced body structure in adolescents.

## Acknowledgement

Research partially sponsored by national founds through the Fundação Nacional para a Ciência e Tecnologia, Portugal - FCT under the project (PEst-OE/MAT/UI0006/2014).

## References

1. ACSM – American College of Sports Medicine. Policy statement regarding the use of human subjects and informed consent. *Medicine and Science in Sports and Exercise*, 21:v, 1989.
2. Barros, H., Lopes, C., Von Hafe, P., Fernando, P., Coelho, R. and Maciel (1997). Risco de enfarte do miocárdio: um estudo comunitário, *Arquivos de Medicina*, 11(5), 285–294.
3. Bellisle, F.; Rolland-Cachera, M.F. and Kellogg Scientific Advisory Committee. (2007). Three consecutive (1993, 1995, 1997) surveys of food intake, nutritional attitudes and knowledge, and lifestyle in 1000 French children, aged 9-11 years. *Journal of Human Nutrition and Dietetics*, 20 (3): 241-251.
4. Bergman, E. and Boyungs, J. (1991). Indoor walking program increases lean body composition in older women. In: Research and Professional Briefs. *Journal of the American Dietetic Association*, 91 (11): 1433-1435.
5. Berning, J.R., Troup, J.P., VanHandel, P.J., Daniels, J. and Daniels. N. (1991). The nutritional habits of young adolescent swimmers. *International Journal of Sport Nutrition*, 1 (3): 240-248.
6. Brouns, F. (1995). Necesidades Nutricionales de los Atletas. *Barcelona: Editorial Paidotribo.*
7. Cisar, C., Housh, T., Johnson, G., Thorland, W. and Hughes, R. (1989). Validity of anthropometric equations for detrmination of changes in body composition in adultes males during training. *Journal of Sports Medicine and Physical Fitness*, 29 (2): 141-148.
8. COMA - Committee On Medical Aspects Of Food Policy (1991).
9. Craplet, C., Craplet, P. and Craplet-Meunier, J. (1995). Alimentacion y Nutricion del Deportista. *Barcelona: Hispano Europea, S.A.*
10. Creff, A. and Bérard, L. (1992). Deporte y Alimentacion - Guia Dietética para el Deportista. *Barcelona: Editorial Hispano Europea, S.A.*, 517 ed.
11. Donoghue, W.C. (1985). How to Measure Your % Bodyfat - An Instruction Manual for the Slim Guide Skinfold Caliper. *Creative Health Products. USA.* 617 ed.
12. DRI - Food and Nutrition Board, Standing Committee on the Scientific Evaluation of Dietary Reference Intakes, Institute of Medicine, National Research Council (2002). Dietary Reference Intakes: Energy, Carbohydrates, Fiber, Fat, Protein, and Amino Acids (Macronutrients). *National Academy Press. Washington, DC. USA.*
13. Durnin, J.V.G.A. and Womersley, J. (1974). Body fat assessed from total body density and its estimation from skinfold thickness: measurements on 481 men and women aged 16 to 72 years. *British Journal of Nutrition*, 32 (1): 77-92.
14. Dwyer, J. (1994). Dietary Assessment. In: Modern Nutrition in Health and Disease. (edited by M. Shils, J. Olson and M. Shike). 817 ed., Vol. 1, pp. 842-860. *Lea & Febiger. USA.*
15. ESHA Research (1992). The Food Processor Plus. *Nutrition & Fitness Software. USA.*

16. Fidler Mis, N., Kobe, H. and Stimec, M. (2012). Dietary intake of macro- and micronutrients in Slovenian adolescents: comparison with reference values. *Annals of Nutrition & Metabolism*, 61 (4): 305-313.
17. Forbes, G. (1987). Human Body Composition: Growth, Aging, Nutrition, and Activity. *New York: Springer-Verlag.*
18. Gibson, R. (1990). Principles of Nutritional Assessment. *New York: Oxoford University Press.*
19. Hamm, M. (1996). La Correcta Nutrición del Deportista. *Barcelona: Editorial Hispano Europea S.A.*, 217 ed.
20. Harrison, G., Buskirk, E., Carter, J., Johnston, F., Lohman, T., Pollock, M., Roche, A. and Wilmore, J. (1988). Skinfold Thickness and Measurement Technique. In: Anthprometric Standardization Reference Manual (edited by T. Lohman, A. Roche and R. Martorell), pp. 55-70. *Champaign. Illinois: Human Kinetics Books.*
21. Hertogh, C., Chavet, P., Gavina, M., Bernard, P., Melin, B. and Jimenez, C. (1995). Méthodes des Mesures et Valeurs de Référence de la Puissance Maximale Développée lors d'Efforts Explosifs. *Cinésiologie, XXXIV* (160) : 61-74.
22. Heyward, V.H. (1991). Advanced Fitness Assessment and Exercise Prescription. *Champaign. Illinois: Human Kinetics Books.* 217 ed.
23. Högström, G.M., Pietil17, T., Nordström, P. and Nordström, A. (2012). Body composition and performance: influence of sport and gender among adolescents. *Journal of Strength Conditioning Research*, 26 (7): 1799-1804.
24. Jeukendrup, A. and Cronin, L. (2011). Nutrition and elite young athletes. *Medicine and Sport Science*, 56, 47-58.
25. Landry, B.W. and Driscoll, S.W. (2012). Physical activity in children and adolescents. *PM & R*, 4(11): 826-832.
26. Leleuch, C. (1997). Eaux minérales et apports calciques et magnesieus pour le sportif. In: Compte Rendu de la 1ere Journee Annuelle de la Pitie Salpetriere. *Cinésiologie, XXXVI* (172) : 75-80.
27. Lohman, T. (1992). Advances in Body Composition Assessment. Current Issues in Exercise Sciences Series, Monograph n17 3. *Human Kinetics Publishers.*
28. Lopes, C. (2000). Alimentação e enfarte agudo do miocárdio: Estudo caso-controlo de base comunitária. *Dissertação de doutoramento apresentada 17 Faculdade de Medicina da Universidade do Porto.*
29. Lopes, C., Fernandes, P., Cabral, S. and Barros, H. (1994). Questionário de Frequência Alimentar - Efeito da Extensão da Lista de Alimentos na Classificação dos Inquéritos. *Arquivos de Medicina*, 8 (5): 291-294.
30. Malina, R.M. (1994). Physical Activity: Relantionship to Growth, Maturation and Physical Fitness. In: Physical Activity Fitness and Health. International Proceedings and Consensus Statement, pp.918-930. *Champaign. Illinois: Human Kinetics, Inc.*
31. Marble, C. (1995). Bilan de deux ans d'éducation nutritionnelle effectuée chez des élèves d'une section sport-étude. *Cinésiologie, XXXIV* (161/162): 139-143.
32. Montecinos, R. and Prat, J. (1982). Incremento de la actividad física en niños y su efecto sobre la composición corporal y la condición física. *Apunts D'Educación Física i Medicina Esportiva, XIX* (75): 169-175.
33. Moreira, P., Sampaio, D. and Almeida, M.D.V. (2003). Validade relativa de um questionário de frequência de consumo alimentar através da comparação com um registo alimentar de quatro dias. *Acta Médica Portuguesa*, 16: 412-420.
34. National Education Programs Working Group Report on The Management of Patients With Hypertension and High Blood Cholesterol (1991). *Annals of Internal Medicine*, 114 , 224-237.

35. Parizkova, J. (1973). Body Composition and Exercise During Growth and Development. In: Physical Activity - Human Growth and Development (edited by G. Rarick), pp. 98-124. *New York: Academic Press.*
36. Pate, R. Slentz, C. and Katz, D. (1989). Relantionships Between Skinfolds Thickness and Performance of Health Related Fitness Test Items. *Research Quarterly for Exercise and Sport*, 60 (2): 183-189.
37. Pendergast, D.R., Meksawan, K., Limprasertkul, A. and Fisher, N.M. (2011). Influence of exercise on nutritional requirements. *European Journal of Applied Physiology*, 111 (3): 379-390.
38. Penteado, V.S., Castro, C.H., Pinheiro, Mde M., Santana, M., Bertolino, S., de Mello, M.T. and Szejnfeld, V.L. (2009). Diet, body composition, and bone mass in well-trained cyclists. *Journal of Clinical Densitometry*, 13 (1): 43-50.
39. Rebelo, D.I., Moreira, P., Rodrigues dos Santos, J.A. and Silva, D.J.L. (2002): Controlo do peso e alimentação em jovens universitários de Desporto e Educação Física. *Revista Portuguesa de Medicina Desportiva*, 20 (101): 111-120.
40. Rybeire, J., Fellmann, N., Montaurier, C., Delaitre, M., Vernet, J. and Vermorel, M. (2000). Daily energy expenditure and its main components as measured by whole-body indirect calorimetry in athletic and non-athletic adolescents. *British Journal of Nutrition*, 83 (4): 355-362.
41. Rodrigues dos Santos, J.A. (1995). A Dietética do Desportista. *Faculdade de Ciências do Desporto e de Educação Física, Universidade do Porto.*
42. Rodrigues dos Santos, J.A., Silva, D.J.L. and Gadelho, S.F.N.A. (2011). Ingestão nutricional de corredores de meio-fundo. *Revista Brasileira de Nutrição Esportiva, São Paulo.* 5 (29): 402-416.
43. Saris, W. (1985). The Assessment and Evaluation of Daily Physical Activity in Children - A Review. *Acta Pediatric Scandinavian Supplement*, 318, 37-48.
44. Silva, D.J.L. (1996). Aptidão Física - Estudo Comparativo da Composição Corporal e dos Níveis de Força entre Alunos da Opção de Desporto e Alunos ≪Sedentários Activos≫, Adolescentes, do Sexo Masculino. *Porto: FCDEF-UP.*
45. Silva, D.J.L. and Rodrigues dos Santos, J.A. (2011): Nutrição e Futebol − estudo com adultos do sexo feminino. *Revista de Educação da ESE de Fafe*, número 1: 1-27, Setembro/2011.
46. Silva, D.J.L., Rodrigues dos Santos, J.A., Kent-Smith, L. and Oliveira, B.M.M. (2005): Ingestão de Micronutrientes em Jovens do sexo masculino, com Diferentes Níveis de Actividade Física. *Revista Portuguesa de Medicina Desportiva*, 23 (113): 27-42.
47. Silva, D.J.L., Silva, N.R.M. and Rodrigues dos Santos, J.A. (2012). Avaliação dos hábitos de ingestão nutricional de jogadores de futsal do sexo masculino: estudo com atletas da 117, 217 e 317 divisão nacional portuguesa. *Revista Brasileira de Futsal e Futebol, São Paulo*, 4 (11): 23-37.
48. Siri, W. (1961). Body Composition From Fluid Spaces and Density - Analysis of Methods. In: Proceedings of the Conference, Anuary. Techniques for Measuring Body Composition (edited by J. Brozec and A. Henschel), pp. 223-244. *Washington DC.: National Academy of Sciences, National Research Council.*
49. Sobral, F. (1981). Perfil Morfológico e Prestação Desportiva - Estudo Antropométrico do Desportista Adolescente de Alto Nível de Rendimento. *Lisboa: Universidade Técnica de Lisboa - Instituto Superior de Educação Física.*
50. Ward, G., Johnson, J. & Stager, J. (1984). Body Composition - Methods of Estimation and Effect Upon Performance. In Clinics in Sport Medicine: Symposium on Nutritional Aspects of Exercise (edited by A. Hecker), pp. 705–722. *Philadelphia: W.B. Saunders Company.*

51. Willett, W.C. (1990). Food Frequency Methods. In: Nutritional Epidemiology (edited by W.C. Willett), pp. 60-90. *Oxford University Press.*
52. Wilmore, J. and Costill, D. (1992). Nutrition and Human Performance. In: Eating, Body Weight and Performance in Athletes - Disorders of Modern Society (edited by K. Brownell, J. Rodin and J. Wilmore), pp. 61–76. *Philadelphia: Lea e Febiger.*
53. Wilmore, J. (1983). Body composition in sport and exercise - directions for future research. *Medicine and Science in Sports and Exercise*, 15 (1): 21-31.

# Comparing the Cumulative Rates of Cancer in two Populations

Christopher T. Lenard[1], Terence M. Mills[2], and Ruth F.G. Williams[3]

[1] Mathematics and Statistics, La Trobe University, Bendigo, Victoria, Australia
(E-mail: c.lenard@latrobe.edu.au)
[2] Loddon Mallee Integrated Cancer Service, Bendigo, Victoria, Australia
(E-mail: tmills@bendigohealth.org.au
[3] Graduate Research School, La Trobe University, Bendigo, Victoria, Australia
(E-mail: ruth.williams@latrobe.edu.au)

**Abstract.** As the incidence of cancer continues to rise, it is natural for a community to want to compare the incidence of cancer in the region with the incidence of cancer in another region, such as the rest of the nation. The cumulative incidence rate is a measure that was introduced in the cancer literature in 1976. This measure is easy to calculate and facilitates comparing the incidence of cancer in two regions. The aim of this paper is to promote this measure by means of a worked example based on illustrative data.
**Keywords:** Epidemiology, Health economics, Health services research, Health funding and financing

## 1 Introduction

"A cancer, or malignant growth, is now known to be a continuous, purposeless, unwanted, uncontrolled and damaging growth of cells." (Stephens and Fox[8].) There are many types of cancer - prostate cancer, lung cancer, bowel cancer, breast cancer to name a few. Although the term "cancer" refers to a broad range of diseases, we will use the term "cancer" to refer, collectively, to all malignant cancers. This is the practice of cancer agencies such as the Australian Institute of Health and Welfare[1].

The incidence of cancer is the number of new cases diagnosed in a particular population and a particular period of time, usually a year. Thus, incidence is a non-negative integer. The incidence rate is the incidence per 100,000 head of population.

It is natural to want to compare the incidence rates of cancer in two populations. One may wish to compare the incidence rate of cancer in a small regional area with that in the rest of the nation. One may wish to compare the incidence of bowel cancer among men with the incidence of bowel cancer among women. One may wish to compare the incidence rate of cancer in a region at a particular

*Stochastic Modeling, Data Analysis and Statistical Applications* (*pp*. 225-232)
Lidia Filus - Teresa Oliveira - Christos H Skiadas (Eds)


time with that in the same region at an earlier time. This could lead to a time series approach to tracking the incidence of cancer in a region over time.

Age is a risk factor associated with cancer (Mills[7]). Hence the incidence rate of cancer will tend to be higher in older populations, all other things being equal. The traditional approach to dealing with this difference in age profiles is to use age-standardized incidence rates. This involves choosing some standard population on which to base the calculations (Estève *et al.*[4], p. 56). This approach has several difficulties. For example, when looking at age-standardized rates in a population, one needs to know the standard population that was used in the calculation.

The concept of cumulative rate of cancer was proposed as an alternative to the age-standardized incidence rate by the distinguished epidemiologist N.E. Day[2] in 1976, although its origins can be traced back to a paper by Yule in 1934 (Yule[9]). The cumulative rate has the advantage that it avoids the arbitrariness of having to choose a pre-defined, standard population - which Yule describes as "superfluous".

The cumulative rate is also directly connected to the cumulative risk, or actuarial risk, of being diagnosed with cancer by a given age. Some cancer agencies quote numerical values of the risk of being diagnosed with cancer. The difficulty with this measure of lifetime risk of being diagnosed with cancer is that the measure is based on an assumption that the only cause of death in the population is cancer. Since this key assumption is often not mentioned in reports, the meaning of lifetime risk can be easily misunderstood. In this paper we do not concern ourselves with risk for these reasons, but simply mention it in passing. The connection between risk and cumulative rate is discussed fully in Day[2], Estève *et al.*([4] p. 60), and Lenard *et al.* [5].

The primary aim of this paper is to demonstrate how one compares the cumulative rates of cancer in two populations. This is a fundamental problem for practitioners. We will achieve this by means of an example that is based on data that are hypothetical, but realistic. The data are purely illustrative. This worked example can be used as a model by those who wish to make such comparisons in practice.

Despite the advantages of the cumulative rate, it is not often used in practice. So, the secondary aim of this paper is to promote further discussion of the cumulative rate.

## 2 Methods

Table 1 contains hypothetical data for two regions. We have chosen to use hypothetical, or illustrative, data because our aim is to demonstrate the method rather than compare the incidence of cancer in two particular regions. The data

are presented in 5-year age groups. For each age group, the number of persons in the population and the incidence of cancer are presented for each region. For example, in Region 1, there are 31,294 persons aged between 40 and 44, and 81 of these persons were diagnosed with cancer in the year in question.

| **Age group** | **Region 1** | | **Region 2** | |
|---|---|---|---|---|
| | **Pop1 (n)** | **Inc1 (x)** | **Pop2 (m)** | **Inc2 (y)** |
| 0-4 | 29289 | 12 | 498381 | 118 |
| 5-9 | 29202 | 6 | 464389 | 55 |
| 10-14 | 31749 | 7 | 461565 | 66 |
| 15-19 | 32427 | 9 | 500763 | 91 |
| 20-24 | 27235 | 6 | 591423 | 175 |
| 25-29 | 24195 | 19 | 612961 | 313 |
| 30-34 | 23986 | 16 | 563386 | 492 |
| 35-39 | 27952 | 48 | 564801 | 793 |
| 40-44 | 31294 | 81 | 567399 | 1186 |
| 45-49 | 32571 | 132 | 540007 | 1969 |
| 50-54 | 33412 | 205 | 512283 | 2883 |
| 55-59 | 31051 | 274 | 455982 | 3675 |
| 60-64 | 30033 | 370 | 421669 | 5064 |
| 65-69 | 23739 | 423 | 325045 | 5382 |
| 70-74 | 18709 | 412 | 251007 | 4845 |

**Table 1: Hypothetical population data and incidence data for two regions**

Details of the methods, and the mathematical ideas that underpin them, have been discussed elsewhere; for example see Estève *et al*.[4] and Lenard *et al*.[6]. Here we present only the formulae that are necessary for the calculations.

Cumulative rate by age 75 for Region 1 is given by

$$CumRate1 = 5\sum(x/n) \tag{1}$$

We use the term "cumulative rate" as an abbreviation for "cumulative incidence rate". One could calculate a cumulative mortality rate in a similar manner using mortality data rather than incidence data in Table 1.

It is clear from formula (1) that the cumulative rate by age 75 is simply the sum of the age-specific incidence rates (expressed as probabilities) from 0 to 75. This interpretation makes the cumulative rate easy to comprehend. It also allows the cumulative rate to be a stand-alone measure almost devoid of assumptions.

The cumulative risk of being diagnosed with cancer by age 75 for Region 1 is approximated by

$$1-\exp\left(-5\sum(x/n)\right).$$

The estimated standard deviation of cumulative rate by age 75 for Region 1 is given by

$$s_1 = 5\sqrt{\left(\sum(x/n^2)\right)}.$$

Alternatively, one could use the approach in Dobson *et al.*[3] for estimating the standard deviation of the cumulative rate.

For Region 2, the formulae are similar: substitute *y* for *x*, and *m* for *n*.

The *z*-statistic for comparing the cumulative rates for the two regions is

$$z = (CumRate1 - CumRate2)/\sqrt{s_1^2 + s_2^2}.$$

Under the null hypothesis that the two populations have the same expected cumulative rates, this *z* statistic has, approximately, the standard Normal distribution.

Suppose that we expect, from experience, that the cumulative rate of cancer in Region 1 is larger than the cumulative rate in Region 2. Then we would conduct a one-sided statistical test and calculate the probability, *p*, that $Z > z$ where *Z* has the standard Normal distribution.

## 3 Results

The results of the analysis of the data are presented in Table 2. We have included the approximate cumulative risks only as a matter of interest; our main focus is on the cumulative rates.

| | **Region 1** | **Region 2** |
|---|---|---|
| Cumulative rate by age 75 | 0.3913 | 0.3553 |
| Approx. cumulative risk by age 75 | 0.3238 | 0.2990 |
| Est. s.d. of cum. rate by age 75 | 0.0089 | 0.0022 |
| *z* | 3.9193 | |
| *p=P(Z > z)* | 4.4404E-05 | |

**Table 2: Results of analysis of data in Table 1.**

In this example, the *p*-value associated with the z-statistic is very small ($p$ = 4.4404E-05). Hence, the data provide strong evidence, in which considerable confidence can be placed, that the cumulative rate of cancer up to age 75 is higher in Region 1 than in Region 2.

## 4 Policy implications

Our discussion of the cumulative rate as a measure is linked to economic policies surrounding cancer care.

Differences in cumulative rates between regions arise from epidemiological factors or demographic structure, or both factors jointly. There are likely to be economic implications from these differences. The allocation of cancer services, whether private, publicly-funded or publicly-provided, can usually be improved between regions. Cancer incidence influences economic decision-making, whether these are the decisions of private agents or government. Policy responses may be warranted. Economic policy formulated by government would need to improve the allocation of cancer resources in ways that private decisions, whether those of the consumer of cancer resources or the producer of cancer services, do not achieve. Appropriate measures of the size and impact of the cancer problem informs both private and public decisions.

The appropriate economic role of government extends even to ensuring the public is correctly informed of the incidence and impact of cancer. For example, alleviating pervasive ill-informed dread in populations is welfare-enhancing. Government action may also improve decisions over cancer resources at the margin in order that cancer resources are allocated to the highest possible outcome, without anyone's welfare being made worse off.

The cumulative rate is likely to vary across regions. Regional disparities occur either because of different population structures (demographic factors) or from differences in the cancer incidence in each age-group (epidemiological reasons). Alternatively, two regions could report similar cumulative rates. This sameness may, on first appearance, suggest to a policy maker that economic rationale for treatment resources for cancer in both regions is similar; however, the population structure in that region may conceal a heightened incidence of cancer in some age groups. Thus, it must be kept in mind that, like other measures, the cumulative rate is a summary measure that has its place in an armamentarium of measures to inform cancer policy. Like all measures, the implications of the measures applied must be clearly understood.

Two regions reporting the same, or similar, cumulative incidence rates may have different cumulative mortality rates. If cumulative mortality rates in two regions are also the same, then cancer treatment resourcing ought to be the same. In other words, cancer survival is approximately the same between this region and the other. If the cancer mortality rates differ, then one must investigate whether the stage of the cancer at diagnosis differs between the two regions. Later stage cancers being detected more frequently in one region, require different resourcing and different site profiles of cancers in two regions also implies that the same resourcing of treatment is not appropriate.

Thus, regional differences in cancer mortality may be related to differences in economic access to cancer resources. People living in one locality (say, a regional or remote area) can have lower incomes. They may face higher prices for cancer treatment, including the cost of travel (the 'time price'). Price differentials can arise despite health insurance arrangements that assert equality and fairness are valued objectives of insurance.

A region with the higher cumulative rate incidence may be able to improve longevity in the region when the cancer resources that are not enhancing health outcomes are redirected to uses that lead to better health outcomes. This outcome can be achieved through the judicious maintenance of the price mechanism.

There is another economic use for developing the appropriate measurement of cancer for policy purposes. Apart from its use in improving economic efficiency in the allocation of cancer resources, cancer measurement can inform equity. Distributive fairness is a widely-accepted objective of the health sector, and thus for cancer.

Weighing the fairness of different cumulative rates of cancer in populations involves notions about the equal treatment of equals and unequal treatment of unequals. One cannot weigh inequity until measurement of the health inequality, or equality, is first undertaken. There are various measures of age-related inequality that can be applied. Each measure (e.g. the coefficient of variation, the Gini coefficient, the Atkinson Index) has different welfare implications. Once the nature and extent of the inequality is measured and known, then one can weigh whether the equality/inequality is fair.

## 5 Conclusions

This paper has been written for practitioners who wish to use the cumulative rate to compare the incidence of cancer in two different populations. The cumulative rate could also be used to compare mortality from cancer in two different populations. The cumulative rate might be used in making decisions about allocating resources for cancer care to different regions.

Although Estève *et al.* ([4], pp. 74-84) discuss methods for comparing the incidence of a disease in two populations, they do not discuss the use of the cumulative rate in this context. The present paper fills this gap in the literature.

The cumulative rate proposed by Day[2] avoids the arbitrariness of a pre-defined standard population on which to base the calculations. The only data required are the population data and incidence data stratified by 5-year age groups. It is possible to deal with age groups of other widths; see Lenard *et al.* [6] as to how this might be done.

The method can be easily adapted to consider the cumulative rate of particular cancers. For example, in considering the cumulative rate of breast cancer among female Australians, one would tabulate the population and incidence of female Australians.

The purpose of a project will guide the researcher in choosing an appropriate maximum age for the cumulative rate. Day[2] recommends that, for whole of life comparisons, 74 is an appropriate maximum age; there are many competing risks for people over this age. However, with increased life expectancy, a higher maximum age may be appropriate for whole of life comparisons. To compare the impact of cancer on younger people, one might set 44 as a maximum age. For childhood cancers, Day[2] suggests that one might consider the maximum age as 14.

One could also use this method to compare the cumulative rates of cancer in one region in two different years. Indeed, one could use the cumulative rate to track how impact of cancer on a particular population is changing over time.

It would be interesting to investigate multiple comparison procedures for comparing the cumulative rates of several populations.

For example, if one were allocating resources for cancer care to four regions A, B, C, D it would be useful to be able to say that the cumulative rate in A was significantly higher than in B, C, and D, but there is no significant difference between the rates in B, C, and D. Then one would have a sound basis for allocating equal resources to regions B, C, D and more to A. However, in comparing the cumulative rates in several populations will involve some technical details to control the size of Type I errors. We will need to draw on the research literature surrounding multiple comparison procedures to explore this matter further.

We will return to some of these issues raised in this section in later papers.

Investigating the cumulative rate as a measure of incidence, or mortality, for the purposes of making comparisons is a contribution to the study of inequalities in cancer care. This touches on matters of justice.

## Acknowledgements

We thank Professor Christos Skiadas and the organisers of SMTDA 2014 for the opportunity to present our ideas in this forum, and Professor Teresa Oliveira for suggesting improvements to this paper. Loddon Mallee Integrated Cancer Service is supported by the Victorian Government.

## References

1. Australian Institute of Health and Welfare & Australasian Association of Cancer Registries. Cancer in Australia: an overview, 2012. Cancer series no. 74. Cat. no. CAN 70. Canberra, AIHW, 2012.
2. N.E. Day. A new measure of age standardized incidence, the cumulative rate. In: Payne R, Waterhouse J. eds. Cancer incidence in Five Continents. Vol. III. IARC Scientific Publications, No. 15. Lyon. International Agency for Research on Cancer, 443-452, 1976.
3. A.J. Dobson, K. Kuulasmaa, E. Eberle and J. Scherer. Confidence intervals for weighted sums of poisson parameters. Statistics in Medicine, 10, 3, 457–462, 1991
4. J. Estève, E. Benhamou, L. Raymond. Statistical Methods in Cancer Research, Vol. IV: Descriptive Epidemiology. Lyon, International Agency for Research on Cancer 1994.
5. C.T. Lenard, T.M. Mills and R.F.G. Williams. The risk of being diagnosed with cancer. Aust N Z J Public Health, 37, 5, 489, 2013.
6. C.T. Lenard, T.M. Mills and R.F.G. Williams. Cumulative incidence rates of cancer. The Mathematical Scientist 39, 2, 83-84, 2014..
7. T.M. Mills. Age and cancer. Significance Magazine. On-line: Available at URL: http://www.statslife.org.uk/health-medicine/892-age-and-cancer , 19 July, 2013.
8. F. Stephens and R. Fox. Cancer explained: The essential guide to diagnosis and management. Second Ed., Random House Australia, North Sydney, 2008.
9. G. Udny Yule. On some points relating to vital statistics, more precisely statis- tics of occupational mortality. Journal of the Royal Statistical Society, 97, 1, 1–84, 1934.

# Impacts of diabetes and homicide mortality on life expectancy in Mexico

Alejandro Aguirre[1] and Fortino Vela[2]

[1]El Colegio de México, Mexico. Camino al Ajusco 20, C. P. 10740, México D. F., MEXICO
(Email: aguirre@colmex.mx)
[2]Universidad Autonoma Metropolitana. Departamento de Producción Económica, Calz. Del Hueso 1100, C. P. 04960, México D. F., MÉXICO
(Email: fvela@correo.xoc.uam.mx)

**Abstract:** Mexico presents sharp contrasts on the evolution of the level of mortality. On one hand, chronic degenerative diseases, especially those related to diabetes, are in an alarming increase. On the other, different criminal groups associated with drug trafficking has increased the number of violent deaths. This has resulted in the decline of life expectancy in certain regions. For example, in regard to the death rate from diabetes mellitus, while in 2000 this figure reached 47.8 per hundred thousand for 2011 was 71.0 per hundred thousand. Meanwhile, in regard to the mortality rate from homicide, while in 2007 it amounted to 8.2 per hundred thousand in 2010 had increased to 22.9 per hundred thousand. In this paper we estimate years of life lost (Arriaga, 1996) for these two causes of death, analyze their trends and relate this indicator with temporary life expectancies. Information from vital statistics, available for 2000 and 2010 at national level is used. The estimations may provide clues to the Mexican authorities to formulate population, health and social policies that help to increase the limits of life expectancy in our country.
**Keywords:** demographic analysis, mortality by cause, years of life lost, temporary life expectancy.

## 1 Introduction

In Mexico the epidemiological transition has followed the expected pattern. That is, there has been a relative increase of chronic-degenerative diseases. Accordingly, in the last decade it has been observed a rise in diabetes mortality, but to levels above those of most developed countries. Apart from bad habits of diet and sedentarism, it seems there is a genetic factor affecting adversely the Mexican population. Therefore, unlike for developed countries, diabetes mellitus has been the first or the second cause of death in Mexico in recent years. For example, according to figures from World Health Organization (WHO, 2011), from a total of 192 countries, Mauritius was the country with the highest diabetes mortality rate in the world (176 per hundred thousand), Mexico occupied the sixth place (83.8 per hundred thousand), above of countries like

*Stochastic Modeling, Data Analysis and Statistical Applications* (*pp*. 233-240)
Lidia Filus - Teresa Oliveira - Christos H Skiadas (Eds)


Portugal (19.3 per hundred thousand), the United States (15.2 per hundred thousand), Canada (13.4 per hundred thousand) and Japan (4.5 per hundred thousand).

Another problem facing Mexican population is the mortality associated with violence which has also presented a rising trend. The so called "war against narco" launched by former president Calderón, provoked a spiral of violence that made increase the number of deaths due to homicide from 8,868 in 2007 to 27,213 2011.
In this paper we estimate the years of life lost (Arriaga, 1996) by two causes of death: diabetes and homicide. As it is known, demographic analysis of mortality often has used different kind of indicators such as crude death rates, specific mortality rates and life expectancies at birth. These indicators aim at portraying the levels and trends of the phenomenon. Nonetheless, each of these indexes present advantages and pitfalls. Thus, for instance, it is known that crude death rates are influenced by age structure, even when the inputs for its calculation are easily available. The years of life lost is an index that not only reflects the number of deaths occurring by each cause. It also takes into account the timing of the deaths.
Information from vital statistics, available for 2000 and 2010, at national level, is used. The estimations may provide clues to the Mexican authorities to formulate population, health and social policies that help to increase the limits of life expectancy in our country.

## 2 Methodology

One way to look at the impact of a certain cause of death on life expectancy is through the years of life lost (YLL). This methodology originally proposed by Arriaga (1996) consists on calculating the years that persons who die before certain age lose in comparison to the hypothesis that they had reached that age. The assumptions to calculate YLL are: The mortality should be null between two ages chosen for the analysis, i.e. those who die should have lived until the upper limit of the interval considered for the analysis. Assuming the analysis is made between the ages a and v (v – a = u). It is also assumed that there is a life table available that reflects the mortality of the population studied. If the distribution of deaths by cause in the life table is equal to the distribution in the deaths registered, then:

$$ndx,j = ndx\ (\ nDx,j\ /\ nDx\ )$$

where:
ndx,j : is the number of deaths due to cause j, between ages x and x+n from the life table
ndx : is the number of deaths between ages x and x+n from the life table
nDx : is the number of deaths registered between ages x and x+n
nDx,j is the number of deaths registered between ages x and x+n , due

to cause j

the volume of YLL by people who die by cause j in the interval of ages between x and x+n is:

$$u,nAPx,j = ndx,j\ [\ (n - nkx) + (v - x - n)\ ]$$

where

nkx : is the average part of the interval [x , x+n] lived by those who die in that interval among those who have survived to age a, the average of YLL is given by the expression:

$$u,napx,j = ndx,j\ [\ (v - nkx - x\ )\ ] / la \qquad (1)$$

It is possible to add the years of life lost in each interval of ages comprised within the large interval of ages between a and v:

$$_{u}ap_{.j} = \sum_{x=a}^{v} {}_{u,n}ap_{x,j}$$

This is the formula we applied for most results presented in this paper considering an initial age a = 20 and the final age v = 80. The causes of death (j) included are diabetes mellitus and homicide.

On the other hand, expression (1) can be added for different causes of death. Considering m causes of death with no intersection and that those m causes comprise all possible causes of death, one can calculate the YLL for an age interval [x, x+n] and for all the causes:

$$_{n}ap_{x.} = \sum_{j=1}^{m} {}_{u,n}ap_{x,j}$$

If in turn, this last expression can be added for all ages between a and v, and in this way we can get the years of life lost between a and v by those who die by any cause. We also analyze those results for 2000 and 2010 and for males and females.

Another index we use in this paper to contrast with the years of life lost, is the temporary life expectancy which can be defined as the average number of years the survivors at certain age (a) are going to live between that age and another age (v). If u = v – a, between the ages a and v, people might live (in theory) a maximum of u years. However, considering mortality they live on average:

$$ {}_{u}e_{a} = \frac{T_{a} - T_{a+u}}{l_{a}} $$

i.e., the person years lived by the cohort between the ages a and v, divided by the number of those that survived t age a.

## 3 Results

We applied the methodology to calculate YLL in the Mexican population between ages 20 and 80 due to diabetes mellitus, homicide, and for all the causes, for the years 2000 and 2010 and by sex (Table 1 and 2). The inputs were life tables by sex for the years 2000 and 2010 and registered deaths by sex, age group and cause (Table 3).

We can see some general results when we considered the YLL by all causes:

1. Men lose more than two additional years than women.
2. The trend over time is to the reduction of YLL. Between 2000 and 2010 YLL reduced around one year for each sex. For men the reduction was from 6.503 to 5.440, whereas for women from 4.222 to 3.340 years of life lost.

Table 1. Mexico, 2000. Deaths by sex, age group and cause (Total, diabetes and homicide).

| Age | Total | | | Diabetes | | | Homicide | | |
|---|---|---|---|---|---|---|---|---|---|
| group | Males | Females | Both | Males | Females | Both | Males | Females | Both |
| 0 | 21,793 | 16,769 | 38,621 | 3 | 2 | 5 | 49 | 38 | 87 |
| 1-4 | 3,726 | 3,236 | 6,963 | 6 | 4 | 10 | 61 | 47 | 108 |
| 5-9 | 2,025 | 1,432 | 3,457 | 4 | 9 | 13 | 66 | 27 | 93 |
| 10-14 | 2,252 | 1,466 | 3,718 | 11 | 20 | 31 | 152 | 45 | 197 |
| 15-19 | 5,106 | 2,282 | 7,389 | 30 | 47 | 77 | 833 | 140 | 973 |
| 20-24 | 7,388 | 2,606 | 9,995 | 60 | 66 | 126 | 1,407 | 147 | 1554 |
| 25-29 | 8,380 | 2,911 | 11,291 | 133 | 104 | 237 | 1,438 | 139 | 1577 |
| 30-34 | 8,737 | 3,271 | 12,009 | 198 | 135 | 333 | 1,233 | 128 | 1361 |
| 35-39 | 9,848 | 4,107 | 13,956 | 359 | 250 | 609 | 1,046 | 115 | 1161 |
| 40-44 | 10,387 | 5,109 | 15,496 | 650 | 500 | 1150 | 777 | 87 | 864 |
| 45-49 | 11,455 | 6,603 | 18,061 | 1,071 | 984 | 2055 | 651 | 72 | 723 |
| 50-54 | 12,574 | 8,493 | 21,068 | 1,622 | 1,677 | 3299 | 432 | 55 | 487 |
| 55-59 | 14,839 | 10,653 | 25,494 | 2,286 | 2,485 | 4771 | 375 | 44 | 419 |
| 60-64 | 17,100 | 13,747 | 30,849 | 2,834 | 3,399 | 6233 | 264 | 51 | 315 |
| 65-69 | 19,510 | 16,467 | 35,978 | 3,036 | 3,999 | 7035 | 195 | 38 | 233 |
| 70-74 | 20,865 | 18,506 | 39,371 | 2,987 | 3,804 | 6791 | 135 | 34 | 169 |
| 75-79 | 21,513 | 19,424 | 40,938 | 2,603 | 3,393 | 5996 | 110 | 22 | 132 |
| 80-99 | 44,356 | 53,462 | 97,822 | 2,928 | 4,769 | 7697 | 92 | 43 | 135 |
| 100+ | 1,023 | 1,952 | 2,975 | 8 | 35 | 43 | 1 | 2 | 3 |
| N. S. | 1,425 | 757 | 2,216 | 34 | 69 | 103 | 127 | 19 | 146 |
| Total | 222,509 | 176,484 | 399,046 | 20,863 | 25,751 | 46,614 | 9,444 | 1,293 | 10,737 |

Source: Elaborated from SINAIS (2013).

When specific causes of death are considered, the panorama changes. The sex differential for homicide mortality is very important. In terms of YLL, men lose about seven times more years than women. As to deaths due to diabetes, in 2000 male mortality was 2% higher than female mortality. In 2010 it was 24% higher. Unlike mortality by all causes, the years of life lost due to homicide rose between 2000 and 2010 for both sexes. In the case of men it went from 0.239 to 0.296: an increase of 24%; for women, at much lower level, went from 0.036 to 0.041: an increase of 14%.

Table 2. Mexico, 2010. Deaths by sex, age group and cause (Total, diabetes and homicide).

| Age | Total | | | Diabetes | | | Homicide | | |
|---|---|---|---|---|---|---|---|---|---|
| group | Males | Females | Both | Males | Females | Both | Males | Females | Both |
| 0 | 16,148 | 12,637 | 28,785 | nd | nd | nd | nd | nd | nd |
| 1-4 | 3,075 | 2,576 | 5,651 | 1 | 4 | 5 | 66 | 51 | 117 |
| 5-9 | 1,603 | 1,276 | 2,882 | 8 | 4 | 12 | 41 | 31 | 73 |
| 10-14 | 2,126 | 1,482 | 3,609 | 9 | 19 | 28 | 168 | 72 | 241 |
| 15-19 | 7,100 | 2,801 | 9,902 | 27 | 37 | 64 | 1,977 | 318 | 2,296 |
| 20-24 | 10,197 | 3,015 | 13,216 | 85 | 99 | 184 | 3,492 | 362 | 3,855 |
| 25-29 | 11,229 | 3,168 | 14,401 | 135 | 145 | 280 | 3,822 | 318 | 4,140 |
| 30-34 | 12,228 | 3,723 | 15,955 | 335 | 193 | 528 | 3,742 | 302 | 4,046 |
| 35-39 | 13,446 | 4,838 | 18,292 | 576 | 384 | 960 | 3,176 | 230 | 3,409 |
| 40-44 | 13,723 | 6,202 | 19,926 | 1,132 | 792 | 1,924 | 2,116 | 189 | 2,306 |
| 45-49 | 15,704 | 8,867 | 24,575 | 1,973 | 1,511 | 3,485 | 1,429 | 168 | 1,597 |
| 50-54 | 18,385 | 11,685 | 30,076 | 3,150 | 2,588 | 5,738 | 1,003 | 102 | 1,106 |
| 55-59 | 20,786 | 14,799 | 35,590 | 4,359 | 3,870 | 8,230 | 604 | 67 | 671 |
| 60-64 | 23,443 | 18,371 | 41,818 | 5,104 | 5,225 | 10,329 | 378 | 54 | 432 |
| 65-69 | 26,005 | 21,237 | 47,247 | 5,412 | 5,820 | 11,232 | 269 | 42 | 311 |
| 70-74 | 29,572 | 25,484 | 55,065 | 5,471 | 6,248 | 11,720 | 174 | 43 | 217 |
| 75-79 | 31,559 | 29,218 | 60,783 | 4,878 | 5,988 | 10,868 | 114 | 19 | 133 |
| 80-99 | 71,869 | 85,025 | 156,912 | 6,975 | 10,227 | 17,202 | 102 | 28 | 130 |
| 100+ | 1,634 | 2,806 | 4,440 | 27 | 79 | 106 | 1 | 0 | 1 |
| N. S. | 2,195 | 459 | 2,813 | 35 | 33 | 68 | 635 | 38 | 708 |
| Total | 332,027 | 259,669 | 592,018 | 39,692 | 43,266 | 82,963 | 23,309 | 2,434 | 25,789 |

Source: SINAIS (2013).

For diabetes mellitus there were mixed results in the trends of YLL. For males the YLL rose from 0.816 in 2000 to 0.927 in 2010; i.e. a 14% increase. For females a reduction took place between 2000 and 2010, from 0.797 to 0.747, a fall of 7%.

The years of life lost is an index that not only reflects the number of deaths occurring by each cause. It also takes into account the timing of the deaths. An early death produces more YLL than a late death. This explains the apparent paradox of having (for the Mexican population) higher mortality rates due to diabetes for women on one hand, and on the other more YLL for men. This is produced because there are more premature male deaths.

Table 3. Mexico: YLL between ages 20 and 80. Males 2000. Homicide.

| Age | ${}_nd(x)^{1}$ | ${}_nD_x$ | ${}_nD_{x,j}$ | ${}_nD_{x,j}/{}_nD_x$ | ${}_nd_{x,j}$ | ${}_nk_x$ | ${}_{u,n}AP_{x,j}$ | ${}_{u,n}ap_{x,j}$ |
|---|---|---|---|---|---|---|---|---|
| 0 | 4062 | 21793 | | | | 0.41 | | |
| 1 | 591 | 3726 | 61 | 0.0164 | 9.6755 | 1.92 | 745.7893 | 0.0079 |
| 5 | 130 | 2025 | 66 | 0.0326 | 4.237 | 2.5 | 307.1852 | 0.0032 |
| 10 | 135 | 2252 | 152 | 0.0675 | 9.1119 | 2.5 | 615.0533 | 0.0065 |
| 15 | 190 | 5106 | 833 | 0.1631 | 30.9969 | 2.5 | 1937.3042 | 0.0204 |
| 20 | 254 | 7388 | 1407 | 0.1904 | 48.3728 | 2.5 | 2781.4341 | 0.0293 |
| 25 | 289 | 8380 | 1438 | 0.1716 | 49.5921 | 2.5 | 2603.5865 | 0.0274 |
| 30 | 412 | 8737 | 1233 | 0.1411 | 58.1431 | 2.5 | 2761.7958 | 0.0291 |
| 35 | 517 | 9848 | 1046 | 0.1062 | 54.9129 | 2.5 | 2333.7972 | 0.0246 |
| 40 | 822 | 10387 | 777 | 0.0748 | 61.4897 | 2.5 | 2305.8655 | 0.0243 |
| 45 | 1336 | 11455 | 651 | 0.0568 | 75.9263 | 2.5 | 2467.6054 | 0.026 |
| 50 | 2273 | 12574 | 432 | 0.0344 | 78.0926 | 2.5 | 2147.5457 | 0.0226 |
| 55 | 3569 | 14839 | 375 | 0.0253 | 90.1931 | 2.5 | 2029.3441 | 0.0214 |
| 60 | 5310 | 17100 | 264 | 0.0154 | 81.9789 | 2.5 | 1434.6316 | 0.0151 |
| 65 | 7893 | 19510 | 195 | 0.01 | 78.8895 | 2.5 | 986.1193 | 0.0104 |
| 70 | 12292 | 20865 | 135 | 0.0065 | 79.5313 | 2.5 | 596.4845 | 0.0063 |
| 75 | 17961 | 21513 | 110 | 0.0051 | 91.838 | 2.5 | 229.5949 | 0.0024 |

[1/] This data come from Mina´s (2001) mortality table.
Source: Elaborated from Mina (2001) and SINAIS (2013).

Temporary life expectancies between ages 20 and 80 are about two years higher for females than for males (Table 6). During the first decade of the XXI century they rose one year. The differences mentioned above are almost the same as the differences existing in the YLL (Table 4) both by sex and between 2000 and 2010, namely, a sex differential of two years, and an improvement of one year in 2010, in comparison with 2000. This means that reduction in years of life lost have a close relationship with life expectancies.

As it was said, the total of years of life lost is equal to the sum of the YLL by each cause. Therefore any reduction in the YLL by each cause will contribute to the reduction of the total YLL and thereby to almost the same increase in the life expectancy.

Table 4. México. YLL 20-80 by causes and sex, 2000 and 2010

| | 2000 | | 2010 | |
|---|---|---|---|---|
| | Males | Females | Males | Females |
| Total | 6.503 | 4.222 | 5.44 | 3.34 |
| Diabetes | 0.816 | 0.797 | 0.927 | 0.747 |
| Homicide | 0.239 | 0.036 | 0.296 | 0.041 |

Source: Estimate.

Table 5. México. Mortality rate by causes and sex, 2000 and 2010(per hundred thounsand people)

| | 2000 | | 2010 | |
|---|---|---|---|---|
| | Males | Females | Males | Females |
| Diabetes | 43.8 | 51.6 | 72.4 | 75.3 |
| Homicide | 19.8 | 2.6 | 42.5 | 4.2 |
| Total* | 4.68 | 3.54 | 6.1 | 4.5 |
| | | | | |
| * This rate is by thousand | | | | |

Source: Estimate.

Table 6. México. Temporary life expectancies ${}_{60}e_{20}$

| Sex | 2000 | 2010 |
|---|---|---|
| Males | 53.5 | 54.56 |
| Females | 55.78 | 56.66 |

## References

1. Aguirre, Alejandro and Fortino Vela, "Una mirada retrospectiva a la evolución de la mortalidad y sus vínculos con la política de población en la materia en México, en los últimos 50 años". 50 años del Centro de Estudios Demográficos, Urbanos y Ambientales, El Colegio de México, in press (2014).
2. Arriaga, Eduardo, "Commments on some indexes to measure the level and change of mortality". Estudios Demográficos y Urbanos, 11, 5-30 (1996).
3. Bocco, Mónica, "La relación entre los años de vida perdidos y la esperanza de vida: aplicaciones para el análisis de la mortalidad". Notas de Población, junio, 39-60 (1996).
4. Mina, Alejandro, "Funciones de sobrevivencia empleadas en el análisis demográfico". Papeles de Población, 28:131-154 (2001).
5. WHO, Global status report on noncommunicable diseases 2010, Italy (2011).

# Estimating the Healthy Life Years Lost: The Health–Mortality Approach Compared to the Global Burden of Disease Studies

**Christos H Skiadas**

ManLab, Technical University of Crete, Chania, Crete, Greece
Email: skiadas@cmsim.net

Abstract. We propose a series of methods and models in order to explore the Global Burden of Disease Study and the provided healthy life expectancy (HALE) estimates from the World Health Organization (WHO) based on the mortality $\mu_x$ of a population provided in a classical life table and a mortality diagram. Our estimates are compared with the HALE estimates for the World territories and the WHO regions. From the mortality point of view we have developed a simple model for the estimation of a characteristic parameter *b* related to the healthy life years lost to disability and providing full application details along with characteristic parameter selection and stability of the coefficients. We also provide a direct estimation method of the parameter *b* from the life tables. We straighten the importance of our methodology by proposing and applying estimates of the parameter *b* by using the Gompertz and the Weibull models.
From the Health State point of view we summarize the main points of the first exit time theory to life table data and present the basic models starting from the first related model published by Janssen and Skiadas (1995). Even more we develop the simpler 2-parameter health state model and an extension of a model expressing the infant mortality to a 4-parameter model which is the simpler model providing very good fitting on the logarithm of the force of mortality, $\ln(\mu_x)$. More important is the use of the Health State Function and the relative impact on mortality to find an estimate for the healthy life years lost to disability.
We have developed simple programs in Excel providing immediately the Life Expectancy, the Loss of Healthy Life Years and the Healthy Life Expectancy estimate.
**Keywords:** Health state function, Healthy life expectancy, Mortality Diagram, Loss of healthy life years, LHLY, HALE, DALE, World Health Organization, WHO, Global burden of Disease, Health status, Gompertz, Weibull.

## 1. Introduction

Starting from the late 80's a Global Burden of Disease (GBD) study was applied in many countries reflecting the optimistic views of many researchers and policy makers worldwide to quantify the health state of a population or a group of persons. In the time course they succeeded in establishing an international network collecting and providing adequate information to calculate health measures under terms as Loss of Healthy Life Years (LHLY) or Healthy Life Expectancy (HALE). The latter tends to be a serious measure important for the policy makers and national and international health programs. So far the process followed was towards statistical measures including surveys and data collection using questionnaires and disability and epidemiological data as well (McDowell, 2006). They faced many views referring to the definition of health and to the inability to count the various health states and of course the different cultural and societal aspects of the estimation of health by various persons worldwide. Further to any objections posed when trying to quantify health, the scientific community had simply to express with strong and reliable measures that millions of people for centuries and thousands of years expressed and

*Stochastic Modeling, Data Analysis and Statistical Applications* (*pp*. 241-254)
Lidia Filus - Teresa Oliveira - Christos H Skiadas (Eds)


continue to repeat every day: That their health is good, fair, bad or very bad. As for many decades the public opinion is seriously quantified by using well established statistical and poll techniques it is not surprising that a part of these achievements helped to improve, establish and disseminate the health state measures. However, a serious scientific part is missing or it is not very much explored that is to find the model underlying the health state measures. Observing the health state measures by country from 1990 until nowadays it is clear that the observed and estimated health parameters follow a rather systematic way. If so why not to find the process underlying these measures? It will support the provided health measures with enough documentation while new horizons will open towards better estimates and data validation.

From the early 90's we have introduced and applied methods, models and techniques to estimate the health state of a population. The related results appear in several publications and we have already observed that our estimates are related or closely related to the provided by the World Health Organization (WHO) and other agencies as Eurostat or experts as the REVES group. However, our method based on a difficult stochastic analysis technique, is not easy to use especially by practitioners. The last four centuries demography and demographers are based on the classical Life Tables. Thus here we propose a very simple model based on the mortality $\mu_x$ of a population provided in a classical life table. To compare our results with those provided by WHO we use the $\mu_x$ included in the WHO abridged life tables. Our estimates are compared with the HALE estimates for all the WHO countries. Even more we provide the related simple program in Excel which provides immediately the Life Expectancy, the Loss of Healthy Life Years and the Healthy Life Expectancy estimate. The comparisons suggest an improved WHO estimate for the majority of the countries. There are countries' results differing from the model and need further study.

**Further Details**

The Global Burden of Disease Study explored the health status of the population of all the countries members of the World Health Organization (WHO). It is a large team work started more than 25 years ago (see Murray and Lopez, 1997,2000, Mathers et al., 2000, Salomon, et al., 2010, 2012, Murray et al., 2015, Hausman, 2012, Vos et al., 2012, Robine, Romieu, Cambois, 1999, WHO, 2000, 2001, 2002, 2004, 2013, 2014 and many other publications). The last years, with the financial support of the Bill and Melinda Gates foundation, the work was expanded via a large international group of researchers. The accuracy of the data collection methods was improved along with the data development and application techniques. So far the health status indicators were developed and gradually were established under terms as healthy life expectancy and loss of healthy life years. Methods and techniques developed during the seventies and eighties as the Sullivan method (Sullivan, 1971) were used quite successfully. Several publications are done with the most important included in The Lancet under the terms DALE and HALE whereas a considerable number can be found in the WHO and World Bank publications. The same half part of a century several works appear in the European Union exploring the same phenomenon and providing more insight to the estimation of the health state of a population and providing tools for the estimation of severe, moderate and light disability. The use of these estimates from the health systems and the governments is obvious.

To a surprise the development of the theoretical tools was not so large. The main direction was towards to surveys and collection of mass health state data instead of developing and using theoretical tools. The lessons learned during the last centuries were towards the introduction of models in the analysis of health and mortality. The classical examples are Edmund Halley for Life Tables and Benjamin Gompertz for the law of mortality and many others. Today our ability to use mass storage tools as the computers and the extensive application of surveys and polls to many political, social and economic activities directed the main health state studies. In other words we give much attention to opinions of the people for their health status followed by extensive health data collection. However, it remains a serious question: **Can we validate the health status results?** *As it is the standard procedure in science, a systematic study as the Global Burden of Disease should be*

*validated by one or more models. Especially as these studies are today the main tool for the health programs of many countries the need of verification is more important.*
People reply according to their experience. Two main approaches arise: The mortality focus approach and the health status approach. Although both look similar responds may have significant differences. The main reason is that health is a rather optimistic word opposed to the pessimistic mortality term. Twenty years ago we provided a model to express the health state of a population. We developed and expanded this model leading to a system providing health status indexes. Here we propose several methodologies to estimate the health indexes and to compare with the provided by WHO.

## 2. The mortality approach

### 2.1. The Simplest Model

We need a simple model to express the health status. The best achievement should be to propose a model in which the health measure should be presented by only one main parameter. We thus propose a two parameter model with one crucial health parameter:

$$\mu_x = \left(\frac{x}{T}\right)^b \tag{1}$$

The parameter $T$ represents the age at which $\mu_x$=1 and $b$ is a crucial health state parameter expressing the curvature of $\mu_x$. As the health state is improved $b$ gets higher values.

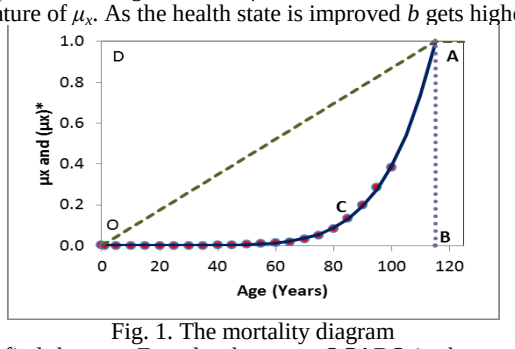


Fig. 1. The mortality diagram

The main task is to find the area $E_x$ under the curve OCABO in the mortality diagram (see Figure 1) which is a measure of the mortality effect. This is done by estimating the integral

$$E_x = \int_0^T \left(\frac{x}{T}\right)^b dx = \frac{T}{(b+1)}\left(\frac{x}{T}\right)^b$$

The resulting value for Ex in the interval [0, T] is given by the simple form:

$$E_{mortality} = \frac{T}{(b+1)}$$

It is clear that the total information for the mortality is the area provided under the curve $\mu_x$ and the horizontal axis. The total area $E_{total}$ of the healthy and mortality part of the life span is nothing else but the area included into the rectangle of length T and height 1 that is $E_{total}$=$T$. The health area is given by

$$E_{health} = T - E_{mortality} = T - \frac{T}{(b+1)} = \frac{bT}{b+1}$$

Then a very simple relation arises for the fraction $E_{health}/E_{mortality}$ that is

$$\frac{E_{health}}{E_{mortality}} = b \tag{2}$$

This is the simplest indicator for the loss of health status of a population. As we have estimated by another method it is more close to the severe disability causes indicator.
The relation $E_{total}/E_{mortality}$ provides another interesting indicator of the form:

$$\frac{E_{total}}{E_{mortality}} = b + 1$$

This indicator is more appropriate for the severe and moderate disability causes indicator (It is compatible with our estimates using the health state approach). It provides larger values

for the disability measures as the $E_{total}$ is larger or the $E_{mortality}$ area is smaller by means that as we live longer the disability period becomes larger.

This method suggests a simple but yet interesting tool for classification of various countries and populations, for the loss of healthy life years. A correction multiplier $\lambda$ should be added for specific situations so that the estimator of the loss of healthy life years should be of the form:

$$LHLY = \frac{E_{total}}{E_{mortality}} = \lambda(b+1)$$

However, for comparisons between countries it is sufficient to select $\lambda$=1. Even more the selection of $\lambda$=1 is appropriate when we would like to develop a quantitative measure for the LHLY without introducing the public opinion for the health status and the estimates for the cause of diseases and other disability measures. From another point of view the influence of the health status of the society to the public opinions related to health may cause differences in the values for LHLY estimated with the HALE method thus a value for $\lambda$ larger or smaller than unity is needed. By means that we will have to measure not exactly the health status but the public opinion related to the health status, the latter leading in a variety of health estimates in connection to socioeconomic and political situation along with crucial health information from the mass media. Both measures, the standard measure with $\lambda$=1 and the flexible one with $\lambda$ different from 1 could be useful for decision makes and health policy administrators and governmental planners.

To our great surprise our model by selecting $\lambda$=1 provided results very close to those provided by WHO as it is presented in the following Tables and in other applications. It is clear that we have found an interesting estimator for the loss of healthy life years.

Our idea to find the loss of healthy life years as a fraction of surfaces in a mortality diagram was proven to be quite important for expressing the health state measures. A more detailed method based on the health state stochastic theory is presented in the book on The Health State Function of a Population and related publications (see Skiadas and Skiadas 2010, 2012, 2015) where more health estimators are found.

**2.2.1. Application details**

As our method needs life table data we prefer to use full life tables when available. The Human Mortality Database is preferred for a number of countries providing full life tables. However, only a small part of the world countries are included and thus we also use the abridged life tables provided by the World Health Organization. The new abridged life tables from WHO including data from 0 to 100 years provide good results when applying our method. Instead the previous life tables (0 to 85 years) are not easily applied. It could be possible to use these life tables by expanding from 85 to 100 years. For both the abridged and the full life table data we have developed the appropriate models and estimation programs in Excel thus make it easy to use.

**2.2.2. Stability of the coefficients of the Simple Model**

Here we discuss some important issues regarding the application of the simple model proposed by equation (1). To apply this model to data we use a non-linear regression analysis technique by using a Levenberg-Marquardt algorithm. The data are obtained from the WHO database providing abridged life tables of the 0-100 years form. The important part of the model is the parameter *b* expressing the loss of healthy life years. Even more *b* can express the curvature of mortality function $\mu_x$. Applying the model to data we need a measure for the selection of the most appropriate value for *b*.

**2.2.3. When *b* should be accepted**

The simpler is to find if *b* follows a systematic change versus age. We start by selecting all the *n* data points ($m_0$, $m_1$,…, $m_n$) for $\mu_x$ to find *b* and then we select *n*-1, n-2,…, *n*-*m* for a sufficient number of $m<n$. As is presented in Figure 2 the parameter *b* follows a systematic change. The example is for USA males and females the year 2000 and the data are from the full life tables of the Human Mortality Database. As it is expected *b* is larger for females than for males. In both cases a distinct maximum value in a specific year of age appears. Accordingly a specific minimum appears for the other not so important parameter *T* (see Figure 3). It is clear that only the specific maximum value for *b* should be selected. Even more the estimates for the maximum *b* account for a local minimum for the first difference

*dx*' of *dx* provided from the life table. Next Figure 4 illustrates this case for USA males the year 2000 along with a fit curve from our model SK-6. The maximum *b* is at 94 years for males and females the same as for the minimum of the first difference corresponding to the right inflection point of the death curve *dx*. Table I includes the parameter estimates for *b* and *T* the year 2000 for USA males and females.

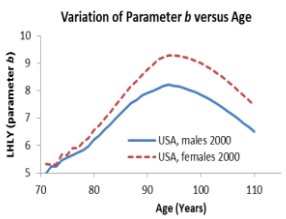


Fig. 2. Development of the health parameter

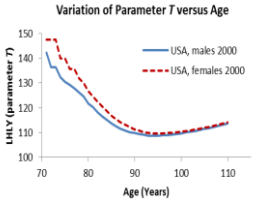


Fig. 3. Development of *T* parameter

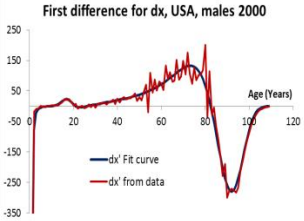


Fig. 4. First difference (derivative) of *dx* versus age

**2.3. Estimation without a model (Direct estimation)**

As the needed data sets in the form of $m_x$ or $q_x$ data are provided from the life tables we have developed a method of direct estimation of the loss of healthy life year estimators directly from the life table by expanding the life table to the right.

$$b+1=\frac{E_{total}}{E_{mortality}}=\frac{xm_x}{\sum_0^x m_x}$$
$$b=\frac{E_{health}}{E_{mortality}}=\frac{xm_x-\sum_0^x m_x}{\sum_0^x m_x}=\frac{xm_x}{\sum_0^x m_x}-1 \quad (3)$$

The only needed is to estimate the above fraction from the life table data. A similar indicator results by selecting the *qx* data from the life table and using the:

$$b+1=\frac{E_{total}}{E_{mortality}}=\frac{xq_x}{\sum_0^x q_x}$$
$$b=\frac{E_{health}}{E_{mortality}}=\frac{xq_x}{\sum_0^x q_x}-1$$

In both cases the results are similar as it is presented in the following Figure 5 (A and B). The estimates from $m_x$ are slightly larger than from $q_x$. In both cases the *b* estimators growth to a maximum at old ages and then decline. The selected *b* or *b*+1 indicator for the life years lost from birth are those of the maximum value. A smoothing technique averaging over 5 years estimators is used to avoid sharp fluctuations in the maximum range area for the direct method. For the Model method a simple 3 point averaging gives good results. The maximum HLYL for the direct estimation is 9.84 for $m_x$ and 9.26 for $q_x$. For the Model estimation with $m_x$ data the related HLYL is 10.0. As we have estimated for other cases both the estimation of the *b* indicator by this direct method and the method by using a model give similar results.

**2.4. More details: The Gompertz and the Weibull Distributions**

It should be noted that a more convenient Gompertz (1825) model form is provided by Jacques F. Carriere (1992) in the form $\mu_x = Bc^x$, where *B* and *c* are parameters. This is close to our simple model selected.

However, we have also selected and applied the following form for the probability density function of the Gompertz model:

$$f_x = e^{-k+bx-e^{-l+bx}} \quad (4)$$

The characteristic parameter expressing the loss of healthy life years is the parameter *l*. this is also demonstrated by observing the cumulative distribution function of the form:

$$F_x = e^{-e^{-l+bx}}$$

The related survival function is

$$S_x = 1 - e^{-e^{-l+bx}}$$

The probability density function is:

$$f_x = be^{-l+bx}e^{-e^{-l+bx}}$$

And the hazard function is

$$h(x) = \frac{f_x}{F_x} = be^{-l+bx} = e^{\ln(b)-l+bx} = e^{-k+bx}$$

Thus explaining the above Gompertz form selected ($k$=$l$-ln($b$)).
The selected value for the estimation of the healthy life years lost is provided by the parameter $l$.
In the same paper Carriere suggests the use the Weibull model. This model has density function ($b$ and $T$ are parameters):

$$f_x = \frac{b}{T}\left(\frac{x}{T}\right)^{b-1} e^{-\left(\frac{x}{T}\right)^b} \quad (5)$$

The Weibull model provides an important form for the hazard function:

$$h(x) = \frac{b}{T}\left(\frac{x}{T}\right)^{b-1}$$

Even more the cumulative hazard is given by:

$$H(x) = \left(\frac{x}{T}\right)^b$$

Another important point is that the Cumulative Hazard provided by the Weibull model is precisely the form for the simple model presented earlier and the parameter $b$ expresses the healthy life years lost.

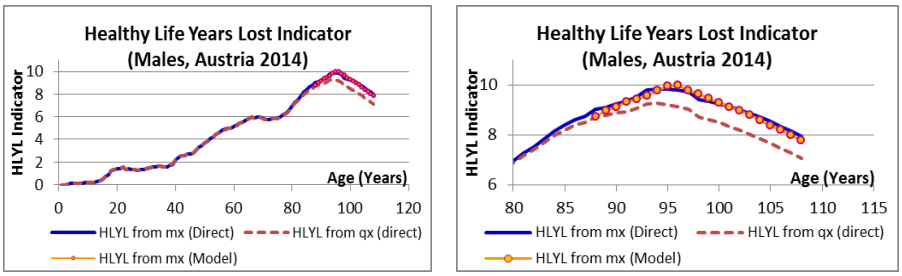


A B

Fig. 5. Estimation of the HLYL indicator ($b$) by the direct method and by the simple model (Full results A and expanded around the maximum B).

## 3. The Health State Models

### 3.1. The Health State Distribution

Although the health state models are introduced from 1995 (see Janssen and Skiadas, 2015 and more publications from Skiadas 2007 and Skiadas and Skiadas 2010, 2012, 2014) few applications appear. The main reason is due to the very laborious first exit time stochastic theory needed and that it is assumed that the use of the Gompertz and the Weibull models along with the related extensions give enough tools for the practical applications. This is not correct as the first exit time stochastic models are produced by using one of the most elegant and accurate methodology to model the health-death process as it is demonstrated in the following. The probability distribution of the general health state model is of the form:

$$f_x = \frac{|H_x - xH'_x|}{\sigma\sqrt{2\pi x^3}} e^{-\frac{H_x^2}{2x\sigma^2}}$$

For the main applications in Demography we can set $\sigma$ = 1 reducing to the simpler from:

$$f_x = \frac{|H_x - xH'_x|}{\sqrt{2\pi x^3}} e^{-\frac{H_x^2}{2x}} \quad (6)$$

While the simpler form arises for the following health state function

$$H(x) = l - (bx)^c \quad (7)$$

That is

$$f_x = \frac{|l+(c-1)(bx)^c|}{\sqrt{2\pi x^3}} e^{-\frac{(l-(bx)^c)^2}{2x}} \quad (8)$$

The simpler model of this form arises when $c = 1$ and it is the so-called Inverse Gaussian expressing the probability density function for the first exit time of a linearly decaying process:

$$f_x = \frac{|l|}{\sqrt{2\pi x^3}} e^{-\frac{(l-bx)^2}{2x}} \quad (9)$$

Applications of this or similar type forms be can found in Ting Lee and Whitmore (2006) and in Weitz and Fraser (2001).

TABLE I

Parameter estimates for the model (USA, 2000)

| Age | Females | | Males | | Age | Females | | Males | |
|---|---|---|---|---|---|---|---|---|---|
| Years | b | T | b | T | Years | b | T | b | T |
| 71 | 5.318 | 147.5 | 4.975 | 142.3 | 91 | 8.942 | 110.7 | 7.992 | 109.4 |
| 72 | 5.308 | 147.5 | 5.244 | 136.4 | 92 | 9.143 | 110.0 | 8.081 | 109.1 |
| 73 | 5.296 | 147.5 | 5.231 | 136.4 | 93 | 9.224 | 109.8 | 8.173 | 108.8 |
| 74 | 5.663 | 140.0 | 5.459 | 132.3 | 94 | **9.291** | **109.6** | **8.218** | **108.6** |
| 75 | 5.649 | 140.0 | 5.559 | 130.5 | 95 | 9.286 | 109.6 | 8.189 | 108.7 |
| 76 | 5.905 | 135.6 | 5.642 | 129.2 | 96 | 9.263 | 109.6 | 8.148 | 108.8 |
| 77 | 5.896 | 135.6 | 5.736 | 127.8 | 97 | 9.224 | 109.7 | 8.094 | 109.0 |
| 78 | 6.146 | 131.9 | 5.844 | 126.3 | 98 | 9.167 | 109.9 | 8.027 | 109.2 |
| 79 | 6.280 | 130.1 | 5.981 | 124.5 | 99 | 9.093 | 110.1 | 7.947 | 109.4 |
| 80 | 6.551 | 126.8 | 6.214 | 121.8 | 100 | 9.002 | 110.3 | 7.856 | 109.7 |
| 81 | 6.748 | 124.6 | 6.368 | 120.2 | 101 | 8.896 | 110.6 | 7.754 | 110.0 |
| 82 | 6.972 | 122.5 | 6.587 | 118.2 | 102 | 8.775 | 110.8 | 7.642 | 110.3 |
| 83 | 7.209 | 120.4 | 6.774 | 116.6 | 103 | 8.641 | 111.2 | 7.521 | 110.7 |
| 84 | 7.453 | 118.5 | 6.981 | 115.0 | 104 | 8.495 | 111.5 | 7.391 | 111.0 |
| 85 | 7.710 | 116.8 | 7.186 | 113.6 | 105 | 8.339 | 111.9 | 7.255 | 111.4 |
| 86 | 7.947 | 115.3 | 7.378 | 112.5 | 106 | 8.173 | 112.3 | 7.114 | 111.8 |
| 87 | 8.185 | 114.0 | 7.546 | 111.5 | 107 | 8.000 | 112.7 | 6.967 | 112.3 |
| 88 | 8.369 | 113.1 | 7.665 | 110.9 | 108 | 7.822 | 113.1 | 6.818 | 112.7 |
| 89 | 8.579 | 112.2 | 7.826 | 110.1 | 109 | 7.638 | 113.5 | 6.666 | 113.2 |
| 90 | 8.778 | 111.3 | 7.916 | 109.8 | 110 | 7.452 | 114.0 | 6.512 | 113.6 |

The last model as right skewed cannot express the human death process expressed by a highly left skewed probability density function. Instead the previous 4-parameter model is applied very successfully. Even more this form is very flexible providing very good fitting in the case of high levels of infant mortality, as it was the case for time periods some decades ago and also for nowadays when infant mortality is relatively low. Two different options arise for the model. That corresponding to the health state estimation with the parameter *l* expressing the high level of the health state and represented with the figures 6A and 6C and another form with low levels for the parameter *l* expressing the Infant Mortality (see the figures 6B and 6D). In the latter case the form of the density function is:

$$f_x = \frac{2|l+(c-1)(bx)^c|}{\sqrt{2\pi x^3}} e^{-\frac{(l-(bx)^c)^2}{2x}} \quad (10)$$

When the parameter *l* is very small a 2-parameter model termed here as the Half-Inverse Gaussian distribution results:

$$f_x = \frac{2(c-1)(bx)^c}{\sqrt{2\pi x^3}} e^{-\frac{(bx)^{2c}}{2x}} \quad (11)$$

The name arises from the similarity of this form with the Half-Normal distribution.
The advantage of the proposed half-inverse Gaussian or IM-Model for the infant mortality modeling is obvious in the case of the application in USA females in 1950. The IM-Model provides a fairly well $R^2$=0.990 instead of $R^2$=0.920 for the Health State Model which provides similar results with the 2-parameter model (see the Table II). The resulting $R^2$ for the year 2010 in USA females are similar as the infant mortality is relatively small (see figures 6C and 6D and Table II).

**3.2. An Important Extension: The simplest IM-Model**

Christel Jennen (1985) suggested a second order approximation to improve the previous model with the first order approximation form:

$$f_x = \frac{|H_x - xH'_x|}{\sqrt{2\pi x^3}} e^{-\frac{H_x^2}{2x}}$$

However, we propose and apply here a simpler form adequate for the applications in demography data:

$$f_x = \left(\frac{2}{\sqrt{2\pi}}\right)\left(\frac{|H_x - xH'_x|}{\sqrt{x^3}} + \frac{k\sqrt{x^3}H''_x}{2|H_x - xH'_x|}\right) e^{-\frac{H_x^2}{2x}} \quad (12)$$

The parameter *k* expresses the level of the influence of the second order correction term. When *k*=0 the last equation form reduces to the first order approximation. The next step is to use the expression $H(x) = l - (bx)^c$ presented earlier for $H(x)$ to find the advanced form of IM-model:

$$f_x = \left(\frac{2}{\sqrt{2\pi}}\right)\left(\frac{|l+(c-1)(bx)^c|}{\sqrt{x^3}} + \frac{k\sqrt{x^3}c(c-1)b^c x^{(c-2)}}{2|l+(c-1)(bx)^c|}\right) e^{-\frac{(l-(bx)^c)^2}{2x}} \quad (13)$$

TABLE II

| Year | 2010 | 2010 | 2010 | 1950 | 1950 | 1950 |
|---|---|---|---|---|---|---|
| Parameter/$R^2$ | Health State | IM Model | 2-Parameter | Health State | IM Model | 2-Parameter |
| *c* | 5.28 | 7.91 | 7.91 | 4.18 | 6.26 | 6.27 |
| *b* | 0.0192 | 0.0148 | 0.0148 | 0.0239 | 0.0173 | 0.0173 |
| *l* | 13.84 | 0.0066 | - | 13.05 | 0.0314 | - |
| $R^2$ | 0.993 | 0.995 | 0.993 | 0.920 | 0.990 | 0.927 |

This is the simpler 4-parameter model providing quite well fitting for the logarithm of the force of mortality, providing not only good estimates for the infant mortality but also very good estimates for all the period of the life time for males and females as is illustrated in Figures 7A-7F. We have thus demonstrated that the model proposed in 1995 and the new versions and advanced forms provided in several publications and in this paper, approach fairly well the mortality data sets provided by the bureau of the census and statistical agencies. This is important in order to straighten the findings when applying the first exit time theory to life table data.

**3.3. The Health State Function and the relative impact on mortality**

Considering the high importance of the proposed model and the related indicator for the verification of the GBD results we proceed in the introduction of a second method based on the health state of the population instead of the previous one which was based on mortality. This model was proposed earlier (see Skiadas and Skiadas, 2010, 2012, 2013, 2014). These works were based on an earlier publication modeling the health state of a population via a first exit time stochastic methodology. Here we develop a special application adapted to WHO data provided as abridged life tables (0 to 100 with 5 year periods). First we expand the abridged life table to full and then we estimate the health indicators and finally the loss of healthy life year indicators.

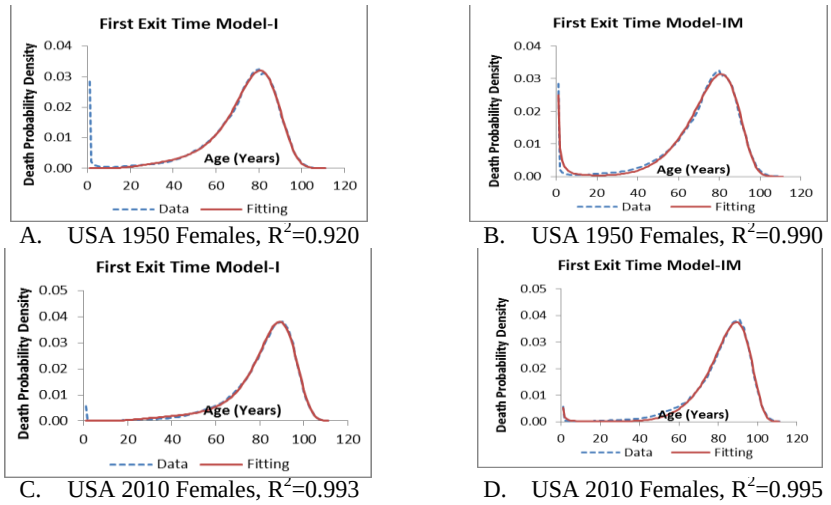


A. USA 1950 Females, $R^2$=0.920 B. USA 1950 Females, $R^2$=0.990

C. USA 2010 Females, $R^2$=0.993 D. USA 2010 Females, $R^2$=0.995

Fig. 6. The First Exit Time Model-IM including the Infant Mortality applied in USA death probability density for females the years 1950 and 2010.

By observing the above graph (Figure 8) we can immediately see that the area between the health state curve and the horizontal axis (OMCO) represents the total health dynamics (THD) of the population. Of particular importance is also the area of the health rectangle (OABC) which includes the health state curve. This rectangle is divided in two rectangular parts the smaller (OAMN) indicating the first part of the human life until reaching the point M at the highest level of health state (usually the maximum is between 30 to 45 years) and the second part (NMBC) characterized by the gradual deterioration of the human organism until the zero level of the health state. This zero point health age C is associated with the maximum death rate. After this point the health state level appears as negative in the graph and characterizes a part of the human life totally unstable with high mortality; this is also indicated by a positively increasing form of the logarithm of the force of mortality $\ln(\mu_x)$.

We call the second rectangle NMBC as the ***deterioration rectangle***. Instead the first rectangle OAMN is here called as the ***development rectangle***. For both cases we can find the relative impact of the area inside each rectangle but outside the health state area to the overall health state. In this study we analyze the relative impact of the ***deterioration area*** MBCM indicated by dashed lines in the ***deterioration rectangle***. It should be noted that if no-deterioration mechanism was present or the repairing mechanism was perfect the health state should continue following the straight line AMB parallel to the X-axis at the level of the maximum health state. The smaller the deterioration area related to the health state area, the higher the healthy life of the population. This comparison can be done by estimating the related areas and making a simple division.

However, when trying to expand the human life further than the limits set by the deterioration mechanisms the percentage of the non-healthy life years becomes higher. This means that we need to divide the total rectangle area by that of the deterioration area to find an estimate for the "lost healthy life years". It is clear that if we don't correct the deterioration mechanisms the loss of healthy years will become higher as the expectation of life becomes larger. This is already observed in the estimates of the World Health Organization (WHO) in the World Health Report for 2000 where the healthy years lost for females are higher than the corresponding values for males. The females show higher life expectancy than males but also higher values for the lost healthy years. The proposed "loss of healthy life years" indicator is given by:

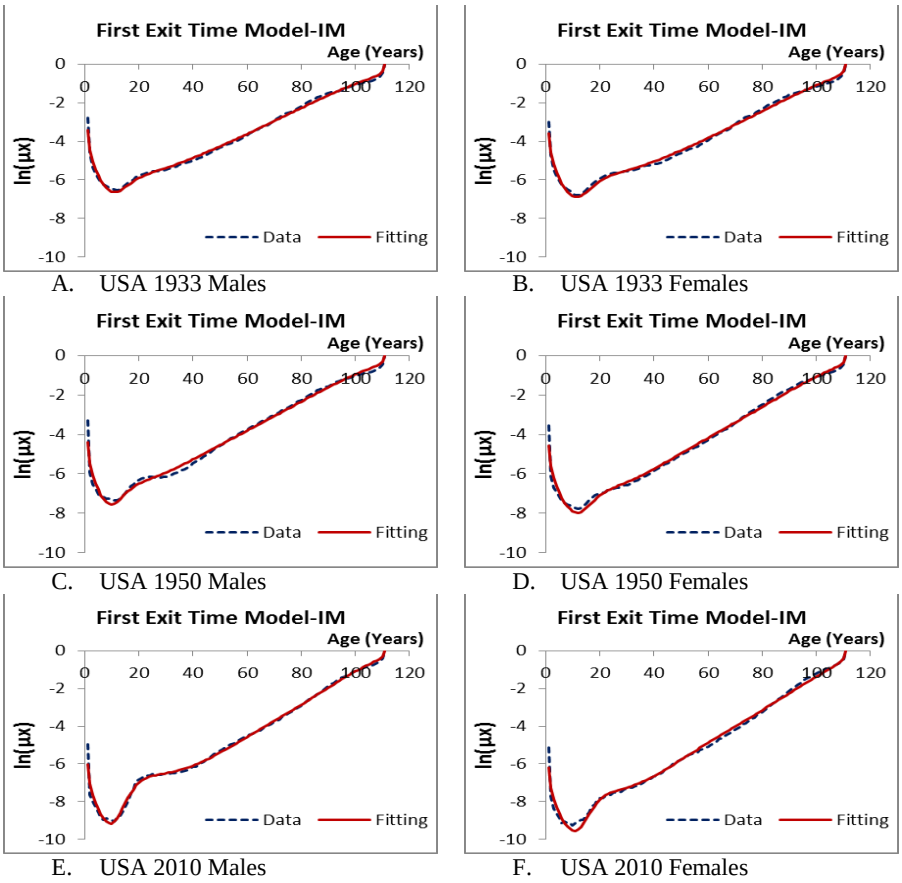


A. USA 1933 Males B. USA 1933 Females

C. USA 1950 Males D. USA 1950 Females

E. USA 2010 Males F. USA 2010 Females

Fig. 7. The First Exit Time Model-IM including the Infant Mortality applied in the USA force of mortality data in logarithmic form for males and females the years 1933, 1950 and 2010.

$$LHLY_1 = \lambda \frac{OABC}{THD_{ideal}} \cdot \frac{THD_{ideal}}{MBCM} = \lambda \frac{OABC}{MBCM}$$

Where $THD_{ideal}$ is the ideal total health dynamics of the population and the parameter $\lambda$ expresses years and should be estimated according to the specific case. For comparing the related results in various countries we can set $\lambda$=1. When OABC approaches the $THD_{ideal}$ as is the case of several countries in nowadays the loss of healthy life years indicator LHLY can be expressed by other forms.

Another point is the use of the (ECD) area in improving forecasts especially when using the 5-year life tables as is the case of the data for all the WHO Countries. In this case the expanded loss of healthy life years indicator LHLY will take the following two forms:

$$LHLY_2 = \lambda \frac{OMCO + ECD}{MBCM} \qquad LHLY_3 = \lambda \frac{OABC + ECD}{MBCM}$$

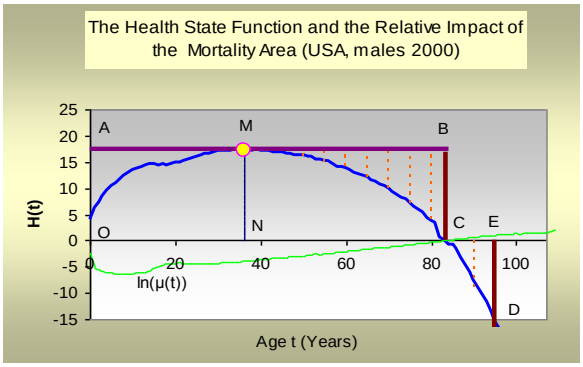


Fig. 8. The impact of mortality area to the health state

It is clear that the second form will give higher values than the previous one. The following scheme applies: $LHLY_1<LHLY_2<LHLY_3$. It remains to explore the forecasting ability of the three forms of the "loss of healthy life years" indicator by applying LHLY to life tables provided by WHO or by the Human Mortality Database or by other sources.
As for the previous case here important is the loss of health state area MBCM whereas the total area including the healthy and non-healthy part is included in OABC+ECD.

$$LHLY_3 = \lambda \frac{OABC + ECD}{MBCM} \tag{14}$$

Details and applications are included in the book on "The Health State Function of a Population", the supplement of this book and other publications (see Skiadas and Skiadas 2010, 2012, 2013, 2016). It is important that we can explore the health state of a population by using the mortality approach with the Simple Model proposed herewith and the health state function approach as well. The latter method provides many important health measures than the simple model.

## 4. Application

### Comparative Application for the World and World Regions

The Table III includes our estimates for the healthy life expectancy at birth for the years 2000 and 2012 by applying the proposed mortality model and the health state model (HSM), and the estimates of WHO referred as HALE and included in the WHO websites (August 2015). Our estimates for the mortality model are based on $LHLY=(b+1)=E_{total}/E_{mortality}$.
The main finding is that our models verify the WHO (HALE) estimates based on the Global Burden of Disease Study. Our results are quite close (with less to one year difference) to the estimates for the World, the High Income Countries, the African region, the European region and Western Pacific and differ by 1-2 years for the Eastern Mediterranean region and the South East Asian region. In the last two cases the collection of data and the accuracy of the information sources may lead to high uncertainty of the related health state estimates. This is demonstrated in the provided confidence intervals for the estimates in countries of these regions in the studies by Salomon et al. (2012) and the Report of WHO (2001) for the HLE of the member states (2000). From the Salomon et al. study we have calculated a mean confidence interval of 5.5 years for males and 6.8 for females for the year 2000. We thus propose to base the future works on the system we propose and to use it to calibrate the estimates especially for the countries providing of low accuracy data.
To support future studies we have formulated an easy to use framework in Excel. The only needed is to insert data for $\mu_x$ in the related column of the program. The program estimates the life expectancy, the loss of healthy life years and the healthy life expectancy.

**TABLE III**

| Comparing WHO (HALE) Results | | | | | | | | | | |
|---|---|---|---|---|---|---|---|---|---|---|
| Sex/Region | Healthy Life Expectancy at Birth | | | | | | Life Expectancy at Birth (LE) | | | |
| | 2000 | | | 2012 | | | 2000 | | 2012 | |
| | WHO HALE | Mortality Model | HSM Model | WHO HALE | Mortality Model | HSM Model | WHO | Mortality | WHO | Mortality Model |
| **Both sexes combined** | | | | | | | | | | |
| World | 58.0 | 58.4 | **58.2** | 61.7 | 62.5 | **61.9** | 66.2 | 66.2 | 70.3 | 70.3 |
| High income | 67.3 | **67.1** | 67.0 | 69.8 | **69.6** | 69.2 | 76.0 | 76.0 | 78.9 | 78.9 |
| African Region | 43.1 | **42.8** | 42.8 | 49.6 | 49.9 | **49.6** | 50.2 | 50.2 | 57.7 | 57.7 |
| Region of the Americas | 64.9 | 65.7 | **65.4** | 67.1 | 67.7 | **67.2** | 73.9 | 73.9 | 76.4 | 76.3 |
| East Med Region | 55.4 | 56.9 | **56.6** | 58.3 | 59.7 | **59.4** | 64.9 | 64.9 | 67.8 | 67.8 |
| European Region | 63.9 | **63.9** | **63.9** | 66.9 | 67.2 | **67.0** | 72.4 | 72.4 | 76.1 | 76.0 |
| South East Asian Region | 54.2 | 56.3 | **55.6** | 58.5 | 60.6 | **60.0** | 62.9 | 63.0 | 67.5 | 67.5 |
| Western Pacific Region | 64.8 | **63.9** | **64.2** | 68.1 | **67.3** | 67.5 | 72.3 | 72.3 | 75.9 | 75.9 |
| **Males** | | | | | | | | | | |
| World | 56.4 | **56.6** | **56.2** | 60.1 | 60.4 | **60.0** | 63.9 | 63.9 | 68.1 | 68.0 |
| High income | 64.7 | 64.1 | **64.2** | 67.5 | **67.0** | **67.0** | 72.4 | 72.3 | 75.8 | 75.7 |
| African Region | 42.4 | 41.6 | **42.3** | 48.8 | **48.6** | **48.6** | 49.0 | 49.0 | 56.3 | 56.3 |
| Region of the Americas | 62.7 | 63.1 | **62.5** | 64.9 | 65.1 | **64.6** | 70.8 | 70.8 | 73.5 | 73.5 |
| East Med Region | 54.8 | 55.7 | **55.6** | 57.4 | 58.2 | **57.9** | 63.6 | 63.6 | 66.1 | 66.1 |
| European Region | 60.7 | **60.4** | 61.1 | 64.2 | **64.3** | 64.5 | 68.2 | 68.2 | 72.4 | 72.4 |
| South East Asian Region | 53.5 | 55.4 | **54.6** | 57.4 | 59.2 | **58.6** | 61.6 | 61.7 | 65.7 | 65.7 |
| Western Pacific Region | 63.0 | 61.8 | **62.0** | 66.6 | 65.2 | **65.7** | 70.0 | 70.0 | 73.9 | 73.9 |
| **Females** | | | | | | | | | | |
| World | 59.7 | 60.3 | **59.9** | 63.4 | 64.3 | **64.1** | 68.5 | 68.5 | 72.7 | 72.6 |
| High income | 70.0 | **69.7** | 69.6 | 72.0 | 71.8 | **72.1** | 79.6 | 79.5 | 82.0 | 81.9 |
| African Region | 43.8 | **43.8** | 43.5 | 50.4 | 51.2 | **50.5** | 51.4 | 51.4 | 59.0 | 59.1 |
| Region of the Americas | 67.2 | 68.0 | **67.8** | 69.1 | 69.9 | **69.8** | 77.0 | 76.9 | 79.3 | 79.2 |
| East Med Region | 56.1 | 58.2 | **57.8** | 59.2 | 61.3 | **61.0** | 66.4 | 66.4 | 69.7 | 69.6 |
| European Region | 67.1 | 67.6 | **67.3** | 69.6 | 70.0 | **69.7** | 76.7 | 76.6 | 79.6 | 79.6 |
| South East Asian Region | 55.0 | 57.2 | **56.4** | 59.7 | 62.0 | **61.7** | 64.3 | 64.4 | 69.4 | 69.4 |
| Western Pacific Region | 66.7 | 65.7 | 66.1 | 69.8 | 68.9 | **69.1** | 74.8 | 74.8 | 78.1 | 78.0 |

**5. Discussion and Conclusions**

The GBD study critisized by Williams (see Murray et al. 2000) whereas many comments from people from social sciences and philosophy refer to the impossibility to define health and, as a consequence, to measure it. The main problem is that we cannot have flexibility in finding an estimate of health the way we do with other measures of the human organism and related activities. So far if we measure health by collecting surveys it is clear that the uncertainty is relatively high. Even more if we decide for an accepted health state estimate (see Sanders, 1964 and related studies during 60's and 70's) it remains the problem of accepting a *unit of measure*. The quantitative methods we propose overcome many of the objections posed. That we have achieved is to propose and apply several quantitative methods and techniques leading to estimates of the healthy life years lost. More than to be close to the WHO results, our calculations provide enough evidence for estimating and quantifying the health state of a population.

## References

Carriere, J.F. Parametric Models for Life Tables, Transactions of the Society of Actuaries, Vol. XLIV, 77-99, 1992.

Chang, M-H, Molla, MT, Truman, BI et al. Differences in healthy life expectancy for the US population by sex, race/ethnicity and geographic region: 2008. Journal of Public Health 2015 Sep;37(3):470-9. doi: 10.1093/pubmed/fdu059. Epub 2014.

Gompertz, B. On the nature of a function expressive of the law of human mortality, and on a new mode of determining the value of life contingencies, Philosophical Transactions of the Royal Society, 115, 513-585, 1825.

Hausman, D. M. Health, well-being, and measuring the burden of disease, Population Health Metrics 10:13, 2012. http://www.pophealthmetrics.com/content/10/1/13.

Janssen, J. and Skiadas, C. H. Dynamic modelling of life-table data, Applied Stochastic Models and Data Analysis, 11, 1, 35-49, 1995.

Mathers, et al. Estimates of DALE for 191 countries: methods and results, Global Programme on Evidence for Health Policy Working Paper No. 16, World Health Organization, June 2000.

McDowell, I. Measuring Health: A Guide to Rating Scales and Questionnaires, Third Edition, Oxford University Press, 2006.

Murray, C.J.L. and Alan D. Lopez, A.D. Global mortality, disability, and the contribution of risk factors: Global Burden of Disease Study, Lancet, May 17; 349(9063):1436-42, 1997.

Murray, C. J. L. et al. Global, regional, and national disability-adjusted life years (DALYs) for 306 diseases and injuries and healthy life expectancy (HALE) for 188 countries, 1990–2013: quantifying the epidemiological transition, The Lancet, August 2015. DOI: http://dx.doi.org/10.1016/S0140-6736(15)61340-X.

Murray, C. J. L. and Lopez, A. D. Progress and Directions in Refining the Global Burden of Disease Approach: A Response to Williams, Health Economics 9: 69–82, 2000. http://down.cenet.org.cn/upfile/40/2006111211716102.pdf

Robine J. M., Isabelle Romieu I. and Cambois, E. Health expectancy indicators, Bulletin of the World Health Organization, 1999, 77 (2).

Salomon, J. A., Wang, H. et al. Healthy life expectancy for 187 countries, 1990-2010: a systematic analysis for the Global Burden Disease Study. Lancet, 380, 2144–2162, 2012. DOI: http://dx.doi.org/10.1016/S0140-6736(12)61690-0

Sanders, B. S. Measuring Community Health Levels. American Journal of Public Health, 54, 1063-1070, 1964.

Skiadas, C. and Skiadas, C. H. Development, Simulation and Application of First Exit Time Densities to Life Table Data, Communications in Statistics - Theory and Methods, 39, 3, 444-451, 2010.

Skiadas, C. H. and Skiadas, C. Estimating the Healthy Life Expectancy from the Health State Function of a Population in Connection to the Life Expectancy at Birth. In: Skiadas, C. H. and Skiadas, C., The Health State function of a population.1st ed. Athens: ISAST, 2012, 2nd ed. 2013. http://www.amazon.com/The-Health-State-Function-Population/dp/6188046505

Skiadas, C. H. The Health State Function, the Force of Mortality and other characteristics resulting from the First Exit Time Theory applied to Life Table Data. In: Skiadas, C. H. and Skiadas, C., The Health State function of a population.1st ed. Athens: ISAST, 69-92, 2012b, 2nd ed. 2013. http://www.amazon.com/The-Health-State-Function-Population/dp/6188046505.

Skiadas, C. H. and Skiadas, C. The Health State Function of a Population, 1st ed. Athens: ISAST, 2012b, 2nd ed. 2013. http://www.amazon.com/The-Health-State-Function-Population/dp/6188046505 .
Skiadas, C. H. and Skiadas, C. Supplement The Health State Function of a Population, Athens, ISAST, 2013. http://www.amazon.com/Supplement-Health-State-Function-Population/dp/6188069831 .
Skiadas, C. H. and Skiadas, C. The First Exit Time Theory applied to Life Table Data: the Health State Function of a Population and other Characteristics, Communications in Statistics-Theory and Methods, 34, 1585-1600, 2014.
Skiadas, C. H. and Skiadas, C. Exploring the State of a Stochastic System via Stochastic Simulations: An Interesting Inversion Problem and the Health State Function, Methodology and Computing in Applied Probability, 17, 973-982, 2015 (published online: June 2014).
Skiadas, C. H. Verifying the Global Burden of Disease Study: Quantitative Methods Proposed, ArXiv.org, October 2015. http://arxiv.org/abs/1510.07346
Skiadas, C. H., Correspondence: On reproducing the results included in the paper on "Differences in healthy life expectancy for the US population by sex, race/ethnicity and geographic region: 2008", communicated to the Journal of Public Health (January 2016).
Salomon, et al. Healthy life expectancy for 187 countries, 1990–2010: a systematic analysis for the Global Burden Disease Study 2010, Lancet 380: 2144–62, 2012.
Sullivan, D. F. A single index of mortality and morbidity, HSMHA Health Reports, 86, 347-354, 1971.
Ting Lee, M-L and Whitmore, G. A. Threshold regression for survival analysis: modelling event times by a stochastic process reaching a boundary, Statistical Science, 21, 4, 501-513, 2006.
Vos, T. M., Flaxman, A. D. et al. Years lived with disability (YLDs) for 1160 sequelae of 289 diseases and injuries 1990–2010: a systematic analysis for the Global Burden of Disease Study 2010. Lancet, 380, 2163–2196, 2012. DOI: http://dx.doi.org/10.1016/S0140-6736(12)61729-2.
Weitz, J. S. and Fraser, H. B., Explaining mortality rate plateaus. Proc. Natl. Acad. Sci. USA, 98(26), 15383 (2001).
WHO. Department of Health Statistics and Information system. "WHO methods and data sources for the global burden of disease estimates 2000-2011". Global Health Estimates Technical Paper WHO/HIS/HSI/GHE/2013.4. November, 2013.
http://www.who.int/healthinfo/statistics/GlobalDALYmethods_2000_2011.pdf
WHO. "WHO methods for life expectancy and healthy life expectancy". Global Health Estimates Technical Paper WHO/HIS/HSI/GHE/2014.5. March, 2014.
http://www.who.int/healthinfo/statistics/LT_method.pdf
WHO, The World Health Report 2001, Statistical Annex, Annex Table 4 Healthy life expectancy (HALE) in all Member States, estimates for 2000. annex4_en_HALE_2000.pdf.
WHO. The World 132 Health Report 2004, Statistical Annex, Annex Table 4 Healthy life expectancy (HALE) in all WHO Member States, estimates for 2002. annex_4_en_2002.pdf.
WHO. The World Health Report 2002, Statistical Annex, Annex Table 4 Healthy life expectancy (HALE) in all Member States, estimates for 2000 and 2001. whr2002_annex4_2001.pdf.
WHO. WHO methods for life expectancy and healthy life expectancy, Global Health Estimates Technical Paper WHO/HIS/HSI/GHE/2014.5, March 2014.
Yong, V. and Saito, Y., Trends in healthy life expectancy in Japan: 1986 – 2004, Demographic Research, Vol. 20, 467-494, 2009.

# 6 CHAPTER

## Statistical Modelling and Applications

# Modeling the relationship between temperature and daily mortality in Cyprus

Haritini Tsangari[1], Zoi Konsoula[2], Stephanie Christou[3], Kyriakos Georgiou[4], and Edna Yamasaki[5]

[1] University of Nicosia Research Foundation, University of Nicosia, Nicosia, Cyprus
(E-mail: tsangari.h@unic.ac.cy)
[2] University of Nicosia Research Foundation, University of Nicosia, Nicosia, Cyprus
(E-mail: konsoula.z@unic.ac.cy)
[3] University of Nicosia Research Foundation, Nicosia, Cyprus
(E-mail: christou.st@unic.ac.cy)
[4] Cyprus Center for European and International Affairs, University of Nicosia, Nicosia, Cyprus
(E-mail: georgiou.k@unic.ac.cy)
[5] University of Nicosia Research Foundation, University of Nicosia, Nicosia, Cyprus
(E-mail: yamasaki.e@unic.ac.cy)

**Abstract.** Climatic changes, such as large temperature fluctuations and increase in the occurrence of heat waves, have been evidenced to affect mortality worldwide. In this paper we examine the effect of high temperatures on mortality in Cyprus, an island which is characterized by a Mediterranean climate. The modeling approach is described. First, the temperature function is created within the newly-developed framework of distributed lag non-linear models, to simultaneously capture non-linearities and delayed effects. The temperature function is, then, incorporated in a Generalized Linear Model with a quasi-Poisson distribution to allow for overdispersion, together with possible confounders such as meteorological indicators, trends and seasonality. Comparisons are additionally made, regarding the effect of temperature on mortality, between inland and coastal areas. All the results are presented in a tabular or graphical form and the conclusions are discussed.
**Keywords:** heat waves, mortality, distributed lag non-linear model, strata constraints, hot threshold, GLM, quasi Poisson, harvesting effect.

## 1 Introduction

Global climate change is projected to further increase the frequency, intensity and duration of heat waves. Exposure to high temperatures can result in a variety of adverse health effects including deaths due to heat-related causes such as heat stroke, but also exacerbating many preexisting health conditions (Rainham and Smoyer-Tomic[34]; Kovats and Hajat[27]; Gosling et al.[18]). Many studies conducted worldwide, have, in fact, indicated a consistent strong

*Stochastic Modeling, Data Analysis and Statistical Applications* (*pp*. 257-272)
Lidia Filus - Teresa Oliveira - Christos H Skiadas (Eds)


association between elevated temperature and all-cause (excluding external causes) mortality, despite any variation observed amongst diseases (Armstrong[3]; Baccini et al.[5]; Michelozzi et al.[29]; Zanobetti and Schwartz[42]; Biggeri and Baccini[7]; Hajat et al.[24]).

The association between temperature and mortality has been evidenced to be non-linear, following a J-, U-, or V-shaped curve, where minimum mortality is detected at moderate temperatures, while an excess health risk is observed at temperatures above a certain threshold, with higher mortality at temperature extremes (Armstrong[3]; Armstrong et al.[4]; Baccini et al.[5]; Curriero et al.[9]; Hajat and Kosatsky[21]).

In addition, many studies have shown evidence of the so-called "delayed effect". They have indicated that temperature can affect not only deaths occurring on the same day, but on several subsequent days, where the converse is also true: deaths on each day depend on the effect of the same day's temperature as well as the lag effects of the previous days' temperatures (Anderson and Bell[2]; Braga et al.[8]; Gasparrini et al.[17]). The estimate of the effect depends on the appropriate specification of the lag dimension of the dependency, defining models flexible enough to represent simultaneously the exposure-response relationship and its temporal structure (Gasparrini et al.[17]).

The island of Cyprus has a typical Mediterranean climate characterized by hot dry summers and rainy changeable winters, separated by short autumn and spring seasons of rapid change. During summertime, it is mainly under the influence of a shallow trough of low pressure extending from the great continental depression centered over Southwest Asia, which results in high temperatures with almost cloudless skies and negligible rainfall (Price et al.[33]). In Cyprus climate change has been observed, with an increase in the average annual temperature by 0.8°C in the last thirty-year period and a drop in precipitation by 17% from the second half of the century. Climate change is expected to act in many ways as a multiplier of existing environment and health problems (Symeou[38]).

Very few studies exist about countries with a Mediterranean climate (Almeida et al.[1]; Garcia-Herrera et al.[15]). The current study, therefore, provides additional evidence on the effect of extreme weather on mortality in a country with a Mediterranean climate, and it is the first that examines this issue for the island of Cyprus. The study, additionally, implements a new methodological approach.

## 2 The GLM modeling framework

A Generalized Linear Model (GLM) framework will be used in our analysis. A general form of the model for the mortality counts, , t=1,….n, is given by:

$$g(\mu_t) = \alpha + \sum_{j=1}^{J} s_j(x_{tj}; \boldsymbol{\beta}_j) + \sum_{k=1}^{K} \gamma_k u_{tk} \quad , \qquad (1)$$

where $\mu = \mathrm{E}(Y)$, g is a monotonic link function and $\mathbf{Y}$ has a distribution from an exponential family (McCullagh and Nelder[28]). In epidemiological studies of the impact of extreme weather on human health, where the response variable is a non-negative daily count (e.g., mortality), overdispersion is often observed, where the variance of the outcome is greater than its mean ($\mathbf{V}(\mathbf{Y}) = \phi\mu, \quad \phi > 1$). GLM models with quasi-Poisson regression have been shown to capture overdispersion well, by extending the Poisson distribution with the estimation of an additional dispersion parameter (Armstrong et al.[4]; Guo et al.[19]; Everitt and Hothorn[13]; Hajat et al.[23]; Schwartz et al.[37]; Zeger[44]). The functions $s_j$ in equation (1) denote smoothed relationships between the variables $x_j$ and the linear predictor, defined by the (unknown) parameter vectors $\beta_j$. The variables $u_k$ include other predictors with linear effects specified by the related coefficients $\gamma_k$. Using mortality counts in the above framework is referred to as the "usual practice" in related research (Armstrong[3]; Dominici[10]) and has been widely implemented in studies of a single city as well as comparisons of various geographical locations (Baccini et al.[5]; Pattenden et al.[31]; Schwartz et al.[37]).

### 2.1 The temperature function in GLM

First, we consider the function $s_1(x_{t1}; \boldsymbol{\beta})$ for temperature, $x$, that will be included in the GLM framework of equation (1), hereafter called the "temperature function". As mentioned in section 1, the relation between temperature and mortality has been evidenced to have two main characteristics: non-linearity and delayed effect. Many methods have been proposed to deal with non-linearity, depending on the shape of the relationship, the degree of approximation required and interpretational issues. Among the most commonly used methods are smooth curves, such as polynomials, quadratic B-splines or natural cubic splines (Dominici et al.[11]) or linear-threshold parameterizations (e.g., "hockey-stick model"), which assume a high temperature threshold, k, and can by represented by a truncated linear function $(x-k)_+$ which equals $(x-k)$ when $x>k$ and 0 otherwise (Armstrong[3]; Hajat et al.[23]; Pattenden et al.[31]; Baccini et al.[5]).

Among the methods that have been proposed to deal with delayed effects, a major role is played by distributed lag models (DLM) (Schwartz[36]; Zanobetti et al.[43]; Braga et al.[8]). When a linear relation is assumed, this methodology allows the effect of a single exposure event to be distributed over a specific period of time, using several parameters to explain the contributions at different lags, thus providing an estimate of the overall effect. The simplest formulation is an unconstrained DLM. However, each individual coefficient at specific lags is often imprecisely estimated and highly correlated with estimates of other coefficients, resulting in collinearity between exposures in adjacent days. To

gain more precision in the estimate of the distributed lag curve, some constraints can be imposed, where an effective choice includes strata constraints (Welty and Zeger[40]; Armstrong[3]; Pattenden et al.[31]; Gasparrini et al.[17]; Gasparrini and Armstrong[16]). In such a "lag-stratified distributed lag model" several days are averaged as the effects of temperature over a period of time rather than from the contribution of one day, assuming a constant effect (equal coefficients) within lag intervals (strata).

Although there exist well-developed methods for dealing with non-linearity or time latency in the temperature-mortality association, these two components are rarely modeled simultaneously. We will use a methodology that unifies many of the previous methods to deal with delayed effects and at the same time provide more flexible alternatives regarding the shape of the relationships, relaxing the assumption of linearity. More specifically, the temperature function will be modeled using the newly-developed framework of Distributed Lag Non-Linear Models (DLNM) (Armstrong[3], Gasparrini et al.[17]; Gasparrini and Armstrong[16]). DLNM can describe non-linear relationships by choosing a "cross-basis", which is a bi-dimensional space of functions describing on the same time the shape of the relationship along the predictor, x, (temperature) and the distributed lag effects. Choosing a cross-basis amounts to specifying two independent sets of "basis" functions, which will be combined (Gasparrini et al.[17]). A DLNM can be specified by

$$s(x_t;\boldsymbol{\eta}) = \sum_{j=1}^{v_x}\sum_{k=1}^{v_l} \mathbf{r}_{tj.}^{T} c_{.k}\eta_{jk} = \boldsymbol{w}_t^{T}\boldsymbol{\eta},$$

where $\mathbf{r}_{tj.}$ is the vector of lagged exposures for the time t transformed through the basis function, the vector $\mathbf{w}_{t.}$ is the $t^{th}$ row of the cross-basis matrix **W, C** is an $(L+1)\times v_l$ matrix of basis variables for the lag vector **l**, and **η** is a vector of unknown parameters. More details regarding the algebraic notation and estimation of DLNMs can be found in Gasparrini et al.[17].

In our study, the choice of the non-linearity dimension of the cross-basis of DLNM will be led by visual inspection of the shape of the temperature-mortality relation, assuming a high threshold temperature (see section 4). Regarding the lag dimension of the cross-basis, we will we assess the effect of temperature on mortality with lags up to 10 days before the day of death, using a constrained distributed lag model, with strata constraints on the coefficients ("lag-stratified distributed lag model"), to avoid collinearity and improve the precision of the estimates. We will define 3 strata intervals with dummy parameterization, assuming constant distributed lag effects along the strata of lags 0-1, 2-5 and 6-10.

### 2.2 Confounding factors in the temperature-mortality relation

The relationship between temperature and mortality may be confounded by measured or unmeasured covariates, which need to be controlled for properly in the GLM model (Peng et al.[32]; Touloumi et al.[39]; Dominici et al.[12]). The meteorological variable relative humidity has been shown to be a confounder of

the mortality-temperature relation and natural cubic splines have been used as a smoothed function (Armstrong et al.[4]; Guo et al.[7]; Braga et al.[8]; Curriero et al.[9]; Anderson and Bell[2]; Armstrong[3]). We will similarly use natural cubic splines to control for the non-linear effect of relative humidity (function $s_2$ in equation (1)). Our GLM model will also control for secular trends and seasonality, by using smooth functions of time (day of the year) (function $s_3$ in equation (1)). Natural cubic splines are most commonly used in this context, where the degree of smoothness is very important, since it determines the amount of residual temporal variation in mortality available to estimate the temperature effect (Armstrong et al.[4]). The relation between temperature and mortality has also been evidenced to be affected by calendar days, where, for example, on weekends the number of hospital admissions can be lower than on weekdays and can also be lower during public holidays (Armstrong et al.[4]; Guo, et al.[19]; Michelozzi et al.[30]; Peng et al.[32]). Thus, any additional confounding by seasonally varying factors which vary on shorter timescales will be controlled by adding categorical/dummy variables for day of the week and public holidays ($\gamma_k u_k$ in equation (1)).

Since our interest is on the heat effect on mortality, the analysis will concentrate on the warm periods of each year, where a warm period is defined as the months from April to September. The same definition was chosen by many previous studies (e.g., Baccini et al.[5]; Michelozzi et al.[30]; Almeida et al.[1]; Pattenden et al.[31]), in order to ensure reasonable statistical power, given the small number of events (mortality), and based on the evidence that heat waves occurring at times other than summer may have just as strong a health impact (Hajat et al.[22]; Michelozzi et al.[29]). Therefore, the data are composed by multiple equally-spaced and ordered series of the same seasons for each year, and do not represent a single continuous time series. We will use the methodology suggested by Gasparrini and Armstrong[16], especially for seasonal analysis, in order to define this multiple series.

The results will be obtained using R statistical software (The R Foundation for Statistical Computing).

## 3 Data

Daily mortality data were provided by the Ministry of Health of the Republic of Cyprus, for each of the five districts in Cyprus (Nicosia, Limassol, Larnaca, Paphos, Ammochostos) for the period between the years 2004 and 2009. The data included total (all-cause) mortality excluding external causes, as classified in the Eurostat Shortlist of 65 causes of death.

Daily meteorological data were collected by the Cyprus Meteorological Service in the five main urban centers of the island. The meteorological parameters that were used for the purpose of this study included measures of temperature and relative humidity. No temperature measure has been shown to be consistently better at predicting mortality and thus there is no standard indicator of heat

stress (Barnett et al.[6]; Michelozzi et al.[30]). We considered the daily surface maximum temperature (in °C), which was used in many related studies (e.g., Armstrong et al.[4]; Filleu et al.[14]; Guo et al.[19]; Rocklöv and Forsberg[35]). Daily values of relative humidity at 8:00 LST and 13:00 LST (in %) were obtained for each district, where the mean of the two values was calculated. We avoided unequal spacing of the observations by imputing missing values as the moving average of surrounding observations (e.g. Rocklöv and Forsberg[35]). Cyprus was considered as a total area, using the combined data from all the stations, but separate analyses were also performed for Nicosia (urban area) and Limassol (coastal area) for comparative purposes.

## 4 Analysis and results

Table 1 presents descriptive statistics for the main variables of the study, all-cause (total) mortality counts, maximum temperature and relative humidity, by district, for the warm periods (April to September) of the years 2004-2009.

| **District** | **Total Mortality** | | **Maximum Temperature (°C)** | | **Relative Humidity (%)** | |
|---|---|---|---|---|---|---|
| | **Mean** | **SD** | **Mean** | **SD** | **Mean** | **SD** |
| Nicosia | 4.56 | 2.19 | 32.84 | 5.48 | 43.02 | 13.66 |
| Limassol | 3.33 | 1.91 | 30.41 | 4.25 | 63.22 | 10.30 |
| Larnaca | 1.75 | 1.38 | 29.81 | 4.28 | 55.11 | 11.89 |
| Paphos | 1.10 | 1.08 | 27.55 | 3.79 | 67.50 | 9.19 |
| Ammochostos | 0.54 | 0.74 | 30.39 | 4.91 | 54.31 | 14.14 |

**Table 1.** Descriptive statistics of the mortality and meteorological variables, per district, for the warm periods (April to September), 2004-2009.

Figure 1 shows the relation between daily all-cause mortality and maximum temperature in Cyprus.

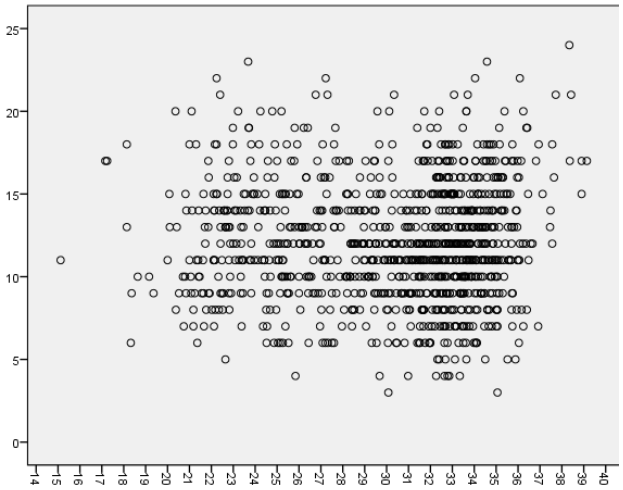


**Fig. 1.** Mortality vs. maximum temperature: Cyprus, warm periods, 2004-2009.

Examination of figure 1 indicates a non-linear effect of temperature. More specifically, it appears to be constant up to one point (zero slope up to temperatures around 29$^{o}$C) and then we have a V-shaped relation with a hot threshold, the common point where two linear terms are constrained to join, which corresponds to a change in the effect estimate and the temperature associated with the minimum mortality rate. Therefore, led by visual inspection, the non-linearity component of the temperature function in DLNM will be captured for our data by the "linear-thresholds" model ("hockey-stick" model), with a high threshold parameterization (see section 2.1). Similar plots were found for Nicosia (urban area) and Limassol (coastal area), when the respective data were examined separately.

Based on figure 1, we tested a grid of temperatures from 31$^{o}$C to 35$^{o}$C, in 0.1$^{o}$C increments, to identify the threshold temperature that satisfied our criteria for model choice (e.g., minimizing residual deviance and Akaike Information Criterion (AIC) (Armstrong[3]; Guo et al.[19]). The hot threshold temperature for Cyprus was found to be 33.7$^{o}$C. Using similar procedures, the threshold temperatures for Nicosia and Limassol were found to be 32.5$^{o}$C and 38$^{o}$C respectively.

The GLM model was then fit to the data, including the temperature function and the potential confounders of the temperature-mortality relation. The final estimated GLM model could be described by the following equation:

$$\log(E(Y_t)) = \boldsymbol{\alpha} + \boldsymbol{\beta}\mathbf{T}_{\mathbf{t,l}} + S_2(RH_t,3) + S_3(d_t,4) + \boldsymbol{\gamma}_1 DOW_t + \gamma_2 Holiday_t$$

where t is the day of observation (days 151 up to 273 of each year, restricted to the periods from April to September), Yt is the observed daily death counts on day t, α is the intercept, $T_{t,l}$ is the temperature function (a matrix obtained by

applying DLNM to temperature), $l$ corresponds to lags of temperature, $\beta$ is the vector of coefficients for $T_{t,l}$ , $S_2(RH_t,3)$ is a natural cubic spline with 3 degrees of freedom to smooth relative humidity, $S_3(d_t,4)$ is a natural cubic spline with 4 degrees of freedom for long-term trends (day of the year), as a smooth function to capture the variation within the warm period, $DOW_t$ is the indicator variable for "day of the week" effect (1=Sunday) on day t ($\gamma$1 is the corresponding coefficient), and $Holiday_t$ is a dummy variable for the holiday effect (1=Public Holiday; $\gamma_2$ is the corresponding coefficient). All the components of the model were significant (p-values<5%), except the Holiday effect. The model had a good fit, satisfying all model criteria and diagnostics tools: first, the abovementioned model had the minimum residual deviance (1032.5) among all models tried (e.g. when removing components such as the day of the week or holiday effect); second, there was no obvious trend in the residual plot and no lag was significantly large (exceeding the range of lower or upper limits) in the Autocorrelation Function (ACF) or Partial Autocorrelation Function (PACF). Therefore, all patterns (autocorrelation and trends) were captured effectively. The corresponding GLM models were also fit for the separate analyses for Nicosia and Limassol. The models similarly had a good fit, where the minimum residual deviance was found (1108.5 and 1162.3 for Nicosia and Limassol respectively) and the model residuals similarly showed that all patterns were captured, with satisfactory residual plots, ACF and PACF plots. The significance of the components was similar, although relative humidity was not found to be a significant confounder for the urban area of Nicosia.

Table 2 shows the relative risk increment per degree of heat sustained per day (effect of lags in the same strata interval is equal), for Cyprus as a total area as well as for Nicosia and Limassol considered separately.

| Lags | Relative risk: % per $^0$C above threshold-per lag (95% CI): Cyprus (threshold=33.7$^0$C) | Relative risk: % per $^0$C above threshold-per lag (95% CI): Nicosia (threshold=32.5$^0$C) | Relative risk: % per $^0$C above threshold-per lag (95% CI): Limassol (threshold=38$^0$C) |
|---|---|---|---|
| 0-1 | 4.24 (2.03 to 5.81) | 1.47 (0.41 to 2.54) | 21.18 (6.18 to 38.30) |
| 2-5 | 0.50 (-0.39 to 1.41) | 0.49 (-0.09 to 1.08) | 15.47 (5.79 to 26.03) |
| 6-10 | 0.41 (-0.29 to 1.11) | 0.30 (-0.15 to 0.76) | -7.79 (-17.04 to 2.48) |
| **0-10** | **13.17 (8.50 to 18.05)** | **6.59 (3.49 to 9.79)** | **73.99 (-6.54, 223.91)** |

**Table 2.** Results for relative risk (increase in mortality) from the Lag-stratified distributed lag linear threshold model - Cyprus, Nicosia, Limassol (2004-2009)

The results in Table 2 show that the effect of heat in Cyprus is much more pronounced for lags 0-1 (4.2% in each of lags 0 and 1, compared to 0.5% in

each of higher lags, more than 8 times higher). In other words, during the same and next day of a heat event, a 1 degree increase in maximum temperature above the threshold of $33.7^0$C is associated with an estimated increase of around 8.5% in all-cause mortality in Cyprus. Table 2 also provides the estimated overall effect of temperature over all 10 lags, which is the total effect from the lag-specific contributions, computed by summing the log relative risks of each lag and it is largely insensitive to constraints (Armstrong[3]; Gasparrini et al.[17]). Looking at the results for Cyprus, the total risk over the 10 lags is around 13% higher for every degree above $33.7^0$C.
Figure 2 presents the overall effect of temperature on all-cause mortality in Cyprus, over lags 0-10.

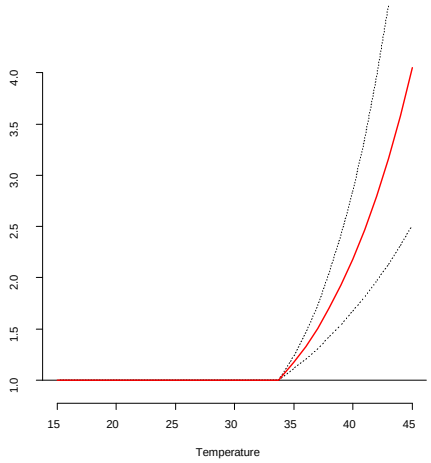


**Fig. 2.** Overall effect (relative risk) over all 10 lags: Cyprus (2004-2009).

As figure 2 indicates, the effect has zero slope up to the threshold temperature and increases after the threshold, with a significant increase in mortality risk at very high temperatures: at temperatures around $40^0$C the risk of dying is around 3 times higher compared to temperatures close to the threshold.
Figure 3 shows a three-dimensional graph of the exposure-response relationship along temperature and lags, with reference at $33.7^0$C, the threshold temperature and provides a general picture of the results. Slices of the 3D plot, for specific temperatures ($35^0$C, $37^0$C, $40^0$C and $42^0$C), appear in the bottom part of the figure.

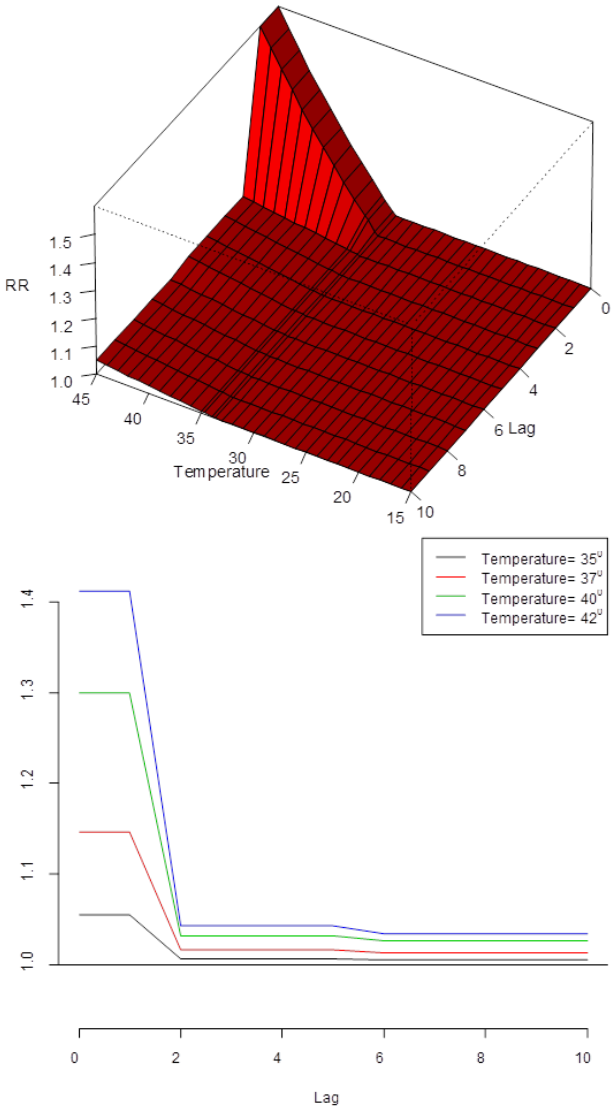


**Fig. 3**. 3-D plot of relative risk along temperature and lags (upper) and slices of the 3-D plot (lag-specific effects) for various temperatures (bottom): Cyprus

Figure 3 shows that heat (i.e. temperatures above the threshold of $33.7^0$C) has a much stronger effect at lags 0 and 1, compared to lags 2-5 and 6-10, and the effect is much stronger at higher temperatures. For example, it is 40% higher at $42^0$C compared to $35^0$C, where at the temperature of $35^0$C the risk is negligible at lags higher than 2. In addition, the effect at lower temperatures (e.g., $35^0$C

and $37^0$C) has a smoother shape, compared to the sudden drop for temperatures above $40^0$C, as we move further away from the event (e.g., a week away).
Focusing on the results obtained from the separate analysis of the data from Nicosia (urban area), showed that, similar to the results for Cyprus, the effect of heat is much more pronounced for lags 0-1, however, the effect in Nicosia is much lower compared to considering Cyprus as a total area (Table 2). A comparison of the 3D plot of Nicosia (not shown) with the plot for Cyprus, showed that the change in effect from lags 0-1 to lags 2-5 is much smoother in Nicosia compared to Cyprus, with the effects in the two strata being very close. In addition, the effect on mortality is stronger at higher temperatures (e.g. $40^0$C and $42^0$C), around 10% higher compared to temperatures around $35^0$C, where the increase in mortality is actually close to zero compared to the threshold temperature of $32.5^0$C and it has an overall smoother shape, with a smaller decrease from lags 0-1 to higher lags. The results regarding Limassol (coastal area) shown in Table 2 similarly show that significant effects occurred within 0-1 lags, which are much higher compared to the total area of Cyprus and the urban area of Nicosia for lags 0-1 and also quite high for lags 2-5 as well. The accumulated effect for Limassol is as high as 74%, but it is associated with a wide confidence interval that ranges from a negative effect to a highly positive effect, reflecting high variability/overdispersion within lags. The most noticeable result is that the relative risk for Limassol for lags 6-10 is highly negative, indicating a deficit of deaths in lags 6-10.

## 5 Discussion

The current study is the first to examine and quantify the effect of high temperatures on all-cause mortality in a Mediterranean island, Cyprus, using a methodology that captures simultaneously any non-linearities and lag effects, based on the general framework of distributed lag non-linear models, while also adjusting for the effect of potential confounders.
The results showed that high temperatures have a significantly adverse effect on public health in Cyprus, irrespective of living in the inner part of the island or the coastal area. In addition, temperature had an effect on all-cause mortality, independent of the effect of relative humidity or seasonal factors, like day of the year (e.g. middle of July or August) or shorter-term effects, like the day of the week (e.g., after a prolonged exposure to the sun during the weekend). An immediate or direct health effect of heat was found, with higher risk within the current and next day of a severe heat event, as opposed to a lower effect in longer lags, as we move further from the event, where the risk drops significantly after two days. The delayed effect of heat could also be seen vice versa: a death due to high temperatures is not due only to the thermal stress of the same day, but also of the previous couple of days. The results of a pronounced direct effect of heat (lags 0-1) on all-cause mortality agree with previous studies that have shown that the heat effect is immediate (Armstrong[3]; Braga et al.[8]; Guo et al.[19]; Pattenden et al.[31]).

In addition to the immediate effect of heat, the results showed that the effect on public health is much more pronounced for higher temperatures, as opposed to temperatures close to the threshold, where the effect is smoother, with a sharp drop from lag 1 to lag 2.

Focusing on the two areas, Nicosia and Limassol, provided similar results of an immediate short-term effect within the first two days, which is reduced in longer lags and for lower temperatures. However, the threshold temperatures corresponding to the lowest observed mortality varied. This variation by latitude and topographical features appeared in other studies (e.g., Baccini et al.[5]) and could reflect population differences in acclimatization or adaptation to high temperatures between coastal and inner-country areas. The meteorological indicator relative humidity should also be considered, since it appeared to play a significant role in the effect of high temperatures on mortality: the mean levels of relative humidity were, as expected, higher in coastal areas, compared to Nicosia, while it was not a significant confounder in the temperature-mortality relation for Nicosia, as opposed to Limassol (and Cyprus as a total area).

In addition, differences in the level of the temperature effect between areas were observed in the study: the effect observed for Nicosia was less pronounced, much smaller and smoother, almost negligible at lags 2-10, indicating a lower risk of mortality in this urban area. The model for the coastal area of Limassol showed a deficit in deaths at longer lags (6-10), with negative relative risk. This reduction in mortality, one week or so after the event, suggests that the heat wave affected especially frail individuals whose health was already so compromised that would have died in the short term anyway (e.g., 2 or 3 weeks later) and whose events were only accelerated by a brief period of time by the effect of exposure. This so called "harvesting effect" or "mortality displacement", has been observed in previous studies, where following heat waves there is a decrease in overall mortality in subsequent weeks, thus representing a short-term forward shift in mortality (Armstrong[3]; Guo et al.[19]; Braga et al.[8]; Hajat et al.[20]; Kinney et al.[26]).

Although the effect of heat appeared to be strong during the first two days and disappeared gradually after this, the choice of including up to 10 lags in our model has led to capturing this harvesting phenomenon for Limassol. In fact, studies of the effect of high temperatures using short lags (up to 2 or 3 lags only) may overestimate the hot effect, as the harvesting effect could only be captured by using longer lags (Anderson and Bell[2]; Guo et al.[19]). To explore better the number of lags for the model, and ensure that any shorter or longer-term effects were captured, sensitivity analysis was additionally performed for the number of total lags, up to 27 lags. The results were very similar to the results for 10 lags, therefore no need for a change in the models was deemed necessary.

## 6 Conclusion

The present study has examined the relationship between temperature and mortality in Cyprus, proposing a new statistical model. The proposed framework provides many advantages, compared to other alternatives for such time series data. For example, it describes simultaneously the two main features of these data, namely non-linearities and delayed dependencies, as opposed to separate models for capturing each of these characteristics: it is flexible and systematizes the linear thresholds models or any other curvilinear distributed lag model previously proposed (Armstrong[3]; Gasparrini and Armstrong[16]; Braga et al.[8]; Curriero et al.[9]; Welty and Zeger[40]).
The adverse health effects of heat waves are largely preventable, especially if appropriate measures are implemented, which include, among others, the setting up of early warning systems (Hayhoe et al.[25]; WHO[41]). As a result, a number of cities across Europe have already begun to develop and implement hot-weather response plans (Rainham & Smoyer-Tomic[34]). The results of the current study can thus be used for the development of early Heat-Health warning systems for the population in Cyprus, targeting climatic variables. Overall the heat effect appears to increase the risk of mortality and requires special attention. The corresponding Governmental departments must shift their focus from surveillance and response to prediction and prevention, to link accurate forecasts of extreme events with effective public health measures and interventions, taking at the same time into consideration the special characteristics of urban and coastal areas.

## Acknowledgments

The Project CYPHEW (ΥΓΕΙΑ/ΔΥΓΕΙΑ/0609(ΒΙΕ)/20) is co-financed by the European Regional Development Fund and the Republic of Cyprus through the Research Promotion Foundation.

## References

1. S. P. Almeida, E. Casimiro and J. Calheiros. Effects of apparent temperature on daily mortality in Lisbon and Oporto, Portugal, Environmental Health, 9, 1-7, 2010.
2. B.G. Anderson and M.L. Bell. Weather-Related Mortality: How Heat, Cold, and Heat Waves Affect Mortality in the United States, Epidemiology, 20, 205-213, 2009.
3. B. Armstrong. Models for the relationship between ambient temperature and daily mortality, Epidemiology, 17, 624-631, 2006.
4. B.G. Armstrong, Z. Chalabi, B. Fenn, S. Hajat, S. Kovats, A. Milojevic and P. Wilkinson. Association of mortality with high temperatures in a temperate climate: England and Wales, J. Epidemiol. Commun. H., 65, 340-345, 2011.
5. M. Baccini, A. Biggeri, G. Accetta, T. Kosatsky, K. Katsouyanni, A. Analitis, H.R. Anderson, L. Bisanti, D. D'Ippoliti, J. Danova, B. Forsberg, S. Medina, A. Paldy, D. Rabczenko, C. Schindler and P. Michelozzi. Heat effects on mortality in 15 European cities, Epidemiology, 19, 711-719, 2008.

6. A.G. Barnett, A.C.A. Tong and S. Clements. What measure of temperature is the best predictor of mortality?, Environmental Research, 110, 604–611, 2010.
7. A. Biggeri and M. Baccini. Modelling Short-Term Effects of Meteorological Variables on Mortality, http://www.sis-statistica.it/files/pdf/atti/CIMe0905p121-130.pdf, 2012.
8. A.L. Braga, A. Zanobetti and J. Schwartz. The time course of weather-related deaths, Epidemiology, 12, 662–667, 2001.
9. F.C. Curriero, K.S. Heiner, J.M Samet,, S.L. Zeger, L. Strug and J.A. Patz. Temperature and mortality in 11 cities of the Eastern United States, Am. J. Epidemiol., 155, 80-87, 2002.
10. F. Dominici. Time-series analysis of air pollution and mortality: a statistical review. Res Rep Health Eff Inst., 123, 3–27; discussion 29–33, 2004.
11. F. Dominici, M. Daniels, S. L. Zeger and J.M. Samet. Air pollution and mortality: estimating regional and national dose–response relationships, Journal of the American Statistical Association, 97, 100-111, 2002.
12. F. Dominici, L. Sheppard and M. Clyde. Health Effects of Air Pollution: A Statistical Review, International Statistical Review, 71, 243–276, 2003.
13. B. S. Everitt and T. A. Hothorn. Handbook of Statistical Analyses Using R, 2nd Edition, Boca Raton, FL.: Chapman & Hall, 2009.
14. L. Filleu, L. Cassadou, S. Médina, P. Fabres, A. Lefranc, D. Eilstein, A. Le Tertre, L. Pascal, B. Chardon, M. Blanchard, C. Declercq, J-F. Jusot, H. Prouvost and M. Ledrans. The Relation Between Temperature, Ozone, and Mortality in Nine French Cities During the Heat Wave of 2003, Environmental Health Perspectives, 114, 1344–1347, 2006.
15. R. Garcia-Herrera, J. Diaz, R.M. Trigo, and E. Hernandez. Extreme summer temperatures in Iberia: health impacts and associated synoptic conditions, Ann. Geophys. 23, 239–251, 2005.
16. A. Gasparrini and B. Armstrong. Distributed lag non-linear models in R: the package dlnm, dlnm version 1.6.3, 2012 ftp://ftp.cn.debian.org/CRAN/web/packages/dlnm/vignettes/dlnmOverview.pdf
17. A. Gasparrini, B. Armstrong and M.G. Kenward. Distributed lag non-linear models, Statistics in Medicine, 29, 2224–2234, 2010.
18. S.N. Gosling, J.A. Lowe, G.R. McGregor, M. Pelling and B.D. Malamud. Associations between elevated atmospheric temperature and human mortality: a critical review of the literature, Climatic Change, 92, 299–341, 2009.
19. Y. Guo, A.G. Barnett, X. Pan, W. Yu and S. Tong. The Impact of Temperature on Mortality in Tianjin, China: A Case-Crossover Design with a Distributed Lag Nonlinear Model, Environmental Health Perspectives, 119, 1719–1725, 2011.
20. S. Hajat, B.G. Armstrong, N. Gouveia and P. Wilkinson. Mortality Displacement of Heat-Related Deaths: A Comparison of Delhi, Sao Paulo, and London, Epidemiology, 16, 613-620, 2005.
21. S. Hajat and T. Kosatky. Heat-related mortality: a review and exploration of heterogeneity, J. Epidemiol. Commun. H., 64, 753-760, 2010.
22. S. Hajat, R.S. Kovats, R.W. Atkinson and A. Haines. Impact of hot temperatures on death in London: a time series approach, Journal of Epidemiology and Community Health, 56, 367-372, 2002.
23. S. Hajat, R.S. Kovats and K. Lachowycz, Heat-related and cold-related deaths in England and Wales: who is at risk?, Occupational and Environmental Medicine, 64, 93-100, 2007 .
24. S. Hajat, S. Vardoulakis, C. Heaviside and B. Eggen, B. Climate change effects on human health: projections of temperature-related mortality for the UK during the

2020s, 2050s, and 2080s, Journal of Epidemiology and Community Health, 68, 641-648, 2014.
25. K. Hayhoe, S. Sheridan, L. Kalkstein and S. Greene. Climate change, heat waves, and mortality projections for Chicago, Journal of Great Lakes Research, 36, 65–73, 2010.
26. P.L. Kinney, M.S. O'Neill, M.L. Bell and J. Schwartz. Approaches for estimating effects of climate change on heat-related deaths: challenges and opportunities, Environ. Sci. Policy, 11, 87–96, 2008.
27. R.S. Kovats and S. Hajat. Heat Stress and Public Health: A Critical Review, Ann. Review of Public Health, 29, 41-55, 2008.
28. P. McCullagh and J.A. Nelder. Generalized Linear Models, 2nd Edition, Boca Raton, FL.: Chapman & Hall/CRC Interdisciplinary Statistics Series, 1989.
29. P. Michelozzi, F.K. De' Donato, A.M. Bargagli, D. D'Ippoliti, M. De Sario, C. Marino, P. Schifano, G. Cappai, M. Leone, U. Kirchmayer, M. Ventura, M. Di Gennaro, M. Leonardi, F. Oleari, A. De Martino and C.A. Perucci. Surveillance of Summer Mortality and Preparedness to Reduce the Health Impact of Heat Waves in Italy, Int. J. Environ. Res. Publ. Health, 7, 2256-2273, 2010.
30. P. Michelozzi, U. Kirchmayer, K. Katsouyanni, A. Biggeri, G. McGregor, B. Menne, P. Kassomenos, H.R. Anderson, M. Baccini, G. Accetta, A. Analytis and T. Kosatsky. Assessment and prevention of acute health effects of weather conditions in Europe, the PHEWE project: background, objectives, design, Environmental Health, 6, 1-10, 2007.
31. S. Pattenden, B. Nikiforov and B.G. Armstrong. Mortality and temperature in Sofia and London, Journal of Epidemiology and Community Health, 57, 628-633, 2003.
32. R.D. Peng, F. Dominici and T.A. Louis. Model choice in time series studies of air pollution and mortality, Journal of the Royal Statistical Society: Series A (Statistics in Society), 169, 179–203, 2006.
33. C. Price, S. Michaelides, S. Pashiardis and P. Alpert. Long term changes in diurnal temperature range in Cyprus, Atmos. Res., 51, 85-98, 1999.
34. D.G.C. Rainham and K.E. Smoyer-Tomic. The role of air pollution in the relationship between a heat stress index and human mortality in Toronto, Environmental Research, 93, 9-19, 2003.
35. J. Rocklöv and B. Forsberg. The Effect of High Ambient Temperature on the Elderly Population in Three Regions of Sweden, International Journal of Environmental Research and Public Health, 7, 2607-2619, 2010.
36. J. Schwartz. The Distributed Lag between Air Pollution and Daily Deaths, Epidemiology, 11, 320-326, 2000.
37. J. Schwartz, C. Spix, G. Touloumi, L. Bachárová, T. Barumamdzadeh, A. Le Tertre, T. Piekarksi, A.P. De Leon, A. Pönkä, G. Rossi, M. Saez and J.P. Schouten. Methodological issues in studies of air pollution and daily counts of deaths or hospital admissions, Journal of Epidemiology and Community Health, 50, S3–11, 1996.
38. C. Symeou. Impacts of climate change on human health in Cyprus, 2009. http://cyprus-institute.us/2009/Symeou_Christina_Global_Climate_Change_project.pdf.
39. G. Touloumi, R. Atkinson, A. Le Tertre, E. Samoli, J. Schwartz, C. Schindler, J.M. Vonk, G. Rossi, M. Saez, D. Rabszenko and K. Katsouyanni. Analysis of health outcome time series data in epidemiological studies, Environmetrics, 15, 101–117, 2004.
40. L.J. Welty and S.L. Zeger. Are the acute effects of particulate matter on mortality in the national morbidity, mortality, and air pollution study the result of inadequate

control for weather and season? A sensitivity analysis using flexible Distributed Lag Model, American Journal of Epidemiology, 162, 80-88, 2005.
41. World Health Organization (WHO). Improving public health responses to extreme weather/heat-waves – EuroHEAT. Technical summary, 2009. http://ccsl.iccip.net/e92474.pdf.
42. A. Zanobetti and J. Schwartz. Temperature and mortality in nine US cities, Epidemiology, 19, 563-570, 2008.
43. A. Zanobetti, M.P. Wand, J. Schwartz and L.M. Ryan. Generalized additive distributed lag models: quantifying mortality displacement, Biostatistics, 1, 279-292, 2000.
44. S.L Zeger. A regression model for time series of counts, Biometrika, 75, 621-629, 1988.

# Statistical Modelling on the antibiotic synthesis process

Carla Noronha[1], Teresa Oliveira[2], and Ruy Costa[3]

[1] Universidade Aberta, Rua da Escola Politécnica, 141-147, 1269-001 Lisboa, Portugal
(E-mail: carla.noronha6@gmail.com)
[2] Universidade Aberta and CEAUL- Center of Statistics and Applications – Faculdade de Ciências de Lisboa, Bloco C6 - Piso 4 Campo Grande 1749-016 Lisboa, Portugal
(E-mail: teresa.oliveira@uab.pt)
[3] Mathematics Dept, Faculdade de Ciências e Tecnologia - Universidade Nova de Lisboa, 2829-516 Caparica, Portugal
(E-mail: ryac@fct.unl.pt)

**Abstract.** The aim of this work is the development of a simulation model capable to allow the comparison of different utilization policies for the rhodium catalyser, used in a complex process of industrial synthesis of an antibiotic – Minocycline. This study was carried out using statistical analysis and statistical modelling. The investigation focused on trying to understand the process, reaching to a possible model, in order to obtain higher yields with lower costs. Kolmogorov-Smirnov and Chi-Square tests were used to make comparisons related to the performance of the catalyzer. Probability distribution fitting and goodness of fit tests were also conducted to the samples of the yields. The purpose was generating pseudorandom numbers in order to help on the conceiving of the simulation model to optimize the synthesis process.

**Keywords:** Minocycline, rhodium, catalyzer, non-parametric tests, statistical analysis, statistical modelling

## 1 Introduction

Minocycline is indicated for the treatment of infections caused by microorganisms sensitive to tetracyclines, as well as infections caused by certain strains of staphylococci resistant to tetracyclines. It is particularly indicated for the treatment of acne and rosacea. The Portuguese pharmaceutical company - Cipan, who kindly provided us the data set, is the world's largest producer of this antibiotic. The synthesis of minocycline is a process that involves multiple steps which are carried out sequentially in this company. The 2$^{nd}$ step of the synthesis process involves a key piece - a metallic catalyzer in activated carbon that since the year when the process was initially developed until now has

*Stochastic Modeling, Data Analysis and Statistical Applications* (*pp*. 273-281)
Lidia Filus - Teresa Oliveira - Christos H Skiadas (Eds)



revealed some inconsistent behavior: the process of synthesis varies greatly in its levels of income. For environmental reasons, in 2009 a change occurred in the solvent used in the process, which may have contributed to this variability.
Minocycline synthesis is a 7 steps process. Our investigation was focused in the 2nd step which includes the intervention of a very expensive rhodium catalyzer. The 2nd step starts with demethylchlorotetracycline (DMC) and ends up with demethyldeoxytetracycline (DOTB) production.
When, after performing its action in the 2nd step, the catalyzer is reusable, we say that it's going to perform another **utilization**. If, on the contrary, it is inactivated with water, both parts A and B are joined and it is reactivated with sulfuric acid. In this case, we say that it has started a new **life**. When the catalyzer is exhausted, it is permanently inactivated and it awaits transportation to England, where the recovery of the metal is made in a specialized company, and this implies very high costs. Our goal was to draw conclusions about the rhodium catalyzer performance, comparing the lives and utilizations yields and also comparing both parts A and B regarding the number of lives and utilizations, as well as the catalyzer behavior over the course of lives and utilizations.

## 2 Material and Methods

Our work was concentrated on the study of the lives and of the utilizations of rhodium metal piece that, after being prepared is divided into two parts to optimize the metal resource. The observed sample consists of 78 yields catalyzers, each having two parts, A and B and a comparison of the number of lives and of the utilizations of different catalyzers was carried out. This sample has been collected from 2007 to 2012 in the pharmaceutical company. The minocycline synthesis process was implemented in 1992, however, the computational data were collected only after 2007. Furthermore, only in 2009 occurred the solvent change, which is why there was no apparent reason to collect the yields data before that. During our study, we tried to answer the following research questions:

1 – Do the catalyzers perform the same number of lives and utilizations?

2 – Did the solvent change cause variations on the 2nd step yields?

3 – Does DOT production differs significantly between the two halves of the rhodium catalyzer?

4 - Does DOT production experience major changes over the course of the lives and utilizations?

We used a sample of 78 catalyzers, parts A and B, collected between 2007 and 2012 in the pharmaceutical company and a 2013 sample was used to validate the computational model that was developed. To determine whether the catalyzers performed the same number of lives and utilizations and also to determine if the 2nd stage of minocycline synthesis process yield suffered oscillations, comparative charts were plotted. Kolmogorov-Smirnov tests and Chi-Square independence tests were conducted to test the hypothesis of parts A and B of the catalyzers being identical (Oliveira, 2004).
From Cipan data files, it was possible to calculate the yield of the 2nd step of the synthesis of minocycline by the ratio between kg DOT.T obtained and the kg raw material used (DMC). These yields were organized by lives and utilizations and their theoretical distribution was determined. For the development of a simulation model, most of the time pseudorandom numbers (PRN) are necessary (Costa, 2002, Anu, 1995). To proceed with its generation concerning minocycline 2$^{nd}$ step, it was necessary to fit a theoretical distribution (or empirical) to each of the samples (Huber, 1999). This procedure extended from life 1 to 3 and from first utilization to the third. These were the samples with significant dimension. After fitting distributions to data, goodness of fit tests were performed to validate the fitting process (Oliveira, 2004, Böhm, 2010).

## 3 Graphical Results – Main findings

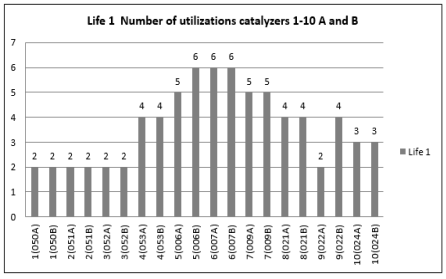


Fig. 1 - Number of utilizations life 1 of the sample's first 10 catalyzers

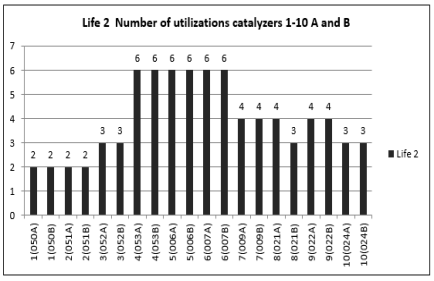


Fig. 2 - Yield and number of utilizations life 1 of the sample's first 8 catalyzers

Figures 1 and 2 represent some of the charts that were drawn to point out the oscillations presented by the number of lives and utilizations. Thus, it is possible to realize that some of the catalyzers performed only 2 utilizations, while others reached 6 utilizations. In the course of the remaining lives, this situation repeats itself, clearly answering our first research question.

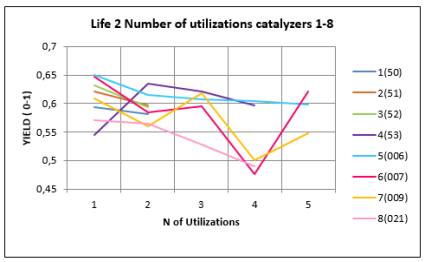


Fig. 3 – Yield in the course of life 1 catalyzers 1 to 8

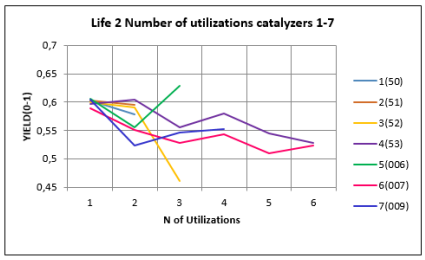


Fig. 4 - Yield in the course of life 2 catalyzers 1 to 7

In figures 3 and 4 we can realize a decreasing tendency in the yields obtained over the course of lives and utilizations. In these charts we can easily compare the yields behavior in the course of lives and utilizations.

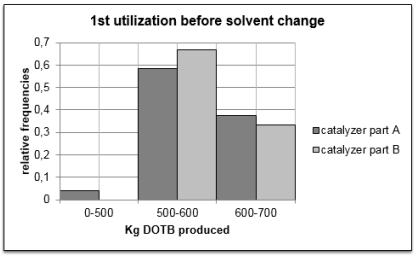


Fig. 5 - Kg of DOTB produced before the solvent change

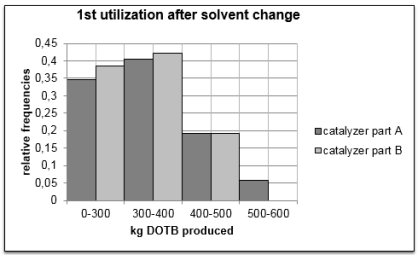


Fig. 6 - Kg of DOTB produced after the solvent change

Trying to determine whether the introduction of the new solvent in 2009 caused significant differences in the performance of the rhodium catalyzers, we set out comparative charts of the yields. As you can see in figures 5 and 6, the differences between both are evident. Before 2009, some of the yields reached 600-700 kgs of DOTB produced, while after that, the production reduced substantially. So, changing from Me-Oxitol to methanol due to environmental reasons caused major decreasing to DOT.T yield.

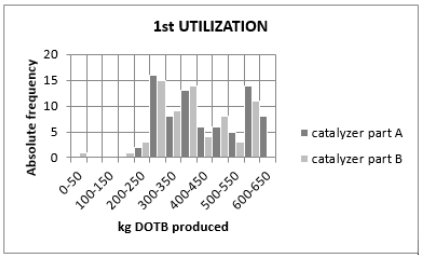


Fig.7 - Kg of DOTB 1st utilization, parts A and B

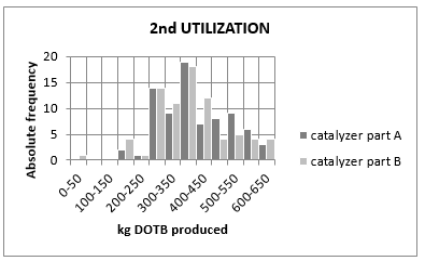


Fig.8 - Kg of DOTB 2nd utilization, parts A and B

Comparing both charts in figures 7 and 8, there seems to be insignificant the differences in the performance of parts A and B of catalyzer. We decided to carry out Kolmogorov Smirnov tests to check this possibility. If this possibility was confirmed, the study could be conducted considering that instead of 78 catalyzers, parts A and B, we could consider a sample of 78 x 2 catalyzers.

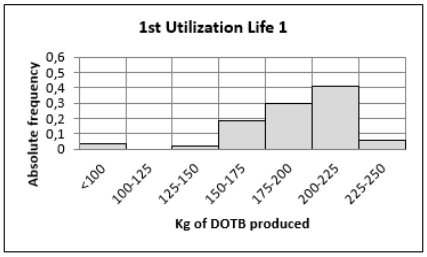


Fig. 9- Kg of DOT.B Life 1 - 1st utilization

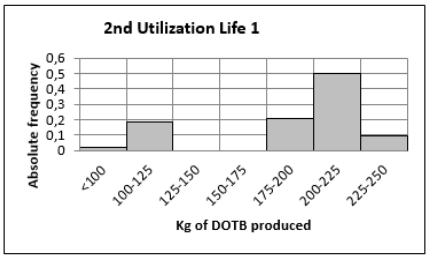


Fig.10 – Kg of DOT.B Life 1– 2nd utilization

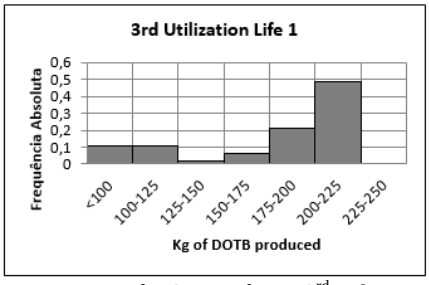


Fig.11 - Kg of DOTB Life 1 – 3rd utilization

Figures 9 to 11 show that there are evidences of discrepancies in the amount of DOT.B produced in the course of lives. The frequency is greatly reduced in classes with smaller amounts of produced DOT.B reaching the highest frequency (about 40%) in the 200-225 kg class, which represents the highest yields. This distribution is consistent with the expected scenario: higher yields in the 1st life were expected.

## 4 Statistical Tests

Kolmogorov-Smirnov tests were performed to investigate whether the samples A and B were collected from identical populations. This process has been carried out for the study of lives. To investigate if the same happened with the utilizations, we decided to use Chi-Square for independent samples (David, 1958).

We also used K-S tests to investigate if was there any difference in the yields of the 2nd step over the course of lives and utilizations. To perform K-S Test, we began by the clustering the amount of DOT.T produced in classes of 50 kg range and calculating its respective frequency. For each of the three lives of the following hypotheses were formulated:

$H_0$: Samples are withdrawn from two identical continuous populations
$H_1$: Samples are not withdrawn from two identical continuous populations

To a significance level of 0.05 we obtained $D_\alpha = 1.36\sqrt{\frac{n_A+n_B}{n_A \cdot n_B}} = 0.26$ and in table 1 the different D values for each life is presented:

| **Life** | D |
|---|---|
| 1 | 0.1667 |
| 2 | 0.0741 |
| 3 | 0.0741 |

Table 1- D levels K-S Test (lives)

Thus, there is no statistical evidence to the 5% significance level that allows to reject the null hypothesis: samples A and B are withdrawn from two identical continuous populations.
Chi-Square Test was applied to the catalyzer parts A and B used in DOT.T productivity, also considering grouping data in equal range classes. However, some of the conditions for the use of this test were not fulfilled: there were classes with frequency equal zero and also classes with expected frequencies less than 5. We overcame these irregularities proceeding to the fusion of adjacent classes.

For each utilization($1^{st}$ and $2^{nd}$) of the sample catalyzers we formulated the following hypotheses:

$H_0$: part A and part B of the catalyzer are identical
$H_1$: part A and part B of the catalyzer are not identical

The Statistical Chi Square test results are presented in table 2.

| Utilization | $\chi^2$ (0.05) | $\chi^2$ (calculated) |
|---|---|---|
| $1^{st}$ | 9.488 | 7.024 |
| $2^{nd}$ | 9.488 | 6.764 |

Table 2 - Chi Square values 1st and 2nd utilizations

For the $3^{rd}$ utilization, the DOT.T productivity was very low, making it difficult to set up classes to screen the necessary conditions for the application of the Chi

Square Test. Thus, we chose to perform Kolmogorov-Smirnov test for two independent samples. The following hypotheses were formulated:

$H_0$: The samples are withdrawn from two identical continuous populations
$H_1$: Samples are not withdrawn from two identical continuous populations

Since D observed was 0.657, which is greater than D (α) = 0.28, we rejected the null hypothesis at 0.05 significance level.

After conducting this test for lives and utilizations, it seems acceptable to consider at 0.05 significance level that the parts A and B of the sample catalyzers (after the change of solvent occurred in 2009) are identical, except for 3rd utilization.

By observation of figures 9, 10 and 11, it appears that DOT.T levels are decreasing. To test this assumption we carried out a K-S Test. The following hypotheses were formulated:

$H_{01}$: DOT.T yield (in kg) of the 1st utilization and 2nd utilization of the 1st life are identical
$H_{11}$: DOT.T yield (in kg) of the 1st utilization and 2nd utilization of the 1st life are not identical

$H_{02}$: DOT.T yield (in kg) of the 1st utilization and 3rd utilization of the 1st life are identical
$H_{12}$: DOT.T yield (in kg) of the 1st utilization and 3rd utilization of the 1st life are not identical

$H_{03}$: DOT.T yield (in kg) of the 2nd and 3rd utilization the 1st life are identical
$H_{13}$: DOT.T yield (in kg) of the 2nd and 3rd utilization the 1st life are not identical

| **Utilization** | $D_{obs}$ | $D_{\alpha}$ |
|---|---|---|
| U1-U2 | 0.1667 | 0.26 |
| U1-U3 | 0.9074 | 0.27 |
| U2-U3 | 0.1032 | 0.27 |

Table 3 – comparing D calculated and Dα between utilizations

As D(obs) between 1st and 2nd utilization and between 2nd and 3rd utilization are lower than Dα at a significance level of 5%, it is acceptable to consider that, 1st and 2nd utilization as well as the 2nd and the 3rd utilization of the 1st life do not differ significantly. However, at that significance level, there are significant differences between the 1st and the 3rd utilization.

## 5 Fitting distributions to data

In order to develop a possible simulation model, it was necessary to generate pseudorandom numbers. With this purpose, we fit continuous distributions to the yields samples (Alves, 2010, Krishnamoorthy, 2006), starting in life one, first utilization and ending in the first utilization from life three.
These were the fitting obtained:

| Life/Utilization | Probability Distribution Parameters |
|---|---|
| Life1,1st Utilization | Weibull $\alpha$=10.067,$\beta$=0.57909 |
| Life1,2nd Utilization | Weibull $\alpha$ =16.855,$\beta$=0.60243 |
| Life1,3rd Utilization | Weibull $\alpha$ =14.92,$\beta$=0.59354 |
| Life 2, 1st Utilization | Gumbel $\sigma$=0.05145, $\mu$=0.54778 |
| Life 2, 2nd Utilization | Weibull a=15.041,$\beta$=0.57493 |
| Life 2, 3rd Utilization | Logistic $\sigma$=0.02053,$\mu$=0.5291 |
| Life 3, 1st Utilization | Weibull $\alpha$ =17.458,$\beta$=0.5441 |

Table 4 - Distribution fitting

Distribution fitting has been performed using *EasyFit*, a software tool which allows us to perform theoretical distributions adjustments to datasets.

Goodness of fit tests were also conducted to determine whether the fitting were suitable. We performed K-S Tests and Chi-Square as well. In some cases, Anderson-Darling Tests have been executed to obtain more accurate conclusions (Böhm, 2010, Justel, 1997).

## Discussion/Results

Based on the analysis and tests carried out, we conclude that the number of lives and utilizations showed differences between the catalyzers in the sample. It was also possible to observe that the parts A and B of the rhodium catalyzer were identical, that is, after the cut performed, the amount of metal contained in both halves was approximately equivalent. The change of solvent due to environmental reasons led to an evident decrease in DOTB production. It has been also possible to realize that the production levels declined over the course of lives and utilizations. Continuous distributions fitting have been performed which enable the generation of pseudorandom numbers, allowing to design a simulation model regarding the comparison of different policies for the use of the rhodium catalyzer. Our investigation allowed to clarify the initial research questions.

## Conclusion

We studied a pharmaceutical company problem connected with the antibiotic synthesis process which led to large financial losses for the company. Our main

goal was to develop a simulation model that allowed to compare different utilization policies for a very expensive process component - the rhodium catalyzer, in order to optimize it. Pseudorandom number generation and goodness of fit tests were performed allowing to develop a useful simulation model for the pharmaceutical (Jain, 2008). Statistical analysis and statistical modelling were the major tools used to carry out this study. The resultant model proved to be a very useful tool, which can be improved in the future by inserting more process variables, besides the yields.

## Acknowledgments

This research was partially sponsored by national funds through the Fundação Nacional para a Ciência e Tecnologia, Portugal - FCT under the project PEst-OE/MAT/UI0006/2014.
The authors are grateful to Cipan for their valuable collaboration collecting all the necessary information to perform this research improving the paper to a great extent.

## References

1. Alves,Isabel Fraga; Neves, Cláudia (2010). Extreme Value Distributions. Lisboa: University of Lisbon, Faculty of Sciences, DEIO, CEAUL.
2. Anu, Maria (1997).Introduction to modeling and simulation. Proceedings of the 1997 Winter Simulation Conference
3. Böhm, Walter; Hornik, Kurt (2010). A Kolmogorov-Smirnov Test for r Samples. Research Report Series / Department of Statistics and Mathematics, 105. Vienna: University of Economics and Business.
4. Costa, Ruy Araújo (2002). Investigação Operacional. Lisboa: Edições Universidade Aberta.
5. David, Herbert (1958). A three sample Kolmogorov-Smirnov Test. The Annals of Mathematical Statistics, JSTOR. 842-851.
6. Krishnamoorthy, K. (2006). Handbook of Statistical Distributions with Applications. Chapman & Hall, Taylor and Francis Group.
7. Huber, Bill (1999).Fitting Distributions to Data: Practical Issues in the Use of Probabilistic Risk Assessment. Sarasota, Florida.
8. Jain, Raj (2008).Analysis of Simulation Results. Washington, Universidade de S. Louis.
9. Jain, Raj (2008).Testing Random Numbers. Washington, Universidade de S. Louis
10. Justel, Ana ; Peña, Daniel; Zamar, Rubén –A Multivariate Kolmogorov-Smirnov Test of Goodness of Fit. Statistics and Probability Letters 35 (1997) p 251-259.
11. Oliveira, Teresa Paula C. (2004). Estatística Aplicada. Lisboa: Edições Universidade Aberta.

# Stochastic Response Surface Methodology – a study on polynomial chaos expansion

**Conceição Leal[1*], Teresa Oliveira[2], Amílcar Oliveira[3]**

[1] Department of Sciences and Technology, Open University, Portugal
Email: conceicao.leal2010@gmail.com
[2] Department of Sciences and Technology, Open University; *CEAUL* Portugal
Email: Teresa.Oliveira@uab.pt
[3] Department of Sciences and Technology, Open University; *CEAUL* Portugal
Email: amilcar.oliveira@uab.pt

**Abstract**: This paper is a review of Stochastic Response Surface Methodology in the context of Risk Analysis, as a tool for modeling uncertainty on the analysis of simulation models. Some applications are reviewed and an application in the survival analysis is implemented with R software.
**Keywords:** Uncertainty, Stochastic Response Surface Methodology, Risk Analysis, Polynomial Chaos, Breast Cancer Prognosis.

## 1 Introduction

Research on complex dynamic systems requires, in most cases, recourse to different simulation techniques in order to estimate models which allow to explore the system and their properties, and to determine the probability of occurrence of an event or of its consequences.
The uncertainties present in a system, and which will propagate in the model simulation, jeopardizing the validity of the information that will be collected, may be due to different causes: the lack of knowledge regarding the true value of a variable, the lack of knowledge about the model that best describes the system or on which the probability distribution function that best represents an amount of interest (Frey et al, 2004). The lack of information about the properties of the system makes the modeling of uncertainties assume such importance that its quantification can become the dominant issue in the tasks modeling, simulation and applications.
The quantification of uncertainty in simulation model can be addressed in two perspectives: one, in which it is assumed that the model and its components do not vary in time and space and, in this case, the uncertainty lies in whether and when the model can be applied to produce reasonable results or when it will fail;

*Stochastic Modeling, Data Analysis and Statistical Applications* (*pp*. 283-295)
Lidia Filus - Teresa Oliveira - Christos H Skiadas (Eds)


another, in which there are variations in time and/or space, and, in this case, the process is a stochastic process, which requires the use of stochastic approaches to quantify uncertainty. Among the several methodologies that have been developed and applied to the propagation of stochastic uncertainty analysis, and that vary with the complexity of the system and the model, the Stochastic Response Surface Methodology (SRSM), is gaining ground for allowing to reduce the high computational cost associated with the numerical simulation of the full models. SRSM is based on the combination of response surface methods with sampling Monte Carlo simulation or Latin Hypercubes.

The simulation of environmental and biological dynamic systems, such as the transport of fluids and gases and their impact on human health, the underground storage of gases like $CO_2$ and their environmental impact, or structural systems and analysis of associated risk, are areas with different applications of the methodology, namely for quantifying the associated uncertainty.

In this study an application of SRSM in medicine is presented. An application in the area of survival analysis is performed in order to estimate the density function of the time to recur (TTR) and the associated hazard function in breast cancer patients who have undergone surgery for excise cancer.

The Wisconsin Prognostic Breast Cancer (WPBC) database, on which the study was developed, has been used in many researches on the breast cancer diagnosis and prognosis with intelligent systems and machine learning. Stands out in this work the Recurrence Surface Approximation, machine learning technique based on linear programming, which allows to predict the expected survival free disease in patients undergoing surgery for excision of breast cancer, according to morphological characteristics of nuclei malignant cells: size, shape and texture. With this technique a hyperplane is estimated which optimizes the estimates time to recur in patients to whom the tumor was excised. Mangasarian et al. (1995), Street et al (1995), Street (1998), Wolberg et al. (1999), Mangasarian et al. (2000) discussed methodological approaches. Anagnostopoulos et al.(2006) use the database to improve the work of Street (1999) on the prediction of disease-free interval with neural networks models. Other researchers, as Veillard et al. (2013), study the same type of prognostic factors, with current data and other evaluation techniques of cell nuclei images.

## 2 Stochastic Response Surface Methodology – polynomials chaos expansion

It is common to use Polynomials Chaos to represent responses of models subject to uncertainties. A mechanical model subject to uncertainties, or a simulation model, can be seen as a function of random variables or stochastic processes, and its response is also a random variable or stochastic process.

According to Isukapalli (1999), SRSM with polynomial chaos expansion, allows to generate a reduced response model, computationally less demanding than the full numerical model and it is statistically equivalent. The estimation of the reduced model coefficients is obtained with the results of a limited number of the full model simulations.

The basic idea of the methodology is to represent the response of a model to changes in input random variables, through a response surface defined with the help of a basis of orthogonal polynomials with respect to a probability measure on the space of parameters.

The classical approach assumes that random variables whose probability density functions are square integrable, can be approximated by the expansion in stochastic series of independent random variables or by direct transformation of these variables (Balakrishnan *et. al*., 2003).

In the classic form of the methodology, a vector of $n$ independent random variables $\xi = (\xi_i), i = 1,..,n,$ is selected, under $N(0,1)$ distribution, to represent uncertain variables of a model $x = (x_i)$, in such that $x_i = h(\xi_i)$. This selection made, response variables are represented as a function of the same vector of random variables: $Y = f(c, \xi)$, with $c$ being the vector of coefficients to estimate. Estimates of the model coefficients are obtained through the response of the complete system model to various achievements of $\xi$. The coefficients $c_i$ quantify the dependence of the response vector Y on the input vector $\xi$, for each realization of $x$.

The form of the $Y$ function is the result of the expansion with P terms in polynomials chaos - polynomials $\Psi_i$ which form a base of orthogonal polynomials to a given probability measure, expressed by $Y = f(c, \xi)$, being

$$f(c,\xi) \approx c_0\Psi_0 + \sum_{i1=1}^{n} c_{i1}\Psi_1(\xi_{i1}) + \sum_{i1=1}^{n}\sum_{i2}^{i1} c_{i1i2}\Psi_2(\xi_{i1},\xi_{i2}) + \dots$$

$P = \sum_{i=0}^{p}\binom{n+i-1}{i}$ is the number of terms retained in the truncated expansion up to terms of degree $p$, in an approximation with $n$ random variables, which corresponds to the total number of expansion coefficients to estimate.

In the most common form of the methodology application it is used a basis of Hermite polynomials and the Gaussian measure (Ghanem and Spanos, 1991).

Since the proposal of Isukapalli and Georgopoulos (1998) and Isukapalli (1999), which present two case studies, other approach proposals have emerged.

Xiu and Karniadakis (2002(a,b), 2003(a,b)) proposed the generalized polynomial chaos expansion. They showed that it is possible to obtain greater precision in the response using non-Gaussian variables and replacing the Hermite polynomials by bases of orthogonal polynomials with respect to probability measure of input variables.

Ernst et. al. (2012) presented conditions on the probability measures involving the mean square convergence of the expansion in polynomials of generalized chaos.

Oladyshkin and Nowak (2012) proposed a new methodology generalization called arbitrary polynomial chaos expansion. In this new approach, the probability distributions of the variables are arbitrary, as well as the probability measures. Statistical moments are the only source of information that is propagated in the stochastic model. Probability distributions of the variables can

be discrete, continuous or continuous discretized. Its specification can be done by analytic via (by PDF or by CFD) histogram representation or by using raw data. In this approach, all distributions are admissible for the input variables of a given model, being sufficient to have a finite number of moments in common. Thus, in the case of considering a truncated polynomial, is not necessary to have the complete knowledge of the probability density function or even of its existence, it suffices to know a finite number of moments. It frees the researcher from the need to take distributions that are not always supported by existing data and gives him freedom to choose the statistical assumptions on which it moves. Oladyshkin et al. (2011) applied the methodology to a problem of underground storage of $CO_2$ and compared the results with those obtained with the conventional method.

Studies show that this expansion converges exponentially and faster than the classical expansion. Estimation of the model parameters depends on their complexity (Isukapalli and Georgopoulos, 1998). If the model is invertible, the model parameters can be obtained directly from the random input variables $(\xi_i)_{i=1}^{n}$. If, despite the nonlinearities, the equations of the model are mathematically manipulable, the model coefficients are determined by an appropriate norm minimization of residuals, after replacing the input random variables by the respective transformations in terms of Gaussian variables $N\,(0,1)$ (Galerkin method). When the model equations are difficult to manipulate or the model is a "*Black Box*" model, the coefficients can be estimated by the collocation point methods or by regression.

If the estimation is made based on collocation methods, each set of points is chosen so that the model estimates are accurate at these points, which causes a set of linear equations whose solution yields the $P$ model parameters.

Isukapalli and Georgopoulus (1998) present some parameter estimation methods, all based on the collocation points methods: Probabilistic Collocation Method, Efficient Collocation Method and regression-based method, and this authors discuss their advantages and disadvantages. In the first two cases, each coefficient of expansion is written as a multidimensional integral, which can be resolved by simulation (Monte Carlo, Latin Hypercube) or quadrature. In regression-based method, coefficients are estimated by minimizing the mean squared error response. This method is more robust than probabilistic methods. Blatman and Sudret (2010) provide detailed descriptions of these methods.

Regardless of the approach, the polynomial chaos expansion is a simple but powerful tool for stochastic modeling. Using the expansion, it is possible to estimate probability density functions (PDF), probability distribution functions (CDF), or other statistics of interest, and quickly evaluate these estimates using Monte Carlo simulation (MCS), once the evaluation of a polynomial function with MCS is faster than the original equations model evaluation, that generally are more complex.

## 3 Literature applications

Isukapalli and Georgopoulos (1998) applied the SRSM to four case studies covering a range of applications, both from the perspective of the model application (biology, air quality and groundwater) and of its complexity.
Datta and Kushwaha (2011) applied the SRSM to study the role of various hydro geologic parameters in the uncertainty assessment of the chemical contaminant concentration in groundwater. This study provides a program of environmental monitoring in the nuclear industry.
Oladyshkin et al. (2012) applied the SRSM, based on the expansion of arbitrary polynomial chaos, to a problem of contaminant transport in 3D heterogeneous aquifer and the risk to human health caused by exposure of the population.
.
Soubra and Ahmed (2012) combined subset simulation method with the SRSM to perform probabilistic analysis of a shallow strip footing.
Bastug et al. (2013) applied the SRSM in a model of gas injection into an incompressible porous media, and showed its effectiveness in uncertainty and sensitivity analysis of complex numerical models.
Sun et. al. (2013) applied the generalized SRSM to assess leakage detectability at geologic carbon storage sites under parameter uncertainty. They demonstrated how SRSM can be used to construct probability maps for assessing the detection of anomalies on the coverage of underground geological storage formations, in space and time.
Li et al. (2014) applied the SRSM to analyze the reliability of an underground cavern, associated with deterministic finite element methods. More specifically, the SRSM was used to perform the probabilistic analysis serviceability performance of the cavern.

## 4 Example of application in medicine

Stochastic Response Surface Methodology will be applied to the Wisconsin Breast Cancer Prognostic (WPBC) database, which is constituted by data of 253 patients with breast cancer who have undergone surgical excision of invasive cancer. Of these 253 cases, 69 will be used, those that correspond to patients that had remission till the end of the study.
The objective of the study is the estimation of a response surface model with Hermite polynomials in which the response variable T is the time to recur (TTR) or disease free survival (DFS) and the uncertainty parameters are three of the ten available covariates, related with morphological characteristics of the nucleus of malignant cells: AREA, TEXTURE and SMOOTHNESS (on average).
This model will be used to estimate the distribution of the response variable and the resulting survival and risk functions. The database is very well described by Mangasarian et al. (1999). In this work the database in regard to the assumptions of normality and independence of the covariates. Different models were simulated with respect to the degree of the polynomial and the number and nature of the covariates included.

Considering the sample size and that used covariates revealed small values of correlation coefficients, although the Shapiro-Wilk variable AREA reveals a significant departure from normality, we assumed this assumption (ecxluding four outliers solve this problem - p-value = 0.1992).

```
shapiro.test
AREA           p-value = 7.995e-07
TEXTURA        p-value = 0.0987
SUAVIDADE      p-value = 0.8454
```

Correlations Matrix

```
                AREAN     SMOOTHN   TEXTUREN
AREAN      1.00000000 -0.08316723 -0.1584508
SMOOTHN   -0.08316723  1.00000000 -0.1572859
TEXTUREN -0.15845076 -0.15728589  1.0000000
```

Various probability distribution models were adjusted to the response variable (R `fitdistrplus` package, `fitdist` function). The distribution with best behaviour was gamma distribution (lower values of statistics and criteria). The Weibull distribution showed very similar values for all statistics and criteria.

```
Goodness-of-fit statistics
                             1-mle-gamma
Kolmogorov-Smirnov statistic  0.09362092
Cramer-von Mises statistic    0.07370940
Anderson-Darling statistic    0.40613205
```

```
Goodness-of-fit criteria
                               1-mle-gamma
Aikake's Information Criterion    609.1817
Bayesian Information Criterion    613.6499
```

The estimation of the model coefficients in the polynomial chaos can be obtained by using experimental design data points, resulting from the combination of roots of a Hermite polynomial of degree a unit higher than the degree of expansion and located closer to zero, because are points more likely. The experiment is implemented in these points, and it is obtained the deterministic model or regression model. It turns out that in this case it is not possible to use experimental points, so the estimation of the model coefficients will be made by regression on the sample data.

To this end, data were prepared and the matrix MRTAS was built with the images of the Hermite polynomials up to the second degree, in the three variables: AREA, TEXTURE and SMOOTHNESS.

```
> PATSMO2005R<-data.frame(MCANCRO=P2005R$CODE_B,AREA=P2005R$AREA,SMOOTH=P2005R$SMOOTH
,
+ TEXTURE=P2005R$TEXTURE,Y=P2005R$TIME_A,Z=P2005R$TIME_B)
> PATSMO2005RN<- data.frame(MCANCRO=P2005R$CODE_B,AREAN=(P2005R$AREA-
mean(P2005R$AREA))/sd(P2005R$AREA),
+ SMOOTHN=(P2005R$SMOOTH-mean(P2005R$SMOOTH))/sd(P2005R$SMOOTH),
+ TEXTUREN=(P2005R$TEXTURE-
mean(P2005R$TEXTURE))/sd(P2005R$TEXTURE),Y=P2005R$TIME_A,Z=P2005R$TIME_B)
> PATSMO2005RNS<- data.frame(AREAN=(P2005R$AREA-mean(P2005R$AREA))/sd(P2005R$AREA),
+ SMOOTHN=(P2005R$SMOOTH-mean(P2005R$SMOOTH))/sd(P2005R$SMOOTH),
+ TEXTUREN=(P2005R$TEXTURE-mean(P2005R$TEXTURE))/sd(P2005R$TEXTURE))
```

The second data-frame contains the variable processed in accordance with appropriate transformation to a normal distribution: $x_i = \mu_i + \sigma_i \xi_i$.

```
> library(EQL)
> x1<-hermite(PATSMO2005RNS,1,prob=TRUE)
> x2<-hermite(PATSMO2005RNS,2,prob=TRUE)
> MR1ATS<-matrix(c(x1[,1]*x1[,2],x1[,1]*x1[,3],x1[,2]*x1[,3]),69,3)
> MRATS<-data.frame(x1,x2,MR1ATS,R= PATSMO2005RN)
```

Was adjusted a first order linear model.

```
PCE1<-lm(Y~AREAN+SMOOTHN+TEXTUREN,data= PATSMO2005RN)
Residuals:
    Min      1Q  Median      3Q     Max
-34.463 -18.451  -5.882   8.033  82.015

Coefficients:
            Estimate Std. Error t value Pr(>|t|)
(Intercept)   30.101      3.096   9.723 2.69e-14 ***
AREAN         -6.295      3.178  -1.981   0.0518 .
SMOOTHN        4.130      3.178   1.300   0.1983
TEXTUREN      -5.117      3.207  -1.596   0.1154
---
Signif. codes:  0 ‘***’ 0.001 ‘**’ 0.01 ‘*’ 0.05 ‘.’ 0.1 ‘ ’ 1

Residual standard error: 25.72 on 65 degrees of freedom
Multiple R-squared: 0.1168,     Adjusted R-squared: 0.07608
F-statistic: 2.866 on 3 and 65 DF,  p-value: 0.04326
```

In the first order model, it is observed that only intersect and variable AREA, gave a significant contribution to the model.
Adjusted the second order model it is observed that intersect and terms AREA, $AREA^2 - 1$ and $SMOOTHNESS^2 - 1$ are significant.

```
> PCERATS<-lm(R~AREAN+TEXTUREN+SMOOTHN+AREAN.1+TEXTUREN.1+SMOOTHN.1+X1+
+ X2+X3,data=MRATS)
Call:
lm(formula = R ~ AREAN + TEXTUREN + SMOOTHN + AREAN.1 + TEXTUREN.1 +
    SMOOTHN.1 + X1 + X2 + X3, data = MRATS)

Residuals:
    Min      1Q  Median      3Q     Max
-40.559 -12.888  -2.928   8.751  79.375

Coefficients:
            Estimate Std. Error t value Pr(>|t|)
(Intercept)  30.2256     3.0888   9.785 5.76e-14 ***
AREAN       -13.5806     4.4800  -3.031  0.00361 **
TEXTUREN     -4.3718     3.6611  -1.194  0.23720
SMOOTHN       2.4267     3.1655   0.767  0.44636
AREAN.1       3.9472     1.4073   2.805  0.00681 **
TEXTUREN.1   -0.9645     2.6137  -0.369  0.71342
SMOOTHN.1     4.7846     2.6628   1.797  0.07749 .
X1           -2.4691     4.2400  -0.582  0.56256
X2            2.2082     4.5419   0.486  0.62864
X3           -0.8439     3.5143  -0.240  0.81105
---
Signif. codes:  0 ‘***’ 0.001 ‘**’ 0.01 ‘*’ 0.05 ‘.’ 0.1 ‘ ’ 1

Residual standard error: 24.12 on 59 degrees of freedom
Multiple R-squared: 0.2946,     Adjusted R-squared: 0.187
F-statistic: 2.738 on 9 and 59 DF,  p-value: 0.009666
```

Fitting a Cox model, none of the three covariates has showed to be statistically significant:

```
             coef   exp(coef)   se(coef)     z Pr(>|z|)
AREA     3.297e-04  1.000e+00  2.040e-04  1.616    0.106
TEXTURE  4.557e-02  1.047e+00  3.127e-02  1.457    0.145
SMOOTH  -1.143e+01  1.088e-05  1.069e+01 -1.069    0.285
```

The assumption test to proportional hazards reveals no statistical evidence that these are not proportional to each variable or to the overall model.

```
            rho  chisq    p
AREA    -0.0443 0.0695 0.792
TEXTURE  0.0707 0.3577 0.550
SMOOTH  -0.0497 0.1355 0.713
GLOBAL       NA 0.6582 0.883
```

Using the second order model, adjusted with Hermite polynomials, it is possible to simulate the probability distribution of the response variable by Monte Carlo sampling (Fig.1).

```
> Nsim<-10^4
> t<-0
> X<-0
> for (i in 1:Nsim) {
+ u1=rnorm(1)
+ u2=rnorm(1)
+ u3=rnorm(1)
+ T<-function(a1,a2,a3) {
+ PCE<- 30.2256 -13.5806  *a1 -4.3718  *a2+ 2.4267*a3+
+ 3.9472 *(a1^2-1)-0.9645*(a2^2-1)+4.7846*(a3^2-1)-2.4691 *(a1*a2)+2.2082   *a1*a3-0.8439
*(a2*a3) }
+   t<-T(u1,u2,u3)
+   X[i]<-t  }
>    X

> X1<-X[X>0] # Eliminar os valores negativos)
> length(X1)
[1] 9866
density(X1)
>   plot(f)
```

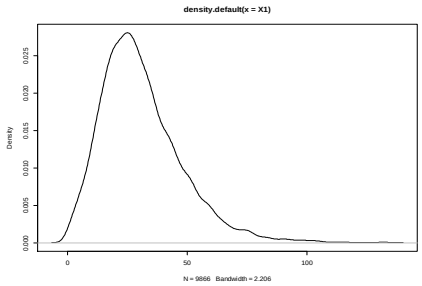


Fig. 1. Simulated density function of the Time to Recur (TTR)

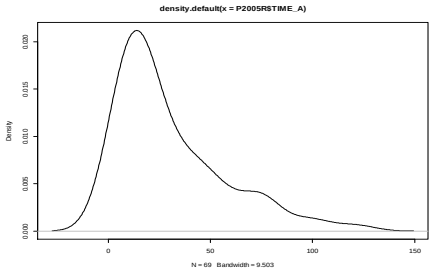


Fig. 2. Empirical density function of the Time to Recur (TTR)

```
> mean(X1)      [1] 30.7739
> sd(X1)        [1] 16.8787
> kurtosis(X1) [1] 2.282831
> skewness(X1) [1] 1.132363
```

```
> mean(P2005R$TIME_A)       [1] 30.10145
> sd(P2005R$TIME_A)         [1] 26.75496
> kurtosis(P2005R$TIME_A)   [1] 1.182963
> skewness(P2005R$TIME_A)   [1] 1.317374
```

From the moment the estimated density function of the response T (Fig.1) is obt ained, it is possible to estimate the survival function (disease-free survival time) by:

$S(t) = 1 - F(t)$= 1, where F is the distribution function of T (Fig.3).

This function can be compared with the Cox model (Fig. 4).

To estimate the hazard function, it is necessary to get the distribution that best fits the survival function. It was concluded that the Gamma function or the Weibull function provides the best fit to the PDF because they result in lower values of statistics and criteria (Fig.5).

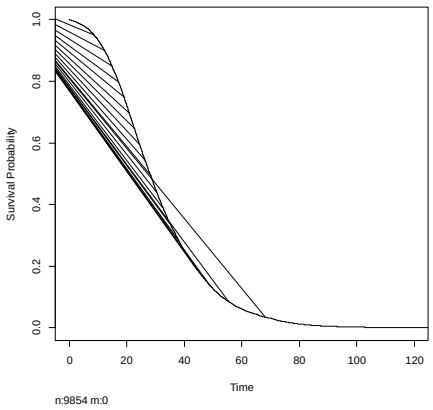


Fig. 3. Simulated survival function

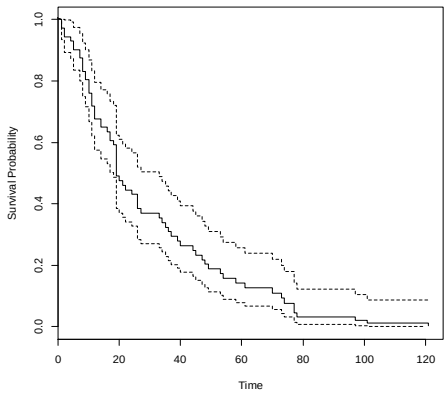


Fig. 4. Cox survival model

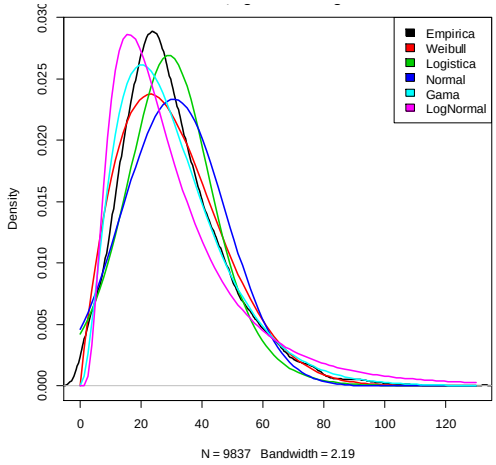


Fig. 5. Empirical density functions

| Weibull | Gama |
|---|---|
| > gofstat(fs2) | > gofstat(fs3) |
| Goodness-of-fit statistics | Goodness-of-fit statistics |
| 1-mle-weibull | 1-mle-gamma |
| Kolmogorov-Smirnov statistic 0.03318575 | Kolmogorov-Smirnov statistic 0.03932581 |
| Cramer-von Mises statistic 4.45026661 | Cramer-von Mises statistic 3.81328090 |
| Anderson-Darling statistic 27.00488424 | Anderson-Darling statistic 25.14518037 |
| Goodness-of-fit criteria | Goodness-of-fit criteria |
| 1-mle-weibull | 1-mle-gamma |
| Aikake's Information Criterion 82226.78 | Aikake's Information Criterion 82352.04 |
| Bayesian Information Criterion 82241.17 | Bayesian Information Criterion 82366.43 |

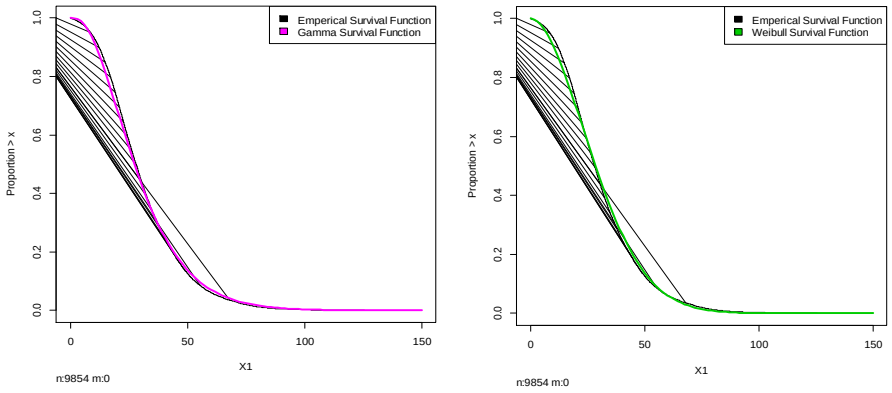


Fig. 6. Comparison of survival function adjusted with simulated data and the survival function obtained with the Weibull or Gamma PDF fitted to simulated data.

Once identified the distribution that best fits the survival function and considering that the function that describes the time until the patient experiences remission, hazard function, is defined by $H(t) = \frac{f(t)}{S(t)}$ , where $f\ (t)$ the density function of T, it is possible to estimate H and to obtain its graphical representation.

```
      > #Função Hazard com a PDF Gamma
      > {x<-runif(10000,0,220)
      + g<-function(x){
      + g<-dgamma(x,2.92905465,0.09507186)}
      + S<-function(x){
      + S<-1-pgamma(x,2.92905465,0.09507186)}
      + h<-g(x)/S(x)}
      > H<-data.frame(x,h)
      > plot(H$x,H$h, main=" Hazard Function(Gamma)",xlab="Disease
Free Survival", ylab="Risk")
```

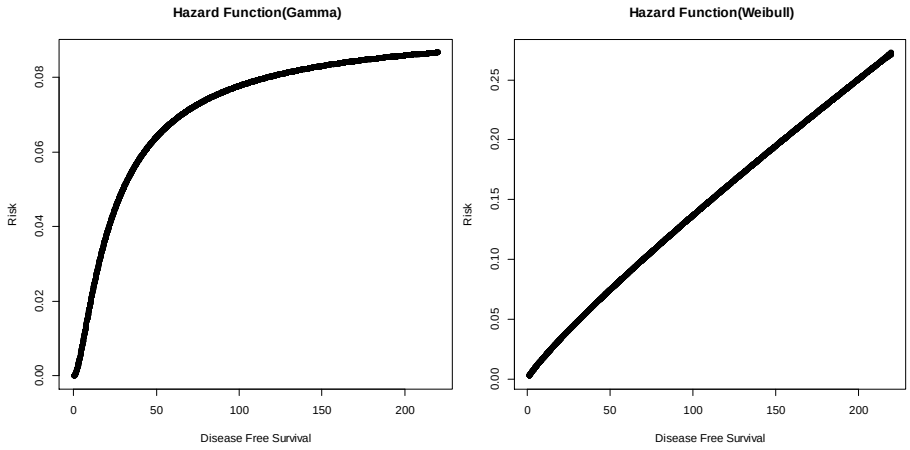


It can be observed that these two functions differ significantly in predicting risk probability.

In a recent work, Ardoino et. al. (2012) investigate a generalization of the gamma model proposed by Cox et al (2006), to study the dynamics of breast cancer and Wahed et. al. (2009) propose a generalization of the Weibull density function, the models are fitted to a previously analyzed breast cancer data set, and its performance is evaluated using conventional methods of assessing the model fit.

## 5 Conclusion

Application of Stochastic Response Surface Methodology has higher expression in the computational modeling of complex systems, since simulation of the complete model usually implies high computational costs. This methodology has been applied mainly to the analysis of environmental risk, in problems of transport of particles and fluids, and in structural reliability analysis. In this work its application was tested to a problem of survival analysis, in breast tumor data related with morphological features of cell nuclei.

Stochastic Response Surface Methodology was used to fit a model, with Hermite polynomials, to estimate time to recur of breast cancer, after excision of the tumor, according to three characteristics of the nuclei of malignant cells: area, texture and smoothness. These characteristics were measured on average, since images collected allow highlight from 10 to 40 tumor cells and were selected from a set of 30 variables, after a study of the correlations and the adjustment to normal distribution. It was observed a significant lack of fit to normality of AREA variable which can be solved excluding four outliers. We opted to keep these observations, since the sample size is significant, but it is

suggested a study of these observations in future work.
We opted to fit the model with the data for which there was recurrence, aware that the results would suffer from a bias. As indicated by Street et al (1999), most observed recurrences were at relatively short times (a mean of 24 months) and therefore a regression method, which uses only these data, result in low prediction of recurrence time, coinciding with the bias of this particular data set. In future work censored data will be considered for the model fit.
By Monte Carlo simulation, the model allow to estimate the probability density function of the response variable $f(t)$, and survival function $S(t)$ which represents the likelihood of a patient to remain free of disease versus time.
The hazard function is obtained with the analytical expressions of $f(t)$ and $S(t)$ functions. Thus, it was necessary to seek a probability density function that would fit well $f(t)$. The gamma function revealed a better fit. The generalized models used by Ardoino et al (2012) and Wahed et. al. (2009) can be explored in future work.

## References

1. Ahmed, A. & Soubra, A. H.: Extension of subset simulation approach for uncertainty propagation and global sensitivity analysis. Georisk: Assessment and Management of Risk for Engineered Systems and Geohazards, 6(3), 162-176 (2012).
2. Balakrishnan, S., Roy, A., Ierapetritou, M. G., Flach, G. P., Georgopoulos, P. G.: Uncertainty reduction and characterization for complex environmental fate and transport models: An empirical Bayesian framework incorporating the stochastic response surface method. Water Resources Research, 39(12) (2003).
3. Bastug, E., Menafoglio, A., Okhulkova, T.: Polynomial Chaos Expansion for an Efficient Uncertainty and Sensitivity Analysis of Complex Numerical Models. Conference Paper. ESREL 2013, Amsterdam, Netherlands (2013).
4. Blatman, G., Adaptive sparse polynomial chaos expansions for uncertainty propagation and sensitivity analysis. Ph.D Thesis, Université Blaise Pascal, Clermont-Ferrand (2009).
5. Datta, D., & Kushwaha, H. S.: Uncertainty Quantification Using Stochastic Response Surface Method Case Study--Transport of Chemical Contaminants through Groundwater. International Journal of Energy, Information & Communications, 2(3) (2011).
6. Ernst, O. G., Mugler, A., Starkloff, H. J., & Ullmann, E.: On the convergence of generalized polynomial chaos expansions. ESAIM Math. Model. Numer. Anal, 46(2), 317-339 (2012).
7. Ghanem, R. G., & Spanos, P. D.: Stochastic finite elements: a spectral approach (Vol. 41). New York: Springer-Verlag (1991).
8. Isukapalli, S. S., Roy, A., Georgopoulos, P. G.: Stochastic response surface methods (SRSMs) for uncertainty propagation: application to environmental and biological systems. Risk analysis, 18(3), 351-363 (1998).
9. Isukapalli SS. An uncertainty analysis of transport transformation models.

Ph.D. Thesis, New Brunswick, New Jersey: The State University of New Jersey (1999).
10. Li, D. Q., Jiang, S. H., Chen, Y. F., & Zhou, C. B.: Reliability analysis of serviceability performance for an underground cavern using a non-intrusive stochastic method. Environmental Earth Sciences, 71(3), 1169-1182 (2014).
11. Li, D., Chen, Y., Lu, W., & Zhou, C. Stochastic response surface method for reliability analysis of rock slopes involving correlated non-normal variables. Computers and Geotechnics, 38(1), 58-68 (2011).
12. Mangasarian, O. L., Street, W. N., & Wolberg, W. H. (1995). Breast cancer diagnosis and prognosis via linear programming. Operations Research, 43(4), 570-577.
13. Oladyshkin, S., Class, H., Helmig, R., & Nowak, W. (2011). A concept for data-driven uncertainty quantification and its application to carbon dioxide storage in geological formations. Advances in Water Resources, 34(11), 1508-1518.
14. Oladyshkin, S., Nowak, W.: Data-driven uncertainty quantification using the arbitrary polynomial chaos expansion. Reliability Engineering and System Safety, 106, 179-190 (2012).
15. Oladyshkin, S., de Barros, F. P. J., & Nowak, W.: Global sensitivity analysis: a flexible and efficient framework with an example from stochastic hydrogeology. Advances in Water Resources, 37, 10-22 (2012).
16. R Development Core Team: R: A Language and Environment for Statistical Computing, R Foundation for Statistical Computing, Vienna, Austria, ISBN 3-900051-07-0 (2012).
17. Sun, A. Y., Zeidouni, M., Nicot, J. P., Lu, Z., & Zhang, D. (2013). Assessing leakage detectability at geologic CO< sub> 2</sub> sequestration sites using the probabilistic collocation method. Advances in Water Resources, 56, 49-60.
18. Xiu, D., Karniadakis, G.E.: Modeling uncertainty in steady state diffusion problems via generalized polynomial chaos. Computer Methods in Applied Mechanics and Engineering, 191(43), 4927-4948 (2002).
19. Xiu, D., Karniadakis, G. E.: Modeling uncertainty in flow simulations via generalized polynomial chaos. Journal of Computational Physics, 187(1), 137-167 (2003a).
20. Xiu, D., Karniadakis, G. E.: A new stochastic approach to transient heat conduction modeling with uncertainty. International Journal of Heat and Mass Transfer, 46(24), 4681-4693 (2003b).
21. Wolberg, W. H., Street, W. N., & Mangasarian, O. L. (1999). Importance of nuclear morphology in breast cancer prognosis. *Clinical Cancer Research*, *5*(11), 3542-3548.

# Is it worth using a fuzzy controller to adjust the mutation probability in a genetic algorithm when the input variable is the number of iterations?

André G. C. Pereira[1], Bernardo B. de Andrade[1], and Enrico Colossimo[2]

[1] Applied Mathematics/Statistics Program, Universidade Federal do Rio Grande do Norte, Natal/RN, Brazil
(E-mail: andre@ccet.ufrn.br, bba@ccet.ufrn.br )
[2] Statistics Department - Universidade Federal de Minas Gerais, Belo Horizonte/MG, Brasil
(E-mail: enricoc@est.ufmg.br)

**Abstract.** In recent years, several attempts to improve the efficiency of the Canonical Genetic Algorithm (CGA) have been presented. One of such attempts was the introduction of the elitist non-homogeneous genetic algorithm whose advantage over the CGA is that variations in the mutation probabilities are allowed. Such variations permit the algorithm to broaden/restrict its search space as the mutation probability increases/deacreases. The problem with this approach is that the way such changes will happen has to be defined before the algorithm is initiated. In general such changes happen in a decreasing way. Another way to vary the mutation probability is to use controllers. Fuzzy controllers have been widely used to adjust the parameters of a genetic algorithm. In this paper a stochastic controller is introduced along with a convergence proof of the genetic algorithm which uses such controller to adjust the mutation probability and a way to construct a stochastic controller from a fuzzy controller. Numerical comparisons between the two types of controllers and the CGA are performed. The general case with several input variables and two output variables (mutation and crossover probabilities) is work in progress.

**Keywords:** Stochastic controller, Fuzzy controller, Genetic Algorithms..

## 1 Introduction

The Canonical Genetic Algorithm (CGA), introduced in Holland[8], is a computational tool that mimics the natural genetic evolutionary process of a population that undergoes three stages: selection, crossover (mating) and mutation. In the CGA, a population of $N$ individuals or chromossomes, $(u_1, u_2, ..., u_N)$, is considered. An evaluation function $f : E \to (0, \infty)$ assigns to each individual $u_i, i = 1, \ldots, N$ a fitness value $0 < f(u_i) < \infty$. In the selection stage, the actual population will be resampled, individuals with higher fitness are more

*Stochastic Modeling, Data Analysis and Statistical Applications* (*pp.* 297-311)
Lidia Filus - Teresa Oliveira - Christos H Skiadas (Eds)



likely to be selected and those with low fitness tends to be eliminated (elitist selection). Following the natural evolutionary process, biological reproduction (crossover) and eventual mutation occur. In the crossover stage, individuals are independently chosen for crossover with a prescribed probability $p_c$. Mutation also operates independently on each individual with a prescribed probability $p_m$. In order to be easier for implementation, each individual is represented by a binary vector of lenght $l$, where $l$ depends on the desired precision. For more details as well as implementation procedures see, for example, Campos *et al.*[2], Pereira and Andrade [12], Goldberg[7] .

In optimization, CGAs are used to solve problems of the type $\max\{f(x), x \in E\}$ with the objective function satisfying $0 < f(x) < \infty$. The individuals represent the feasible solutions and the selection stage preserves with higher probability the best fitted/searched points. In the crossover stage, neighboring points are searched, allowing a refined comparison in the surrounding. In the mutation stage, random points, possibly away from the preserved ones, are visited and constitute a strategy to avoid being trapped in local optimum points.

The non-homogeneous Genetic Algorithms (NHGA) was analysed in Campos *et al.*[1] focusing on the improvement of eficiency upon the CGA, by allowing the mutation and crossover probabilities to vary under certain conditions. The elitist genetic algorithm (EGA), which was introduced in Rudolph[15], was a modification in the CGA that solved the problem of eficiency of the CGAs. A non-homogeneous version of the EGA, called elitist non-homogeneous genetic algorithm (ENHGA), was introduced in Rojas Cruz and Pereira[14] in order to improve the eficiency of the EGA. Other attempts to improve the eficiency of the CGA, without changing the mutation and crossover probabilities can be seen in [3,5], some numerical comparisons between ENHGA and EGA, can be seen in Campos *et al.*[2], and the proper way of running the ENHGA can be seen in Pereira and Andrade[12].

The advantage of the ENHGA over the EGA is that variation of the mutation probabilities (starting high and decreasing) permits the algorithm to broaden its search space at the start and restrict it later on. The way in which the mutation probabilities vary is defined before the algorithm is initiated. The ideal would be for the parameters to vary, rather than only diminish, depending on a certain measure of dispersion of the elements of the current population, as well as the number of iterations of the algorithm. To this end, controllers are introduced in the intermediate stages of the algorithm in order to adjust such changes. Various types of controllers can be used for this task, ranging from deterministic methods to those that employ fuzzy logic. Many simulation studies have used fuzzy controllers to adjust the parameters in order to improve the performance of the genetic algorithm. However, it has been only recently [13] discussed the conditions that must be met by the controller in order to ensure convergence of the genetic algorithm.

In [6] the authors describe a series of parameters of the GA and simulations were developed to illustrate that variations on those parameters interfere with the output of the algorithm. In [10] it is reported that, based on [6], one attempt of defining the way of varying the parameters in order to improve the performance of the algorithm was unsuccessfully tried. For this reason a fuzzy

controller was proposed as a tool to control the parameters substantiated only by simulations. In [14] sufficient conditions are given on the crossover and mutation probabilities in order to guarantee the convergence of the GA. In many others papers GA and fuzzy controllers are used but in a different way than the one that is presented in this work: The GA is used to obtain a rule basis and membership functions in a dynamic way, so that the performance of the fuzzy controller is improved. An example of that use can be seen in [9] where a GA, called "improved GA", is used to adjust the rules and functions mentioned above. However, no additional piece of information is given to explain why that GA is better, but in [14] it is explained that an elitist version of this GA converges. The contribution of our work is to define a naive stochastic controller, to give sufficient conditions to the stochastic controller that is used to adjust the mutation probability, has to satisfy in order to guarantee the convergence of the GA. It also shows that this kind of controller is statistically as efficient as the fuzzy one.

In this work, a fuzzy controller and a stochastic controller were constructed where the input variable is the number of iterations $N_g$ and the output variable is the mutation probability ($p_m$) . The convergence of the genetic algorithm using fuzzy controller can be seen in [13] while the convergence of the stochastic controller is presented in this work. The stochastic controller will be constructed in the simplest way possible, using a Uniform distribution. This work thus illustrates that if the input variable is the number of interations, although the use of fuzzy controllers improves, in some sense, the genetic algorithm it is not worth using it because the same improvement can be obtained using a faster and lighter controller such as a stochastic controller. Many other input variables can be used in a fuzzy controller as those presented in [10] and in the references therein.

In Section 2 definitions and results concerning the non-homogeneous Markov Chains that will be used in the rest of the paper are presented. In Section 3 the fuzzy controller with $N_g$ as input variable and $p_m$ as output variable is shortly described (which is extensively done in [4]). The stochastic controller is lighter but expresses the relevant characteristics of fuzzy controllers by means of statistical distributions. In addition convergence results are obtained. In Section 4, numerical comparisons between the elitst non-homogeneous genetic algorithm that uses a fuzzy controller and a stochastic controller for five special functions are presented and statistical properties are obtained.

## 2 Preliminaries

Following notation from the previous section let $f : E \to (0, \infty)$ be a function subject to a genetic algorithm in order to find

$$x^* = \text{argmax}\{f(x), x \in E\},$$

where $E$ is a discretization of the domain of the function $f$. To proceed the following steps of the algorithm, such points are represented as binary vectors of length $l$, where $l$ depends on the desired precision. A population of size $N$

is considered, let $Z = \{(u_1, u_2, ..., u_N); u_i \in E, i = 1, 2, ..., N\}$ be the set of all populations of size $N$. $Z$ is the state space of the Markov Chain that is used to prove the convergence of the algorithm (see Campos *et al.*[1], Dorea *et al.*[5], Rojas Cruz and Pereira[14] and Rudolph[15]).

The evolution of the ENHGA is different from the evolution of the EGA just in the update of the values of the parameters $p_m$ and $p_c$. Thus, the elitist algorithm can be summarized in the following sketch:

a)Choose randomly an initial population having $N$ elements, each one being represented by a binary vector of length $l$, and create one more position, the $(N + 1)$-th entry of the population vector, which will keep the best element from the $N$ previous elements.

b)Repeat

1. perform selection with the first $N$ elements
2. perform crossover with the first $N$ elements
3. perform mutation with the first $N$ elements
4. If the best element from this new population is better than that of the $(N + 1)$-th position, change the $(N + 1)$-th position by this better element, otherwise, keep the $(N + 1)$-th position unchanged
5. perform $p_c$ and $p_m$ changes, as previously planned.

c) until some stopping criterion applies.

Denote this new state space by $\tilde{Z}$.

In Rojas Cruz and Pereira[14], it is shown that the ENHGA is a non-homogeneous Markov Chain, with a finite state space $\tilde{Z}$, whose transition matrices are given by $P_n = SC_nM_n, \forall n \in \mathbb{N}$, where $S, C_n, M_n$ are transition matrices which represent the selection, crossover and mutation stages respectively. Here the $M_n$ is composed by the third and fourth steps described in the above sketch. In the same paper it is shown that there is a sequence $\{\alpha_n\}_{n\in\mathbb{N}}$ such that

$$\inf_{i\in\tilde{Z}, j\in\tilde{Z}^*} P_n(i, j) \geq \alpha_n,$$

where $\tilde{Z}^* \subset \tilde{Z}$, which contains all populations that have the optimum point as one of its points. The following results were obtained as corollaries to their main result.

**Corollary 1:** Let $\{X_n\}_{n\in\mathbb{N}}$ be the Markov Chain which models the elitist non-homogeneous genetic algorithm, if the sequence above is such that $\sum_{k\geq 1} \alpha_k = \infty$ then

$$P(\lim_{n\to\infty} X_n \in \tilde{Z}^*) = 1. \tag{1}$$

A simpler condition to verify in actual implementations which guarantee the above result is

**Corollary 2:** Let $\{X_n\}_{n\in\mathbb{N}}$ be the Markov Chain which models the elitist non-homogeneous genetic algorithm, if the mutation probabilities $\{p_m(n)\}_{n\in\mathbb{N}}$ are such that $p_m(n) > \gamma > 0$ for all $n \in \mathbb{N}$ or $\sum_n p_m(n)^l < \infty$ then (1) holds.

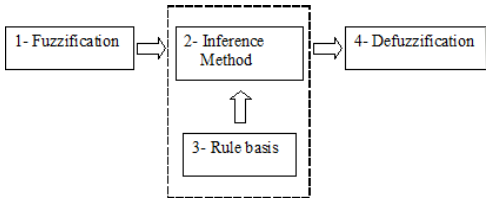


**Figure 1.** Fuzzy controler scheme

## 3 The Fuzzy Controller/The Stochastic Controller

A fuzzy controller has the ability to associate an output value with an input value. Its implementation involves four essential components: fuzzification, the inference method, the base rule and defuzzification, as shown in Figure 1 [11].

Fuzzification is the first part of the process, and it consists of converting the numerical input into fuzzy sets. The second part involves definition of the inference method that provides the fuzzy output (or control) to be adopted by the controller, from each fuzzy input. The third step in the process (the rule base) involves a mathematical "translation" of the information comprising the knowledge base of the fuzzy system. Finally, defuzzification is an operation that converts a fuzzy set to a numerical value, which can be achieved using a technique such as the Center of Gravity method described by the formula (of weighted average of the membership function $\varphi_{(A)}$ of set $A$)

$$C(A) = \frac{\int u\varphi_{(A)}(u)du}{\int \varphi_{(A)}(u)du} \tag{2}$$

Consider the following construction of fuzzy sets for the variables $N_g$ and $p_m$, using the state variables: low (L), average (A), and high (H). These sets were characterized by their membership functions, which define the extent to which a determined element does or does not belong to the set. Figures 2 and 3 show the membership functions for $Ng$ and $p_m$.

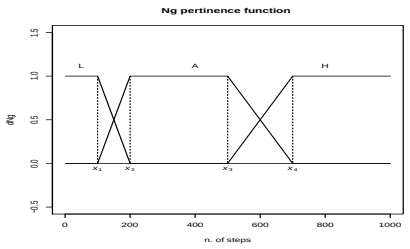


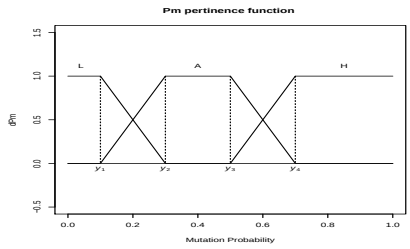


**Figure 2.** Membership function for $N_g$ **Figure 3.** Membership function for $p_m$

It was proved in [13] that

**Theorem 1:** If we use membership functions like those presented in figures 2

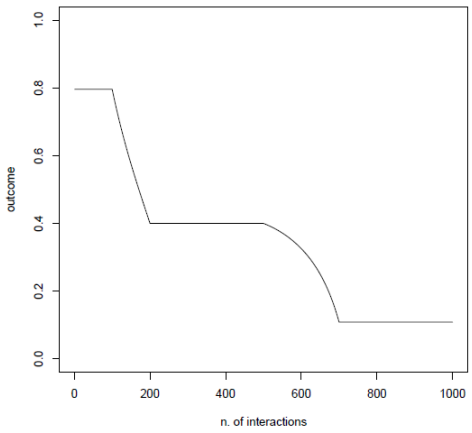


**Figure 4.** Fuzzy controler outcome

and 3 and the Mamdani inference method, based on max-min operators and the base rule consisting of three rules:

1. If $Ng$ is low (L), then $p_m$ is high (H);
2. If $Ng$ is average (A), then $p_m$ is average (A);
3. If $Ng$ is high (H), then $p_m$ is low (L).

Then the non-homogeneous genetic algorithm controlled by this fuzzy controller converges.
Now, let's observe more closely the possible outcomes of this controller. As time goes by, the number of iterations makes the rules be triggered, starting with $N_g = L$ what implies that $p_m = H$ is triggered, then $N_g = L$ and $N_g = A$ are trigged together and that implies $p_m = H$ and $p_m = A$ are triggered together too, and so on. Taking these rules into consideration and calculating (2) we obtain the outcome of the fuzzy controller as a function of the number of iterations illustrated in Figure 4.

Let us set up the following stochastic controller based on the outcome of the fuzzy controller

$$\text{out}(n) = \begin{cases} 0.8,\ 0 < n < 100 \\ U_1,\ 100 \leq n < 200 \\ 0.4,\ 200 \leq n < 500 \\ U_2,\ 500 \leq n < 700 \\ 0.1,\ n \geq 700 \end{cases}$$

where $U_1 \sim U[0.4, 0.8]$ and $U_2 \sim U[0.1, 0.4]$.

**Remark.** We note that the numbers in the definition of the stochastic controller are obtained by the membership functions. If the membership functions change, then these values are likely to change too.

Using this stochastic controller to adjust the mutation probability in the elitist non-homogeneous genetic algorithm, by corollary 2 of the former section,

it converges. More generally

**Theorem 2:** If a stochastic controller is set up to adjust the mutation probability of an elistist non-homogeneous genetic algorithm, if its output satisfies the hypothesis of corollary 2, then (1) holds.

**Remark.** In Theorem 2, the input variable(s) were not estabilished, that is because we just need the output to satisfy the hypotheses of corollary 2.

## 4 Numerical Evaluations

We have used five test functions to compared the performance of three versions of the GA: (i) the EGA; (ii) the ENHGA using a fuzzy controller on the mutation probability $p_m$ and (iii) the ENHGA using a stochastic controler on $p_m$. The functions are:

1. $f : [-2, 1] \times [-2, 1] \to \mathbb{R}$ given by

$$f(x) = 6 + x^2 - 3\cos(2\pi x) + y^2 - 3\cos(2\pi y)$$

2. $f : [-\frac{1280}{63}, \frac{1240}{63}] \times [-\frac{1280}{63}, \frac{1240}{63}] \to \mathbb{R}$ given by

$$f(x) = 0.5 - \frac{\sin(\sqrt{x^2 + y^2})^2 - 0.5}{(1 + 0.001(x^2 + y^2))^2}$$

3. $f : [-4, 2] \times [-4, 2] \to \mathbb{R}$ given by

$$f(x) = \frac{1}{0.3 + x^2 + y^2}$$

4. $f : [-2, 2] \times [-2, 2] \to \mathbb{R}$ given by

$$\begin{aligned} f(x) = [1 + (19 - 14x + 3x^2 - 14y + 6xy + 3y^2)(x + y + 1)^2] \\ \times [30 + (18 - 32x + 12x^2 + 48y - 36xy + 27y^2)(2x - 3y)^2] \end{aligned}$$

5. $f : [-5, 10] \times [0, 15] \to \mathbb{R}$ given by

$$f(x) = \left(y - \frac{5.1x^2}{4\pi^2} + \frac{5x}{\pi} - 6\right)^2 + 10\left(1 - \frac{1}{8\pi}\right)\cos(x) + 10$$

All of the above domains were discretized so that $x$ would lie in a grid of $2^{12}$ points. The maximum is known for each function within the respective grid. In the simulations we considered population sizes $N$ of 10, 30 and 50 individuals. For each $N$ and each function we run 1000 trials and we recorded the number of trials in which the optimum was found within 1000 interations. These counts are displayed in the fourth column of Table 1. We also report in Table 1 the maximum number of interations needed to reach the optimum (worst case) for those instances where all 1000 trials were succesful. For example: given the

first function, with $N = 10$, the EGA was succesful (before our fixed limit of 1000 interations) in 813 out of 1000 trials; still with the first function, with $N = 30$, the ENHGA with the fuzzy controller was succesful in all 1000 trials and all of them reached the maximum before the 716th interation.

Figures 5–9 show the evolution of our simulations and generally suggest that either form of controller provides an improvement over the simple EGA. Statistics from those simulations are provided in Table 1. The results in Table 1, specifically the third column ($S$), show an enormous gain in performance when using a controller (either fuzzy (ii) or stochastic (iii)) over the standard algorithm, except for function 3 and perhaps 4 where all versions seem equally good. In other words, except for functions 3 and 4, the successes under algorithm (i), $S_i$, is much smaller than $S_{ii}$ and $S_{iii}$. For function 1 with $N = 10$ the counts $S$ seem less distant but a $\chi^2$ test for equality of those three proportions (.813, .976, .980) reveal a significant difference (p-value $< 0.001$) which we attribute to $S_i$ being smaller than $S_{ii}$ and $S_{iii}$. The same test for equality of two proportions was carried out for those cases where neither $S_{ii}$ nor $S_{iii}$ is equal to 1000. These cases occurred in (Function, $N$) = (1, 10), (2, 10), (2, 30) and (5, 10). The corresponding $\chi^2$ tests resulted in p-values bounded below by 0.18 so we can safely conclude that there is no statistical difference between the performances of algorithms (ii) and (iii) in terms of proportion of succesful trials. In addition, the worst-case statistic (Table 1, fourth column) strongly indicates that GA with the stochastic controller (iii) seems to require less interations to reach the maximum then the GA the fuzzy controller (ii): most such cases favour (iii) over (ii); the largest difference – 299 iterations – favouring (iii) was observed in case (3, 50) and the largest difference – 87 interations – favouring (ii) was observed in case (1, 30). Finally, there is an enormous gain in execution time when comparing (iii) with (ii) given the simplicity of the stochastic controller over the fuzzy controller. Since our functions were rather simple we did not experience prohibite execution times but this can be an issue in larger problems.

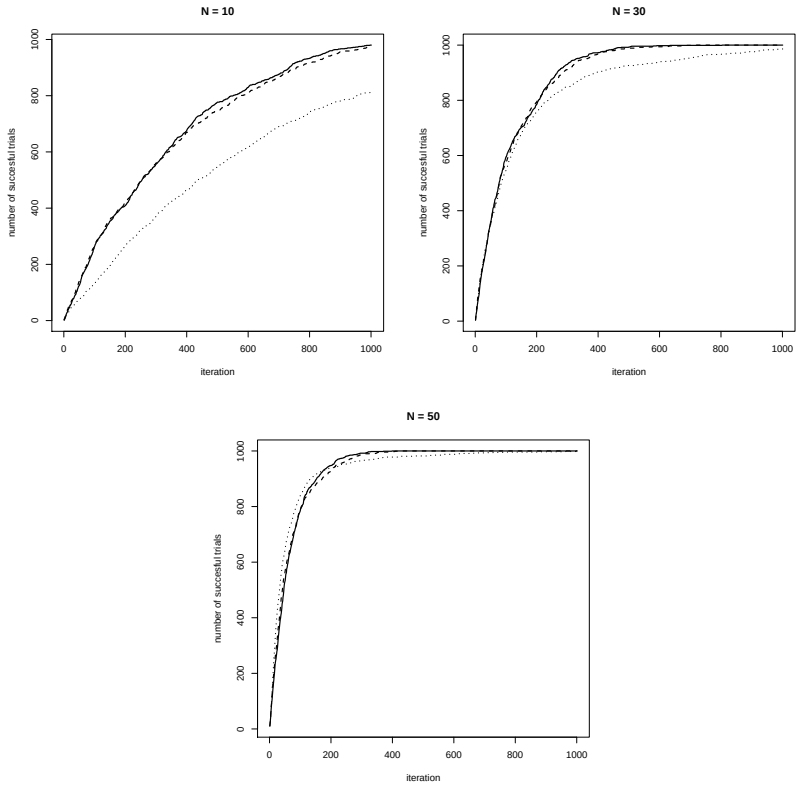


**Figure 5.** Number of succesful trials across 1000 simulations each limited to 1000 iterations using function 1 and different population sizes $N$. Dotted line represents scheme (i)–no controller, dashed line scheme (ii)–fuzzy, and full line scheme (iii)–stochastic.

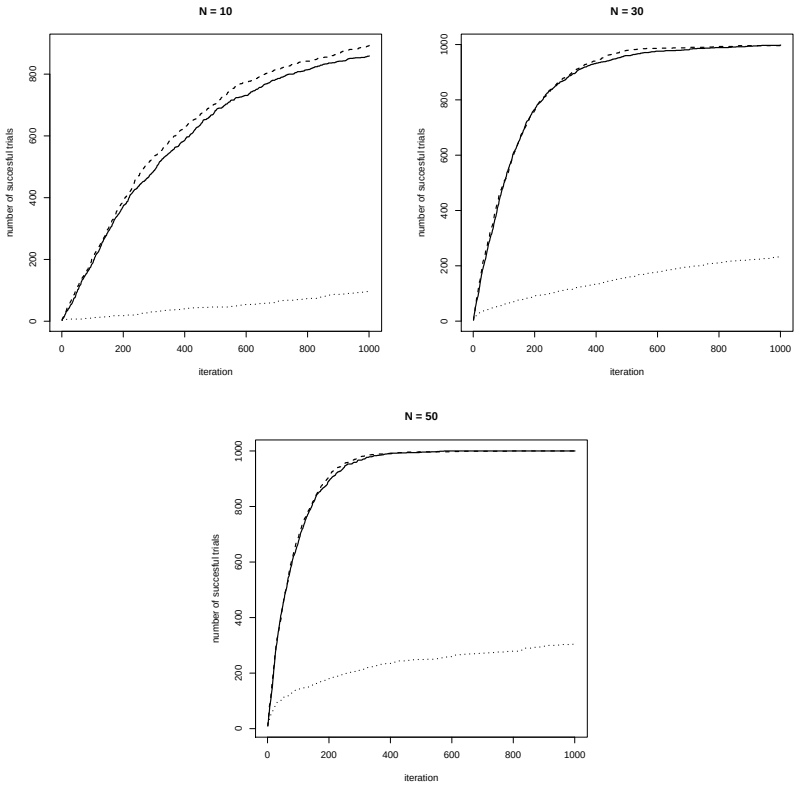


**Figure 6.** Number of succesful trials across 1000 simulations each limited to 1000 iterations using function 2 and different population sizes $N$. Dotted line represents scheme (i)–no controller, dashed line scheme (ii)–fuzzy, and full line scheme (iii)–stochastic.

## 5 Conclusions

The literature has many studies in which fuzzy controllers have been used to adjust the parameters of a genetic algorithm, some of them using the number of iterations of the algorithm as input variable. This work presents a very light stochastic controller to adjust the mutation probability which does not require any expensive calculation in its evolution. The idea was to compare this stochastic controller with a fuzzy one. We have given conditions under which such controllers make the elitist non-homogeneous genetic algorithm converge. Our simulations using five test functions suggest that the elitist genetic algorithm is greatly improved by the use of the two controllers considered. Most interestingly is the fact that we observed no statistical difference between the fairly expensive fuzzy controller and the much simpler stochastic one. In fact, the performance was even better under the simple stochastic controller in many cases. Thus, when the input variable is the number of interations, the computa-

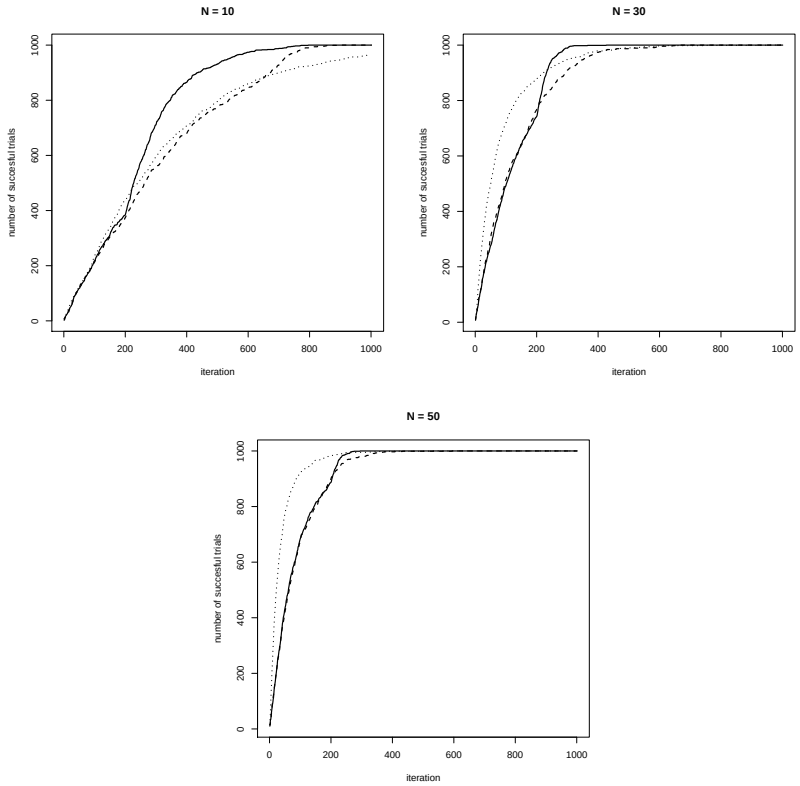


**Figure 7.** Number of succesful trials across 1000 simulations each limited to 1000 iterations using function 3 and different population sizes $N$. Dotted line represents scheme (i)–no controller, dashed line scheme (ii)–fuzzy, and full line scheme (iii)–stochastic.

tional effort can be reduced by using the light stochastic controller to adjust the mutation rate instead of the fuzzy controller without any loss in performance.

## Acknowledgment

The authors are grateful to PROCAD/CAPES and CNPq for financial support.

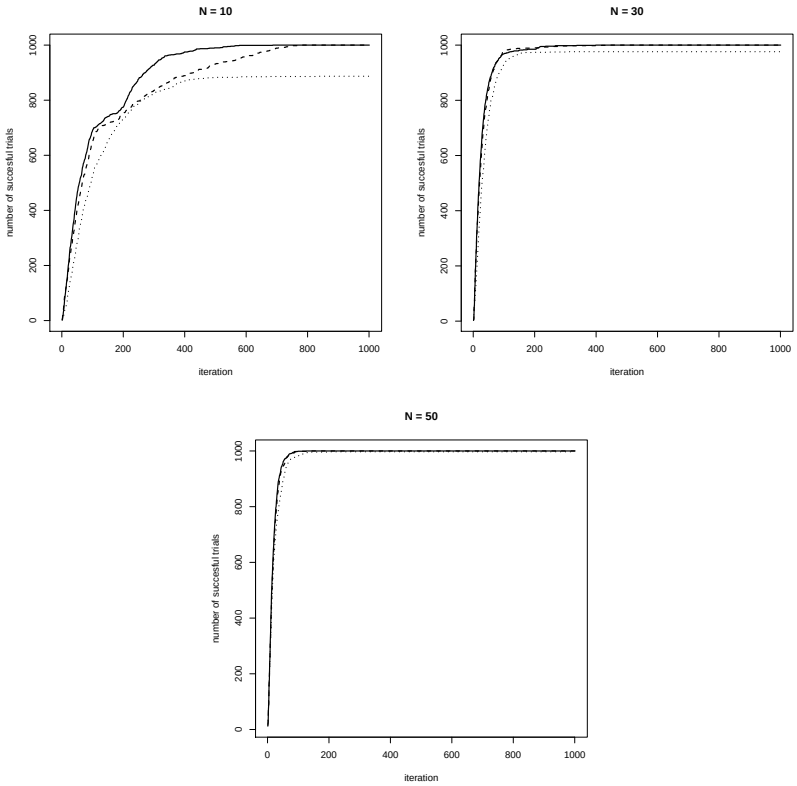


**Figure 8.** Number of succesful trials across 1000 simulations each limited to 1000 iterations using function 4 and different population sizes $N$. Dotted line represents scheme (i)–no controller, dashed line scheme (ii)–fuzzy, and full line scheme (iii)–stochastic.

## References

1. Campos, V.S.M., Pereira, A.G.C. and Rojas Cruz, J.A., *Modeling the Genetic Algorithm by a Non-Homogeneous Markov Chain: Weak and Strong Ergodicity.* Theory of Probability and its Applications, v.57,Issue 1(2012),p.185-192.
2. V.S.M. Campos, A.G.C. Pereira, L.A. Carlos and I.A.S. de Assis. Algoritmo Genético por cadena de Markov homogénea versus no-homogénea : Un estudio comparativo. *Journal of the Chilean Institute of Operations Research*, vol 2 (2012) p. 30-35.
3. V.S.M. Campos and A.G.C. Pereira, *A study on the Elitist Non-homogeneous Genetic Algorithm.* Biometrie und Medizinische Informatik. Greifswalder Seminarberichte (to appear).
4. L.A. Carlos, *Genetic Algorithms Convergence Analysis: A Markov Chain approach.* PhD Thesis presented at Electric Engineering Program of the Federal University of Rio Grande do Norte- Brazil (in portuguese)(2013).
5. Dorea, C.C.Yu, Guerra Júnior, J.A., Morgado, R., Pereira, A.G.C. *Multistage Markov Chain Modeling of the Genetic Algorithm and Convergence Results..* Numerical Functional Analysis and Optimization, v.31, (2010) p. 164-171.

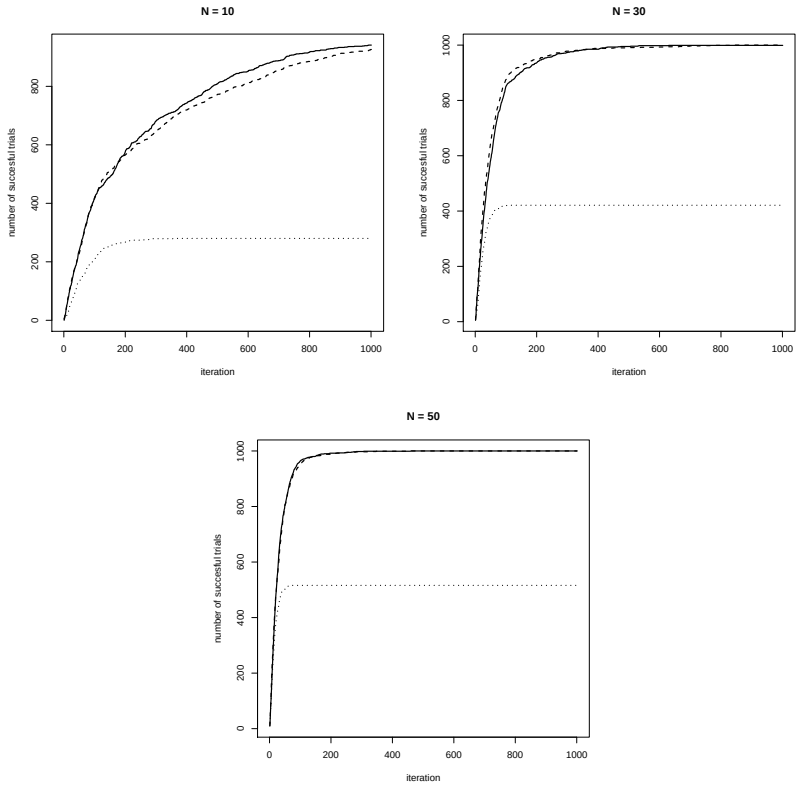


**Figure 9.** Number of succesful trials across 1000 simulations each limited to 1000 iterations using function 5 and different population sizes $N$. Dotted line represents scheme (i)–no controller, dashed line scheme (ii)–fuzzy, and full line scheme (iii)–stochastic.

6. Grefenstette, J.J., *Optimization of control parameters for genetic algorithm*, IEEE Transactions on systems, man, and cybernetics, vol. smc-16, n.1, pp.122-128, (1986).
7. Goldberg, D.E. *Genetic Algorithms in Search, Optimizations and Machine Learning*. Assison Wesley, Teading, MA (1989).
8. Holland, J.H. *Adaptation in natural and artificial systems*. Ann Arbor: The University of Michigan Press,(1975).
9. Lam, H.K., Ling, S.H., Leung F.H.F. and Tam, P.K.S., *Function estimation using a fuzzy neural-fuzzy network and an improved genetic algorithm*. International Journal of Approximate Reasoning, Volume 36, Issue 3, pp. 243–260 (2004).
10. Lee, M.A. and Takagi,H., *Dynamic control of genetic algorithms using fuzzy logic techniques*, Procceding of 5th International conference on Genetic Algorithms (ICGA'93), Urbana-Champaign, IL, pp. 76-83, (1993).
11. Pedrycz, W., *Fuzzy Sets Engineering*. CRC Press (1995).
12. Pereira, A.G.C. and Andrade, B.B. On the Genetic Algorithm with Adaptive Mutation Rate and Statistical Applications (submitted).

13. Pereira, A.G.C.. and Roveda,J.A.F., *Convergence analysis of an elitist non-homogeneous genetic algorithm with mutation probability adjusted by a fuzzy controller*, (submitted) .
14. Rojas Cruz, J.A., Pereira, A.G.C., *The Elitist Non-homogeneous Genetic Algorithm: Almost sure convergence*. Statistics and Probability Letters, v.83 (2013), p. 2179-2185.
15. Rudolph, G. *Convergence Analysis of Canonical Genetic Algorithms*. IEEE Transactions on Neural Networks, V.5, (1994),96-101.
16. Yun, Y., Gen, M. *Performance Analysis of Adaptative Genetic Algorithms with Fuzzy Logic and Heuristics*. Fuzzy Optimization and Decision Making, V.2, (2003), 161-175.

**Table 1.** Simulation results considering the five functions described in the text and three versions of the GA: (i) the EGA, (ii) the ENHGA using a fuzzy controller on $p_m$ and (iii) the ENHGA using a stochastic controler on $p_m$.

| Function | $N$ | GA | Successes ($S$) | Worst case (iterations) |
|---|---|---|---|---|
| 1 | 10 | (i) | 813 | - |
| | | (ii) | 976 | - |
| | | (iii) | 980 | - |
| | 30 | (i) | 986 | - |
| | | (ii) | 1000 | 716 |
| | | (iii) | 1000 | 803 |
| | 50 | (i) | 998 | - |
| | | (ii) | 1000 | 416 |
| | | (iii) | 1000 | 398 |
| 2 | 10 | (i) | 96 | - |
| | | (ii) | 894 | - |
| | | (iii) | 859 | - |
| | 30 | (i) | 232 | - |
| | | (ii) | 996 | - |
| | | (iii) | 998 | - |
| | 50 | (i) | 304 | - |
| | | (ii) | 1000 | 779 |
| | | (iii) | 1000 | 574 |
| 3 | 10 | (i) | 964 | - |
| | | (ii) | 1000 | 904 |
| | | (iii) | 1000 | 795 |
| | 30 | (i) | 1000 | 945 |
| | | (ii) | 1000 | 660 |
| | | (iii) | 1000 | 426 |
| | 50 | (i) | 1000 | 517 |
| | | (ii) | 1000 | 593 |
| | | (iii) | 1000 | 294 |
| 4 | 10 | (i) | 887 | - |
| | | (ii) | 1000 | 776 |
| | | (iii) | 1000 | 686 |
| | 30 | (i) | 976 | - |
| | | (ii) | 1000 | 445 |
| | | (iii) | 1000 | 398 |
| | 50 | (i) | 997 | - |
| | | (ii) | 1000 | 125 |
| | | (iii) | 1000 | 126 |
| 5 | 10 | (i) | 280 | - |
| | | (ii) | 926 | - |
| | | (iii) | 941 | - |
| | 30 | (i) | 421 | - |
| | | (ii) | 1000 | 833 |
| | | (iii) | 999 | - |
| | 50 | (i) | 516 | - |
| | | (ii) | 1000 | 453 |
| | | (iii) | 1000 | 459 |

# 7 CHAPTER

## Experimental Design and Related Topics

# Estimation in Models with Commutative Orthogonal Block Structure, Imbedded Orthogonality

Sandra S. Ferreira, Célia Nunes, Dário Ferreira, and João Tiago Mexia

Department of Mathematics and Center of Mathematics, University of Beira Interior, Covilhã, Portugal, Emails: sandraf@ubi.pt, celian@ubi.pt , dario@ubi.pt , jtm@fct.unl.pt

**Abstract.** As a branch of Block Designs, research on Balanced Incomplete Block Designs (BIBD) arose several interesting and defying problems within Combinatory Mathematics. Hadamard Matrices are present in our daily life and it give rise to a class of block designs named Hadamard configurations. It is easy and current to find different applications of it based on new technologies and codes of figures such as Quick Response Codes (QR Codes). These are bi-dimensional barcodes that can be easily read by common devices which have image capture function, such as mobile phones. Risk is the potential of losing something of value, weighed against the potential to gain something of value. There are several types of risk and we will focus on information security risk, namely on the information loss for QR Codes. Connections between the various methodologies and QR Codes will be discussed.
**Keywords:** BIBD, Combinatorial Designs, Hadamard Matrices, QR Codes.

## 1 Introduction

Models with orthogonal block structure, OBS, are mixed models with the family $\nu = \left\{\sum_{j=1}^{m} \gamma_j Q_j; \quad \gamma \in \mathbb{R}_+^m\right\}$, of variance-covariance matrices where the $Q_1, ..., Q_m$ are pairwise orthogonal orthogonal projection matrices, POOPM, summing to the identity matrix, $I_n$. These designs were introduced by [10] and [11], and continue to play an important part in the theory of randomized block designs, see for instance [1] and [2]. Refer to [6] and [13] for historical developments of the mixed model. The inference for these models is centered on the estimation of treatment contrasts, see [7].
We will consider a special class of models with OBS, the commutative orthogonal block structure, COBS, in which $T$, the orthogonal projection matrix on the space $\Omega$ spanned by the mean vector commutes with the matrices in principal basis of a CJA $\mathcal{A}$, $pb(\mathcal{A})$, see [4].

Imbedded orthogonality will be within a submodel or submodels of a larger model. We will consider two situations in which the submodel or submodels

*Stochastic Modeling, Data Analysis and Statistical Applications* (*pp.* 315-323)
Lidia Filus - Teresa Oliveira - Christos H Skiadas (Eds)



have COBS. A model has such a structure if it has variance-covariance matrix

$$V = \sum_{j=1}^{m} \gamma_j Q_j, \tag{1}$$

where $\gamma_1, ..., \gamma_m$ will be the canonical variance components.
As we shall see it may worthwhile to use results on COBS in developing the inference for the full model.
The first situation we will consider, in section 3, will be $L$ extensions of COBS. Then the full model will have observations vector

$$Y = LY^o + e, \tag{2}$$

where $L$ is a matrix with linearly independent column vectors and $Y^o$ will correspond to a model with COBS and $e$ will be an error vector with null mean vector and variance covariance matrix $\sigma^2 I_n$ assumed to be independent from $Y^o$.

The second situation, in section 4, is that of structured families of COBS. Given a fixed effects orthogonal models we will have for each of its treatments a model with COBS. These submodels will have the same space spanned by their mean vectors and the same variance covariance matrix. Then their family will be isomorphic.
In the first situation $Y^o$ will be at the core of the global model so we will call it the core model. In the second situation we have two strata. The first strata will correspond to the fixed effects model which we will call the base model while the second strata will correspond to the family of COBS.
When analyzing $L$ extensions we will be generalizing the treatment we have for the core model which is quite different of our purpose for the third section. Then we will study the factors of the base design on the estimable vectors of the models of the family. Thus our purpose will be quite distinct in the two situations. Nevertheless the algebraic structure of COBS will provide, in both cases, the base for inference.

## 2 Mixed models with COBS

A mixed model

$$Y = \sum_{i=0}^{w} X_i \beta_i, \tag{3}$$

where $\beta_0$ is fixed and the $\beta_1, ..., \beta_w$ are random, independent, with null mean vectors and variance-covariance matrices $\theta_1 I_{c_1}, ..., \theta_w I_{c_w}$, will have mean vector $\mu = X_0 \beta_0$ and variance-covariance matrix

$$U = \sum_{i=1}^{w} \theta_i I_{c_i}, \tag{4}$$

where the matrices $M_i = X_i X_i^\top, i = 1, ..., w$. The orthogonal projection matrix on the space spanned by $\mu$ will be

$$T = X_0(X_0^\top X_0)^+ X_0^\top, \tag{5}$$

where $(X_0^\top X_0)^+$ is the MOORE-PENROSE inverse of $X_0^\top X_0$. Moreover, see for instance [8],

$$\psi = G\beta_0 \tag{6}$$

is estimable if and only if $G = CX_0$ and it's Least Square Estimator, LSE, will be

$$\widetilde{\psi} = G\widetilde{\beta}_0 \tag{7}$$

where

$$\widetilde{\beta}_0 = (X_0^\top X_0)^+ X_0^\top Y. \tag{8}$$

When the matrices $T, X_1, ..., X_w$ commute there will be POOPM $Q_1, ..., Q_m$, see [5], such that

$$\begin{cases} T = \sum_{j=1}^{z} Q_j \\ M_i = \sum_{j=1}^{m} b_{i,j} Q_j, i = 1, ..., w. \end{cases} \tag{9}$$

Let $R(W)$ be the range space of $W$. If

$$R[X_1, ..., X_w] = \mathbb{R}^n \tag{10}$$

we have

$$R(\sum_{i=1}^{w} M_i) = R([X_1, ..., X_w]) = \mathbb{R}^n \tag{11}$$

and since

$$\sum_{i=1}^{w} M_i = \sum_{j=1}^{m} \left( \sum_{i=1}^{w} b_{i,j} \right) Q_j \tag{12}$$

we must have

$$\sum_{j=1}^{m} Q_j = I_n, \tag{13}$$

otherwise $\sum_{i=1}^{w} M_i$ would not be invertible. Moreover we will have

$$V = \sum_{j=1}^{m} \gamma_j Q_j \tag{14}$$

with

$$\gamma_j = \sum_{i=1}^{w} b_{i,j} \sigma_i^2, j = 1, ..., m. \tag{15}$$

Then when the matrices $T, M_1, ..., M_w$ commute and $R[X_1, ..., X_w] = \mathbb{R}^n$ the model is COBS.

Since, then, $T$ and $V$ commute the Least Square Estimator, LSE, will be, see [15], Best Linear Unbiased Estimator, BLUE.

Considering

$$\gamma(1) = \begin{bmatrix} \gamma_1 \\ \vdots \\ \gamma_z \end{bmatrix}, \gamma(2) = \begin{bmatrix} \gamma_{z+1} \\ \vdots \\ \gamma_m \end{bmatrix}, \sigma^2 = \begin{bmatrix} \sigma_1^2 \\ \vdots \\ \sigma_w^2 \end{bmatrix},$$

and partitioning matrix $B = [b_{i,j}]$ on

$$B = [B(1) \quad B(2)], \tag{16}$$

where $B(1)$ has $z$ columns, we get

$$\gamma(l) = B(l)^\top \sigma^2. \tag{17}$$

We now point out that

$$R(Q_j) \subset R(T), j = 1, ..., z, \tag{18}$$

and so we can only directly estimate the $\gamma_{z+1}, ..., \gamma_m$, which correspond to the components of $\gamma(2)$. But, when the row vectors of $B(2)$, that are the column vectors of $B(2)^\top$, are linearly independent we will have

$$\begin{cases} \sigma^2 = (B(2)^\top)^+ \gamma(2) \\ \\ \gamma_1 = B(1)^\top (B(2)^\top)^+ \gamma(2). \end{cases} \tag{19}$$

In this case $\gamma(2)$ and $\sigma^2$, the relevant parameters for the random effects part of the model determine each other. Then this part segregates a submodel and we say there is segregation.

Let the row vectors of $A_j$ constitute an orthonormal basis for $R(Q_j), j = 1, ..., m$, and put

$$\begin{cases} \eta_j = A_j \mu, j = 1, ..., m \\ \\ \widetilde{\eta}_j = A_j Y, j = 1, ..., m, \end{cases} \tag{20}$$

then $\eta_j = 0, j = z + 1, ..., m$, since the row vectors of $A_j, j = z + 1, ..., m$, are orthogonal to $\Omega = R(X_0)$ and $\mu \in \Omega$. The $\widetilde{\eta}_j = 0, j = 1, ..., m$, will have mean vectors $\eta_j, j = 1, ..., m$, and variance-covariance matrix

$$A_j V A_j^\top = \gamma_j Q_j, j = 1, ..., m, \tag{21}$$

since

$$A_j Q_{j'} A_j^\top = 0_{g_j \times g_{j'}}, j \neq j', \tag{22}$$

where $g_j$ =rank $A_j$ =rank $(Q_j), j = 1, ..., m$. Thus, with

$$S_j = \|A_j Y\|, j = 1, ..., m, \tag{23}$$

we have

$$E(S_j) = g_j\gamma_j, j = z+1, ..., m, \tag{24}$$

and, consequently, the unbiased estimators

$$\widetilde{\gamma}_j = \frac{S_j}{g_j}, j = z+1, ..., m. \tag{25}$$

Moreover, if $\psi = G\beta$ is estimable we have $G = CX_0$ as well as

$$\psi = C\mu_0 = CT\mu_0. \tag{26}$$

Now $Q_j = A_j^\top A_j, j = 1, ..., m$, and $T = \sum_{j=1}^z Q_j = \sum_{j=1}^z A_j^\top A_j$ so that

$$\psi = C\sum_{j=1}^z A_j^\top \eta_j = \sum_{j=1}^z C_j\eta_j, \tag{27}$$

with $C_j = CA_j^\top$, so the estimable vectors are generalized linear combinations of the canonical estimable vectors $\eta_1, ..., \eta_m$. The $\widetilde{\eta}_1, ..., \widetilde{\eta}_m$ are the LSE of the $\eta_1, ..., \eta_m$ and

$$\widetilde{\psi} = \sum_{j=1}^z C_j\widetilde{\eta}_j. \tag{28}$$

## 3 L extensions

The orthogonal projection matrix on $\ominus = R(L)$ is

$$P = LL^+ = L(L^\top L)^+L^\top. \tag{29}$$

Given

$$Y = LY^o + e, \tag{30}$$

we take $Z = L^+Y$ having, since the column vectors of $L$ are linearly independent, $Z = Y^o + e^o$, where $e^o$ has null mean vector and variance-covariance matrix $\sigma^2L^+L^{+^\top}$ and is independent of $Y^o$. Then $Z$ will have mean vector $\mu$ and variance-covariance matrix

$$\sum_{j=1}^m \gamma_j Q_j + \sigma^2 L^+L^{+\top}. \tag{31}$$

But now the LSE for $\psi$ will be

$$\widetilde{\psi}^o = G\widetilde{\beta}_0^o \tag{32}$$

with

$$\widetilde{\beta}_0^o = (X_0^\top X_0)^+X_0^\top Z. \tag{33}$$

With

$$\begin{cases} \eta_j = A_j\mu, j = 1, ..., m \\ \\ \widetilde{\eta}_j^o = A_j Z, j = 1, ..., m, \end{cases} \tag{34}$$

where in the expression of the $\widetilde{\eta}_j^o$ we replaced $Y^o$ by $Z, j = 1, ..., m$, we have

$$\widetilde{\psi} = \sum_{j=1}^{z} C_j \widetilde{\eta}_j^o. \tag{35}$$

Moreover $\widetilde{\eta}_j^o$ will have mean vector $\eta_j$ and variance-covariance matrix

$$\sum_{j=1}^{m} \gamma_j Q_j + \sigma^2 A_j L^+ L^{+^\top} A_j^\top, j = 1, ..., m, \tag{36}$$

so,

$$S_j^o = \|\widetilde{\eta}_j^o\|^2, j = z+1, ..., m, \tag{37}$$

will have mean value $g_j\gamma_j + t_j\sigma^2, j = z+1, ..., m$ when $t_j$ is the trace of

$$A_j L^+ L^{+^\top} A_j^\top, j = z+1, ..., m. \tag{38}$$

Then for applying the previous results on estimation of variance components we have only to estimate $\sigma^2$. The orthogonal projection matrix on the orthogonal complement $\ominus^\perp$ of $\ominus$ is

$$P^\perp = I_{\overline{n}} - P \tag{39}$$

where $\overline{n}$ is the number of components of $Y$. Since

$$P^\perp Y = P^\perp e \tag{40}$$

and $P^\perp e$ has null mean vector and variance covariance matrix $\sigma^2 P^\perp$, the mean value of

$$\overline{S} = \|P^\perp Y\|^2 \tag{41}$$

will be $\overline{g}\sigma^2$, with $\overline{g} = \overline{n} - n$, where $n$ is the number of components of $Y$. Thus we have the unbiased estimators

$$\begin{cases} \widetilde{\sigma}^2 = \frac{\overline{S}}{\overline{g}} \\ \\ \widetilde{\gamma}_j = \frac{S_j^o - t_j\widetilde{\sigma}^2}{g_j}, j = z+1, ..., m, \end{cases} \tag{42}$$

from which we estimate the components of $\sigma^2$ and $\gamma(1)$ if there is segregation.

## 4 Families and Regressional Families

Let us consider COBS

$$Y(u) = \sum_{i=0}^{w} X_i \beta_i(u), u = 1, ..., \overline{u} \tag{43}$$

with the same model matrices, and also the same covariance components $\sigma_i^2, i = 1, ..., w$. The observation vectors $Y(u), u = 1, ..., \overline{u}$, are assumed to be independent.
These models will have mean vectors

$$\mu(u) = X_0 \beta_0(u), u = 1, ..., \overline{u}, \tag{44}$$

so there estimable vectors will be the

$$\psi(u) = G\beta_0 = C\mu(u), u = 1, ..., \overline{u}, \tag{45}$$

since we must have $G = CX_0$, for $\psi(u), u = 1, ..., \overline{u}$ to be estimable.
The orthogonal projection matrix on $\Omega = R(X_0)$ will be

$$T = X_0 (X_0^\top X_0)^+ X_0^\top, \tag{46}$$

the same for all these COBS, as well as their variance-covariance matrix

$$V = \sum_{j=1}^{w} \sigma^2 M_i, \tag{47}$$

with, as before, $M_i = X_i X_i^\top, i = 1, ..., w$. Since these models are COBS,

$$T, M_1, ..., M_w \tag{48}$$

commute and there will be POOPM $Q_1, ..., Q_m$, such that

$$\begin{cases} T = \sum_{j=1}^{z} Q_j \\ \\ M_i = \sum_{j=1}^{m} b_{i,j} Q_j, i = 1, ..., w. \end{cases} \tag{49}$$

So, as before

$$V = \sum_{j=1}^{m} \gamma_j Q_j \tag{50}$$

with

$$\gamma_j = \sum_{i=1}^{w} b_{i,j} \sigma_i^2, j = 1, ..., m, \tag{51}$$

this is the variance components, both usual and canonical, are the same for all the COBS. Moreover assuming that the row vectors of $A_j$ constitute an orthonormal basis for $R(Q_j)$ we can define the

$$\begin{cases} \eta_j(u) = A_j \mu(u), u = 1, ..., \overline{u} \\ \\ \widetilde{\eta}_j(u) = A_j Y(u), u = 1, ..., \overline{u} \end{cases}, \tag{52}$$

continuing to have $\eta_j(u) = 0, j = z+1, ..., m$, as well as

$$\psi(u) = \sum_{j=1}^{z} C_j \eta_j(u), \tag{53}$$

where $C_j = CA_j^{\top}, j = 1, ..., u$. The $\eta_j(u) = 0, j = 1, ..., z, u = 1, ..., \overline{u}$ will be the estimable vectors for the COBS. As before, the

$$S_j(u) = \|\widetilde{\eta}_j(u)\|^2, j = z+1, ..., m, u = 1, ..., \overline{u}, \tag{54}$$

will have mean vectors $g_j\gamma_j$, with $g_j$ =rank $(Q_j), j = z+1, ..., m$. Since the $Y(u), u = 1, ..., \overline{u}$, are independent so the $S_j(u), u = 1, ..., \overline{u}, j = z+1, ..., m$ will be independent. So we are led to use the unbiased estimators

$$\widetilde{\gamma}_j = \frac{\sum_{u=1}^{\overline{u}} S_j(u)}{\overline{u} g_j(u)}, j = z+1, ..., m, \tag{55}$$

for the components of $\gamma(1)$. If the COBS are segregated we will also have the unbiased estimators

$$\begin{cases} \widetilde{\sigma}^2 = (B(2)^{\top})^{+}\widetilde{\gamma}_2 \\ \widetilde{\gamma}_1 = B(1)^{\top}(B(2)^{\top})^{+}\widetilde{\gamma}_2 \end{cases}. \tag{56}$$

Let us now assume that the COBS in the family correspond to the rows of a model matrix $K = [k_{l,h}]$ with linearly independent row vectors. We can consider the columns of $K$ as containing levels of $\overline{h}$ quantitative factors. Our purpose in the joint analysis of the COBS will be to study the action of these factors on the estimable vectors of the COBS. To do this we will consider linear regression with model matrix $K$ for dependent variables with values

$$\widetilde{\lambda}(u) = a^{\top}\widetilde{\psi}(u), u = 1, ..., \overline{u}, \tag{57}$$

so we may say that the COBS constitute a regressional family. It is easy to see that all conditions required for adjusting linear regression hold for these families.

## 5 Final Remarks

The two situations we considered are quite distinct. In the first of these there was an unique COBS located "up-stream" while in the second one we had several COBS located "down-stream." The COBS orthogonality was relevant in both cases so it is not location bounded.
Then imbedded orthogonality may be relevant in many cases.

## Acknowledgements

This work was partially supported by the Center of Mathematics, University of Beira Interior through the project PEst-OE/MAT/UI0212/2013 and CMA through the project PEst-OE/MAT/UI0297/2013.

## References


1. Caliński, T., Kageyama, S. *Block Designs: A Randomization Approach*, Volume I: Analysis, Lect. Notes Stat. **150**, Springer, New York, 2000.
2. Caliński, T., Kageyama, S. *Block Designs: A Randomization Approach*, Volume II: Design, Lect. Notes Stat., **170**, Springer, New York, 2003.
3. Fonseca, M., Mexia, J.T., Zmyślony, R. *Binary operations on Jordan algebras and orthogonal normal models*, Linear Algebra Appl., **417**, 75-86, 2006.
4. Fonseca, M., Mexia, J.T., Zmyślony, R. *Inference in normal models with commutative orthogonal block structure*. Acta Comment. Univ. Tartu. Math., **12**, 3-16, 2008.
5. Fonseca, M., Jesus, V., Mexia, J.T. and Zmyślony, R. *Binary Operations and Canonical Forms for Factorial and Related Models*. Linear Algebra Appl. **430**, 2781-2797, 2009.
6. Henderson, C. R. *Statistical Methods in Animal Improvement: Historical Overview*. In Gianola, Daniel and Hammond, Keith. Advances in Statistical Methods for Genetic Improvement of Livestock. Springer-Verlag Inc., 2-14, 1990.
7. Houtman, A.M., Speed, T.P. *Balance in designed experiments with orthogonal block structure*. Ann. Statist., **11**, 1069-1085, 1983.
8. Mexia, J.T. *Best linear unbiased estimates, duality of F tests and the Scheffé multiple comparison method in the presence of controlled heteroscedasticity*. Comput. Stat. Data An., **10**(3) 271-281, 1990.
9. Mexia, J.T., Vaquinhas, R., Fonseca, M., Zmyślony, R. *COBS: Segregation, Matching, Crossing and Nesting*. Latest Trends on Applied Mathematics, Simulation, Modeling, 4th International Conference on Applied Mathematics, Simulation, Modelling (ASM'10) 249-255, 2010.
10. Nelder, J.A. *The analysis of randomized experiments with orthogonal block structure*. I. Block structure and the null analysis of variance. Proceedings of the Royal Society (London), Series A, **273**, 147-162, 1965a.
11. Nelder, J.A. *The analysis of randomized experiments with orthogonal block structure*. II. Treatment structure and the general analysis of variance. Proceedings of the Royal Society (London), Series A, **273**, 163-178, 1965b.
12. Schott, J.R. *Matrix Analysis for Statistics*. John Wiley & Sons, New York, 1997.
13. Searle, S.R., Casella, G., McCulloch, C.E. *Variance Components*. John Wiley & Sons, New York, 1992.
14. Seely, J. *Quadratic subspaces and completeness*. Ann. Math. Stat., **42**(2), 710-721, 1971.
15. Zmyślony, R. *A characterization of best linear unbiased estimators in the general linear model*, Mathematical Statistics and Probability Theory, Proceedings Sixth International Conference, Wisla, Lecture Notes in Statistics, Springer, New York-Berlin, **2**, 365-373, 1978.

# Optimal design for parameters of stochastic processes

Milan Stehlík[1,2] and Philipp Hermann[2]

[1] Departamento de Matemática, Universidad Técnica Federico Santa María, Casilla 110-V, Valparaíso, Chile.
(E-mail: mlnstehlik@gmail.com)
[2] Department of Applied Statistics, Johannes Kepler University, 4040 Linz, Altenbergerstrasse 69, Austria
(E-mail: philipp.hermann@aon.at)

**Abstract.** The determination of optimal designs for models with correlated errors is substantially more difficult and for this reason not so well developed. Stochastic process with parametrized mean and covariance is observed over a compact set. The information obtained from observations is measured through the information functional (defined on the Fisher information matrix). In this paper we will focus on efficient designs for the parameters of correlated processes observed on plane. We will discuss the role of equidistant designs for the correlated process. Such designs have been proven to be optimal for parameters of trend of stationary Ornstein-Uhlenbeck process. More complex geometry of planes allows us to construct monotonic and space-filling designs. In the first case we relate to non-reversibility of diffusion, naturally modeled by Ornstein-Uhlenbeck sheet. In the manuscript a comparison between space filling designs and monotonic designs is made.
**Keywords:** monotonic design, Latin hypercube design, Ornstein-Uhlenbeck sheet.

## 1 Introduction

The determination of optimal designs for models with correlated errors is substantially more difficult and for this reason not so well developed. Stochastic process with parametrized mean and covariance is observed over a compact set. The information obtained from observations is measured through the information functional (defined on the Fisher information matrix). We focus on efficient designs for parameters of correlated processes and discuss the role of equidistant designs for the correlated processes. Such designs have been proven to be optimal for parameters of trend of stationary Ornstein-Uhlenbeck process (see Kiseľák and Stehlík[5]). For such a process we provided a study of small samples and asymptotical comparisons of the efficiencies of equidistant designs whilst taking both the parameters of trend as well as the parameters of covariance into account. If only trend parameters are of interest, the designs covering more or less uniformly the whole design space will rather be

*Stochastic Modeling, Data Analysis and Statistical Applications* (*pp.* 325-331)
Lidia Filus - Teresa Oliveira - Christos H Skiadas (Eds)



efficient when correlation decreases exponentially (see Kiseľák and Stehlík[5]). Some other issues on designs for spatial processes, i.e. identifiablity and existence of optimal designs, are given in Dette *et al.*[4], Müller and Stehlík[7] and Stehlík *et al.*[9]. For the case of a complicated setup we shall introduce a compound criterion (see Müller and Stehlík[6]) and an integrated compound criterion to discuss their potential of optimal designing for parameters of correlated processes. The role of heteroscedasticity is studied in Boukouvalas *et al.*[3]. Finally, the application in troposphere methane modelling will illustrate the developed methods (see Rodríguez-Díaz *et al.*[8]). In this paper we provide a comparison between monotonic and space-filling designs, introduced in the case of Ornstein-Uhlenbeck sheets in Baran *et al.*[2] and Baran and Stehlík[1].

## 2 Calculation of Fisher Information

Fisher information (FIM hereafter), obtained from observations and measured through the information functional, was the parameter of interest in this simulation study. It was calculated on basis of the following equations (1) and (2). The first approach (1) assumes equidistant design points on the diagonal of a square [0,1]x[0,1]. With the aid of equation (2) FIM can be calculated, e.g. for factorial design with points in [0,1]x[0,1]. The third approach is done on the basis of Latin Hypercube designs, whereby Fisher information matrix calculation is based on equation (2). However, the third approach can be split in two procedures where the first is built on S-optimality and the second on optimal euclidean distances between the points. The following equations show the differences in the computation of $M_\theta(n)$, representing FIM of $\theta$ with respect to $n$, the number of design points.

$$M_\theta(n) = 1 + \sum_{i=1}^{n-1} \frac{1-q_i}{1+q_i}, \qquad \text{where } q_i = \exp(-\alpha d_i - \beta\delta_i) \tag{1}$$

$$M_\theta(n) = \mathbf{1}_n C^{-1}(n,r)\mathbf{1}_n, \qquad \text{with} \tag{2}$$

$$C(\varepsilon(s_1,t_1),\varepsilon(s_2,t_2)) = \frac{\tilde{\sigma}^2}{4\alpha\beta} \cdot \exp(-\alpha \cdot |t_1 - t_2| - \beta|s_1 - s_2|)$$

and $\alpha > 0, \beta > 0, \tilde{\sigma} > 0$. The parameters $\alpha$ and $\beta$ were set 1 and $\tilde{\sigma} = 2$ such that the fraction of the covariance matrix equals to 1, wherefore no influence on behalf of this term is given.

The results of the computations for several design points are listed in Table 1. Obviously, $M_\theta(n)$ increases with increasing number of design points. Different starting values for FIM were calculated in addition to different magnitudes of the increase between the approaches, however, the parameter of interest does not exceed 2.18 for any design. As the header of the table shows, the first column displays the number of generated design points and the second one FIM with equidistant design points. In the third column FIM resulting from factorial design is shown and the last two columns present the results for the two different optimizing options with Latin Hypercube designs. Fisher

information for the factorial design equals to 2.1378 for every $n$, because this computation can only be performed for the four possible points on a [0,1]x[0,1] square {(0,0), (0,1), (1,0), (1,1)}. Further computations of this design are impossible in this setup without additional conditions.

| n | Equidistant | Factorial | LHS | Impr. LHS |
|---|---|---|---|---|
| 2 | 1.7616 | 2.1378 | 1.5883 | 1.4209 |
| 3 | 1.9242 | 2.1378 | 1.7496 | 1.7804 |
| 4 | 1.9645 | 2.1378 | 1.6522 | 1.6809 |
| 5 | 1.9797 | 2.1378 | 1.7203 | 1.8714 |
| 6 | 1.9869 | 2.1378 | 1.8007 | 1.8282 |
| 7 | 1.9908 | 2.1378 | 1.7953 | 1.8324 |
| 8 | 1.9933 | 2.1378 | 1.9036 | 1.9029 |
| 9 | 1.9948 | 2.1378 | 1.8871 | 1.8816 |
| 10 | 1.9959 | 2.1378 | 1.9135 | 1.9291 |
| 15 | 1.9983 | 2.1378 | 1.9773 | 2.0257 |
| 20 | 1.9991 | 2.1378 | 2.0223 | 2.0324 |
| 30 | 1.9996 | 2.1378 | 2.0668 | 2.0797 |
| 40 | 1.9998 | 2.1378 | 2.1189 | 2.1131 |
| 50 | 1.9999 | 2.1378 | 2.1100 | 2.1294 |
| 100 | 2.0000 | 2.1378 | 2.1742 | 2.1789 |

**Table 1.** FIM for different number of design points (n) and the introduced designs

In order to have a graphical overview of the development of FIM concerning the number of generated design points, the results are plotted in the Figures 1 and 2. Figure 1 shows that equidistant design leads to higher FIM with less than 15 design points. The calculated FIM for the two LHS designs are overtaking equidistant design at a threshold between 10 and 20 and keep increasing slightly. However, FIM for equidistant design is increasing rarely (from n = 10 to n = 100, $\Delta = 0.0041$; see Table 1), hence, the higher the number of observations the larger is the difference in terms of FIM to the other approaches. In Figure 2 we highlight the development of FIM for the first 15 observations which enables a comparison for the LHS designs with different optimization rules. Thereby, optimizing with respect to euclidean differences results in a higher Fisher information, however, the difference decreases with increasing observation numbers. Moreover, it is shown that more than 15 observations are needed to compute higher FIM from Latin Hypercube designs compared to equidistant design.

## 3 Computation and Comparison for different Parameters

Aim of this section is to emphasize the impact on Fisher information for the four introduced designs due to changes in the parameters, i.e. $\beta$ in the following simulation study.

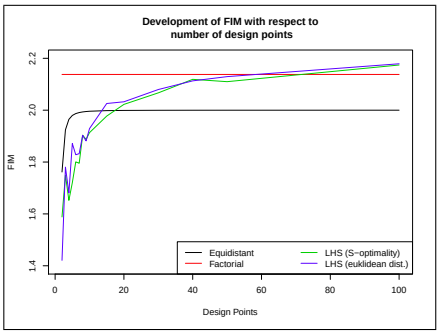


**Fig. 1.** Overall development of FIM for number of design Points

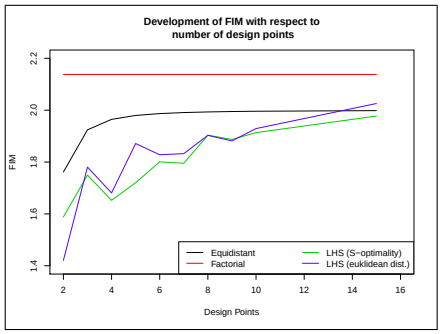


**Fig. 2.** Development of FIM for number of design points. Zoom to $2 \leq n \leq 15$

### 3.1 Analysis for $\alpha = 1$, $\beta = 10$, $\tilde{\sigma} = 1$

The values of the parameters $\alpha, \beta, \tilde{\sigma}$ have changed to 1, 10 and 1. Therefore, the effect of an increase in $\beta$ on the Fisher information can be observed. Moreover, this leads to the fact that the fraction in the correlation structure is unequal to 1. Table 2 and Figure 3 show the Fisher information calculated with the defined designs given the introduced change in $\beta$, which enables checking the four designs against each other and with respect to the number of observations. In this setup it can be seen that FIM is higher for the LHS designs than for equidistant design, beginning with 4 generated design points. Recall that for $\beta = 1$ the FIM of LHS designs overtake FIM of equidistant design with more than 15 observations. Hence, it can be assumed that an increase in $\beta$, ceteris paribus, leads to the fact that fewer observations (4 instead of 15 due to an increase of $\beta$ from 1 to 10) are needed to compute higher FIM for Latin Hypercube than for equidistant design. The differences between the two LHS approaches are rarely noticeable (not exceeding 0.04), wherefore in Figure 3 Latin Hypercube designs optimized with respect to euclidean difference also represent S-optimality. Moreover, the difference between LHS and equidistant design by comparing FIM is increasing with increasing number of design points.

### 3.2 Simulation Study for different $\beta$ and $n$

Table 3 shows the calculations of FIM for the introduced designs, where $\alpha$ respectively $\tilde{\sigma}$ are equal to 1 and $\beta$ uses every integer between 1 and 10. Hence, 10 calculations for every number of observations are necessary, whereby the first column for each designs is a calculation with $\beta = 2$. The purpose behind this sensitivity check is to see the impact of a misclassification of $\beta$, given the known true parameter is 2. The main result of this comparison is that an increase in $\beta$ leads to larger increases in LHS designs compared to equidistant design, regardless of the number of observation. Equidistant design leads to higher FIM for small numbers of design points, although, by increasing $\beta$ and $n$ one will compute higher FIM from Latin Hypercube designs. The underlying randomness in the computation of the LHS design points is responsible for the

| | Equidistant | factorial | LHS | Impr. LHS |
|---|---|---|---|---|
| 2 | 2.0000 | 3.9147 | 1.9866 | 1.9850 |
| 3 | 2.9837 | 3.9147 | 2.9192 | 2.9402 |
| 4 | 3.8505 | 3.9147 | 3.8603 | 3.8578 |
| 5 | 4.5193 | 3.9147 | 4.7733 | 4.7796 |
| 6 | 5.0025 | 3.9147 | 5.6652 | 5.6703 |
| 7 | 5.3459 | 3.9147 | 6.5539 | 6.5220 |
| 8 | 5.5918 | 3.9147 | 7.3766 | 7.3605 |
| 9 | 5.7710 | 3.9147 | 8.2137 | 8.1866 |
| 10 | 5.9042 | 3.9147 | 9.0017 | 8.9738 |
| 15 | 6.2335 | 3.9147 | 12.7110 | 12.7123 |
| 20 | 6.3514 | 3.9147 | 16.0476 | 16.0391 |
| 30 | 6.4350 | 3.9147 | 21.7060 | 21.7431 |
| 40 | 6.4638 | 3.9147 | 26.4036 | 26.4125 |
| 50 | 6.4770 | 3.9147 | 30.3338 | 30.3173 |
| 100 | 6.4943 | 3.9147 | 43.1648 | 43.1954 |

**Table 2.** FIM for different number of design points (n), $\alpha = 1$, $\beta = 10$, $\tilde{\sigma} = 1$

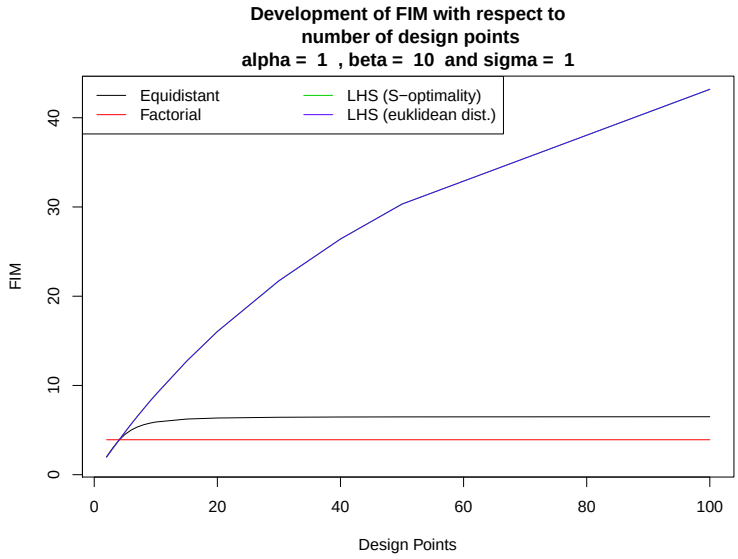


**Fig. 3.** Development of FIM for number of Design Points, $\alpha = 1$, $\beta = 10$, $\tilde{\sigma} = 1$

fact that in this simulation example 40 observations, defined as $n^*$, would be needed to compute higher FIM of LHS than for equidistant design, given $\beta = 1$. Increasing $\beta$ leads to a monotonic decrease in $n^*$ such that only 8 observations for $\beta = 2$ and solely 4 observations for $\beta = 10$ are needed.

Table 4 shows the calculated differences, defined as $\Delta$, between FIM with true parameters $\beta = 2, \alpha = 1$ and misclassifications of $\alpha = 1$ and $\beta = 1 - 10$ (except for 2). Obviously, larger differences are observed for larger deviations from the true parameter $\beta$. The same effect can be observed for increasing number of observations.

## 4 Conclusions

In this paper we illustrated that monotonic design should be taken as an interesting benchmark design for cases when researchers expect non-reversibility of time (process cannot step back in time). In fact we have seen that efficiencies for monotonic designs are comparable (if not better in certain setups) to the efficiency of space-filling designs. More discussion and statistical derivation can be found in Baran and Stehlík[1].

## 5 Acknowledgement

We acknowledge the support of the ANR project DESIRE FWF I 833-N18. First author also acknowledges FONDECYT Regular 2015, ingresada con el No1151441: "Statistical and mathematical modelling as a knowledge bridge between Society and Ecology Sustainability".

## References

1. S. Baran and M. Stehlík. Optimal designs for parameters of shifted Ornstein-Uhlenbeck sheets measured on monotonic sets, *Statistics and Probability Letters*, DOI: 10.1016/j.spl.2015.01.006, 2015.
2. S. Baran, K. Sikolya and M. Stehlík. On the optimal designs for prediction of Ornstein-Uhlenbeck sheets, *Statistics and Probability Letters*, 83, **6**, 1580–1587, 2013.
3. A. Boukouvalas, D. Cornford and M. Stehlík. Optimal Design for Correlated processes with input-dependent noise, *Computational Statistics and Data Analysis*, 71, 1088–1102, 2014.
4. H. Dette, J. Kunert and A. Pepelyshev. Exact optimal designs for weighted least squares analysis with correlated errors, *Statistica Sinica*, 18, 135–154, 2008.
5. J. Kiseľák and M. Stehlík. Equidistant D-optimal designs for parameters of Ornstein-Uhlenbeck process, *Statistics and Probability Letters*, 78, 1388–1396, 2008.
6. W.G. Müller and M. Stehlík. Compound optimal spatial designs, *Environmetrics*, 21, 354–364, 2010.
7. W.G. Müller and M. Stehlík. Issues in the Optimal Design of Computer Simulation Experiments, *Applied Stochastic Models in Business and Industry*, 25, 163–177, 2009.
8. J.M. Rodríguez-Díaz, T. Santos-Martín, H. Waldl, and M. Stehlík. Filling and D-optimal designs for the correlated Generalized Exponential models, *Chemometrics and Intelligent Laboratory Systems*, 114, 10–18, 2012.
9. M. Stehlík, J.M. Rodríguez-Díaz, W.G. Müller, and J. López-Fidalgo. Optimal allocation of bioassays in the case of parametrized covariance functions: an application in lung's retention of radioactive particles, *Test*, 17, 56–68, 2008.

| | Equi- | Factorial | | | | | | | | | | LHS with S-Optimality | | | | | | | | | | LHS with optimal euclidean distances | | | | | | | | | |
|---|---|---|---|---|---|---|---|---|---|---|---|---|---|---|---|---|---|---|---|---|---|---|---|---|---|---|---|---|---|---|---|
| n/$\beta$ | distant | 2 | 1 | 3 | 4 | 5 | 6 | 7 | 8 | 9 | 10 | 2 | 1 | 3 | 4 | 5 | 6 | 7 | 8 | 9 | 10 | 2 | 1 | 3 | 4 | 5 | 6 | 7 | 8 | 9 | 10 |
| 2 | 2.00 | 3.61 | 3.28 | 3.73 | 3.79 | 3.83 | 3.86 | 3.88 | 3.89 | 3.91 | 3.91 | 1.92 | 1.84 | 1.94 | 1.96 | 1.97 | 1.97 | 1.98 | 1.98 | 1.98 | 1.98 | 1.90 | 1.82 | 1.94 | 1.95 | 1.96 | 1.97 | 1.97 | 1.98 | 1.98 | 1.98 |
| 3 | 2.98 | 3.61 | 3.28 | 3.73 | 3.79 | 3.83 | 3.86 | 3.88 | 3.89 | 3.91 | 3.91 | 2.70 | 2.45 | 2.79 | 2.84 | 2.87 | 2.89 | 2.91 | 2.92 | 2.93 | 2.93 | 2.73 | 2.51 | 2.82 | 2.86 | 2.89 | 2.91 | 2.92 | 2.93 | 2.94 | 2.94 |
| 4 | 3.85 | 3.61 | 3.28 | 3.73 | 3.79 | 3.83 | 3.86 | 3.88 | 3.89 | 3.91 | 3.91 | 3.39 | 2.94 | 3.57 | 3.67 | 3.73 | 3.77 | 3.80 | 3.83 | 3.84 | 3.86 | 3.40 | 2.96 | 3.58 | 3.68 | 3.74 | 3.78 | 3.81 | 3.83 | 3.85 | 3.86 |
| 5 | 4.52 | 3.61 | 3.28 | 3.73 | 3.79 | 3.83 | 3.86 | 3.88 | 3.89 | 3.91 | 3.91 | 4.02 | 3.36 | 4.30 | 4.45 | 4.55 | 4.62 | 4.67 | 4.71 | 4.74 | 4.77 | 4.03 | 3.37 | 4.31 | 4.46 | 4.56 | 4.63 | 4.68 | 4.72 | 4.75 | 4.77 |
| 6 | 5.00 | 3.61 | 3.28 | 3.73 | 3.79 | 3.83 | 3.86 | 3.88 | 3.89 | 3.91 | 3.91 | 4.67 | 3.82 | 5.04 | 5.25 | 5.38 | 5.48 | 5.55 | 5.60 | 5.64 | 5.68 | 4.65 | 3.80 | 5.03 | 5.24 | 5.37 | 5.47 | 5.54 | 5.59 | 5.64 | 5.67 |
| 7 | 5.35 | 3.61 | 3.28 | 3.73 | 3.79 | 3.83 | 3.86 | 3.88 | 3.89 | 3.91 | 3.91 | 5.12 | 4.04 | 5.63 | 5.92 | 6.10 | 6.24 | 6.34 | 6.41 | 6.47 | 6.52 | 5.12 | 4.05 | 5.63 | 5.92 | 6.10 | 6.24 | 6.34 | 6.41 | 6.47 | 6.52 |
| 8 | 5.59 | 3.61 | 3.28 | 3.73 | 3.79 | 3.83 | 3.86 | 3.88 | 3.89 | 3.91 | 3.91 | 5.67 | 4.40 | 6.28 | 6.64 | 6.87 | 7.04 | 7.16 | 7.25 | 7.33 | 7.39 | 5.63 | 4.36 | 6.25 | 6.61 | 6.85 | 7.02 | 7.14 | 7.24 | 7.31 | 7.38 |
| 9 | 5.77 | 3.61 | 3.28 | 3.73 | 3.79 | 3.83 | 3.86 | 3.88 | 3.89 | 3.91 | 3.91 | 5.97 | 4.48 | 6.73 | 7.18 | 7.48 | 7.70 | 7.86 | 7.99 | 8.09 | 8.17 | 6.01 | 4.52 | 6.75 | 7.20 | 7.50 | 7.71 | 7.87 | 8.00 | 8.10 | 8.18 |
| 10 | 5.90 | 3.61 | 3.28 | 3.73 | 3.79 | 3.83 | 3.86 | 3.88 | 3.89 | 3.91 | 3.91 | 6.42 | 4.74 | 7.29 | 7.82 | 8.17 | 8.43 | 8.62 | 8.77 | 8.89 | 8.99 | 6.44 | 4.77 | 7.30 | 7.83 | 8.18 | 8.44 | 8.63 | 8.78 | 8.90 | 9.00 |
| 15 | 6.23 | 3.61 | 3.28 | 3.73 | 3.79 | 3.83 | 3.86 | 3.88 | 3.89 | 3.91 | 3.91 | 7.94 | 5.42 | 9.41 | 10.38 | 11.06 | 11.56 | 11.95 | 12.26 | 12.52 | 12.73 | 7.94 | 5.43 | 9.41 | 10.38 | 11.05 | 11.56 | 11.95 | 12.26 | 12.52 | 12.73 |
| 20 | 6.35 | 3.61 | 3.28 | 3.73 | 3.79 | 3.83 | 3.86 | 3.88 | 3.89 | 3.91 | 3.91 | 9.02 | 5.86 | 11.03 | 12.42 | 13.44 | 14.21 | 14.82 | 15.32 | 15.73 | 16.07 | 8.97 | 5.82 | 10.97 | 12.36 | 13.38 | 14.16 | 14.77 | 15.27 | 15.68 | 16.03 |
| 30 | 6.43 | 3.61 | 3.28 | 3.73 | 3.79 | 3.83 | 3.86 | 3.88 | 3.89 | 3.91 | 3.91 | 10.40 | 6.35 | 13.27 | 15.40 | 17.05 | 18.37 | 19.44 | 20.34 | 21.09 | 21.73 | 10.44 | 6.40 | 13.29 | 15.42 | 17.07 | 18.38 | 19.45 | 20.34 | 21.10 | 21.74 |
| 40 | 6.46 | 3.61 | 3.28 | 3.73 | 3.79 | 3.83 | 3.86 | 3.88 | 3.89 | 3.91 | 3.91 | 11.26 | 6.63 | 14.75 | 17.49 | 19.70 | 21.51 | 23.02 | 24.30 | 25.41 | 26.37 | 11.30 | 6.68 | 14.79 | 17.52 | 19.72 | 21.53 | 23.04 | 24.32 | 25.42 | 26.38 |
| 50 | 6.48 | 3.61 | 3.28 | 3.73 | 3.79 | 3.83 | 3.86 | 3.88 | 3.89 | 3.91 | 3.91 | 11.93 | 6.88 | 15.92 | 19.15 | 21.82 | 24.07 | 25.98 | 27.63 | 29.07 | 30.34 | 11.95 | 6.92 | 15.92 | 19.14 | 21.81 | 24.05 | 25.95 | 27.60 | 29.04 | 30.30 |
| 100 | 6.49 | 3.61 | 3.28 | 3.73 | 3.79 | 3.83 | 3.86 | 3.88 | 3.89 | 3.91 | 3.91 | 13.47 | 7.38 | 18.79 | 23.48 | 27.66 | 31.40 | 34.78 | 37.84 | 40.62 | 43.16 | 13.55 | 7.45 | 18.86 | 23.55 | 27.72 | 31.46 | 34.83 | 37.88 | 40.66 | 43.20 |

**Table 3.** FIM for different number of design points and different beta

| | Equi- | Factorial | | | | | | | | | | LHS with S-Optimality | | | | | | | | | | LHS with optimal euclidean distances | | | | | | | | | |
|---|---|---|---|---|---|---|---|---|---|---|---|---|---|---|---|---|---|---|---|---|---|---|---|---|---|---|---|---|---|---|---|
| n/$\beta$ | distant | 2 | 1 | 3 | 4 | 5 | 6 | 7 | 8 | 9 | 10 | 2 | 1 | 3 | 4 | 5 | 6 | 7 | 8 | 9 | 10 | 2 | 1 | 3 | 4 | 5 | 6 | 7 | 8 | 9 | 10 |
| 2 | 2.00 | 3.61 | -0.32 | 0.12 | 0.19 | 0.23 | 0.25 | 0.27 | 0.29 | 0.30 | 0.31 | 1.92 | -0.08 | 0.03 | 0.04 | 0.05 | 0.05 | 0.06 | 0.06 | 0.06 | 0.07 | 1.90 | -0.09 | 0.03 | 0.05 | 0.06 | 0.06 | 0.07 | 0.07 | 0.07 | 0.08 |
| 3 | 2.98 | 3.61 | -0.32 | 0.12 | 0.19 | 0.23 | 0.25 | 0.27 | 0.29 | 0.30 | 0.31 | 2.70 | -0.25 | 0.09 | 0.14 | 0.17 | 0.20 | 0.21 | 0.22 | 0.23 | 0.24 | 2.73 | -0.22 | 0.08 | 0.13 | 0.15 | 0.17 | 0.18 | 0.19 | 0.20 | 0.21 |
| 4 | 3.85 | 3.61 | -0.32 | 0.12 | 0.19 | 0.23 | 0.25 | 0.27 | 0.29 | 0.30 | 0.31 | 3.39 | -0.45 | 0.18 | 0.28 | 0.34 | 0.39 | 0.42 | 0.44 | 0.46 | 0.47 | 3.40 | -0.44 | 0.18 | 0.27 | 0.34 | 0.38 | 0.41 | 0.43 | 0.45 | 0.46 |
| 5 | 4.52 | 3.61 | -0.32 | 0.12 | 0.19 | 0.23 | 0.25 | 0.27 | 0.29 | 0.30 | 0.31 | 4.02 | -0.66 | 0.28 | 0.44 | 0.54 | 0.61 | 0.66 | 0.70 | 0.73 | 0.75 | 4.03 | -0.65 | 0.28 | 0.43 | 0.53 | 0.60 | 0.65 | 0.69 | 0.72 | 0.74 |
| 6 | 5.00 | 3.61 | -0.32 | 0.12 | 0.19 | 0.23 | 0.25 | 0.27 | 0.29 | 0.30 | 0.31 | 4.67 | -0.85 | 0.37 | 0.58 | 0.72 | 0.81 | 0.88 | 0.93 | 0.98 | 1.01 | 4.65 | -0.85 | 0.38 | 0.59 | 0.72 | 0.82 | 0.89 | 0.94 | 0.99 | 1.02 |
| 7 | 5.35 | 3.61 | -0.32 | 0.12 | 0.19 | 0.23 | 0.25 | 0.27 | 0.29 | 0.30 | 0.31 | 5.12 | -1.08 | 0.50 | 0.79 | 0.98 | 1.11 | 1.21 | 1.29 | 1.35 | 1.40 | 5.12 | -1.08 | 0.50 | 0.79 | 0.98 | 1.11 | 1.21 | 1.29 | 1.35 | 1.40 |
| 8 | 5.59 | 3.61 | -0.32 | 0.12 | 0.19 | 0.23 | 0.25 | 0.27 | 0.29 | 0.30 | 0.31 | 5.67 | -1.27 | 0.61 | 0.96 | 1.20 | 1.36 | 1.49 | 1.58 | 1.66 | 1.72 | 5.63 | -1.28 | 0.61 | 0.97 | 1.21 | 1.38 | 1.51 | 1.60 | 1.68 | 1.74 |
| 9 | 5.77 | 3.61 | -0.32 | 0.12 | 0.19 | 0.23 | 0.25 | 0.27 | 0.29 | 0.30 | 0.31 | 5.97 | -1.50 | 0.75 | 1.21 | 1.51 | 1.72 | 1.89 | 2.01 | 2.11 | 2.20 | 6.01 | -1.48 | 0.75 | 1.19 | 1.49 | 1.71 | 1.87 | 1.99 | 2.09 | 2.17 |
| 10 | 5.90 | 3.61 | -0.32 | 0.12 | 0.19 | 0.23 | 0.25 | 0.27 | 0.29 | 0.30 | 0.31 | 6.42 | -1.68 | 0.87 | 1.40 | 1.75 | 2.01 | 2.20 | 2.35 | 2.48 | 2.57 | 6.44 | -1.67 | 0.86 | 1.39 | 1.74 | 2.00 | 2.19 | 2.34 | 2.46 | 2.56 |
| 15 | 6.23 | 3.61 | -0.32 | 0.12 | 0.19 | 0.23 | 0.25 | 0.27 | 0.29 | 0.30 | 0.31 | 7.94 | -2.52 | 1.47 | 2.43 | 3.11 | 3.62 | 4.01 | 4.32 | 4.58 | 4.79 | 7.94 | -2.51 | 1.47 | 2.43 | 3.11 | 3.62 | 4.01 | 4.32 | 4.57 | 4.78 |
| 20 | 6.35 | 3.61 | -0.32 | 0.12 | 0.19 | 0.23 | 0.25 | 0.27 | 0.29 | 0.30 | 0.31 | 9.02 | -3.17 | 2.01 | 3.40 | 4.41 | 5.19 | 5.80 | 6.29 | 6.70 | 7.05 | 8.97 | -3.15 | 2.00 | 3.39 | 4.41 | 5.19 | 5.80 | 6.30 | 6.71 | 7.06 |
| 30 | 6.43 | 3.61 | -0.32 | 0.12 | 0.19 | 0.23 | 0.25 | 0.27 | 0.29 | 0.30 | 0.31 | 10.40 | -4.05 | 2.87 | 5.00 | 6.66 | 7.97 | 9.05 | 9.94 | 10.69 | 11.33 | 10.44 | -4.04 | 2.86 | 4.99 | 6.64 | 7.95 | 9.02 | 9.91 | 10.66 | 11.30 |
| 40 | 6.46 | 3.61 | -0.32 | 0.12 | 0.19 | 0.23 | 0.25 | 0.27 | 0.29 | 0.30 | 0.31 | 11.26 | -4.62 | 3.50 | 6.24 | 8.44 | 10.25 | 11.76 | 13.05 | 14.15 | 15.11 | 11.30 | -4.62 | 3.49 | 6.22 | 8.42 | 10.23 | 11.74 | 13.02 | 14.12 | 15.08 |
| 50 | 6.48 | 3.61 | -0.32 | 0.12 | 0.19 | 0.23 | 0.25 | 0.27 | 0.29 | 0.30 | 0.31 | 11.93 | -5.05 | 3.99 | 7.22 | 9.89 | 12.14 | 14.05 | 15.70 | 17.14 | 18.41 | 11.95 | -5.03 | 3.97 | 7.19 | 9.85 | 12.09 | 14.00 | 15.65 | 17.09 | 18.35 |
| 100 | 6.49 | 3.61 | -0.32 | 0.12 | 0.19 | 0.23 | 0.25 | 0.27 | 0.29 | 0.30 | 0.31 | 13.47 | -6.09 | 5.32 | 10.01 | 14.19 | 17.93 | 21.31 | 24.36 | 27.15 | 29.69 | 13.55 | -6.10 | 5.31 | 10.00 | 14.17 | 17.91 | 21.27 | 24.33 | 27.10 | 29.65 |

**Table 4.** Differences in FIM for different number of design points and different beta compared to calculation with "true parameter" $\beta = 2$, $\alpha = 1$

# BIBD, Hadamard Matrices and Risk Of Data Loss on QR Codes

Carla Francisco[1] and Teresa A. Oliveira[1,2]

[1] Departamento de Ciências e Tecnologia, Universidade Aberta, Portugal
(E-mail: carlasusete@hotmail.com)
[2] Centro de Estatística e Aplicações, Universidade de Lisboa
(E-mail: teresa.oliveira@uab.pt)

**Abstract** Experimental design with blocks was first presented by Sir Ronald A. Fisher in the beginning of the $20^{th}$ century, considering applications in agriculture. It became one of the areas of mass development for research in various fields, from agriculture to medicine, playing a central role not only on the research process but also on the new technological advances.

As a branch of block designs, research on Balanced Incomplete Block Designs (BIBD) arose several interesting and defying problems within combinatory mathematics.

BIBD designs can be constructed and analysed more easily with the aid of computer tools, such as the The R Project for Statistical Computing, which, as will be shown, contains several different tools just for this purpose.

Hadamard matrices are present in our daily life, they give rise to a class of block designs named Hadamard configurations. It is easy and current to find their different applications based on new technologies and codes of figures such as Quick Response Codes (QR Codes). These are bi-dimensional bar codes that can be easily read by common devices which have image capture function, such as mobile phones. The use of such codes is very popular nowadays in simple things like to send a simple text message, a picture or for a batch of information regarding a product or more.

Risk is the potential of losing something of value, weighed against the potential to gain something of value. There are several types of risk, one of them is the information loss for QR Codes and that will be presented in this paper. QR Codes can get damaged, and their data can be lost. Data recovery mechanisms for QR Codes are implemented as a compromise between error correction level and data storage capacity. The more the recovery capability the less data that can be stored. Connections between the various methodologies and QR Codes will be discussed.

**Keywords:** BIBD, R Statistics, Hadamard Matrices, Quick Response Codes (QR Codes), Risk.

*Stochastic Modeling, Data Analysis and Statistical Applications* (*pp.* 333-345)
Lidia Filus - Teresa Oliveira - Christos H Skiadas (Eds)



## 1 Introduction

Jacques Salomon Hadamard was a french mathematician that during his life has tirelessly published papers and books of high quality. One of the works for which he is remembered is the Hadamard matrices.

The foundations of block designs were laid down by *Sir* Ronald Fisher in the early 1930's. It became one of the areas of mass development for research in various fields from agriculture to medicine, as well as to other areas of research.

Following his seminar work, several techniques were presented in order to analyse data and to present new kinds of designs of experiments.

Research on block designs began with randomized block designs which play an important role in the design and analysis of experiments, see e.g., Caliński & Kageyama (2000)[3], (2003)[4], Research in this area was followed by developments considering Incomplete Block Designs (IBD). Balanced Incomplete Block Designs (BIBD) and Partially Balanced Incomplete Block Designs (PBIBD). The adjective incomplete refers to the block size ($k$) and the variety set ($v$), with $k < v$, while balanced refers to each pair of varieties occurring in the same number of blocks. In BIBD every pair of varieties concur in the same number of blocks. A review of some main concepts associated to BIBD will be presented.

The Hadamard matrices are a class of matrices introduced by Jacques Hadamard in 1893. In this class of matrices, entries are $+1$ and $-1$ so that rows are mutually orthogonal. A Hadamard matrix, $\mathbf{H}$, is said to be skewed if the relation $\mathbf{H}^\top + \mathbf{H} = 2\mathbf{I}$ holds, where $\mathbf{H}^\top$ stands for the matrix transpose of $\mathbf{H}$ and $\mathbf{I}$ represents the identity matrix. Besides this condition, the matrix rows are mutually orthogonal, which will have direct impact to their use, namely if one thinks in geometric terms, this means that every pair of rows $(i, j)$, with $i \neq j$, will represent two perpendicular vectors. To better understand these matrices the concept of tensors is crucial. These are geometrical entities introduced in mathematics and physics to generalize the notion of scalars, vectors and matrices. A tensor is a form of representation associated with a set of operations like sum and product. A finite body with $q$ elements is denominated a Galois Field, $GF(q)$. If the order of $a$ is $q - 1$ then $a$ is a primitive element of $GF(q)$.

The notation BIBD $(v, b, r, k, \lambda|b^*)$ is used to describe a BIBD $(v, b, r, k, \lambda)$ with precisely $b^*$ distinct blocks. Oliveira (2010)[15] presents some developments on this matter.

The most primeval of all block designs is the completely randomized design (complete blocks design). However, in many practical situations, the adoption of a design like that is not appropriate and in some cases, is not at all feasible. This fact led to the development of various types of incomplete block designs, which in turn have been used extensively for experiments in many areas. It was observed by Fisher that the random allocation of treatments to experimental units, eliminates the bias in the evaluation of differences between treatments. In certain experimental situations there may exist systematic variations present in the experimental units.

For example, in an agricultural field experiment, the experimental units are typically ground portions (parcels). In this kind of experiment, there may be a

fertility gradient such that portions having the same level of fertility are more homogeneous than those which have a different level of fertility. In experiments with pigs, which were considered the experimental unit, it is very likely that the pigs belonging to the same litter are genetically closer to each other than those belonging to different litters. Similarly, in experiments with cattle, several breeds may be involved and animals that belong to the same race are expected to be statistically more similar than those belonging to different races. In clinical trials with patients, these form the experimental units. The assays can be performed in different centers, and patients in the same center may be more similar than those from other centers due to differences in treatment practices and management procedures followed in different centers. In the situations of the previous examples using totally random experimental design is not appropriate. In fact one must take advantage of *a priori* information about the systematic variations, so that this information can be used to eliminate the effect of this variability, which will be reflected in a smaller experimental error, thus increasing the accuracy of the experiment. Incomplete block designs are used when it is impractical to use all treatments in each block. In incomplete block designs no variety occurs more than once in the same block. Due to the wide application of experimental design using incomplete block designs on areas of cutting edge research, and also on many questions still open in the theoretical framework, these designs are of particular interest.

The QR Codes are two-dimensional barcodes that can be easily read by a device capable of image capture, as is the case of most existing mobile phones. These codes can represent text, an address for a web site (URL), a phone number, a geo-referenced location, an email, a contact or an SMS. They were initially used for cataloging parts in vehicle production. Nowadays many QR codes are used for several different tasks such as inventory management and stock control, from industry to trade. Recently mobile applications, were developed so that they can allow their users to read these codes using a camera phone. QR Codes are common in magazines and advertisements, where they are used to encode different kinds of information, or for instance to provide contact information, as detailed as if they were a personal or business card. QR Codes have become a focus of advertising companies, since they provide an effortless way to access the advertised brand's website. On a personal computer these codes can be read with the aid of a scanner. QR codes have, as the base of their error correcting structure, Hadamard matrices.

## 2 Objectives

This paper proposes to illustrate error correction on QR Codes through the use of Hadamard matrices as error correction promoters and their connection to incomplete block designs.

These Hadamard matrices form an important part of the family of error correction codes, denominated ReedMuller codes. These are used in practice on the QR Codes, CDs, DVDs, DSL internet, digital tape devices, digital tv and satellite transmission of signals. This paper will focus in particular on the error correction applied to QR Codes.

In the next section will be presented the basic foundations of BIB designs, followed by a review of Paley Hadamard matrices and how these two are related. Then it will be illustrated how these matrices are used on the Reed-Solomon error correction code, and how these apply to QR Code error correction. Some examples will be presented.

## 3 BIBD and R Project for Statistical Computing

A Balanced Incomplete Block Design is an arrangement of $v$ treatments (varieties) in $b$ blocks, each of size $k(< v)$, where each variety occur exactly $r$ times and every pair of varieties concur in exactly $\lambda$ blocks. The necessary, but not sufficient conditions for the existence of a BIBD are:

$$\begin{cases} v < b \\ vr = bk \\ \lambda(v-1) = r(k-1) \end{cases}$$

A balanced incomplete block design consists of five parameters, such that:

$v$ represents the number of varieties
$b$ represents the number of blocks
$r$ is the number of occurrences of each variety
$k$ the block length
$\lambda$ the number of blocks each pair occurs in

In order to generate balanced incomplete block designs with the aid of the computational statistical program 'R', we can use the extra 'package', 'crossdes'. This 'package' includes several functions that assist in building balanced designs. Each BIBD produced with the aid of this 'package', has five parameters described above. To install the 'package' the command 'install.packages ("crossdes")' is used. To load the 'package' in order to be able to use the functions contained herein, the command 'library ("crossdes")' is used. The 'find.BIB' function is used to generate a block design with a specific number of treatments, blocks (which correspond to the lines of the generated plan) and elements per block (corresponding to the columns of the generated plan). It is also possible to use another function to test if the generated plan meets the conditions to be a BIBD. For instance, to create a design with five treatments in four blocks of three elements the function is as follows:

> find.BIB(5, 4, 3)

The R output is:

```
     [,1] [,2] [,3]
[1,]    2    3    5
[2,]    1    2    4
[3,]    3    4    5
[4,]    1    3    5
```

**Figure1.** Output of instruction find.BIB(5,4,3).

The resulting structure is not a BIBD because the treatments are not all repeated the same number of times. This observation can be confirmed by using the 'isGYD' function as follows: 'isGYD (find.BIB (5, 4, 3))'. The result of executing this function in 'R' is:

```
> isGYD(find.BIB(5, 4, 3))

[1] The design is neither balanced w.r.t. rows nor w.r.t. columns.
```

**Figure2.** Output of instruction isGYD(find.BIB(5,4,3)).

Consider now another example, this time with seven treatments and seven blocks of three elements:

```
> other.plan = find.BIB(7,7,3)
> other.plan
     [,1] [,2] [,3]
[1,]    1    2    6
[2,]    3    5    6
[3,]    4    6    7
[4,]    2    3    7
[5,]    1    3    4
[6,]    2    4    5
[7,]    1    5    7
```

**Figure3.** Output of instruction find.BIB(7,7,3)

It is confirmed through the use of the 'isGYD' function that this experimental design is indeed a BIBD:

```
> isGYD(find.BIB(7,7,3))

[1] The design is a balanced incomplete block design w.r.t. rows.
```

**Figure4.** Output of instruction isGYD(find.BIB(7,7,3)).

Another useful 'package' to generate outlines plans for balanced incomplete block designs, is the 'dae'. As the one above, this package has several different functions targeted to aid in obtaining experimental designs. The following example illustrates the use of one of the features of "dae", the "fac.layout " to generate an experiment of balanced incomplete block design consisting of randomized factors:

```
> BIBD.unit<-list(Blocks=4, Plots=3)
> BIBD.nest<-list(Plots="Blocks")
> Treats<-factor(c(1,2,3, 1,2,4, 1,3,4, 2,3,4), labels=c("A","B","C","D"))
> BIBD.lay<-fac.layout(unrandomized=BIBD.unit, nested.factors=BIBD.nest,
  randomized=Treats, seed=987)
> BIBD.lay
   Units Permutation Blocks Plots Treats
1      1           2      1     1      C
2      2           3      1     2      A
3      3           1      1     3      B
4      4          10      2     1      B
5      5          12      2     2      C
6      6          11      2     3      D
7      7           9      3     1      C
8      8           7      3     2      D
9      9           8      3     3      A
10    10           4      4     1      A
11    11           5      4     2      D
12    12           6      4     3      B
>
```

**Figure5.** Randomized factors BIBD with 3 treatments and 4 blocks.

A page from CRAN - The Comprehensive R Archive Network, aggregates all the existing information about the various 'packages' related to experimental design with the aid of the 'R'. This page can be found at the url: http://cran.r-project.org/web/views/ExperimentalDesign.html. This page presents first the general-purpose packages and proceeds to those that perform more specific tasks such as the ones used in the design of experiments for agriculture, industry and clinical trials among others.

## 4 Hadamard Matrices

A Hadamard matrix is a square matrix $\mathbf{H}_n$ of order $n$ with entries $\pm 1$ if $\mathbf{H}_n\mathbf{H}_n^\top = n\mathbf{I}_n$. If $\mathbf{H}_n$ is Hadamard matrix then $\mathbf{H}_n\mathbf{H}_n^\top = n\mathbf{I}_n$. A Hadamard matrix remains so when any row or column is multiplied by $-1$. Having this into consideration, one can always write a Hadamard matrix with its first row and first column having only $+1$'s, that it is a normal form an Hadamard matrix.

If, $\mathbf{H}_n$ exists for $n = 1$ then $\mathbf{H}_2$, can be written like the one bellow:

$\mathbf{H}_2 = \begin{bmatrix} 1 & 1 \\ 1 & -1 \end{bmatrix}$.

More examples of Hadamard Matrices:

$$\mathbf{H}_4 = \left[\begin{array}{cc|cc} 1 & 1 & 1 & 1 \\ 1 & -1 & 1 & -1 \\ \hline 1 & 1 & -1 & -1 \\ 1 & -1 & -1 & 1 \end{array}\right]; \mathbf{H}_8 = \left[\begin{array}{cccc|cccc} 1 & 1 & 1 & 1 & 1 & 1 & 1 & 1 \\ 1 & -1 & 1 & -1 & 1 & -1 & 1 & -1 \\ 1 & 1 & -1 & -1 & 1 & 1 & -1 & -1 \\ 1 & -1 & -1 & 1 & 1 & -1 & -1 & 1 \\ \hline 1 & 1 & 1 & 1 & -1 & -1 & -1 & -1 \\ 1 & -1 & 1 & -1 & -1 & 1 & -1 & 1 \\ 1 & 1 & -1 & -1 & -1 & -1 & 1 & 1 \\ 1 & -1 & -1 & 1 & -1 & 1 & 1 & -1 \end{array}\right]$$

$4 \times 4$ Hadamard matrix $\qquad$ $8 \times 8$ Hadamard matrix

The necessary condition for the existence of a Hadamard matrix $\mathbf{H}_n$, $n > 2$ is that $n \equiv 0(mod 4)$; more about this can be found on Hall (1986)[7]. Hadamard matrices for all permissible values of $n \leq 100$, with the exception of $n = 92$ can be found on Plackett and Burman (1946)[16]. Only later on Baumert et al. (1962)[1], presented a Hadamard matrix of order 92.

According to Hedayat and Wallis (1978)[8] and Sawade (1985)[19] Hadamard matrices have their existence confirmed for all permissible values of $n \leq 424$. If $\mathbf{H}_m$ and $\mathbf{H}_n$ are Hadamard matrices of orders $m$ e $n$, respectively, then their tensor product $\mathbf{H}_m \otimes \mathbf{H}_n$ is a Hadamard matrix of order $mn$. So, in particular, a Hadamard matrix $\mathbf{H}_n$ of order $n$ where $n = 2s$ and $s \geq 2$ is an integer, can be built by taking the $s$-fold tensor product of $\mathbf{H}_2$ with itself, as it is given above:

$$\mathbf{H}_{2^s} = \underbrace{\mathbf{H}_2 \otimes \mathbf{H}_2 \otimes \cdots \otimes \mathbf{H}_2}_{s \text{ times}}$$

## 5 Relationship between Hadamard matrices and BIBD

Consider a Hadamard matrix $\mathbf{H}_{4u}$, which without loss of generality, is assumed to be in its normal form. Delete from $\mathbf{H}_{4u}$, its first row and first column of all ones to obtain a matrix $\mathbf{A}$ of order $(4u-1) \times (4u-1)$.

Define, $\mathbf{N} = \frac{1}{2}(\mathbf{A} + \mathbf{J}_{4u-1})$.

This means that $\mathbf{N}$ is obtained from $\mathbf{A}$, by replacing the $-1$'s in $\mathbf{A}$ by zero and keeping $+1$'s unaltered. Then, it is not hard to see that $\mathbf{N}$ is the incidence matrix of a BIB design with parameters:

$$v = 4u - 1 = b \; ; \; r = 2u - 1 = k \; ; \; \lambda = u - 1 \tag{1}$$

Conversely, if $\mathbf{M}$ is the incidence matrix of a BIB design with parameters given by (1), then by replacing the zeros in $\mathbf{M}$ by $-1$ and bordering the resultant matrix by a row and column of all ones, a Hadamard matrix of order $4u$ is obtained.

**Theorem 1.** *The existence of a Hadamard matrix of order* $4u$ *is equivalent to the existence of a BIB design with parameters given by (1).*

Example 1 - Consider a Hadamard matrix $\mathbf{H}_{16}$ which can be obtained by forming the tensor product $\mathbf{H}_4 \otimes \mathbf{H}_4$, where $\mathbf{H}_4$ is as below:

$$\mathbf{H}_4 = \begin{bmatrix} 1 & 1 & 1 & 1 \\ 1 & -1 & 1 & -1 \\ 1 & 1 & -1 & -1 \\ 1 & -1 & -1 & 1 \end{bmatrix}$$

Following the construction method described above, a solution of a BIBD structure with parameters $v = 15 = b$, $r = 7 = k$, $\lambda = 3$ is obtained.

## 6 Application of Hadamard Matrices to Error Correction

ReedMuller codes are a family of linear error-correcting codes used in communications. Special cases of ReedMuller codes include the Hadamard code, the Walsh-Hadamard code and the ReedSolomon code.

The Hadamard code is an error-correcting code that is used for error detection and correction when transmitting messages over very noisy or unreliable channels. A famous application of the Hadamard code was the NASA space probe Mariner 9 in 1971, where the code was used to transmit photos of Mars back to Earth.

Generalized Hadamard codes are obtained from a $n \times n$ Hadamard matrix $\mathbf{H}$. To obtain a code over the alphabet $\{0, 1\}$, the mapping $1 \mapsto 1$, $1 \mapsto 0$, or, equivalently, $x \mapsto (1x)/2$, is applied to the matrix elements.

To get the punctured Hadamard code with $n = 2^{k-1}$ the chosen Hadamard matrix $\mathbf{H}$ has to be of Sylvester type, which gives rise to a message length of $\log_2(2n) = k$. QR-Codes contain codewords that are 8 bits long and use the ReedSolomon error correction algorithm with four different error correction levels. The higher the error correction level, the less the available storage capacity there is.

The Reed-Solomon algorithm was created by Irving Reed and Gustave Solomon, both engineers at MIT's Lincoln Labs. It was published in the paper: "Polynomial Codes over Certain Finite Fields". Reed-Solomon codes are of the

same family of error correcting codes as the Hadamard codes. The rows of a $k \times v$ generating matrix, for a generalised Reed Solomon (RS) code $GR_k(c, 1)$, where $c = (1, c, \ldots, c^{v-1})$ for some $c \in GF(q)$, of order $v$, are rows of a cocyclic matrix. For $v = p$, an odd prime number, the resulting Reed-Solomon codes are cocyclic Hadamard codes. Reed-Solomon codes are thus closely related to Hadamard matrices as well.

## 7 Risk

Risk is a probability or threat of damage, injury, liability, loss, or any other negative occurrence that is caused by external or internal vulnerabilities, and that might be avoided through a preemptive action. There are several types of risk, meaning different classes or various forms of risk such as, project risk which are the factors that could cause a project to fail, business risk which are associated with the level of exposure a business will face if a project fails, production system risk which considers the running costs of a project, economic risk which can be manifested in lower incomes or higher expenditures than expected, health, safety, and environmental risk even though these are separate areas, they are often linked because a single risk event may have impacts in all these three areas. Other types of risk are security risk which concerns the protection of assets from harm caused by deliberate acts and information technology and information security risk, among many others. The one that concerns QR Codes the most, is the information security risk in its area of information loss risk. Here, information loss risk refers to the problematic of losing important data, contained in the QR Code.

Risk assessment is the process of identifying potential hazards and analyze what could happen if a hazard occurs. A hazard is a recognized threat. Therefore risk assessment is the determination of quantitative or qualitative value of risk related to a concrete situation and a recognized threat. There are various methods for performing risk assessment, however there is one believed to be the most straightforward for most organisations. This method consists of five steps: identify the hazards, decide who might be harmed and how, evaluate the risks and decide on precaution, record the findings and implement them and the final step is to review the assessment and update it if necessary.

For QR Codes there is a significant risk of damage and therefore risk of loss of the information contained in it. As an exemplification a risk assessment can be determined for a QR Code. This particular QR Code is assumed to be part of a publicity campaign and it is assumed to be exposed to the elements, therefore the chance of damage to this code is enlarged. Here the exposure factor is assumed to be .30, meaning the code endures a damage of 30%. The asset is assumed to be really valuable for the company conducting the publicity campain, therefore the single loss expectancy or SLE is, considering the previous factors, also high. Therefore it is really important to try and maintain the information contained on the QR Code as retrievable as possible,even under this risky conditions. To prevent the loss of information on this QR Code a greater error correction level should be used when the code is created. As said previously there are four levels of error correction that can be used: Level L −

up to 7% damage, Level M − up to 15% damage, Level Q − up to 25% damage and Level H − up to 30% damage. This values are described on the ISO/IEC 18004:2000(E) setion 8.5.1, table 12[20]. In this conditions where the QR Code is exposed to the environmental elements, such as rain, wind, sun, dirt, etc. the H level should be used, so even though there was 30% of damage to this QR Code, the information contained in it would still be totally readable. Examples of damaged QR Codes are presented in figures 6., 7. and 8. As such, when creating QR Codes for example for business cards, the chances of it getting dirty are rather low and it is desirable to have a QR code as small as possible. Here a standard 7% error threshold is enough and very suitable for cards and other printed matter. However if QR codes are going to be used outdoors, on cars and trucks or any place where data may be obscured by dirt then setting the error correction to a higher setting is advisable. Unfortunately the higher the error correction level that is used the less information that can be written on to the QR Code. So there is a compromise between risk mitigation and information providing.

**Figure6.** QR Code exposed to the environmental elements

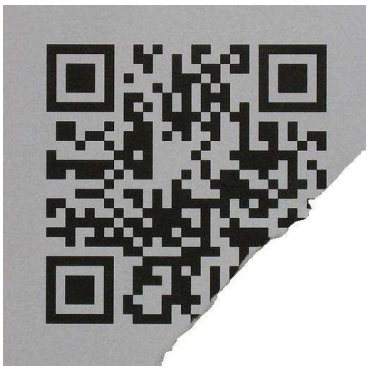

**Figure7.** Damaged QR code, is still decodable thanks to error correction. Image source: WikiPedia.

**Figure8.** Another example of a damaged QR Code.

This QR code contains the url to the SMTDA Conference, even with the paint on it, the code is still readable.

## 8 Final considerations and Conclusions

This work explores connections between BIBD, Hadamard matrices and QR Codes. Nowadays BIB Designs find the most diverse applications in various fields and it is important to explore new applications and also to improve the existing ones using this knowledge area as a new challenge to innovation. Hadamard matrices are of extreme importance and we can find them in various aspects of our daily life. It is quite easy and current to see their different applications based on new technologies mainly on computational level. QR codes can fully take advantage of the classical concepts, by combining and exploring theoretical and practical connections, they are related also with error-correcting codes and with visual cryptography. The relation between BIBD and

Hadamard matrices can be explored as there are so many optimal properties in these designs and several open issues to explore. QR Codes are sometimes exposed to conditions where their data can be lost, therefore it is very important to limit that risk by the use of error-correcting strategies. Links to risk analysis should not be ignored. This has been illustrated through the use of several examples.

## 9 Acknowledgements

This research was partially sponsored by national funds through the Fundao Nacional para a Cincia e Tecnologia, Portugal - FCT under the project PEst-OE/MAT/UI0006/2014.

## References

1. Baumert, L. D.; Golomb, S. W. and Hall Jr., M. Discovery of an Hadamard matrix of order 92. *Bull. Amer. Math. Soc.* 68 (3) 237-238, 1962.
2. Bose, R. C. On the construction of balanced incomplete block designs. *Annals of Eugenics* 9, 358-399, 1939.
3. Caliński, T. and Kageyama, S. , Block Designs: A Randomization Approach. Vol. I: Analysis. *Lecture Notes in Statistics*, Springer, 150, 2000.
4. Caliński, T. and Kageyama, S. , Block Designs: A Randomization Approach. Vol. II: Design. *Lecture Notes in Statistics*, Springer, 170, 2003.
5. Foody, W. and Hedayat, A. On theory and applications of BIB Designs with repeated blocks. *The Annals of Statistics*, 5(5), 932 - 945, 1977.
6. Georgiou, S.; Koukouvinos, C.; Seberry, J. Hadamard matrices, orthogonal designs and construction algorithms, *in Wallis, WD (ed), Designs 2002: Further Combinatorial and Constructive Design Theory. Kluwer Academic Publishers, Norwell, Massachusetts*, 133-205, 2002.
7. Hall Jr, M. , Combinatorial Theory, 2nd edition. New York, Wiley, 1986.
8. Hedayat, A. and Wallis, W. D. , Hadamard matrices and their applications. *The Annals of Statistics*, 6 (6), 1184-1238, 1978.
9. Hedayat, A and Hwang, H. , *Construction of BIB Designs with Various Support Sizes.* Chicago, Illionois, 1980.
10. Hedayat, A. S. and Hwang, H. L. , BIB (8,56,21,3,6) and BIB(10,30,9,3,2) Designs with Repeated Blocks. *Journal of Combinatorial Theory, Series A 36*, 73-91, 1984.
11. Jennifer Seberry. Hadamard matrices. *University of Wollongong*, 2012.
12. Launey, W., Combinatorial Designs: A tribute to Jennifer Seberry on her 60th Birthday, *Discrete Mathematics*, 308 (13), 27232731, 2008.
13. Mathon, R.and Rosa, A. , CRC Handbook of Combinatorial Designs, *Edited by Charles J. Colbourn and Jeffrey H Dinitz.* CRC Press, 2010.
14. Oliveira , T. A. Ceranka, B , Graczyk, M. , The variance of the difference of block effects in the balanced incomplete block designs with repeated blocks, *Colloquium Biometrycczne*, 36 , 115-124, 2006.

15. Oliveira, T. A. , BIB designs with repeated blocks: review and perspectives, *in "Proceedings of the Tenth Islamic Countries Conference on Statistical Sciences (ICCS-X)". Cairo: The Islamic Countries Society of Statistical Sciences*, 1 , 82-96, 2010.
16. Plackett, R. L. and Burman, J. P.,The design of optimum multifactorial experiments. *Biometrika* 33 (4), 305-325, 1946.
17. Raghvarao, D. Constructions and Combinatorial Problems in Design of Experiments. New York: Wiley, 1971.
18. Bart Preneel, Hans Dobbertin, Antoon Bosselaers, The Cryptographic Hash Function RIPEMD-160, CryptoBytes 3(2), pp. 9-14, 1997.
19. Sawade, K. "A Hadamard Matrix of Order-268." Graphs Combinatorics 1, 185-187, 1985.
20. http://www.iso.org/iso/home/store/catalogue$_tc$/$catalogue_detail.htm?csnumber = 43655 consultedontheSeptember5th$, 2014.

# Combinatorial Approach to Statistical Design of Experiments

Petya Valcheva

Sofia University "St. Kliment Ohridski"
(e-mail: pvalcheva@unwe.bg)

**Abstract.** The paper describes the various types of combinatorial designs applied in Statistical Design of Experiments. We give more detailed information about Balanced Incomplete Block Designs (*BIBDs*) and Orthogonal Arrays (*OAs*). The "difference matrix"- method for achievement of *OAs* is also described. Based on it two new constructions of orthogonal arrays $(6,15)$ and $(6,20)$ are obtained. They are non-isomorphic to the already known constructions of such arrays. The known $(7,12) - OA$ is also discussed.

**Keywords:** balanced incomplete block design, difference matrix, orthogonal array, quasi-difference matrix.

## 1 Introduction

Orthogonal arrays(*OAs*), first introduced by Rao in 1947, are essential combinatorial structures. Their mathematical theory is inspiring, beautiful and closely related to combinatorics, geometry, finite fields and error-correcting codes. They are used in various scientific fields such as computer science, cryptography and statistics. The Statistical Design of Experiments is that branch of the statistics, where these structures are widely applied and that is the reason to be immensely important in areas, where a lot of research interests are concentrated, like manufacturing, medicine, agriculture and many others. More detailed information can be found in [1].
The statistical theory of the Experimental design was mainly initiated by R.A.Fisher [2] in the 1935*s* at the Rothamsted Experimental Station as a performance of agricultural experiments, but later it has been applied successfully in the military and industry. For example, Besse Day, working at the U.S. Naval Experimentation Laboratory, used the methods to solve problems such as finding the cause of bad welds at a naval shipyard during World War II [3].
Many experiments involve the study of the effects of two or more factors. The most efficient way to see the relationship between the independent variables(factors) is so called *factorial design*. By this technique, we mean that in each complete trial or replication of the experiment all possible combinations of the levels of the factors are investigated. But in many cases the number of treatments to be tested is large, which need more materials and respectively will increase the cost of experimentation in terms of labor, time and moreover money. In certain situations, we may not be able

*Stochastic Modeling, Data Analysis and Statistical Applications,* (*pp.* 347-352)
Lidia Filus, Teresa Oliveira, Christos H Skiadas (Ed)



to run all the treatment combinations in each block. In incomplete block designs, the block size is smaller than the total number of treatments to be compared. But when all comparisons are equally important, the combinations used in each block should be selected in so called *balanced manner*, that is, we must construct such block that any pair of treatments occur together in the same number of times as any other pair. These are the balanced incomplete block designs (*BIBD*), in which any two treatments occur together an equal number of times. Such designs are introduced by Yates in 1936 [6] and are similar to the construction of the orthogonal arrays, as we will see below.
Consider two sets $T$ and $B$, whose elements are $t$ treatments and $b$ blocks respectively in a *BIBD*, that satisfy the following conditions:
(i) each block contains exactly $k$ members
(ii) each treatment occurs in exactly $r$ blocks(or is replicated $r$ times)
(iii) each pair of treatments occurs in the same block exactly $\lambda$ times.
A balanced incomplete block design has five parameters $t, b, r, k, \lambda$ and can be defined as a collection of $b$ subsets of size $k$ from a set of $t$ treatments, such that (i),(ii) and (iii) are satisfied. The parameter $\lambda$ must be an integer. If we denote by $n$ the total number of observations, we have the following relations between the parameters:
(i) $r.t = b.k = n$
(ii) $\lambda(t-1) = r(k-1)$
If $t = b$, the *BIBD* is said to be a symmetric *BIBD*.
The statistical model for the *BIBD* is

$$y_{ij} = \mu + \tau_i + \beta_j + \varepsilon_{ij}$$

where $y_{ij}$ is the $i-th$ observation in the $j-th$ block, $\mu$ is the overall mean, $\tau_i$ is the effect of the $i-th$ treatment, $\beta_j$ is the effect of the $j-th$ block and $\varepsilon_{ij}$ is the $NID(0,\sigma^2)$ random error component.
The second part of the article gives detailed information about the technique for finding difference matrix and quasi-difference matrix, which will help us to construct orthogonal array. As we mentioned, they are used extensively in factorial designs because of their similar structure to the block designs.
The last section demonstrates some results, derived by computer realization of the methods, described in the previous part.

## 2 On the Construction of Difference Matrices

The purpose of this section is to describe some different techniques for finding combinatorial designs. It will be discussed various approaches with so called *difference matrix(DM)* and *quasi-difference matrix(QDM)*. Such matrices are constructed via algebraic arguments. More detailed information is given in [4,5].
One of the relevant and interesting questions in the theory of Latin squares is how to determine the maximum possible number, denoted by $N(v)$, of *mutually orthogonal Latin squares of order* $v$ *(MOLS*$(v)$*)*. It is well known that for each $v \geq 2$, $N(v) \leq v-1$. Summarized results for $N(v)$ can be found in [7].

Let $S$ be a non-empty set of order $\nu$. A *Latin square of order* $\nu$ is a $\nu \times \nu$ matrix L, in which $\nu$ distinct symbols are arranged so that each element of S appears once in each row and column. Let $L_1$ and $L_2$ be Latin squares of same order, say $\nu \geq 2$. We say that $L_1$ and $L_2$ are orthogonal if, when superimposed, each of the possible $\nu^2$ ordered pairs occur exactly once. A set $\{L_1, ..., L_t\}$ of $t \geq 2$ Latin squares of order $\nu$ is orthogonal if any two distinct Latin squares are orthogonal. We call this a set of mutually orthogonal Latin squares(*MOLS*).
The existence of $k-2$ $MOLS((\nu))$ is equivalent to the existence of an orthogonal array $OA(k,\nu)$, which is defined as a $k \times \nu^2$ matrix

$$A = \{(a_{ij}), i = 1, ..., k, j = 1, ..., \nu^2\}$$

over a $\nu$-set $S$, such that any two rows contain all the ordered pairs of elements from $S$ exactly once. In this case, it is customary to say that the orthogonal array has index unity ($\lambda = 1$) and strength $k$. It is known that $k \leq \nu + 1$. A $k \times \nu$ sub-matrix of an $OA(k,\nu)$ is called a *parallel class*, if every row in it is a permutation of the elements of $S$. An $OA(k,\nu)$ is called *resolvable*, if its columns can be split into $\nu$ disjoint parallel classes. The existence of an $OA(k,\nu)$ possessing a parallel class is equivalent to the existence of $k-2$ *idempotent* $MOLS((\nu))$. The existence of a resolvable $OA(k,\nu)$ is equivalent to the existence of $k-1$ $MOLS((\nu))$ [4,5]. Orthogonal arrays are combinatorial designs, that can be obtained from difference and quasi-difference matrices, which will be defined below.
Let $\Gamma = \{1, g_2, ..., g_\nu\}$ be a group of order $\nu$. A $k \times \lambda\nu$ matrix

$$D = \{(d_{ij}), i = 1, ..., k, j = 1, ..., \lambda\nu\}$$

with entries from $\Gamma$ is called a $(\nu, k; \lambda)$-difference matrix over $\Gamma$ and is denoted by $DM(\nu, k, ; \lambda)$ if it satisfies the *difference property*: for each $1 \leq i < j \leq k$, the multi-set

$$\{d_{il} d_{jl}^{-1}; 1 \leq l \leq \lambda\nu\}$$

(the difference list) contains every element of $\Gamma$ $\lambda$ times. When $\Gamma$ is *abelian*, i.e. $\Gamma = \{0, g_2, ..., g_\nu\}$, typically additive notation is used, so that differences $d_{il} - d_{jl}$ are employed. Removing any row from a $(\nu, k; \lambda)$-difference matrix gives a $(\nu, k-1; \lambda)$-difference matrix, i.e. the difference property still holds. A $DM(\nu, k; \lambda)$ does not exist if $k > \lambda\nu$. A $(\nu, k)$-difference matrix over $\Gamma$ gives rise to a resolvable $OA(k,\nu)$ and hence to an $OA(k+1,\nu)$.
In the case when $\lambda = 1$ a $(\nu, k; 1)$-difference matrix, denoted by $DM(\nu, k)$, gives rise to $OA(k,\nu)$ by developing it through the group $\Gamma$ in the following way:

$$OA(k,\nu) = (DM|DM.g_2|\ldots|DM.g_\nu)$$

In many cases *MOLS* are obtained from quasi-difference matrices, that is a matrix which contains an additional to the group elements point often denoted by $\infty$. Below we discuss the construction of these matrices.
Extend the group $\Gamma$ by an additional element $\{\infty\}$(point infinity) and denote it by $\Gamma_\infty = \Gamma \cup \{\infty\} = \{1, g_2, ..., g_n, \infty\}$. Consider a $k \times \lambda(\nu+2)$ matrix over the group $\Gamma_\infty$, so that:

(i) each row contains the point $\{\infty\}$ exactly $\lambda$ times and each column contains it at most once
(ii) for any two distinct rows, the difference property stay in force, i.e. for every $i,t \in \{1,2,...,k\}, i \neq t$ the list of differences $\{d_{ij}d_{tj}^{-1}\}$ contains each element of $\Gamma$ exactly $\lambda$ times (differences with the additional element $\infty$ are undefined).
Such matrix is called $(v,k;\lambda)$ quasi-difference matrix over $(\Gamma_\infty, G)$ and is denoted by $QDM(v,k;\lambda)$. In case when $\lambda = 1$, denote it by $QDM(v,k)$.An orthogonal array $OA(k,v+1)$ can be obtained developing $QDM(v,k;\lambda)$ over the subgroup G and adding an additional column consisting of points infinity - $(\infty,\infty,...,\infty)^T$ in the following way:

$$OA(k,v+1) = \left( \begin{array}{c|c|c|c} QDM & QDM.u_2 & \dots & QDM.u_n \end{array} \begin{array}{|c} \infty \\ \infty \\ \vdots \\ \infty \end{array} \right)$$

Another way of deriving orthogonal arrays and *MOLS* from difference matrices with $\lambda > 1$ was introduced in [8]. Let $\Gamma$ be a group of order $v = \lambda.n$ and let $G = \{1,u_2,...,u_n\}$ be a subgroup of $\Gamma (G \leq \Gamma)$ of order n, where $n = \frac{v}{\lambda}$. A $(v,k;\lambda)$-difference matrix $DM = (d_{ij})$ is said to be a difference matrix over $(\Gamma, G)$, and denoted by $DM(v,k;\lambda)$, if the difference property stay true, but is of the form: $d_{ij}d_{tj}^{-1} = d_{is}d_{ts}^{-1}$ yields $d_{ij}^{-1}d_{is} \notin G$, i.e. $d_{ij}, d_{is}$ are from different left cosets of G. In this case $OA(k,v)$ is obtained from $DM(v,k;\lambda)$, developing it over the subgroup G in the following way:

$$OA(k,v) = (DM|DM.u_2|\dots|DM.u_v)$$

## 3 Some Results on *MOLS* of order 12,15 and 20

3.1. The case $v = 12$
A construction of a resolvable $DM(12,6)$ over the group $C_6 \times C_2$ was obtained in [8], which leads to the existence of 5 $MOLS(12)$. We try to improve this result by investigation of $DM(12,k;2)$. There exist 5 groups of order 12, but from the Proposition 1 in [10], it is sufficient to consider $Z_{12}$ and $S_3 \times C_2$ only. After being developed C Sharp project, the exhaustive computer search for $(12,6;2)$-difference matrix, over these groups with respect to their order 6 subgroups, shows that there exists no $DM(12,k;2)$ when $k > 6$. Moreover all the resolvable $DM(12,6;2)$ found this way give no new $OA(7,12)$, i.e. under the above restrictions the construction of 5 $MOLS(12)$ obtained in [8] is unique.

3.2. The case $v = 15$
Four *MOLS* of order 15 were obtained in [9] by a construction of $DM(15,6)$ over the group $Z_{15}$. We performed an exhaustive computer search, using self-prepared C Sharp project, for $QDM(14,k;2)$ over $Z_{14} \cup \{\infty\}$. All of the obtained $QDM(14,4;2)$ were developed to the orthogonal array $OA(4,15)$. None of these arrays can be extended to $OA(7,15)$ for 5 $MOLS(15)$. Using *Todorov's* program package *OADM* for *OAs* and *DMs* processing it was shown that this construction is not isomorphic to the one in [9].

Below is given one example of $QDM(14,4;2)$ and its extension to 4 $MOLS(15)$.

$QDM(14,4;2)$

$$\left\|\begin{array}{cccccccccccccc|cccccccccccccc}
\infty & 0 & 0 & 0 & 0 & 0 & 0 & 0 & 0 & 0 & 0 & 0 & 0 & 0 & \infty & 1 & 1 & 1 & 1 & 1 & 1 & 1 & 1 & 1 & 1 & 1 & 1 & 1 \\
0 & 0 & 1 & 2 & 3 & 4 & 5 & 6 & 7 & 8 & 9 & 10 & 11 & 12 & 13 & \infty & 1 & 0 & 1 & 2 & 3 & 4 & 5 & 6 & 7 & 8 & 9 & 10 & 11 & 12 & 13 & \infty \\
0 & \infty & 0 & 3 & 11 & 1 & 10 & 8 & 2 & 12 & 5 & 13 & 9 & 4 & 6 & 7 & 1 & 7 & \infty & 1 & 4 & 12 & 2 & 11 & 9 & 3 & 13 & 6 & 0 & 10 & 5 & 8 \\
0 & 10 & 6 & \infty & 2 & 8 & 0 & 4 & 13 & 11 & 3 & 7 & 12 & 5 & 1 & 9 & 1 & 2 & 11 & 7 & \infty & 3 & 9 & 1 & 5 & 0 & 12 & 4 & 8 & 13 & 6 & 10
\end{array}\right\|$$

Extension to 4 $MOLS(15)$

$$\begin{array}{cccccccccccccc}
\infty & 0 & 3 & 11 & 1 & 10 & 8 & 2 & 12 & 5 & 13 & 9 & 4 & 6 & 7 \\
7 & \infty & 1 & 4 & 12 & 2 & 11 & 9 & 3 & 13 & 6 & 0 & 10 & 5 & 8 \\
6 & 8 & \infty & 2 & 5 & 13 & 3 & 12 & 10 & 4 & 0 & 7 & 1 & 11 & 9 \\
12 & 7 & 9 & \infty & 3 & 6 & 0 & 4 & 13 & 11 & 5 & 1 & 8 & 2 & 10 \\
3 & 13 & 8 & 10 & \infty & 4 & 7 & 1 & 5 & 0 & 12 & 6 & 2 & 9 & 11 \\
10 & 4 & 0 & 9 & 11 & \infty & 5 & 8 & 2 & 6 & 1 & 13 & 7 & 3 & 12 \\
4 & 11 & 5 & 1 & 10 & 12 & \infty & 6 & 9 & 3 & 7 & 2 & 0 & 8 & 13 \\
9 & 5 & 12 & 6 & 2 & 11 & 13 & \infty & 7 & 10 & 4 & 8 & 3 & 1 & 0 \\
2 & 10 & 6 & 13 & 7 & 3 & 12 & 0 & \infty & 8 & 11 & 5 & 9 & 4 & 1 \\
5 & 3 & 11 & 7 & 0 & 8 & 4 & 13 & 1 & \infty & 9 & 12 & 6 & 10 & 2 \\
11 & 6 & 4 & 12 & 8 & 1 & 9 & 5 & 0 & 2 & \infty & 10 & 13 & 7 & 3 \\
8 & 12 & 7 & 5 & 13 & 9 & 2 & 10 & 6 & 1 & 3 & \infty & 11 & 0 & 4 \\
1 & 9 & 13 & 8 & 6 & 0 & 10 & 3 & 11 & 7 & 2 & 4 & \infty & 12 & 5 \\
13 & 2 & 10 & 0 & 9 & 7 & 1 & 11 & 4 & 12 & 8 & 3 & 5 & \infty & 6 \\
0 & 1 & 2 & 3 & 4 & 5 & 6 & 7 & 8 & 9 & 10 & 11 & 12 & 13 & \infty
\end{array}$$

$$\begin{array}{cccccccccccccc}
10 & 6 & \infty & 2 & 8 & 0 & 4 & 13 & 11 & 3 & 7 & 12 & 5 & 1 & 9 \\
2 & 11 & 7 & \infty & 3 & 9 & 1 & 5 & 0 & 12 & 4 & 8 & 13 & 6 & 10 \\
7 & 3 & 12 & 8 & \infty & 4 & 10 & 2 & 6 & 1 & 13 & 5 & 9 & 0 & 11 \\
1 & 8 & 4 & 13 & 9 & \infty & 5 & 11 & 3 & 7 & 2 & 0 & 6 & 10 & 12 \\
11 & 2 & 9 & 5 & 0 & 10 & \infty & 6 & 12 & 4 & 8 & 3 & 1 & 7 & 13 \\
8 & 12 & 3 & 10 & 6 & 1 & 11 & \infty & 7 & 13 & 5 & 9 & 4 & 2 & 0 \\
3 & 9 & 13 & 4 & 11 & 7 & 2 & 12 & \infty & 8 & 0 & 6 & 10 & 5 & 1 \\
6 & 4 & 10 & 0 & 5 & 12 & 8 & 3 & 13 & \infty & 9 & 1 & 7 & 11 & 2 \\
12 & 7 & 5 & 11 & 1 & 6 & 13 & 9 & 4 & 0 & \infty & 10 & 2 & 8 & 3 \\
9 & 13 & 8 & 6 & 12 & 2 & 7 & 0 & 10 & 5 & 1 & \infty & 11 & 3 & 4 \\
4 & 10 & 0 & 9 & 7 & 13 & 3 & 8 & 1 & 11 & 6 & 2 & \infty & 12 & 5 \\
13 & 5 & 11 & 1 & 10 & 8 & 0 & 4 & 9 & 2 & 12 & 7 & 3 & \infty & 6 \\
\infty & 0 & 6 & 12 & 2 & 11 & 9 & 1 & 5 & 10 & 3 & 13 & 8 & 4 & 7 \\
5 & \infty & 1 & 7 & 13 & 3 & 12 & 10 & 2 & 6 & 11 & 4 & 0 & 9 & 8 \\
0 & 1 & 2 & 3 & 4 & 5 & 6 & 7 & 8 & 9 & 10 & 11 & 12 & 13 & \infty
\end{array}$$

$$\begin{array}{cccccccccccccc}
0 & 1 & 2 & 3 & 4 & 5 & 6 & 7 & 8 & 9 & 10 & 11 & 12 & 13 & \infty \\
12 & 11 & \infty & 7 & 6 & 0 & 5 & 4 & 10 & 1 & 3 & 8 & 13 & 2 & 9 \\
7 & 2 & 13 & 9 & 10 & 4 & 11 & 5 & 0 & 8 & \infty & 6 & 1 & 12 & 3 \\
2 & 10 & 7 & 12 & 3 & 8 & 0 & 13 & 5 & 11 & 1 & 9 & 4 & \infty & 6 \\
9 & 7 & 8 & 10 & 2 & 6 & 1 & 11 & 12 & 5 & 13 & \infty & 3 & 0 & 4 \\
11 & 3 & 10 & 1 & 8 & 7 & 4 & \infty & 13 & 2 & 5 & 12 & 9 & 6 & 0 \\
4 & 13 & 6 & 8 & \infty & 1 & 10 & 0 & 9 & 12 & 7 & 5 & 2 & 3 & 11 \\
6 & 0 & 12 & 4 & 1 & 9 & \infty & 8 & 11 & 3 & 2 & 10 & 5 & 7 & 13 \\
10 & 4 & 11 & 2 & 0 & \infty & 3 & 9 & 1 & 13 & 6 & 7 & 8 & 5 & 12 \\
5 & 8 & 0 & 13 & 7 & 11 & 9 & 6 & 3 & \infty & 12 & 4 & 10 & 1 & 2 \\
\infty & 5 & 1 & 11 & 12 & 10 & 13 & 3 & 4 & 6 & 9 & 2 & 0 & 8 & 7 \\
1 & 9 & 5 & \infty & 13 & 2 & 8 & 12 & 6 & 0 & 4 & 3 & 7 & 11 & 10 \\
13 & \infty & 3 & 5 & 9 & 12 & 7 & 1 & 2 & 4 & 11 & 0 & 6 & 10 & 8 \\
8 & 12 & 9 & 6 & 5 & 3 & 2 & 10 & \infty & 7 & 0 & 13 & 11 & 4 & 1 \\
3 & 6 & 4 & 0 & 11 & 13 & 12 & 2 & 7 & 10 & 8 & 1 & \infty & 9 & 5
\end{array}$$

$$\begin{array}{cccccccccccccc}
0 & 1 & 2 & 3 & 4 & 5 & 6 & 7 & 8 & 9 & 10 & 11 & 12 & 13 & \infty \\
13 & 10 & 9 & 4 & 7 & 1 & 0 & 3 & \infty & 6 & 5 & 12 & 2 & 8 & 11 \\
6 & 13 & 12 & 5 & 1 & \infty & 9 & 10 & 7 & 11 & 3 & 0 & 8 & 4 & 2 \\
1 & 3 & 13 & 8 & 0 & 9 & 11 & 5 & 12 & \infty & 2 & 7 & 10 & 6 & 4 \\
3 & 9 & 7 & 13 & 6 & 10 & 5 & 2 & 0 & 8 & 11 & 4 & \infty & 12 & 1 \\
8 & 7 & 5 & \infty & 13 & 3 & 12 & 0 & 4 & 10 & 6 & 2 & 1 & 11 & 9 \\
2 & 6 & \infty & 0 & 11 & 13 & 7 & 8 & 10 & 1 & 12 & 3 & 4 & 9 & 5 \\
5 & 4 & 3 & 11 & 10 & 2 & 13 & \infty & 6 & 12 & 9 & 8 & 7 & 1 & 0 \\
9 & 0 & 1 & 7 & 2 & 12 & 4 & 13 & 11 & 3 & 8 & 5 & 6 & \infty & 10 \\
11 & 5 & 10 & 9 & \infty & 4 & 8 & 1 & 13 & 2 & 7 & 6 & 0 & 3 & 12 \\
7 & 2 & 0 & 12 & 5 & 11 & 1 & 6 & 9 & 13 & 4 & \infty & 3 & 10 & 8 \\
12 & \infty & 4 & 10 & 8 & 0 & 2 & 9 & 3 & 5 & 13 & 1 & 11 & 7 & 6 \\
\infty & 8 & 11 & 1 & 12 & 6 & 10 & 4 & 5 & 7 & 0 & 13 & 9 & 2 & 3 \\
4 & 11 & 6 & 2 & 9 & 8 & 3 & 12 & 1 & 0 & \infty & 10 & 13 & 5 & 7 \\
10 & 12 & 8 & 6 & 3 & 7 & \infty & 11 & 2 & 4 & 1 & 9 & 5 & 0 & 13
\end{array}$$

3.3. The case $v = 20$

Here we give our version of four $MOLS(20)$, which are constructed in [11] and [12] in a $QDM(19,6;1)$ form. We investigate $DM(20,k;2)$ over $Z_{20}$ with respect to its order 10 subgroup. It was supposed that corresponding orthogonal array admits an order 3 automorphism. An example of $DM(20,6;2)$ is given below, but no $DM(20,7;2)$ was obtained. By the construction, it is obviously that the corresponding $OA(6,20)$ possesses an order 5 automorphism and since the constructions in [11] and [12] admit no such automorphism, our example is non-isomorphic to them.

$DM(20,6;2)$

$$\left\|\begin{array}{cccccccccccccccccccc}
0 & 0 & 0 & 0 & 0 & 0 & 0 & 0 & 0 & 0 & 0 & 0 & 0 & 0 & 0 & 0 & 0 & 0 & 0 & 0 \\
0 & 1 & 2 & 3 & 4 & 5 & 6 & 7 & 8 & 9 & 10 & 11 & 12 & 13 & 14 & 15 & 16 & 17 & 18 & 19 \\
12 & 2 & 17 & 7 & 13 & 10 & 5 & 4 & 8 & 16 & 15 & 1 & 0 & 9 & 11 & 18 & 3 & 6 & 19 & 14 \\
18 & 19 & 6 & 17 & 15 & 1 & 5 & 11 & 13 & 12 & 3 & 2 & 9 & 0 & 14 & 8 & 10 & 7 & 4 & 16 \\
9 & 4 & 10 & 12 & 16 & 19 & 2 & 0 & 6 & 18 & 11 & 3 & 5 & 18 & 1 & 13 & 7 & 14 & 17 & 15 \\
5 & 6 & 15 & 7 & 12 & 13 & 1 & 14 & 17 & 11 & 9 & 3 & 18 & 10 & 8 & 4 & 16 & 0 & 2 & 19
\end{array}\right\|$$

$$\left\|\begin{array}{cccccccccccccccccccc}
1 & 1 & 1 & 1 & 1 & 1 & 1 & 1 & 1 & 1 & 1 & 1 & 1 & 1 & 1 & 1 & 1 & 1 & 1 & 1 \\
0 & 1 & 2 & 3 & 4 & 5 & 6 & 7 & 8 & 9 & 10 & 11 & 12 & 13 & 14 & 15 & 16 & 17 & 18 & 19 \\
11 & 1 & 0 & 15 & 6 & 18 & 16 & 9 & 12 & 3 & 4 & 10 & 5 & 19 & 17 & 13 & 2 & 8 & 14 & 7 \\
3 & 16 & 4 & 11 & 19 & 10 & 15 & 8 & 0 & 9 & 18 & 13 & 2 & 12 & 1 & 7 & 17 & 6 & 14 & 5 \\
2 & 16 & 6 & 14 & 10 & 5 & 9 & 17 & 3 & 15 & 4 & 13 & 12 & 0 & 11 & 19 & 1 & 18 & 8 & 7 \\
3 & 16 & 19 & 2 & 14 & 15 & 17 & 0 & 4 & 7 & 11 & 12 & 10 & 9 & 6 & 1 & 18 & 8 & 5 & 13
\end{array}\right\|$$

## 4 Conclusion

These two examples for $v = 15$ $v = 20$ were put to computer extension(again using own program project) without preserving the "difference" property. Unfortunately, the derived constructions are not resolvable, which means that they do not lead to obtaining more orthogonal Latin squares. Therefore, the question of their existence is still open.

## Acknowledgement

**This work was supported by the European Social Fund through the Human Resource Development Operational Programme under contract** $BG051PO001-3.3.06-0052(2012/2014)$**.**

## References

1. Hedayat, A.S., Sloane, N, J.A., Stufken, John, *Orthogonal arrays: theory and application.*, Springer, 1999.
2. John, Peter William Meredith, *Incomplete block designs.*, Marcel Dekker, 1980.
3. Davim, J.Paulo (Editor), *Statistical and Computational Techniques in Manufacturing.*, Springer, 2012.
4. C. Colbourn and J. Dinitz (Editors), *CRC Handbook of Combinatorial Designs.*, CRC Press, Boca Raton, 2007.
5. T. Beth, D. Jungnickel, and H. Lenz, *Design Theory.*, Cambridge University Press, Cambridge, England, 1999.
6. Montgomery, Douglas.C, *Design and analysis of experiments - 5th edition.*, John Wiley and Sons, 2001.
7. Brouwer, A.E., *The number of mutually orthogonal Latin squares - a table up to order 10000.*, Report ZW 123, Math. Centr., Amsterdam 1978
8. Johnson, D.M., Dulmage, A.I., Mendelson, N.S., *Orthomorphisms of group and orthogonal Latin squares.*, Canadian J. Math., 13, 356-372, 1961.
9. Schellenberg, P.J., van Rees, G.M., Vanstone, S.A., *Four pairwise orthogonal Latin squares of order 15.*, Ars Combinatoria, 6, 141-150, 1978.
10. Todorov, D.T., *Four mutually orthogonal Latin squares of order 14.*, Journal of Combinatorial Designs, 20, 1-5, 2012.
11. Todorov, D.T., *Four mutually orthogonal Latin squares of order 20.*, Ars Combinatoria, 27-C, 63-65, 1989.
12. Abel, R.J.R., Todorov, D.T., *Four mutually orthogonal Latin squares of orders 20, 30, 38 and 44.*, J. Comb. Theory(A), 64, 144-148, 1993.

# 8 CHAPTER

## Information Theory and Risk Analysis

# Entropy Measures and the Generalized Fisher's Information

Thomas L. Toulias[1] and Christos P. Kitsos[1]

Department of Informatics, Technological Educational Institute of Athens
12243 Egaleo, Athens, Greece
(E-mail: {t.toulias, xkitsos}@teiath.gr)

**Abstract.** This paper investigates the generalized Fisher's entropy type information measure with respect to the multivariate $\gamma$–order Normal distribution and certain boundaries are obtained. Also the Rényi and Shannon entropies are evaluated and discussed.
**Keywords:** Fisher's entropy type information measure, $\gamma$–order Normal distribution, Rényi entropy.

## 1 Introduction

In principle, the information measures are divided to three main categories: parametric (typical example Fisher's information), non parametric (with Shannon information measure to be the most well known) and entropy type, see Cover and Thomas [1], which are adopted at this paper. The introduced new entropy type measure of information $\mathrm{J}_\alpha(X)$ is a function of the density $f_X$ of the $p$-variate random variable $X$, see Kitsos and Tavoularis [2], defined as

$$\mathrm{J}_\alpha(X) := \mathrm{E}\left(\|\nabla \log f(X)\|^\alpha\right) = \int_{\mathbb{R}^p} f(x)\, \|\nabla \log f_X(x)\|^a \, dx. \tag{1}$$

Notice that, $\mathrm{J}_2 = \mathrm{J}$, with J being the known Fisher's entropy type information measure.

Moreover, the known entropy power $\mathrm{N}(X)$, defined through Shannon entropy $\mathrm{H}(X)$, has been extended to

$$\mathrm{N}_\alpha(X) = \nu_\alpha \exp\{\tfrac{\alpha}{p}\mathrm{H}(X)\}, \tag{2}$$

with

$$\nu_\alpha = (\tfrac{\alpha-1}{e})\pi^{-\alpha/2}\left[\frac{\Gamma(\frac{p}{2}+1)}{\Gamma(p\frac{\alpha-1}{\alpha}+1)}\right]^{\frac{\alpha}{p}},\ \alpha > 1,$$

see Kitsos and Tavoularis [2] for details. Notice that, $\nu_2 = (2\pi e)^{-1}$ and $\mathbf{N}_2 = \mathbf{N}$, where N the known Shannon entropy power for the normal distribution.

*Stochastic Modeling, Data Analysis and Statistical Applications* (*pp.* 355-364)
Lidia Filus - Teresa Oliveira - Christos H Skiadas (Eds)



Moreover, it can be proved that

$$\mathrm{J}_\alpha(X)\mathrm{N}_\alpha(X) \geq p, \tag{3}$$

which extends the well known result with $\alpha = 2$, see Kitsos and Tavoularis [2].

The so called Information Inequality, is generalized due to the introduced information measures, Kitsos and Tavoularis [2]. The Generalized Information Inequality (GII) is given by

$$\left[\tfrac{2\pi e}{p}\mathrm{Var}(X)\right]^{1/2}\left[\tfrac{1}{p}\nu_\alpha \mathrm{J}_\alpha(X)\right]^{1/\alpha} \geq 1.$$

When $\alpha = 2$ we have $\mathrm{Var}(X)\mathrm{J}_2(X) \geq p$, and therefore, the Cramer–Rao inequality (Cover and Thomas [1], Th. 11.10.1) holds. The lower boundary $B_\alpha^p$ for the introduced generalized information $\mathrm{J}_\alpha(X)$ is

$$\mathrm{J}_\alpha(X) \geq B_\alpha^p := \tfrac{p}{\nu_\alpha}\left[\tfrac{2\pi e}{p}\,\mathrm{Var}(X)\right]^{-\alpha/2}. \tag{4}$$

In Fig. 1 the lower boundaries $B_\alpha^p$ across $\alpha$ are depicted, assuming $\mathrm{Var}(X) = 1$ and for all dimensions $p$. Moreover, Fig. 2 depicts the boundaries $B_\alpha^1$ across $\mathrm{Var}(X)$ and for parameter values $\alpha = 1, 2, \ldots, 100$.

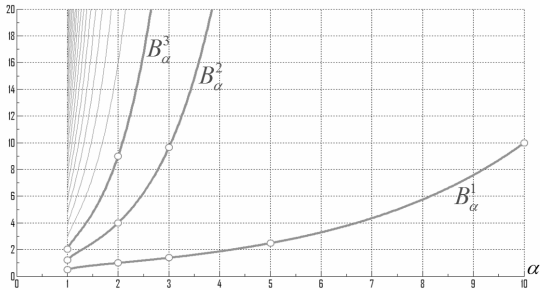


**Fig. 1.** Graphs of the boundaries $B_\alpha^p$ across $\alpha$, with fixed $\mathrm{Var}\, X = 1$ for every dimension $p \geq 1$.

Let H denote the Shannon (differential) entropy of a r.v. X with p.d.f. $f_X$, i.e.

$$\mathrm{H}(X) := \int_{\mathbb{R}^p} f_X(x)\log f(x)dx. \tag{5}$$

For any multivariate random variable $X$ with zero mean and covariance matrix $\Sigma$, it holds

$$\mathrm{H}(X) \leq \tfrac{1}{2}\log\{(2\pi e)^p\,|\det\Sigma|\}, \tag{6}$$

while the equality in (6) holds if and only if $X$ is a normally distributed variable, i.e $X \sim N^p(\mu, \Sigma)$, see Cover and Thomas [1]. Moreover, the Normal distribution, according to Information Measures Theory, is adopted for the noise, acting additively to the input variable when an input–output time discrete channel is formed.

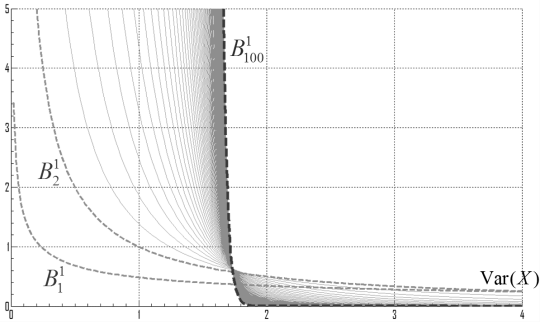


**Fig. 2.** Graphs of the boundaries $B^p_\alpha$ across Var $X$ for parameters $\alpha = 1, 2, \ldots, 100$.

Kitsos and Tavoularis in ([2] and [3]) introduced and studied the multivariate (and elliptically contoured) $\gamma$–ordered Normal distribution, i.e. $\mathcal{N}^p_\gamma(\mu, \Sigma)$, see also Kitsos and Toulias [4] and Kitsos *et al.* [5] for further reading. Recall the definition of $\mathcal{N}_\gamma$:

**Definition 1.** The $p$–dimensional random variable $X$ follows the $\gamma$–order Normal, $\mathcal{N}^p_\gamma(\mu, \Sigma)$ with mean vector $\mu \in \mathbb{R}^p$ and positive definite scale matrix $\Sigma \in \mathbb{R}^{p\times p}$, when the density function, $f_X$, is of the form

$$f_X(x;\ \mu, \Sigma) = C^p_\gamma |\det \Sigma|^{-1/2}\ \exp\left\{-\tfrac{\gamma-1}{\gamma} Q(x)^{\frac{\gamma}{2(\gamma-1)}}\right\}, \quad x \in \mathbb{R}^p, \tag{7}$$

with $Q$ the quadratic form $Q(x) = (x-\mu)\Sigma^{-1}(x-\mu)^{\mathrm{T}}$, $x \in \mathbb{R}^p$. We shall write $X \sim \mathcal{N}^p_\gamma(\mu, \Sigma)$. The normality factor $C^p_\gamma$ is defined as

$$C^p_\gamma = \pi^{-p/2}\ \frac{\Gamma\left(\frac{p}{2}+1\right)}{\Gamma(p\frac{\gamma-1}{\gamma}+1)} (\tfrac{\gamma-1}{\gamma})^{p\frac{\gamma-1}{\gamma}}. \tag{8}$$

Notice that, for $\gamma = 2$, $\mathcal{N}^p_2(\mu, \Sigma)$ is the well known multivariate normal distribution. Moreover, the function $\phi(\alpha) = f_\alpha(\mu, \Sigma)^{1/\alpha}$ with $\Sigma = (\sigma^2/\alpha)^{2(\alpha-1)/\alpha}\mathbb{I}_p$, corresponds to extremal function for an inequality extending LSI due to Del Pino *et al.* [6]. The essential result is that the defined $\gamma$-ordered Normal distribution works as an extremal function to a generalized form of the Logarithmic Sobolev Inequality.

The family of $\mathcal{N}^p_\gamma(\mu, \Sigma)$, i.e. the family of the elliptically contoured $\gamma$–ordered Normals, provides a smooth bridging between the multivariate (and elliptically countered) Uniform, Normal and Laplace r.v. $U$, $N$ and $L$, i.e. between $U \sim \mathcal{U}^p(\mu, \Sigma)$, $Z \sim \mathcal{N}^p(\mu, \Sigma)$, and $L \sim \mathcal{L}^p(\mu, \Sigma)$ respectively, with density functions

$$f_U(x;\ \mu, \Sigma) = \begin{cases} \frac{\Gamma(\frac{p}{2}+1)}{\pi^{p/2}\sqrt{|\det \Sigma|}}, & x \in \mathbb{R}^p,\ \text{with } Q(x) \le 1, \\ 0, & x \in \mathbb{R}^p,\ \text{with } Q(x) > 1, \end{cases} \tag{9}$$

$$f_Z(x;\ \mu, \Sigma) = \frac{1}{(2\pi)^{p/2}\sqrt{|\det \Sigma|}} \exp\left\{-\tfrac{1}{2}Q(x)\right\}, \quad x \in \mathbb{R}^p, \tag{10}$$

$$f_L(x;\ \mu,\Sigma)=\frac{\Gamma(\frac{p}{2}+1)}{p!\pi^{p/2}\sqrt{|\det\Sigma|}}\exp\left\{-\sqrt{Q(x)}\right\},\quad x\in\mathbb{R}^p, \tag{11}$$

respectively. That is, the $\mathcal{N}_\gamma^p$ family of distributions, not only generalizes the Normal one but also two other very significant distributions, as the Uniform and Laplace distributions, are induced. Indeed:

**Theorem 1.** *The multivariate $\gamma$-ordered Normal distribution, $\mathcal{N}_\gamma^p(\mu,\Sigma)$, for order values of $\gamma=0,1,2,\pm\infty$ coincides with*

$$\mathcal{N}_\gamma^p(\mu,\Sigma)=\begin{cases}\mathcal{D}^p(\mu), & \gamma=0 \ \ and \ \ p=1,2,\\ 0, & \gamma=0 \ \ and \ \ p\geq 3,\\ \mathcal{U}^p(\mu,\Sigma), & \gamma=1,\\ \mathcal{N}^p(\mu,\Sigma), & \gamma=2,\\ \mathcal{L}^p(\mu,\Sigma), & \gamma=\pm\infty.\end{cases} \tag{12}$$

## 2 Entropy and Information Measures

Besides the generalized entropy power $\mathrm{N}_\alpha$, another significant entropy measure that generalizes the Shannon entropy is the Rényi entropy. For a $p$–variate continues random variable with p.d.f. $f_X$, the Rényi entropy $\mathrm{R}_\alpha(X)$ is defined, through the $\alpha$–norm of $f_X\in\mathscr{L}^\alpha(\mathbb{R}^p)$, by

$$\mathrm{R}_\alpha(X):=-\tfrac{\alpha}{\alpha-1}\log\|f_X\|_\alpha=\tfrac{1}{1-\alpha}\log\int_{\mathbb{R}^p}|f_X(x)|^\alpha dx,\quad \alpha>0,\ \alpha\neq 1. \tag{13}$$

For the limiting case of $\alpha\to 1$ the Rényi entropy converges to the usual Shannon entropy $\mathrm{H}(X)$ as in (5). Notice that we use the minus sign for $\mathrm{R}_\alpha$ to be in accordance with the definition of (5).

Considering now a r.v. from the $\gamma$–GND family, the following holds.

**Theorem 2.** *For the $p$–variate, spherically contoured $\gamma$–order normally distributed $X_\gamma\sim\mathcal{N}_\gamma^p(\mu,\sigma^2\mathbb{I}_p)$, the Rényi entropy of $X_\gamma$ is given by*

$$\mathrm{R}_\alpha(X_\gamma)=p\tfrac{\gamma-1}{\gamma(\alpha-1)}\log\alpha-\log(C_\gamma^p\sigma^{-p}). \tag{14}$$

*Proof.* Consider the p.d.f. $f_{X_\gamma}$ as in (7). From the definition (13) it is

$$\mathrm{R}_\alpha(X_\gamma)=\tfrac{\alpha}{1-\alpha}\log(C_\gamma^p\sigma^{-p})+\tfrac{1}{1-\alpha}\log\int_{\mathbb{R}^p}\exp\left\{-\tfrac{\alpha(\gamma-1)}{\gamma}\|\tfrac{x-\mu}{\sigma}\|^{\frac{\gamma}{\gamma-1}}\right\}dx,$$

and applying the linear transformation $z=(x-\mu)\sigma^{-1}$ with $dz=d\{(x-\mu)/\sigma\}=\sigma^{-p}dx$, the $\mathrm{R}_\alpha$ above is reduced to

$$\begin{aligned}\mathrm{R}_\alpha(X_\gamma)&=\tfrac{\alpha}{1-\alpha}\log\left(C_\gamma^p\sigma^{-p}\right)+\tfrac{1}{1-\alpha}\log\left(\sigma^p\int_{\mathbb{R}^p}\exp\left\{-\tfrac{\alpha(\gamma-1)}{\gamma}\|z\|^{\frac{\gamma}{\gamma-1}}\right\}dz\right)\\ &=\tfrac{\alpha}{1-\alpha}\log(C_\gamma^p\sigma^{p\frac{1-\alpha}{\alpha}})+\tfrac{1}{1-\alpha}\log\int_{\mathbb{R}^p}\exp\left\{-\tfrac{\alpha(\gamma-1)}{\gamma}\|z\|^{\frac{\gamma}{\gamma-1}}\right\}dz.\end{aligned}$$

Switching to hyperspherical coordinates, we get

$$\mathrm{R}_\alpha(X_\gamma) = \tfrac{\alpha}{1-\alpha}\log K(\sigma) + \tfrac{1}{1-\alpha}\log \int\limits_{\mathbb{R}_+} \exp\left\{-\tfrac{\alpha(\gamma-1)}{\gamma}\rho^{\frac{\gamma}{\gamma-1}}\right\}\rho^{p-1}d\rho,$$

where $K(\sigma) = C_\gamma^p \sigma^{p(1-\alpha)/\alpha}\omega_{p-1}^{1/\alpha}$ with $\omega_{p-1} = 2\pi^{p/2}/\,\Gamma(p/2)$ denoting the volume of the $(p-1)$–sphere. Transforming $du := d(\frac{\gamma-1}{\gamma}\rho^{\gamma/(\gamma-1)}) = \rho^{1/(\gamma-1)}d\rho$ we obtain successively

$$\begin{aligned}
\mathrm{R}_\alpha(X_\gamma) &= \tfrac{\alpha}{1-\alpha}\log K(\sigma) + \tfrac{1}{1-\alpha}\log \int\limits_{\mathbb{R}_+} e^{-\alpha u}\rho^{\frac{(p-1)(\gamma-1)-1}{\gamma-1}}du \\
&= \tfrac{\alpha}{\alpha-1}\log K(\sigma) + \tfrac{1}{1-\alpha}\log \int\limits_{\mathbb{R}_+} e^{-\alpha u}\left(\rho^{\frac{\gamma}{\gamma-1}}\right)^{\frac{(p-1)(\gamma-1)-1}{\gamma}}du \\
&= \tfrac{\alpha}{1-\alpha}\log K(\sigma) + \tfrac{1}{1-\alpha}\log(\tfrac{\gamma}{\gamma-1})^{p\frac{\gamma-1}{\gamma}-1} + \tfrac{1}{1-\alpha}\log \int\limits_{\mathbb{R}_+} e^{-\alpha u}u^{p\frac{\gamma-1}{\gamma}-1}du \\
&= \tfrac{\alpha}{1-\alpha}\log K(\sigma) + \tfrac{1}{1-\alpha}\log(\tfrac{\gamma}{\gamma-1})^{p\frac{\gamma-1}{\gamma}-1} - p\tfrac{\gamma-1}{\gamma}\cdot\tfrac{\log\alpha}{1-\alpha} + \tfrac{1}{1-\alpha}\log\Gamma(p\tfrac{\gamma-1}{\gamma}).
\end{aligned}$$

Finally, by substitution of the expressions for $K(\sigma)$, $\omega_{p-1}$ and the normalizing factor $C_\gamma^p$, we obtain

$$\mathrm{R}_\alpha(X_\gamma) = p\log\sigma - \tfrac{\alpha}{1-\alpha}\log C_\gamma^p + \tfrac{1}{1-\alpha}\log C_\gamma^p + p\tfrac{\gamma-1}{\gamma}\cdot\tfrac{\log\alpha}{\alpha-1},$$

and hence (14) holds true.

**Corollary 1.** *For the special cases of $\alpha = 0, 1, 2, +\infty$ Rényi entropy of $X_\gamma \sim \mathcal{N}_\gamma(\mu, \Sigma)$ reduces to*

$$\mathrm{R}_\alpha(X_\gamma) = \begin{cases} +\infty, & \alpha = 0, \quad (\textit{Hartley entropy}) \\ p\frac{\gamma-1}{\gamma} - \log(C_\gamma^p/\sigma^p), & \alpha = 1, \quad (\textit{Shannon entropy}) \\ p\frac{\gamma-1}{\gamma}\log 2 - \log(C_\gamma^p/\sigma^p), & \alpha = 2, \quad (\textit{collision entropy}) \\ -\log(C_\gamma^p/\sigma^p), & \alpha = +\infty. \quad (\textit{min–entropy}) \end{cases}$$

Rényi entropy $\mathrm{R}_\alpha(X_\gamma)$, as in (14), is an decreasing function of parameter $\alpha$, and hence

$$\mathrm{R}_{+\infty}(X_\gamma) < \mathrm{R}_2(X_\gamma) < \mathrm{R}_1(X_\gamma) < \mathrm{R}_0(X_\gamma).$$

*Example 1.* For the multivariate and spherically contoured Uniform random variable $U \sim \mathcal{U}(\mu, \sigma^2\mathbb{I}_p)$, the Hartley, Shannon, collision and the min– entropies coincide as,

$$\mathrm{R}_\alpha(U) = \log\frac{\pi^{p/2}\sigma^p}{\Gamma(\frac{p}{2}+1)}, \quad \alpha \in \mathbb{R}_+,$$

while for the univariate case of $U \sim \mathcal{U}(\mu-\sigma, \mu-\sigma)$ we are reduced to

$$\mathrm{R}_\alpha(U) = \log(2\sigma), \quad \alpha \in \mathbb{R}_+.$$

Notice that for a uniformly distributed r.v. the Rényi entropy $\mathrm{R}_\alpha$ is $\alpha$–invariant, depending only on the dimension $p \in \mathbb{N}$ and the scale parameter $\sigma$.

*Example 2.* For the multivariate and elliptically contoured Laplace random variable $L \sim \mathcal{L}(\mu, \sigma^2 \mathbb{I}_p)$, the Hartley, Shannon, collision and the min– entropies are given by,

$$\mathrm{R}_\alpha(L) = \begin{cases} +\infty, & \alpha = 0, \quad \text{(Hartley entropy)} \\ p + \log\{p!\pi^{p/2}\sigma^p\,\Gamma(\frac{p}{2}+1)^{-1}\}, & \alpha = 1, \quad \text{(Shannon entropy)} \\ \log\{2^p p!\pi^{p/2}\sigma^p\,\Gamma(\frac{p}{2}+1)^{-1}\}, & \alpha = 2, \quad \text{(collision entropy)} \\ \log\{p!\pi^{p/2}\sigma^p\,\Gamma(\frac{p}{2}+1)^{-1}\}, & \alpha = +\infty. \quad \text{(min–entropy)} \end{cases}$$

*Example 3.* According to the classification Theorem 1 and Corollary 1, we can evaluate the usual Shannon entropy for the multivariate (and spherically contoured) Uniform, Normal and Laplace distributions with $\Sigma = \sigma^2 \mathbb{I}_p$, i.e.

$$\mathrm{H}(X) = \begin{cases} \log \frac{\pi^{p/2}}{\Gamma(\frac{p}{2}+1)} \sqrt{|\det \Sigma|}, & \text{for } X \sim \mathcal{N}_1^p(\mu, \Sigma) = \mathcal{U}^p(\mu, \Sigma), \\ \frac{1}{2}\log\{(2\pi e)^p\,|\det \Sigma|\}, & \text{for } X \sim \mathcal{N}_2^p(\mu, \Sigma) = \mathcal{N}^p(\mu, \Sigma), \\ p + \log \frac{p!\pi^{p/2}}{\Gamma(\frac{p}{2}+1)} \sqrt{|\det \Sigma|}, & \text{for } X \sim \mathcal{N}_{\pm\infty}^p(\mu, \Sigma) = \mathcal{L}^p(\mu, \Sigma), \end{cases}$$

see also (6) for the Normal case, while for the univariate case $p = 1$, we are reduced to

$$\mathrm{H}(X) = \begin{cases} \log 2\sigma, & \text{for } X \sim \mathcal{N}_1^1(\mu, \sigma^2) = \mathcal{U}^1(\mu, \sigma^2) = \mathcal{U}(\mu - \sigma, \mu - \sigma), \\ \log \sqrt{2\pi e}\sigma, & \text{for } X \sim \mathcal{N}_2^1(\mu, \sigma^2) = \mathcal{N}(\mu, \sigma^2), \\ 1 + \log 2\sigma, & \text{for } X \sim \mathcal{N}_{\pm\infty}^1(\mu, \sigma^2) = \mathcal{L}^1(\mu, \sigma^2) = \mathcal{L}(\mu, \sigma). \end{cases}$$

where $\mathcal{U}(\mu - \sigma, \mu - \sigma)$, $\mathcal{N}(\mu, \sigma^2)$ and $\mathcal{L}(\mu, \sigma)$ are the usual notations for the univariate Uniform, Normal and Laplace distributions respectively.

Now, we shall evaluate the generalized Fisher's entropy type information of a random variable following the multivariate $\gamma$-order Normal, $\mathcal{N}_\gamma^p$.

**Theorem 3.** *The generalized Fisher's information* $\mathrm{J}_\alpha$ *of a r.v.* $X_\gamma \sim \mathcal{N}_\gamma^p(\mu, \lambda\Sigma^*)$ *where* $\lambda \in \mathbb{R}_+ \setminus 0$ *and* $\Sigma^*$ *is a real matrix with unit orthogonal vectors, i.e.* $\Sigma^* \in \mathbb{R}_\perp^{p\times p}$*, is given by*

$$\mathrm{J}_\alpha(X_\gamma) = (\tfrac{\gamma}{\gamma-1})^{\frac{\alpha}{\gamma}} \frac{\Gamma\left(\frac{\alpha+p(\gamma-1)}{\gamma}\right)}{\lambda^{\alpha/2}\,\Gamma\left(p\frac{\gamma-1}{\gamma}\right)}. \tag{15}$$

*Proof.* From (1) we have

$$\mathrm{J}_\alpha(X_\gamma) = \alpha^\alpha \int_{\mathbb{R}^p} \left\| \nabla f_{X_\gamma}^{1/\alpha}(x) \right\|^\alpha dx,$$

while from the definition of the density function $f_{X_\gamma}$, in (7), we have

$$\begin{aligned} \mathrm{J}_\alpha(X_\gamma) &= \alpha^\alpha C_\gamma^p \int\limits_{\mathbb{R}^p} \left\| \nabla \exp\left\{ -\tfrac{\gamma-1}{\alpha\gamma} Q(x)^{\frac{\gamma}{2(\gamma-1)}} \right\} \right\|^\alpha dx \\ &= \alpha^\alpha (\tfrac{\gamma-1}{\alpha\gamma})^\alpha C_\gamma^p \int\limits_{\mathbb{R}^p} \exp\left\{ -\tfrac{\gamma-1}{\gamma} Q^{\frac{\gamma}{2(\gamma-1)}}(x) \right\} \left\| \nabla Q^{\frac{\gamma}{2(\gamma-1)}}(x) \right\|^\alpha dx. \end{aligned} \tag{16}$$

For the gradient of the quadratic form $Q(x)$ we have $\nabla Q(x) = \lambda^{-1}\nabla\{(x-\mu)\Sigma^{*-1}(x-\mu)^{\mathrm{T}}\} = 2\lambda^{-1}\Sigma^{*-1}(x-\mu)^{\mathrm{T}}$, while from the fact that $\Sigma^*$ is an orthogonal matrix we have $\|\Sigma^{*-1}(x-\mu)^{\mathrm{T}}\| = \|x-\mu\|$. Therefore, (16) can be written as

$$\mathrm{J}_\alpha(X_\gamma) = \lambda^{-\alpha} C_\gamma^p \int\limits_{\mathbb{R}^p} \exp\left\{ -\tfrac{\gamma-1}{\gamma} Q^{\frac{\gamma}{2(\gamma-1)}}(x) \right\} Q^{\frac{\alpha\gamma}{2(\gamma-1)}-\alpha}(x) \, \|x-\mu\|^\alpha \, dx.$$

Applying the linear transformation $z = (x-\mu)(\lambda\Sigma^*)^{-1/2}$ in the above integral, it is $dx = d(x-\mu) = \sqrt{\lambda^p \, |\det \Sigma^*|} dz = \lambda^{p/2} dz$, the quadratic form $Q$ is reduced to

$$Q(x) = (x-\mu)(\lambda\Sigma)^{*-1}(x-\mu)^{\mathrm{T}} = (x-\mu)(\lambda\Sigma^*)^{-1/2}[(x-\mu)(\lambda\Sigma^*)^{-1/2}]^{\mathrm{T}} = \|z\|^2,$$

and thus,

$$\mathrm{J}_\alpha(X_\gamma) = \lambda^{(p-\alpha)/2} C_\gamma^p \int\limits_{\mathbb{R}^p} \|z\|^{\frac{\alpha}{\gamma-1}} \exp\left\{ -\tfrac{\gamma-1}{\gamma} \|z\|^{\frac{\gamma}{\gamma-1}} \right\} dz.$$

Switching to hyperspherical coordinates, we get

$$\mathrm{J}_\alpha(X_\gamma) = \lambda^{(p-\alpha)/2} C_\gamma^p \omega_{p-1} \int\limits_0^{+\infty} \rho^{\frac{\alpha}{\gamma-1}} \exp\left\{ -\tfrac{\gamma-1}{\gamma} \rho^{\frac{\gamma}{\gamma-1}} \right\} \rho^{p-1} d\rho,$$

where $\omega_{p-1} = \frac{2\pi^{p/2}}{\Gamma(p/2)}$ is the volume of the $(p-1)$–sphere, $\mathbb{S}_{p-1}$, and hence

$$\mathrm{J}_\alpha(X_\gamma) = 2\frac{\pi^{p/2}}{\Gamma(\frac{\pi}{2})} \lambda^{(p-\alpha)/2} C_\gamma^p \int\limits_0^{+\infty} \rho^{\frac{\alpha+(p-1)(\gamma-1)}{\gamma-1}} \exp\left\{ -\tfrac{\gamma-1}{\gamma} \rho^{\frac{\gamma}{\gamma-1}} \right\} d\rho.$$

From the fact that $d(\frac{\gamma-1}{\gamma}\rho^{\frac{\gamma}{\gamma-1}}) = \rho^{\frac{1}{\gamma-1}}d\rho$ and the definition of the gamma function, we obtain successively

$$\begin{aligned}
\mathrm{J}_\alpha(X_\gamma) &= 2\frac{\pi^{p/2}}{\Gamma(\frac{\pi}{2})}\lambda^{(p-\alpha)/2}C_\gamma^p \int_0^{+\infty} \rho^{\frac{\alpha+(p-1)(\gamma-1)}{\gamma-1}-\frac{1}{\gamma-1}} \exp\left\{-\tfrac{\gamma-1}{\gamma}\rho^{\frac{\gamma}{\gamma-1}}\right\} d(\tfrac{\gamma-1}{\gamma}\rho^{\frac{\gamma}{\gamma-1}}) \\
&= 2\frac{\pi^{p/2}}{\Gamma(\frac{\pi}{2})}\lambda^{(p-\alpha)/2}C_\gamma^p \int_0^{+\infty} \rho^{\frac{\alpha+p\gamma-\gamma-p}{\gamma-1}} \exp\left\{-\tfrac{\gamma-1}{\gamma}\rho^{\frac{\gamma}{\gamma-1}}\right\} d(\tfrac{\gamma-1}{\gamma}\rho^{\frac{\gamma}{\gamma-1}}) \\
&= 2\frac{\pi^{p/2}}{\Gamma(\frac{\pi}{2})}\lambda^{(p-\alpha)/2}(\tfrac{\gamma}{\gamma-1})^{\frac{\alpha-\gamma+p(\gamma-1)}{\gamma}}C_\gamma^p \times \\
&\quad \int_0^{+\infty} (\tfrac{\gamma-1}{\gamma}\rho^{\frac{\gamma}{\gamma-1}})^{\frac{\alpha-\gamma+p(\gamma-1)}{\gamma}} \exp\left\{-\tfrac{\gamma-1}{\gamma}\rho^{\frac{\gamma}{\gamma-1}}\right\} d(\tfrac{\gamma-1}{\gamma}\rho^{\frac{\gamma}{\gamma-1}}) \\
&= 2\frac{\pi^{p/2}}{\Gamma(\frac{\pi}{2})}\lambda^{(p-\alpha)/2}(\tfrac{\gamma}{\gamma-1})^{\frac{\alpha-\gamma+p(\gamma-1)}{\gamma}}C_\gamma^p\,\Gamma(\tfrac{\alpha+p(\gamma-1)}{\gamma}),
\end{aligned}$$

and, finally, applying the normalizing factor $C_\gamma^p$ as in (8), we derive (15) and the Theorem has been proved.

For the defined generalized Fisher's information measure and the $\gamma$–ordered Normal, it is clear that the values of $\mathrm{J}_\alpha(X_\gamma)$ depends on the two parameters $\alpha$ and $\gamma$. Therefore, we shall investigate under what values of $\alpha$ and $\gamma$ there are bounds for $\mathrm{J}_\alpha(X_\gamma)$.

In the following Proposition we provide some inequalities for the generalized Fisher's entropy type information measure $\mathrm{J}_\alpha$ for the family of the $\gamma$–order Normal distributions with positive order $\gamma$, i.e. for $\mathrm{J}_\alpha(X_\gamma)$ where $X_\gamma \sim \mathcal{N}_\gamma^p(\mu, \sigma^2\mathbb{I}_p)$, considering parameters $\alpha > 1$ and $\gamma > 2$.

**Proposition 1.** *The generalized Fisher's information measure* $\mathrm{J}_\alpha$ *of a random variable* $X_\gamma$ *following the multivariate and spherically contoured* $\gamma$*–order Normal distribution, i.e.* $X_\gamma \sim \mathcal{N}_\gamma^p(\mu, \sigma^2\mathbb{I}_p)$, $\alpha, \gamma \geq 2$, *satisfy the inequalities*

$$\mathrm{J}_\alpha(X_\gamma) \begin{cases} > p\sigma^{-\alpha}, & \text{for } \alpha > \gamma, \\ = p\sigma^{-\alpha}, & \text{for } \alpha = \gamma, \\ < p\sigma^{-\alpha}, & \text{for } \alpha < \gamma. \end{cases} \tag{17}$$

*Proof.* For the spherically contoured r.v. $X_\gamma \sim \mathcal{N}_\gamma^p(\mu, \sigma^2\mathbb{I}_p)$ we are reduced to (15) where $\lambda = \sigma^2$. Thus, for the proof the first branch of (17) we assume $\alpha > \gamma$, i.e. $\frac{\alpha}{\gamma} > 1$. Then, we have $\frac{\alpha+p(\gamma-1)}{\gamma} > 1 + p\frac{\gamma-1}{\gamma}$. This implies,

$$\Gamma(\tfrac{\alpha+p(\gamma-1)}{\gamma}) > \Gamma(1 + p\tfrac{\gamma-1}{\gamma}) = p^{\frac{\gamma-1}{\gamma}}\,\Gamma(p\tfrac{\gamma-1}{\gamma}), \tag{18}$$

if $1 + p\frac{\gamma-1}{\gamma} \geq \Gamma_0$, where $\Gamma_0 \approx 1.4628$ denotes the point of minimum for the positive gamma function, $\Gamma(x)$, $x > 0$. That is, if the inequality $x = 1 + p\frac{\gamma-1}{\gamma} \geq \Gamma_0$ holds, then $\Gamma(x) \geq \Gamma(\Gamma_0)$, as the gamma function is an increasing function

for $x \geq \Gamma_0$. Inequality, $1 + p\frac{\gamma-1}{\gamma} \geq \Gamma_0$, is equivalent to, $\gamma \geq \frac{p}{p+1-\Gamma_0} \approx \frac{p}{p-0.4628} > 1$, which is true as $\gamma \geq 2$ in our assumption for the values of parameter $\gamma$. Thus, (18) holds indeed, for orders $\gamma \geq \frac{p}{p+1-\Gamma_0}$, and so,

$$\frac{\Gamma(\frac{\alpha+p(\gamma-1)}{\gamma})}{\Gamma(p\frac{\gamma-1}{\gamma})} > p^{\frac{\gamma-1}{\gamma}}. \tag{19}$$

Our assumption, $\frac{\alpha}{\gamma} > 1$, together with the fact that, $\frac{\gamma}{\gamma-1} > 1$ for all defined orders $\gamma \in \mathbb{R}\backslash[0,\, 1]$, leads us to $(\frac{\gamma}{\gamma-1})^{\alpha/\gamma} > \frac{\gamma}{\gamma-1}$. Then, inequality (19) provides

$$\Big(\frac{\gamma}{\gamma-1}\Big)^{\frac{\alpha}{\gamma}} \frac{\Gamma(\frac{\alpha+p(\gamma-1)}{\gamma})}{\Gamma(p\frac{\gamma-1}{\gamma})} > \frac{\gamma}{\gamma-1} p^{\frac{\gamma-1}{\gamma}} = p,$$

and, using (15), we derive that, $\mathrm{J}_\alpha(X_\gamma) > p\sqrt{|\det \Sigma|}$ for $\alpha > \gamma$, i.e. the first branch of (17) holds. Similarly the other two branches also hold.

**Corollary 2.** *The generalized Fisher's information* $\mathrm{J}_\alpha$ *of a spherically contoured r.v.* $X_\gamma \sim \mathcal{N}_\gamma^p(\mu, \sigma^2 \mathbb{I}_p)$*, with* $\alpha/\gamma \in \mathbb{N}^*$*, is reduced to*

$$\mathrm{J}_\alpha(X_\gamma) = \sigma^{-\alpha}(\gamma-1)^{-\alpha\gamma} \prod_{k=1}^{\alpha/\gamma} \{\alpha - p + (p-k)\gamma\}.$$

The following Fig. 3 depicts the generalized Fisher's information $\mathrm{J}_\alpha$ of the bi–variate (and spherically contoured) $\gamma$–order normally distributed random variables $X_\gamma \sim \mathcal{N}_\gamma^2(\mu, \mathbb{I}_2)$ across the parameter $\alpha > 1$, and for various shape parameters $\gamma = 1, 1.1, \ldots, 1.9, 2, 3, \ldots, 10$. The usual Normal distribution case of $\gamma = 2$ is also highlighted.

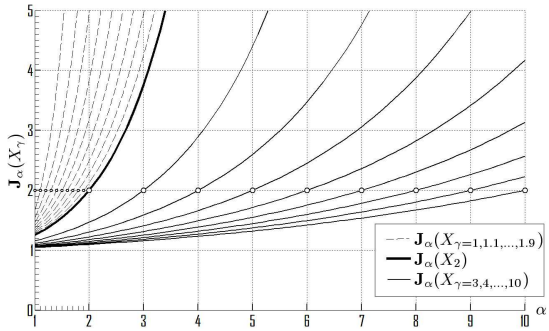


**Fig. 3.** Graphs of $\mathrm{J}_\alpha(X_\gamma)$ across parameter $\alpha > 1$, with $X_\gamma \sim \mathcal{N}_\gamma^2(\mu, \mathbb{I}_2)$, and for various $\gamma$ values.

## 3 Discussion

In this paper we considered the generalized form of the multivariate normal distribution, namely the $\gamma$–order Normal distribution, $\mathcal{N}_{\gamma}^{p}$. This generalization is obtained as an extremal of the LSI corresponding a power–generalization of the entropy type Fisher's information $\mathrm{J}_{\alpha}$. This generalized entropy type information measure, which extends the known entropy type Fisher's information, is discussed and evaluated for the $\gamma$–order normally distributed random variable, say $X_{\gamma}$.

Moreover, the corresponding Rényi and Shannon entropy were evaluated for $X_{\gamma}$, including the specific cases of the multivariate (and elliptically contoured) Uniform, Normal and Laplace distributions, resulting from $\mathcal{N}_{\gamma}^{p}$. Finally, certain boundaries of the $\mathrm{J}_{\alpha}$ were obtained for the spherically contoured $\mathcal{N}_{\gamma}^{p}$ family of distributions.

## References

1. T.M. Cover and J.A. Thomas. *Elements of Information Theory*, 2nd Ed., Wiley, 2006.
2. C.P. Kitsos and N.K. Tavoularis. Logarithmic Sobolev inequalities for information measures, *IEEE Trans. Inform. Theory*, 55, 6, 2554–2561, 2009.
3. C.P. Kitsos and N.K. Tavoularis. New entropy type information measures, in *Information Technology Interfaces*, V. Luzar–Stiffer, Z. Jarec and Z. Bekic (Eds), 255–259, 2009.
4. C.P. Kitsos and T.L. Toulias. New information measures for the generalized normal distribution, *Information*, 1, 13–27, 2010.
5. C.P. Kitsos, T.L. Toulias and P.C. Trandafir On the multivariate $\gamma$–ordered normal distribution, *Far East J. of Theoretical Statistics*, 38, 1, 49–73, 2012.
6. M. Del Pino, J. Dolbeault and I. Gentil. Nonlinear diffusions, hypercontractivity and the optimal $L^{p}$–Euclidean logarithmic Sobolev inequality, *J. Math. Anal. Appl.*, 293, 2, 375–388, 2004.

# Entropy and Information Measures for the Generalized Normal Distribution

Thomas L. Toulias

Department of Informatics, Technological Educational Institute of Athens
12243 Egaleo, Athens, Greece
(E-mail: t.toulias@teiath.gr)

**Abstract.** This paper presents and discusses two generalized forms of the Shannon entropy, as well as a generalized information measure. These measures are applied on a exponential–power generalization of the usual multivariate Normal distribution, i.e. the $\gamma$–order Normal distribution $\mathcal{N}_\gamma$, which is linked to the generalized Fisher's entropy type information measure. Finally, three univariate $\mathcal{N}_\gamma$–based extensions were also given, i.e the $\gamma$–order Lognormal distribution $\mathcal{LN}_\gamma$, the left/right truncated cases of $\mathcal{N}_\gamma$ and $\mathcal{LN}_\gamma$ distributions, and a two–way asymmetric for of the $\mathcal{N}_\gamma$ distribution.
**Keywords:** Fisher's entropy type information measure, $\gamma$–order Normal distribution, Rényi entropy.

## 1 Introduction

A fundamental concept in Information Theory is the so–called information measures (or information). There are several kinds of information measures which all quantify the uncertainty of an outcome of a random experiment, and therefore, in principal, information is a measure of the reduction of uncertainty. Signal Processing and Cryptography are two main fields of applicable aspects of information measures, see Bauer [1], Hoffstein *et al.* [8] and Stinson [17].

In principle, the information measures are divided into three main categories: parametric (Fisher's information being a typical example), non parametric (with Shannon information measure being the most well known) and entropy type, see Cover and Thomas [4], and Ferentinos and Papaioannou [6], which are adopted in this paper.

Let $X$ be a multivariate random variable (r.v.) with parameter vector $\theta = (\theta_1, \theta_2, \ldots, \theta_p) \in \mathbb{R}^p$ and p.d.f. $f_X = f_X(x;\ \theta)$, $x \in \mathbb{R}^p$. The parametric type Fisher's Information Matrix $\mathrm{I}_{\mathrm{F}}(X;\ \theta)$ (also denoted as $\mathrm{I}_\theta(X)$) defined as the covariance of $\nabla_\theta \log f_X(X;\ \theta)$ (where $\nabla_\theta$ is the gradient with respect to the parameters $\theta_i$, $i = 1, 2, \ldots, p$) is a parametric type information measure, expressed also as

$$\begin{aligned} \mathrm{I}_\theta(X) &= \operatorname{Cov}\left(\nabla_\theta \log f_X(X;\ \theta)\right) = \mathrm{E}_\theta\left[\nabla_\theta \log f_X \cdot (\nabla_\theta \log f_X)^{\mathrm{T}}\right] \\ &= \mathrm{E}_\theta\left[\|\nabla_\theta \log f_X\|^2\right], \end{aligned}$$

*Stochastic Modeling, Data Analysis and Statistical Applications* (*pp.* 365-383)
Lidia Filus - Teresa Oliveira - Christos H Skiadas (Eds)



where $\|\cdot\|$ is the usual $\mathscr{L}^2(\mathbb{R}^p)$ norm, while $\mathrm{E}_\theta[\cdot]$ denotes the expected value operator applied to random variables, with respect to parameter $\theta$.

In the same vein, the Fisher's entropy type information measure $\mathrm{I_F}(X)$, or $\mathrm{J}(X)$, of a r.v. $X$ with p.d.f. $f$ on $\mathbb{R}^p$ is defined as the covariance of the r.v. $\nabla \log f(X)$, i.e. $\mathrm{J}(X) := \mathrm{E}[\|\nabla \log f(X)\|^2]$, with $\mathrm{E}[\cdot]$ denoting the usual expected value operator of a random variable with respect to the its p.d.f. Hence, $\mathrm{J}(X)$ can be written as

$$\begin{aligned}\mathrm{J}(X) &= \int\limits_{\mathbb{R}^p} f(x)\|\nabla \log f(x)\|^2 dx = \int\limits_{\mathbb{R}^p} f(x)^{-1}\|\nabla f(x)\|^2 dx \\ &= \int\limits_{\mathbb{R}^p} \nabla f(x)\cdot \nabla \log f(x) dx = 4\int\limits_{\mathbb{R}^p} \left\|\nabla \sqrt{f(x)}\right\|^2 dx. \end{aligned} \tag{1}$$

Generally, the family of the entropy type information measures $\mathrm{I}(X)$, of a $p$–variate r.v. $X$ with p.d.f. $f$, is defined through the *score function* of $X$, i.e.

$$U(X) := \|\nabla \log f(X)\|,$$

as

$$\mathrm{I}(X) := \mathrm{I}(X;\ g, h) := g\left(\mathrm{E}[h(U(X))]\right),$$

where $g$ and $h$ are real–valued functions. For the case of $g = \text{i.d.}$ and $h(X) = X^2$ we obtain the entropy type Fisher's information measure of $X$ as in (31), i.e.

$$\mathrm{I_F}(X) := \mathrm{E}[\|\nabla \log f(X)\|^2]. \tag{2}$$

Besides $\mathrm{I_F}$, other entropy type information measures as the Vajda's, Mathai's and Boeke's information measures, denoted with $\mathrm{I_V}$, $\mathrm{I_M}$ and $\mathrm{I_B}$ respectively, are defined as:

$$\begin{array}{lll} \mathrm{I_F}(X) := \mathrm{I}(X), \text{ with } g := \mathrm{id.} & \text{and } h(U) := U^2, \\ \mathrm{I_V}(X) := \mathrm{I}(X), \text{ with } g := \mathrm{id.} & \text{and } h(U) := U^\lambda,\ \lambda \geq 1, \\ \mathrm{I_M}(X) := \mathrm{I}(X), \text{ with } g(X) := X^{1/\lambda} & \text{and } h(U) := U^\lambda,\ \lambda \geq 1, \\ \mathrm{I_B}(X) := \mathrm{I}(X), \text{ with } g(X) := X^{\lambda-1} & \text{and } h(U) := U^{\frac{\lambda}{\lambda-1}},\ \lambda \in \mathbb{R}_+ \setminus 1. \end{array}$$

Consider now the Vajda's parametric type measure of information $\mathrm{I_V}(X;\ \theta, \alpha)$, which is a generalization of $\mathrm{I_F}(X;\ \theta)$, defined by Vajda [18],

$$\mathrm{I}_V(X;\ \theta, \alpha) := \mathrm{E}_\theta[\|\nabla_\theta \log f(X)\|^\alpha], \quad \alpha \geq 1. \tag{3}$$

Similarly, the Vajda's entropy type information measure $\mathrm{J}_\alpha(X)$ generalizes Fisher's entropy type information $\mathrm{J}(X)$, and is defined as

$$\mathrm{J}_\alpha(X) := \mathrm{E}[\|\nabla \log f(X)\|^\alpha], \quad \alpha \geq 1, \tag{4}$$

see Kitsos and Tavoularis [9]. We shall refer to $\mathrm{J}_\alpha(X)$ as the generalized Fisher's entropy type information measure or $\alpha$–GFI. The second–GFI is reduced to the

usual J, i.e. $\mathrm{J}_2(X) = \mathrm{J}(X)$. Equivalently, from the definition of the $\alpha$–GFI above we can obtain

$$\begin{aligned}\mathrm{J}_\alpha(X) &= \int_{\mathbb{R}^p} \|\nabla \log f(x)\|^\alpha f(x)dx = \int_{\mathbb{R}^p} \|\nabla f(x)\|^\alpha f^{1-\alpha}(x)dx \\ &= \alpha^\alpha \int_{\mathbb{R}^p} \|\nabla f^{1/\alpha}(x)\|^\alpha dx. \end{aligned} \tag{5}$$

The Shannon (or relative) entropy $\mathrm{H}(X)$ of a continuous r.v. $X$ with p.d.f.$f$ is a also a fundamental concept in Information Theory, applied heavily in Cryptography, Stinson [17], and defined as,

$$\mathrm{H}(X) := \mathrm{E}[\log f(X)] = \int_{\mathbb{R}^p} f(x) \log f(x)dx, \tag{6}$$

Cover and Thomas [4], where we omit here the usual minus sign. For any multivariate random variable $X$ with zero mean and covariance matrix $\Sigma$, it holds

$$\mathrm{H}(X) \leq \tfrac{1}{2} \log\{(2\pi e)^p \, |\det \Sigma|\}, \tag{7}$$

while the equality in (7) holds if and only if $X$ is a normally distributed variable, i.e $X \sim N^p(\mu, \Sigma)$, Cover and Thomas [4].

The corresponding entropy power $\mathrm{N}(X)$ is defined by

$$\mathrm{N}(X) := \nu e^{\frac{2}{p}\mathrm{H}(X)}, \tag{8}$$

where $\nu := (2\pi e)^{-1}$. The generalized entropy power $\mathrm{N}_\alpha(X)$, introduced in Kitsos and Tavoularis [9], is of the form

$$\mathrm{N}_\alpha(X) := \nu_\alpha e^{\frac{\alpha}{p}\mathrm{H}(X)}, \tag{9}$$

with normalizing factor $\nu_\alpha$ given by the appropriate generalization of $\nu$, namely

$$\nu_\alpha := \left(\tfrac{\alpha-1}{\alpha e}\right)^{\alpha-1} \pi^{-\frac{\alpha}{2}} \left[\frac{\Gamma\left(\frac{p}{2}+1\right)}{\Gamma\left(p\frac{\alpha-1}{\alpha}+1\right)}\right]^{\frac{\alpha}{p}}, \quad \alpha \in \mathbb{R} \setminus [0,1]. \tag{10}$$

For the parameter case of $\alpha = 2$, (9) is reduced to the known entropy power $\mathrm{N}(X)$, i.e. $\mathrm{N}_2(X) = \mathrm{N}(X)$ and $\nu_2 = \nu$.

The known information inequality $\mathrm{J}(X)\mathrm{N}(X) \geq p$ still holds under the generalized entropy type Fisher's information, as $\mathrm{J}_\alpha(X)\mathrm{N}_\alpha(X) \geq p$, $\alpha > 1$, see Kitsos and Tavoularis [9]. As a result the Cramér–Rao inequality, $\mathrm{J}(X)\,\mathrm{Var}(X) \geq p$ (Cover and Thomas [4], Th. 11.10.1), can be extended to

$$\left[\tfrac{2\pi e}{p}\,\mathrm{Var}(X)\right]^{1/2} \left[\tfrac{\nu_\alpha}{p}\mathrm{J}_\alpha(X)\right]^{1/\alpha} \geq 1, \quad \alpha > 1, \tag{11}$$

see Kitsos and Tavoularis [9]. Under the normality parameter $\alpha = 2$, (11) is reduced to the usual Cramér–Rao inequality.

A lower boundary $B_\alpha^p$ for the introduced generalized information $\mathrm{J}_\alpha(X)$ is then found, as

$$\mathrm{J}_\alpha(X) \geq B_\alpha^p := \tfrac{p}{\nu_\alpha}\left[\tfrac{2\pi e}{p}\operatorname{Var}(X)\right]^{-\alpha/2}. \tag{12}$$

In Fig. 1 the lower boundaries $B_\alpha^p$ across $\alpha$ are depicted, assuming $\operatorname{Var}(X) = 1$ and for all dimensions $p$. Moreover, Fig. 2 depicts the boundaries $B_\alpha^1$ across $\operatorname{Var}(X)$ and for parameter values $\alpha = 1, 2, \ldots, 100$.

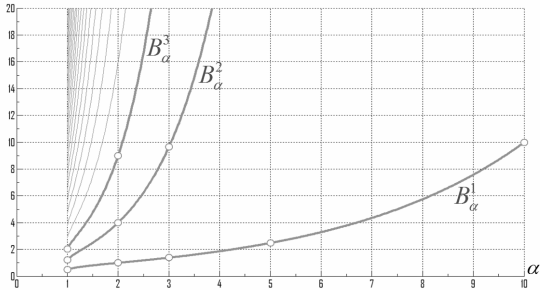


**Fig. 1.** Graphs of the boundaries $B_\alpha^p$ across $\alpha$, with fixed $\operatorname{Var} X = 1$ for every dimension $p \geq 1$.

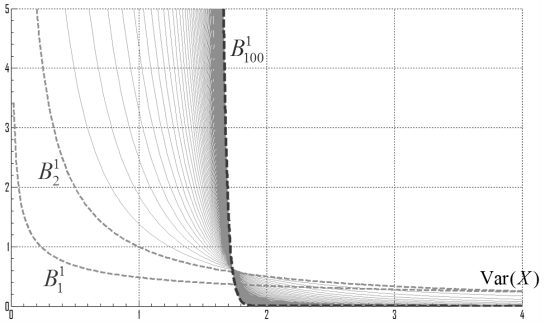


**Fig. 2.** Graphs of the boundaries $B_\alpha^p$ across $\operatorname{Var} X$ for parameters $\alpha = 1, 2, \ldots, 100$.

Through the generalized entropy power $\mathrm{N}_\alpha$ a generalized form of the usual Shannon entropy can be produced, as the Shannon entropy whose entropy power is $\mathrm{N}_\alpha$ (instead of the usual N), i.e.

$$\mathrm{N}_\alpha(X) = \nu \exp\{\tfrac{2}{p}\mathrm{H}_\alpha(X)\}, \quad \alpha \in \mathbb{R} \setminus [0,\, 1], \tag{13}$$

called the *generalized Shannon entropy*, or *$\alpha$–Shannon entropy*. Therefore, from (9) a linear relation between the generalized Shannon entropy $\mathrm{H}_\alpha(X)$ and the usual Shannon entropy $\mathrm{H}(X)$ is obtained, i.e.

$$\mathrm{H}_\alpha(X) = \tfrac{p}{2}\log\tfrac{\nu_\alpha}{\nu} + \tfrac{\alpha}{2}\mathrm{H}(X), \quad \alpha \in \mathbb{R} \setminus [0,\, 1]. \tag{14}$$

Essentially, (14) represents a linear transformation of $\mathrm{H}(X)$, which depends on the parameter $\alpha$ and the dimension $p \in \mathbb{N}$. It is also clear that the generalized Shannon entropy for $\alpha = 2$ is the usual Shannon entropy, i.e. $\mathrm{H}_2 = \mathrm{H}$.

## 2 Entropy and information of the generalized Normal distribution

The Normal distribution, according to Information Theory, is adopted for the noise, acting additively to the input variable when an input–output time discrete channel is formed. Kitsos and Tavoularis in [9,10] introduced and studied a three parameter entropy–power generalization of the multivariate Normal distribution, and its construction is related to the generalized entropy power. See also Kitsos and Toulias [11], and Kitsos *et al.* [14] for further reading. We recall its definition:

**Definition 1.** The $p$–dimensional random variable $X$ follows the $\gamma$–order Normal distribution $\mathcal{N}_\gamma^p(\mu, \Sigma)$ with location parameter vector $\mu \in \mathbb{R}^p$ and positive definite scale matrix $\Sigma \in \mathbb{R}^{p\times p}$, when the density function, $f_X$, is of the form

$$f_X(x;\ \mu, \Sigma, \gamma) = C_\gamma^p |\det \Sigma|^{-1/2}\ \exp\left\{-\tfrac{\gamma-1}{\gamma} Q_\theta(x)^{\frac{\gamma}{2(\gamma-1)}}\right\}, \quad x \in \mathbb{R}^p, \tag{15}$$

with the $p$–quadratic form $Q_\theta(x) := (x-\mu)\,\Sigma^{-1}(x-\mu)^{\mathrm{T}}$, $x \in \mathbb{R}^p$, and $\theta := (\mu, \Sigma) \in \mathbb{R}^{p\times p\times p}$. We shall write $X \sim \mathcal{N}_\gamma^p(\mu, \Sigma)$. The normality factor $C_\gamma^p$ is defined as

$$C_\gamma^p := \pi^{-p/2}\ \frac{\Gamma\left(\frac{p}{2}+1\right)}{\Gamma(p\frac{\gamma-1}{\gamma}+1)} (\tfrac{\gamma-1}{\gamma})^{p\frac{\gamma-1}{\gamma}}. \tag{16}$$

Notice that, for $\gamma = 2$, $\mathcal{N}_2^p(\mu, \Sigma)$ is the well known multivariate normal distribution. It can be also easily noticed that the parameter vector $\mu$ is in fact the mean vector of the $\mathcal{N}_\gamma^p$ distribution, i.e. $\mu = \mathrm{E}[X]$ for all parameters $\gamma \in \mathbb{R} \setminus [0, 1]$.

Denote now with $\mathbb{E}_\theta$ the area of the $p$–ellipsoid $Q_\theta(x) \le 1$, $x \in \mathbb{R}^p$. The family of $\mathcal{N}_\gamma^p(\mu, \Sigma)$, i.e. the family of the elliptically contoured $\gamma$–order Normals, provides a smooth bridging between the multivariate (and elliptically countered) Uniform, Normal and Laplace r.v. $U$, $Z$ and $L$, i.e. between $U \sim \mathcal{U}^p(\mu, \Sigma)$, $Z \sim \mathcal{N}^p(\mu, \Sigma)$ and Laplace $L \sim \mathcal{L}^p(\mu, \Sigma)$ r.v. as well as the multivariate degenerate Dirac distributed r.v. $D \sim \mathcal{D}^p(\mu)$ (with pole at

the point $\mu$), with density functions

$$f_U(x) = f_U(x;\ \mu, \Sigma) := \begin{cases} \dfrac{\Gamma(\frac{p}{2}+1)}{\pi^{p/2}\sqrt{|\det \Sigma|}}, & x \in \mathbb{E}_\theta, \\ 0, & x \notin \mathbb{E}_\theta, \end{cases} \tag{17}$$

$$f_Z(x) = f_Z(x;\ \mu, \Sigma) := \frac{1}{(2\pi)^{p/2}\sqrt{|\det \Sigma|}} \exp\left\{-\tfrac{1}{2}Q_\theta(x)\right\}, \quad x \in \mathbb{R}^p, \tag{18}$$

$$f_L(x) = f_L(x;\ \mu, \Sigma) := \frac{\Gamma(\frac{p}{2}+1)}{p!\pi^{p/2}\sqrt{|\det \Sigma|}} \exp\left\{-\sqrt{Q_\theta(x)}\right\}, \quad x \in \mathbb{R}^p, \tag{19}$$

$$f_D(x) = f_D(x;\ \mu) := \begin{cases} +\infty, & x = \mu, \\ 0, & x \in \mathbb{R}^p \setminus \mu, \end{cases} \tag{20}$$

respectively. That is, the $\mathcal{N}_\gamma^p$ family of distributions, not only generalizes the usual Normal but also two other very significant distributions, as the Uniform and Laplace distributions, are induced. The above discussion is summarized in the following Theorem, see Kitsos *et al.* [14].

**Theorem 1.** *The elliptically contoured $p$–variate $\gamma$–order Normal distribution $\mathcal{N}_\gamma^p(\mu, \Sigma)$ for order values of $\gamma = 0, 1, 2, \pm\infty$ coincides with*

$$\mathcal{N}_\gamma^p(\mu, \Sigma) = \begin{cases} \mathcal{D}^p(\mu), & \text{for } \gamma = 0 \text{ and } p = 1, 2, \\ 0, & \text{for } \gamma = 0 \text{ and } p \geq 3, \\ \mathcal{U}^p(\mu, \Sigma), & \text{for } \gamma = 1, \\ \mathcal{N}^p(\mu, \Sigma), & \text{for } \gamma = 2, \\ \mathcal{L}^p(\mu, \Sigma), & \text{for } \gamma = \pm\infty. \end{cases} \tag{21}$$

*Remark 1.* Considering the above Theorem, the definition values of the shape parameter $\gamma$ of $\mathcal{N}_\gamma^p$ distributions can be extended to include the limiting extra values of $\gamma = 0, 1, \pm\infty$ respectively, i.e. $\gamma$ can now be considered as a real number outside the open interval $(0, 1)$. Particularly, when $X_\gamma \sim \mathcal{N}_\gamma^p(\mu, \Sigma)$, $\gamma \in \mathbb{R} \setminus (0, 1) \cup \{\pm\infty\}$ then the r.v. $X_0$, $X_1 \sim \mathcal{U}^p(\mu, \Sigma)$ and $X_{\pm\infty} \sim \mathcal{L}^p(\mu, \Sigma)$ can be defined as

$$X_0 := \lim_{\gamma \to 0^-} X_\gamma, \quad X_1 := \lim_{\gamma \to 1^+} X_\gamma, \quad X_{\pm\infty} := \lim_{\gamma \to \pm\infty} X_\gamma. \tag{22}$$

Eventually, the Uniform, Normal, Laplace and also the degenerate distribution $\mathcal{N}_0^p$ (like Dirac for dimensions $p = 1, 2$) can be considered as members of the "extended" $\mathcal{N}_\gamma^p$ family of generalized Normal distributions, with $\gamma \in (\mathbb{R} \cup \{\pm\infty\}) \setminus (0,\ 1)$.

Notice also that $\mathcal{N}_1^1(\mu, \sigma)$ coincides with the known (continuous) Uniform distribution $\mathcal{U}(\mu - \sigma, \mu + \sigma)$. Specifically, for every Uniform distribution expressed with the usual notation $\mathcal{U}(a, b)$, it holds that $\mathcal{U}(a, b) = \mathcal{N}_1^1(\frac{a+b}{2}, \frac{b-a}{2}) = \mathcal{U}^1(\mu, \sigma)$. Also $\mathcal{N}_2(\mu, \sigma^2) = \mathcal{N}(\mu, \sigma^2)$, $\mathcal{N}_{\pm\infty}(\mu, \sigma^2) = \mathcal{L}(\mu, \sigma)$ and also $\mathcal{N}_0(\mu, \sigma) = \mathcal{D}(\mu)$. Therefore the following holds.

**Corollary 1.** *The univariate $\gamma$–ordered Normal distributions $\mathcal{N}_\gamma^1(\mu, \sigma^2)$ for order values $\gamma = 0, 1, 2, \pm\infty$ coincides with the usual (univariate) Dirac $\mathcal{D}(\mu)$, Uniform $\mathcal{U}(\mu - \sigma, \mu + \sigma)$, Normal $\mathcal{N}(\mu, \sigma^2)$ and Laplace $\mathcal{L}(\mu, \sigma)$ distributions respectively.*

For the multivariate normally distributed $X \sim \mathcal{N}^p(\mu, \Sigma)$ it is clear, from (15), that the maximum density value $\max f_X = f_X(\mu) = (2\pi)^{-p/2} |\det \Sigma|^{-1/2}$ decreases as dimension $p \in \mathbb{N}$ rises, providing "flattened" probability densities. This is also true for the multivariate Laplace distributed $X \sim \mathcal{L}^p(\mu, \Sigma) = \mathcal{N}^p_{\pm\infty}(\mu, \Sigma)$. In fact, from 19, it holds that $\max f_X = \pi^{-p/2} \frac{1}{p!} \Gamma(\frac{p}{2}+1) |\det \Sigma|^{-1/2}$ and therefore, the high–dimensional Laplace distributions densities are "flattened", since the maximum density values decreases as $p \in \mathbb{N}$ increases. This is true because, for dimensions $2p$, the maximum density is

$$\max f_X = C^p_{\pm\infty} |\det \Sigma|^{-1/2} = \pi^{-p/2} \frac{1}{(p+1)(p+2)...2p} |\det \Sigma|^{-1/2}.$$

Hence, as in the Normal distribution case, $X$ obtains, in principle, heavy tails as the dimension increases. However, this is not the case for the multivariate (and elliptically contoured) Uniform distributed $X \sim \mathcal{U}^p(\mu, \Sigma) = \mathcal{N}^p_1(\mu, \Sigma)$, because the volume of the corresponding $p$–elliptical–cylinder shape of their density functions, as in (17), must always equal 1, although $\mathcal{U}^p$ have no tails to "absorb" probability mass when dimension increases, as the Normal or the Laplace distributions does. Considering the above Remark, the following Proposition shows that, among all elliptical multivariate Uniform distributions $\mathcal{U}^p(\mu, \Sigma)$ with fixed scale matrix $\Sigma$, the $\mathcal{U}^5(\mu, \Sigma)$ has the minimum $\max f_X$, see Kitsos *et al.* [14].

**Theorem 2.** *For the elliptically contoured Uniformly distributed $X \sim \mathcal{U}^p(\mu, \Sigma)$, we have*

$$\min_{p \in \mathbb{N}} \{\max f_X\} = \tfrac{15}{6\pi^2} |\det \Sigma|^{-1} = \max \mathcal{U}^5(\mu, \Sigma),$$

*i.e. the 5–dimensional Uniform distribution provides the least of all maximum density values among all $\mathcal{U}^p(\mu, \Sigma)$ with fixed scale matrix $\Sigma$.*

Recall now the cumulative distribution function (c.d.f.) $\Phi_Z(z)$ of the standardized normally distributed $Z \sim \mathcal{N}(0, 1)$, i.e.

$$\Phi_Z(z) = \tfrac{1}{2} + \tfrac{1}{2} \operatorname{erf}(\tfrac{z}{2}), \quad z \in \mathbb{R}, \tag{23}$$

with $\operatorname{erf}(\cdot)$ being the usual error function. Similarly, for the generalized $\mathcal{N}_\gamma$ family of distributions, the generalized error function $\operatorname{Erf}_{\gamma/(\gamma-1)}$, Gradshteyn and Ryzhik [7], is involved. Indeed, the following holds.

**Theorem 3.** *Let $X$ be a univariate $\gamma$–order normally distributed random variable, i.e. $X \sim \mathcal{N}^p_\gamma(\mu, \sigma^2)$ with p.d.f. $f_X$. Then the c.d.f. $F_X$ of $X$ is the c.d.f. $\Phi_Z$ of the standardized r.v. $Z = \frac{1}{\sigma}(X - \mu) \sim \mathcal{N}_\gamma(0, 1)$, and is given by*

$$F_{X_\gamma}(x) = \Phi_Z(\tfrac{x-\mu}{\sigma}) = \tfrac{1}{2} + \frac{\sqrt{\pi}}{2\,\Gamma(\frac{\gamma-1}{\gamma})\,\Gamma(\frac{\gamma}{\gamma-1})} \operatorname{Erf}_{\frac{\gamma}{\gamma-1}} \left\{ (\tfrac{\gamma-1}{\gamma})^{\frac{\gamma-1}{\gamma}} \tfrac{x-\mu}{\sigma} \right\} \tag{24}$$

$$= 1 - \frac{1}{2\,\Gamma(\frac{\gamma-1}{\gamma})} \Gamma\left( \tfrac{\gamma-1}{\gamma}, \tfrac{\gamma-1}{\gamma} (\tfrac{x-\mu}{\sigma})^{\frac{\gamma}{\gamma-1}} \right), \quad x \in \mathbb{R}, \tag{25}$$

*with $\Gamma(\cdot, \cdot)$ being the upper (complementary) incomplete gamma function.*

Applying the Shannon entropy on a $\gamma$–order normally distributed random variable we obtain the following.

**Proposition 1.** *The Shannon entropy of a random variable $X \sim \mathcal{N}_\gamma^p(\mu, \Sigma)$, with p.d.f. $f_X$, is of the form*

$$\mathrm{H}(X) = p\tfrac{\gamma-1}{\gamma} - \log\{C_\gamma^p |\det \Sigma|^{-1/2}\} = p\tfrac{\gamma-1}{\gamma} - \log\max f_X. \tag{26}$$

*Proof.* Let $C(\Sigma) := C_\gamma^p \det \Sigma\,|^{-1/2}$. From (15) and the definition (6) we have that the Shannon entropy of $X$ is

$$\mathrm{H}(X) = -\log C(\Sigma) + C(\Sigma)^{\frac{\gamma-1}{\gamma}} \int\limits_{\mathbb{R}^p} Q_\theta(x)^{\frac{\gamma}{2(\gamma-1)}} \exp\left\{-\tfrac{\gamma-1}{\gamma} Q_\theta(x)^{\frac{\gamma}{2(\gamma-1)}}\right\} dx.$$

Applying the linear transformation $z = (x-\mu)^{\mathrm{T}} \Sigma^{-1/2}$ with $dx = d(x-\mu) = \sqrt{|\det \Sigma|}dz$, the $\mathrm{H}(X)$ above is reduced to

$$\mathrm{H}(X) = -\log C(\Sigma) + C_\gamma^p \tfrac{\gamma-1}{\gamma} \int\limits_{\mathbb{R}^p} \|z\|^{\frac{\gamma}{\gamma-1}} \exp\left\{-\tfrac{\gamma-1}{\gamma}\|z\|^{\frac{\gamma}{\gamma-1}}\right\} dz.$$

Switching to hyperspherical coordinates, we get

$$\mathrm{H}(X) = -\log C(\Sigma) + C_\gamma^p \tfrac{\gamma-1}{\gamma} \omega_{p-1} \int\limits_{\mathbb{R}_+} \rho^{\frac{\gamma}{\gamma-1}} \exp\left\{-\tfrac{\gamma-1}{\gamma}\rho^{\frac{\gamma}{\gamma-1}}\right\} \rho^{p-1} d\rho,$$

where $\omega_{p-1} := 2\pi^{p/2}/\,\Gamma\left(\frac{p}{2}\right)$ is the volume of the $(p-1)$–sphere. Applying the variable change $du := d(\frac{\gamma-1}{\gamma}\rho^{\gamma/(\gamma-1)}) = \rho^{1/(\gamma-1)} d\rho$ we obtain successively

$$\begin{aligned}
\mathrm{H}(X) &= -\log C(\Sigma) + C_\gamma^p \omega_{p-1} \int\limits_{\mathbb{R}_+} u e^{-u} \rho^{\frac{(p-1)(\gamma-1)-1}{\gamma-1}} du \\
&= \log C(\Sigma) - C_\gamma^p \omega_{p-1} \int\limits_{\mathbb{R}_+} u e^{-u} \left(\rho^{\frac{\gamma}{\gamma-1}}\right)^{\frac{(p-1)(\gamma-1)-1}{\gamma}} du \\
&= -\log C(\Sigma) + C_\gamma^p \omega_{p-1} (\tfrac{\gamma}{\gamma-1})^{p\frac{\gamma-1}{\gamma}-1} \int\limits_{\mathbb{R}_+} u^{p\frac{\gamma-1}{\gamma}} e^{-u} du \\
&= -\log C(\Sigma) + p\tfrac{\gamma-1}{\gamma}\,\Gamma(p\tfrac{\gamma-1}{\gamma}) C_\gamma^p \omega_{p-1}.
\end{aligned}$$

Finally, by substitution of the volume $\omega_{p-1}$ and the normalizing factor $C(\Sigma)$ and $C_\gamma^p$, as in (16), relation (26) is obtained.

**Corollary 2.** *According to the classification Theorem 1, one can evaluate the Shannon entropy for the multivariate (and elliptically contoured) Uniform, Normal and Laplace distributions, i.e.*

$$\mathrm{H}(X) = \begin{cases} \log \frac{\pi^{p/2}}{\Gamma(\frac{p}{2}+1)} \sqrt{|\det \Sigma|}, & \text{for } X \sim \mathcal{N}_1^p(\mu,\Sigma) = \mathcal{U}^p(\mu,\Sigma), \\ \frac{1}{2}\log\{(2\pi e)^p |\det \Sigma|\}, & \text{for } X \sim \mathcal{N}_2^p(\mu,\Sigma) = \mathcal{N}^p(\mu,\Sigma), \\ p + \log \frac{p!\pi^{p/2}}{\Gamma(\frac{p}{2}+1)} \sqrt{|\det \Sigma|}, & \text{for } X \sim \mathcal{N}_{\pm\infty}^p(\mu,\Sigma) = \mathcal{L}^p(\mu,\Sigma), \end{cases} \tag{27}$$

*while for the univariate case $p = 1$, the Shannon entropy is reduced to*

$$\mathrm{H}(X) = \begin{cases} \log 2\sigma, & \text{for } X \sim \mathcal{N}_1^1(\mu, \sigma^2) = \mathcal{U}^1(\mu, \sigma^2) = \mathcal{U}(\mu - \sigma, \mu - \sigma), \\ \log\sqrt{2\pi e}\sigma, & \text{for } X \sim \mathcal{N}_2^1(\mu, \sigma^2) = \mathcal{N}(\mu, \sigma^2), \\ 1 + \log 2\sigma, & \text{for } X \sim \mathcal{N}_{\pm\infty}^1(\mu, \sigma^2) = \mathcal{L}^1(\mu, \sigma^2) = \mathcal{L}(\mu, \sigma). \end{cases}$$

*where $\mathcal{U}(\mu - \sigma, \mu - \sigma)$, $\mathcal{N}(\mu, \sigma^2)$ and $\mathcal{L}(\mu, \sigma)$ are the usual notations for the univariate Uniform, Normal and Laplace distributions respectively.*

*Proof.* Let $X_\gamma \sim \mathcal{N}_\gamma^p(\mu, \Sigma)$ and recall (22). Applying Theorem 1 into (26) the top branch of (27) for $\gamma = 1$ is obtained (in limit), i.e. $\mathrm{H}(X_1) := \lim_{\gamma \to 1^+} \mathrm{H}(X_\gamma)$, the middle branch of (27) for $\gamma = 2$ (normality), while the last branch of (27) is obtained for $\gamma = \pm\infty$ (in limit), i.e. $\mathrm{H}(X_{\pm\infty}) := \lim_{\gamma \to \pm\infty} \mathrm{H}(X_\gamma)$.

Besides the generalized entropy power $\mathrm{N}_\alpha$ (Section 1), another significant entropy measure that generalizes the Shannon entropy is the Rényi entropy. For a $p$–variate continuous random variable with p.d.f. $f_X$, the Rényi entropy $\mathrm{R}_\alpha(X)$ is defined, through the $\alpha$–norm of $f_X \in \mathscr{L}^\alpha(\mathbb{R}^p)$, by

$$\mathrm{R}_\alpha(X) := -\tfrac{\alpha}{\alpha - 1} \log \|f_X\|_\alpha = \tfrac{1}{1-\alpha} \log \int_{\mathbb{R}^p} |f_X(x)|^\alpha dx, \quad \alpha \in \mathbb{R}_+^* \setminus 1, \tag{28}$$

where $\mathbb{R}_+^* := \{\alpha \in \mathbb{R} : \ \alpha > 0\}$. For the limiting case of $\alpha \to 1$ the Rényi entropy converges to the usual Shannon entropy $\mathrm{H}(X)$ as in (6). Notice that the minus sign is used in (28) to be in line with the definition of (6).

Considering now a r.v. from the $\mathcal{N}_\gamma$ family of distributions, the following holds.

**Theorem 4.** *For the $p$–variate, spherically contoured $\gamma$–order normally distributed $X_\gamma \sim \mathcal{N}_\gamma^p(\mu, \sigma^2 \mathbb{I}_p)$, the Rényi entropy of $X_\gamma$ is given by*

$$\mathrm{R}_\alpha(X_\gamma) = p \tfrac{\gamma - 1}{\gamma(\alpha - 1)} \log \alpha - \log(C_\gamma^p \sigma^{-p}), \quad \alpha \in \mathbb{R}_+^* \setminus 1. \tag{29}$$

*Proof.* Consider the p.d.f. $f_{X_\gamma}$ as in (15). From the definition (28) it is

$$\mathrm{R}_\alpha(X_\gamma) = \tfrac{\alpha}{1-\alpha} \log(C_\gamma^p \sigma^{-p}) + \tfrac{1}{1-\alpha} \log \int_{\mathbb{R}^p} \exp\left\{ -\tfrac{\alpha(\gamma-1)}{\gamma} \| \tfrac{x-\mu}{\sigma} \|^{\frac{\gamma}{\gamma-1}} \right\} dx,$$

and applying the linear transformation $z = (x - \mu)\sigma^{-1}$ with $dz = d\{(x - \mu)/\sigma\} = \sigma^{-p} dx$, the $\mathrm{R}_\alpha$ above is reduced to

$$\begin{aligned} \mathrm{R}_\alpha(X_\gamma) &= \tfrac{\alpha}{1-\alpha} \log\left(C_\gamma^p \sigma^{-p}\right) + \tfrac{1}{1-\alpha} \log \left( \sigma^p \int_{\mathbb{R}^p} \exp\left\{ -\tfrac{\alpha(\gamma-1)}{\gamma} \|z\|^{\frac{\gamma}{\gamma-1}} \right\} dz \right) \\ &= \tfrac{\alpha}{1-\alpha} \log(C_\gamma^p \sigma^{p \frac{1-\alpha}{\alpha}}) + \tfrac{1}{1-\alpha} \log \int_{\mathbb{R}^p} \exp\left\{ -\tfrac{\alpha(\gamma-1)}{\gamma} \|z\|^{\frac{\gamma}{\gamma-1}} \right\} dz. \end{aligned}$$

Switching to hyperspherical coordinates, it holds

$$\mathrm{R}_\alpha(X_\gamma) = \tfrac{\alpha}{1-\alpha}\log K(\sigma) + \tfrac{1}{1-\alpha}\log \int\limits_{\mathbb{R}_+} \exp\left\{-\tfrac{\alpha(\gamma-1)}{\gamma}\rho^{\frac{\gamma}{\gamma-1}}\right\}\rho^{p-1}d\rho,$$

where $K(\sigma) := C_\gamma^p \sigma^{p(1-\alpha)/\alpha}\omega_{p-1}^{1/\alpha}$, with $\omega_{p-1} := 2\pi^{p/2}/\,\Gamma(p/2)$ denoting the volume of the $(p-1)$–sphere. Transforming $du := d(\frac{\gamma-1}{\gamma}\rho^{\gamma/(\gamma-1)}) = \rho^{1/(\gamma-1)}d\rho$, it holds successively

$$\begin{aligned}
\mathrm{R}_\alpha(X_\gamma) &= \tfrac{\alpha}{1-\alpha}\log K(\sigma) + \tfrac{1}{1-\alpha}\log \int\limits_{\mathbb{R}_+} e^{-\alpha u}\rho^{\frac{(p-1)(\gamma-1)-1}{\gamma-1}}du \\
&= \tfrac{\alpha}{\alpha-1}\log K(\sigma) + \tfrac{1}{1-\alpha}\log \int\limits_{\mathbb{R}_+} e^{-\alpha u}\left(\rho^{\frac{\gamma}{\gamma-1}}\right)^{\frac{(p-1)(\gamma-1)-1}{\gamma}}du \\
&= \tfrac{\alpha}{1-\alpha}\log K(\sigma) + \tfrac{1}{1-\alpha}\log(\tfrac{\gamma}{\gamma-1})^{p\frac{\gamma-1}{\gamma}-1} + \tfrac{1}{1-\alpha}\log \int\limits_{\mathbb{R}_+} e^{-\alpha u}u^{p\frac{\gamma-1}{\gamma}-1}du \\
&= \tfrac{\alpha}{1-\alpha}\log K(\sigma) + \tfrac{1}{1-\alpha}\log(\tfrac{\gamma}{\gamma-1})^{p\frac{\gamma-1}{\gamma}-1} - p\tfrac{\gamma-1}{\gamma}\cdot\tfrac{\log\alpha}{1-\alpha} + \tfrac{1}{1-\alpha}\log\Gamma(p\tfrac{\gamma-1}{\gamma}).
\end{aligned}$$

Finally, by substitution of the expressions for $K(\sigma)$, $\omega_{p-1}$ and the normalizing factor $C_\gamma^p$, the Rényi entropy entropy is then given by

$$\mathrm{R}_\alpha(X_\gamma) = p\log\sigma - \tfrac{\alpha}{1-\alpha}\log C_\gamma^p + \tfrac{1}{1-\alpha}\log C_\gamma^p + p\tfrac{\gamma-1}{\gamma}\cdot\tfrac{\log\alpha}{\alpha-1},$$

and hence (29) holds true.

The collision and the mean–entropy are certain entropy measures often used in Cryptology. There measures are provided by the Rényi entropy, for specific parameter values, through the following:

**Corollary 3.** *For the special cases of $\alpha = 0, 1, 2, +\infty$, the Rényi entropy of $X_\gamma \sim \mathcal{N}_\gamma(\mu, \Sigma)$ is reduced to*

$$\mathrm{R}_\alpha(X_\gamma) = \begin{cases} +\infty, & \alpha = 0, \quad (\textit{Hartley entropy}) \\ p\frac{\gamma-1}{\gamma} - \log(C_\gamma^p/\sigma^p), & \alpha = 1, \quad (\textit{Shannon entropy}) \\ p\frac{\gamma-1}{\gamma}\log 2 - \log(C_\gamma^p/\sigma^p), & \alpha = 2, \quad (\textit{collision entropy}) \\ -\log(C_\gamma^p/\sigma^p), & \alpha = +\infty. \quad (\textit{min–entropy}) \end{cases}$$

Rényi entropy $\mathrm{R}_\alpha(X_\gamma)$, as in (29), is an decreasing function of parameter $\alpha$, and therefore

$$\mathrm{R}_{+\infty}(X_\gamma) < \mathrm{R}_2(X_\gamma) < \mathrm{R}_1(X_\gamma) < \mathrm{R}_0(X_\gamma), \quad \gamma \in \mathbb{R}\setminus[0\,1].$$

*Example 1.* For the multivariate and spherically contoured Uniform random variable $U \sim \mathcal{U}(\mu, \sigma^2\mathbb{I}_p)$, the Hartley, Shannon, collision and the min– entropies coincide as,

$$\mathrm{R}_\alpha(U) = \log\frac{\pi^{p/2}\sigma^p}{\Gamma(\frac{p}{2}+1)}, \quad \alpha \in \mathbb{R}_+\setminus 1,$$

while for the univariate case of $U \sim \mathcal{U}(\mu-\sigma, \mu-\sigma)$ the Rényi entropy is reduced to

$$\mathrm{R}_\alpha(U) = \log(2\sigma), \quad \alpha \in \mathbb{R}_+ \setminus 1.$$

Notice that for a uniformly distributed r.v. the Rényi entropy $\mathrm{R}_\alpha$ is $\alpha$–invariant, depending only on the dimension $p \in \mathbb{N}$ and the scale parameter $\sigma$.

*Example 2.* For the multivariate and spherically contoured Laplace random variable $L \sim \mathcal{L}(\mu, \sigma^2 \mathbb{I}_p)$, the Hartley, Shannon, collision and the min– entropies are given by,

$$\mathrm{R}_\alpha(L) = \begin{cases} +\infty, & \alpha = 0, \quad \text{(Hartley entropy)} \\ p + \log\{p!\pi^{p/2}\sigma^p\,\Gamma(\frac{p}{2}+1)^{-1}\}, & \alpha = 1, \quad \text{(Shannon entropy)} \\ \log\{2^p p!\pi^{p/2}\sigma^p\,\Gamma(\frac{p}{2}+1)^{-1}\}, & \alpha = 2, \quad \text{(collision entropy)} \\ \log\{p!\pi^{p/2}\sigma^p\,\Gamma(\frac{p}{2}+1)^{-1}\}, & \alpha = +\infty. \quad \text{(min–entropy)} \end{cases}$$

Now, the generalized Fisher's entropy type information of a random variable following the multivariate $\mathcal{N}_\gamma^p$, is evaluated.

**Theorem 5.** *The generalized Fisher's information* $\mathrm{J}_\alpha$ *of a r.v.* $X_\gamma \sim \mathcal{N}_\gamma^p(\mu, \lambda\Sigma^*)$ *where* $\lambda \in \mathbb{R}_+^*$ *and* $\Sigma^*$ *is a real matrix with unit orthogonal vectors, i.e.* $\Sigma^* \in \mathbb{R}_\perp^{p\times p}$*, is given by*

$$\mathrm{J}_\alpha(X_\gamma) = (\tfrac{\gamma}{\gamma-1})^{\frac{\alpha}{\gamma}} \frac{\Gamma\left(\frac{\alpha+p(\gamma-1)}{\gamma}\right)}{\lambda^{\alpha/2}\,\Gamma\left(p\frac{\gamma-1}{\gamma}\right)}, \quad \alpha \in \mathbb{R}_+ \setminus 1. \tag{30}$$

*Proof.* From (5),

$$\mathrm{J}_\alpha(X_\gamma) = \alpha^\alpha \int\limits_{\mathbb{R}^p} \left\| \nabla f_{X_\gamma}^{1/\alpha}(x) \right\|^\alpha dx,$$

while from the definition of the density function $f_{X_\gamma}$, as in (15),

$$\begin{aligned} \mathrm{J}_\alpha(X_\gamma) &= \alpha^\alpha C_\gamma^p \int\limits_{\mathbb{R}^p} \left\| \nabla \exp\left\{ -\tfrac{\gamma-1}{\alpha\gamma} Q(x)^{\frac{\gamma}{2(\gamma-1)}} \right\} \right\|^\alpha dx \\ &= \alpha^\alpha (\tfrac{\gamma-1}{\alpha\gamma})^\alpha C_\gamma^p \int\limits_{\mathbb{R}^p} \exp\left\{ -\tfrac{\gamma-1}{\gamma} Q^{\frac{\gamma}{2(\gamma-1)}}(x) \right\} \left\| \nabla Q^{\frac{\gamma}{2(\gamma-1)}}(x) \right\|^\alpha dx. \end{aligned} \tag{31}$$

For the gradient of the quadratic form $Q(x)$ it holds that $\nabla Q(x) = \lambda^{-1}\nabla\{(x-\mu)\Sigma^{*-1}(x-\mu)^{\mathrm{T}}\} = 2\lambda^{-1}\Sigma^{*-1}(x-\mu)^{\mathrm{T}}$, while from the fact that $\Sigma^*$ is an orthogonal matrix we have $\|\Sigma^{*-1}(x-\mu)^{\mathrm{T}}\| = \|x-\mu\|$. Therefore, (5) can be written as

$$\mathrm{J}_\alpha(X_\gamma) = \lambda^{-\alpha} C_\gamma^p \int\limits_{\mathbb{R}^p} \exp\left\{ -\tfrac{\gamma-1}{\gamma} Q^{\frac{\gamma}{2(\gamma-1)}}(x) \right\} Q^{\frac{\alpha\gamma}{2(\gamma-1)}-\alpha}(x)\, \|x-\mu\|^\alpha\, dx.$$

Applying the linear transformation $z := (x-\mu)(\lambda\Sigma^*)^{-1/2}$ in the above integral, it is $dx = d(x-\mu) = \sqrt{\lambda^p\,|\det\Sigma^*|}dz = \lambda^{p/2}dz$, the quadratic form $Q$ is reduced to

$$Q(x) = (x-\mu)(\lambda\Sigma)^{*-1}(x-\mu)^{\mathrm{T}} = (x-\mu)(\lambda\Sigma^*)^{-1/2}[(x-\mu)(\lambda\Sigma^*)^{-1/2}]^{\mathrm{T}} = \|z\|^2,$$

and thus,

$$\mathrm{J}_\alpha(X_\gamma) = \lambda^{(p-\alpha)/2}C_\gamma^p \int\limits_{\mathbb{R}^p} \|z\|^{\frac{\alpha}{\gamma-1}} \exp\left\{-\tfrac{\gamma-1}{\gamma}\|z\|^{\frac{\gamma}{\gamma-1}}\right\} dz.$$

Switching to hyperspherical coordinates, it holds

$$\mathrm{J}_\alpha(X_\gamma) = \lambda^{(p-\alpha)/2}C_\gamma^p\omega_{p-1} \int\limits_0^{+\infty} \rho^{\frac{\alpha}{\gamma-1}} \exp\left\{-\tfrac{\gamma-1}{\gamma}\rho^{\frac{\gamma}{\gamma-1}}\right\} \rho^{p-1}d\rho,$$

where $\omega_{p-1} := \frac{2\pi^{p/2}}{\Gamma(p/2)}$ is the volume of the $(p-1)$–sphere, $\mathbb{S}_{p-1}$, and hence

$$\mathrm{J}_\alpha(X_\gamma) = 2\frac{\pi^{p/2}}{\Gamma(\frac{\pi}{2})}\lambda^{(p-\alpha)/2}C_\gamma^p \int\limits_0^{+\infty} \rho^{\frac{\alpha+(p-1)(\gamma-1)}{\gamma-1}} \exp\left\{-\tfrac{\gamma-1}{\gamma}\rho^{\frac{\gamma}{\gamma-1}}\right\} d\rho.$$

From the fact that $d(\frac{\gamma-1}{\gamma}\rho^{\frac{\gamma}{\gamma-1}}) = \rho^{\frac{1}{\gamma-1}}d\rho$ and the definition of the gamma function, we obtain successively

$$\begin{aligned}
\mathrm{J}_\alpha(X_\gamma) &= 2\frac{\pi^{p/2}}{\Gamma(\frac{\pi}{2})}\lambda^{(p-\alpha)/2}C_\gamma^p \int\limits_0^{+\infty} \rho^{\frac{\alpha+(p-1)(\gamma-1)}{\gamma-1}-\frac{1}{\gamma-1}} \exp\left\{-\tfrac{\gamma-1}{\gamma}\rho^{\frac{\gamma}{\gamma-1}}\right\} d(\tfrac{\gamma-1}{\gamma}\rho^{\frac{\gamma}{\gamma-1}}) \\
&= 2\frac{\pi^{p/2}}{\Gamma(\frac{\pi}{2})}\lambda^{(p-\alpha)/2}C_\gamma^p \int\limits_0^{+\infty} \rho^{\frac{\alpha+p\gamma-\gamma-p}{\gamma-1}} \exp\left\{-\tfrac{\gamma-1}{\gamma}\rho^{\frac{\gamma}{\gamma-1}}\right\} d(\tfrac{\gamma-1}{\gamma}\rho^{\frac{\gamma}{\gamma-1}}) \\
&= 2\frac{\pi^{p/2}}{\Gamma(\frac{\pi}{2})}\lambda^{(p-\alpha)/2}(\tfrac{\gamma}{\gamma-1})^{\frac{\alpha-\gamma+p(\gamma-1)}{\gamma}}C_\gamma^p\times \\
&\quad \int\limits_0^{+\infty} (\tfrac{\gamma-1}{\gamma}\rho^{\frac{\gamma}{\gamma-1}})^{\frac{\alpha-\gamma+p(\gamma-1)}{\gamma}} \exp\left\{-\tfrac{\gamma-1}{\gamma}\rho^{\frac{\gamma}{\gamma-1}}\right\} d(\tfrac{\gamma-1}{\gamma}\rho^{\frac{\gamma}{\gamma-1}}) \\
&= 2\frac{\pi^{p/2}}{\Gamma(\frac{\pi}{2})}\lambda^{(p-\alpha)/2}(\tfrac{\gamma}{\gamma-1})^{\frac{\alpha-\gamma+p(\gamma-1)}{\gamma}}C_\gamma^p\,\Gamma(\tfrac{\alpha+p(\gamma-1)}{\gamma}),
\end{aligned}$$

and, finally, applying the normalizing factor $C_\gamma^p$ as in (16), we derive (30) and the Theorem has been proved.

For the defined generalized Fisher's information measure and the $\gamma$–ordered Normal, it is clear that the values of $\mathrm{J}_\alpha(X_\gamma)$ depends on the two parameters $\alpha$ and $\gamma$. Therefore, we shall investigate for which values of $\alpha$ and $\gamma$ the $\mathrm{J}_\alpha(X_\gamma)$ is bounded.

In the following Proposition we provide some inequalities for the generalized Fisher's entropy type information measure $\mathrm{J}_\alpha$ for the family of the $\gamma$–order Normal distributions with positive order $\gamma$, i.e. for $\mathrm{J}_\alpha(X_\gamma)$ where $X_\gamma \sim \mathcal{N}_\gamma^p(\mu, \sigma^2 \mathbb{I}_p)$, considering parameters $\alpha > 1$ and $\gamma > 2$.

**Proposition 2.** *The generalized Fisher's information measure* $\mathrm{J}_\alpha$ *of a random variable* $X_\gamma$ *following the multivariate and spherically contoured* $\gamma$*–order Normal distribution, i.e.* $X_\gamma \sim \mathcal{N}_\gamma^p(\mu, \sigma^2 \mathbb{I}_p)$, $\alpha, \gamma \geq 2$, *satisfy the inequalities*

$$\mathrm{J}_\alpha(X_\gamma) \begin{cases} > p\sigma^{-\alpha}, \ \textit{for } \alpha > \gamma, \\ = p\sigma^{-\alpha}, \ \textit{for } \alpha = \gamma, \\ < p\sigma^{-\alpha}, \ \textit{for } \alpha < \gamma. \end{cases} \tag{32}$$

*Proof.* For the spherically contoured r.v. $X_\gamma \sim \mathcal{N}_\gamma^p(\mu, \sigma^2 \mathbb{I}_p)$ we are reduced to (30) where $\lambda = \sigma^2$. Thus, for the proof of the first branch of (32) we assume $\alpha > \gamma$, i.e. $\frac{\alpha}{\gamma} > 1$. Then, we have $\frac{\alpha + p(\gamma-1)}{\gamma} > 1 + p\frac{\gamma-1}{\gamma}$. This implies,

$$\Gamma(\tfrac{\alpha+p(\gamma-1)}{\gamma}) > \Gamma(1 + p\tfrac{\gamma-1}{\gamma}) = p^{\frac{\gamma-1}{\gamma}}\, \Gamma(p\tfrac{\gamma-1}{\gamma}), \tag{33}$$

if $1 + p\frac{\gamma-1}{\gamma} \geq \Gamma_0$, where $\Gamma_0 \approx 1.4628$ denotes the point of minimum for the positive gamma function, $\Gamma(x)$, $x > 0$. That is, if the inequality $x = 1 + p\frac{\gamma-1}{\gamma} \geq \Gamma_0$ holds, then $\Gamma(x) \geq \Gamma(\Gamma_0)$, as the gamma function is an increasing function for $x \geq \Gamma_0$. Inequality, $1 + p\frac{\gamma-1}{\gamma} \geq \Gamma_0$, is equivalent to, $\gamma \geq \frac{p}{p+1-\Gamma_0} \approx \frac{p}{p-0.4628} > 1$, which is true as $\gamma \geq 2$ in our assumption for the values of parameter $\gamma$. Thus, (33) holds indeed, for orders $\gamma \geq \frac{p}{p+1-\Gamma_0}$, and so,

$$\frac{\Gamma(\frac{\alpha+p(\gamma-1)}{\gamma})}{\Gamma(p\frac{\gamma-1}{\gamma})} > p^{\frac{\gamma-1}{\gamma}}. \tag{34}$$

Our assumption, $\frac{\alpha}{\gamma} > 1$, together with the fact that, $\frac{\gamma}{\gamma-1} > 1$ for all defined orders $\gamma \in \mathbb{R} \backslash [0,\, 1]$, leads us to $(\frac{\gamma}{\gamma-1})^{\alpha/\gamma} > \frac{\gamma}{\gamma-1}$. Then, inequality (34) provides

$$\left(\tfrac{\gamma}{\gamma-1}\right)^{\frac{\alpha}{\gamma}} \frac{\Gamma(\frac{\alpha+p(\gamma-1)}{\gamma})}{\Gamma(p\frac{\gamma-1}{\gamma})} > \tfrac{\gamma}{\gamma-1} p^{\frac{\gamma-1}{\gamma}} = p,$$

and, using (30), we derive that, $\mathrm{J}_\alpha(X_\gamma) > p\sqrt{|\det \Sigma|}$ for $\alpha > \gamma$, i.e. the first branch of (32) holds. Similarly the other two branches also hold.

**Corollary 4.** *The generalized Fisher's information* $\mathrm{J}_\alpha$ *of a spherically contoured r.v.* $X_\gamma \sim \mathcal{N}_\gamma^p(\mu, \sigma^2 \mathbb{I}_p)$, *with* $\alpha/\gamma \in \mathbb{N}^*$, *is reduced to*

$$\mathrm{J}_\alpha(X_\gamma) = \sigma^{-\alpha}(\gamma - 1)^{-\alpha\gamma} \prod_{k=1}^{\alpha/\gamma} \{\alpha - p + (p-k)\gamma\}. \tag{35}$$

*Proof.* From (30) and the gamma function additive identity, i.e. $\Gamma(x+1) = x\,\Gamma(x)$, $x \in \mathbb{R}_+^*$, relation (35) holds

The following Fig. 3 depicts the generalized Fisher's information $\mathrm{J}_\alpha$ of the bi– and tri–variate (and spherically contoured) $\gamma$–order normally distributed random variables $X_\gamma \sim \mathcal{N}_\gamma^2(\mu, \mathbb{I}_{p=1,2})$, across the parameter $\alpha > 1$, and for various shape parameters $\gamma = 1, 1.1, \ldots, 1.9, 2, 3, \ldots, 10$. The bivariate case $p = 2$ is presented in the left sub–figure, while the trivariate case $p = 3$ in the right sub–figure. The usual Normal distribution case of $\gamma = 2$ is also highlighted.

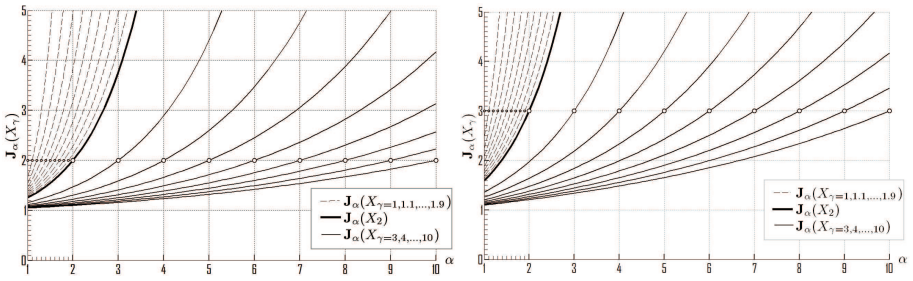


**Fig. 3.** Graphs of $\mathrm{J}_\alpha(X_\gamma)$ across parameter $\alpha > 1$, with $X_\gamma \sim \mathcal{N}_\gamma^2(\mu, \mathbb{I}_{p=2,3})$, and for various $\gamma$ values.

## 3 Other $\mathcal{N}_\gamma$–based extensions

We present here some distributions that are based on the $\gamma$–order Normal distribution.

### 3.1 Generalized Lognormal distribution

The Lognormal distribution is defined as the distribution of a random variable whose logarithm is normally distributed, and usually is formulated with two parameters. It is widely applied in life sciences, including Biology, Ecology, Geology, Meteorology as well as Economics, Finance, and Risk Analysis, see Crow and Shimizu [5]. Also, it plays an important role in Astrophysics and Cosmology, see Bernardeau and Kofman [2], Blasi *et al.* [3] among others.

Furthermore, Log–Uniform and Log–Laplace distribution can be similarly defined with applications in Finance, see Yan and Hanson [19], Kozubowski and Podgórski [15]. Especially, the power–tail phenomenon of the Log–Laplace distribution, Kozubowski and Podgórski [16], attracts, very often, attention in Environmental Sciences, Physics and Economics.

The Lognormal distribution can be also extended to the $\gamma$–order Lognormal distribution, denoted with $\mathcal{LN}(\mu, \sigma^2)$, in the sense that if $X \sim \mathcal{N}_\gamma^1(\mu, \sigma^2)$, with p.d.f. $f_X$, then $Y = e^X$ follows the $\mathcal{LN}_\gamma(\mu, \sigma)$ with p.d.f.

$$g_Y(y) := \tfrac{1}{y} f_X(\log y) = C_\gamma^1(\sigma y)^{-1} \exp\left\{ -\tfrac{\gamma-1}{\gamma} \left| \tfrac{\log y - \mu}{\sigma} \right|^{\frac{\gamma}{\gamma-1}} \right\}, \quad y \in \mathbb{R}_+^*. \quad (36)$$

Moreover, if $X \sim \mathcal{LN}_\gamma(\mu, \sigma)$ then $\log X \sim \mathcal{N}_\gamma^1(\mu, \sigma^2)$.

For certain shape parameter values $\gamma$ the $\mathcal{LN}_\gamma$ distribution is reduced to Log–Uniform and Log–Laplace distribution. See [12] for further reading on the subject.

Figure 4 illustrates, in a compact form, all the density functions $f_{X_\gamma}(x)$, $x \in [-3, 3]$, for all $\gamma \in [-10, 0) \cup [1, 10]$, where $X_\gamma \sim \mathcal{LN}_\gamma(0, 1)$. The known densities of Log–Uniform ($\gamma = 1$) and Lognormal ($\gamma = 2$) distributions are also depicted. Moreover the densities of $\mathcal{LN}_{\gamma=\pm 10}(0, 1)$, which approximate the density of Log–Laplace distribution $\mathcal{LL}(0, 1) = \mathcal{LN}_{\pm\infty}(0, 1)$, as well as the density of $\mathcal{LN}_{-0.005}(0, 1)$, which approximates the degenerate Dirac distribution $\mathcal{D}(1)$, are clearly presented. One can notice the smooth–bringing between these significant distributions that are included in the family of the $\gamma$–order Lognormal distribution.

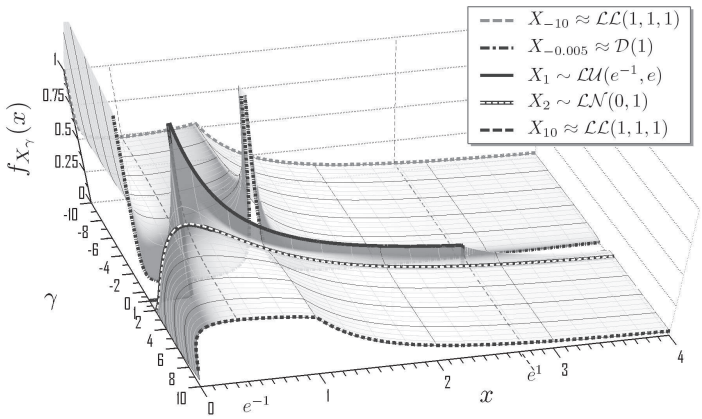


**Fig. 4.** Graph of all the densities $f_{X_\gamma}(x)$, $x \in [-3, 3]$, for various shape parameters $\gamma$, where $X_\gamma \sim \mathcal{LN}_\gamma(0, 1)$.

### 3.2 Truncated $\gamma$–order Normal and Lognormal distribution

Let $X$ be a univariate r.v. from $\mathcal{N}_\gamma(\mu, \sigma^2)$ with p.d.f. $f_X$, as in (15), and c.d.f. $F_X$, as in (24) or (25). Then, the r.v. $X_\rho^+$ is said to follow the *right–truncated $\gamma$–order Normal distribution at the point* $\rho \in \mathbb{R}$, when its p.d.f. $f_{X_\rho^+}$ is of the form

$$f_{X_\rho^+}(x) := \begin{cases} 0, & \text{if } x > \rho, \\ \dfrac{f_X(x)}{F_X(\rho)} = \dfrac{C_\gamma^1}{\sigma F_X(\rho)} \exp\left\{ -\frac{\gamma-1}{\gamma} \left| \frac{x-\mu}{\sigma} \right|^{\frac{\gamma}{\gamma-1}} \right\}, & \text{if } x \le \rho, \end{cases}$$

while $X_\tau^-$ is said to follow the *left–truncated $\gamma$–order Normal distribution at the point* $\tau \in \mathbb{R}$, when its p.d.f. $f_{X_\tau^-}$ is given by

$$f_{X_\tau^-}(x) := \begin{cases} 0, & \text{if } x < \tau, \\ \dfrac{f_X(x)}{1-F_X(\tau)} = \dfrac{C_\gamma^1}{\sigma - \sigma F_X(\tau)} \exp\left\{-\frac{\gamma-1}{\gamma}\left|\frac{x-\mu}{\sigma}\right|^{\frac{\gamma}{\gamma-1}}\right\}, & \text{if } x \geq \tau. \end{cases}$$

For the generalized Lognormal case $Y := e^X \sim \mathcal{LN}_\gamma(\mu, \sigma^2)$, through (36), the r.v. $Y_\rho^+$ follows the *right–truncated $\gamma$–order Lognormal distribution at the (log–scaled) point* $\rho \in \mathbb{R}_+^*$, when its p.d.f. $g_{Y_\rho^+}$ is of the form

$$g_{Y_\rho^+}(y) := \begin{cases} 0, & \text{if } y > \rho, \\ \dfrac{f_X(\log y)}{y F_X(e^\rho)} = \dfrac{C_\gamma^1}{\sigma y F_X(e^\rho)} \exp\left\{-\frac{\gamma-1}{\gamma}\left|\frac{\log y-\mu}{\sigma}\right|^{\frac{\gamma}{\gamma-1}}\right\}, & \text{if } y \leq \rho, \end{cases}$$

while the r.v. $Y_\tau^-$ follows the *left–truncated $\gamma$–order Lognormal distribution at the (log–scaled) point* $\tau \in \mathbb{R}_+^*$, when its p.d.f. $g_{Y_\tau^-}$ is given by

$$g_{Y_\tau^-}(y) := \begin{cases} 0, & \text{if } y < \tau, \\ \dfrac{f_X(\log y)}{y - y F_X(e^\tau)} = \dfrac{C_\gamma^1}{\sigma y[1-F_X(e^\tau)]} \exp\left\{-\frac{\gamma-1}{\gamma}\left|\frac{\log y-\mu}{\sigma}\right|^{\frac{\gamma}{\gamma-1}}\right\}, & \text{if } y \geq \tau. \end{cases}$$

### 3.3 Asymmetric form of the $\gamma$–order Normal Distribution

A two–way asymmetric form of the $\mathcal{N}_\gamma$ family can be constructed using a pair $(\sigma_1, \sigma_2)$ of asymmetric scale parameters, and/or a pair $(\gamma_1, \gamma_2)$ of asymmetric shape parameters.

A r.v. $X$ follows the (two–way) *asymmetric ($\gamma_1$,$\gamma_2$)–order Normal distribution*, denoted by $\mathcal{AN}_{\gamma_1,\gamma_2}(\mu, \sigma_1^2, \sigma_2^2)$, when its p.d.f. $f_X$ is defined as

$$f_X(x) := \begin{cases} C \exp\left\{-\frac{\gamma_1-1}{\gamma_1}\left|\frac{x-\mu}{\sigma_1}\right|^{\frac{\gamma_1}{\gamma_1-1}}\right\}, & x < \mu, \\ C \exp\left\{-\frac{\gamma_2-1}{\gamma_2}\left|\frac{x-\mu}{\sigma_2}\right|^{\frac{\gamma_2}{\gamma_2-1}}\right\}, & x \geq \mu, \end{cases}$$

with $\mu$ being the (maximum density) turning point, and $C$ being the (mutual) normalizing factor

$$C := \frac{2C_{\gamma_1}^1 C_{\gamma_2}^1}{\sigma_1 C_{\gamma_2}^1 + \sigma_2 C_{\gamma_1}^1} = \frac{1}{\sigma_1 \Gamma(\frac{\gamma_1-1}{\gamma_1})(\frac{\gamma_1-1}{\gamma_1})^{1/\gamma_1} + \sigma_2 \Gamma(\frac{\gamma_2-1}{\gamma_2})(\frac{\gamma_2-1}{\gamma_2})^{1/\gamma_1}}.$$

Equivalently, when $X_1$, $X_2$ are two univariate (and symmetric) r.v. from $\mathcal{N}_{\gamma_1}(\mu, \sigma_1^2)$ and $\mathcal{N}_{\gamma_2}(\mu, \sigma_2^2)$, for the asymmetric r.v. $X$ with p.d.f. $f_{X_1}$ and $f_{X_2}$, it is

$$f_X(x) = \frac{2}{1 + \left(\frac{\sigma_2 C_{\gamma_2}^1}{\sigma_1 C_{\gamma_1}^1}\right)^{\operatorname{sgn}(\mu-x)}} \times \begin{cases} f_{X_1}(x), & x < \mu, \\ f_{X_2}(x), & x \geq \mu. \end{cases}$$

where $\mathrm{sgn}(\cdot)$ is the sign function. See Fig. 5 for the visualization of some "shape–asymmetric" $\mathcal{AN}_{2;\gamma}(0,1,1)$ distributions (with fixed shape parameter $\gamma_1 = 2$ for the left part of the p.d.f. and various $\gamma$ parameter values for the right part of the asymmetric p.d.f.). For some "scale–asymmetric" distributions $\mathcal{AN}_{\gamma,\gamma}(0,1,\sigma^2)$ see Fig. 6 (depicting four cases of shape parameter values $\gamma = 6/5, 2, 4, -2$, with fixed scale parameter $\sigma_1 = 1$ for the p.d.f.'s left part, and various $\sigma$ parameter values for the right part of the asymmetric p.d.f.).

The c.d.f. $F_X$ of the asymmetric r.v. $X \sim \mathcal{AN}_{\gamma_1,\gamma_2}(\mu, \sigma_1^2, \sigma_2^2)$ is then given by

$$F_X(x) = \begin{cases} \frac{1+\mathrm{sgn}(x-\mu)}{1+k} + \frac{\mathrm{sgn}(x-\mu)}{(1+k)\,\Gamma(\frac{\gamma-1}{\gamma})}\,\Gamma\left(\frac{\gamma-1}{\gamma}, \frac{\gamma-1}{\gamma}\left|\frac{x-\mu}{\sigma}\right|^{\frac{\gamma}{\gamma-1}}\right), & x < \mu, \\ \frac{1}{1+k} + \frac{1}{1+k^{-1}}\left[2 - \Gamma(\frac{\gamma-1}{\gamma})^{-1}\,\Gamma\left(\frac{\gamma-1}{\gamma}, \frac{\gamma-1}{\gamma}\left(\frac{x-\mu}{\sigma}\right)^{\frac{\gamma}{\gamma-1}}\right)\right], & x \geq \mu, \end{cases}$$

where $k = (\sigma_2 C^1_{\gamma_2})(\sigma_1 C^1_{\gamma_1})^{-1}$.

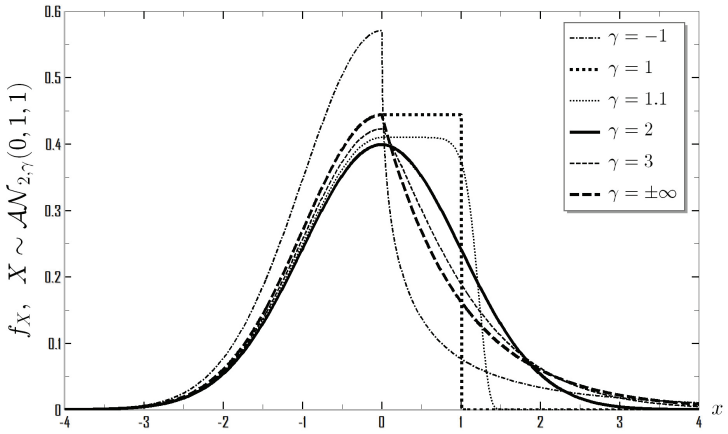


**Fig. 5.** Graph of the densities $f_X$, with $X \sim \mathcal{AN}_{2;\gamma}(0,1,1)$, for various "right" shape parameter values $\gamma$.

## 4 Discussion

In this paper we considered an exponential–power generalized form of the multivariate normal distribution, namely the $\gamma$–order Normal distribution, $\mathcal{N}^p_\gamma$. This generalization was obtained through the study of the generalized entropy power, Kitso and Tavoularis [9]. The Shannon entropy as well as the Rényi entropy was evaluated and discussed (including the specific cases of the multivariate Uniform, Normal and Laplace distributions) for the $\gamma$–order normally distributed random variables. Moreover, the generalized entropy type information measure, $\mathrm{J}_\alpha$, which extends the known entropy type Fisher's information, was investigated through these random variables and certain boundaries of the

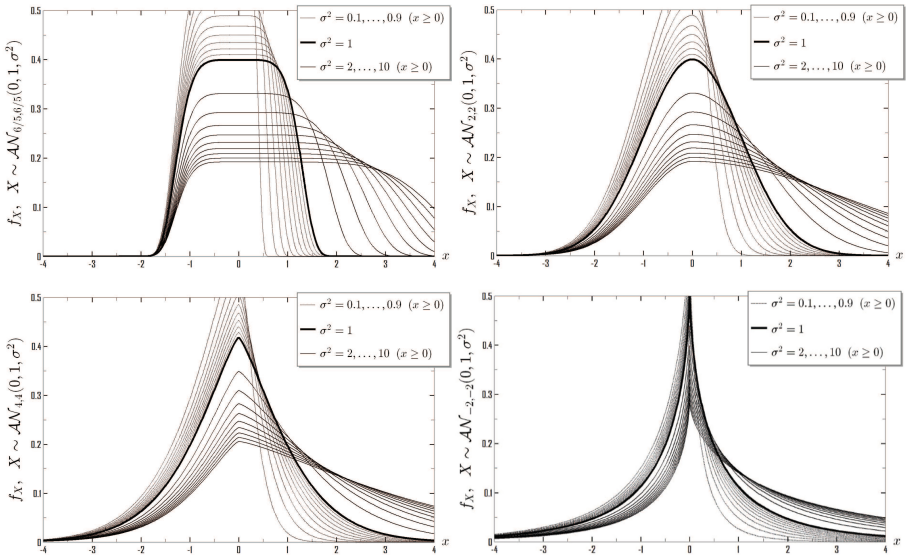

**Fig. 6.** Graphs of the densities $f_X$, with $X \sim \mathcal{AN}_{\gamma,\gamma}(0,1,\sigma^2)$, for various "right" scale parameter values $\sigma$ $(<,=,>1)$, in four cases of shape parameter $\gamma$ values.

$\mathrm{J}_\alpha$ were obtained. Finally, three univariate $\mathcal{N}_\gamma$–based extensions were also given, i.e. the $\gamma$–order Lognormal distribution $\mathcal{LN}_\gamma$, the left/right truncated cases of $\mathcal{N}_\gamma$ and $\mathcal{LN}_\gamma$ distributions, and a two–way asymmetric $\mathcal{N}_\gamma$ distribution.

## References


1. L.F. Bauer. *Kryptologie, Methoden und Maximen*, Springer–Verlag, London (1994)
2. F. Bernardeau and L. Kofman. Properties of the cosmological density distribution function, *Monthly Notices of the Royal Astrophys. J.*, 443, 479–498, 1995.
3. P. Blasi, S. Burles and A.V. Olinto. Cosmological magnetic field limits in an inhomogeneous Universe. *The Astrophysical Journal Letters*, 2, L79–L82, 1999.
4. T.M. Cover and J.A. Thomas. *Elements of Information Theory*, 2nd Ed., Wiley, 2006.
5. E.L. Crow and K. Shimizu. *Lognormal Distributions, Theory and Applications*, M. Dekker, New York & Basel, 1998.
6. K. Ferentinos and T. Papaioannou. New parametric measures of information, *Inform. and Control*, 51, 193–208, 1981
7. I.S. Gradshteyn and I.M. Ryzhik. *Table of Integrals, Series, and Products*, Elsevier, 2007.
8. J. Hoffstein, J. Pipher and J.H. Silverman. *An Introduction to Mathematical Cryptography*, Springer, 2008.
9. C.P. Kitsos and N.K. Tavoularis. Logarithmic Sobolev inequalities for information measures, *IEEE Trans. Inform. Theory*, 55, 6, 2554–2561, 2009.
10. C.P. Kitsos and N.K. Tavoularis. New entropy type information measures, in *Information Technology Interfaces*, V. Luzar–Stiffer, Z. Jarec and Z. Bekic (Eds), 255–259, 2009.
11. C.P. Kitsos and T.L. Toulias. New information measures for the generalized normal distribution, *Information*, 1, 13–27, 2010.

12. C.P. Kitsos and T.L. Toulias. On the generalized Lognormal distribution, *J. Prob. and Stat.*, vol. 2013, 1–16, 2013.
13. C.P. Kitsos and T.L. Toulias. Inequalities for the generalized entropy type Fisher's information, in *Handbook f Functional Equations: Functional Inequalities*, T.M. Rassias (Ed.), Springer (ISBN: 978-1-4939-1245-2), 2014.
14. C.P. Kitsos, T.L. Toulias and P.C. Trandafir On the multivariate $\gamma$–ordered normal distribution, *Far East J. of Theoretical Statistics*, 38, 1, 49–73, 2012.
15. T.J. Kozubowski and K. Podgórski. Asymmetric Laplace laws and modeling financial data, *Math. Comput. Modelling*, 34, 1003–1021, 2000.
16. T.J. Kozubowski and K. Podgórski. Asymmetric Laplace distributions, *Math. Sci.*, 25, 37–46, 2001.
17. D.R. Stinson. *Cryptography: Theory and Practice*, 3rd Ed., CRC Press, 2006.
18. I. Vajda. $\mathcal{X}^2$–divergence and generalized Fisher's information, in *Transactions of the 6th Prague Conference on Information Theory, Statistical Decision Functions and Random Processes*, 873–886, 1973.
19. G. Yan and F.B. Hanson. Option pricing for a stochastic–volatility jump-diffusion model with log–uniform jump–amplitudes, in *Proceedings of the American Control Conference*, 2006. (DOI: 10.1109/ACC.2006.1657175)

# Quantization dimension and Iterated function system generation of chaos with applications in ecology

Jozef Kiseľák[1], Mrinal Kanti Roychowdhury[2], Jiří Dušek[3], and Milan Stehlík[4]

[1] Institute of Mathematics, Faculty of Science,P.J.Šafárik University in Košice, Slovakia
(E-mail: jozef.kiselak@gmail.com )
[2] Dept of Mathematics, The University of Texas-Pan American, Edinburg, TX
(E-mail: roychowdhurymk@utpa.edu )
[3] Global Change Research Centre AS CR, České Budějovice, Czech Republic,
(E-mail: dusek.j@czechglobe.cz)
[4] Corresponding author. Department of Applied Statistics, Johannes Kepler University in Linz. Altenberger Strasse 69, A4040 Linz a. D., Austria,
Departamento de Matemática, Universidad Técnica Federico Santa María, Casilla V 110, Valparaíso, Chile
(E-mail: Milan.Stehlik@jku.at)

**Abstract.** Chaos can appear in ecological systems from many sources. There are several possibilities how to model chaos. Principal question of methane emissions released from wetland can be formulated, whether there is a chaotical part of methane emission. In this paper, we will provide reconstruction of Pareto based chaos based on Iterated Function System (IFS). We will mention several open problems and relate them to already developed statistical methodology for measuring of entropy as well as related statistical inference for methane emissions released from wetland.

**Keywords:** Chaos, entropy, methane emissions, iterated function system.

## 1 Introduction

Biogeochemical processes on the different time scales are measurable by change of entropy having a thermodynamic meaning [7], [1]. Chaos can appear in ecological systems from many sources. There are several possibilities for chaos modelling, let us mention entropies, topological dimension, quantization dimension, ergodic theorems and dynamical systems. Principal question of methane emissions released from wetland can be formulated, whether there is a chaotical part of methane emission. We developed a statistical methodology for measuring of entropy and related statistical inference for methane emissions released from wetland in [6]. We concentrated on paradigm question how much stochasticity and how much chaos is present in the methane emission model,

*Stochastic Modeling, Data Analysis and Statistical Applications* (*pp.* 385-391)
Lidia Filus - Teresa Oliveira - Christos H Skiadas (Eds)



using the residua from the process of methane emissions from wetlands in the sedge-grass marsh, in South Bohemia, Czech Republic.

Methane emissions are modelled via trend fitting. In [4] we have modelled this dependence by a time-series model. The trend component is estimated by the Ordinary Least Squares and the noise component is represented by the sum of an infinite moving average model with Pareto-like positive and negative parts of the innovations and independent identically distributed (i.i.d.) innovations. The process of methane release from soil has also chaotic features. Relation to entropy and a specific version of Kullback-Leibler divergence can be given (see [8]). Reconstruction of Pareto based chaos based on an Iterated function system (IFS) will be also provided in this paper.

An interesting connection between the quantization dimension and temperature function, $\beta(q)$, such that $\beta(0)$ defines Hausdorff dimension of attractor for some Moran measures, has been developed in [5]. However, to better understand underlying mechanism of ecological emissions also other values of $\beta(q)$, $q > 0$ are of interest. Nevertheless, classical theory of chaos considered only the extremal case of $\beta(0)$ and its estimates.

## 2 Iterated function system: reconstructing chaos from Pareto

Our approach is based on the results achieved by [9]. We considered iterated function system (IFS) $\{\mathbb{R}, f_i, p_i\}_{i=1}^n$ with probabilities. That is, $f_i : \mathbb{R} \to \mathbb{R}, i = 1, \ldots, n$ are functions and $p_i$ are associated non-negative numbers with $\sum_{i=1}^{n} p_i = 1$. It is known that if $f_i$ are contractions, see [3], then there exists a unique nonempty compact set $A$ (set-attractor) satisfying

$$A = \bigcup_{i=1}^{n} f_i(A)$$

and a unique probability measure $\mu$ (unique measure-attractor), supported on $A$, satisfying the invariance equation $\mu(\cdot) = \sum_{i=1}^{n} p_i \mu(f_i^{-1}(\cdot))$. If an IFS has a unique measure-attractor $\mu$, then $\mu$ is the unique stationary distribution of $\{X_k\}_{k=0}^{\infty}$, i.e. for the Markov chain obtained by random (independent) iterations with the functions, $f_i$, chosen with the corresponding probabilities, $p_i$. The inverse problem is to, given a probability distribution $\mu$, find an IFS having $\mu$ as its unique measure-attractor. A simple solution to the inverse problem for continuous probability measures on $\mathbb{R}$, see [9]. Let $\mu$ be a probability measure on $\mathbb{R}$ with its distribution $F$. The generalised inverse distribution function is defined by

$$F^{-1}(z) = \inf_{x \in \mathbb{R}} \{F(x) \geq z\}, \ 0 \leq z \leq 1.$$

It is true, see [9], that if $Z \sim U(0, 1)$, then $F^{-1}(Z)$ is a $\mu$-distributed random variable. This basic property helps us to simulate from an arbitrary distribution on $\mathbb{R}$, by simulating uniform random numbers on the unit interval. Moreover,

if $\mu$ is continuous then $F(F^{-1}(z)) = z$ for $0 < z < 1$. This is a crucial property for the following result, again see [9].

**Theorem 1.** *A continuous distribution, $\mu$, on $\mathbb{R}$ with distribution function, $F$, is the measure-attractor of the IFS with monotone maps $f_i(x) = (F^{-1} \circ u_i \circ F)(x)$, for any $x$ with $F(x) > 0$, and probabilities $p_i = \frac{1}{n}$, where $u_i(z) = \frac{z}{n} + \frac{i-1}{n},\ 0 \le z \le 1,\ i = 1, 2, \ldots, n$, for any $n \ge 2$.*

Note that this theorem cannot be generalized to discrete distributions. As it is stated in [9], from Theorem 1 it follows that any continuous probability distribution on $\mathbb{R}$ can be approximated by the empirical distribution of a Markov chain $\{X_k\}$ on $\mathbb{R}$ generated by an IFS with trivial randomness generated e.g. by a coin or dice.

Our problem is to illustrate possible chaos generation by iteration of Pareto-based functions. This justifies our approach in [6], since methane emissions are aggregated in a similar way. Accordingly, we considered Pareto distribution with probability density function

$$h(x) = \begin{cases} \alpha\, x_m^{\alpha}\, x^{-(\alpha+1)}, & x \ge x_m \\ 0, & x < x_m \end{cases},$$

where $x_m > 0$ is a threshold and $\alpha > 0$ is a shape parameter, which is known as the tail index. Using Theorem 1 we obtain $f_i$ in the following form

$$f_i(x) = \begin{cases} \dfrac{x_m\, n^{\frac{1}{\alpha}}}{\left(n - i + \left(\frac{x_m}{x}\right)^{\alpha}\right)^{\frac{1}{\alpha}}}, & x \ge x_m \\ \dfrac{x_m\, n^{\frac{1}{\alpha}}}{(n-i+1)^{\frac{1}{\alpha}}}, & x < x_m \end{cases}, \quad i = 1, \ldots, n.$$

In Figure 1 are first three continuous monotone maps with $n = 4,\ \alpha = 1.3$ and threshold $x_m = 1$.

Notice that almost all the well-known fractals (Cantor set, Sierpinski triangle etc.), as well as many less well known ones, are the attractors of appropriate IFSs. An approximation of attractor computed by a simple algorithm given in section 4 is displayed in Figure 2.

Notice that one can show that $f_i,\ i = 1, \ldots, n$, are Lipschitz continuous with constant $L = n^{\frac{1}{\alpha}}(n-i+1)^{\frac{-(\alpha+1)}{\alpha}}$, but they are not contractive in general. In practice software that implements IFS only require that the whole system be contractive on average, see [2]. We setup the configuration as follows: $n = 2,\ p_1 = p_2 = \frac{1}{2},\ \alpha = 1.3$ and $x_m = 1$. This represents a reliable choice of parameters, see e.g. [6], where authors modelled $CH_4$ flux "emissions" by the infinite moving average process. We computed tenth-order composition of functions $f_1, f_2$, which were chosen randomly with probabilities $p_1, p_2$. This procedure has been repeated 1000 times (due to time complexity). We obtain observations at given value $x = 3$, the histogram of which (compared to real density) can be seen in Figure 3. Various situations where parameters $\alpha$ and $x_m$ are perturbated are plotted in figures 4, 5, 6. From this, we can see the self-similarity of chaos (and heavy tails, respectively), since iteration of density of the tail of emission creates heavy-tailed pattern density.

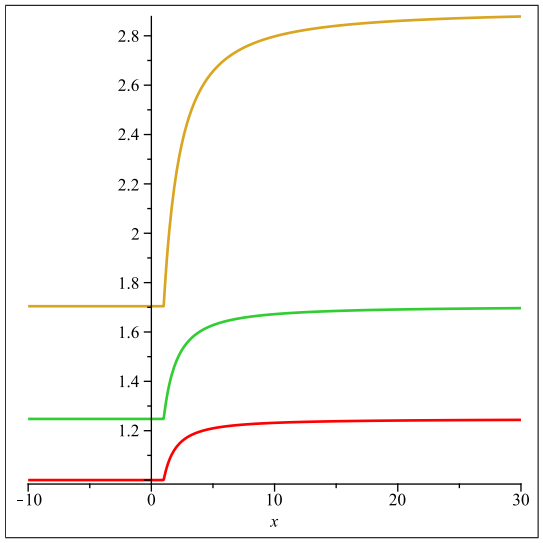


**Fig. 1.** Graphs of the functions $f_1, f_2, f_3$ $(red, green, orange)$ for $n = 4$ with $x_m = 1,\ \alpha = 1.3$.

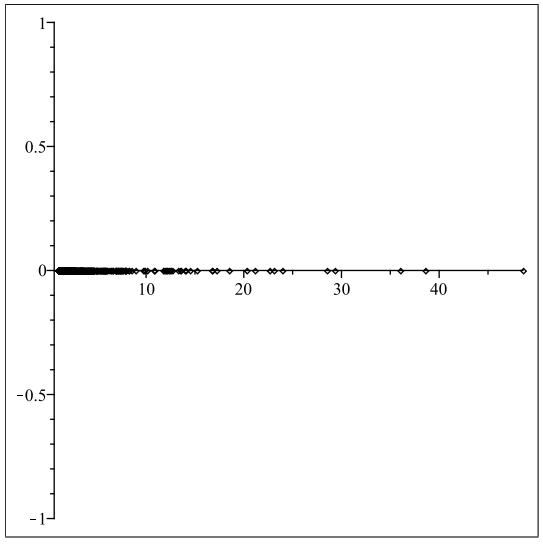


**Fig. 2.** Graphical illustration of an attractor on the real line generated by IFS $f_1, f_2$ for $n = 2$ with $x_m = 1,\ \alpha = 1.3$.

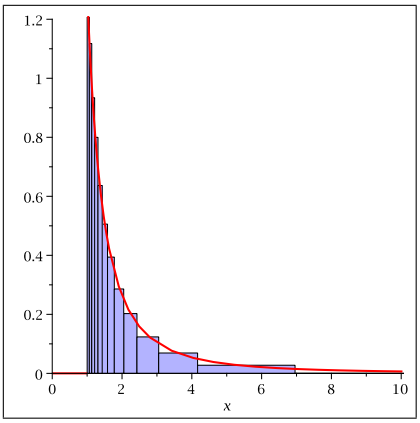


**Fig. 3.** Approximation of Pareto density $\alpha = 1.3$ and $x_m = 1$.

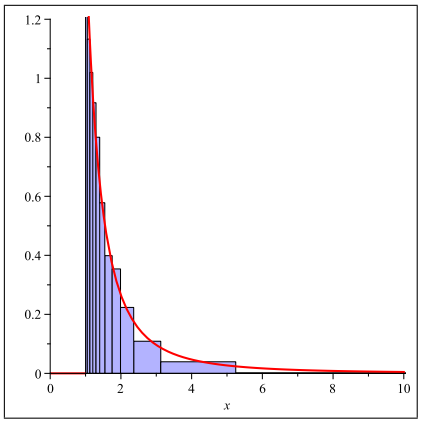


**Fig. 4.** Approximation of Pareto density $\alpha = 1.5$ and $x_m = 1$.

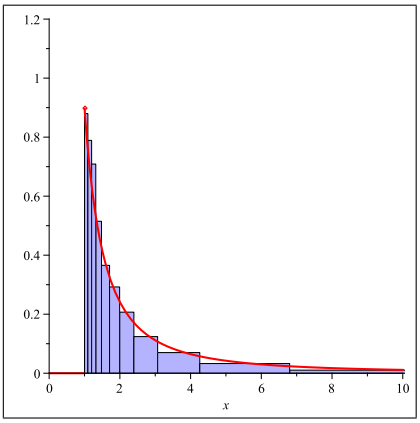


**Fig. 5.** Approximation of Pareto density with $\alpha = 0.9$ and $x_m = 1$.

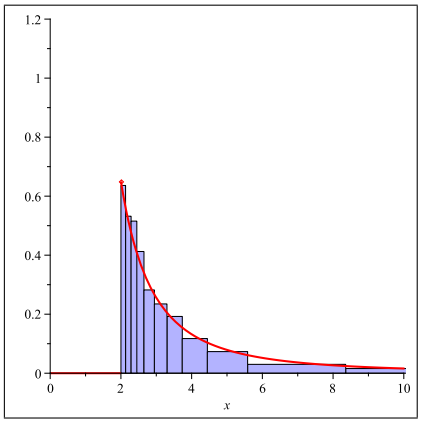


**Fig. 6.** Approximation of Pareto density $\alpha = 1.3$ and $x_m = 2$.

## 3 Conclusions

As is stated in [6], the complexities of methane emissions from wetlands, especially many dependencies and interactions may lead an experimenter to a conclusion that it is a complicated and chaotic system. IFS is a typical and also appropriate tool for generating chaos. In this paper, we show how to relate IFS with extreme value distribution of Pareto type. Such relations could be very useful for better understanding of the self-similar stochastic processes in emissions. The ecological aspect of ebullition given by such approach is an open question.

## 4 Maple codes of simple procedures

We have used MAPLE 14 to calculate an approximation of Pareto density as well as an approximation of attractor. These algorithms can be implemented using a few lines of MAPLE.

Following procedure generates observations at given point $X$ and specific choice of parameters.

active1dgenerate := proc(N,NN,X,XM,A,m) NN - number of f$_i$ $functions, N-numberofrepeatedprocedures, Xgivenpoint, XM-threshold, A-alpha, m-numberofiterationslocalroll, f, i, j, p, fun, function, FUN : roll := rand(1..NN)$ :
f :=i-¿ piecewise(x ¡ XM,XM*NN^(1/A)/(NN-i+1)^(1/A), XM*NN^(1/A)/(NN-i+(XM/x)^A)^(1/A)):
for i from 1 to N do p[1]:=roll(): fun[1]:=unapply(f(p[1]),x): FUN[1]:=unapply(f(p[1]),x): for j from 2 to m do p[j]:=roll(): fun[j]:=unapply(f(p[j]),x): FUN[j]:=unapply(fun[j](FUN[j-1](x)),x): od: function[i]:=FUN[m](X): od:
return(seq(function[i],i=1..N)): end proc:

The next script generates points, which form an approximation of attractor.

active1dattractor := proc(N,NN,XM,A,x0) x0 is a starting point of attractor local X, i, p, fun, roll, f: X[0]:=x0: roll := rand(1 .. NN): f :=i-¿ piecewise(x ¡ XM,XM*NN^(1/A)/(NN-i+1)^(1/A), XM*NN^(1/A)/(NN-i+(XM/x)^A)^(1/A)):
for i from 1 to N do p:=roll(): fun:=unapply(f(p),x): X[i]:=fun(X[i-1]): od: return(seq([X[i],0],i=1..N)): end proc:

## Acknowledgement

Jozef Kiseľák was partially supported by grant VEGA MŠ SR 1/0344/14. Milan Stehlík acknowledges the support of Fondecyt Proyecto Regular N 1151441.

## References

1. T.M. Addiscott. Entropy, non-linearity and hierarchy in ecosystems, *Geoderma* 160, 57–63, 2010.
2. S. Draves, E. Reckase. The Fractal Flame Algorithm, Revised November 2008. Retrieved from http://flam3.com/flame.pdf.
3. J. E. Hutchinson, Fractals and self-similarity, *Indiana Univ. Math. J.*, 30(5), 1981, 713-747.
4. P. Jordanova, J. Dušek,and M. Stehlík. Modeling methane emission by the infinite moving average process, *Chemometrics and Intelligent Laboratory Systems* 122, 40–49, 2013.
5. M.K. Roychowdhury. Quantization dimension for some Moran measures, *Proc.of the Am.Math.Soc.* 138, 4045–4057, 2010.
6. R. Sabolová, V. Sečkárova, J. Dušek and M. Stehlík. Entropy based statistical inference for methane emissions released from wetland. *Chemometrics and Intelligent Laboratory Systems* 141, 125–133, 2015.

7. E. Schrödinger. *What is Life?* Cambridge University Press, Cambridge, 1967.
8. M. Stehlík. Decompositions of information divergences: Recent development, open problems and applications, AIP Conf. Proc., 1493 , 972-976, 2012.
9. Ö. Stenflo, Iterated function systems with a given continuous stationary distribution, *Fractals* 20(3,4), 197-202, 2012.

# Accuracy of the Risk Estimators

Georgios C. Zachos*

Department of Mathematics, University of the Aegean, Samos, Greece
(E-mail: zachosg@aegean.gr)

**Abstract.** The purpose of this paper is to evaluate the accuracy of the beta estimations that are suggested to be free of intervalling effect bias. The accuracy of the asymptotic estimators of betas is examined by comparing them to OLS assessments as well as to beta estimations adjusted according to their tendency to regress towards one. Furthermore the above measurement is employed for different intervals among data observations and the findings are reexamined by taking into account the 'Corhay effect'. In addition, models that take into account Heteroskedasticity in residuals are used to perform the same comparisons.
**Keywords:** Adjusted Risk Coefficients, Intervalling Effect Bias, Asymptotic Beta
**JEL classification:** C22, G12, G14

**Georgios C. Zachos is indebted to D. Konstantinides for his invaluable advice, E. Lamprou for providing datasets and D. Kokonakis and E. Papanagiotou for their valuable help.*

## 1 Introduction

Measuring non-diversifiable risk in an investment like a fund or a security is the most common practice in financial analysis. Thanks to Sharpe [29] systematic risk of a security can be quantified simply by its regressing returns to the market returns and consequently the slope, or the beta of this procedure will eventually produce a figure exposing how volatile and risky the security in relation to the market is. Apart from this practical use, the systematic risk measuring is prolific in academic terms. There is a vast academic literature investigating the best model that can provide the most accurate systematic risk measure. For example, many variations of the model can be formulated. In a single dimension, it appeared in the Sharpe and Lintner's [21] Capital Asset Pricing Model (CAPM) and the Market Model (MM) while in multidimensional versions the Three Factor Model of Fama and French [12] and Carhart's [4] four factor model are among the most popular.

The aim of this paper is to evaluate the accuracy of the beta estimations that are suggested to be free of intervalling effect bias. In particular, we examine whether the methodology of reducing price adjustment delays due to microstructure of capital markets contributes to the accuracy of the risk estimations. A number of works have evaluated the validity of this method, for instance McInish and Wood [23] so this issue appears to interest both academics and practitioners. To our knowledge there are no studies on evaluation of the accuracy of intervalling effect

*Stochastic Modeling, Data Analysis and Statistical Applications* (*pp*. 393-407)
Lidia Filus - Teresa Oliveira - Christos H Skiadas (Eds)


free-betas by straightforwardly comparing them to betas corrected according to their tendency to regress towards the grand beta mean.

To that end, let employ two methodologies. The first methodology was suggested by Cohen *et al.* [6] and the second one by Blume [2]. The first considers price adjustment delays that are present into microstructure of markets and leads to interavalling-effect bias, so it suggested a procedure to reduce this phenomenon. It appears as a two-stage procedure: In the first stage the Market Model and Ordinary Least Squares (OLS) time series regression betas are calculated for a number of intervals, typically from one day to one month. In the second stage an asymptotic estimator of the systematic risk coefficient by cross-sectional regress OLS betas towards a monotonically decreased equation is calculated. Consequently the asymptotic estimator reduces the intervalling-effect bias. The methodology is significant as far as the researchers include it in their agenda, see for instance in Fung *et al.* [16]. More recent studies that use this methodology are Diakogiannis and Makri [9] and Milonas and Rompotis [26].
Furthermore Blume's technique [2] attempts to calculate future risk coefficients by taking into consideration the fact that betas aren't constant over time, yet they have the tendency to regress towards the market mean. By dividing a time dataset to sub-periods, for instance three or five year periods, he calculates betas for each time period. Afterwards he regresses the betas of the earlier period towards the betas of the later period.
With the use of the regression equation and first period's beta a researcher is able to recalculate betas of the second period, thus the adjusted assessment according to his phraseology. Final step of this methodology is an examination of the accuracy of the assessments that are based on historical data compared to the risk factors that take into account the tendency of the betas to regress toward the grand mean. Apart for Blume's methodology, there are other techniques that attempt to correct the beta estimations according to the aforementioned principal, with most important the Bayesian technique. Initially inducted by Vasicek [31], the Bayesian method is widely used by prestigious companies like Merrill Lynch and as Elton *et al.* [10] suggests it could be more favorable in comparison to Blume's technique in certain occasions. Concerning beta adjustment techniques we should mention Mantripragada [22] who applied a plethora of those methodologies to Canadian stock datasets and more recently the Sarker [27] who used both Vasicek and Blume's technique to data from Dhaka Stock Exchange and concluded that there are no significant differences in their results.
Taking into account all the above I:

1) Investigate the accuracy of the asymptotic estimators of betas by comparing them to OLS naïve assessments and to beta estimations adjusted according to Blume [2] method.
2) I employ above comparison for different intervals among data observations (daily and monthly intervals).

3) I also re-examine my results by taking into account the Corhay [8] effect in results[1].
4) Finally I extract asymptotic estimators of betas by using models that take into account Heteroskedasticity in residuals (GARCH and Exponential-GARCH) and I proceed with the same accuracy inspection.
In terms of data daily closing time security prices of the entire universe of Athens Stock Exchange are selected for calculating returns, while market returns are presented from Athens Stock General Index. Also data are collected for ten consecutive years. Moreover since Blume [2] and Cohen *et al.* [5] use the Market Model, same method should apply here hence risk free rate is not necessary. The rest of the paper is organized as follows. Section 2 includes literature review. Section 3 discusses data, Section 4 analyzes methodology approach while results are included in section 5. Section 6 concludes.

## 2 Literature Review

### 2.1 The Model

In line with methodology used by Blume [2] and Cohen *et al.* [6], for my analysis I will use the Market Model. Formula is

$$E(ri)=\alpha_i+\beta_i E\ (r_m) \qquad (1)$$

Where $E(ri)$ is the expected return on the capital asset, $\alpha_i$ is the residual return of asset I. $\beta_i$ (the beta coefficient) represents sensitivity of the asset returns compared to market returns or $\beta_i = COV(Ri,Rm)/Var(Rm)$. Total risk of the portfolio can be viewed as beta. Rephrasing, the model uses time series regression to calculate beta, so $E\ (r_1m)$ stands for expected return of the market.
Compared to the single index CAPM model it differs in two ways: First there is absence of risk free rate as in realistic terms it makes no countable difference and second, Elton *et al*. [11] points out that MM lacks the assumption that all covariances among securities occur because of a common covariance with the market. Also multifactor models, like Fama and French three factors model [12], [14] or Carhart's [4] four factor model are not selected. As Elton et al [10] points out, maybe historical prices are better interpreted by a multi-dimensional model but in terms of predictive ability a single-index model should be preferred. Moreover

[1] As Corhay [8] points out if the interval between data observations is more than a day we might get a different result every time we choose a different starting day. To this end I perform tests by selecting every possible starting day within the interval and the final beta estimation is the average of those results.

multi-dimensional model might include more noise than information in their factors in certain occasions.

## 2.2 Adjusted Risk Coefficient

Blume [2] argued with a common practice of investors to act as if beta coefficients are constant over time. After examining correlations of unadjusted risk coefficients he suggested a methodology where he extracted future adjusted betas according to past prices. Most important in this methodology is the assumption that betas tend to regress toward market mean and consequently his methodology measures this phenomenon. Furthermore, he examined accuracy of adjusted assessment through mean square errors and found that they are significantly more accurate compared to assessments based simply on historical prices. In terms of methodology he separated his data into sub-periods and calculated via Ordinary Least Squares (OLS) time series regression the betas of those periods. In addition he performed cross section regression where betas of one period are the explanatory variables and betas of the next period are the dependent. Finally, with the use of the regression equation and the data of the first period, second period's beta can be extracted and according to Blume's [2] findings, they are more accurate compared to historical prices results.

Definitely promising, yet Blume's technique has been further investigated by the academic community and proved to be less than flawless. For instance, Klemkosky *et al.* [18] indicated bias occurring and recommended three procedures to reduce those effects. On the contrary Blume [3] addressed the issue of order bias which leads to non-stationarity in estimated beta coefficients. He argued that it is not of major importance by suggesting that extreme betas of investments tend to become less extreme both for new or existing investments. Summing up, two types that effect Blume's technique should be mentioned. One is the fact that it fails to forecast a trend in beta and assumes that any trends occurring are random. Second it fails to spot other factors except correlation with the market that effect beta changes, for instance industry effects.

In line with Blume's concept, other techniques have been suggested with most important the Bayesian technique, initially suggested by Vasicek [31]. It is widely used by prestigious firms like Merrill Lynch and as Elton *et al.* [11] explains, it assumes that beta of investments tend to be closer to average beta than historical prices suggest so adjusts each historical beta towards the average. Suffering from its own bias, for instance when a beta is greater than one, it is corrected by a bigger percentage compared to a less than the market beta, yet it is suggested to be a slightly better technique compare to Blume's by many authors like Elton *et al.* [10] and Klemkosky and Martin [18].

## 2.3 Asymptotic Beta

The second methodology employed in this paper is the asymptotic estimation of betas proposed by Cohen *et al.* [6]. As the majority of empirical researchers in

financial economics presume no friction, Hawanini *et al.* [17], based on microstructure theory, argued by confirming the importance of friction in trading process and by indicating the complex and persistent impact friction has on generating returns practice. Also Hawanini *et al.* [17] points out in the same study that when differencing interval is increasing, price adjustment delay impact will reduce. Concluding, in their paper it is suggested that if differencing intervals are greater than aforementioned delays, then the latter will lessen. Giving a simple example of what intervalling-effect bias is, it can be stated that if an investor estimates beta for a security with daily data with OLS regression procedure, he will get a figure that will differ compared to a procedure with weekly data, and again he will get different beta for monthly intervals among observations.

Also Cohen *et al.* [6], in line with previous findings points out that when working with short differencing interval data the variation between true and observed beta is considerable. True are the beta that should be obtained in case of a frictionless environment and observed beta are the beta that can be calculated and actually observed by investors. Also Cohen *et al.* [7] denoted that price adjustment delays are associated with market value of the shares included in sample investigated. In the same work it is suggested that if intervals are increasing gradually then bias will reduce and eventually diminish. In formula terms Fung *et al.* [16] suggested the following:

$$\beta_i^* = \lim_{l \to \infty} \beta_i^0(l) \tag{2}$$

Where $\beta_i^*$ represents an inconsistent estimator of $\beta_i$, while $\beta_i^0(l)$ is the beta estimator for interval l.

The most important in Cohen *et al.* [6] work is their suggestion of a methodology where the true beta can be estimated, thus the asymptotic estimator of beta. It is a two stages procedure. First step is to calculate systematic risk coefficient, thus the slope or the beta in the Market Model with regression method for intervals from 1,2,…, l days. Regression formula is

$$r_{jLT} = a_{jL}^1 + b_{jL}^1 r_{MLT} + e_{jLT}^1 \tag{3}$$

Prescript 1 denotes the first stage. The second stage is occurring in order to estimate the intervalling effect on risk coefficient. For that procedure all the estimated betas for all intervals and for each security are cross-sectional regressed with the interval effect which reduces as intervals are increasing and is expressed from the monotonically decreased equation $f_j(l) = L^{-k}$ where it is assumed that:

$$\lim_{l \to \infty} f_j(l) = 0 \forall j \tag{4}$$

Formula of the second stage is:

$$b_{jL}^{1} = a_j^{2} + b_j^{2} L^{-n} + e_{jL}^{2} \quad (5)$$

Where 2 denotes the second stage of the procedure and $a_j^{2}$ stands for the asymptotic estimator of beta. Clearly as L increases without bound the intervalling effect reduces. Consequently $L^{-n}$ diminishes and thus true beta will be approaching the figures of observed beta. Concerning n we follow the same methodology as in Cohen *et al.* [6] and Fung *et al.* [16] [2]. Finally Cohen *et al.* [7] highlights the importance of $b_j^{2}$ as quantitative proxy to measure intervalling effect. If it is statistically significant, a negative price of $b_j^{2}$ will suggest that as differencing interval lengthens beta coefficient will rise and vice versa. If it is statistically insignificant there is no intervalling effect at all.

## 3 Data

Sample data were collected from Bloomberg's terminal database. Daily closing time observations are selected due to homogeneity reasons. In case an observation misses due to unforeseen constraints, the average of the previous and next day is calculated and serves as the missing observation. Moreover all securities are valued in euro currency. In addition, the sample set consists of the whole universe of securities traded in Athens Stock Exchange for ten consecutive years, from 02/01/2002 until 30/12/2011. In case a security was excluded from trading during the time sample was chosen, it will be excluded from the sample as well. For Market returns ASE General Index (capitalization weighted) is used in calculations. ASE appears to be an interesting selection for a number of reasons. First it does not present features like big capitalization of more mature markets like New York Stock Exchange or Frankfurt Stock Exchange, which habitually provide data for research. Moreover it was excluded from emerging markets (and harmonized with standards of mature markets) in 2001, yet it downgraded again in 2013 by index provider MSCI so it is expected to produce very interesting results which can be compared to results provided from a mature market. In addition, it is expected to be more volatile compared to a mature market as it lacks capitalization, which is another thing that makes ASE more appealing. Finally, Athens Stock Exchange was selected because there is evidence that friction in trading processes appears to be present. As it is suggested by Alexakis and Alexakis [1] there is evidence that Hellenic Market follows patterns of global markets with delay.
From initial observations continuously compounded rate of return on each security is calculated according to formula presented below[3].

---

[2] Cohen *et al.* [6] n estimation is approximately 0.8 and as exposed in table 1 we get a similar result only on second period (07-11) and only when we take into account Corhay's effect (OLS 0.61, GARCH 0.75 and EGARCH 0.69 respectively)

[3] Continuously compounded rate of return was also used for market returns

$$r_{pt} = \ln\left(\frac{P_{pt}}{Ppt-1}\right) \quad (6)$$

$Ppt$ stands for price observation of security P, at day t and $Ppt-1$ represents observation of the same security one day before. ln is the natural logarithm. Working with differences, and therefore interpreting coefficients as elasticities, is a common practice when analyzing such data. As Koop [19] highlights a data set of financial data will behave well in terms of stationarity[4].

## 3.1 Visual Inspection of Market

Appendix presents graphs for ASE General Index and the continuously compounded rate of return of the same index. ASE index appears to exhibit from 2003 onwards an excessively positive uptrend which appears to finish at the end of 2008. Reason for that inarguably is the global crisis emerging from last semester of 2007 onwards. Mortgage subprime crisis in U.S. market seem to be initial reason as Krugman [20] explains, nevertheless crisis spread worldwide afterwards. As Friedman and Schwartz [15] denoted, an economic collapse could be a cumulative type process. Concerning returns of ASE index, while in uptrend almost in no occasion a 5% change is observed, on the other hand when market index is falling graphs become volatile exhibiting percentage changes even more than 10% and up to 15%. Such conclusion is to be taken into consideration, as volatility in market indicates risk and uncertainty. Concluding visual inspection, two downturns and one peak at the end of 2008 are observed in period selected for sample.

# 4 Methodology Approach

The purpose is to examine the accuracy of the asymptotic estimated betas compared to accuracy of betas obtained both from adjusted and naïve assessments. Initially from the whole universe of Athens Stock Exchange shares in the sample, the ones that are not traded throughout the whole ten year period are excluded. Afterwards, in accordance with Blume [2], the ten year period of data is separated into two five year sub periods. Continuously compounded rates of returns of shares are calculated. Next Market Model OLS style regressions will be performed for each share return and for each five year period. The same pattern applies when I work OLS in conjunction with GARCH and EGARCH methodology. Athens Stock Exchange General Index's returns are also calculated and stand as Market variable in equation. In accordance with Cohen *et al.* [6] regressions take place for intervals

[4] Further information can be provided by the author on request

from 1 to 30 days. Moreover asymptotic estimations of betas are obtained with the use of second stage Cohen *et al.* [6] recommend for same intervals. It is important to consider Corhay's [8] suggestion that estimated betas differ in case differencing interval starts on a different day so when differencing interval is bigger than a day, then betas will be calculated by taking as a starting date every observation included in the interval. Then the average of betas obtained is the final estimated beta. Finally we examine a set of results that takes into account Corhay effect and a set that does not do so. All regressions take place in Matlab software package.

Furthermore, in accordance with Blume's technique, betas of the 07-11 period are cross-sectionally regressed towards the 02-06 period[5]. The outcome of this procedure is a regression formula with the later period's betas as the dependent variable and earlier betas as explanatory[6]. Having in mind Blume's technique once again we are able to retrospectively make estimations of later period's betas with the use of this formula and first period's beta.

The result of the aforementioned procedures are assessments of betas for the period 2007-2011 that are based on historical data, results that are adjusted to Blume's correction and asymptotic estimated beta results. Final step is a valuation of accuracy of those results with the use of mean square errors as Blume suggested in his methodology. Consequently, we are able to examine if the asymptotic estimation of betas provide more accurate beta estimations compared to naïve ones and also compared to beta adjustments proposed by Blume [2].

## 5 Results

Results are presented in table 3 and table 4 in appendix. As I am working with mean square errors the smallest price denotes the more accurate estimation. Furthermore the key finding (bolded in tables) occurs when I use as benchmark (1st period 02-06) OLS and daily results and as comparison periods OLS and daily Blume adjustment (0.2862), daily asymptotic estimator (0.2708) and daily naïve estimation (0.3882). Evidence suggests that asymptotic estimators are more accurate compared to both naïve and adjusted assessments. Furthermore, when I take into account the Corhay effect in asymptotic estimator (0.2537) the results are the same and further more evidence suggest that asymptotic estimations of betas are even more accurate[7].

In addition, in every other test I performed, evidence suggests that asymptotic estimators are more accurate compared to naïve assessments yet less accurate compared to assessments compared to blume's technique. More specifically:

---

[5] I don't follow the exact pattern of Blume [2] only in terms we don't put beta prices in ascending order and also I don't categorize stocks into portfolios according to their beta prices

[6] All regression formulas are presented in table in appendix

[7] Concerning naïve assessments and adjusted ones results are the same when Corhay effect is not taken into account since these are results taken from daily data thus the interval among observations is one

1) When I use as benchmark (02-06) OLS and monthly results (No Corhay) I have the following MSE figures (Blume 0.2573, asymptotic 0.3679, naïve 0.3791).
2) When I use as benchmark (02-06) OLS and monthly results (Corhay) I have the following MSE figures (Blume 0.375, asymptotic OLS 0.4672, naïve 0.4869).
3) When I use as benchmark (02-06) GARCH[8] and daily results (No Corhay) I have the following MSE figures (Blume 0.2641, asymptotic GARCH 0.2736, naïve 0.373).
4) When I use as benchmark (02-06) GARCH and daily results (Corhay) I have the following MSE figures (Blume 0.2603, asymptotic GARCH 0.2706, naïve 0.3728).
5) When I use as benchmark (02-06) GARCH and monthly results (No Corhay) I have the following MSE figures (Blume 0.3197, asymptotic GARCH 0.4202, naïve 0.4796).
6) When I use as benchmark (02-06) GARCH and monthly results (Corhay) I have the following MSE figures (Blume 0.3678, asymptotic GARCH 0.4457, naïve 0.5003).
7) When I use again as benchmark (02-06) GARCH and daily results (No Corhay) and I examine asymptotic EGARCH, I have the following MSE figures (Blume 0.2641, asymptotic EGARCH 0.3007, naïve 0.373).
8) When I use again as benchmark (02-06) GARCH and daily results (Corhay) and we examine asymptotic EGARCH, I have the following MSE figures (Blume 0.2603, asymptotic EGARCH 0.2956, naïve 0.3728).
9) When I use again as benchmark (02-06) GARCH and monthly results (No Corhay) and I examine asymptotic EGARCH, I have the following MSE figures (Blume 0.3197, asymptotic EGARCH 0.4534, naïve 0.4796).
10) When I use again as benchmark (02-06) GARCH and monthly results (Corhay) and I examine asymptotic EGARCH, I have the following MSE figures (Blume 0.3678, asymptotic EGARCH 0.4936, naïve 0.5003).
Some caveats that should be discussed seem to be present because of the special features of the ASE index composition. Specifically, the capitalization of the ASE is included in only 60 shares (almost 100% of Cap), yet I have been working with 224 stocks. In other words, almost ¾ of the stocks seem to contribute nothing to the index weight and as a consequence the index does not seem to be correlated to the majority of the sample. When we regress relatively uncorrelated time series we are not expected to get good R*2 values and the same applies here[9]. In an intuitive sense the capitalization's issue seems to have an effect on Blume's regressions formulas, as the larger slope factor we notice gets a value of approximately 0.30 as observed in table 2, while Blume observes values that reach up to 0.75.

## 6 Conclusions

[8] In terms of GARCH and EGARCH results I select according to AIC

[9] For instance the R*2 mean for OLS regressions (07-11 period, daily and not Corhay effect) is only 0.15

Inarguably the main finding in the paper is the fact that Asymptotic estimators of beta seem to provide accurate estimations of risk. In all cases examined (OLS, GARCH and E-GARCH) the aforementioned technique provided more accurate beta compared to naïve assessments. When I test for daily and monthly interval between observations, evidence favours the previous result. Conclusions drawn under are the same if I also take into account Corhay [8] effect. Furthermore, there are two occasions where asymptotic estimations of beta give more accurate risk factors even compared to the ones Blume's [2] adjustment provides: when I am working with OLS daily data and I don't consider Corhay effect and when I am working with OLS daily data but take into account Corhay effect.
Promising as they might be, those findings signify the need for more research in order to provide robust evidence. More specifically I suggest:
a) A study with the same data set and methodology but only with stocks that have a considerable weight in the ASE general index. Evidence suggests that some drawbacks will be avoided if this pattern is followed.
b) In line with the previous suggestion, a selection of stocks should occur according to how good the regression fits, for instance according to R*2 of regressions.
c) Apart from daily and monthly also other intervals should be examined.
d) Moreover the same methodology should apply to another market with other features compared to the ones ASE markets exposes, preferably a mature market. The comparison between the results of an emerging and mature market will contribute to solid conclusions.
e) Apart from Blume's [2] also Bayesian techniques could be applied to the analysis. As they appear to perform slightly better (Elton *et al.* [10]) and they are used extensively by practitioners in order to correct estimations of risk, they should be used as an alternative method of adjusting betas and therefore as an extra comparison measurement.

## References

1. Alexakis, P., Alexakis, A. C., *Issues Concerning Efficiency in Interconnections of Big Financial Markets and Greek Financial Market,* Studies Concerning Greek Financial System, Economic university of Athens Publications, Athens (Text in Greek), 2010.
2. Blume, E. M., On the Assessment of Risk, *The Journal of Finance*, 26, 1, 1{10, 1971.
3. Blume, E. M., Betas and Their Regression Tendencies, *The Journal of Finance*, 30, 3, 785{795, 1975.
4. Carhart, M. M., On Persistence in Mutual Fund Performance, *The Journal of Finance*, 52, 1, 57{81, 1997.
5. Cohen, K., Hawanini, G, Maier, S., Schwartz, R. and Whitecomb, D., Implications of Microstructure Theory for Empirical Research on Stock Price Behavior, *The Journal of Finance*, 35, 2, 249{257, 1980.
6. Cohen, K., Hawanini, G, Maier, S., Schwartz, R. and Whitecomb, D., Estimating and Adjusting for the Intervalling Effect bias in Beta, *Management Science*, 29,1,135{148, 1983a.
7. Cohen, K., Hawanini, G, Maier, S., Schwartz, R. and Whitecomb, D., Friction in the Trading Process and the Estimation of Systematic Risk, *Journal of Financial Economics*, 12, 12, 263{278, 1983b.

8. Corhay, A. (1992), The intervalling effect bias in beta: A note, *Journal of Banking and Finance*, 16, 1, 61{73, 1992.
9. Diacogiannis, G., and Makri, P., Estimating Betas in Thinner Markets: The Case of The Athens Stock Exchange, *International Research Journal of Finance and Economis*, 1, 13, 108{123, 2008.
10. Elton, J. E., Gruber, J. M., Urich, J. T., Are Betas Best?, *The Journal of Finance*, 33, 5,1375{1384, 1978.
11. Elton, J. E., Gruber, J. M., Brown, J. S., Goetzmann, N. W., *Modern Portfolio Theory and Investment Analysis,* John Wiley & Sons (Asia) Pte Ltd, Eighth Edition, 2011.
12. Fama E., French K., Common Risk Factors in the Returns on Stocks and Bonds, *The Journal of Financial Economics*, 33, 1,3{56, 1993.
13. Fama, E. and French, K., Size and Book-to-Market Factors in Earnings and Returns, *Journal of Finance*, 50, 1, 131{156, 1995.
14. Fama E., French K., Multifactor Explanations of Asset Pricing Anomalies, *The Journal of Finance*, 51, 1, 55{84, 1996.
15. Friedman, M. and Schwartz J. A. , *A Monetary History of the United States*, Princeton University Press, 1963.
16. Fung, W., Schwartz, R. and Whitecomb, D., Adjusting for the Intervalling Effect bias in Beta: A Test using Paris Bourse Data, *Journal of Banking and Finance,* 9, 3,443-460, 1985.
17. Hawawini, G. A., Intertemporal Cross Dependence in Securities' Daily Returns and the Short-Run Intervalling Effect on Systematic Risk, *Financial Quantitave Anal.,* 15, 1, 139-150, 1980.
18. Klemkosky, C. R., Martin, D. J., The Adjustment of Beta Forecasts, *The Journal of Finance*, 30, 4, 1123{1128, 1975.
19. Koop, G., *Analysis of Economic Data,* 2nd edition, John Wiley & Sons Ltd, 2002.
20. Krugman, P., A (Subprime) Catastrophe Foretold *http://www.spiegel.de/international/0,1518,513748,00.html, Spiegel on Line,* 2007.
21. Lintner, J., The Valuation of Risk Assets and the Selection of Risky Investments in Stock Portfolios and Capital Budgets, *The Review of Economics and Statistics*, 47, 1, 13{37, 1965.
22. Mantripragada, K. , Beta Adjustment Methods, *Journal of Business Research*, 8, 3,329{339, 1980.
23. McInish, H. T. and Wood, A. R., Adjusting for Beta Bias: An Assessment of Alternate Techniques: A Note, *the Journal of Financial*, 41, 1 277{286, 1986.
24. Milionis E. A., A conditional CAPM; implications for systematic risk estimation, *The Journal of Risk Finance*, 12 4, 306{314, 2011.
25. Milonas, T. N. and Rompotis, G. G., Does Intervalling Effect Affect ETF's?, *Managerial Finance*, 39, 9, 863{882, 2013.
26. Sarker, R. M., Forecast Ability of the Blume's and Vasicek's Technique: Evidence from Bangladesh, *Journal of Business and Management,* 9, 6, 22{27, 2013.
27. Semushin, A., Parshakov, P., 'The Impact of Data Frequency on Performance Measures' *9th International Conference on Applied Financial Economics*, INEAG, 495-502, 2012.
28. Sharpe, F. W., Capital Asset Prices: A Theory of Market Equilibrium Under Conditions of Risk, *Journal of Finance,* 19, 3, 425{442, 1964.
29. Stoukas, T., 'Greece Downgraded to Emerging Market at MSCI in World First' *Bloomberg Business week*, 11th June 2013, 2013.
30. Vasicek, A. O., A note on Using Cross-Sectional information in Bayesian Estimation of Security Betas, *The Journal of Finance*, 28, 5, 1233{1239, 1973.

# Appendix

## Graph 1 ASE Index

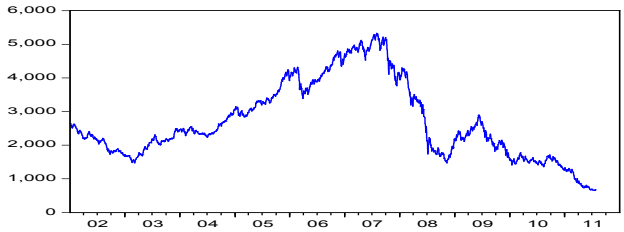


## Graph 2 Continuously Compounded Rate of Return of ASE Index

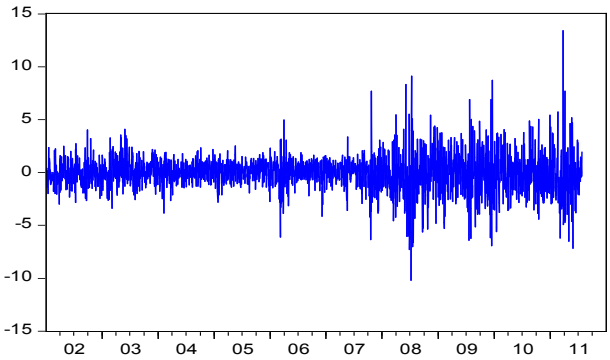


## Table 1 Exponent k Prices

| PRICES FOR EXPONENT K | | | | | |
|---|---|---|---|---|---|
| PERIOD 02-06 | | | | | |
| NO CORHAY | | | CORHAY | | |
| OLS | GARCH | EGARCH | OLS | GARCH | EGARCH |
| 1.46366071 | 1.2540625 | 1.38691964 | 0.44526786 | 0.40174107 | 0.41767857 |
| PERIOD 07-11 | | | | | |
| 1.13620536 | 1.25848214 | 1.17584821 | 0.60973214 | 0.74915179 | 0.69383929 |

**Table 2 Blume's Regression Formulas**

| BLUME'S REGRESSION FORMULAS | |
|---|---|
| REGRESSION METHODOLOGY | FORMULA |
| OLS DAILY AND NO CORHAY | y=0.264683+0.298818*x |
| OLS MONTHLY AND NO CORHAY | y=0.469163+0.234048*x |
| GARCH DAILY AND NO CORHAY | y=0.258781+0.281737*x |

| BLUME'S REGRESSION FORMULAS | |
|---|---|
| **REGRESSION METHODOLOGY** | **FORMULA** |
| GARCH MONTHLY AND NO CORHAY | y=0.4591+0.19378*x |
| ASYM OLS AND NO CORHAY | y=0.43205+0.244549*x |
| ASYM GARCH AND NO CORHAY | y=0.381777+0.274477*x |
| ASYM EGARCH AND NO CORHAY | y=0.373206+0.248492*x |
| OLS MONTHLY AND CORHAY | y=0.481481+0.20592*x |
| GARCH MONTHLY AND CORHAY | y=0.424121+0.215524*x |
| ASYM OLS AND CORHAY | y=0.548167+0.164256*x |
| ASYM GARCH AND CORHAY | y=0.502987+0.175038*x |
| ASYM EGARCH AND CORHAY | y=0.456146+0.175427*x |

**Table 3 MSE Results (no Corhay correction)**

| MEAN SQUARE ERRORS BETWEEN ADJ OR ASYMPT AND NAÏVE BETAS (no corhay) | | | |
|---|---|---|---|
| **OLS DAILY AS BENCHMARK (02-06)** | **ADJ OLS 07-11** | **ASYMP OLS 07-11** | **NAÏVE OLS 07-11** |
| | **0.286191552** | **0.270828** | **0.388213724** |
| **result: asymptotic OLS assesments more accurate** | | | |
| **OLS MONTHLY AS BENCHMARK (02-06)** | **ADJ OLS 07-11** | **ASYMP OLS 07-11** | **NAÏVE OLS 07-11** |
| | 0.257303968 | 0.367929 | 0.379163204 |
| **result: asymptotic OLS assesments less accurate but more compare to naïve** | | | |
| | | | |
| **GARCH DAILY AS BENCHMARK (02-06)** | **ADJ GARCH 07-11** | **ASYMP GARCH 07-11** | **NAÏVE GARCH 07-11** |
| | 0.264122376 | 0.273596 | 0.372973585 |
| **result: asymptotic GARCH assesments less accurate but more compare to naïve** | | | |
| **GARCH MONTHLY AS BENCHMARK (02-06)** | **ADJ GARCH 07-11** | **ASYMP GARCH 07-11** | **NAÏVE GARCH 07-11** |
| | 0.319749826 | 0.420151 | 0.479564789 |
| **result: asymptotic GARCH assesments less accurate** | | | |
| **GARCH DAILY AS BENCHMARK (02-06)** | **ADJ GARCH 07-11** | **ASYMP EGARCH 07-11** | **NAÏVE GARCH 07-11** |
| | 0.264122376 | 0.300656 | 0.372973585 |
| **result: asymptotic EGARCH assesments less accurate but more compare to naïve** | | | |
| **GARCH MONTHLY AS BENCHMARK (02-06)** | **ADJ GARCH 07-11** | **ASYMP EGARCH 07-11** | **NAÏVE GARCH 07-11** |
| | 0.319749826 | 0.453409 | 0.479564789 |
| **result: asymptotic EGARCH assesments less accurate but more compare to naïve** | | | |

**Table 4 MSE Results (Corhay correction)**

| MEAN SQUARE ERRORS BETWEEN ADJ OR ASYMPT AND NAÏVE BETAS (corhay) | | | |
|---|---|---|---|
| **OLS DAILY AS BENCHMARK (02-06)** | **ADJ OLS 07-11** | **ASYMP OLS 07-11** | **NAÏVE OLS 07-11** |
| | **0.286191552** | **0.253697139** | **0.388213724** |
| **result: asymptotic OLS assesments more accurate** | | | |
| **OLS MONTHLY AS BENCHMARK (02-06)** | **ADJ OLS 07-11** | **ASYMP OLS 07-11** | **NAÏVE OLS 07-11** |
| | 0.375046614 | 0.467201 | 0.486873048 |
| **result: asymptotic OLS assesments less accurate but more compare to naïve** | | | |
| | | | |
| **GARCH DAILY AS BENCHMARK (02-06)** | **ADJ GARCH 07-11** | **ASYMP GARCH 07-11** | **NAÏVE GARCH 07-11** |
| | 0.260343182 | 0.270565 | 0.372767352 |
| **result: asymptotic GARCH assesments less accurate but more compare to naïve** | | | |
| **GARCH MONTHLY AS BENCHMARK (02-06)** | **ADJ GARCH 07-11** | **ASYMP GARCH 07-11** | **NAÏVE GARCH 07-11** |
| | 0.367789325 | 0.445706 | 0.500254781 |
| **result: asymptotic GARCH assesments less accurate but more compare to naïve** | | | |
| **GARCH DAILY AS BENCHMARK (02-06)** | **ADJ GARCH 07-11** | **ASYMP EGARCH 07-11** | **NAÏVE GARCH 07-11** |
| | 0.260343182 | 0.295568 | 0.372767352 |
| **result: asymptotic EGARCH assesments less accurate but more compare to naïve** | | | |
| **GARCH MONTHLY AS BENCHMARK (02-06)** | **ADJ GARCH 07-11** | **ASYMP EGARCH 07-11** | **NAÏVE GARCH 07-11** |
| | 0.367789325 | 0.493591 | 0.500254781 |
| **result: asymptotic EGARCH assesments less accurate but more compare to naïve** | | | |

# A Partially Reduced-Bias Value-at-Risk Estimation Procedure

M. Ivette Gomes[1], Frederico Caeiro[2], and Fernanda Figueiredo[3]

[1] Centro de Estatística e Aplicações, Faculdade de Ciências, Universidade de Lisboa
Lisboa, Portugal
(e-mail: ivette.gomes@fc.ul.pt)
[2] Centro de Matemática e Aplicações, Faculdade de Ciências e Tecnologia, Universidade Nova de Lisboa
Caparica, Portugal
(e-mail: fac@fct.unl.pt)
[3] Centro de Estatística e Aplicações, Universidade de Lisboa, and Faculdade de Economia, Universidade do Porto
Porto, Portugal
(e-mail: otilia@fep.up.pt)

**Abstract.** For any level $q$, $0 < q < 1$, and on the basis of a sample $\underline{\mathbf{X}} := (X_1, \ldots, X_n)$ of either independent, identically distributed or possibly weakly dependent and stationary random variables from an unknown model $F$ with a heavy right-tail function, the value-at-risk at the level $q$, the size of the loss that occurred with a small probability $q$, is estimated by a new partially reduced-bias semi-parametric procedure. With the notation $(X_{1:n} \leq \cdots \leq X_{n:n})$ for the set of ascending order statistics associated with the available sample $\underline{\mathbf{X}}$, such a procedure is based on the mean-of-order-$p$ of the set of statistics $\underline{\mathbf{U}} := \{U_{ik} := X_{n-i+1:n}/X_{n-k:n},\ 1 \leq i \leq k < n\}$, with $p$ a non-negative number and $k+1$ the number of top order statistics used in the estimation.
**Keywords:** Heavy right-tails, Monte-Carlo simulations, Semi-parametric estimation, Statistics of univariate extremes, Value-at-risk.

## 1 Introduction

On the basis of a sample $(X_1, \ldots, X_n)$ of independent, identically distributed or possibly weakly dependent and stationary random variables (r.v.'s), from an underlying cumulative distribution function (c.d.f.) $F$, let us denote by $(X_{1:n} \leq \cdots \leq X_{n:n})$ the sample of associated ascending order statistics. If we can find attraction coefficients $(a_n, b_n)$, with $a_n > 0$ and $b_n \in \mathbb{R}$, such that the sequence of linearly normalized maxima, $\{(X_{n:n} - b_n)/a_n\}_{n \geq 1}$, converges to a non-degenerate r.v., then (Gnedenko, 1943, [8]) such a r.v. is of the type of a general *extreme value* (EV) c.d.f.,

$$\mathrm{EV}_\xi(x) = \begin{cases} \exp(-(1+\xi x)^{-1/\xi}, 1+\xi x > 0, & \text{if } \xi \neq 0, \\ \exp(-\exp(-x)),\ x > 0, & \text{if } \xi = 0. \end{cases} \tag{1}$$

*Stochastic Modeling, Data Analysis and Statistical Applications* (*pp.* 409-419)
Lidia Filus - Teresa Oliveira - Christos H Skiadas (Eds)



We then say that $F$ is in the max-domain of attraction of $\mathrm{EV}_\xi$, use the notation $F \in \mathcal{D}_{\mathcal{M}}(\mathrm{EV}_\xi)$, and the parameter $\xi$ is the *extreme value index* (EVI), a crucial parameter in the field of statistics of extremes.

For heavy right tails, i.e. for $\xi > 0$, in (1), we are interested in the semi-parametric estimation of the *value-at-risk* ($\mathrm{VaR}_q$) at the level $q$, i.e. the size of the loss that occurred with a small probability $q$. Equivalently, we are dealing with a high quantile

$$\chi_{1-q} \equiv \mathrm{VaR}_q := F^{\leftarrow}(1-q),$$

of an unknown c.d.f. $F$, with $F^{\leftarrow}(y) = \inf\{x : F(x) \geq y\}$ denoting the generalized inverse function of $F$. As usual, let us denote by $U(t)$ the reciprocal tail quantile function, i.e.

$$U(t) := F^{\leftarrow}(1-1/t), \quad t \geq 1,$$

the generalized inverse function of $1/(1-F)$. For small $q$, we thus want to estimate the parameter

$$\mathrm{VaR}_q = U\left(1/q\right), \quad q = q_n \to 0, \quad nq_n \leq 1,$$

i.e. we want to extrapolate beyond the sample, possibly working in the whole $\mathcal{D}_{\mathcal{M}}(\mathrm{EV}_{\xi>0}) =: \mathcal{D}^{+}_{\mathcal{M}}$, assuming thus that

$$U(t) \ \sim \ Ct^{\xi}, \quad \text{as } t \to \infty, \tag{2}$$

where the notation $a(t) \ \sim \ b(t)$ means that $a(t)/b(t) \to 1$, as $t \to \infty$.

Weissman (1978, [22]) proposed the following semi-parametric $\mathrm{VaR}_q$-estimator:

$$\mathrm{Q}^{(q)}_{\hat{\xi}}(k) := X_{n-k:n}\left(\frac{k}{nq}\right)^{\hat{\xi}}, \tag{3}$$

where $\hat{\xi}$ can be any consistent estimator for $\xi$ and Q stands for quantile. For $\xi > 0$, the classical EVI-estimator, usually the one which is used in (3), for a semi-parametric quantile estimation, is the Hill estimator $\hat{\xi} = \hat{\xi}(k) =: \mathrm{H}(k)$ (Hill, 1975, [21]), with the functional expression,

$$\mathrm{H}(k) := \frac{1}{k}\sum_{i=1}^{k} V_{ik}, \quad V_{ik} = \ln \frac{X_{n-i+1:n}}{X_{n-k:n}}, \ 1 \leq i \leq k. \tag{4}$$

If we plug in (3) the Hill estimator, $\mathrm{H}(k)$, we get the so-called Weissman-Hill quantile or $\mathrm{VaR}_q$-estimator, with the obvious notation,

$$\mathrm{Q}^{(q)}_{\mathrm{H}}(k) = X_{n-k:n}\left(\frac{k}{nq}\right)^{\mathrm{H}(k)}. \tag{5}$$

To derive the asymptotic behavior of $\mathrm{Q}^{(q)}_{\mathrm{H}}(k)$, as well as of alternative $\mathrm{VaR}_q$-estimators, it is useful to impose a second-order expansion on the tail function

$$\overline{F}(x) := 1 - F(x)$$

or on the function $U$, in (2), often assuming that we are working in Hall-Welsh class of models (Hall and Welsh, 1985, [20]), where, as $t \to \infty$, and with $C,\ \xi > 0$, $\rho < 0$ and $\beta$ non-zero,

$$U(t) = Ct^{\xi}\big(1 + A(t)/\rho + o\left(t^{\rho}\right)\big), \qquad A(t) = \xi\ \beta\ t^{\rho}. \tag{6}$$

The class in (6) is a wide class of models, that contains most of the heavy-tailed parents useful in applications, like the $\mathrm{EV}_{\xi}$, in (1), if $\xi > 0$, the associated *Generalized Pareto* $\big(\mathrm{GP}_{\xi}(x) = 1 + \ln \mathrm{EV}_{\xi}(x),\ x \geq 0\big)$, and the Student-$t_{\nu}$, with $\nu$ degrees of freedom and a probability density function,

$$f(x;\nu) = \frac{\Gamma(\nu+1)/2}{\sqrt{\pi\nu}\ \Gamma(\nu/2)}\big(1 + x^2/\nu\big)^{-(\nu+1)/2}, \quad x \in \mathbb{R}. \tag{7}$$

Indeed, (6) implies (2).

Note next that we can write

$$\mathrm{H}(k) = \sum_{i=1}^{k} \ln\left(\frac{X_{n-i+1:n}}{X_{n-k:n}}\right)^{1/k} = \ln\left(\prod_{i=1}^{k} \frac{X_{n-i+1:n}}{X_{n-k:n}}\right)^{1/k}, \quad 1 \leq i \leq k < n.$$

The Hill estimator is thus the logarithm of the geometric mean (or mean-of-order-0) of

$$\underline{\mathbb{U}} := \{U_{ik} := X_{n-i+1:n}/X_{n-k:n},\ 1 \leq i \leq k < n\}. \tag{8}$$

More generally, Brilhante *et al.* (2013, [1]), considered as basic statistics the mean-of-order-$p$ of $\underline{\mathbb{U}}$, in (8), with $p \geq 0$, i.e., the class of statistics

$$A_p(k) = \begin{cases} \left(\frac{1}{k}\sum\limits_{i=1}^{k} U_{ik}^{p}\right)^{1/p}, \text{ if } p > 0, \\ \left(\prod\limits_{i=1}^{k} U_{ik}\right)^{1/k}, \quad \text{if } p = 0, \end{cases}$$

and the class,

$$\mathrm{H}_p k) := \begin{cases} \Big(1 - A_p^{-p}(k)\Big)/p, \text{ if } p > 0, \\ \ln A_0(k) = \mathrm{H}(k), \text{ if } p = 0, \end{cases} \tag{9}$$

with $\mathrm{H}_0(k) \equiv \mathrm{H}(k)$, given in (4). The class of MOP EVI-estimators in (9) depends now on this tuning parameter $p \geq 0$, and was shown to be valid for $0 \leq p < 1/\xi$, whenever $k = k_n$ is an intermediate sequence, i.e. a sequence of integers $k = k_n$, $1 \leq k < n$, such that

$$k = k_n \to \infty \quad \text{and} \quad k_n = o(n), \text{ as } n \to \infty.$$

If we plug in (3) the MOP EVI-estimator, $\mathrm{H}_p(k)$, we get the so-called MOP quantile or $\mathrm{VaR}_q$-estimator, with the obvious notation,

$$\mathrm{Q}_{\mathrm{H}_p}^{(q)}(k) = X_{n-k:n}\left(\frac{k}{nq}\right)^{\mathrm{H}_p(k)}, \tag{10}$$

studied asymptotically and for finite samples in Gomes *et al.* (2013, [18]).

The MOP EVI-estimators in (9) can often have a high asymptotic bias, and bias reduction has recently been a vivid topic of research in the area of statistics of extremes. Working just for technical simplicity in the particular class of models in (6), the asymptotic distributional representation of $\mathrm{H}_p(k)$ for $p = 0$ led Caeiro *et al.* (2005, [3]), to directly remove the dominant component of the bias of the Hill EVI-estimator, given by $\xi\beta(n/k)^\rho/(1-\rho)$, considering the *corrected-Hill* (CH) EVI-estimators,

$$\mathrm{CH}(k) \equiv \mathrm{CH}_{\hat\beta,\hat\rho}(k) := \mathrm{H}(k)\Big(1 - \frac{\hat\beta}{1-\hat\rho}\left(\frac{n}{k}\right)^{\hat\rho}\Big), \tag{11}$$

a *minimum-variance reduced-bias* (MVRB) class of EVI-estimators for adequate second-order parameters' estimators, $(\hat\beta, \hat\rho)$. Estimators of $\rho$ can be found in Gomes *et al.* (2002, [14]), Fraga Alves *et al.* (2003, [7]), and more recently in Goegebeur *et al.* (2008, [9]; 2010, [10]), Ciuperca and Mercadier (2010, [6]) and Caeiro and Gomes (2012, [5]), among others. Regarding the $\beta$-estimation, we refer Gomes and Martins (2002, [11]), Caeiro and Gomes (2006, [4]) and Gomes *et al.* (2010, [15]), also among others. Gomes and Pestana (2007, [13]) have used the EVI-estimator in (11) to build $\mathrm{VaR}_q$-estimators, that we obviously denote by $\mathrm{Q}^{(q)}_{\mathrm{CH}}(k)$.

Working with values of $p$ such that the asymptotic normality of the estimators in (9) holds, i.e. $0 \le p < 1/(2\xi)$, Brilhante *et al.* (2014, [2]) noticed that there is an optimal value

$$p \equiv p_{_M} = \varphi_\rho/\xi, \quad \text{with} \quad \varphi_\rho = 1 - \rho/2 - \sqrt{(1-\rho/2)^2 - 1/2}, \tag{12}$$

which maximises the asymptotic efficiency of the class of estimators in (9). Then, they considered the optimal r.v. $\mathrm{H}_{p_{_M}}(k)$, with $\mathrm{H}_p(k)$ and $p_{_M}$ given in (9) and (12), respectively, deriving its asymptotic behaviour. Such a behaviour has led Gomes *et al.* (2014, [19]) to introduce a partially reduced-bias (PRB) class of MOP EVI-estimators based on $\mathrm{H}_p(k)$, in (9), with the functional expression

$$\mathrm{PRB}_p(k;\hat\beta,\hat\rho) := \mathrm{H}_p(k)\Big(1 - \frac{\hat\beta(1-\varphi_{\hat\rho})}{1-\hat\rho-\varphi_{\hat\rho}}\left(\frac{n}{k}\right)^{\hat\rho}\Big), \tag{13}$$

still dependent on a tuning parameter $p$ and with $\varphi_\rho$ defined in (12). On the basis of a large-scale simulation study, it was shown in the aforementioned paper that these PRB EVI-estimators, in (13), are able to outperform the CH EVI-estimators, in (11), for a large variety of models. It is thus sensible to work with the new $\mathrm{VaR}_q$-estimator $\mathrm{Q}^{(q)}_{\mathrm{PRB}_p}(k)$, with the obvious functional form

$$\mathrm{Q}^{(q)}_{\mathrm{PRB}_p}(k) := X_{n-k:n}\left(\frac{k}{nq}\right)^{\mathrm{PRB}_p(k;\hat\beta,\hat\rho)}, \tag{14}$$

with $\mathrm{PRB}_p(k;\hat\beta,\hat\rho)$ given in (13), $p$ any non-negative number and $k+1$ the number of top order statistics used in the estimation. The small-scale Monte-Carlo simulation performed in Section 2 shows the potentiality of the $\mathrm{VaR}_q$ semi-parametric estimators in (14).

Under adequate regularity conditions all the aforementioned classes of EVI and VaR estimators are asymptotically normal.

## 2 Monte-Carlo simulation

We have implemented multi-sample Monte-Carlo simulation experiments of a large size, $5000 \times 20$, essentially for the new classes of VaR-estimators, $\mathrm{Q}^{(q)}_{\mathrm{PRB}_p}(k)$, in (14), with $\mathrm{PRB}_p$ given in (13), for a few values of $p$, comparatively with the VaR-estimators in (5) and (10). We have considered sample sizes $n = 100, 500, 1000, 2000$ and 5000, and $\xi = 0.1, 0.25, 0.5$ and 1, from the following models:

1. Extreme value model, with c.d.f. $F(x) = \mathrm{EV}_\xi(x)$, in (1) ($\rho = -\xi$), and
2. Student-$t_\nu$ underlying parents, with $\nu = 4$ ($\xi = 1/\nu = 0.25$; $\rho = -2/\nu = -0.5$), with probability density function given in (7).

For details on multi-sample simulation, see Gomes and Oliveira (2001, [12]).

### 2.1 Mean values and MSE patterns as functions of *k*

For each value of $n$ and for each of the aforementioned models, we have first simulated the mean values (E) and root MSE (RMSE) of the VaR-estimators under consideration, as functions of the number of top order statistics $k$ involved in the estimation, and on the basis of the first run of size 5000. Just as an illustration, we present Figure 1, associated with $\mathrm{EV}_{0.25}$ parents. In this figure, we show, for $n = 1000$, $q = 1/n$, and on the basis of the first $N = 5000$ runs, the simulated patterns of mean value, $\mathrm{E}_Q[\cdot]$, and root mean squared error, $\mathrm{RMSE}_Q[\cdot]$, of $\mathrm{Q}^{(q)}_{\hat{\xi}}(k)/\chi_{1-q}$, based on $\mathrm{Q}^{(q)}_{\hat{\xi}}(k)$ in (3), with $\hat{\xi}$ replaced by both $\mathrm{PRB}_p$, in (13), for $p = p_\ell = \ell/(8\xi)$, $\ell = 1(1)7$, representing only some of these $\ell$-values, and CH, in (11). We have also plotted the Weissman-Hill VaR-estimator, based on H, in (4).

To enhance the fact that for $n = 1000$ the $\mathrm{PRB}_p$ VaR-estimators do not overpass the CH VaR-estimator, we further present Figure 2, similar to Figure 1, but associated with an underlying Student $t_4$ ($\xi = 0.25, \rho = -0.5$) parent.

### 2.2 Behaviour at optimal levels

We have further computed the Weissman-Hill VaR-estimator $\mathrm{Q}^{(q)}_{\mathrm{H}}(k) \equiv \mathrm{Q}^{(q)}_{\mathrm{H}_0}(k)$ at the simulated value of $k^{(q)}_{0|\mathrm{H}_0} := \arg\min_k \mathrm{RMSE}\big(\mathrm{Q}^{(q)}_{\mathrm{H}_0}(k)\big)$, the simulated optimal $k$ in the sense of minimum RMSE, and with $\mathrm{Q}^{(q)}_{\hat{\xi}}(k)$ defined in (3). Such a value is not highly relevant in practice, but provides an indication of the best possible performance of the Weissman-Hill VaR-estimator. Such an estimator is denoted by $\mathrm{Q}_{00} := \mathrm{Q}_{\mathrm{H}|0}$. We have also computed $\mathrm{Q}_{p0} := \mathrm{Q}_{\mathrm{H}_p|0}$, the

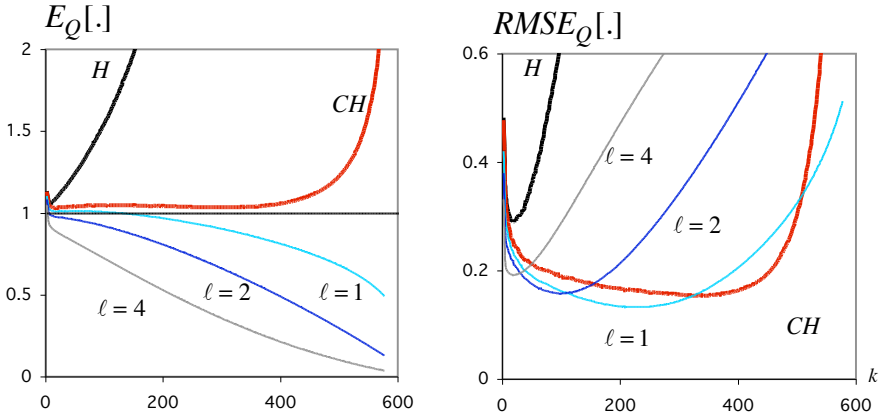


**Fig. 1.** Underlying $EV$ parent with $\xi = 0.25$ ($\rho = -0.25$)

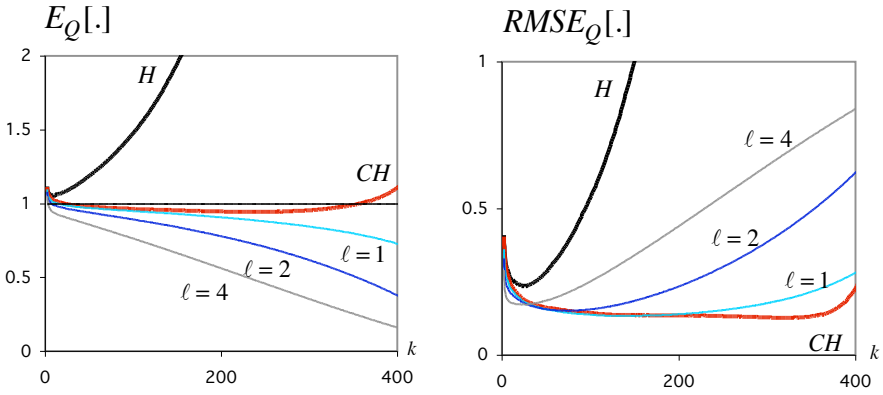


**Fig. 2.** Underlying Student $t_4$ ($\xi = 0.25, \rho = -0.5$) parent

estimator in (14) at optimal levels, for a few values of $p$, and the simulated indicators,

$$\text{REFF}_{p|0} := \text{RMSE}\,(\text{Q}_{00})/\text{RMSE}\,(\text{Q}_{p0}). \tag{15}$$

A similar REFF-indicator, $\text{REFF}_{\text{CH}|0}$ has also been computed for the VaR-estimator based on CH EVI-estimators, in (11).

*Remark 1.* The indicator in (15) has been conceived so that an indicator higher than one means a better performance than the one of the Weissman-Hill VaR-estimator. Consequently, the higher these indicators are, the better the associated VaR-estimators perform, compared to $\text{Q}_{00}$.

As an illustration of the results obtained for the different VaR-estimators under consideration, we present Tables 1 and 2. In the first row, we provide the RMSE of $\text{Q}_{00}$, denoted by $\text{RMSE}_0$, so that we can easily recover the RMSE of all other estimators. The subsequent rows provide the REFF-indicators of the VaR-estimators based on CH and on $\text{PRB}_p$. The highest REFF indicator is underlined and **bolded**.

**Table 1.** Simulated RMSE of $Q_{00}$, $q = 1/n$ (first row) and REFF-indicators of $Q_{\text{CH}|0}$ and $Q_{\text{PRB}_{p_\ell}|0}$, for $p_\ell = \ell/(8\xi)$, $\ell = 1(1)7$, for $\text{EV}_\xi$ parents, with $\xi = 0.25$ ($\rho = -0.25$), together with 95% CIs

| **EV parent,** $\xi = 0.25$ | | | | |
|---|---|---|---|---|
| $n$ | 100 | 500 | 1000 | 5000 |
| $\text{RMSE}_0$ | $0.469 \pm 0.0046$ | $0.329 \pm 0.0029$ | $0.294 \pm 0.0023$ | $0.231 \pm 0.0016$ |
| CH | $1.393 \pm 0.0144$ | $1.681 \pm 0.0215$ | $1.908 \pm 0.0103$ | $1.196 \pm 0.0045$ |
| $\ell = 1$ | $1.491 \pm 0.0152$ | $\underline{\mathbf{1.722}} \pm 0.0204$ | $\underline{\mathbf{2.186}} \pm 0.0233$ | $\underline{\mathbf{4.595}} \pm 0.0781$ |
| $\ell = 2$ | $1.605 \pm 0.0140$ | $1.609 \pm 0.0154$ | $1.850 \pm 0.0165$ | $3.558 \pm 0.0254$ |
| $\ell = 3$ | $1.694 \pm 0.0148$ | $1.558 \pm 0.0133$ | $1.612 \pm 0.0135$ | $2.357 \pm 0.0220$ |
| $\ell = 4$ | $\underline{\mathbf{1.718}} \pm 0.0157$ | $1.569 \pm 0.0126$ | $1.528 \pm 0.0130$ | $1.655 \pm 0.0147$ |
| $\ell = 5$ | $1.677 \pm 0.0167$ | $1.551 \pm 0.0132$ | $1.496 \pm 0.0121$ | $1.379 \pm 0.0111$ |
| $\ell = 6$ | $1.607 \pm 0.0165$ | $1.516 \pm 0.0110$ | $1.455 \pm 0.0116$ | $1.291 \pm 0.0097$ |
| $\ell = 7$ | $1.535 \pm 0.0159$ | $1.473 \pm 0.0114$ | $1.414 \pm 0.0112$ | $1.245 \pm 0.0095$ |

**Table 2.** Simulated RMSE of $Q_{00}$, $q = 1/n$ (first row) and REFF-indicators of $Q_{\text{CH}|0}$ and $Q_{\text{PRB}_{p_\ell}|0}$, for $p_\ell = \ell/(8\xi)$, $\ell = 1(1)7$, for Student $t_4$ ($\xi = 0.25, \rho = -0.5$) parents, together with 95% CIs

| **Student** $t_4$ **parent,** $(\xi, \rho) = (0.25, -0.5)$ | | | | |
|---|---|---|---|---|
| $n$ | 100 | 500 | 1000 | 5000 |
| $\text{RMSE}_0$ | $0.378 \pm 0.0039$ | $0.270 \pm 0.0021$ | $0.240 \pm 0.0014$ | $0.185 \pm 0.0007$ |
| CH | $1.211 \pm 0.1316$ | $1.480 \pm 0.0134$ | $\underline{\mathbf{1.881}} \pm 0.0156$ | $1.531 \pm 0.0095$ |
| $\ell = 1$ | $1.281 \pm 0.1408$ | $\underline{\mathbf{1.516}} \pm 0.0133$ | $1.844 \pm 0.0167$ | $1.939 \pm 0.0795$ |
| $\ell = 2$ | $1.364 \pm 0.1496$ | $1.442 \pm 0.0107$ | $1.603 \pm 0.0093$ | $\underline{\mathbf{2.821}} \pm 0.0284$ |
| $\ell = 3$ | $1.453 \pm 0.1544$ | $1.411 \pm 0.0112$ | $1.447 \pm 0.0084$ | $1.856 \pm 0.0144$ |
| $\ell = 4$ | $1.499 \pm 0.1410$ | $1.442 \pm 0.0107$ | $1.392 \pm 0.0073$ | $1.418 \pm 0.0098$ |
| $\ell = 5$ | $\underline{\mathbf{1.504}} \pm 0.1025$ | $1.464 \pm 0.0108$ | $1.397 \pm 0.0063$ | $1.246 \pm 0.0080$ |
| $\ell = 6$ | $1.481 \pm 0.0559$ | $1.452 \pm 0.0107$ | $1.385 \pm 0.0066$ | $1.171 \pm 0.0077$ |
| $\ell = 7$ | $1.441 \pm 0.0263$ | $1.430 \pm 0.0100$ | $1.356 \pm 0.0064$ | $1.134 \pm 0.0076$ |

Again as an illustration, now of the bias of the new VaR-estimators at optimal levels, see Tables 3 and 4. We present there, for the same values of $n$ as before, the simulated mean values at optimal levels of the VaR-estimators under study. Information on 95% confidence intervals (CIs), computed on the basis of the 20 replicates with 5000 runs each, is also provided. Again, and among the estimators considered, the one providing the smallest squared bias is underlined, and written in **bold**.

For a better visualisation of the tables above, we represent Figures 3 and 4, again related to $\text{EV}_{0.25}$ and Student-$t_4$ parents, respectively.

**Table 3.** Simulated mean values, at optimal levels, of $Q_{\mathrm{T}|0}/\chi_{1-q}$, $q = 1/n$, with T =H, CH and $\mathrm{PRB}_{p_\ell}$, $p_\ell = \ell/(10\xi)$, $\ell = 1(1)7$, for $\mathrm{EV}_\xi$ parents, with $\xi = 0.25$ ($\rho = -0.25$), together with 95% CIs

| **$\mathrm{EV}_\xi$ parent, $\xi = 0.25$** | | | | |
|---|---|---|---|---|
| $n$ | 100 | 500 | 1000 | 5000 |
| H | $1.143 \pm 0.0068$ | $1.108 \pm 0.0048$ | $1.106 \pm 0.0052$ | $1.094 \pm 0.0036$ |
| CH | $0.848 \pm 0.0092$ | $\underline{\mathbf{0.925}} \pm 0.0027$ | $1.036 \pm 0.0041$ | $1.093 \pm 0.0035$ |
| $\ell = 1$ | $\underline{\mathbf{0.868}} \pm 0.0069$ | $0.913 \pm 0.0023$ | $\underline{\mathbf{0.953}} \pm 0.0027$ | $\underline{\mathbf{1.000}} \pm 0.0008$ |
| $\ell = 2$ | $0.868 \pm 0.0056$ | $0.893 \pm 0.0013$ | $0.921 \pm 0.0019$ | $0.9889 \pm 0.0006$ |
| $\ell = 3$ | $0.865 \pm 0.0063$ | $0.888 \pm 0.0022$ | $0.896 \pm 0.0015$ | $0.958 \pm 0.0007$ |
| $\ell = 4$ | $0.839 \pm 0.0027$ | $0.884 \pm 0.0022$ | $0.887 \pm 0.0017$ | $0.916 \pm 0.0006$ |
| $\ell = 5$ | $0.804 \pm 0.0024$ | $0.873 \pm 0.0026$ | $0.880 \pm 0.0023$ | $0.882 \pm 0.0012$ |
| $\ell = 6$ | $0.775 \pm 0.0021$ | $0.872 \pm 0.0031$ | $0.872 \pm 0.0037$ | $0.882 \pm 0.0020$ |
| $\ell = 7$ | $0.750 \pm 0.0019$ | $0.850 \pm 0.0010$ | $0.870 \pm 0.0009$ | $0.880 \pm 0.0026$ |

**Table 4.** Simulated mean values, at optimal levels, of $Q_{\mathrm{T}|0}/\chi_{1-q}$, $q = 1/n$, with T =H, CH and $\mathrm{PRB}_{p_\ell}$, $p_\ell = \ell/(10\xi)$, $\ell = 1(1)7$, for Student $t_4$ ($\xi = 0.25, \rho = -0.5$) parents, together with 95% CIs

| $n$ | 100 | 500 | 1000 | 5000 |
|---|---|---|---|---|
| **Student $t_4$ parent, $(\xi, \rho) = (0.25, -0.5)$** | | | | |
| H | $1.114 \pm 0.0056$ | $1.089 \pm 0.0037$ | $1.085 \pm 0.0037$ | $1.077 \pm 0.0037$ |
| CH | $0.905 \pm 0.0351$ | $\underline{\mathbf{0.922}} \pm 0.0030$ | $\underline{\mathbf{0.978}} \pm 0.0028$ | $1.056 \pm 0.0015$ |
| $\ell = 1$ | $\underline{\mathbf{0.930}} \pm 0.0669$ | $0.912 \pm 0.0025$ | $0.940 \pm 0.0011$ | $1.049 \pm 0.0057$ |
| $\ell = 2$ | $0.927 \pm 0.0428$ | $0.904 \pm 0.0024$ | $0.919 \pm 0.0014$ | $\underline{\mathbf{0.978}} \pm 0.0011$ |
| $\ell = 3$ | $0.898 \pm 0.0098$ | $0.906 \pm 0.0018$ | $0.908 \pm 0.0014$ | $0.946 \pm 0.0009$ |
| $\ell = 4$ | $0.866 \pm 0.0028$ | $0.909 \pm 0.0029$ | $0.907 \pm 0.0016$ | $0.923 \pm 0.0009$ |
| $\ell = 5$ | $0.839 \pm 0.0016$ | $0.899 \pm 0.0019$ | $0.905 \pm 0.0024$ | $0.907 \pm 0.0012$ |
| $\ell = 6$ | $0.815 \pm 0.0014$ | $0.892 \pm 0.0030$ | $0.896 \pm 0.0020$ | $0.897 \pm 0.0020$ |
| $\ell = 7$ | $0.795 \pm 0.0013$ | $0.890 \pm 0.0008$ | $0.890 \pm 0.0020$ | $0.894 \pm 0.0017$ |

## 3 Concluding remarks

- It is clear that Weissman-Hill VaR-estimation leads to a strong over-estimation of VaR and the MOP methodology can provide a more adequate VaR-estimation, being even able to beat the MVRB VaR-estimators in a large variety of situations.
- The obtained results lead us to strongly advise the use of the quantile estimator $\mathrm{Q}_{\mathrm{PRB}_p}$ for any adequate choice of $p$, provided by an algorithm like for instance the bootstrap algorithm of the type devised for an EVI-estimation in Gomes *et al.* (2011, [16]) and Gomes *et al.* (2013, [17]), among others.

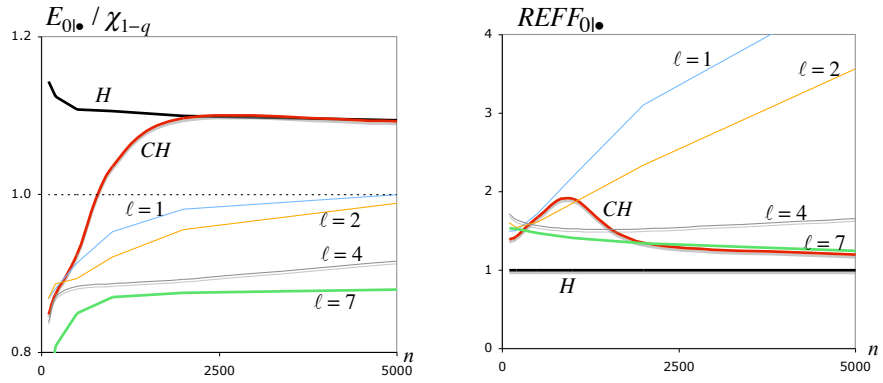


**Fig. 3.** Normalized mean values (*left*) and REFF-indicators (*right*) of the $\mathrm{VaR}_q$-estimators under study, at optimal levels, for $q = 1/n$ and $\mathrm{EV}_{0.25}$ parents

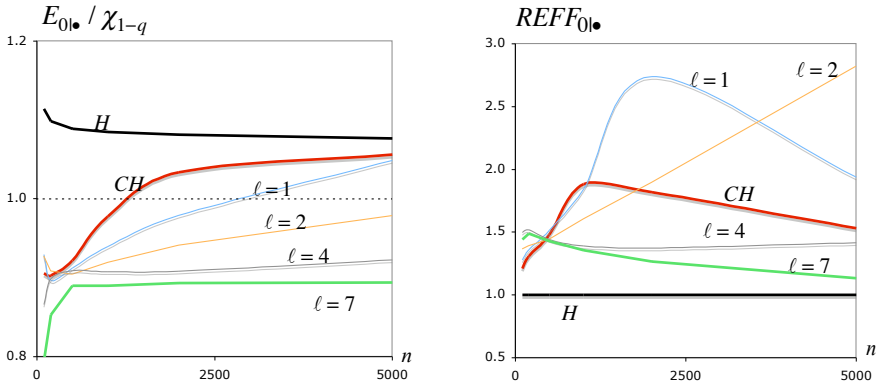


**Fig. 4.** Normalized mean values (*left*) and REFF-indicators (*right*) of the $\mathrm{VaR}_q$-estimators under study, at optimal levels, for $q = 1/n$ and Student $t_4$ parents

- For small values of $|\rho|$ the use of $\mathrm{Q}_{\mathrm{PRB}_p}$, with an adequate value of $p$, always enables a reduction in RMSE regarding the Weissman-Hill estimator and even the CH $\mathrm{VaR}_q$-estimator. Moreover, the bias is also reduced comparatively with the bias of the Weissman-Hill VaR-estimator with the obtention of estimates closer to the target value $\mathrm{VaR}_q$, for $q = 1/n$.
- Such a reduction is particularly high for values of $\rho$ close to zero, even when we work with models out of $\mathcal{D}^{+}_{\mathcal{M}}$, like the the log-gamma and the log-Pareto. This is surely due to the high bias of the Weissman-Hill lnVaR-estimators for models with $\rho = 0$.
- The patterns of the estimators' sample paths are always of the same type, in the sense that for all $k$ the VaR-estimator, $\mathrm{Q}^{(q)}_{\mathrm{PRB}_p}$ decreases as $p$ increases.

## References


1. Brilhante, M.F., Gomes, M. I., and Pestana, D., "A simple generalization of the Hill estimator", *Computational Statistics and Data Analysis* 57:1, 518–535 (2013).
2. Brilhante, M.F., Gomes, M. I., and Pestana, D., "The mean-of-order $p$ extreme value index estimator revisited", in *New Advances in Statistical Modeling and Application*, A. Pacheco, R. Santos, M.R. Oliveira, and C.D. Paulino, Eds., Springer-Verlag, Berlin, Heidelberg, 163–175 (2014).
3. Caeiro, F., Gomes, M.I., and Pestana, D., "Direct reduction of bias of the classical Hill estimator", *Revstat* 3:2, 113–136 (2005).
4. Caeiro, F., and Gomes, M. I., "A new class of estimators of the 'scale' second order parameter", *Extremes* 9, 193–211 (2006).
5. Caeiro, F., and Gomes, M. I., "A Semi-parametric estimator of a shape second order parameter", in *New Advances in Statistical Modeling and Application*, A. Pacheco, R. Santos, M.R. Oliveira, and C.D. Paulino, Eds., Springer-Verlag, Berlin, Heidelberg, 137–144 (2014).
6. Ciuperca, G., and Mercadier, C., "Semi-parametric estimation for heavy tailed distributions", *Extremes* 13:1, 55–87 (2010).
7. Fraga Alves, M. I., Gomes, M. I., and de Haan, L., " A new class of semi-parametric estimators of the second order parameter", *Portugaliae Mathematica* 60:1, 193–213 (2003).
8. Gnedenko, B. V., "Sur la distribution limite du terme maximum d'une série aléatoire", *Annals of Mathematics* 44:6, 423–453 (1943).
9. Goegebeur, Y., Beirlant, J., and de Wet, T. "Linking pareto-tail kernel goodness-of-fit statistics with tail index at optimal threshold and second order estimation" *Revstat* 6:1, 71–81 (2008).
10. Goegebeur, Y., Beirlant, J., and de Wet, T. "Kernel estimators for the second order parameter in extreme value statistics" *J. Statist. Plann. Inference* 140:9, 2632–2654 (2010).
11. Gomes, M. I., and Martins, M. J., "Asymptotically unbiased' estimators of the tail index based on external estimation of the second order parameter", *Extremes* 5:1, 5–31 (2002).
12. Gomes, M. I., and Oliveira, O. "The bootstrap methodology in Statistics of Extremes—choice of the optimal sample fraction', *Extremes* 4:4, 331–358 (2001).
13. Gomes, M. I., and Pestana, P., "A sturdy reduced-bias extreme quantile (VaR) estimator", *J. American Statistical Association* 102:477, 280–292 (2007).
14. Gomes, M. I., de Haan, L., and Peng, L. "Semi-parametric estimation of the second order parameter–asymptotic and finite sample behaviour", *Extremes* 5:4, 387–414 (2002).
15. Gomes, M. I., Henriques-Rodrigues, L., Pereira, H., and Pestana, D., "Tail index and second order parameters' semi-parametric estimation based on the log-excesses", *J. Statist. Comput. and Simul.* 80:6, 653–666 (2010).
16. Gomes, M. I., Mendonça, S., and Pestana, D. "Adaptive reduced-bias tail index and VaR estimation via the bootstrap methodology", *Comm. in Statistics—Theory and Methods* 40:16, 2946–2968 (2011).
17. Gomes, M. I., Figueiredo, F., and Neves, M. M. "Adaptive estimation of heavy right tails: resampling-based methods in action", *Extremes* 15, 463–489 (2012).

18. Gomes, M. I., Brilhante, M. F., and Pestana, D., "A mean-of-order-$p$ class of Value-at-Risk estimators, In C. Kitsos, T. Oliveira, A. Rigas and S. Gulati (eds.), *Theory and Practice of Risk Assessment*, Springer Proceedings in Mathematics and Statistics, in press (2013).
19. Gomes, M. I., Brilhante, M. F., Caeiro, F., and Pestana, D., "A New Partially Reduced Mean-of-order-$p$ Class of Extreme Value Index Estimators", under submission (2014).
20. Hall, P., and Welsh, A. W., "Adaptive estimates of parameters of regular variation", *Ann. Statist.* 13, 331–341 (1985).
21. Hill, B. M., "A simple general approach to inference about the tail of a distribution", *Ann. Statist.* 3, 1163–1174 (1975).
22. Weissman, I., "Estimation of parameters and large quantiles based on the $k$ largest observations", *J. Amer. Statist. Assoc.* 73, 812–815 (1978).

# Strong Approximation of the Random Sums with Applications in Queuing and Risk Theories

Nadiia Zinchenko

Department of Informatics and Applied Mathematics, Nizhyn State Mukola Gogol University, Kropyv'yanskogo 2, 16600, Nizhyn, Ukraine
(e-mail: znm@univ.kiev.ua)

**Abstract.** We present sufficient conditions, which provide the strong approximation of the random sums, and use them to investigate certain models in the risk and queuing theories.
**Keywords:** Invariance principle, Law of the iterated logarithm, Queuing models, Random sums, Risk process, Risk process with stochastic premiums, Strong approximation, Strong limit theorem.

## 1 Introduction

Limit theorems for the random sums $D(t) = \sum_{i=1}^{N(t)} X_i$, where $\{X_i, i \geq 1\}$ are random variables (r.v.) and $N(t)$ is a counting process, became rather popular during last 20 years or so, see, for is instance, Gnedenko and Korolev[7], Whitt[15] and Silvestrov[14]. This topic is interesting not only from theoretical point of view, but also due to numerous practical applications, since mentioned random sums often appear in useful applications in queuing theory (accumulated workload input into queuing system in time interval (0,t)), in risk theory (total claim amount to insurance company up to time t), in financial mathematics (total market price change up to time t) and in certain statistical procedures. In the present work main attention is focused on the strong limit theorems for random sums. Below we consider two classes of strong limit theorem. The first class is *a strong invariance principle* (SIP), other terms are *strong approximation* or *almost sure approximation*.

We say that a random process $\{D(t), t \geq 0\}$ admits strong approximation by the random process $\{\eta(t), t \geq 0\}$ if $D(t)$ (or stochastically equivalent $D^*(t)$) can be constructed on the rich enough probability space together with $\eta(t)$ in such a way that a.s.

$$|D(t) - \eta(t)| = o(r(t)) \vee O(r(t)) \text{ as } t \to \infty, \tag{1}$$

where approximating error (error term ) $r(.)$ is a non-random function.

While week invariance principle provides the convergence of distributions, the strong invariance principle describes how "small" can be the difference between trajectories of $D(t)$ and approximating process $\eta(t)$.

*Stochastic Modeling, Data Analysis and Statistical Applications* (*pp.* 421-432)
Lidia Filus - Teresa Oliveira - Christos H Skiadas (Eds)



We present some general results concerning sufficient conditions for strong approximation of random sums $D(t)$ by a Wiener or $\alpha$-stable Lévy process under various conditions on the counting process N(t) and random summands $\{X_i, i \geq 1\}$. Corresponding proofs are based on the rather general theorems about the strong approximation of superposition of càd-làg processes, not obligatory connected with partial sums, Zinchenko[22]. It worth mentioning that SIP-type results itself can serve as a source of a number of limit theorems. Indeed, using (1) with appropriate error term we can easily transfer the results about the asymptotic behavior of the Wiener or $\alpha$-stable Lévy process on the asymptotic behavior of random sums. Thus, the second class of limit theorems deal with the rate of growth of $D(T)$ and it's increments. As a consequence a number of limit theorems for risk processes in classical Cramér-Lundberg and renewal Sparre Andersen risk models can be obtained, particularly, strong and weak invariance principle for risk processes, diffusion and stable approximation of ruin probabilities, various modifications of the LIL and Erdös-Rényi-Csörgő-Révész-type SLLN for risk processes, which describe the rate of growth and fluctuations of mentioned processes and are useful for planning the insurance activities and reserves. The case of risk models with stochastic premiums is investigated in details.

## 2 SIP for superposition of the random processes

In this section we present two theorems (Zinchenko[22]), which provide strong approximation of the superposition of the random processes $X(M(t))$, when càd-làg random processes $X(t)$ and $M(t)$ themselves admit a.s. approximation by a Wiener or stable Lévy processes.

So, let $X(t)$ and $M(t)$ be independent separable real measurable càd-làg processes, $X(0) = 0$, $M(0) = 0$, $M(t)$ does not decrease with probability 1.

**Theorem 1.** *Suppose that there are standard Wiener processes $W_1(t)$ and $W_2(t)$, constants $m \in R^1$, $\lambda > 0$, $\tau > 0$, $\delta > 0$, for which a.s.*

$$\sup_{0 \leq t \leq T} |M(t) - \lambda t - \tau W_1(t)| = O(r(T)), \tag{2}$$

$$\sup_{0 \leq t \leq T} |X(t) - mt - \sigma W_2(t)| = O(q(T)), \tag{3}$$

*where $r(t) \uparrow \infty$, $r(t)/t \downarrow 0$ , $t \to \infty$ , $q(t) \uparrow \infty$, $q(t)/t \downarrow 0$ as $t \to \infty$.*

*Let $\nu^2 = \sigma^2\lambda + m^2\tau^2\lambda^3$. Then $X(t)$ and $M(t)$ can be redefined on the one probability space together with a standard Wiener process $W(t)$ in such a way that a.s.*

$$\sup_{0 \leq t \leq T} |X(M(t)) - m\lambda t - \nu W(t)| = O(r(T) + q(T) + \ln T). \tag{4}$$

Now let us regard a case when $X(t)$ admits a.s. approximation by $\alpha$-stable process with $1 < \alpha < 2$. Condition $\alpha > 1$ is important for applications.

**Theorem 2.** *Suppose that $M(t)$ satisfies (2), $X(t)$ admits a.s. approximation*

$$\sup_{0\le t\le T}\left|X(t)-mt-Y_{\alpha,\beta}(t)\right|=O(q(T)), \tag{5}$$

*where $Y_{\alpha,\beta}(t)$, $t\ge 0$ is $\alpha$-stable process independent of $W_2(t)$, $1<\alpha<2$, $|\beta|\le 1$, $m\in R_1$. Then $M(t)$ and $X(t)$ can be redefined on the one probability space in such a way that $\forall\varepsilon>0$ a.s.*

$$\Delta^*(T)=\sup_{0\le t\le T}\left|X(M(t))-(m\lambda)t-(Y_{\alpha,\beta}(t\lambda)+(m\tau)W_2(t))\right|=$$

$$=O\Big(q(T)+r(T)\Big)+o\Big(\big(r(T)+(T\ln\ln T)^{1/2}\big)^{1/(\alpha-\varepsilon)}\Big). \tag{6}$$

## 3 SIP for random sums

Let $\{X_i, i\ge 1\}$ be i.i.d.r.v with common distribution function (d.f.) $F(x)$, characteristic function (ch.f.) $f(u)$, $EX_1=m$, $VarX_1=\sigma^2$ if $E|X_1|^2<\infty$. Denote

$$S(t)=\sum_{i=1}^{[t]}X_i,\quad S(0)=0,\quad t>0.$$

Also suppose that $\{Z_i, i\ge 1\}$ is another sequence of i.i.d.r.v. independent of $\{X_i, i\ge 1\}$ with d.f. $F_1(x)$, ch.f. $f_1(u)$ and $EZ_1=1/\lambda>0$,

$$Z(n)=\sum_{i=1}^{n}Z_i,\quad Z(0)=0,\quad Z(x)=Z([x]),$$

and define the *renewal (counting) process* $N(t)$ associated with partial sums $Z(n)$ as

$$N(t)=\inf\{x\ge 0: Z(x)>t\}.$$

In the most interesting applications $\{Z_i\}$ are non-negative r.v. Here and in the next sections we consider *random sums (randomly stopped sums)* defined as

$$D(t)=S(N(t))=\sum_{i=1}^{N(t)}X_i,$$

where i.i.d.r.v. $\{X_i, i\ge 1\}$ and renewal process $N(t)$ are given above.

General SIP-type Theorems 1, 2 are rather convenient for investigation random sums. Really, random sum $D(t)=S(N(t))$ is a typical example of the superposition of the random processes $S(t)$ and $N(t)$, furthermore strong approximation of the partial sum processes $S(t)$ and renewal processes was rather intensively investigated since the middle of 60-th, for the wide bibliography see Csörgő and L. Horváth[5], Alex and Steinebach[1], Zinchenko[18] and more recent Bulinski and Shashkin[3], Zinchenko[22]. Concrete assumptions on summands clear up the type of approximating process and the form of error term.

When $\{X_i, i \geq 1\}$ and $\{Z_i, i \geq 1\}$ have finite moments of order $p \geq 2$ both $S(t)$ and $N(t)$ admit strong approximation by a Wiener process with optimal error terms $q(t)$ and $r(t)$ presented by Csörgő and L. Horváth[5]. Denote by $\sigma^2 = VarX_1$, $\tau^2 = VarZ_1$, $\nu^2 = \lambda\sigma^2 + \lambda^3 m^2 \tau^2$. Substituting explicit expressions for $q(t)$ and $r(t)$ in (4), we obtain following result (see also Csörgő and Horváth[5]):

**Theorem 3.** *(i) Let $E|X_1|^{p_1} < \infty$, $E|Z_1|^{p_2} < \infty$, $p = \min\{p_1, p_2\} > 2$, then $\{X_i\}$ and $N(t)$ can be constructed on the same probability space together with a Wiener process $\{W(t), t \geq 0\}$ in such a way that a.s.*

$$\sup_{0 \leq t \leq T} |S(N(t)) - \lambda m t - \nu W(t)| = o(T^{1/p}); \tag{7}$$

*(ii) if $p = 2$ then right side of (7) is $o(T \ln \ln T)^{1/2}$;*
*(iii) if $E \exp(uX_1) < \infty$, $E \exp(uZ_1) < \infty$ for all $u \in (0, u_o)$, then right-hand side of (7) is $O(\ln T)$.*

Next suppose that $\{X_i\}$ are attracted to $\alpha$-stable law with $1 < \alpha < 2$, $|\beta| \leq 1$, then approximating process for $S(t)$ is a stable process $Y_\alpha(t)$ (condition $\alpha > 1$ is needed to have a finite mean). SIP in this case was studied by Berkes *et al.*[2] in the case of symmetric stable law ($\alpha = 0$) and by Zinchenko[16] in general case with additional assumptions on ch.f. or pseudo-moments of $\{X_i, i \geq 1\}$, see also Mijnheer[13]. Below we use following
**Assumption (C)** : *there are $a_1 > 0, a_2 > 0$ and $l > \alpha$ such that for $|u| < a_1$*

$$|f(u) - g_{\alpha,\beta}(u)| < a_2 |u|^l, \tag{8}$$

*where $f(u)$ is a ch.f. of $(X_1 - EX_1)$ if $1 < \alpha < 2$ and ch.f. of $X_1$ if $0 < \alpha \leq 1$, $g_{\alpha,\beta}(u)$ is a ch.f. of the stable law.*

Assumption (C) not only provides normal attraction of $\{X_i, i \geq 1\}$ to the stable law $G_{\alpha,\beta}(x)$, but also leads to the rather "good" error term $q(t) = t^{1/\alpha - \varrho}$, $\varrho > 0$, in SIP for $S(t)$ (Zinchenko[16]). Thus, in this case random sum process $S(N(t))$ also admits a.s. approximation by $\alpha$-stable process according to Theorem 2. More precise, we have

**Theorem 4 (Zinchenko[21], [22]).** *Let $\{X_i\}$ satisfy **(C)** with $1 < \alpha < 2$, $|\beta| \leq 1$, $EZ_1^2 < \infty$. Then $\{X_i\}$, $\{Z_i\}$, $N(t)$ can be defined together with $\alpha$-stable process $Y_\alpha(t) = Y_{\alpha,\beta}(t)$, $t \geq 0$, so that a.s.*

$$\left|S(N(t)) - m\lambda t - Y_{\alpha,\beta}(\lambda t)\right| = o(t^{1/\alpha - \varrho_1}), \quad \varrho_1 \in (0, \rho_0), \tag{9}$$

*for some $\varrho_0 = \varrho_0(\alpha, l) > 0$.*

**Corollary 1 (SIP for compound Poisson process).** *Theorems 3, 4 hold if $N(t)$ is a homogeneous Poisson process with intensity $\lambda > 0$.*

## 4 The rate of grows of the random sums

In this section we demonstrate the possible way of application of the SIP: using SIP with appropriate error term one can easily extend the results about the asymptotic behavior of the Wiener or stable processes on the rate of growth of random sums $D(t) = S(N(t))$.

**Corollary 2 (Classical LIL for random sums).** *Let $\{X_i\}$ and $\{Z_i\}$ be independent sequences of i.i.d.r.v. with $EX_1 = m < \infty$, $0 < EZ_1 = 1/\lambda < \infty$, $\sigma^2 = VarX_1 < \infty$, $\tau^2 = VarZ_1 < \infty$. Then a.s.*

$$\limsup_{t\to\infty} \frac{|D(t) - m\lambda t|}{\sqrt{2t \ln\ln t}} = \nu, \quad \nu^2 = \lambda\sigma^2 + \lambda^3 m^2 \tau^2. \tag{10}$$

Statement (10) is a straightforward consequence of the classical LIL for a Wiener process and form of error term in Theorem 3.

On the other hand, from Chung's LIL for Wiener process and Theorem 3 it easily follows

**Corollary 3 (Chung's LIL for random sums).** *Let $\{X_i\}$ and $\{Z_i\}$ be as in Corollary 2, then a.s.*

$$\liminf_{t\to\infty} \left(\frac{8 \ln\ln T}{\pi^2 T}\right)^{1/2} \sup_{0\le t\le T} |D(t) - m\lambda t| = \nu, \quad \nu^2 = \lambda\sigma^2 + \lambda^3 m^2 \tau^2. \tag{11}$$

Moreover, if the stable distribution $G_{\alpha,\beta}$, $\alpha \neq 1$, is not concentrated on the half of the axe, i.e. $|\beta| \neq 1$ if $\alpha < 1$ and $|\beta| \le 1$ if $1 < \alpha < 2$, then a.s.

$$\liminf_{T\to\infty} \left(\frac{\ln\ln T}{T}\right)^{1/\alpha} \sup_{0\le t\le T} |Y_{\alpha,\beta}(t)| = C_{\alpha,\beta}, \tag{12}$$

where the constant $C_{\alpha,\beta}$ is defined with the help of so-called "I-functional of the stable process" ( Donsker and Varadhan[6]). Thus, from (12) and Theorem 3 we get

**Corollary 4.** *Let $\{X_i, i \ge 1\}$ satisfy (**C**) with $1 < \alpha < 2$ and $\{Z_i, i \ge 1\}$ be as in Corollary 2, then a.s.*

$$\liminf_{T\to\infty} \left(\frac{\ln\ln T}{T}\right)^{1/\alpha} \sup_{0\le t\le T} |D(t) - m\lambda t| = C_{\alpha,\beta} \lambda^{1/\alpha}. \tag{13}$$

When summands $\{X_i, i \ge 1\}$ are attracted to asymmetric stable law $G_{\alpha,-1}$, we have

**Corollary 5.** *Let $\{X_i, i \ge 1\}$ satisfy (**C**) with $1 < \alpha < 2$, $\beta = -1$. Assume that $EZ_1^2 < \infty$. Then a.s.*

$$\limsup_{t\to\infty} \frac{D(t) - m\lambda t}{t^{1/\alpha} (B^{-1} \ln\ln t)^{1/\theta}} = \lambda^{1/\alpha}, \tag{14}$$

$$B = B(\alpha) = (\alpha - 1)\alpha^{-\theta} |\cos(\pi\alpha/2)|^{1/(\alpha-1)}, \quad \theta = \alpha/(\alpha - 1). \tag{15}$$

Proof follows from Theorem 4 and one-side LIL for the stable process $Y_{\alpha,-1}$.

**Corollary 6.** *Corollaries 2 – 5 hold for a compound Poisson process.*

## 5 How big are increments of the random sums?

When both $\{X_i\}$ and $\{Z_i\}$ have finite variance, SIP for $D(t)$ gives the possibility to extend the Erdös-Rényi-Csörgő-Révész LLN for increments of Wiener process $W(T+a_T)-W(T)$ ( Csörgő and Révész[4]) on the asymptotics of $D(T+a_T)-D(T)$. Notice that additional assumptions on $\{X_i, i \geq 1\}$ and $\{Z_i, i \geq 1\}$, which determine the form of approximation term, have impact on the possible length of intervals $a_T$.

**Theorem 5.** *Let $\{X_i, i \geq 1\}$ and $\{Z_i, i \geq 1\}$ be independent sequences of i.i.d.r.v., $EX_1 = m$, $varX_1 = \sigma^2$, $EZ_1 = 1/\lambda > 0$, $varZ_1 = \tau^2$,*

$$E\exp(uX_1) < \infty, \quad E\exp(uZ_1) < \infty, \tag{16}$$

*as $|u| < u_0$, $u_0 > 0$, function $a_T, T \geq 0$ satisfies following conditions: (i) $0 < a_T < T$, (ii) $T/a_T$ does not decrease in $T$. Also assume that*

$$a_T/\ln T \to \infty \text{ as } T \to \infty. \tag{17}$$

*Then a.s.*

$$\limsup_{T\to\infty} \frac{|D(T+a_T) - D(T) - m\lambda a_T|}{\gamma(T)} = \nu, \tag{18}$$

*where*

$$\nu^2 = \lambda\sigma^2 + \lambda^3 m^2 \tau^2, \quad \gamma(T) = \{2a_T(\ln\ln T + \ln T/a_T)\}^{1/2}.$$

**Theorem 6.** *Let $\{X_i, i \geq 1\}$, $\{Z_i, i \geq 1\}$ and $a_T$ satisfy all conditions of previous Theorem 5 with following assumption used instead of (16)*

$$EX_1^{p_1} < \infty, \quad p_1 > 2, \quad EZ_1^{p_2} < \infty, \quad p_2 > 2.$$

*Then (18) is true if $a_T > c_1 T^{2/p}/\ln T$ for some $c_1 > 0$, $p = \min\{p_1, p_2\}$.*

When $\{X_i, i \geq 1\}$ are attracted to an asymmetric stable law, Theorem 4 and variant of Erdös-Rényi-Csörgő-Révész type law for $\alpha$-stable Lévy process without positive jumps (Zinchenko[17]) yield

**Theorem 7.** *Suppose that $\{X_i, i \geq 1\}$ satisfy (**C**) with $1 < \alpha < 2$, $\beta = -1$, $EZ_1^2 < \infty$, $EX_1 = m$, $EZ_1 = 1/\lambda > 0$. Function $a_T$ is non-decreasing, $0 < a_T < T$, $T/a_T$ is also non-decreasing and provides ${d_T}^{-1} T^{1/\alpha - \varrho_2} \to 0$ for certain $\varrho_2 > 0$ determined by the error term in SIP-type Theorem 4. Then a.s.*

$$\limsup_{T\to\infty} \frac{D(T+a_T) - D(T) - m\lambda a_T}{d_T} = \lambda^{1/\alpha}, \tag{19}$$

*where normalizing function $d_T = a_T^{1/\alpha}\{B^{-1}(\ln\ln T + \ln T/a_T)\}^{1/\theta}$, constants $B$, $\theta$ are defined in (15).*

More results in this area are presented by Zinchenko and Safonova[19], Frolov[8]–[10], Martikainen and Frolov[12].

## 6 How small are increments of the random sums?

The answer on such question for a Wiener and partial sum processes was obtained by Csörgő and Révész[4]. For instance, they proved that for increasing $a_T > 0$ such that $(\ln(T/a_T))/(\ln \ln T) \uparrow \infty$ a.s.

$$\lim_{T\to\infty} \gamma(T, a_T) \inf_{0\le t\le T-a_T} \sup_{0\le s\le a_T} |W(t+s) - W(t)| = 1, \tag{20}$$

where

$$\gamma(T, a_T) = \left(\frac{8(\ln T/a_T + \ln \ln T)}{\pi^2 a_T}\right)^{1/2}.$$

Thus SIP for random sums with appropriate error term leads to the following statement, which holds when summands $\{X_i\}$ as well as inter-occurrence times $\{Z_i\}$ satisfy the Cramer's condition:

**Corollary 7.** *Assume that i.i.d.r.v.* $\{X_i, i \ge 1\}$ *and* $\{Z_i, i \ge 1\}$ *satisfy all conditions of the Theorem 5,* $\nu^2 = \lambda\sigma^2 + \lambda^3 m^2 \tau^2$ *and* $a_T(\ln T)^{-3} \to \infty$ *as* $t \to \infty$*, then a.s.*

$$\lim_{T\to\infty} \gamma(T, a_T) \inf_{0\le t\le T-a_T} \sup_{0\le s\le a_T} |D(t+s) - D(t) - m\lambda a_T| = \nu. \tag{21}$$

## 7 Applications in queuing and risk theories

In the M/G/1 *queuing system* customers arrive according to a Poisson process $N(t)$ and $i$th customer requires a service time of length $X_i$, i.i.d.r.v. $\{X_i, i \ge 1\}$ are independent of $N(t)$. In this case the random sum process $D(t) = \sum_{i=1}^{N(t)} X_i$ is the compound Poisson process and represent the accumulated workload input in time interval (0,t]. Obviously all results of the previous sections are applicable to $D(t)$ and provide SIP-type theorems (Theorems 3, 4; Corollary 1) for the accumulated workload input $D(t)$ and describe the rate of grows of $D(t)$ (Corollaries 2–6). Clearly the conditions, which provide mentioned results, are, in fact, conditions on the distributions of service times. The simplest form they have in the case of M/M/1 system. The same approach can be used for investigation the more general system G/G/1, where $N(t)$ is a renewal process. In this case conditions on inter-arrival intervals are also needed.

As the next step we consider the popular Sparre-Anderssen *collective risk model*. Within this model the risk process, which describes the evolution of reserve capital, is defined as

$$U(t) = u + ct - \sum_{i=1}^{N(t)} X_i, \tag{22}$$

where: $u \ge 0$ denotes an initial capital; $c > 0$ stands for the gross premium rate; renewal (counting) process $N(t) = \inf\{n \ge 1 : \sum_{i=1}^{n} Z_i > t\}$ counts the number of claims to insurance company in time interval [0,t]; positive i.i.d.r.v. $\{Z_i, i \ge 1\}$ are time intervals between claim arrivals; positive i.i.d.r.v.$\{X_i\}$

with d.f. $F(x)$ denote claim sizes; the sequences $\{X_i, i \geq 1\}$ and $\{Z_i, i \geq 1\}$ are independent; $EX_1 = m$, $EZ_1 = 1/\lambda > 0$.

*Classical Cramér-Lundberg risk model* is model (22), where $N(t)$ is a homogeneous Poisson process with intensity $\lambda > 0$.

In the framework of collective risk model random sum $D(t) = \sum_{i=1}^{N(t)} X_i = S(N(t))$ can be interpreted as a total claim amount arising during time interval $[0, t]$, and increments

$$D(T + a_T) - D(T) = \sum_{i=N(T)+1}^{N(T+a_T)} X_i$$

as claim amounts during the time interval $[T, T + a_T]$.

Since process $D(t)$ is a typical example of the random sum, main results of the Sections 2 – 6 can be applied to investigation of the risk process $U(t)$. First of all, Theorems 3 – 4 yield the SIP-type results for $D(t)$ and $U(t)$ under various assumptions on the claim sizes $\{X_i, i \geq 1\}$ and inter-arrival times $\{Z_i, i \geq 1\}$. In the actuarial mathematics individual claim sizes are usually divided in two classes, i.e. *small* claims and *large* claims, according to the tail behavior of their distribution function $F(x)$.

Claims are called *small* if $F(x)$ is light-tailed satisfying Cramér's condition, i.e. when $M(u) = E \exp(uX_1) < \infty$ for $u \in (0, u_0)$; in opposite case, when moment generating function does not exist for any $u > 0$, the claims are called *large* ($F(x)$ is heavy-tailed). It is natural to assume that inter-arrival times $Z_i$ have finite variance.

Thus, for small claims and $\{Z_i\}$ satisfying Cramér's condition, processes $D(t)$ and $U(t)$ admit strong approximation by a Wiener process with the error term $O(\ln t)$; for large claims with finite moments of order $p > 2$ the error term is $o(t^{1/p})$, if $p = 2$ then error term is $o((t \ln \ln t)^{1/2})$. For catastrophic events claims can be so large that their variance is infinite. In this case we assume that $\{X_i\}$ are in domain of normal attraction of asymmetric stable law $G_{\alpha,1}$ with $1 < \alpha < 2$, $\beta = 1$, and additionally satisfy condition (C). Then by Theorem 4 an approximating process for $D(t)$ is $\alpha$-stable process $Y_{\alpha,1}$ with $1 < \alpha < 2$, $\beta = 1$, and risk (reserve) process $U(t)$ admits a.s. approximation by $\alpha$-stable process $Y_{\alpha,-1}$, $1 < \alpha < 2$, $\beta = -1$, which has only negative jumps; the error term is presented in Theorem 4.

The form of error term in SIP is "good" enough for investigation the rate of growth of total claims and asymptotic behavior of the reserve process. Due to results of Section 4 various modifications of the LIL for $D(T)$ can be obtained almost without a proof. So, in the case of small claims or large claims ( but with finite moments of order $p \geq 2$) for large $t$ we can a.s. indicate upper/lower bounds for growth of total claim amounts $D(t)$ as $m\lambda t \pm \nu\sqrt{2t \ln \ln t}$ and for reserve capital $U(t)$ as $u + t\rho m\lambda \pm \nu\sqrt{2t \ln \ln t}$, where $\sigma^2 = VarX_1$, $\tau^2 = VarZ_1$, $\nu^2 = \lambda\sigma^2 + \lambda^3 m^2 \tau^2$, $\rho = (c - \lambda m)/\lambda m > 0$ is a safety loading.

For large claims in domain of normal attraction of asymmetric stable law $G_{\alpha,1}$ with $1 < \alpha < 2$, $\beta = 1$ (for instance, Pareto type r.v. with $1 < \alpha < 2$) Corollary 5 for large $t$ provides a.s. upper bound for the risk process

$$U(t) \leq u + \rho m\lambda t + \lambda^{1/\alpha} t^{1/\alpha} (B^{-1} \ln \ln t)^{1/\theta}.$$

SIP-type results also help to answer on the question: how large can be fluctuations of the total claims/payments on the intervals whose length $a_T$ increases as $T \to \infty$ ? Indeed, under appropriate conditions on claim size distributions and for rather "large" intervals $a_T$ (but growing not faster then $T$) increments $D(T+a_T)-D(T)$ satisfy variants of Erdös-Rényi-Csörgő-Révész LLN similarly to (18) or (19).

Our general approach gives a possibility to study also more complicated risk models with stochastic premiums.

## 8 Strong limit theorems for the risk process with stochastic premiums

Within the **risk model with stochastic premiums** the risk process $U(t)$, $t \geq 0$, is defined as

$$U(t) = u + Q(t) = u + \Pi(t) - S(t) = u + \sum_{i=1}^{N_1(t)} y_i - \sum_{i=1}^{N(t)} x_i, \tag{23}$$

where: $u \geq 0$ is an initial capital; point process $N(t)$ models the number of claims in the time interval $[0,t]$; positive r.v. $\{x_i : i \geq 1\}$ are claim sizes; $Ex_1 = \mu_1$; point process $N_1(t)$ is interpreted as a number of polices bought during $[0,t]$; r.v. $\{y_i : i \geq 1\}$ stand for sizes of premiums paid for corresponding polices, $Ey_1 = m_1$.

We call $U(t)$ (or $Q(t)$) the ***Cramér-Lundberg risk process with stochastic premiums*(CLSP)** if $N(t)$ and $N_1(t)$ are two independent *Poisson processes* with intensities $\lambda > 0$ and $\lambda_1 > 0$; $\{x_i\}$ and $\{y_i\}$ are two sequences of positive i.i.d.r.v. independent of the Poisson processes and of each other with d.f. $F(x)$ and $G(x)$, respectively, $\lambda_1 Ey_1 > \lambda Ex_1$.

This model, being a natural generalization of the classical Cramér -Lundberg risk model, was studied by Zinchenko and Andrusiv[20]. Korolev *et al.*[11] present an interesting example of using (23) for modeling the speculative activity of money exchange point and optimization of its profit.

Notice that process $Q(t) = \Pi(t) - S(t)$ is again a compound Poisson process with intensity $\lambda^* = \lambda + \lambda_1$ and d.f. of the jumps $G^*(x) = \frac{\lambda_1}{\lambda^*} G(x) + \frac{\lambda}{\lambda^*} F^*(x)$, where $F^*(x)$ is a d.f. of the random variable $-x_1$. In the other words

$$Q(t) = \sum_{i=1}^{N^*(t)} \xi_i, \tag{24}$$

where $N^*(t)$ is homogeneous Poisson process with intensity $\lambda^* = \lambda + \lambda_1$ and i.i.d.r.v. $\xi_i$ have d.f. $G^*(x)$.

**Theorem 8 (SIP for CLSP, finite variance case).** *(I)If in model (23) both premiums $\{y_i\}$ and claims $\{x_i\}$ have moments of order $p > 2$, $y_1^2 = m_2$, $Ex_1^2 = \mu_2$, then there is a standard Wiener process $\{W(t), t \geq 0\}$ such that a.s.*

$$\sup_{0 \leq t \leq T} |Q(t) - (\lambda_1 m_1 - \lambda \mu_1)t - \tilde{\sigma} W(t)| = o(T^{1/p}), \quad \tilde{\sigma}^2 = \lambda_1 m_2 + \lambda \mu_2. \tag{25}$$

*(II) If premiums* $\{y_i\}$ *and claims* $\{x_i\}$ *are light-tailed with finite moment generating function in some positive neighborhood of zero, then a.s.*

$$\sup_{0\le t\le T} |Q(t) - (\lambda_1 m_1 - \lambda\mu_1)t - \tilde{\sigma}W(t)| = O(\log T), \tag{26}$$

Proof immediately follows from Corollary 1 since $Q(t)$ is a compound Poisson process (see (24)) with intensity $\lambda^* = \lambda + \lambda_1$, whose jumps have mean $\frac{\tilde{a}}{\lambda^*} = \frac{\lambda_1}{\lambda^*}m_1 - \frac{\lambda}{\lambda^*}\mu_1$, and second moment $\frac{\tilde{\sigma}^2}{\lambda^*} = \frac{\lambda_1}{\lambda^*}m_2 + \frac{\lambda}{\lambda^*}\mu_2$.

*Remark.* In model (23) it is natural to suppose that premiums have distributions with light tails or tails which are lighter than for claim sizes. Therefore moment conditions, which determine the error term in SIP, are in fact conditions on claim sizes.

For catastrophic accidents claims can be so large that they have infinite variance, i.e. belong to the domain of attraction of a certain stable law. Thus, for Cramér-Lundberg risk process with stochastic premiums we have:

**Theorem 9 (SIP for CLSP, large claims attracted to $\alpha$-stable law).** *Suppose that claim sizes* $\{x_i\}$ *satisfy* ***(C)*** *with* $1 < \alpha < 2$, $\beta \in [-1, 1]$, *premiums* $\{y_i\}$ *are i.i.d.r.v. with finite variance, then a.s.*

$$\left|Q(t) - (\lambda_1 m_1 - \lambda\mu_1)t - (\lambda + \lambda_1)^{1/\alpha} Y_{\alpha,\beta}(t)\right| = o(t^{1/\alpha - \varrho_2}), \quad \varrho_2 \in (0, \rho_0), \tag{27}$$

*for some* $\varrho_0 = \varrho_0(\alpha, l) > 0$.

On the next step we focus on investigation the rate of growth of risk process $Q(t)$ as $t \to \infty$ and its increments $Q(t + a_t) - Q(t)$ on intervals whose length $a_t$ grows but not faster than $t$.

The key moments are representation of $Q(t)$ as compound Poisson process (24 ) and application of the results obtained in Sections 4–6, namely, various modifications of the LIL and Erdös-Rényi-Csörgő-Révész law for random sums.

**Theorem 10 ( LIL for CLSP).** *If in model (23) both premiums* $\{y_i\}$ *and claims* $\{x_i\}$ *have moments of order* $p > 2$, *then*

$$\limsup_{t\to\infty} \frac{|Q(t) - \tilde{a}t|}{\sqrt{2t \ln\ln t}} = \tilde{\sigma}, \ \textit{where } \tilde{a} = \lambda_1 m_1 - \lambda\mu_1, \quad \tilde{\sigma}^2 = \lambda_1 m_2 + \lambda\mu_2.$$

Notice that Theorem 10 covers not only the case of small claims, but also the case of large claims with finite moments of order $p > 2$.

Next result deals with the case of large claims with infinite variance. More precise, we shall consider the case when r.v. $\{x_i, i \ge 1\}$ in CLSP-model (23) are attracted to an asymmetric stable law $G_{\alpha,1}$, but premiums have $Ey_1^2 < \infty$.

**Theorem 11.** *Let* $\{x_i, i \ge 1\}$ *satisfy condition* ***(C)*** *with* $1 < \alpha < 2$, $\beta = 1$ *and* $Ey_1^2 < \infty$. *Then a.s.*

$$\limsup_{t\to\infty} \frac{Q(t) - (\lambda_1 m_1 - \lambda\mu_1)t}{t^{1/\alpha}(B^{-1}\ln\ln t)^{1/\theta}} = (\lambda + \lambda_1)^{1/\alpha},$$

*where* $B = B(\alpha) = (\alpha - 1)\alpha^{-\theta}|\cos(\pi\alpha/2)|^{1/(\alpha-1)}, \quad \theta = \alpha/(\alpha - 1)$.

Next theorem clarify the asymptotics of increments of the risk process with stochastic premiums and present the Erdös-Rényi-Csörgő-Révész type law for $Q(t)$.

**Theorem 12 (Small claims).** *Let in CLSP-model (23) claims* $\{x_i, i \geq 1\}$ *and premiums* $\{y_i, i \geq 1\}$ *be independent sequences of i.i.d.r.v. with* $Ex_1 = \mu_1$, $Ex_1^2 = \mu_2$, $Ey_1 = m_1 > 0$, $y_1^2 = m_2$, *and finite moment generating functions*

$$E\exp(ux_1) < \infty, \quad E\exp(uy_1) < \infty \text{ as } |u| < u_0, \quad u_0 > 0.$$

*Assume that non-decreasing function* $a_T$, $T \geq 0$, *satisfies following conditions: (i)* $0 < a_T < T$, *(ii)* $T/a_T$ *does not decrease in* $T$. *Also let*

$$a_T/\ln T \to \infty \text{ as } T \to \infty.$$

*Then a.s.*

$$\limsup_{T\to\infty} \frac{|Q(T + a_T) - Q(T) - a_T(\lambda_1 m_1 - \lambda\mu_1)|}{\gamma(T)} = \tilde{\sigma},$$

*where*

$$\gamma(T) = \{2a_T(\ln\ln T + \ln T/a_T)\}^{1/2}, \quad \tilde{\sigma}^2 = \lambda_1 m_2 + \lambda\mu_2.$$

*Remark.* General Sip-type theorems give also the possibility to investigate more general cases when $\{y_i\}$ and $\{x_i\}$ are sequences of dependent r.v., for example, associated or weakly dependent, $N(t)$ and $N_1(t)$ can be renewal processes, Cox processes, ets.

## References


1. M. Alex, J. Steinebach. Invariance principles for renewal processes and some applications. *Teor. Jmovirn. Mat. Stat.* 50, 22–54, 1994.
2. I. Berkes, H. Dehling, D. Dobrovski, W. Philipp. A strong approximation theorem for sums of random vectors in domain of attraction to a stable law. *Acta Math. Hung.*, 48, 161–172, 1986.
3. A.V. Bulinski, A.P. Shashkin. *Limit theorems for associated random fields and related systems*, Fizmatlit, Moscow, 2008.
4. M. Csörgő, P. Révész. *Strong Approximation in Probability and Statistics*, Acad. Press, New York, 1981.
5. M. Csörgő, L. Horváth. *Weighted Approximation in Probability and Statistics*, Wiley, New York, 1993.
6. M. D. Donsker, S. R. Varadhan. On LIL for local times. *Communs. Pure and Appl. Math.* 30, 707–753, 1977.
7. B.V. Gnedenko, V.Yu. Korolev. *Random Summation: Limit Theorems and Applications*, CRT Press, Boca - Raton, Florida, 1996.
8. A. Frolov. On Erdös-Rényi Laws for renewal processes. *Teor. Jmovirn. Mat. Stat.* 68, 164–173, 2003.
9. A. Frolov. Limit theorems for increments of sums of independent random variables. *Journal of Math. Sciences* 128, 1, 2604–2613, 2006.
10. A. Frolov. Strong limit theorems for increments of compound renewal processes. *Journal of Math. Sciences* 152, 6, 944–957, 2008.

11. V. Yu. Korolev, V.E. Bening, S.Ya. Shorgin. *Mathematical Foundations of Risk Theory*, Fizmatlit, Moscow, 2007, (in Russian).
12. A. Martikainen, A. Frolov. On the Chung law for compound renewal processes. *Journal of Math. Sciences*, 145, N 2, 4866–4870, 2007.
13. J. Mijnheer. Limit theorems for sums of independent random variables in domain of attraction of a stable law: a survey. *Teor. Jmovirn. Mat. Stat.* 53, 109–115, 1995.
14. D. Silvestrov. *Limit Theorems for Randomly Stopped Stochastic Processes*, Springer-Verlag, London, 2004.
15. W. Whitt. *Stochastic-Processes Limits: An Introduction to Stochastic-Process Limits and Their Application to Queues*, Springer-Verlag, New York, 2002.
16. N. Zinchenko. The strong invariance principle for sums of random variables in the domain of attraction of a stable law. *Teor. Verojatnost. i Primenen.* 30, 131–135, 1985.
17. N. Zinchenko. Asymptotics of increments of the stable processes with the jumps of one sign. *Teor. Veroyatnost. i Primenen.* 32, 793–796, 1987.
18. N. Zinchenko. The Skorokhod representation and strong invariance principle. *Teor. Jmovirn. Mat. Stat.* 60, 51–63, 2000.
19. N. Zinchenko, M. Safonova. Erdös-Renyi type law for random sums with applications to claim amount process. *Journal of Numerical and Applied Mathematics* 1(96), 246–264, 2008.
20. N. Zinchenko, A. Andrusiv. Risk processes with stochastic premiums. *Theory of Stoch. Processes* 14, 3–4 , 189–208, 2008.
21. N. Zinchenko. Strong invariance principle for a superposition of random processes. *Theory of Stoch. Processes* 16(32), 130–138, 2010.
22. N. Zinchenko. Almost sure approximation of the superposition of the random processes. *Methodology and Computing in Applied Probability*, DOI 10.1007/s 11009-013-9350-y, 2013.

# 9 CHAPTER

## Time Series, Signals, Networks

# Diffusion Maps in the Reconstruction of Nonlinear Signals

Lúcia M. S. Pinto[1], Ricardo Fabbri[2], and Francisco D. Moura Neto[2]

[1] Escola Nacional de Ciências Estatísticas
Instituto Brasileiro de Geografia e Estatística
Rua André Cavalcanti, 106, Rio de Janeiro, RJ 20231-050, Brazil
(e-mail: lumasapin@hotmail.com)
[2] Polytechnic Institute, Rio de Janeiro State University
Rua Bonfim, 25, Nova Friburgo, RJ 28625-570, Brazil,
(e-mail: [rfabbri,fmoura]@iprj.uerj.br)

**Abstract.** Diffusion maps have proven to be very useful for dimensionality reduction of high dimensional data sets. This method has been introduced by Coifman *et al.* citecoifman2005geometric. Following the program set forth by Munford and Desolneux [10], which establishes a feedback architecture for data recognition and reconstruction, we construct a procedure for the regularized reconstruction of signals, based on the distance from the training data set and otimization of diffused data. The results show the robustness of the methodology.
**Keywords:** Diffusion maps, Dimensionality reduction, PCA, Regularization.

## 1 Introduction

The aim of this work is to investiate one of the most recent techniques for dimensionality reduction of data in data modeling, looking in particular at pattern recognition and the related problem of reconstruction from a few parameters.

In a general sense, given $n$ data points in $\mathbb{R}^d$, $X^1, X^2, \ldots, X^n$, the dimensionality reduction algorithms attempt to find $n$ points in $\mathbb{R}^k$, $Y^1, Y^2, \ldots, Y^n$, such that each $Y^i$ represents the corresponding $X^i$, preferably with $k$ much less than $d$ (in fact, we are interested in reducing the dimensionality of the data) in such a way as to preserve, as much as possible, the inter-relation of the data points in the new set, in the same way as in the original data set. Several methods have been used with this aim since the classic PCA (Principal Components Analysis) till the Spectral MDS, Aflalo and Kimmel[1], which shows the continued importance of this topic.

In this article we explore the diffusion maps method as a powerful tool for dimensionality reduction, in special for the recognition and reconstruction of signals coming from the quatification of qualities of physical systems.

We are interested in the problem in the perspective of *pattern theory* which consists in the search for a feedback structure, where *bottom-up* and *top-down*

*Stochastic Modeling, Data Analysis and Statistical Applications* (*pp.* 435-441)
Lidia Filus - Teresa Oliveira - Christos H Skiadas (Eds)



algorithms are re-feed and modified for a better understanding of the physical system. In general terms we can interpret a bottom-up algorithm as being represented by a function $G$, an algorithm, mapping the space of signals in a space of signal features,

$$\begin{array}{ccc} \text{Signals space} & \text{Analysis} & \text{Signal features space} \\ \mathbb{R}^d \supset E & \xrightarrow{G} & F \subset \mathbb{R}^k \ , \end{array}$$

that is, atributing parameters (in $F$) to the signals (in $E$).

The set of features can have high dimension. When $E$ is a diferentiable manifold of dimension $e$, it would be adequate that the dimensionality reduction algorithm $G$ would take $E$ into $G(E) \subset F$, possibly still a manifold of dimension $e$ in $\mathbb{R}^k$, with $e \leq k < d$, (hopefully $k \ll d$). Therefore, a signal that required $d$ real numbers to its apecification, would be represented by just $k$ real numbers.

In this setting, the recognition of a signal $X^*$ would be to identify $\tilde{X} \in E$ sharing similar features with $X^*$, that is,

$$G(X^*) \text{ near, or in the same class as, } G(\tilde{X}) \ .$$

Having the features of a signal, $Y^* \in F$, or near to $F$, the aim of reconstruction would be to determine a signal, $X^* \in \mathbb{R}^d$ (not necessarily belonging to te training set $E$ but, preferably, close), such that

$$G(X^*) \cong Y^*$$

and that $X^*$ could be accepted as a real signal of the physical system. In ths way we can imagine a function, or an algorithm, close to an inverse of $G$,

$$\begin{array}{ccc} \text{Space of signals} & \text{Synthesis} & \text{Signal features space} \\ \mathbb{R}^d \supset E & \xleftarrow{H} & F \subset \mathbb{R}^k \end{array}$$

in such a way that $X^* \cong H(Y^*)$.

Appart from the *bottom-up* stage, there is the *top-down* stage, and the two algorithms interact. Given $X^*$, a signal with the properties close to the detected ones $G(X^*)$ (in low dimension) it is synthetized, possibly following a stochastic model sufficiently simple and compared with the input signal. In essence, one computes $\tilde{X} \cong H(G(X^*))$ and compares $X^*$ with $\tilde{X}$, adopting a feedback architecture.

Diffusion maps have great potential in this scenario. However this method has not been conceived with the full set of tools for the construction of machine learning systems based on *recognition by synthesis* in the framework of pattern theory. One of the contributions of this work is that we exploit these ideas to shed light on the problem of recognition.

## 2 Diffusion maps

Diffusion maps is one of the most recent and promissing non-linear dimensionality reduction techniques. This technique allows mapping distances in a

convenient form, in the sense that a diffusion distance discussed below between the input data (training set) approaches the euclidean distance between their images by the diffusion mapping.

The initial step is to construct a graph where each element $X^i$ of a data set $E = \{X^1, X^2 \ldots, X^n\}$ becomes a node of the graph, while the weight of edge joining $X^i$ e $X^j$, $w_{ij}$, are recorded as the $ij$ entry of an afinity matrix, $W$.

It is usual to express the afinity by means of a gaussian kernel given by $W(X^i, X^j) = \exp(-\frac{\|X^i - X^j\|^2}{\varepsilon})$, where $\varepsilon$ depends on the problem. One can interpret $\sqrt{\varepsilon}$ as the size of a neighborhood and it is based on the knowledge of the structure and the density of the data set. This kernel defines a local geometry of the data set. Here we choose $\varepsilon$ as a function of the diameter, $r$, of the data set.

Coifman and Lafon [4] present three normalizations for a family of diffusion maps: $(W^\alpha)_{ij} = \frac{w_{ij}}{d_i^\alpha d_j^\alpha}$, where $d_i^\alpha = (\sum_{k=1}^n w_{ik})^\alpha$ is the degree of the $i^{th}$ node of the original graph to the power $\alpha$ and $w_{ij}$ is computed by the gaussian kernel. They emphasize three values for $\alpha$. When $\alpha = 0$ this corresponds to the classical normalized laplacian of a graph, $\alpha = 1/2$ corresponds to the Fokker-Plank operator and $\alpha = 1$ leads to the Laplace-Beltrami operator. Here we stick to $\alpha = 1$.

We normalize the weight matrix $W$. Let $d_i = (D)_{ii} = \sum_{j=1}^n w_{ij}$ and $p_{ij} = \frac{w_{ij}}{d_i}$. Matrix $P = D^{-1}W$, whose entries are $p_{ij}$, is a Markov matrix, for a Markov process where the states are the nodes of the graph and the transition probability matrix is $P$.

Considering increasing powers of $P$, $P^t = (D^{-1}W)^t$, the Markov process incorporates more and more the intrinsec geometry of the data set. Since $p_{ij}$ is the one-step transition probability from $X^i$ to $X^j$, the $ij$ entry of $P^t$, $p_{ij}^t$, is the transition probability from $X^i$ to $X^j$ in $t$ steps, that is, the probability associated with the set of all paths of lenght $t$ leaving $X^i$ and arriving at $X^j$, reconstructing the geometry of the data set from local connectivity.

## 3 Diffusion distance

To the Markov process described previously, there corresponds a family of diffuion distances, $D_t(X^i, X^j)$. This family measures the connectivity between points $X^i$ and $X^j$ by paths of lenght $t$ in the data set. The *diffusion distance* between $X^i$ e $X^j$, for each fixed $t$, is defined by

$$D_t(X^i, X^j) = \left( \sum_{X^r \in E} \frac{(p_{ir}^t - p_{jr}^t)^2}{\sigma_r} \right)^{1/2},$$

where $\sigma_r = \frac{d_r}{\sum_{i=1}^n d_i}$.

The difusion distance can be rewritten as

$$D_t(X^i, X^j) = (\mathrm{tr}\,(D))^{\frac{1}{2}} \left( \sum_{k=1}^{n-1} \lambda_k^{2t} (v_k(i) - v_k(j))^2 \right)^{1/2}, \qquad (1)$$

where $\boldsymbol{v_k}$ , $\lambda_k$ are, respectively, the eigenvectors and the eigenvalues of the Markov matrix.

Motivated by this expression, the diffusion map is defined in the following way. Let $\mathbf{v}_0, \mathbf{v}_1, \ldots, \mathbf{v}_{n-1}$ be eigenvectors from the right of $P = D^{-1}W$ associated to $\lambda_0 = 1 \geq \lambda_1 \geq \ldots \geq \lambda_{n-1} \geq -1$. For each fixed $t$, the diffusion map is $\mathcal{D}_t$ such that

$$\mathcal{D}_t(X^i) = \begin{pmatrix} \lambda_1^t v_1(i) \\ \lambda_2^t v_2(i) \\ \vdots \\ \lambda_{n-1}^t v_{n-1}(i) \end{pmatrix}, \tag{2}$$

for each $X^i$ in the training data set. (There is no need to use $\lambda_0$ since $\boldsymbol{v}_0$ is a constant vector.)

We can verify that $D_t(X^i, X^j) = (\mathrm{tr}\,(D))^{\frac{1}{2}} \parallel \mathcal{D}_t(X^i) - \mathcal{D}_t(X^j) \parallel$, and in this way the diffusion distance between the original data is proportional to the euclidean distance of its features.

The parameter $t$ of the Markov process works as a type of scaling factor. The larger $t$ is the bigger is the scale considered in the modeling of the data. By varying $t$ one gets a kind of multi-scale analysis of the data set.

Since the absolute value of the eigenvalues are between 0 and 1, for increasing values of $t$ in the stochastic process allow us to keep few components in the diffusion map to analyse data. In fact, for $t$ large enough, we shall have several insignificant $(\lambda_k)^t$, and several terms in $\parallel \mathcal{D}_t(X^i) - \mathcal{D}_t(X^j) \parallel$ contributing very little for the distance between $X^i$ and $X^j$, and can be neglected. Therefore, for large $t$, it is possible to consider few components of the diffusion map.

If, in addition, $W$ is positive semi-definite then the eigenvalues of $P$ are between zero and one. In this case, if we let $k$ be the number of components, chosen as a function of $t$, we can rewrite (1) in an approximate way,

$$D_t(X^i, X^j) \cong (\mathrm{tr}\,(D))^{\frac{1}{2}} \left( \sum_{s=1}^{k} \lambda_s^{2t} (v_s(i) - v_s(j))^2 \right)^{1/2}$$

$$\cong (\mathrm{tr}\,(D))^{\frac{1}{2}} \parallel \mathcal{D}_t(X^i) - \mathcal{D}_t(X^j) \parallel,$$

where

$$\mathcal{D}_t(X^i) \cong \begin{pmatrix} \lambda_1^t v_1(i) \\ \lambda_2^t v_2(i) \\ \vdots \\ \lambda_k^t v_k(i) \end{pmatrix} .$$

Therefore, the diffusion distance between $X^i$ and $X^j$ is almost the same as the euclidean distance between their images in $\mathbb{R}^k$ which, in many practical applications, has dimension $k \ll n$, Lafon and Lee [8]. We also remark that, as the scale parameter $t$ increases, the features of the data, that is, their images by the diffusion map, tend to merge together since $\mathcal{D}_t(X^i) \to 0$, when $t \to +\infty$, for every single data point.

## 4 Pre-image

The pre-image problem consists in finding in the input space an element of the training set which better approximates the inverse image of an element in the reduced space. In general, the exact pre-image does not exist, or it is not unique, and we need an approximate solution Mika *et al.* [9].

We consider here the pre-image problem in the context of the reconstruction of signals by means of a cost function, which differs from previous approaches, Etyngier *et al.* [6], Arias *et al.*[2] and Arif *et al.* [3] We use Nystrom's extension of $\mathcal{D}$ to other vectors in $I\!R^d$, which do not belong to the training set, Lafon *et al.* [7]. We represent it by $\tilde{\mathcal{D}}$.

Since $\mathcal{D}$ is injective in the training set, the pre-image problem has a unique solution in the set of features of training signals. For features outside that set that question is more complicated. The problem of the pre-image of an arbitrary point of $I\!R^{n-1}$ is an ill-posed problem and, in general, the pre-image of a unique point, if it exits, will be a set of vectors in the input space Arias *et al.* [2]. In order to circunvent this difficulty and to look for adequate modifications, we can consider a regularization of the problem by means of the training set.

Assume we are given a point $b \in I\!R^{n-1}$. We look for a good approximation of a possible pre-image, $x$, of that point. We want that $x$ be as close as possible to the data set, in such a way to regularize the inversion. Clearly, we also want that the image of $x$ by the diffusion map be $b$ or near by it. For each $b$ we can represent these requirements by means of an objetive function $f : I\!R^d \to I\!R$, as follows,

$$f(x) = \|\tilde{\mathcal{D}}(x) - b\| + \gamma \min_k(\|x - X^k\|). \tag{3}$$

That is, given $b \in I\!R^{n-1}$, its pre-image, if it exits, will be the vector $x \in I\!R^d$ minimzing $f$ above.The parameter $\gamma$ is used so that it is possible to adjust the level of influence of the second term with respect to the first term, in the right hand side of (3). These ideas can also be used for the reconstruction of PCA.

If we wish to consider the pre-image problem for several points, $b \in I\!R^{n-1}$, we may extend the previous cost function to explicitely consider its dependence not only on $x$ but also on $b$, $f : I\!R^d \times I\!R^{n-1} \to I\!R$, defined by $f(x, b) = \|\tilde{\mathcal{D}}(x) - b\| + \gamma \min_k(\|x - X^k\|)$. Therefore, we consider a function $G$ defined by minimizing $f$, $G : I\!R^{n-1} \to I\!R^d$, such that

$$G(b) = \arg\min_x f(x, b). \tag{4}$$

In general $G(b)$ may be a subset of $I\!R^d$ since $f(\cdot, b)$ can have several minimum points.

The point of minimum, denoted by $\tilde{X}$, when $b = G(X^*)$, is the reconstructed sinal $X^*$. The residue $X^* - \tilde{X}$, has to be verified to check the quality of the reconstruction and the power of analysis and synthesis of the prposed method.

## 5 Experiment

We applied the discussion of extension and pre-image problem to a set of known geometric structure in $I\!R^3$, representing an helix. We considered just

38 points in $\mathbb{R}^3$ consisting of an helix with three turns. Further, random noise was added to 189 points distributed with equal spacing between the points of the helix. The calculation of the features of these noisy points was done by means of Nystrom extension. The pre-images were computed by minimization of the cost function, equation (3), using a simulated annealing algorithm. The regularization parameter was set $\gamma = 0.09$. For the diffusion map we let $\varepsilon = 0,001r^2, t = 50$ e $\alpha = 1$.

Figure 1 presents the results of this experiment. There is a small part of it which has been amplified. In blue are represented the points of the ideal helix, the noisy points are in red, and the pre-images are in green.

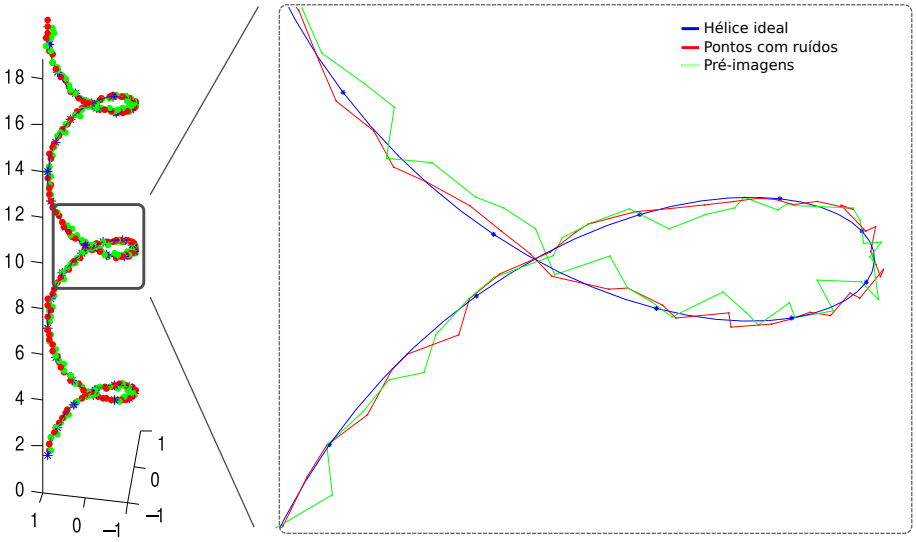


**Fig. 1.** Helix with a small stretch amplified where one can see its noisy points (red) and the corresponding pre-images (green) for the diffusion maps.

## 6 Conclusion

This article presents the diffusion map method for dimensionality reduction focussed on pattern theory in respect to the non-linear reconstruction of signals.

We also formulate and exploit a cost function to compute pre-images for the diffusion maps, which constitutes a significant contribution of this work.

## References

1. Aflalo, Y. and Kimmel, R.,"Spectral multidimensional scaling", *Proceedings of the National Academy of Sciences*, 110(45):18052–18057 (2013).

2. Arias, P., Randall, G. and Sapiro, G., "Connecting the out-of-sample and pre-image problems in kernel methods", *IEEE Conference on Computer Vision and Pattern Recognition*, 1–8 (2007).
3. Arif, O., Vela, P. A. and Daley, W., *Pre-image problem in manifold learning and dimensional reduction methods*, *IEEE Ninth International Conference on Machine Learning and Applications*, 921–924 (2010).
4. Coifman, R. R. and Lafon, S., "Diffusion maps", *Applied and computational harmonic analysis*, 21(1):5–30 (2006).
5. Coifman, R.R. and Lafon, S. and Lee, A.B. and Maggioni, M. and Nadler, B. and Warner, F. and Zucker, S.W. "Geometric diffusions as a tool for harmonic analysis and structure definition of data: Diffusion maps", *Proceedings of the National Academy of Sciences of the United States of America*, 102(21):7426 (2005).
6. Etyngier, P., Segonne,F. and Keriven, R. "Shape priors using manifold learning techniques", *IEEE 11th International Conference on Computer Vision*, 1–8 (2007).
7. Lafon, S., Keller, Y. and Coifman, R. R., "Data fusion and multicue data matching by diffusion maps" *IEEE Transactions on Pattern Analysis and Machine Intelligence*, 28(11):1784–1797 (2006).
8. Lafon, S. and Lee, A., "Diffusion maps and coarse-graining: A unified framework for dimensionality reduction, graph partitioning, and data set parameterization", *IEEE Transactions on Pattern Analysis and Machine Intelligence*, 28(9):1393–1403 (2006).
9. Mika, S., Schlkopf, B., Smola, A. J., Mller, K.-R., Scholz, M. and Rtsch, G., "Kernel pca and de-noising in feature spaces", *NIPS* 11:536–542 (1998).
10. Mumford, D., and Desolneux, A., *Pattern theory: the stochastic analysis of real-world patterns*, A K Peters, Ltd., Natick (2010).

# Weighted Multivariate Fuzzy Trend Model for Seasonal Time Series

Erika Watanabe[1] and Norio Watanabe[2]

[1] Graduate School of Chuo University
Tokyo, Japan
(e-mail: a09.3ng6@g.chuo-u.ac.jp)
[2] Industrial and Systems Engineering, Chuo University
Tokyo, Japan
(e-mail: watanabe@indsys.chuo-u.ac.jp)

**Abstract.** Analyzing trends in multivariate time series is an important issue. A fuzzy trend model has been proposed for estimating trends in multivariate time series. This fuzzy trend model can decompose trends into common and individual trends. However, seasonality is not considered in this model. In this paper we propose a model including seasonality. Another problem of the former model is that common trend might differ from each series when there are large differences among series. Therefore we propose a scaling model which can decompose trends effectively by introducing weights. Usability of proposed models is demonstrated by a numerical example.
**Keywords:** Decomposition of trend, Common trend, Seasonal component, Fuzzy system.

## 1 Introduction

It is important to analyze trend included in multivariate time series. Most of models and methods are proposed for stationary time series or time series whose trends are removed previously. Models or methods for analyzing trend have not been developed sufficiently.

The moving average method and polynomial regression are typical methods for estimating trend. However, it is not easy to determine the length of interval for moving average. Polynomial regression can estimate trend easily but cannot follow irregular movement. On the other hand the fuzzy trend model ([1]) occupies an intermediate position between moving average method and polynomial regression and can analyze trend objectively and flexibly. Fuzzy trend models are also available for multivariate time series and can decompose trends into common and individual trends ([2], [3]). Whether time series is multivariate or scalar, most time series have seasonality or periodic components. However, seasonality is not considered in these models. In this paper we propose a multivariate fuzzy trend model including seasonal components.

*Stochastic Modeling, Data Analysis and Statistical Applications* (*pp.* 443-450)
Lidia Filus - Teresa Oliveira - Christos H Skiadas (Eds)



The former model has another problem that the common trend might differ from each series when there are large differences among series. In this case standardization is difficult, since time series with trends are nonstationary, and mean values and variances depend on time points generally. To resolve this problem we propose a weighted model which can decompose trends effectively by introducing weights for scaling. We also consider a non-weighted fuzzy trend model with seasonal components and weighted fuzzy trend model without seasonal components. We provide an identification method for our models. Applicability of proposed models is demonstrated by a numerical example.

## 2 Fuzzy trend model

Let $\{y_{ln}|n = 1, ..., N,\ l = 1, 2, ..L\}$ denote the observed time series, where $L$ is a number of time series and $N$ is a length of time series. The new model proposed in this paper is defined as follows:

$$y_{ln} = \frac{1}{r_l}(\mu_{ln} + u^S_{ln} + x_{ln}) \tag{1}$$

$$\mu_{ln} = \sum_{k=1}^{K} \nu_{lk}(n)\mu_k \tag{2}$$

$$R_{lk}\text{: If } n \text{ is } A_{lk}, \text{ then } \mu_k = \alpha_{lk}(n - a_k) + \beta_{lk}, \tag{3}$$

where $R_{lk}$ is a fuzzy if-then rule, $\nu_{lk}(n)$ is a membership function of a fuzzy set $A_{lk}$, $u_{lk} = \{(\alpha_{lk}\ \beta_{lk})'\}$ is an unobserved bivariate series ($u'$ means the transpose of $u$), and $x_{ln}$ is a zero-mean stationary process with variance $\sigma^2$.

When $u_{lk}$ is a stochastic process, we assume that $x_{ln}$ and $u_{lk}$ are independent. The weight $r_l$ is for standardization and we assume that $\sum_{l=1}^{L} r_l = 1$ and $r_l > 0$. The parameter $a_k$ satisfies the equation:

$$a_k = a_{k-1} + d, \tag{4}$$

where $d$ is a positive integer and $a_1 = 1$. We use the following membership function:

$$\nu_{lk}(n) = \frac{1}{2}\{\cos(\pi(n - a_k)/d) + 1\}. \tag{5}$$

Fig. 1 shows the membership functions of $A_{l1}, ..., A_{lK}$. The model given by (2)-(3) is a kind of Takagi-Sugeno's fuzzy system ([4]).

The term $u^S_{ln}$ is a deterministic seasonal component, where $u^S_{l,n+p} = u^S_{ln}$ and $p$ is the period. As a constraint we set $\sum_{n=1}^{p} u^S_{ln} = 0$ for all $l$. In this paper we assume that $p$ is known.

Each trend is lead by the latent process $u_l = (u'_{l1}, ..., u'_{lK})'$ in this model. We assume that $u_{lk}$ can be decomposed as follows:

$$u_l = u^C + u^I_l, \tag{6}$$

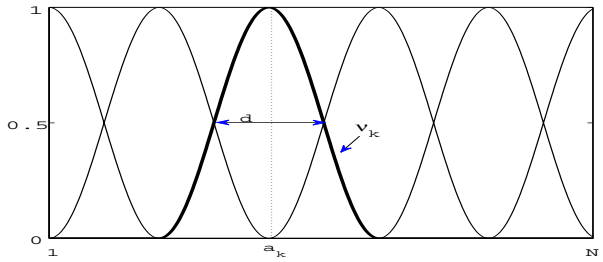


**Fig. 1.** Membership functions

where the latent processes $u^C$ and $u_l^I$ imply the common and individual trends respectively. Such decomposition requires a constraint condition. We will describe this condition later (cf. Eq. (26)).

As special cases of the model (1), the non-weighted model with seasonal components is given by

$$y_{ln} = \mu_{ln} + u_{ln}^S + x_{ln}, \tag{7}$$

and the weighted model without seasonal components is given by

$$y_{ln} = \frac{1}{r_l}(\mu_{ln} + x_{ln}). \tag{8}$$

When $u_{ln}^S = 0$ in (7), this model is identical with the former one.

## 3 Identification

In this section we consider the weighted model (1) only. Identification methods for the models (7) and (8) are derived easily.

In fuzzy trend models estimation of latent processes plays an important role. We rewrite the model as follows:

$$z^R = G_1 u^C + G_2 u^I + x, \tag{9}$$

where

$$z^R = \begin{pmatrix} z_1 \\ \vdots \\ \vdots \\ z_L \end{pmatrix} = \begin{pmatrix} r_1 y_1 - B^S u_1^S \\ \vdots \\ \vdots \\ r_L y_L - B^S u_L^S \end{pmatrix} \tag{10}$$

$$y_l = (y_{l1}, ..., y_{lN})' \tag{11}$$

$$u^I = (u_1^{I\prime}, ..., u_L^{I\prime})' \tag{12}$$

$$u_l^S = (u_{l1}^S, ..., u_{lp}^S)' \tag{13}$$

$$G_1 = (B_1', ..., B_L')' \tag{14}$$

$$G_2 = \begin{pmatrix} B_1 & \cdots & \cdots & 0 \\ \vdots & B_2 & \cdots & \vdots \\ \vdots & \vdots & \ddots & \vdots \\ 0 & 0 & \cdots & B_L \end{pmatrix} \tag{15}$$

$$B_l = \begin{pmatrix} \nu_{l1}(1) & \nu_{l1}(1)(1-a_1) & \cdots & \nu_{lK}(1) & \nu_{lK}(1)(1-a_K) \\ \vdots & \vdots & & \vdots & \vdots \\ \nu_{l1}(N) & \nu_{l1}(N)(N-a_1) & \cdots & \nu_{lK}(N) & \nu_{lK}(N)(N-a_K) \end{pmatrix}. \tag{16}$$

The matrix $B^S$ is the upper $N \times p$ submatrix of the matrix consisting of sufficient numbers of $p$-dimensional identity matrices. The vector $x$ is defined similarly.

Now we consider an estimation procedure. First we estimate a seasonal component for each series by the least squares method for given $d$ and $r_l$. From (1) – (16) we can rewrite

$$y_l = \frac{1}{r_l} B_l u_l + \frac{1}{r_l} B^S u_l^S + \frac{1}{r_l} x_l \tag{17}$$

$$= B_l \tilde{u}_l + \tilde{B}^S \tilde{u}_l^S + \tilde{x}_l \tag{18}$$

$$= [B_l \quad \tilde{B}^S] \begin{pmatrix} \tilde{u}_l \\ \tilde{u}_l^S \end{pmatrix} + \tilde{x}_l, \tag{19}$$

where

$$\tilde{u}_l^S = \frac{1}{r_l} (u_{l1}^S, ..., u_{l,p-1}^S)', \tag{20}$$

$$\tilde{B}^S = B^S \begin{pmatrix} 1 & 0 & \cdots & 0 \\ 0 & 1 & \cdots & 0 \\ \vdots & \vdots & & \vdots \\ 0 & 0 & \cdots & 1 \\ -1 & -1 & \cdots & -1 \end{pmatrix}, \tag{21}$$

and so on. The size of the last matrix in (21) is $p \times (p-1)$. Note that $u_l^S$ follows the constraint condition. From (19) the ordinary least squares method can be applied for estimation of $\tilde{u}_l^S$. We represent the estimated seasonal component by $\hat{u}_l^S$. The latent processes $u_l$'s are re-estimated by using all series in the following way.

We define the new series by removing the seasonal component from the original series as follows:

$$\hat{z}^R = (\hat{z}_1', ..., \hat{z}_L')' \tag{22}$$

$$\hat{z}_l = r_l y_l - B^S \hat{u}_l^S. \tag{23}$$

From (9) the latent process can be estimated by the least squares method also. However, we cannot apply the ordinary least squares method to our model directly. Then we propose a two stage estimation procedure. The least squares estimators $\hat{u}^C$ and $\hat{u}^I$ are given by

$$\hat{u}^C \equiv (G_1'G_1)^{-1}G_1'\hat{z}^R \tag{24}$$

and

$$\hat{u}^I \equiv (G_2'G_2)^{-1}G_2'(\hat{z}^R - G_1\hat{u}^C) \tag{25}$$

respectively. We can show that the estimator $\hat{u}^I$ satisfies the equation:

$$G_1'G_2\hat{u}^I = 0. \tag{26}$$

Thus we adopt the condition (26) as a restriction. That is, the constraint of our model is $G_1'G_2u^I = 0$.

Next we propose a recursive procedure for estimating $r_l$.

Step 1. Set $r_l = 1/L$ $(l = 1, ..., L)$.
Step 2. Estimate $\hat{u}^C$ by (24).
Step 3. Calculate $r_l$ as follows:
$r_l^{(0)} = \hat{z}_l'B_l\hat{u}^C/\hat{z}_l'\hat{z}_l$
$\lambda = (\sum_{l=1}^{L} r_l^{(0)} - 1)/(\sum_{l=1}^{L} 1/\hat{z}_l'\hat{z}_l)$
$r_l = r_l^{(0)} - \lambda/\hat{z}_l'\hat{z}_l$.
Step 4. Go to Step 2, if $r_l$'s are not converged.
Step 5. Estimate $\hat{u}^I$ by (25).

The step 3 in the above procedure is lead by the method of Lagrange multiplier. Finally we have to determine $d$ from data, since $d$ is unknown generally. We apply the quasi Bayesian Information Criterion given by the equation:

$$BIC = NL\log(\hat{\sigma}^2) - N\sum_{l=1}^{L}\log r_l^2 + (2KL + L + p - 1)\log NL, \tag{27}$$

where

$$\hat{\sigma}^2 = (\hat{z}^R - G_1\hat{u}^C - G_2\hat{u}^I)'(\hat{z}_R - G_1\hat{u}^C - G_2\hat{u}^I)/NL. \tag{28}$$

The width parameter $d$ is selected by minimizing $BIC$. The length of the latent process $K$ is determined from $d$.

## 4 Numerical example

We apply the proposed models to artificial time series shown by Fig. 2 for demonstration. The length of series $N$ is 116 and number of series $L$ is three. (These series are real data of carbon dioxide concentration at three places in Japan. However, this multivariate time series is not real, since the original time points are not aligned.)

We fit the non-weighted model (7) and weighted model (1), since seasonality appears clearly. Both selected $d$'s of two models are 68. The result by the non-weighted model (7) is shown by Fig. 3. The bold line is the common trend, solid line is the original series and dotted line is the sum of common and original trends and seasonal component. The figure shows that seasonality is estimated well. However, the common trend differs from each series, since there are large differences among series. This means that the common movement in each series is not estimated appropriately.

The result by the weighted model (1) is shown by Fig. 4. The solid line is the weighted series $r_l y_l$. Comparing Figs. 3 and 4 it is found that the weighted model provides more natural results. The estimated weight is (0.3430, 0.3292, 0.3278). Fig. 5 shows the estimated seasonal components and individual trends. Similarity or dissimilarity of three series can be considered from Fig. 5.

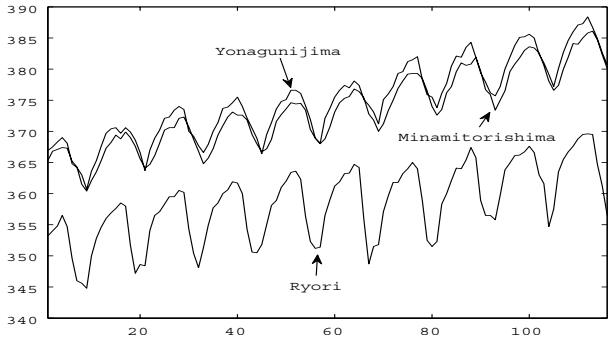


**Fig. 2.** Original series

## 5 Conclusion

In this paper we proposed the non-weighted and weighted fuzzy trend models for multivariate time series with or without seasonality.

The non-weighted model cannot estimate common trend well, when there are large differences among series. The weighted model resolves this problem. Moreover the proposed models can estimates seasonal components directly. The numerical example shows that the proposed identification method works well.

It is expected to apply our models to multivariate time series widely. However, simulation studies and practical examples are required for further evaluation of the identification procedure.

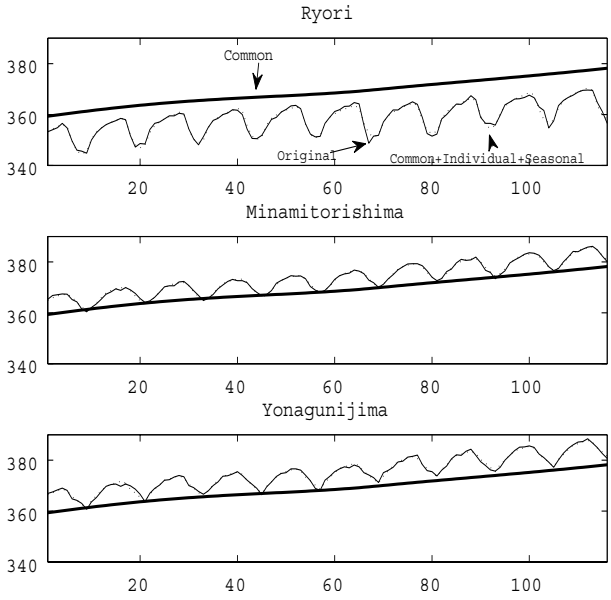


**Fig. 3.** Result by non-weighted model

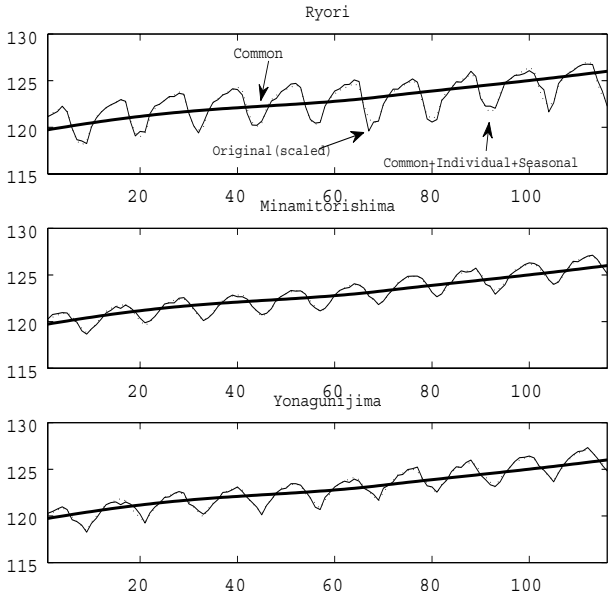


**Fig. 4.** Result by weighted model

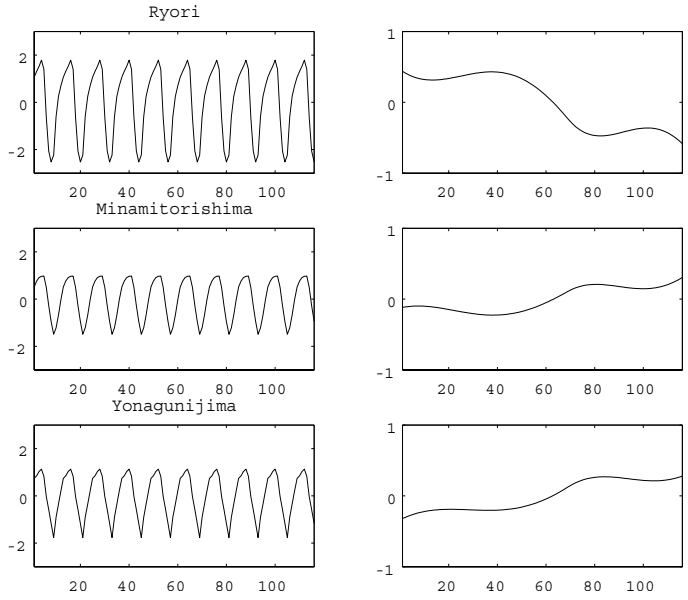


**Fig. 5.** Seasonal components and individual trends

## References

1. Kuwabara, M. and Watanabe, N., "Correlation analysis of long-term financial time series by a fuzzy trend model", *The Porceedings of 11th IASTED International Conference on Artificial Intelligence and Soft Computing* 63–67 (2007).
2. Kuwabara, M. and Watanabe, N., "Financial time series analysis based on a fuzzy trend model" (in Japanese), *Journal of Japan Society for Fuzzy Theory and Intelligent Informatics*, 20, 2, 244–254 (2008).
3. Kuwabara, M. and Watanabe, N., "A multivariate fuzzy trend model for analysis of common and individual trends", *The Proceedings of Joint 4th International Conference on Soft Computing and Intelligent Systems and 9th International Symposium on advanced Intelligent Systems*, 110–114 (2008).
4. Takagi, T. and Sugeno, M., "Fuzzy identification of systems and its application to modeling and control", *IEEE Trans. on Systems and Cybernetics*, 15(1), 116–132 (1985)

# Management of technical maintenance of water pipeline networks on the basis of reliability characteristics

Boli Ya. Yarkulov
Samarkand State Institute of Building and Architecture,
Samarkand, Uzbekistan

Email: yarkulov@rambler.ru

## Abstract

This article considers the new devising methodological approach on the basis of reliability characteristics (failure intensity), to be applied in the system of controlling the technical maintenance of water pipeline networks. Specifically:
- Define the types of reliability characteristics of the controlling objects, which characterizes on its actual condition.
- Define the main parameters of controlling object (spare parts, workers) technique maintenance on the basis of reliability characteristics.
This approach needs solving the problem in the following sequence:
- Define the types of failure of water pipeline networks;
- Determine algorithm for each type of failure flow of water pipeline networks;
- Define the quantity of resources that is necessary for the maintenance of workability of water pipeline networks on each type of failure;
- Estimate the reliability of water pipeline networks operation for various types of failure.

Carried out research allowed to distinguish four types of failure of elements and pipelines of water-supply networks dependent on time of their introduction, putting into exploitation, and outer influences:
- Running-in failure, which occurs in the initial period of exploitation;
- Failures in condition of system's normal operation;
- Failures in condition of system's physical depreciation (aging);
- Instantaneous (random) or gradual failures that occur as a result of outer strikes, i.e. earthquakes.

To determinate the amount of spare parts, the mathematical model in the form of optimization problem with one non-linear restriction and algorithm that builts on the base of quickest and descent method, which its solution under the increasing intensity of failures of elements and pipelines of water-supply networks was formulated.

*Stochastic Modeling, Data Analysis and Statistical Applications* (pp. 451-460)
Lidia Filus - Teresa Oliveira - Christos H Skiadas (Eds)



**Keywords:** Water pipeline networks, technique maintenance, reliability, failures, modeling, earthquakes, algorithm, workability, probability.

## 1. Introduction

It is known fact that engineering networks including water pipeline network in big cities and settlements is not built simultaneously because the water pipeline networks are constructed as result of cities and settlements widening. That is why there are buildings (constructions) of water pipeline networks of different remoteness year in the same city.

This situation complicates in a certain extent the process of controlling technical maintenance of water pipeline networks, as the intensity of failure flows in districts differs from one another dependent on their construction time remoteness. The traditional method causes insufficient or excess planning of amount of spare parts and employee group, which is necessary for the maintenance of workability of water pipeline networks.

The reasons are: existence of input information in a big capacity, missing information on some of networks' characteristics, insufficiency of data information on some parameters (on network state, influence of outer strikes), which require the special approach to solving this problem.

The dynamical character of development of water pipeline network system requires a constant improvement of system of controlling the technical maintenance, as lagging in development of subject of control from object of control causes huge social-economical losses.

On the other hand, the condition of water networks may change as a result of various earthquakes. Especially, during strong earthquakes, the condition of water networks will change instantly. As a result of earthquake, the water supply and distribution system will be partially or fully out of order. In hot climates, this situation leads not only to social and economic losses, but also increases the danger of expansion of epedemii. For example, as a result of earthquake in Armenia in 1989, there was the danger of expansion of the epidemic, even though it was the winter time. Because the water supply system was not restored by the deadline, and there was no beforehand developed system management.

## 2. Research of Changing the Failure Intensity Properties and Solving the Problem of Technical Maintenance of Water Pipeline Networks

Let the system of water pipeline networks consist of $a_r$, ($r = \overline{1,R}$)elements (r - signifies element's type). The system is concentrated in a sufficiently big territory, i.e. it is territorially dispersed system, object of control (water pipeline networks) is divided onto definite repair-exploitation areas and technique control carried out for the maintenance of their workability. Controlling system consists of two levels, i.e. upper level represents city

municipal government of water pipeline network, and lower level includes repair-exploitation area administration.

The failures of one or several elements do not cause the general failure in system. This depends on exactly in what part of system of water pipeline network the failure element (area) is situated, i.e. in the lines of main water pipeline (in initial network), in crosspieces and so on. We mark out four types of failure.

1. Running-in, early failure, occurring in the initial period of exploitation;
2. Failures in condition of system's normal operation;
3. Failures in condition of system's physical aging, depreciation (obsolescence);
4. Random, chance or gradual failures, that occur as a result of outer strikes, i.e. earthquakes, strikes of heavy transport means and so on.

Random, chance failure occurs at the same moment after one or series of strikes under strong earthquakes. Gradual failure occurs as a result of saving of deformation of several not strong strikes under not strong or insensible earthquakes.

It is known that failure characteristics (intensity, deepness) reflect the system state. To control the technical systems first their state should be determined. For that we introduce the parameter of system's elements condition $x_r(t)$, $r = \overline{1,R}$

$x_r(t)$ = { 0 on faultless r element in the moment t }

$x_r(t)$ = {1 on defective r element in the moment t }

If to mark through $\lambda_r(t_i)$ the intensity of failures of r- element in the moment $t_i$ (i =1,4) then vector of systems condition is determined:

In the periods of running-in failures

$X_r(t_1)=\{X_1(t_1),\ \lambda_1(t_1);\ X_2(t_1),\lambda_2(t_1);...;\ X_R(t_1),\ \lambda_R(t_1)\ \}$,

In the periods of normal operating

$X_r(t_2)=\{X_1(t_2),\ \lambda_1(t_2);\ X_2(t_2),\ \lambda_2(t_2);...;\ X_R(t_2),\ \lambda_R(t_2)\}$,

In the periods of physical depreciation

$X_r(t_3)=\{X_1(t_3),\ \lambda_1(t_3);\ X_2(t_3),\ \lambda_2(t_3);...;\ X_R(t_3),\ \lambda_R(t_3)\}$,

In earthquakes (extraordinary, force major situations)

$X_r(t_4)=\{X_1(t_4),\ \lambda_1(t_4);\ X_2(t_4);\ \lambda_2(t_4);...;\ X_R(t_4),\ \lambda_R(t_4)\}$

Besides, arises necessity in defining the function of allotment of failure intensity on appropriate periods. Proceeding from features of changing of the failure intensity of water pipeline networks there considered four types of functions of failure intensity allotment $\lambda_r(t_i)$ :

1. Running-in failure is corresponded by Weibull-Gnedenko distribution, as on $\beta<1$ the intensity of failures decreases.

   In the period of normal operation of failures intensity system is usually considered by constant value, i.e. $\lambda$=const and Weibull-

Gnedenko distribution corresponds to this, (and also exponential distribution), as if $\beta=1$, $\lambda$ is constant value.

2. In case of occurring of many deterioration failures, i.e. obsolescence occurrence is essential, then it causes strong change in intensity of failures during time (Figure 1).

Besides, intensity of failures monotonously increase (period $t_2,t_3$) and intensity of failures change corresponded by Weibull-Gnedenko distribution, where $\lambda(t)$ increases if $\beta>1$ (Beichelt& Franken, 1988 ).

3. In case of weak earthquakes, i.e. when there is outer strike influence, it is accepted that operating time of the equipment and pipelines of water-supply networks have distribution of increasing in average function intensity. Usually, in the models of impact load occur operating times from the class of increasing in average functions intensity. This means that equipments and pipelines of water-supply networks have undergone outer strikes that occur in casual moments of time and cause damage (accident) in the system. Damages accumulate in the equipments and pipelines until some of critical level won't be reached or exceeded, if this critical level is reached, then in equipments and pipelines occur failure (gradual).

Besides, in case of strong earthquakes instantaneous, chance failures usually occur, which happen in seismic active areas of the Globe. For example, such cases were observed in 1966 in Tashkent (Republic of Uzbekistan), in 1968 in Ashgabat(Turkmenistan) earthquakes and these earthquakes reached up to 9 points on the Richter scale.

It should be marked that analysis of failure intensity quality for all period of exploitation of water-supply pipeline networks shows that there exists the following determination.

In running-in stage of exploitation of water-supply pipeline networks an interval of $(0,t_1)$ in real probability of faultless operation begins to grow after the beginning of exploitation.

*Determination 1.* Probability of faultless operation of technical system elements $\overline{F}_t(a_r)$, that are worked less $t_1$, monotonously increases on t, $0<t<t_1$.

According to the given determination, the intensity of failures in the interval of $(0,t_1)$ monotonously decreases, it is considered decreasing function of intensity.

*Determination 2.* Probability of faultless operation of works of elements of technical system $\overline{F}_t(a_r)$, that worked for a time $t_2$, monotonously decreases on t, $t_2<t<\infty$, $t_2$ – beginning of obsolescence stage of the elements of technical systems.

**Fig. 1**. Failures intensity change dependent on water networks exploitation time.

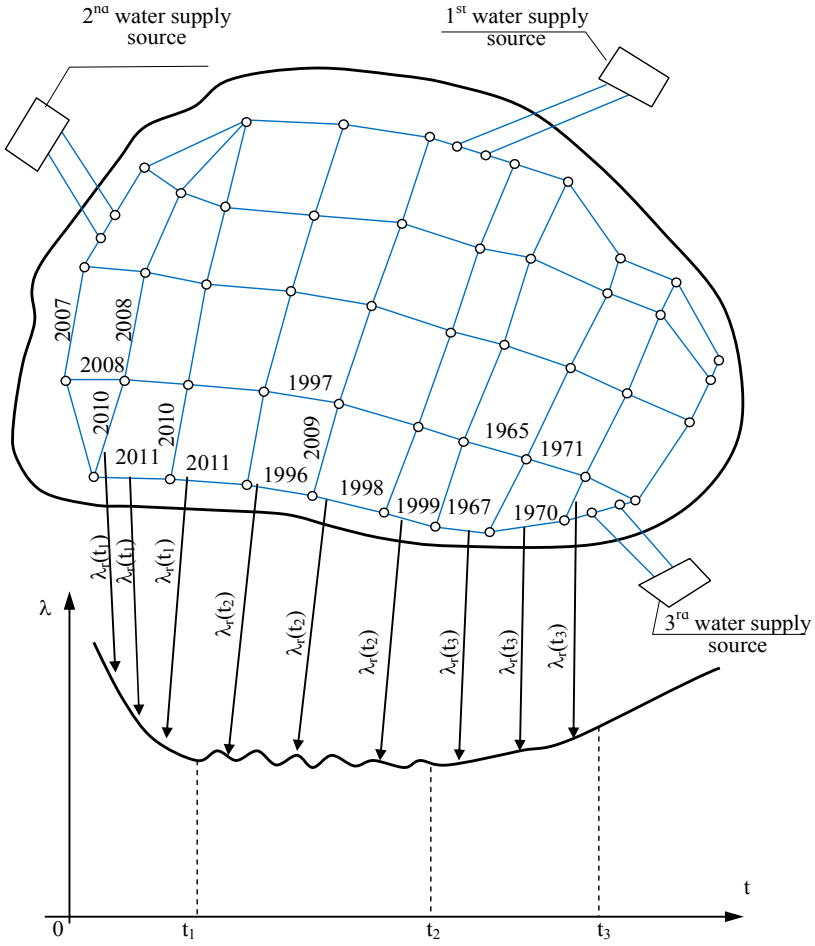


According to this determination, beginning from $t_2$ time failure intensity monotonously arises, i.e. increasing function of intensity.

Now we will examine the process of the task solution of the quantity determination of the resources (spare parts), which are necessary for the workability efficiency support in the condition of the little-studied gradual failure, which happens as a result of weak earthquakes.

It is established that resources quantity determination task in weak earthquake conditions should be solved in three stages:

1. Determination of failure flow.
2. Determination of the probability of the faultless work.

3. Determination of resources quantity necessary for the liquidation of the earthquakes aftereffects.

Under the supervision of professor Abramov N.N. (Sabitov,1977), it is established that failure flow dependent on earthquakes intensity is expressed by the following dependency formula:

$\lambda = a + b\,m - c\,m^2$ (1)

where - a, b, c are the unknown parameters, m earthquakes intensity scale.

As it is seen from formula (1), failure flow depends from random factors, at the same time for determination of their meaning we used the Monte-Carlo method which is given in work (Yarkulov, 2004).

On the second stage with the known meaning of the failure flow intensity the water-supply networks' system faultless work probability is determined.

**3.Algorithm for the Faultless Work Probability Determination of the Water Pipeline Networks at the External Influences.**

At the imperceptible and weak earthquakes the water plumbing networks are subject to the weak influences and as a result critical failure crashes (damages) appear. It leads to damages accumulation and this process will continue till certain critical level will be achieved and exceeded, afterward the failure comes in the system.

When damages accumulate till the failure threshold, the system's faultless work probability is expressed not by the exponential law, but by the Weibull's distribution law (close to Weibull's distribution). It is explained by the fact that at the damages stack as a result of external influences and physical wear and tear, and the time among the failures will be decreased.

Therefore, at the gradual failure the system's faultless work probability is determined on the base of the full probability formula:

$$F(t) = \sum_0^\infty e^{-\lambda_t} \frac{\lambda k}{k!}\, P[x_1 + x_2 + \cdots + x_k \lessdot x] \qquad (2)$$

Where P $[x_1+x_2+\ldots+x_k<x]$ – is a probability that common damages that present k-hits sum, don't exceed acceptable limits equal to x.

$(\lambda e)^k e^{-\lambda t} / k!$ is a probability that by $(0, t_1)$ time k hits sharp ensue.

As it is seen from formula (2) numerical values of probability P $[x_1+x_2+\ldots+x_k<x]$ are not always possible to get. At the same time it's possible to determine the limiting boundaries of failure origin probability on the basis of the past (registered) earthquakes.

It leads to the imitation of the given process, i.e. probability enactment, exceeding the possible, limiting boundaries, equal to x at k-hits.

Algorithm imitating the given process must provide the possibility of modeling interval change and change boundaries of damages origin possibility. Suppose that during a month 10-15 imperceptible earthquakes happen, it means that hits quantity equal to k=10÷15 (usually it happens in Central Asia country). In the capacity of modeling interval length t=30 days, i.e. a month period should be taken.

When considering the water supply system it's possible to divide the whole system into the R equivalent elements, i.e. every area is accepted as one equivalent element. Now we will consider the algorithm, enacting system's faultless work probability.

**Algorithm's Description**

1. Determination of equivalent elements quantity and elements types $a_r(r=1,R)$.
2. x=0.1 is specified.
3. Modeling interval is determined (0,t), t=30 days.
4. Hits quantity is specified, i.e. k (k=10÷15).
6. Random value is enacted $\xi_i$ .
7. The necessary tests number is specified $n_g \geq \log(1-p)/\log(1-\varepsilon)$, where p= 0.95, ε = 0.01 .
8. $i \geq n_g$ is verified. If $i \geq n_g$, then transition to the following paragraph, otherwise - to the paragraph 6.
9. $\xi_i = \sum_i \xi_i / n_g, \quad (i = \overline{1, n_g}, j = \overline{1,k})$ is calculated.
10. j≥ k conditions verification. If this condition is satisfied, then transition to the following paragraph, otherwise - to the paragraph 6.
11. $\xi_1 + \xi_2 + ... + \xi_k < x$ conditions verification. If this condition is satisfied, then $P[\xi_1 + \xi_2 + ... + \xi_k \leq x] = 0$ and transition to the paragraph 12, otherwise $P[\xi_1 + \xi_2 + ... + \xi_k \leq x] = p(\eta)$ and transition to the following paragraph (where $0 < p(\eta) \leq 1$).

p(η) – probable value, which is determined by big numbers law depending on tests and factors quantity.

12. $F_r(t) = \sum_{k=0}^{L} e^{-\lambda_r a_r t} \frac{(\lambda_r a_r t)^k}{k!}$ P $[\xi_1 + \xi_2 + ... + \xi_k < x]$ is calculated

Where $a_r$ – r type element quantity, (r=1,R), L – possible hits quantity.

13. r< R conditions verification. If this condition is satisfied, then transition to the paragraph 6, otherwise - to the following paragraph.
14. Printing $F_r(t)$ and algorithm end.

The developed algorithm allows taking into account water supply network condition change under the impact of the imperceptible and weak earthquakes gradual failures can occur.

On the third stage for spare parts quantity determination originally singularity of the given system should be taken into account. As it is known, water supply networks are connected logically serial, chained and in parallel.

We will consider logically connected elements of the water supply network.

4. **The Task of Spare Parts Quantity Determination**

If take the designations such as $m_r$ – spare elements quantity, $T_D$ – acceptable probability of the system's faultless work, (reliability norm $\alpha$ – water supply percentage), then the spare elements optimal quantity determination task in damages stacking conditions is presented in this way, i.e. find $m_r$, which may be solved at different criteria and limitations.

$$\min C_N = \sum_{r=1}^{R} C_r m_r \tag{3}$$

We choose in the capacity of limitations system:

$$\prod_{r=1}^{R} F_r m_r \geq T_D \tag{4}$$

Conditions (3)-(4) are the task of the multidimensional optimization with one limitation. Its solution practically comes to the one-dimensional tasks sequence solution on every step of optimization. Therefore, for (3)-(4) tasks solution it is possible to use the fastest descent method. On the basis of the last we will compose their solution algorithm.

**The Algorithm Description**

1. $m_r = 1$, $r = \overline{(1, R)}$ are specified.

2. $\theta = \prod_{r=1}^{R} F_r m_r$ is calculated.

3. $\prod_{r=1}^{R} F_r m_r \geq T_D$ Conditions of verification. If this condition is satisfied, then transition to the paragraph 9, otherwise - to the following paragraph.

4. $F_r(m_r) = \sum_{k=0}^{m_r} \frac{(\lambda_r a_r t)^k}{k!} e^{-\lambda_r a_r t}$ is calculated

5. $\Delta F_r(m_r) = F_r(m_r) - F_r(m_r+1)$, $(r = \overline{1,R})$ is calculated.

6. $C_r/\Delta F_r(m_r)$, $(r = \overline{1,R})$ is calculated.

7. $\min_{m_r} C_r / \Delta F_r (m_r)$, $(r = \overline{1,R})$ is found.

8. The variable $(m_r)$ is increased on one unit to which $\min_{m_r} C_r/\Delta F_r(m_r)$ corresponds and transition to the paragraph 3.

9. Objective function value calculation $\min C_N = \sum_{r=1}^{R} C_r m_r.$

10. The end of the algorithm.

The analysis of the results obtained shows that the developed algorithm is suitable for the practical accounts of the spare elements quantity when under the influence of the external hits gradual failures arise. The main sources of the gradual refusals emergence in seismic active districts (zones) are the weak earthquakes.

The given task was solved for the consecutively serial connected elements of the system, and for the systems with parallel joined elements it is solved analogically, only with the limitations change (4).

## 5.Conclusions:

1. It is necessary to manage the technical maintenance (efficiency support) of the water-supply networks only by their condition, as it

allows minimizing the exploitation expenses and water loss. To support the water plumbing networks efficiency at minimal expenses it is necessary to determine the failure flow intensity on the network areas. In the inhabited districts and cities, which are situated in seismic active zones, it is necessary to determine the failure flow in condition of imperceptible, weak and strong earthquakes.

2. With due regard for the data of the failure flow intensity it is necessary to determine the optimal resources quantity (spare parts, working teams) on the basis of the above mentioned models and algorithms which do not admit shortage or plenty of the resources.
3. To develop the complete system of models and algorithms, which are necessary for the water plumbing network efficiency support, and as a result, to create the information system of the network technique maintenance management.

## 6.Recommendation

This project is virtually internationl project because no country is safe from earthquakes in the world. It would be good if the concerned organizations (enterprises) from other countries will be able to support (finans support) for this project.

Create emergency reserve resources for individual cities in the region (e.g., state or province), which is enough to rebuild water systems within the same city. Create a separate section "control in extreme situations" in the system engineering management.

## References

1. Beichelt F., Franken P.(1988) Reliability and Technical Maintenance. Mathematical approach. Translated from German, edited by I.A. Ushakov.“ Radio and communication”, Moscow.

2. Sabitov A.D.(1977) Water in Areas with Research Reliability of Systems Supply and Distribution of Increased Seismicity .Thesis of diss. Ph.D., Moscow.

3. Yarkulov B. Ya. (2004) Management of Technical Maintenance and Appraisal of Reliability of Water Line Networks. “Fan” Publishing House, Tashkent.

4. Bakhvalov N.S.(1973) Numerical methods.Moskow.

4. Barlow ,R.E.,Proshan, F.(1965) Mathematical theory of reliability.New York: J. Wiley & Sons

5. Barlow, R.E., Proshan, F.(1976) Theory of maintained systems: distribution of time to first system failure. Math.oper.Res.1,32-42

# Singular extremals in control problems for wireless sensor networks

Larisa Manita

National Research University Higher School of Economics
Moscow Institute of Electronics and Mathematics
Bolshoy Trehsviatitelskiy Per. 3, 109028 Moscow, Russia
(E-mail: lmanita@hse.ru)

**Abstract.** Energy-saving optimization is very important for various engineering problems related to modern distributed systems. We consider here a control problem for a wireless sensor network with a single time server node and a large number of client nodes. The problem is to minimize a functional which accumulates clock synchronization errors in the clients nodes and the energy consumption of the server over some time interval $[0, T]$. The control function $u = u(t)$, $0 \le u(t) \le u_1$, corresponds to the power of the server node transmitting synchronization signals to the clients. For all possible parameter values we find the structure of extremal trajectories. We show that for sufficiently large $u_1$ the extremals contain singular arcs.

**Keywords:** Pontryagin maximum principle, bilinear control system, singular extremals, wireless sensor network, energy-saving optimization.

## 1 Model

Power consumption, clock synchronization and optimization are very popular topics in analysis of wireless sensor networks [1]–[7]. In the majority of modern papers their authors discuss and compare communication protocols (see, for example, [4]), network architectures (for example, [3]) and technical designs by using numerical simulations or dynamical programming methods (e.g., [6]). In the present talk we consider a mathematical model related with large scale networks which nodes are equipped with noisy non-perfect clocks [2]. The task of optimal clock sychronization in such networks is reduced to the classical control problem. Its functional is based on the trade-off between energy consumption and mean-square synchronization error. This control problem demonstrates surprisingly deep connections with the theory of singular optimal solutions [8]-[13].

The network consists of a single server node (denoted by 1) and $N$ client nodes (sensors) numbered as $2, \dots, N + 1$.

Let $x_i$ be a state of the node $i$ having the meaning of a local clock value at this node. The network evolves in time $t \in \mathbb{R}_+$ as follows.

*Stochastic Modeling, Data Analysis and Statistical Applications* (*pp.* 461-474)
Lidia Filus - Teresa Oliveira - Christos H Skiadas (Eds)



1) The node 1 is a time server with the perfect clock:

$$\frac{d\,x_1(t)}{dt} = v > 0$$

2) The client nodes are equipped with non-perfect clocks with a random Gaussian noise

$$\frac{d\,x_j(t)}{dt} = v + \sigma dB_j(t) + \text{synchronizing jumps},$$

where $B_j(t)$, $j = 2, \dots, N+1$, are independent standard Wiener processes, $\sigma > 0$ corresponds to the strength of the noise and "synchronizing jumps" are explained below.

3) At random time moments the server node 1 sends messages to randomly chosen client nodes, $u$ is the *intensity* of the Poissonian message flow issued from the server. The client $j$, $j = 2, \dots, N+1$, that receives at time $\tau$ a message from the node 1 immediately ajusts its clock to the current value of $x_1$:

$$\begin{aligned} x_j(\tau + 0) &= x_1(\tau), \\ x_k(\tau + 0) &= x_k(\tau), \qquad k \neq j. \end{aligned}$$

Hence the client clocks $x_j(t)$, $t \geq 0$, are stochastic processes which interact with the time server.

The function

$$R(t) = \mathsf{E}\frac{1}{N}\sum_{j=2}^{N+1} \left(x_j(t) - x_1(t)\right)^2$$

is a cumulative measure of desynchronization between the client and server nodes. Here $\mathsf{E}$ stands for the expectation.

It was proved in [2] that the function $R(t)$ satisfies the differential equation

$$\dot{R} = -uR + N\sigma^2$$

## 2 Optimal control problem

Consider the following optimal control problem

$$\int_0^T (\alpha R(t) + \beta u(t))\, dt \to \inf \tag{1}$$

$$\dot{R}\,(t) = -u(t)R(t) + N\sigma^2 \tag{2}$$

$$R\,(0) = R_0 \tag{3}$$

$$0 \leq u(t) \leq u_1 \tag{4}$$

Here $\alpha$, $\beta$ are some positive constants. The control function $u\,(t)$ corresponds to the power of the server node transmitting synchronization signals to the clients. The functional (1) accumulates clock synchronization errors in the

clients nodes and the energy consumption of the server over some time interval $[0, T]$.

The admissible solutions to (1)-(4) are absolutely continuous functions, the admissible controls belong to $L^\infty[0, T]$.

We prove that the problem (1)-(4) has a unique solution. We find a structure of optimal control. We show that optimal solutions may contain singular arcs.

## 3 Existence of solution

**Lemma 1** *For any $R_0$ and any parameter values $T$, $\alpha$, $\beta$, $N$, $\sigma^2$, $u_1$ there exists a solution $(\hat{R}(t), \hat{u}(t))$ to the problem (1)-(4).*

*Proof.* Let $\mathcal{B}_{R_0}$ denote the set of continuous functions $R:\ [0, T] \to \mathbb{R}$ such that $R(0) = R_0$. Consider the map $K:\ L^\infty[0, T] \to \mathcal{B}_{R_0}$ defined as follows:

$$(Ku)(t) = R_0 \exp\left(-\int_0^t u(\xi)d\xi\right) + N\sigma^2 \int_0^t \exp\left(-\int_s^t u(\xi)d\xi\right) ds$$
$$=:\ A(u, t) + B(u, t). \tag{5}$$

This operator assigns to the control function $u$ the corresponding solution $R$ of (1)-(4).

**1.** Let $\left\{u^{(n)}(t)\right\}_{n=1}^{\infty}$ be a minimizing sequence for the fuctional

$$\int_0^T (\alpha R(t) + \beta u(t))\ dt,$$

i.e.,

$$\int_0^T \left(\alpha K u^{(n)}(t) + \beta u^{(n)}(t)\right)\ dt \to \inf_{u\in V}\left\{\int_0^T (\alpha R(t) + \beta u(t))\ dt\right\}, \qquad (n \to \infty),$$

where $V = \{v \in L^\infty[0, T]:\ 0 \le v(t) \le u_1\}$. Recall that the space $L^1[0, T]$ is the adjoint space to $L^\infty[0, T]$. By $\langle\phi, u\rangle$ we denote the value of the functional $\phi \in (L^\infty[0, T])^* \cong L^1[0, T]$ at $u \in L^\infty[0, T]$:

$$\langle\phi, u\rangle = \int_0^T \phi(\xi)u(\xi)\, d\xi\,.$$

Since $u^{(n)}(t) \in [0, u_1]$, one can extract a weakly-$*$ converging in $L^\infty[0, T]$ subsequence $u^{(n_k)}(t)$ by virtue of Banach-Alaoglu theorem. Without loss of generality one can assume that $u^{(n)}$ weakly-$*$ converges to some $\hat{u} \in L^\infty[0, T]$. This means that for each $\rho \in L^1[0, T]$ one has

$$\int_0^T \rho(\xi)u^{(n)}(\xi)\, d\xi \to \int_0^T \rho(\xi)\hat{u}(\xi)\, d\xi, \quad n \to \infty. \tag{6}$$

**2.** Let us prove that the sequence $R^{(n)}(t) := Ku^{(n)}(t)$ converges pointwise to $\hat{R}(t) := K\hat{u}(t)$ as $n \to \infty$.

Further let $\phi_s^t(\xi) := -\mathbf{1}_{[s,t]}(\xi) = \begin{cases} -1, \xi \in [s,t], \\ 0, \ \xi \notin [s,t]. \end{cases}$ Taking $\rho(\xi) = \phi_0^t(\xi)$ in (6) we obtain

$$\int_0^t u^{(n)}(\xi)\, d\xi \to \int_0^t \hat{u}(\xi)\, d\xi, \quad n \to \infty,$$

hence

$$A(u^{(n)}, t) \to A(\hat{u}, t), \quad n \to \infty$$

for each fixed $t$. Note that $B(u^{(n)}, t) = N\sigma^2 \int_0^t \exp\left\langle \phi_s^t, u^{(n)} \right\rangle ds$. The functions $\exp\left\langle \phi_s^t, u^{(n)} \right\rangle$ are uniformly bounded and pointwise convergent, hence Lebesgue's dominated theorem yields the convergence

$$B(u^{(n)}, t) \to B(\hat{u}, t), \quad n \to \infty$$

for each fixed $t$. So we established the required convergence.

**3.** Let us show that $\hat{R}(t)$ is a solution to (1)–(4).

Obviously $R^{(n)}(t)$ are uniformly bounded (this follows straightforward from the explicit formula (5)). Since they form a pointwise convergent sequence, Lebesgue's dominated theorem yields

$$\int_0^T \alpha R^{(n)}(t)\, dt \to \int_0^T \alpha \hat{R}(t)\, dt, \quad n \to \infty.$$

Moreover, due to weak-$*$ convergence, one has

$$\int_0^T \beta u^{(n)}(t)\, dt = \beta \int_0^T \phi_0^T(t) u^{(n)}(t) dt \to \beta \int_0^T \phi_0^T(t) \hat{u}(t) dt = \beta \int_0^T \hat{u}(t) dt.$$

This yields

$$\int_0^T \left( \alpha R^{(n)}(t) + \beta u^{(n)}(t) \right) dt \to \int_0^T \left( \alpha \hat{R}(t) + \beta \hat{u}(t) \right) dt.$$

Thus $(\hat{R}(t), \hat{u}(t))$ is an optimal solution to (1)–(4). □

## 4 Pontryagin maximum principle

We will apply Pontryagin Maximum Principle [14] to the problem (1)-(4). Let $\left( \widehat{R}(t), \widehat{u}(t) \right)$ be an optimal solution. Then there exist a constant $\lambda_0$ and a continuous function $\psi(t)$ such that for all $t \in (0, T)$ we have

$$H\left( \widehat{R}(t), \psi(t), \widehat{u}(t) \right) = \max_{0 \le u \le u_1} H\left( \widehat{R}(t), \psi(t), u \right) \tag{7}$$

where the Hamiltonian function

$$H(R, \psi, u) = -\lambda_0 (\alpha R + \beta u) + \psi\left( -uR + N\sigma^2 \right)$$

Except at points of discontinuity of $\widehat{u}(t)$

$$\dot{\psi}(t) = -\frac{\partial H\left(\widehat{R}(t), \psi(t), \widehat{u}(t)\right)}{\partial R} = \lambda_0 \alpha + \widehat{u}(t)\psi \tag{8}$$

And $\psi$ satisfies the following transversality condition

$$\psi(T) = 0 \tag{9}$$

The function $\psi(t)$ is called an adjoint function. The condition (7) is called the **maximum condition.**

The dynamics equation (2) and the adjoint equation (8) form a Hamiltonian system

$$\begin{array}{l} \dot{\psi} = \lambda_0 \alpha + \widehat{u}(t)\psi \\ \dot{R} = -\widehat{u}(t) R + N\sigma^2 \end{array} \tag{10}$$

where $\widehat{u}(t)$ satisfies the maximum condition (7). The solutions $(R(t), \psi(t))$ of (10) are called extremals. If $\lambda_0 \neq 0$, we say that $(R(t), \psi(t))$ is normal. One can show [3] that in the problem (1)-(4) every extremal is normal. So we can put $\lambda_0 = 1$.

## 5 Switching function and singular extremals

Denote

$$H_0(R, \psi) = -\alpha R + \psi N \sigma^2, \quad H_1(R, \psi) = -\beta - R\psi \tag{11}$$

then $H = H_0 + uH_1$. The Hamiltonian $H$ is linear in $u$. Hence to maximize it over the interval $u \in [0, u_1]$ we need to use boundary values depending on the sign of $H_1$.

$$\hat{u}(t) = \begin{cases} 0, & H_1(R(t), \psi(t)) < 0 \\ u_1, & H_1(R(t), \psi(t)) > 0 \end{cases} \tag{12}$$

The function $H_1$ is called a switching function.

Suppose that there exists an interval $(t_1, t_2)$ such that

$$H_1(R(t), \psi(t)) = 0, \quad \forall t \in (t_1, t_2) \tag{13}$$

then the extremal $(R(t), \psi(t)), \quad t \in (t_1, t_2)$, is called a ***singular*** one. In this case we can't find an optimal control from the maximum condition (7). We will differentiate the identity $H_1(R(t), \psi(t)) \equiv 0$ by virtue of the Hamiltonian system (10) until a control $u$ appears with a non-zero coefficient.

We say that a number $q$ is the order of the singular trajectory iff

$$\frac{\partial}{\partial u}\frac{d^k}{dt^k}\bigg|_{(10)} H_1(R, \psi) = 0, \qquad k = 0, \ldots, 2q-1,$$

$$\frac{\partial}{\partial u}\frac{d^{2q}}{dt^{2q}}\bigg|_{(10)} H_1(R, \psi) \neq 0$$

in some open neighborhood of the singular trajectory $(R(t), \psi(t))$.

It is known that $q$ is an integer.

Singular solutions arise frequently in control problems [8]-[12] and are therefore of practical significance. We prove that for suffiently large $u_1$ a singular control is realised in the problem (1)-(4).

**Lemma 2** *Let*

$$\sqrt{\frac{\alpha N\sigma^2}{\beta}} \leq u_1$$

*then in the problem (1)-(4) there exists a singular extremal of order* 1

$$\hat{R}_s(t) \equiv \sqrt{N\sigma^2\frac{\beta}{\alpha}}, \quad \psi_s(t) \equiv -\sqrt{\frac{\alpha\beta}{N\sigma^2}} \tag{14}$$

*and the corresponding singular control is*

$$u_s = \sqrt{\frac{\alpha N\sigma^2}{\beta}}$$

*Proof.* Assume that (13) holds. We will differentiate this identity along the extremal with respect to $t$:

$$\left.\frac{d}{dt}\right|_{(10)} H_1(R(t), \psi(t)) = 0 \quad \Rightarrow -N\sigma^2\psi(t) - \alpha R(t) = 0 \tag{15}$$

$$\left.\frac{d^2}{dt^2}\right|_{(10)} H_1(R(t), \psi(t)) = 0 \quad \Rightarrow u\left(\alpha R(t) - N\sigma^2\psi(t)\right) - 2\alpha N\sigma^2 = 0 \tag{16}$$

From (13)–(15) we have

$$R(t) = \sqrt{N\sigma^2\frac{\beta}{\alpha}}, \quad \psi(t) = -\sqrt{\frac{\alpha\beta}{N\sigma^2}} \tag{17}$$

Substituting (17) in (16) we obtain

$$2\sqrt{N\sigma^2\alpha\beta}\cdot u - 2\alpha N\sigma^2 = 0$$

Thus

$$R(t) \equiv \sqrt{N\sigma^2\frac{\beta}{\alpha}}, \quad \psi(t) \equiv -\sqrt{\frac{\alpha\beta}{N\sigma^2}}$$

is a singular extremal of order 1 and $u_s = \sqrt{\frac{\alpha N\sigma^2}{\beta}}$ is the corresponding singular control.

Note that if $\sqrt{\frac{\alpha N\sigma^2}{\beta}} > u_1$ then $u_s$ does not satisfy the condition $0 \leq u(t) \leq u_1$ hence optimal solutions to the problem (1)-(4) are nonsingular. □

Recall the well-known generalized Legendre-Clebsch condition [8], the necessary condition for optimality of the singular extremal of order 1:

$$\frac{\partial}{\partial u}\frac{d^2}{dt^2}H_1(\widehat{R}(t), \psi(t)) \geq 0$$

We see that this condition holds in our problem. One can show that any concatenation of the singular control with a bang control $u = 0$ or $u = u_1$ satisfies the necessary conditions of the maximum principle [8].

From the transversality condition (9) it is easily seen that on the final time interval the optimal control $\widehat{u}\,(t)$ in the problem (1)-(4) is nonsingular. Namely, for all initial condition $R_0$ and for all parameter values $\alpha$, $\beta$, $N$, $\sigma^2$, $u_1$ we have the following result.

**Lemma 3** *There exists $\varepsilon > 0$ such that $\widehat{u}\,(t) = 0$ for all $t \in (T - \varepsilon, T)$ .*

*Proof.* Using the transversality condition (9) we obtain $H_1(\widehat{R}\,(T)\,, \psi\,(T)) = -\beta < 0$. The continuity of the switching function $H_1$ implies that

$$H_1(\widehat{R}\,(t)\,, \psi\,(t)) < 0 \quad \forall t \in (T - \varepsilon, T)$$

for some $\varepsilon > 0$. The maximum condition (7) yields $\widehat{u}\,(t) = 0,\ \ t \in (T - \varepsilon, T)$. □

## 6 The orbits of the Pontryagin maximum principle system

Consider the behaviour of the extremals on the plane $(R, \psi)$. Let $\Gamma$ be a switching curve, that is, a set of point such that $H_1\,(R, \psi) = 0$. By (11) we have $\Gamma = \{\,(R, \psi)|\,\beta + R\psi = 0\}$. We are interested in the domain $\{(R, \psi) :\ R > 0\}$. Denote

$$\Gamma^+ = \Gamma \cap \{(R, \psi) :\ R > 0\}$$

Above $\Gamma^+$ the optimal control $\hat{u}$ equals 0, below $\Gamma^+$ the optimal control $\hat{u}$ equals $u_1$ (see (12)). Let $u = 0$ then the Hamiltonian system (10) has the form

$$\dot{R} = N\sigma^2, \quad \dot{\psi} = \alpha \tag{18}$$

The general solution of (18) is

$$R\,(t) = N\sigma^2 t + C, \quad \psi\,(t) = \alpha t + w$$

On the plane $(R, \psi)$ the orbits of the system (18) are straight lines

$$\psi = \frac{\alpha}{N\sigma^2} R + B$$

Let $u = u_1$ than the Hamiltonian system (10) has the form

$$\dot{R} = -u_1 R + N\sigma^2, \quad \dot{\psi} = \alpha + u_1 \psi \tag{19}$$

The general solution of (19) is

$$R(t) = \widetilde{C} e^{-u_1 t} + \frac{N\sigma^2}{u_1}, \quad \psi\,(t) = \widetilde{w} e^{u_1 t} - \frac{\alpha}{u_1}$$

On the plane $(R, \psi)$ if $\widetilde{C} \neq 0$, $\widetilde{w} \neq 0$, the orbits of the system (19) are hyperbolas

$$|\alpha + \psi u_1| \cdot \left|N\sigma^2 - u_1 R\right| = \omega$$

If $\widetilde{C} = 0$, $\widetilde{w} \neq 0$, the orbit is the straight line $R = \frac{N\sigma^2}{u_1}$, directed upward if $\widetilde{w} > 0$ or downward if $\widetilde{w} < 0$. If $\widetilde{w} = 0$, the orbit is the straight line $\psi = -\frac{\alpha}{u_1}$, directed to the left if $\widetilde{C} > 0$ or to the right if $\widetilde{C} < 0$. If $\widetilde{C} = 0$, $\widetilde{w} = 0$ , the point $\left(\frac{N\sigma^2}{u_1}, -\frac{\alpha}{u_1}\right)$ is the stationary orbit.

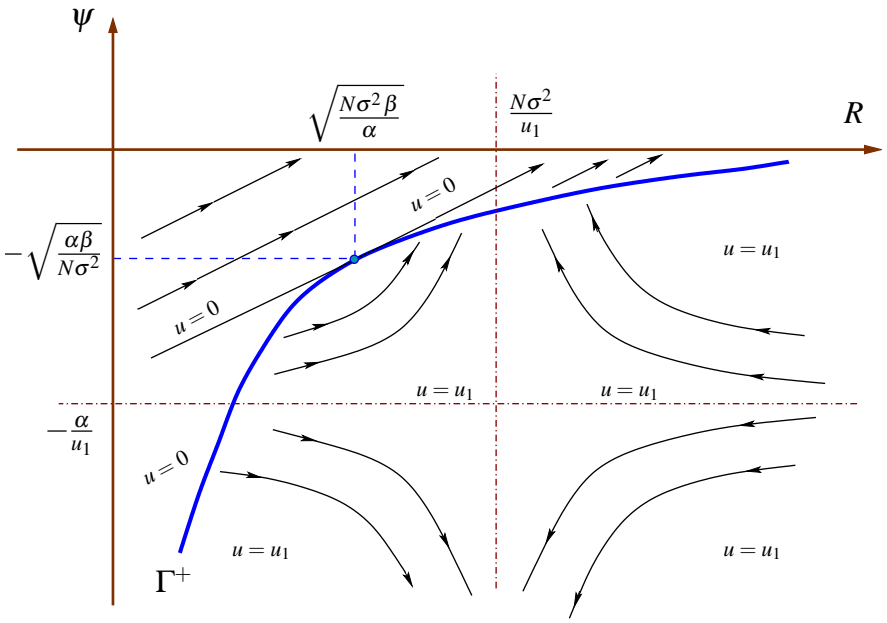


**Fig 1.** Orbits in the nonsingular case: $\sqrt{\frac{\alpha N\sigma^2}{\beta}} > u_1$

**Remark.** On Fig. 1 and Fig. 2 we don't show trajectories $(R(t), \psi(t))$ with $\psi(0) > 0$ because they cannot satisfy the transversality condition.

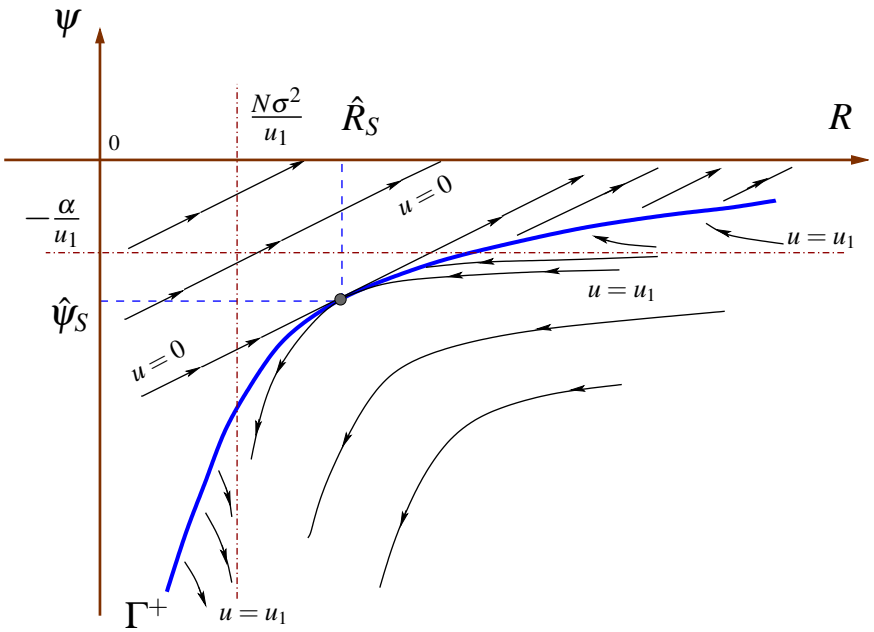


**Fig 2.** Orbits in the singular case: $\sqrt{\dfrac{\alpha N\sigma^2}{\beta}} \le u_1$

Note that in the case $\sqrt{\alpha N\sigma^2/\beta} \le u_1$ two extremals go out of the singular point $\left(\sqrt{N\sigma^2\frac{\beta}{\alpha}}, -\sqrt{\frac{\alpha\beta}{N\sigma^2}}\right)$ (with $u=0$ and $u=u_1$). But only one extremal (going of the singular point) satisfies the transversality condition (9).

Thus for any $R_0 \ge 0$ there exists a unique extremal such that $R(0) = R_0$, $\psi(T) = 0$. Since we prove that a solution to problem (1)-(4) exists hence the constructed extremals are optimal.

To summarize the above analysis in the next two sections we consider separately the nonsingular and singular cases. In each case we provide a plot with optimal solutions and state a conclusion on the structure of the optimal control $\hat{u}(t)$ (Theorems 1 and 2). It is interesting also to see how the structure of $\hat{u}(t)$ depends on the parameter $R_0$ and $T$. The answer is presented on Figures 4 and 6.

## 7 Optimal solutions. Nonsingular case

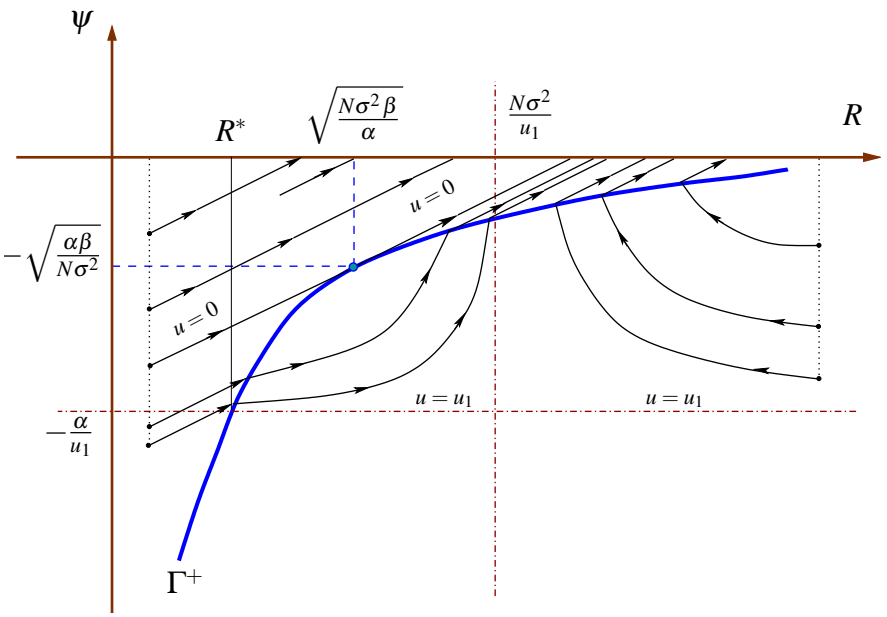


**Fig 3.** Optimal solutions for different values of the problem parameters. *Nonsingular case.*

**Theorem 1** *Let* $\sqrt{\dfrac{\alpha N\sigma^2}{\beta}} > u_1$, *that is, optimal solutions are nonsingular (Lemma 2). Then, depending of values* $R(0)$ *and* $T$, *the optimal control* $\hat{u}(t)$ *has one of the following forms*

$$1.1. \quad \hat{u}(t) = 0,\ t \in (0,T)$$

$$1.2. \quad \hat{u}(t) = \begin{cases} u_1,\ t \in (0,t_1) \\ 0,\ t \in (t_1,T) \end{cases}$$

$$1.3. \quad \hat{u}(t) = \begin{cases} 0,\ t \in (0,t_1) \\ u_1,\ t \in (t_1,t_2) \\ 0,\ t \in (t_2,T) \end{cases}$$

*i.e., the optimal control switches between* $u = 0$ *and* $u = u_1$ *and the number of switchings does not exceed 2.*

The Fig. 4 shows how the *structure* of optimal controls $\hat{u} = \hat{u}(t)$, $t \in [0, T]$, depends on $T$ and on the initial value $R(0)$.

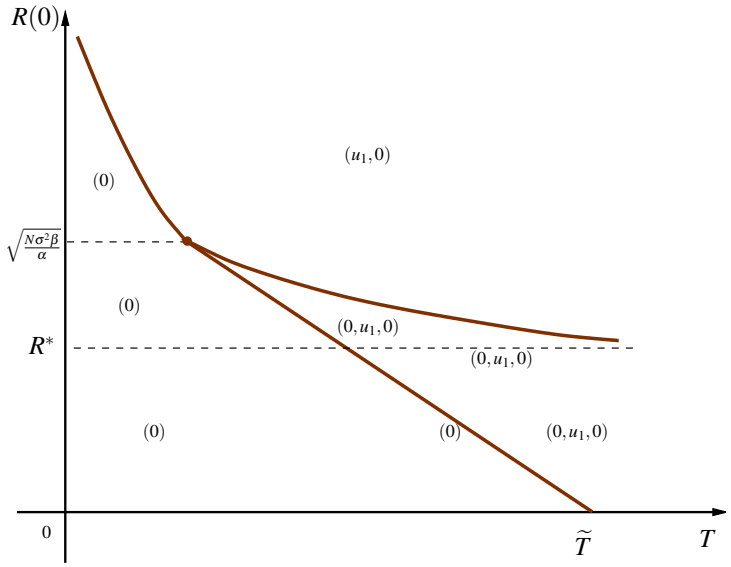


**Fig 4.**

Let $(\theta, \rho)$ be some point on the plane $(T, R(0))$. Assume that $(\theta, \rho)$ belongs to a domain labeled, *for example*, by $(a, b, c)$. This means that for the optimal control problem with $T = \theta$ and $R(0) = \rho$ the optimal control function $\hat{u} = \hat{u}(t)$ has the following form

$$\hat{u}(t) = \begin{cases} a, & t \in (0, \tau_1), \\ b, & t \in (\tau_1, \tau_2), \\ c, & t \in (\tau_2, \theta). \end{cases}$$

Here $\tau_1$ and $\tau_2$ are some numbers satisfying the condition $0 < \tau_1 < \tau_2 < \theta$. The numbers $\tau_1$ and $\tau_2$ depend on $(\theta, \rho)$ and on all parameters $(\alpha, \beta, N, \sigma)$ of the model. For points $(\theta, \rho)$ in the domain labeled by $(0)$ we have $\hat{u}(t) = 0$ for all $t \in [0, T]$.

## 8 Optimal Solutions. Singular case

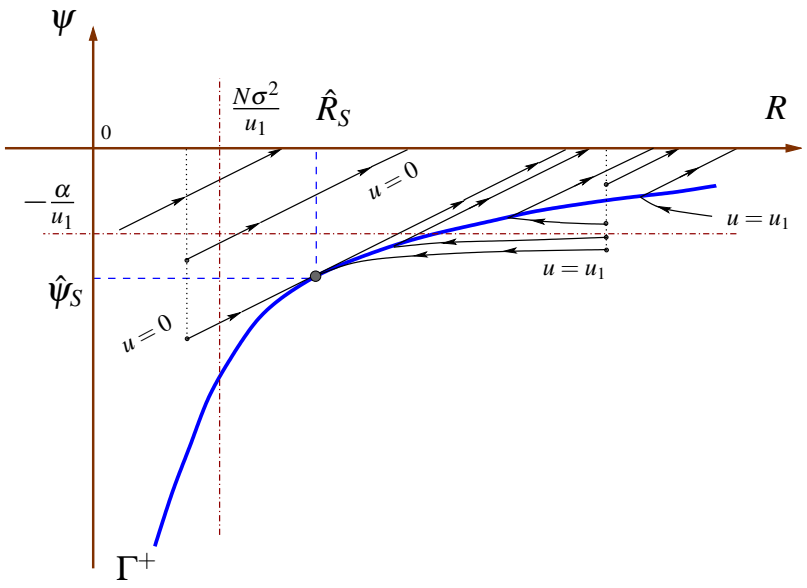


**Fig 5.** Optimal solutions for different values of the model parameters. *Singular case.*

**Theorem 2** *Let* $\sqrt{\frac{\alpha N\sigma^2}{\beta}} \le u_1$. *Then, depending of values* $R(0)$ *and* $T$, *the optimal control* $\hat{u}(t)$ *has one of the following forms*

$$2.1. \quad \hat{u}(t) = 0,\ t \in (0,T)$$

$$2.2. \quad \hat{u}(t) = \begin{cases} u_1,\ t \in (0,t_1) \\ 0,\ t \in (t_1,T) \end{cases} \qquad 2.3. \quad \hat{u}(t) = \begin{cases} u_s,\ t \in (0,t_1) \\ 0,\ t \in (t_1,T) \end{cases}$$

$$2.4. \quad \hat{u}(t) = \begin{cases} 0,\ t \in (0,t_1) \\ u_s,\ t \in (t_1,t_2) \\ 0,\ t \in (t_2,T) \end{cases}, \qquad 2.5. \quad \hat{u}(t) = \begin{cases} u_1,\ t \in (0,t_1) \\ u_s,\ t \in (t_1,t_2) \\ 0,\ t \in (t_2,T) \end{cases}$$

*i.e., the number of control switchings does not exceed 2 and the optimal solutions may contain the singular arcs (cases 2.3-2.5).*

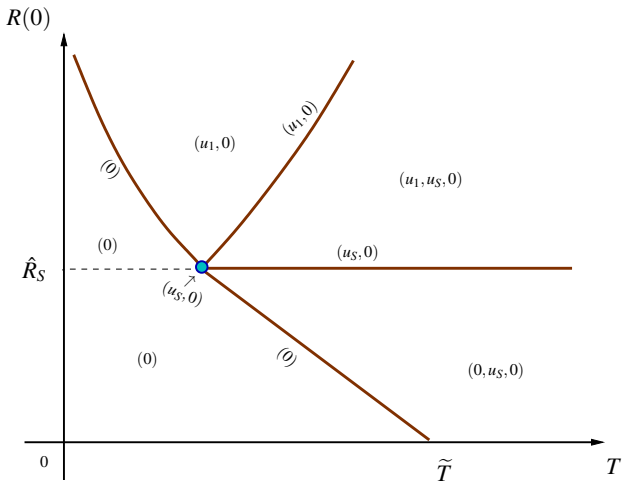


**Fig 6.**

As it is seen from Fig. 6 in the *singular case* on the plane $(T, R(0))$ we have more domains with different structures of the optimal control $\hat{u} = \hat{u}(t)$. These additional domains are labeled as $(u_S, 0)$ or $(a, u_S, 0)$. Note that on that intervals $t \in \Delta$ where $\hat{u}(t) = u_S$ the function $\hat{R}(t)$ takes the constant value $\hat{R}_S$:

$$\hat{R}(t) = \hat{R}_S, \qquad t \in \Delta.$$

## 9 Conclusions

We considered the control problem for wireless sensor networks with a single time server node and a large number of client nodes. The cost functional of this control problem accumulates clock synchronization errors in the clients nodes and the energy consumption of the server over some time interval $[0, T]$. For all possible parameter values we found the structure of optimal control function. It was proved that for any optimal solution $\widehat{R}\,(t)$ there exist a time moment $\tau$, $0 \le \tau < T$, such that $\hat{u}(t) = 0$, $t \in [\tau, T]$, i.e., the sending messages at times close to $T$ is not optimal. We showed that for sufficiently large $u_1$ the optimal solutions contain singular arcs. We found conditions on the model parameters under which different types of the optimal control are realized.

We hope that our study of the energy-saving optimization will also be usefull for analysis of other engineering problems related to modern distributed systems. In future we plan to extend these results to more general models.

## References

1. Sundararaman, B., Buy, U., Kshemkalyani, A.D., Clock synchronization for wireless sensor networks: a survey. Ad Hoc Networks, 3, 3, 281–323, 2005
2. Manita A., Clock synchronization in symmetric stochastic networks, Queueing Systems, 76, 2, 149-180, 2014

3. Feistel A., Wiczanowski M., Stanczak S., Optimization of Energy Consumption in Wireless Sensor Networks, Proc. ITG/IEEE International Workshop on Smart Antennas (WSA), 2007, Wien, Austria.
4. Albu R., Labit Y., Gayraud T., Berthou P., An Energy-efficient Clock Synchronization Protocol for Wireless Sensor Networks, Computing Research Repository - CORR , vol. abs/1012.2, 2010
5. Lan Wang, Yang Xiao, Energy Saving Mechanisms in Sensor Networks. Broadband Networks, 2005. BroadNets 2005, 724 - 732, Vol. 1.
6. Xu Ning, Christos G. Cassandras, Dynamic Sleep Time Control in Wireless Sensor Networks, ACM Transactions on Sensor Networks, Vol. 6, No. 3, Article 21, 2010.
7. Moshaddique Al Ameen, S. M. Riazul Islam, Kyungsup Kwak, Energy Saving Mechanisms for MAC Protocols in Wireless Sensor Networks, International Journal of Distributed Sensor Networks Volume 2010, Article ID 163413.
8. Heinz Schattler, Urszula Ledzewicz, Geometric Optimal Control Theory: Methods and Examples. Springer, 2012
9. Volker Michel, Singular Optimal Control: The State of the Art, Berichte der Arbeitsgruppe Technomathematik, V.169, 1996
10. Zelikin M.I., Borisov V.F. Theory of chattering control with applications to Astronautics, Robotics, Economics and Engineering. Boston et al.: Birkhauser, 1994.
11. M.I. Zelikin, L.A. Manita, Optimal control for a Timoshenko beam, C.R. Mécanique 334, Issue 5 (2006) 292-297
12. Manita L., Optimal Chattering Regimes in Nonhomogeneous Bar Model. In C.H. Skiadas, "Theoretical and Applied Issues in Statistics and Demography" (book devoted to ASMDA2013, Barcelona), ISAST, 2014.
13. Powers W. F., On the Order of Singular Optimal Control Problems, J. of Optimization Theory and Applications:V. 32, No, 4, 1980
14. Pontryagin L.S., Boltyanskii V.G., Gamkrelidze R.V., Mishchenko E.F., The Mathematical Theory of Optimal Processes. John Wiley, 1962

# Sommerfeld's Integrals and Hallén's Integral Equation in Data Analysis for Horizontal Dipole Antenna above Real Ground

Farid Monsefi[1], Milica Rančić[1,2], Sergei Silvestrov[1], and Slavoljub Aleksić[2]

[1] Division of Applied Mathematics, UKK, Mälardalen University, MDH Västerås, Sweden
(e-mail: farid.monsefi, milica.rancic, sergei.silvestrov@mdh.se)
[2] Dept. of Theoretical Electrical Engineering, ELFAK, University of Niš Niš, Serbia
(e-mail: slavoljub.aleksic@elfak.ni.ac.rs)

**Abstract.** High frequency (HF) analysis of the horizontal dipole antenna above real ground, which is employed in this paper, is based on the electric-field integral equation method and formulation of the Hallén's integral equation solved for the current using the point-matching method. The Sommerfeld's integrals, which express the influence of the real ground parameters, are solved approximately. Influence of different parameters of the geometry and ground on current distribution and input admittance is investigated. Furthermore, the method validation is done by comparison to the full-wave theory based exact model, and available measured data.
**Keywords:** Horizontal dipole antenna, Hallén's integral equation, Point-matching method, Polynomial current approximation, Real ground, Sommerfeld's integrals.

## 1 Introduction

Increase of the radiation power in different frequency bands during the last decades, has called for a study of harmful effects of the radio frequency energy on the living organisms and electronic equipment. An accurate determination of the near field strength in the vicinity of higher-power transmitting antennas is necessary for assessing any possible radiation hazards. In that sense, it is of great importance to account for the influence of the finite ground conductivity on the electromagnetic field structure in the surroundings of these emitters. The estimation of this influence has been intensively studied by Wait and Spies[1], Popović[2], Bannister[3], Popović and Djurdjević[4], Popović and Petrović[5], Rančić and Rančić[7], [8], Rančić and Aleksić[9], [11], Rančić[10], Arnautovski-Toseva *et al.*[12], [13], Nicol and Ridd[14], and a number of approaches has been applied in that sense, ranging from the exact full-wave based ones (Popović and Djurdjević[4], Arnautovski-Toseva *et al.*[12], [13]) to different forms of approximate, less time-consuming ones (Wait and Spies[1], Popović[2],

*Stochastic Modeling, Data Analysis and Statistical Applications* (*pp.* 475-486)
Lidia Filus - Teresa Oliveira - Christos H Skiadas (Eds)



Bannister[3], Popović and Petrović[5], Rančić and Rančić[7], [8], Rančić and Aleksić[9], [11], Rančić[10]). Although the approximate methods introduce a certain level of calculation error, their simplicity is of interest in the electromagnetic compatibility (EMC) studies. For that reason, finding an approximate, but satisfyingly accurate method applicable to wide range of parameters is often a goal of researches done in this field.

In this paper, the authors perform analysis of a thin horizontal dipole antenna (HDA) above lossy half-space (LHS) of known electrical parameters. The approach is based on the electric-field integral equation method, and formulation of the Hallén's integral equation (HIE), Balanis[6]. This equation is then solved for the current, which is assumed in a polynomial form Popović[2], using the point-matching method (PMM) (Balanis[6]). This way obtained system of linear equations involves improper Sommerfeld's integrals, which express the influence of the real ground, and are here solved approximately using simple, so-called OIA and TIA, approximations (Rančić and Rančić[7], [8], Rančić and Aleksić[9], [11], Rančić[10]). Both types of approximations are in an exponential form, and therefore, are similar to those obtained applying the method of images. It should be kept in mind that the goal of this approach is to develop approximations that have a simple form, whose application yields satisfyingly accurate calculations of the Sommerfeld's type of integrals, and are widely applicable, i.e. their employment is not restricted by the values of electrical parameters of the ground, or the geometry, Rančić and Rančić[7], [8], Rančić and Aleksić[9], [11], Rančić[10].

Thorough analysis is performed in order to observe the influence of different parameters of the geometry, and the ground, on current distribution and the input impedance/admittance of the HDA. Furthermore, the verification of the method is done by comparison to the exact model based on the full-wave theory (Arnautovski-Toseva *et al.*[12], [13]), and experimental data from Nicol and Ridd[14]. Obtained results indicate a possibility of applying the described methodology to inverse problems involving evaluation of electrical parameters of the ground (or detection of ground type change) based on measured input antenna impedance/admittance.

## 2 Theory

Considered HDA is positioned in the air (conductivity $\sigma_0 = 0$, permittivity $\epsilon_0$, permeability $\mu_0$) at height $h$ above semi-conducting ground that can be considered a homogeneous and isotropic medium of known electrical parameters. Antenna conductors are of equal lenght $l_1 = l_2 = l$ and cross-section radius $a_1 = a_2 = a$ ($a \ll l$ and $a \ll \lambda_0$, $\lambda_0$ – wavelength in the air). The HDA is fed by an ideal voltage generator of voltage $U$ and frequency $f$, and is oriented along the $x$-axis.

For such antenna structure, the Hertz's vector potential has two components, i.e. $\mathbf{\Pi}_{00} = \Pi_{x00}\ \hat{x} + \Pi_{zx00}\ \hat{z}$, which are described, at an the arbitrary field point $\mathrm{M}_0(x, y, z)$, by the following expressions:

$$\Pi_{x00} = \frac{1}{4\pi\underline{\sigma}_0}\int_{-l}^{l} I(x')\left[K_0(r_{1k}) + S^h_{00}(r_{2k})\right]\mathrm{d}x', \tag{1}$$

$$\Pi_{zx00} = \frac{1}{4\pi\underline{\sigma}_0}\frac{\partial}{\partial x}\int_{-l}^{l} I(x')\int_{\alpha=0}^{\infty}\left[-\underline{n}^{-2}\tilde{T}_{z10}(\alpha) + \tilde{T}_{\eta 10}(\alpha)\right]\frac{\tilde{K}_{00}(\alpha, r_{2k})}{u_0}\,\mathrm{d}\alpha\,\mathrm{d}x'. \tag{2}$$

where $I(x')$ - current distribution ($x'$ - axis assigned to the HDA); $\underline{\gamma}_i$ - propagation constant and $\underline{\sigma}_i$ - equivalent complex conductivity of the $i$-th medium ($i = 0$ for the air, and $i = 1$ for the lossy ground); $\underline{n} = \underline{\gamma}_1/\underline{\gamma}_0 = \sqrt{\underline{\epsilon}_{r1}}$ - complex refractive index ($\underline{\gamma}_0 = \mathrm{j}\beta_0$ in the air); $\underline{\epsilon}_{r1} \approx \epsilon_{r1} - \mathrm{j}60\sigma_1\lambda_0$ - complex relative permittivity; $\alpha$ - continual variable over which the integration is done; $\tilde{K}_{00}(\alpha, r_{2k})$ - spectral form of the potential kernel, $K_0(r_{ik}) = e^{-\underline{\gamma}_0 r_{ik}}/r_{ik}$ - standard potential kernel, $i = 1, 2$; $S^h_{00}(r_{2k})$ - a type of the Sommerfeld's integral; $\tilde{T}_{z10}(\alpha)$ and $\tilde{T}_{\eta 10}(\alpha)$ - spectral transmission coefficients; $r_{1k} = \sqrt{\rho_k'^2 + (z-h)^2}$, $r_{2k} = \sqrt{\rho_k'^2 + (z+h)^2}$, $\rho_k'^2 = (x - x_k')^2 + (y - y_k')^2$, $k = 1, 2$; $u_0 = \sqrt{\alpha^2 + \underline{\gamma}_0^2}$, $x_k'$ and $y_k'$ - coordinates of the $k$-th current source element.

Boundary condition for the total tangential component of the electric field vector must be satisfied at any given point on the antenna surface, i.e.:

$$E_x + U\delta(x) = 0, \quad -l \le x \le l,\ y = a,\ z = h, \tag{3}$$

where $E_x$ - $x$-component (tangential one) of the electric field vector $\boldsymbol{E}$

$$E_x = \boldsymbol{E}\hat{x} = \left[\mathrm{graddiv}\ \boldsymbol{\Pi}_{00} - \underline{\gamma}_0^2\ \boldsymbol{\Pi}_{00}\right]\hat{x} = \frac{\partial^2\Pi_{x00}}{\partial x^2} + \frac{\partial^2\Pi_{zx00}}{\partial x\partial z} - \underline{\gamma}_0^2\ \Pi_{x00}. \tag{4}$$

The second term in (4) can be written in the following manner:

$$\frac{\partial^2\Pi_{zx00}}{\partial x\partial z} = \frac{\partial^2\Pi^*_{zx00}}{\partial x^2}, \tag{5}$$

where $\Pi^*_{zx00}$ denotes the modified $z$-component of the Hertz's vector potential

$$\Pi^*_{zx00} = \frac{-1}{4\pi\underline{\sigma}_0}\int_{-l}^{l} I(x')\int_{\alpha=0}^{\infty}\left[-\underline{n}^{-2}\tilde{T}_{z10}(\alpha) + \tilde{T}_{\eta 10}(\alpha)\right]\tilde{K}_{00}(\alpha, r_{2k})\,\mathrm{d}\alpha\,\mathrm{d}x' =$$

$$= \frac{-1}{4\pi\underline{\sigma}_0}\int_{-l}^{l} I(x')\left[(1 - \underline{n}^{-2})K_0(r_{2k}) - \underline{n}^{-2}S^v_{00}(r_{2k}) + S^h_{00}(r_{2k})\right]\mathrm{d}x'. \tag{6}$$

where $S^v_{00}(r_{2k})$ - another type of the Sommerfeld's integral. Substituting (4) into (3) and adopting (5), the boundary condition (3) becomes:

$$\underline{\gamma}_0^2\ \Pi^*_{x00} - \frac{\partial^2\Pi^*_{x00}}{\partial x^2} = \underline{\gamma}_0^2\ \Pi^*_{zx00} + U\delta(x), \quad -l \le x \le l,\ y = a,\ z = h, \tag{7}$$

where $\Pi^*_{x00}$ denotes the *modified* $x$-component of the Hertz's vector potential

$$\Pi^*_{x00} = \Pi_{x00} + \Pi^*_{zx00} =$$

$$= \frac{1}{4\pi\underline{\sigma}_0}\int_{-l}^{l} I(x')\left[K_0(r_{1k}) + (\underline{n}^{-2}-1)K_0(r_{2k}) + \underline{n}^{-2}S_{00}^{v}(r_{2k})\right]\mathrm{d}x'. \quad (8)$$

Equation (7) presents the second order nonhomogeneus partial differential equation whose solution can be expressed as:

$$\Pi_{x00}^{*} = C_1'\cos\beta_0 x + C_2'\sin\beta_0 x -$$

$$-\frac{1}{\beta_0}\int_{s=0}^{x}\left[\underline{\gamma}_0^2\ \Pi_{zx00}^{*} + U\delta(x)\right]_{\substack{x=s\\y=a\\z=h}}\sin\beta_0(x-s)\mathrm{d}s, \quad (9)$$

i.e.

$$4\pi\underline{\sigma}_0\Pi_{x00}^{*} = C_1\cos\beta_0 x + C_2\sin\beta_0 x +$$

$$+\mathrm{j}\underline{\gamma}_0\int_{-l}^{l} I(x')\int_{s=0}^{x}\left[\begin{matrix}(1-\underline{n}^{-2})K_0(r_{2k})-\\ -\underline{n}^{-2}S_{00}^{v}(r_{2k})+\\ +S_{00}^{h}(r_{2k})\end{matrix}\right]_{\substack{x=s\\y=a\\z=h}}\sin\beta_0(x-s)\mathrm{d}s\ \mathrm{d}x', \quad (10)$$

where $C_1 = 4\pi\underline{\sigma}_0 C_1'$, and $C_2 = 4\pi\underline{\sigma}_0(C_2' - \mathrm{j}U/\underline{\gamma}_0)$ is a constant that will be obtained from the potential gap condition $\varphi_{00}(x=0^+) - \varphi_{00}(x=0^-) = U$ at feeding points. The electric scalar potential can be expressed as:

$$\varphi_{00} = -\mathrm{div}\mathbf{\Pi}_{00} = -\frac{\partial\Pi_{x00}}{\partial x} - \frac{\partial\Pi_{zx00}}{\partial z} = -\frac{\partial\Pi_{x00}}{\partial x} - \frac{\partial\Pi_{zx00}^{*}}{\partial x} = -\frac{\partial\Pi_{x00}^{*}}{\partial x}, \quad (11)$$

and substituting (10) in (11) we get

$$\varphi_{00} = -\mathrm{j}30C_1\sin\beta_0 x + \frac{U}{2}\cos\beta_0 x -$$

$$-\mathrm{j}30\frac{\partial}{\partial x}\int_{-l}^{l} I(x')\int_{s=0}^{x}\left[\begin{matrix}(1-\underline{n}^{-2})K_0(r_{2k})-\\ -\underline{n}^{-2}S_{00}^{v}(r_{2k})+\\ +S_{00}^{h}(r_{2k})\end{matrix}\right]_{\substack{x=s\\y=a\\z=h}}\sin\beta_0(x-s)\mathrm{d}s\ \mathrm{d}x'. \quad (12)$$

Knowing (12), the potential gap condition yields $C_2 = -\mathrm{j}U/60$. Finally (10) becomes:

$$4\pi\underline{\sigma}_0\Pi_{x00}^{*} = C_1\cos\beta_0 x - \mathrm{j}\frac{U}{60}\sin\beta_0 x +$$

$$+\mathrm{j}\underline{\gamma}_0\int_{-l}^{l} I(x')\int_{s=0}^{x}\left[\begin{matrix}(1-\underline{n}^{-2})K_0(r_{2k})-\\ -\underline{n}^{-2}S_{00}^{v}(r_{2k})+\\ +S_{00}^{h}(r_{2k})\end{matrix}\right]_{\substack{x=s\\y=a\\z=h}}\sin\beta_0(x-s)\mathrm{d}s\ \mathrm{d}x'. \quad (13)$$

Expression (13) presents the Hallén's integral equation (HIE) (Balanis[6]), having the current distribution $I(x')$ and the integration constant $C_1$ as unknowns. With a suitable function chosen to approximate the current distribution, HIE (13) is transformed to a system of linear equations appying the point-matching method at so-called matching points along the antenna.

It is of great importance to select an appropriate approximation for the current distribution since it will affect the calculation accuracy of both the near- and the far-field characteristics. There is a variety of proposed functions in the literature, but the polynomial current approximation proposed in

Popović[2] was repeatedly proven as a very accurate one when analysing different wire antenna structures, Popović[2], Popović and Djurdjević[4], Popović and Petrović[5], Rančić and Rančić[7], [8], Rančić[10], Rančić and Aleksić[9], [11]. The form that will be used in this paper is as follows:

$$I(x') = \sum_{m=0}^{M} I_m \left(\frac{x'}{l}\right)^m, \tag{14}$$

where $I_m$, $m = 0, 1, 2, \cdots, M$, present unknown complex current coefficients.

Adopting (14), HIE (13) becomes:

$$\sum_{m=0}^{M} I_m \int_{-l}^{l} \left(\frac{x'}{l}\right)^m \left[\begin{array}{c} K_0(r_{1k})+(\underline{n}^{-2}-1)K_0(r_{2k})+\underline{n}^{-2}S_{00}^{v}(r_{2k})- \\ -\mathrm{j}\underline{\gamma}_0 \int_{s=0}^{x} \left[\begin{array}{c}(1-\underline{n}^{-2})K_0(r_{2k})- \\ -\underline{n}^{-2}S_{00}^{v}(r_{2k})+ \\ +S_{00}^{h}(r_{2k})\end{array}\right]_{\substack{x=s\\y=a\\z=h}} \sin\beta_0(x-s)\mathrm{d}s \end{array}\right] \mathrm{d}x' -$$

$$-C_1 \cos\beta_0 x = -\mathrm{j}\frac{U}{60}\sin\beta_0 x. \tag{15}$$

Unknown complex current coefficients $I_m$, $m = 0, 1, 2, \cdots, M$, are determined from the system of linear equations obtained matching (15) at points:

$$x_i = \frac{i}{M} l, \; i = 0, 1, 2, \cdots, M. \tag{16}$$

This way, system of $(M + 1)$ linear equations is formed, lacking one additional equation to account for the unknown integration constant $C_1$. This remaining linear equation is obtained applying the condition for the current at the conductor's end. Standardly, the vanishing of the current is assumed at the end of antenna arm (Popović[2], Popović and Djurdjević[4], Popović and Petrović[5], Rančić and Rančić[7], [8], Rančić and Aleksić[9], [11], Rančić[10]), which corresponds to $I(-l) = I(l) = 0$, i.e. based on (14) to

$$\sum_{m=0}^{M} I_m = 0. \tag{17}$$

(Note: A more realistic condition for the current at the conductor's ending, derived satisfying the continuity equation at the end of an antenna arm, can also be used.)

This way, the system of equations needed for computing the current distribution of the observed antenna is formed. Based on that, for the given generator voltage $U$, the input admittance is determined from $Y_{in} = I_0/U$, where $I_0 = I_m|_{m=0}$.

Remaining problem are two Sommerfeld's integrals appearing in (15) expressed by

$$S_{00}^{v}(r_{2k}) = \int_{\alpha=0}^{\infty} \tilde{R}_{z10}\tilde{K}_{00}(\alpha, r_{2k})\mathrm{d}\alpha, \tag{18}$$

$$S_{00}^{h}(r_{2k}) = \int_{\alpha=0}^{\infty} \tilde{R}_{\eta 10}\tilde{K}_{00}(\alpha, r_{2k})\mathrm{d}\alpha, \tag{19}$$

where the first terms in both integrands represent spectral reflection coefficients (SRCs):

$$\tilde{R}_{z10}(\alpha) = \frac{\underline{n}^2 u_0 - u_1}{\underline{n}^2 u_0 + u_1},\ u_i = \sqrt{\alpha^2 + \underline{\gamma}_i^2},\ i = 0, 1, \tag{20}$$

$$\tilde{R}_{\eta 10}(\alpha) = \frac{u_0 - u_1}{u_0 + u_1},\ u_i = \sqrt{\alpha^2 + \underline{\gamma}_i^2},\ i = 0, 1. \tag{21}$$

In order to solve the type of Sommerfeld's integral given by (18) the methodology proposed in Rančić and Rančić[7] will be applied. Let us assume the SRC (20) in a so-called - TIA (*two-image approximation*) form:

$$\tilde{R}_{z10}(u_0) \cong B_v + A_{1v} e^{-(u_0 - \underline{\gamma}_0)\underline{d}_v}, \tag{22}$$

where $B_v$, $A_{1v}$ and $\underline{d}_v$ are unknown complex constants. When (22) is substituted into (18), the following general TIA approximation is obtained:

$$S_{00}^v(r_{2k}) \cong B_v K_0(r_{2k}) + A_v K_0(r_{2kv}), \tag{23}$$

where $r_{2kv} = \sqrt{\rho_k'^2 + (z + h + \underline{d}_v)^2}$, presents the distance between the second image and the observation point $\mathrm{M}_0$, and $A_v = A_{1v} \exp(\underline{\gamma}_0 \underline{d}_v)$. Now, matching expressions (20) and (22) at $u_0 \to \infty$ and $u_0 = \underline{\gamma}_0$, and the first derivative of the same expressions at $u_0 = \underline{\gamma}_0$, the following values for the unknown complex constants in (22) are obtained:

$$B_v = R_\infty, A_{1v} = R_0 - R_\infty, \underline{d}_v = (1 + \underline{n}^{-2})/\underline{\gamma}_0, \tag{24}$$

where: $R_\infty = \tilde{R}_{z10}(u_0 \to \infty) = (\underline{n}^2 - 1)/(\underline{n}^2 + 1)$ and $R_0 = (\underline{n} - 1)/(\underline{n} + 1)$.

Substituting (24) into (23), the following TIA form of (18) is obtained:

$$S_{00}^v(r_{2k}) \cong R_\infty K_0(r_{2k}) + (R_0 - R_\infty) e^{\underline{\gamma}_0 \underline{d}_v} K_0(r_{2kv}). \tag{25}$$

Similarly, we can assume (21) in the following form (Rančić and Rančić[8], Rančić and Aleksić[9], [11], Rančić[10]):

$$\tilde{R}_{\eta 10}(u_0) \cong B_h + A_{1h} e^{-(u_0 - \underline{\gamma}_0)\underline{d}_h}, \tag{26}$$

where $B_h$, $A_{1h}$ and $\underline{d}_h$ - unknown complex constants. Substituting (26) into (19), the following general approximation is obtained:

$$S_{00}^h(r_{2k}) \cong B_h K_0(r_{2k}) + A_h K_0(r_{2kh}), \tag{27}$$

where $A_h = A_{1h} \exp(\underline{\gamma}_0 \underline{d}_h)$, and $r_{2kh} = \sqrt{\rho_k'^2 + (z + h + \underline{d}_h)^2}$.

After matching (21) and (26) at points $u_0 \to \infty$ and $u_0 = \underline{\gamma}_0$, and their first derivatives at $u_0 = \underline{\gamma}_0$, we get values $B_h = 0$, $A_{1h} = -R_0$, and $\underline{d}_h = 2/(\underline{\gamma}_0 \underline{n})$, i.e. (27) gets the OIA (*one-image approximation*) form, Rančić and Aleksić[9], [11], Rančić[10]:

$$S_{00}^h(r_{2k}) \cong -R_0 e^{\underline{\gamma}_0 \underline{d}_h} K_0(r_{2kh}). \tag{28}$$

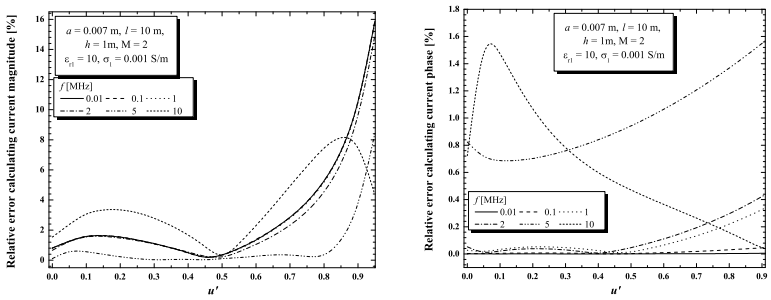


**Fig. 1.** Relative error of the current magnitude (left) and phase (right) along the HDA arm.

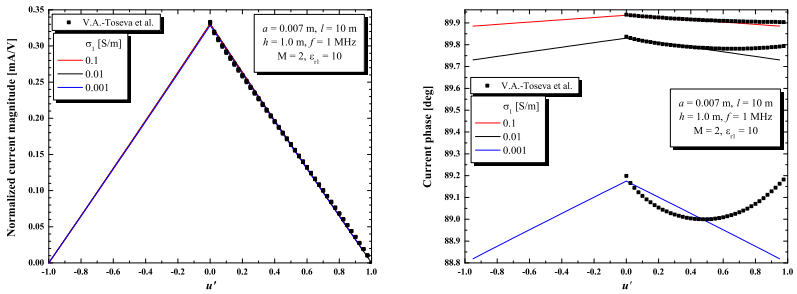


**Fig. 2.** Current magnitude (left) and phase (right) along the HDA for different ground conductivities.

## 3 Numerical results

Described numerical procedure is applied to near-field analysis of the symmetrical HDA fed by an ideal voltage generator of voltage $U$.

Firstly, results of the relative error of current distribution calculation are given in Figure 1. The conductor is $2l = 20$ m long with the cross-section radius of $a = 0.007$ m, and it is placed at $h = 1.0$ m above lossy ground with electrical permittivity $\epsilon_{r1} = 10$. In this case, the variable parameter is the frequency that takes values from a wide range (10 kHz to 10 MHz). The relative error is shown separately for the current magnitude and phase along the HDA arm for the case of the specific conductivity of $\sigma_1 = 0.001$ S/m. As a reference set of data, those from Arnautovski-Toseva *et al.*[12], [13] are taken.

Current distribution's magnitude and phase at 1 MHz, can be observed from Figure 2. The HDA has the same dimensions as previously, and it is placed at $h = 1.0$ m above lossy ground with electrical permittivity $\epsilon_{r1} = 10$. The value of the specific conductivity has been taken as a parameter: $\sigma_1 = 0.001, 0.01, 0.1$ S/m. Comparison has been done with the results from Arnautovski-Toseva *et al.*[12], [13].

Further, the influence of the conductor's position on the current distribution has been analysed. The results are graphically illustrated in Figure 3 together

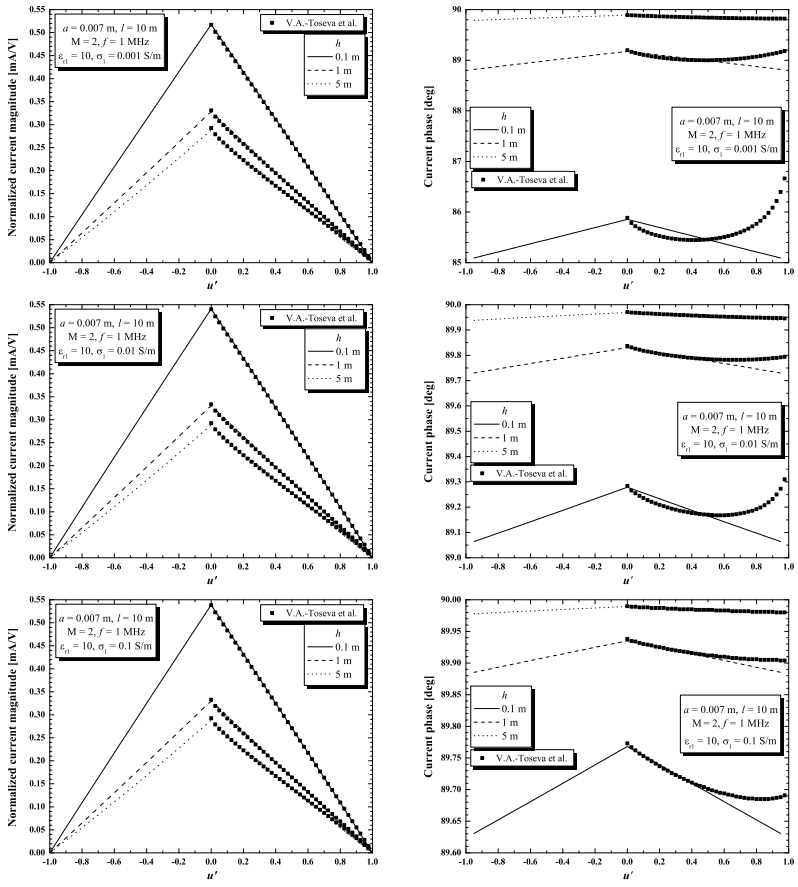


**Fig. 3.** Current magnitude (left) and phase (right) along the HDA above LHS at different heights.

with the ones from Arnautovski-Toseva *et al.*[12], [13]. Three cases were observed that correspond to heights $h = 0.1, 1.0, 5.0$ m. The current has been calculated at frequency of 1 MHz, and analysis has been done for the following values of the specific ground conductivity: $\sigma_1 = 0.001, 0.01, 0.1$ S/m. HDA dimensions are the same as previously.

Next example explores the dependence of the current (its magnitude and phase) on different ground conductivities calculated at the feeding point A($l =$ 0 m), which can be observed from Figure 4. Two cases are considered: solid line represents the value of $\sigma_1 = 0.001$ S/m, and the dashed one corresponds to $\sigma_1 = 0.1$ S/m. The first row of Figure 4 corresponds to HDA height of $h = 2.5$ m, and the second one to $h = 5.0$ m. The same influence for height $h = 0.5$ m is given in Rančić and Aleksić[11].

Similarly, the dependence of the current (its magnitude and phase) at specific points along the HDA arm in the frequency range from 10 kHz to 10 MHz,

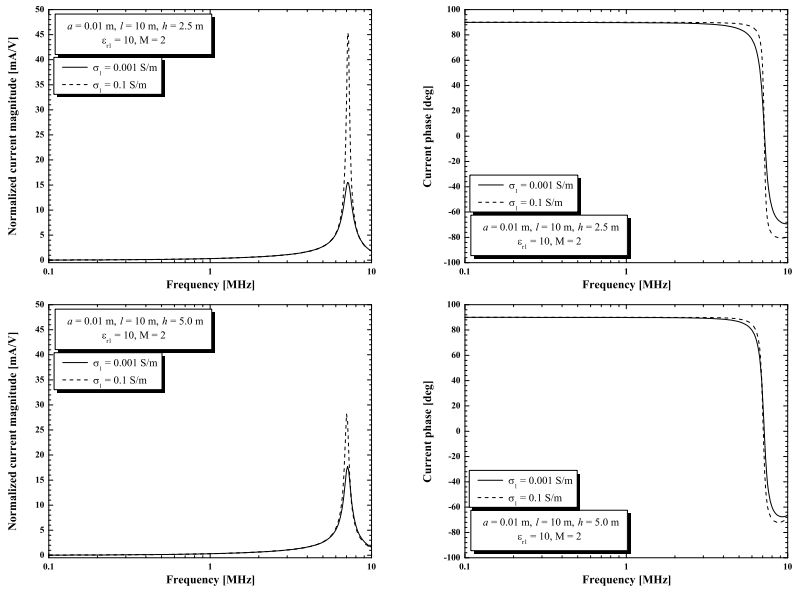


**Fig. 4.** HDA current magnitude (left) and phase (right) at point A for different ground conductivities.

is presented in Figure 5. The antenna is $2l = 20$ m long with a cross-section radius of $a = 0.01$ m, and considered heights are: $h = 0.5, 2.5, 5.0$ m. Electrical parameters' values of the ground are: electrical permittivity $\epsilon_{r1} = 10$, and specific conductivity $\sigma_1 = 0.1$ S/m. Current is calculated at points: A($l = 0$ m), B($l = 2.5$ m), C($l = 5.0$ m), and D($l = 7.5$ m). This example for $\sigma_1 = 0.001$ S/m and $h = 0.5$ m is given in Rančić and Aleksić[11].

Finally, Figure 6 shows comparison between theoretical calculations performed using the methodology described in this paper, and the results of the admittance measurements for the frequency range of $7 - 12$ MHz (Nicol and Ridd[14]). Observed HDA is 15 m long suspended at height of 0.3 m above the LHS. Two boundary cases of the ground are observed: a perfect dielectric (blue data), and a highly conducting plane (black data). Corresponding results obtained by the method of images are also shown (open circles). It can be observed that the better accordance is achieved using the method described here, which was expected since the observed antenna is very close to the ground (for the frequency of 10 MHz, height of 0.3 m corresponds to $0.01\lambda_0$), and the accuracy of the method of images decreases when the antenna is at height less than $h/\lambda_0 = 0.025$ (Popović and Petrović[5]).

## 4 Conclusions

Approximate method for the analysis of horizontal dipole antenna has been applied in this paper for the purpose of the current distribution and input admittance evaluation for the HDA positioned in the air at arbitrary height

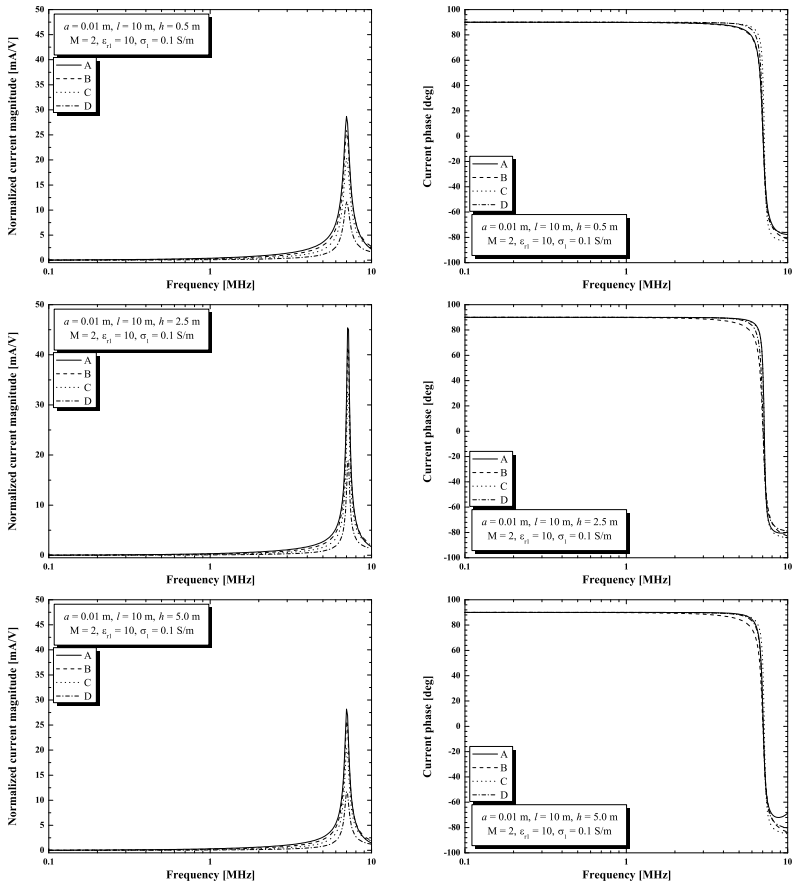


**Fig. 5.** HDA current magnitude (left) and phase (right) at different points along the antenna.

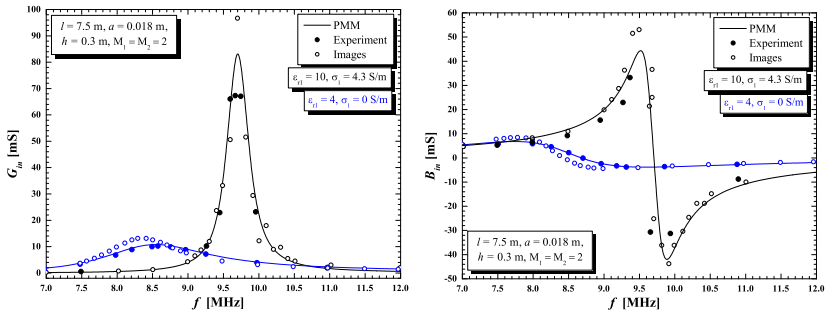


**Fig. 6.** HDA input conductance (left) and susceptance (right) versus frequency.

above LHS, which is considered a homogenous medium. The aim of the paper was to validite the applied method for the cases of interest in the EMC studies.

The analysis has been performed in a wide frequency range, and for different positions of the antenna, as well as for various values of the LHS's conductivity. It has been proven, based on the comparison with the exact model from Arnautovski-Toseva *et al.*[12], [13], that the methodology used here yields very accure results in the observed parameters' ranges. This indicates a possibilty of applying this method for analysis of different wire structures in the air above LHS, and more importantly, very close to the ground where the finite conductivity's influence is the greatest.

## 5 Acknowledgement

This work is partly supported by the RALF3 project funded by the Swedish Foundation for Strategic Research (SSF), and the EUROWEB Project funded by the Erasmus Mundus Action II programme of the European Commission.

The second author would like to thank members of the Division of Applied Mathematics at the MDH University, Sweden for inspiring and fruitful collaboration.

## References

1. Wait, J. R. and Spies, K. P., "On the Image Representation of the Quasi-Static Fields of a Line Current Source above the Ground", *Can. J. Phys.* 47, 2731–2733 (1969).
2. Popović, B. D., "Polynomial Approximation of Current along thin Symmetrical Cylindrical Dipoles", *Proc. Inst. Elec. Eng.* 117, 5, 873–878 (1970).
3. Bannister, P. R., "Extension of Quasi-Static Range of Finitely Conducting Earth Image Theory Technique to other Ranges", *IEEE Trans. on AP* 26, 3, 507-508 (1978).
4. Popović, B. D. and Djurdjević, D. Ž., "Entire-Domain Analysis of Thin-Wire Antennas near or in Lossy Ground", *IEE Proc., Microw. Antennas Propag.* 142, 213-219 (1995).
5. Popović, B. D. and Petrović, V. V., "Horizontal Wire Antenna above Lossy Half-Space: Simple Accurate Image Solution", *International journal of numerical modelling: Electronic networks, devices and fields* 9, 194-199 (1996).
6. Balanis, C. A., *Antenna Theory: Analysis and Design, Chapter 8*, 3rd Edition: J. Wiley and Sons, Inc., Hoboken, New Jersey (2005).
7. Rančić, M. P. and Rančić, P. D., "Vertical Dipole Antenna above a Lossy Half-Space: Efficient and Accurate Two-Image Approximation for the Sommerfeld's Integral", in Proc. of *EuCAP 2006* Nice, France, paper No121 (2006).
8. Rančić, M. and Rančić, P., "Horizontal Linear Antennas above a Lossy Half-Space: A New Model for the Sommerfeld's Integral Kernel", *Int. J. El. Commun. AEU* 65, 879-887 (2011).
9. Rančić, M. and Aleksić, S., "Horizontal Dipole Antenna very Close to Lossy Half-Space Surface", *Electrical Review* 7b, 82-85 (2012).
10. Rančić, M., *Analysis of Wire Antenna Structures in the Presence of Semi-Conducting Ground*, Ph.D dissertation, Faculty of electronic engineering, University of Niš, Niš, Serbia (2012).

11. Rančić, M. and Aleksić, S., "Analysis of Wire Antenna Structures above Lossy Homogeneous Soil", in Proc. of *21st Telecommunications Forum (TELFOR)* Belgrade, Serbia, 640-647 (2013).
12. Arnautovski-Toseva, V., Khamlichi Drissi, K. El, and Kerroum, K., "Comparison of Approximate Models of Horizontal Wire Conductor above Homogeneous Ground", in Proc. of *EuCAP 2012* Prague, Czech Republic, 678-682 (2012).
13. Arnautovski-Toseva, V., Khamlichi Drissi, K. El, Kerroum, K., Grceva, S. and Grcev, L., "Comparison of Image and Transmission Line Models of Energized Horizontal Wire above Two-Layer Soil", *Automatika* 53, 38-48 (2012).
14. Nicol, J.L. and Ridd, P.V., "Antenna Input Impedance: Experimental Confirmation and Gological Application", *Can. J. Phys.* 66, 818-823 (1988).

# Sensitivity Analysis of the GI/M/1 Queue with Negative Customers

Sofiane Ouazine[1] and Karim Abbas[2]

[1] Department of Mathematics
University of Bejaia, Campus of Targua Ouzemour, Algeria
(e-mail: wazinesofi@gmail.com)
[2] LAMOS Laboratory,
University of Bejaia, Campus of Targua Ouzemour, Algeria
(e-mail: kabbas.dz@gmail.com)

**Abstract.** In this paper we discuss the applicability of the Taylor series approach to the numerical analysis of the GI/M/1 queue with negative customers. In other words, we use the Taylor series expansions to examine the robustness of the GI/M/1 (FIFO, $\infty$) queueing model having RCH (Removal of Customer at the Head) to perturbations in the negative customers process (the occurrence rate of RCH). We analyze numerically the sensitivity of the entries of the stationary distribution vector of the GI/M/1 queue with negative customers to those perturbations, where we exhibit these entries as polynomial functions of the occurrence rate of RCH parameter of the considered model. Numerical examples are sketched out to illustrate the accuracy of our approach.
**Keywords:** Taylor series expansion, Sensitivity analysis, GI/M/1 queue with negative customers, Numerical methods, Performance measures.

## 1 Introduction

Recently there has been a rapid increase in the literature on queueing systems with negative arrivals. Queues with negative arrivals, called G-queues, were first introduced by Gelenbe [5]. When a negative customer arrives, it immediately removes an ordinary (positive) customer if present. Negative arrivals have been interpreted as inhibiter and synchronization signals in neural and high speed communication network. For example, we can use negative arrivals to describe the signals, which are caused by the client, cancel some proceeding.

There is a lot of research on queueing system with negative arrivals. But most of these contributions considered continuous-time queueing model: Boucherie and Boxma [6], Jain and Sigman [8], Bayer and Boxma [2], Harrison and Pitel [9] all of them investigated the same M/G/1 model but with the different killing strategies for negative customers; Harrison, Patel and Pitel [10] considered the M/M/1 G-queues with breakdowns and repair; Yang [11] considered GI/M/1 model by using embedded Makov chain method.

*Stochastic Modeling, Data Analysis and Statistical Applications* (*pp.* 487-493)
Lidia Filus - Teresa Oliveira - Christos H Skiadas (Eds)



In this paper we investigate the GI/M/1/N with Poisson negative arrivals to test the robustness of the model to perturbation in the negative customers process (the occurrence rate of RCH). In deed, we use the Taylor series expansions to examine the robustness of the GI/M/1/N queue to perturbations in the arrival process. Specifically, we analyse numerically the sensitivity of the entries of the stationary distribution vector of the GI/M/1/N queue to that perturbations, where we exhibit these entries as polynomial functions of the occurrence rate of RCH.

The remainder of this paper is organized as follows. In Section 2, we introduce the necessary notations for analyzing of the considered queueing model, and present closed-form expressions for the sensitivity of the stationary distribution to model parameter as a function of the deviation matrix. In Section 3, we outline the numerical framework to compute the relative absolute error in computing the stationary distribution. Concluding remarks are provided in Section 4.

## 2 Queueing Model Analysis

We investigate the GI/M/1/N queue with negative customers, where $N$ is the capacity of the system including the one who is in service. Assume that customer arrivals occur at discrete-time instants $\tau_k$, where $\tau_0 = 0$, customers arrive at the system according to a renewal process with interarrival time distribution $G(t)$ and mean $1/\lambda$. The service time $T_s$ of each server is assumed to be distributed exponentially with service rate $\mu$. Its density function is given by

$$s(t) = \mu e^{-\mu t}, \quad t \geq 0.$$

Additionally, we assume that there is another kind of customers, namely RCH, arriving in the system according to an independent Poisson process of parameter $h$. Let $L_k$ denote the number of customers left in the system immediately after the kth departing customer. A sequence of random variables $L_k; k = 1, 2, \ldots, N$ constitutes a Markov chain. Its transition probabilities matrix is given by:

$$P = \begin{pmatrix} b_0 & a_0 & 0 & 0 & 0 & \ldots & 0 \\ b_1 & a_1 & a_0 & 0 & 0 & \ldots & 0 \\ b_2 & a_2 & a_1 & a_0 & 0 & \ldots & 0 \\ b_3 & a_3 & a_2 & a_1 & a_0 & 0 & 0 \\ \vdots & \vdots & \vdots & \vdots & \vdots & \vdots & \vdots \\ b_{N-1} & a_{N-1} & a_{N-2} & a_{N-3} & a_{N-4} & \ldots & a_0 \\ b_{N-1} & a_{N-1} & a_{N-2} & a_{N-3} & a_{N-4} & \ldots & a_0 \end{pmatrix}_{(N+1)\times(N+1)}$$

where $a_j = \frac{(\mu+h)^j}{(-1)^j j!} \frac{\partial^j F^*}{\partial \alpha^j}(\alpha)$, $b_j = 1 - \sum_{i=0}^{j} a_i$, $\alpha = \mu + h$ and $F^*$ is the Laplace transformation corresponding to pdfs $f$(i.e $dG(t) = f(t)dt$) of the interarrival process.

Let $\pi$ denote the stationary distribution of the Markov chain $L_k$. We define the traffic intensity $\rho$ =(arrival rate)/(service rate) = $\lambda/\mu$. It can be shown

that the Markov chain $L_k$ is positive recurrent for all $\rho$. In this paper, we consider the stationary distribution $\pi$ as a mapping of some real-valued parameter $\theta$, in notation $\pi_\theta$. For example, $\theta$ may denote the occurrence rate of RCH parameter of the model. We are interested in obtaining higher-order sensitivity of stationary distribution with respect to parameter $\theta$. In the sequel we derive formulas for the higher order derivatives of $\pi_\theta$ with respect to $\theta$. Then, by using these formulas we obtain a Taylor series expansions in $\theta$ for $\pi_{\theta+\Delta}$, where its coefficients are expressed in closed form as functions of the *deviation matrix* (denoted by $D_\theta$) associated to the Markov chain $L_k$. It is well know that if $P_\theta$ is irreductible, then $(I - P_\theta + \Pi_\theta)$ is invertible, where $\Pi_\theta = e\,\pi_\theta$. Then, the matrix $D_\theta = (I - P_\theta + \Pi_\theta)^{-1} - \Pi_\theta$ exists and it is called the deviation matrix. The deviation matrix can be obtained in explicit form by:

$$\begin{aligned} D_\theta &= \sum_{n=0}^{\infty} (P_\theta^n - \Pi_\theta), \\ &= \sum_{n=0}^{\infty} (P_\theta - \Pi_\theta)^n - \Pi_\theta, \\ &= (I - P_\theta + \Pi_\theta)^{-1} - \Pi_\theta. \end{aligned}$$

In the following theorem we give the higher-order derivatives of the stationary distribution $\pi_\theta$ with respect to $\theta$ in terms of the deviation matrix $D_\theta$, which is a key result used in the framework proposed subsequently.

**Theorem 1.** *[7]* Let $\theta \in \Theta$ and let $\Theta_0 \subset \Theta$, with $\Theta \subset \mathbf{R}$ be a closed interval with $\theta$ an interior point such that the Markov chain is ergodic on $\Theta_0$. Provided that the entries of the transition matrix $P_\theta$ are $n$-times differentiable with respect to $\theta$, let

$$K_\theta(n) = \sum_{\substack{1 \le m \le n; \\ 1 \le l_k \le n; \\ l_1 + \cdots + l_m = n}} \frac{n!}{l_1! \cdots l_m!} \prod_{k=1}^{m} \left( P_\theta^{(l_k)}\, D_\theta \right) ..$$

Then, it holds that

$$\pi_\theta^{(n)} \;=\; \pi_\theta\, K_\theta(n)\,, \tag{1}$$

where $P_\theta^{(k)}$ (respectively $\pi_\theta^{(k)}$) is the matrix (respectively vector) of the elementwise $k$th order derivative of $P_\theta$ (respectively $\pi_\theta$) with respect to parameter $\theta$.

In the following, we propose a numerical approach to compute the stationary distribution $\pi_\theta$ for some parameter value $\theta$, and we demonstrate how this stationary distribution can be evaluated for the case where the control parameter $\theta$ is changed in some interval. In other words, we will compute the function $\pi(\theta+\Delta)$ on some $\Delta$-interval. More specifically, we will approximately compute $\pi(\theta + \Delta)$ by an polynomial in $\Delta$. To achieve this we will use the Taylor series

expansion approach established in [7]. Under some mild conditions it holds that $\pi_{\theta+\Delta}$ can be developed into a Taylor series of the following form:

$$\pi_{\theta+\Delta} = \sum_{n=0}^{k} \frac{\Delta^n}{n!} \pi_\theta^{(n)}, \tag{2}$$

where $\pi_\theta^{(n)}$ denotes the $n$-th order derivative of $\pi_\theta$ with respect to $\theta$ (see formula (1)).

We call

$$H_\theta(k, \Delta) = \sum_{n=0}^{k} \frac{\Delta^n}{n!} \pi_\theta^{(n)} \tag{3}$$

the $k$-th order Taylor approximation of $\pi_{\theta+\Delta}$ at $\theta$.

Under the conditions put forward in Theorem 1 it holds for $k < n$ that:

$$\pi_\theta^{(k+1)} = \sum_{m=0}^{k} \binom{k+1}{m} \pi_\theta^{(m)} P_\theta^{(k+1-m)} D_\theta \,. \tag{4}$$

An explicit representation of the lower derivatives of $\pi_\theta$ is given by [1]:

$$\pi_\theta^{(1)} = \pi_\theta P_\theta^{(1)} D_\theta \tag{5}$$

and

$$\pi_\theta^{(2)} = \pi_\theta P_\theta^{(2)} D_\theta + 2\pi_\theta (P_\theta^{(1)} D_\theta)^2. \tag{6}$$

Elaborating on the recursive formula for higher order derivatives (4), the second order derivative can be written as:

$$\pi_\theta^{(2)} = \pi_\theta P_\theta^{(2)} D_\theta + 2\pi_\theta^{(1)} P_\theta^{(1)} D_\theta. \tag{7}$$

In the same vein, we obtain for the third order derivative:

$$\pi_\theta^{(3)} = \pi_\theta P_\theta^{(3)} D_\theta + 3\pi_\theta^{(2)} P_\theta^{(1)} D_\theta + 3\pi_\theta^{(1)} P_\theta^{(2)} D_\theta. \tag{8}$$

## 3 Numerical Application

In this section, we apply the numerical approach based on the Taylor series expansions introduced above to the GI/M/1/N queue with negative customers, where we consider the model with perturbed the occurrence rate of RCH parameter. In this case, we estimate numerically the sensitivity of the stationary distribution of the queueing model with respect to the perturbation.

Let $\Theta = (a, b) \subset \mathbf{R}$, for $0 < a < b < \infty$.

**(H)** For $0 \leq j \leq N$ it holds that $a_j$ is $n$-times differentiable with respect to $h$ on $\Theta$.

Under **(H)** it holds that the first $n$ derivatives of $P$ exists. Let $P^{(k)}$ denote the $k$th order derivative of $P$ with respect to $h$, then it holds that

$$P^{(k)}(i,j) = \frac{d^{(k)}}{dh^{(k)}} P(i,j), 0 \leq \quad i,j \leq N, \tag{9}$$

or, more specifically,

$$P^{(k)} = \begin{pmatrix} b_0^{(k)} & a_0^{(k)} & 0 & 0 & 0 & \dots & 0 \\ b_1^{(k)} & a_1^{(k)} & a_0^{(k)} & 0 & 0 & \dots & 0 \\ b_2^{(k)} & a_2^{(k)} & a_1^{(k)} & a_0^{(k)} & 0 & \dots & 0 \\ b_3^{(k)} & a_3^{(k)} & a_2^{(k)} & a_1^{(k)} & a_0^{(k)} & 0 & 0 \\ \vdots & \vdots & \vdots & \vdots & \vdots & \vdots & \vdots \\ b_{N-1}^{(k)} & a_{N-1}^{(k)} & a_{N-2}^{(k)} & a_{N-3}^{(k)} & a_{N-4}^{(k)} & \dots & a_0^{(k)} \\ b_{N-1}^{(k)} & a_{N-1}^{(k)} & a_{N-2}^{(k)} & a_{N-3}^{(k)} & a_{N-4}^{(k)} & \dots & a_0^{(k)} \end{pmatrix}_{(N+1)\times(N+1)} \tag{10}$$

where

$$a_j^{(k)} = \frac{(-1)^k(\mu+h)^j}{(-1)^{j+k}j!} \frac{\partial^{j+k} F^*}{\partial \alpha^{j+k}}(\alpha) + \sum_{n=1}^{k} \frac{C_{k-1}^n (-1)^{k-n}(\mu+h)^{j-n}}{(-1)^{k+j-n}(j-n)!} \frac{\partial^{k+j-n} F^*}{\partial \alpha^{k+j-n}}(\alpha) + \frac{(\mu+h)^{j-k}}{(-1)^j (j-k)!} \frac{\partial^j F^*}{\partial \alpha^j}(\alpha)$$

and $b_j^{(k)} = -\sum_{i=0}^{j} a_j^{(k)}$

Consider the M/M/1/N queue with service rate $\mu$ and exponential inter-arrival time with rate $\lambda$. First, we present the numerical results obtained by applying our approach to this case. Therefore, we set $\mu = 2$, $\lambda = 1$ . For the implementation of our algorithm in MATLAB, we require a finite version of our queueing model. Figures 1, 2 and 3 depict the relative error on the stationary distributions $\pi_\theta^{(k)}(i)$ for $0 \leq i \leq N$ and $k = 1, 2, 3$, of the M/M/1/N queue versus the perturbation parameter $\Delta \in [-\delta, \delta]$, where $\delta = 0.1$. As expected, the relative error on the stationary distributions decreases as the perturbation parameter $h$ decreases.

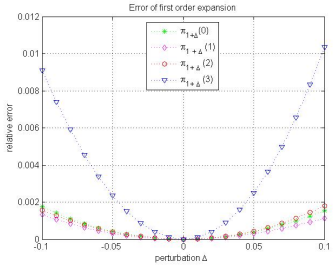


**Fig. 1.** The relative error in computing $\pi_{1+\Delta}$ by Taylor series of 1st order.

series coefficients are given in terms of the deviation matrix corresponding to the embedded Markov chain. We have presented some numerical examples

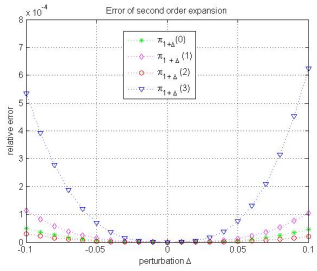


**Fig. 2.** The relative error in computing $\pi_{1+\Delta}$ by Taylor series of 2nd order.

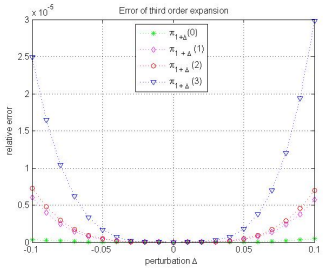


**Fig. 3.** The relative error in computing $\pi_{1+\Delta}$ by Taylor series of 3rd order.

that illustrate our numerical approach. In fact, the convergence rate of the Taylor series is such that already a Taylor polynomial of degree 2 or 3 yields good numerical results. As part of future work, we will further investigate the multi-server queues with vacations. We will also further provide a simplified and easily computable expression bounding the remainder of the Taylor series and, thereby provide an algorithmic way of deciding which order of the Taylor polynomial is su?cient to achieve a desired precision of the approximation Abbas, Heidergott and Aissani (2013).

## 4 Conclusion

This paper has developed a numerical, method to analyze the effect of the perturbation of the negative customers process in the performance measures of the queuing model considered (Stationary distribution), our numerical investigation are based on the Taylor series expansion; see [7], where the Taylor series coefficients are given in terms of the deviation matrix corresponding to the embedded Markov chain. Therefore, we have presented different examples that illustrate our numerical approach, and as illustrated by the numerical examples the convergence rate of the Taylor series is such that already a Taylor polynomial of degree 2 or 3 yields good numerical results, we will further investigate the multi-server queues with vacations. We will also further provide a simplified and easily computable expression bounding the remainder of the Taylor series and, thereby provide an algorithmic way of deciding which or-

der of the Taylor polynomial is sufficient to achieve a desired precision of the approximation [1].

## References

1. Abbas, K., Heidergott, B. and Aïssani, D. A Functional Approximation for the M/G/1/N Queue. Discrete Event Dynamic Systems , pages 93–104, 2013.
2. Bayer, N., Boxma, O.J. WienerHopf analysis of an M/G/1 queue with negative customers and of a related class of random walks, Queueing Syst.23 (1996) 30117316.
3. Boucherie, R.J. , Boxma, O.J. The workload in the M/G/1 queue with work removal, Probab. Eng.Inform.Sci.10 (1995) 26117277.
4. Cao, X.R. Realization Probabilities: The Dynamics of Queueing Systems, Springer-Verlag, New York, 1994.
5. Gelenbe,E. Product-form queueing networks with negative and positive customers, J.Appl. Probab.28 (1991) 65617663.
6. Boucherie, R.J. , Boxma, O.J. The workload in the M/G/1 queue with work removal, Probab. Eng.Inform.Sci.10 (1995) 26117277.
7. Heidergott, B., Hordijk, A.: Taylor series expansions for stationary Markov chains. Advances in Applied Probability 35, 1046–1070 (2003)
8. Jain, G., Sigman, K. A pollaczek-Khintchine formula for M/G/1 queues with disasters, J.Appl. Probab.33 (1996) 1191171200.
9. Harrison, P.G., Pitel, E. The M/G/1 queue with negative customers, Adv. Appl. Probab. 28 (1996) 54017566.
10. Harrison, P.G., Patel, N.M. Pitel, E. Reliability modelling using G-queues, Eur. J. Oper. Res. 126 (2000) 27317287.
11. Yang, W.S., Chae, K.C. A note on the GI/M/1 queue with poisson negative arrivals, J. Appl. Probab.38 (2001) 1081171085.

# 10 CHAPTER

## Statistical Quality Control

# Monitoring the Coefficient of Variation with Run Rules in Short Production Runs

Asma Amdouni[1,2], Philippe Castagliola[1],
Hassen Taleb[3], and Giovanni Celano[4]

[1] Université de Nantes & IRCCyN UMR CNRS 6597, Nantes, France
(e-mail: philippe.castagliola@univ-nantes.fr)
[2] Institut Supérieur de Gestion, Université de Tunis, Tunisie
(e-mail: asma.amdouni@etu.univ-nantes.fr)
[3] University of Gafsa, Tunisia
(e-mail: Hassen.Taleb@isg.rnu.tn)
[4] Università di Catania, Catania, Italy
(e-mail: gcelano@dii.unict.it)

**Abstract.** Monitoring the coefficient of variation (CV) is an effective approach to Statistical Process Control when both the process mean and standard deviation are not constant but, nevertheless, proportional. Until now, research has not yet investigated the monitoring of the CV for short production runs. This paper proposes a new efficient method to monitor the CV by means of one-sided Run Rules type charts and provides the derivation of the corresponding Truncated Run Length properties (i.e. $TARL$, $TSDRL$ and $TRL_r$).
**Keywords:** Coefficient of variation, Short production runs, Markov chain, Truncated run length.

## 1 Introduction

A control chart is one of the most effective techniques in Statistical Process Control (SPC) used to improve the quality and productivity of a production process. It generally assumes that a normally distributed process is *in-control* as long as it has a constant mean and variance. As soon as a change occurs in the mean and / or the standard-deviation, a control chart is supposed to trigger an alarm corresponding to an *out-of-control* situation. But they are some situations where the mean and the standard-deviation may not be constant all the time but they are proportional and the process is nevertheless operating in-control. In this case, monitoring the mean ($\bar{X}$ chart) and / or the standard-deviation ($S$ chart) is useless and a possible alternative is to consider the on-line monitoring of the coefficient of variation (CV, in short) $\gamma$.

Kang *et al.* [14] were the first to develop a Shewhart-type control chart for monitoring the CV using rational subgroups and applied it to a clinical chemistry-control process in order to show that the CV is a potentially attractive tool in quality improvement, where neither the process mean nor the

*Stochastic Modeling, Data Analysis and Statistical Applications* (*pp.* 497-504)
Lidia Filus - Teresa Oliveira - Christos H Skiadas (Eds)



variance are constant. Hong *et al.* [11], were the first to propose an EWMA-CV (Exponentially Weighted Moving Average) control chart in order to improve the CV chart proposed by Kang *et al.* [14] and detect small shifts more efficiently. More recently, Castagliola *et al.* [6] suggested a new method to monitor the CV by means of two one-sided EWMA charts of the CV squared. Calzada and Scariano [2] suggested a synthetic control chart (denoted SynCV) for monitoring the CV and Castagliola *et al.* [3,4] proposed alternative approaches to monitor the CV based on Run Rules and Variable Sampling Interval strategy, respectively.

The researches presented above are aimed at monitoring a process over a production horizon considered as *infinite*. But, there are many situations where the production horizon is very short, i.e. a few hours or a few days, and is considered as *finite*. Control charts specifically designed for finite production run processes have been first introduced by Ladany [16] who presents a methodology for the economic optimization of a $p$-chart for short runs. Later, Ladany and Bedi [17] extended this work to allow time $H$ to be a decision variable. More recently, the design of Shewhart-type $\bar{X}$ control charts for short runs have been discussed in Del Castillo and Montgomery [8,9]. Bayesian type control charts for monitoring the sample mean during a short run have been proposed by Calabrese [1], Tagaras [25], Tagaras and Nikolaidis [26] and Nenes and Tagaras [21]. The statistical measures of performance of the Fixed Sampling Rate (FSR) Shewhart and EWMA $t$ and $\bar{X}$ control charts, monitoring the process mean in short horizon processes, have been investigated by Celano *et al.* [7]. Nenes and Tagaras [20,22] investigated the performance of the CUSUM control chart, again under the assumption of a finite run. Very recently, Castagliola *et al.* [5] investigated the statistical properties of VSS (Variable Sample Size) Shewhart control charts monitoring the mean in a short production run context.

If several $\bar{X}$ type control charts have been proposed for short run processes, as far as we know, no research has been done concerning the monitoring of the CV in a *short run* context. Consequently, the purpose of this paper is to fill this gap by proposing one-sided Run Rules type charts for monitoring the coefficient of variation i.e. an upward (downward) Run Rules CV control chart aiming at detecting an increase (decrease) in the CV for short run processes and by investigating their truncated run length properties.

The remainder of the paper is organized as follows. In Section 2, the main distribution properties of the sample coefficient of variation are briefly introduced. In Section 3, two one-sided Run Rules CV charts for short production runs are defined. The truncated run length properties $TARL$ (average of the truncated run length), $TSDRL$ (standard deviation of the truncated run length), $TRL_{0.5}$ (interpolated 50%-quantile, i.e. the median, of the truncated run length distribution) and $TRL_{0.95}$ (interpolated 95%-quantile of the truncated run length distribution) are presented in Section 4 as measures of statistical performance. Finally, conclusions and future research directions, in Section 5, complete the paper.

## 2 Properties of the (Sample) Coefficient of Variation

Let $X$ be a random variable and let $\mu = E(X)$ and $\sigma = \sigma(X)$ be the mean and standard-deviation of $X$, respectively. By definition, the *coefficient of variation* $\gamma$ of the random variable $X$ is defined as

$$\gamma = \frac{\sigma}{\mu}.$$

Now, let us assume that $\{X_1, \ldots, X_n\}$ is a sample of $n$ normal i.i.d. $(\mu, \sigma)$ random variables. Let $\bar{X}$ and $S$ be the sample mean and the sample standard-deviation of $X_1, \ldots, X_n$, i.e.,

$$\bar{X} = \frac{1}{n}\sum_{i=1}^{n} X_i,$$

and

$$S = \sqrt{\frac{1}{n-1}\sum_{i=1}^{n}(X_i - \bar{X})^2}.$$

The sample coefficient of variation $\hat{\gamma}$ is defined as

$$\hat{\gamma} = \frac{S}{\bar{X}}.$$

By definition, $\hat{\gamma}$ is defined on $(-\infty, +\infty)$. The distributional properties of the sample coefficient of variation $\hat{\gamma}$ have been studied by McKay [19], Hendricks and Robey [10], Iglewicz *et al.* [13], Iglewicz and Myers [12], Warren [28], Vangel [27] and Reh and Scheffler [24]. Among these authors, Iglewicz *et al.* [13] noticed that $\frac{\sqrt{n}}{\hat{\gamma}}$ follows a noncentral $t$ distribution with $n-1$ degrees of freedom and noncentrality parameter $\frac{\sqrt{n}}{\gamma}$. Based on this property, it is easy to derive approximations for the c.d.f. (cumulative distribution function) $F_{\hat{\gamma}}(x|n,\gamma)$ and inverse c.d.f. $F_{\hat{\gamma}}^{-1}(\alpha|n,\gamma)$ of $\hat{\gamma}$ as

$$F_{\hat{\gamma}}(x|n,\gamma) \simeq 1 - F_t\left(\frac{\sqrt{n}}{x}\,\middle|\, n-1, \frac{\sqrt{n}}{\gamma}\right), \tag{1}$$

and

$$F_{\hat{\gamma}}^{-1}(\alpha|n,\gamma) \simeq \frac{\sqrt{n}}{F_t^{-1}\left(1-\alpha\,\middle|\, n-1, \frac{\sqrt{n}}{\gamma}\right)}. \tag{2}$$

## 3 One-sided CV charts with Run Rules for short production runs

A manufacturing process is scheduled to produce a small lot of $N$ parts during a production horizon having finite length $H$. Let $I$ be the number of scheduled inspections within the production horizon $H$. The interval between two

consecutive inspections, i.e. the sampling frequency is $h = \frac{H}{I+1}$ hours since no inspection takes place at the end of the run. Let us suppose that we observe subgroups $\{X_{i,1}, X_{i,2}, \ldots, X_{i,n}\}$ of size $n$, at time $i = 1, 2, \ldots, I$. We assume that there is independence within and between these subgroups and we also assume that each random variable $X_{i,j}$ follows a normal $N(\mu_i, \sigma_i)$ distribution where parameters $\mu_i$ and $\sigma_i$ are constrained by the proportionality relation $\gamma_i = \frac{\sigma_i}{\mu_i} = \gamma_0$, $i = 1, 2, \ldots, I$, when the process is in-control. This implies that from one subgroup to another, the values of $\mu_i$ and $\sigma_i$ may change, but the coefficient of variation $\gamma_i = \frac{\sigma_i}{\mu_i}$ is *constant* and equal to some predefined in-control value $\gamma_0 = \frac{\sigma_0}{\mu_0}$, common to all the subgroups, where $\mu_0$ is the in-control mean and $\sigma_0$ is the in-control standard-deviation.

In the 2-out-of-3 Run Rules, an out-of-control signal is obtained if two out-of-three successive values $\hat{\gamma}_i$ are plotted above an upper warning limit $UWL$ or two out-of-three successive points are plotted below a lower warning limit $LWL$. In this paper, we propose to define two separate one-sided control charts:

- a downward chart (denoted as $RR_{2,3} - \gamma^-$ chart) aiming at detecting a decrease in the CV, with the following limits

$$\begin{aligned} LWL &= \mu_0(\hat{\gamma}) - K_{2,3}^- \sigma_0(\hat{\gamma}), \\ UWL &= +\infty, \end{aligned} \tag{3}$$

- an upward control chart (denoted as $RR_{2,3} - \gamma^+$ chart) aiming at detecting an increase in the CV, with the following limits

$$\begin{aligned} LWL &= 0, \\ UWL &= \mu_0(\hat{\gamma}) + K_{2,3}^+ \sigma_0(\hat{\gamma}), \end{aligned} \tag{4}$$

where $K_{2,3}^- > 0$ and $K_{2,3}^+ > 0$ are the warning limit parameters and where $\mu_0(\hat{\gamma})$ and $\sigma_0(\hat{\gamma})$ are the mean and standard-deviation of the sample coefficient of variation $\hat{\gamma}$, respectively, when the process is in-control. Since there is no closed form for $\mu_0(\hat{\gamma})$ and $\sigma_0(\hat{\gamma})$, the following approximations proposed by Reh and Scheffler [24] can be used

$$\begin{aligned} \mu_0(\hat{\gamma}) \simeq \gamma_0 \Bigg(1 &+ \frac{1}{n}\left(\gamma_0^2 - \frac{1}{4}\right) + \frac{1}{n^2}\left(3\gamma_0^4 - \frac{\gamma_0^2}{4} - \frac{7}{32}\right) \\ &+ \frac{1}{n^3}\left(15\gamma_0^6 - \frac{3\gamma_0^4}{4} - \frac{7\gamma_0^2}{32} - \frac{19}{128}\right)\Bigg), \end{aligned} \tag{5}$$

$$\begin{aligned} \sigma_0(\hat{\gamma}) \simeq \gamma_0 \Bigg(\frac{1}{n}&\left(\gamma_0^2 + \frac{1}{2}\right) + \frac{1}{n^2}\left(8\gamma_0^4 + \gamma_0^2 + \frac{3}{8}\right) \\ &+ \frac{1}{n^3}\left(69\gamma_0^6 + \frac{7\gamma_0^4}{2} + \frac{3\gamma_0^2}{4} + \frac{3}{16}\right)\Bigg)^{1/2}. \end{aligned} \tag{6}$$

The sequence of points plotted on both the $RR_{2,3} - \gamma^-$ and $RR_{2,3} - \gamma^+$ charts can be modelled as a stochastic process. Therefore, to compute the statistical properties of the control charts the following Markov Chain matrix

**P** can be used

$$\mathbf{P} = \begin{pmatrix} \mathbf{Q} & \mathbf{r} \\ \mathbf{0}^T & 1 \end{pmatrix} = \left(\begin{array}{ccccccc|c} 0 & 0 & 0 & p_C & p_L & 0 & 0 & p_U \\ 0 & 0 & 0 & 0 & 0 & 0 & p_C & p_L + p_U \\ p_C & p_L & 0 & 0 & 0 & 0 & 0 & p_U \\ 0 & 0 & p_U & p_C & p_L & 0 & 0 & 0 \\ 0 & 0 & 0 & 0 & 0 & p_U & p_C & p_L \\ p_C & 0 & 0 & 0 & 0 & 0 & 0 & p_L + p_U \\ 0 & 0 & p_U & p_C & 0 & 0 & 0 & p_L \\ \hline 0 & 0 & 0 & 0 & 0 & 0 & 0 & 1 \end{array}\right),$$

where $\mathbf{0} = (0, 0, \ldots, 0)^T$, $\mathbf{Q}$ is the $(7, 7)$ matrix of transient probabilities, the $(7, 1)$ vector $\mathbf{r}$ satisfies $\mathbf{r} = \mathbf{1} - \mathbf{Q1}$ (i.e. row probabilities must sum to 1), with $\mathbf{1} = (1, 1, 1, 1, 1, 1, 1)^T$. The corresponding $(7, 1)$ vector $\mathbf{q}$ of initial probabilities associated with the transient states is equal to $\mathbf{q} = (0, 0, 0, 1, 0, 0, 0)^T$ (i.e. the initial state is the fourth one). The probabilities $p_L = P(\hat{\gamma} < LWL)$, $p_U = P(\hat{\gamma} > UWL)$ and $p_C = P(LWL \leq \hat{\gamma} \leq UWL)$ are equal to:

- For the $RR_{2,3} - \gamma^-$ chart:

$$\begin{aligned} p_L &= F_{\hat{\gamma}}(LWL|n, \gamma_1), \\ p_U &= 1 - F_{\hat{\gamma}}(LWL|n, \gamma_1), \\ p_C &= 0, \end{aligned}$$

- For the $RR_{2,3} - \gamma^+$ chart:

$$\begin{aligned} p_L &= 0, \\ p_U &= F_{\hat{\gamma}}(UWL|n, \gamma_1), \\ p_C &= 1 - F_{\hat{\gamma}}(UWL|n, \gamma_1), \end{aligned}$$

where $F_{\hat{\gamma}}(\ldots|n, \gamma_1)$ is the c.d.f. (cummulative distribution function) of $\hat{\gamma}$ as defined in (1) and where $\gamma_1 = \tau\gamma_0$ is an out-of-control value for the CV. Values of $\tau \in (0, 1)$ correspond to a decrease of the nominal CV, while values of $\tau > 1$ correspond to an increase of the nominal CV.

## 4 Truncated Run Length Properties

In an *infinite* horizon context, the run length $RL$ of the one-sided Run Rules control charts presented in the previous section is a *Discrete PHase-type* (or DPH) random variable of parameters $(\mathbf{Q}, \mathbf{q})$, (see Neuts [23] or Latouche and Ramaswami [18]). Consequently, the p.m.f. (probability mass function) $f_{RL}(\ell)$ and the c.d.f. $F_{RL}(\ell)$ of the run length $RL$ are defined for $\ell = 1, 2, \ldots$ and are equal to

$$f_{RL}(\ell) = \mathbf{q}^T \mathbf{Q}^{\ell-1} \mathbf{r}, \tag{7}$$

$$F_{RL}(\ell) = 1 - \mathbf{q}^T \mathbf{Q}^{\ell} \mathbf{1}. \tag{8}$$

In an *finite* horizon context, the short run measures of statistical performance of a control chart have been originally proposed by Nenes and Tagaras [22]

who assume that the truncated run length $TRL$ of the short run chart is defined for $\ell = 1, 2, \ldots, I+1$ and the p.m.f. $f_{TRL}(\ell)$ and the c.d.f. $F_{TRL}(\ell)$ of the truncated run length $TRL$ are equal to

$$f_{TRL}(\ell) = \begin{cases} f_{RL}(\ell) & \text{if } \ell = 1, 2, \ldots, I \\ 1 - F_{RL}(I) & \text{if } \ell = I+1, \end{cases}$$

and

$$F_{TRL}(\ell) = \begin{cases} F_{RL}(\ell) & \text{if } \ell = 1, 2, \ldots, I \\ 1 & \text{if } \ell = I+1 \end{cases}$$

The *finite* horizon counterpart of $ARL = E(RL)$ for *infinite* horizon is $TARL = E(TRL)$. It can be proved that

$$TARL = \mathbf{q}^T \left( \sum_{\ell=0}^{I} \mathbf{Q}^\ell \right) \mathbf{1} \tag{9}$$

It can be also proved that the second non-central moment $TRL2 = E(TRL^2)$ of the truncated run length $TRL$ is equal to

$$TRL2 = \mathbf{q}^T \left( \sum_{\ell=0}^{I} (2\ell+1) \mathbf{Q}^\ell \right) \mathbf{1} \tag{10}$$

This allows to compute the standard-deviation of the truncated run length as

$$TSDRL = \sqrt{TRL2 - TARL^2}$$

In order to gain more insight concerning the variability of the $TRL$, we have also decided to derive the interpolated $r$-quantile, $r \in (0, 1)$, of the truncated run length distribution $TRL_r$. The computation of $TRL_r$ depends on the value of $r$:

- if $r \in (0, F_{TRL}(1))$ then $TRL_r$ is not defined.
- if $r \in [F_{TRL}(1), F_{TRL}(I))$ then we have $F_{TRL}(\ell) = F_{RL}(\ell)$, $\ell = 1, 2, \ldots, I$. The idea is then to replace the *discrete* c.d.f. $F_{RL}(\ell)$ by some *continuous* c.d.f. Investigating different possible distributions led us to choose the *continuous* gamma c.d.f. $F_\gamma(\ell | a, b, c)$ with parameters $(a > 0, b > 0, c)$ as a good candidate, where $a = \frac{4\mu_2^3}{\mu_3^2}$, $b = \frac{\mu_3}{2\mu_2}$, $c = \mu - \frac{2\mu_2^2}{\mu_3}$ and where $\mu = \nu_1$, $\mu_2 = \nu_2 - \nu_1^2 + \nu_1$ and $\mu_3 = \nu_3 + 3(1-\nu_1)\nu_2 + 2\nu_1^3 - 3\nu_1^2 + \nu_1$ are the mean, second and third central moments of $RL$, respectively, and $\nu_1$, $\nu_2$ and $\nu_3$ are the first three factorial moments of $RL$, i.e.

$$\begin{aligned} \nu_1 &= \mathbf{q}^T (\mathbf{I} - \mathbf{Q})^{-1} \mathbf{1}, \\ \nu_2 &= 2\mathbf{q}^T (\mathbf{I} - \mathbf{Q})^{-2} \mathbf{Q} \mathbf{1}, \\ \nu_3 &= 6\mathbf{q}^T (\mathbf{I} - \mathbf{Q})^{-3} \mathbf{Q}^2 \mathbf{1}. \end{aligned}$$

An approximation for $TRL_r$ is then

$$TRL_r \simeq F_\gamma^{-1}(r | a, b, c),$$

where $F_{\gamma}^{-1}(r|a,b,c)$ is the inverse c.d.f. of the gamma distribution with parameters $(a,b,c)$. The choice of the gamma distribution is motivated by its actual ability to accurately fit DPH type distributions.

- if $r \in [F_{TRL}(I),1)$ we suggest to linearly interpolate $TRL_r$ between the points $(F_{TRL}(I),I)$ and $(1,I+1)$, i.e.

$$TRL_r \simeq \frac{(I+1)F_{TRL}(I) - I - r}{F_{TRL}(I) - 1}$$

## 5 Conclusions

In this paper, we have proposed two separate one-sided Run Rules type control charts monitoring the coefficient of variation in a short production run context: a downward (upward) Shewhart-type chart denoted as $RR_{2,3}-\gamma^{-}$ ($RR_{2,3}-\gamma^{+}$) aiming at detecting a shift decreasing (increasing) the in-control CV $\gamma_0$. We have also derived the Truncated Run Length properties of these charts, i.e. $TARL$, $TSDRL$ and $TRL_r$. Since monitoring the CV in a short production run is a new subject of SPC research, there is room for many extensions like, for instance, the use of adaptive strategies like the VSI (Variable Sampling Interval), VSS (Variable Sampling Size) or DS (Double Sampling) and the design of advanced schemes like EWMA or CUSUM.

## References

1. J. Calabrese. Bayesian Process Control for Attributes. *Management Science*, 41(4):637–645, 1995.
2. M.E. Calzada and S.M. Scariano. A Synthetic Control Chart for the Coefficient of Variation. *Journal of Statistical Computation and Simulation*, 85(5):853–867, 2013.
3. P. Castagliola, A. Achouri, H. Taleb, G. Celano, and S. Psarakis. Monitoring the Coefficient of Variation Using a Variable Sampling Interval control chart. *Quality and Reliability Engineering International*, 2012. DOI: 10.1002/qre.1465.
4. P. Castagliola, A. Achouri, H. Taleb, G. Celano, and S. Psarakis. Monitoring the Coefficient of Variation Using Control Charts with Run Rules. *Quality Technology and Quantitative Management*, 10(1):75–94, 2013.
5. P. Castagliola, G. Celano, S. Fichera, and G. Nenes. The Variable Sample Size $t$ Control Chart for Monitoring Short Production Runs. *International Journal of Advanced Manufacturing Technology*, 66(9):1353–1366, 2013.
6. P. Castagliola, G. Celano, and S. Psarakis. Monitoring the Coefficient of Variation Using EWMA Charts. *Journal of Quality Technology*, 43(3):249–265, 2011.
7. G. Celano, P. Castagliola, S. Fichera, and E. Trovato. Shewhart and EWMA $t$ Charts for Short Production Runs. *Quality Reliability Engineering International*, 27(3):313–326, 2011.
8. E. Del Castillo and D.C. Montgomery. Optimal Design of Control Charts for Monitoring Short Production Runs. *Economic Quality Control*, 8(4):225–240, 1993.
9. E. Del Castillo and D.C. Montgomery. A General Model for the Optimal Economic Design of $\bar{X}$ Charts used to Control Short or Long Run Processes. *IIE Transactions*, 28(3):193–201, 1996.

10. W.A. Hendricks and W.K. Robey. The Sampling Distribution of the Coefficient of Variation. *Annals of Mathematical Statistic*, 7(3):129–132, 1936.
11. E.P. Hong, C.W. Kang, J.W. Baek, and H.W. Kang. Development of CV Control Chart Using EWMA Technique. *Journal of the Society of Korea Industrial and Systems Engineering*, 31(4):114–120, 2008.
12. B. Iglewicz and R.H. Myers. Comparisons of Approximations to the Percentage Points of the Sample Coefficient of Variation. *Technometrics*, 12(1):166–169, 1970.
13. B. Iglewicz, R.H. Myers, and R.B. Howe. On the Percentage Points of the Sample Coefficient of Variation. *Biometrika*, 55(3):580–581, 1968.
14. C.W. Kang, M.S. Lee, Y.J. Seong, and D.M. Hawkins. A Control Chart for the Coefficient of Variation. *Journal of Quality Technology*, 39(2):151–158, 2007.
15. M. Klein. Two Alternatives to the Shewhart $\overline{X}$ Control Chart. *Journal of Quality Technology*, 32(4):427–431, 2000.
16. S.P. Ladany. Optimal Use of Control Charts for Controlling Current Production. *Management Science*, 19(7):763–772, 1973.
17. S.P. Ladany and D.N. Bedi. Selection of the Optimal Setup Policy. *Naval Research Logistics Quaterly*, 23(2):219–233, 1976.
18. G. Latouche and V. Ramaswami. *Introduction to Matrix Analytic Methods in Stochastic Modelling*. ASA SIAM, 1999.
19. A.T. McKay. Distribution of the Coefficient of Variation and Extended $t$ Distribution. *Journal of the Royal Statistical Society*, 95(4):695–698, 1932.
20. G. Nenes and G. Tagaras. The CUSUM Chart for Monitoring Short Production Run. In *Proceedings of 5th International Conference on Analysis of Manufacturing Systems – Production Management*, pages 43–50, Zakynthos Island, Greece, May 2005.
21. G. Nenes and G. Tagaras. The Economically Designed two Sided Bayesian $\bar{X}$ Control Chart. *European Journal of Operational Research*, 183(1):263–277, 2007.
22. G. Nenes and G. Tagaras. Evaluation of CUSUM Charts for Finite-Horizon Processes. *Communications in Statistics – Simulation and Computation*, 39(3):578–597, 2010.
23. M.F. Neuts. *Matrix-Geometric Solutions in Stochastic Models: an Algorithmic Approach*. Dover Publications Inc., 1981.
24. W. Reh and B. Scheffler. Significance Tests and Confidence Intervals for Coefficients of Variation. *Computational Statistics & Data Analysis*, 22(4):449–452, 1996.
25. G. Tagaras. Dynamic Control Charts for Finite Production Runs. *European Journal of Operational Research*, 91(1):38–55, 1996.
26. G. Tagaras and Y. Nikolaidis. Comparing the Effectiveness of Various Bayesian $\bar{X}$ Control Charts. *Operations Research*, 50(5):878–888, 2002.
27. M.G. Vangel. Confidence Intervals for a Normal Coefficient of Variation. *American Statistician*, 15(1):21–26, 1996.
28. W.G. Warren. On the Adequacy of the Chi-Squared Approximation for the Coefficient of Variation. *Communications in Statistics – Simulation and Computation*, 11(6):659–666, 1982.

# Control charts implemented on the basis of a bootstrap reference sample

Fernanda Otília Figueiredo[1] and M. Ivette Gomes[2]

[1] Faculdade de Economia da Universidade do Porto, and CEAUL, Rua Dr. Roberto Frias, 4200-464 Porto, Portugal
(E-mail: otilia@fep.up.pt)
[2] FCUL, DEIO and CEAUL, Universidade de Lisboa, Bloco C6, Piso 4 - Campo Grande, 1749-016 Lisboa, Portugal
(E-mail: ivette.gomes@fc.ul.pt)

**Abstract.** The bootstrap methodology is used in Phase I of control charting to estimate the nominal process parameters, together with the use of robust estimates. We evaluate the performance of the Mean-chart with estimated parameters for monitoring the process location, where the estimates are obtained on the basis of a simple reference sample or via bootstrapping from such sample. The run-length distribution of the corresponding charts for samples of size 5 and 10 is obtained by Monte Carlo simulations, and the values obtained for some parameters of interest are discussed.

**Keywords:** Bootstrap, Control charts, Robust statistics, Statistical Process Control.

## 1 Introduction

The control charts, introduced by Shewhart in 1924, are one of the main tools in Statistical Process Control (SPC), but their domain has been successively enlarged, with applications to areas as diverse as Health, Medicine, Genetics, Biology, Environmental Sciences, Finance, Metrology, Sports and Justice, among others. For an overview of standard and non-standard applications of control charts see, for instance, Montgomery[18], Woodall and Montgomery[27],[28], MacCarthy and Wasusri[17], Dull and Tegarden[11], Vardeman *et al.*[26], and references therein.

To develop any control chart the nominal process parameters must be either assumed known or estimated. In practice the distribution of the process data as well as the process parameters are usually unknown, being the process parameters usually estimated from an in-control Phase I reference sample, made up of $m$ subgroups of size $n$, before we proceed to the building of a (non-)parametric control chart.

A strong emphasis has been given to the analysis of the real performance of control charts implemented on the basis of estimated parameters, and to the effect of the non-normality in the performance of the usual control charts. Apart

*Stochastic Modeling, Data Analysis and Statistical Applications* (*pp.* 505-514)
Lidia Filus - Teresa Oliveira - Christos H Skiadas (Eds)



from the pioneer works of Schilling and Nelson[25], Balakrishnan and Kocherlakota[1], Chan *et al.*[3], Rocke[21],[22], Quesenberry[20], Chen[8], Nedumaran and Pignatiello[19], Champ and Jones[4], Chakraborti[5],[6],[7], and Jensen *et al.*[16], we mention, among others, the recent works of Zhang and Castagliola[29], Schoonhoven *et al.*[23],[24], and Castagliola and Figueiredo[2]. From these studies we easily conclude that to obtain control charts implemented with estimated control limits with the same run-length properties as the corresponding charts with true limits, the choice of the number of subgroups, $m$, and the sample size, $n$, cannot be heuristic. Besides the need of a very large number $m$ of subgroups, which is a limitation from a practical point of view, and in some cases even impossible, we must determine the control limits in a robust way. Other approach consists of modifying the chart parameters' in order to take into consideration the variability introduced by the estimation of the nominal process values in Phase I, allowing that way to maintain the expected false alarm rate.

Our aim in this paper is only to investigate the benefits of using the bootstrap methodology in Phase I of control charting to obtain a larger reference sample to estimate the nominal process parameters, together with the use of robust estimates. More precisely, from an in-control reference sample of $m$ subgroups (20 or 30) of size $n = 5, 10$, we set out to construct a larger reference sample of $M_b$ subgroups (100, 500 or 1000) of size $n$ by bootstrapping from the pooled sample of size $m \times n$. The nominal process parameters are then estimated through the use of a few location and scale statistics. To illustrate the effect of these parameters' estimates on the properties of the chart we will consider the traditional Mean-chart with 3-sigma (exact and estimated) control limits to monitor the mean value of a normal process. The paper is organized as follows. Section 2 provides some information about the implementation of the Mean-chart with estimated control limits, the bootstrap methodology and the statistics considered in the estimation of the nominal process parameters. Section 3 presents some relevant parameters of the run-length distribution of the traditional Mean-chart implemented on the basis of previous estimates, obtained by Monte Carlo simulations, and Section 4 concludes with some comments about the performance of the implemented control charts.

## 2 Mean-chart with estimated control limits based on bootstrap estimates

### 2.1 Mean-chart with estimated control limits

Let $Y$ be a random variable associated with a normal process, being the in-control mean value, $\mu_0$, and the in-control standard deviation, $\sigma_0$, both unknown. The most popular control chart for the process location monitoring is the Mean-chart with estimated control limits, $\overline{Y}$, obtained by plotting the sample means of the Phase II samples $(Y_{i,1}, \ldots, Y_{i,n})$, $i = 1, 2, \ldots$, of $n$ independent normal random variables, $N(\mu_0 + \delta\sigma_0, \sigma_0)$, where $i$ is the subgroup number and $\delta$ is the magnitude of the standardized mean shift. If $\delta = 0$ the

process is in-control, otherwise the process is out-of-control due to a shift in the mean process.

The (estimated) control limits (CL's) of the $\overline{Y}$-chart are random variables, which can be written in the form

$$\widehat{CL}'s = \hat{\mu}_0 \pm K\hat{\sigma}_0, \tag{1}$$

where the chart parameter $K$ depends on the sample size $n$, and is determined in order to obtain a given in-control performance, say, a fixed in-control Average Run-Length (ARL). For instance, the $\overline{Y}$-chart with exact 3-sigma control limits, $CL's = \mu_0 \pm \frac{3}{\sqrt{n}}\sigma_0$, leads to an in-control ARL=370.4. If we consider $K = 3/\sqrt{n}$ in (1), the corresponding Mean-chart does not have the same performance of the chart with exact 3-sigma control limits, unless the process nominal values $\mu_0$ and $\sigma_0$ are adequately estimated.

### 2.2 A reference sample for the estimation of the nominal process parameters

The standard procedure is to estimate $\mu_0$ and $\sigma_0$ from $m = 20, 30$ subgroups $(X_{i,1}, \ldots, X_{i,n})$, $i = 1, \ldots, m$ of size $n$, usually 4 or 5, assuming independence between and within subgroups, and that $X_{i,j} \sim N(\mu_0, \sigma_0)$. However, the literature refer that for an adequate estimation of $\mu_0$ and $\sigma_0$, the number $m$ of initial subgroups must be very large, at least $400/n$ (see, for instance, Quesenberry[20] and Castagliola and Figueiredo[2]). In this study we apply the bootstrap methodology to the pooled sample of size $m \times n$ in order to obtain a larger number $M_b = 100, 500, 1000$ of subgroups of size $n = 5, 10$ that will be used for the estimation of $\mu_0$ and $\sigma_0$.

### 2.3 How does the bootstrap methodology work?

Let $(W_1, \ldots, W_n)$ be a random sample of size $n$ from a $d.f.$ $F(.)$. The bootstrap sample, $(W_1^*, \ldots, W_n^*)$, is obtained by randomly sampling $n$ times, with replacement, from the observed sample $(w_1, \ldots, w_n)$. These variables $W_i^*$ are independent and identically distributed $(i.i.d.)$ replicates from a random variable $W^*$, with $d.f.$ equal to the empirical $d.f.$ of our observed sample, given by

$$F_n^*(w) := \frac{1}{n}\sum_{i=1}^{n} I_{\{w_i \leq w\}}, \tag{2}$$

where $I_A$ denotes the indicator function of the set $A$. For other details about the bootstrap methodology see, for instance, Davison and Hinkley[10], Efron[12] and Efron and Tibshirani[13].

In our case, by bootstrapping from the empirical $d.f.$ associated to the pooled reference sample of size $m \times n$, $(x_{1,1}, \ldots, x_{1,n}, \ldots, x_{m,1}, \ldots, x_{m,n})$, we generate $M_b$ random samples of size $n$, say $(X_{r,1}^*, \ldots, X_{r,n}^*)$, $r = 1, \ldots, M_b$.

In the sequel $(X_{i,1}, \ldots, X_{i,n})$ denotes the $i$-th subgroup of size $n$ used in the estimation of the nominal values and let $X_{i,(j)}$ be the $j$-th ascending order statistics (o.s.) associated to the subgroup $(X_{i,1}, \ldots, X_{i,n})$.

### 2.4 Estimates of the nominal process parameters under consideration

To estimate the in-control mean value $\mu_0$ and the in-control standard deviation $\sigma_0$, we have carried out the following procedure:

1. From $k$ subgroups of size $n$ (5, 10), with $k$ denoting either $m$ (20, 30) or $M_b$ (100, 500, 1000), we compute $k$ partial estimates, $\widehat{\mu}_{0i}$ and $\widehat{\sigma}_{0i}$, $i = 1, \cdots, k$;
2. Then, we consider the overall estimates of $\mu_0$ and $\sigma_0$, $\widehat{\mu}_0 = \sum_{i=1}^{k} \widehat{\mu}_{0i}/k$ and $\widehat{\sigma}_0 = \sum_{i=1}^{k} \widehat{\sigma}_{0i}/k$, to be used in the 3-sigma control limits of the $\overline{Y}$-chart.

We must point out that even when we are working with potential normal processes, in practice we can have some disturbances in the data, and in particular, in the $m$ subgroups collected in Phase I. Thus, to obtain the partial estimates $\widehat{\mu}_{0i}$ and $\widehat{\sigma}_{0i}$, apart from the usual estimators for $\mu_0$ and $\sigma_0$, we also consider the Total Median ($TMd$) and the Total Range ($TR$) statistics, defined and studied in Cox and Iguzquiza[9], Figueiredo[14] and Figueiredo and Gomes[15]. The statistics $TMd$ and $TR$ are resistant to changes in the underlying model, and are similar to a special trimmed-mean, in which the ideal percentage of trimming does not depend on the data distribution. The distributional behaviour of the $TMd$ and the $TR$ estimators has already been investigated, and these statistics have revealed to be efficient and robust estimators of the mean value and the standard deviation, respectively.

Thus, to obtain the partial estimates $\widehat{\mu}_{0i}$, we consider, for $n = 5, 10$, the *sample mean*,

$$\overline{X}_i = \frac{1}{n} \sum_{j=1}^{n} X_{i,j},$$

and the *total median*, defined by

$$TMd_i = 0.058 \left( X_{i,(1)} + X_{i,(5)} \right) + 0.366 X_{i,(3)} + 0.259 \left( X_{i,(2)} + X_{i,(4)} \right)$$

for samples of size $n = 5$, and by

$$TMd_i = 0.001(X_{i,(1)} + X_{i,(10)}) + 0.019(X_{i,(2)} + X_{i,(9)}) + 0.078(X_{i,(3)} + X_{i,(8)}) + 0.168(X_{i,(4)} + X_{i,(7)}) + 0.234(X_{i,(5)} + X_{i,(6)})$$

for samples of size $n = 10$.

To obtain the partial estimates $\widehat{\sigma}_{0i}$, unbiased whenever the underlying model is normal, we consider, for $n = 5, 10$, the following statistics divided by the normalizing scale constant $c$, next given: the *sample standard deviation*,

$$S_i = \sqrt{\frac{1}{n-1} \sum_{j=1}^{n} \left( X_{i,j} - \overline{X}_i \right)^2}, \; c = c_4 = \begin{cases} 0.940, \, if \, n = 5 \\ 0.921, \, if \, n = 10, \end{cases}$$

the *sample range*,

$$R_i = X_{i,(n)} - X_{i,(n)}, \; c = d_2 = \begin{cases} 2.326, \, if \, n = 5 \\ 2.058, \, if \, n = 10, \end{cases}$$

and the *total range*, defined by

$$TR_i = 0.737\left(X_{i,(5)} - X_{i,(1)}\right) + 0.263\left(X_{i,(4)} - X_{i,(2)}\right),\ c = 1.801,$$

for samples of size $n = 5$, and by

$$TR_i = 0.654(X_{i,(10)} - X_{i,(1)}) + 0.241(X_{i,(9)} - X_{i,(2)}) + 0.079(X_{i,(8)} - X_{i,(3)}) + 0.022(X_{i,(7)} - X_{i,(4)}) + 0.004(X_{i,(6)} - X_{i,(5)}),\ c = 1.513,$$

for samples of size $n = 10$.

In the sequel the two overall estimates of $\mu_0$ will be denoted by $\overline{\overline{X}}$ and $\overline{TMd}$, and the three overall estimates of $\sigma_0$ will be denoted by $\overline{S}/c_4$, $\overline{R}/d_2$ and $\overline{TR}/c$.

## 3 Run-length distribution of the Mean-chart with control limits estimated via bootstrapping

The ability of a control chart to detect process changes is usually measured by the expected number of samples taken before the chart signals, i.e., by its ARL (*Average Run Length*), together with the standard deviation of the Run Length distribution, SDRL. When we have to estimate some process parameters to determine the control limits of the chart, the RL variable (i.e., the number of samples taken before the chart signals) has not a geometric distribution as it happens in the known parameters case, but a more right-skewed distribution.

Some authors, Chakraborti[5],[6],[7] and Jensen *et al.*[16], for instance, refer that in this case the ARL and the SDRL parameters are not the best measures of performance of a control chart, due to the high asymmetry of the RL distribution, and one might prefer the use of the Median Run-Length, MRL, as a measure performance, and the 5th and the 95th percentiles of the RL distribution to represent the spread of the RL. Additionally, for a more complete understanding of the chart performance, they suggest the analysis of the conditional RL distribution, i.e., the RL distribution conditional on the observed estimates, together with the analysis of the marginal RL distribution. Such a marginal distribution is computed by integrating the conditional RL distribution over the range of the parameter estimators and takes thus into account the random variability introduced into the charting procedure through parameter estimation without requiring the knowledge of the observed estimates.

In order to get information about the in-control and the out-of-control performance of the previous $\overline{Y}$ charts with estimated 3-sigma control limits to monitor normal data, we compute the (conditional) RL distribution of the $\overline{Y}$-charts by Monte Carlo simulation, using 250000 runs in the simulation experiment. Tables 1 and 2 present estimates of some parameters of the in-control and out-of-control RL distribution for the case of known nominal process values (exact limits obtained by replacing $\mu_0 = 0$ and $\sigma_0 = 1$), and when the estimated control limits are based on the overall estimates ($\overline{\overline{X}}$,$\overline{S}/c_4$), ($\overline{\overline{X}}$,$\overline{R}/d_2$) and ($\overline{TMd}$,$\overline{TR}/c$), obtained from a reference sample of $m$ (20 and 30) subgroups of size $n = 5$ and from $M_b$ (100, 500 and 1000) subgroups of size $n = 5$ obtained by bootstrapping from the pooled reference sample of size $m \times n$.

| Mean-chart with | | ARL | | | SDRL | | |
|---|---|---|---|---|---|---|---|
| Estimated CL's # subgroups | | Estimates | | | Estimates | | |
| $m$ | $M_b$ | $(\overline{\overline{X}}, \overline{S}/c_4)$ | $(\overline{\overline{X}}, \overline{R}/d_2)$ | $(\overline{TMd}, \overline{TR}/c)$ | $(\overline{\overline{X}}, \overline{S}/c_4)$ | $(\overline{\overline{X}}, \overline{R}/d_2)$ | $(\overline{TMd}, \overline{TR}/c)$ |
| 20 | | 458 | 444 | 445 | 891 | 817 | 836 |
| | 100 | 404 | 386 | 375 | 728 | 713 | 676 |
| | 500 | 388 | 366 | 370 | 671 | 576 | 627 |
| | 1000 | 378 | 365 | 368 | 608 | 602 | 615 |
| 30 | | 415 | 418 | 409 | 640 | 695 | 628 |
| | 100 | 394 | 374 | 375 | 633 | 620 | 588 |
| | 500 | 373 | 363 | 364 | 543 | 494 | 508 |
| | 1000 | 378 | 364 | 367 | 533 | 499 | 518 |
| Exact CL's | | 371 | | | 371 | | |

**Table 1.** In-control ARL and SDRL of the 3-sigma $\overline{Y}$-chart for samples of size $n = 5$. For the estimation we consider $m = 20, 30$ or $M_b = 100, 500, 1000$ subgroups of size $n = 5$.

| Mean-chart with | | | ARL | | | SDRL | | |
|---|---|---|---|---|---|---|---|---|
| Estimated CL's # subgroups | | | Estimates | | | Estimates | | |
| $m$ | $M_b$ | $\delta$ | $(\overline{\overline{X}}, \overline{S}/c_4)$ | $(\overline{\overline{X}}, \overline{R}/d_2)$ | $(\overline{TMd}, \overline{TR}/c)$ | $(\overline{\overline{X}}, \overline{S}/c_4)$ | $(\overline{\overline{X}}, \overline{R}/d_2)$ | $(\overline{TMd}, \overline{TR}/c)$ |
| 30 | | 0.3 | 132.4 | 134.4 | 135.2 | 209.5 | 216.4 | 224.0 |
| | | 0.5 | 42.3 | 42.5 | 42.9 | 62.3 | 64.1 | 65.4 |
| | | 0.7 | 15.7 | 15.9 | 15.8 | 20.3 | 20.5 | 20.9 |
| | | 1.0 | 5.0 | 5.0 | 4.9 | 5.4 | 5.5 | 5.2 |
| | | 1.5 | 1.6 | 1.6 | 1.6 | 1.1 | 1.1 | 1.1 |
| | 500 | 0.3 | 124.8 | 121.5 | 123.3 | 196.0 | 181.5 | 188.2 |
| | | 0.5 | 39.7 | 39.4 | 39.3 | 57.4 | 56.0 | 56.6 |
| | | 0.7 | 14.9 | 14.7 | 14.8 | 18.8 | 18.9 | 18.6 |
| | | 1.0 | 4.8 | 4.7 | 4.8 | 5.2 | 5.0 | 5.0 |
| | | 1.5 | 1.6 | 1.6 | 1.6 | 1.1 | 1.0 | 1.0 |
| Exact CL's | | 0.3 | 99.2 | | | 98.4 | | |
| | | 0.5 | 33.1 | | | 32.5 | | |
| | | 0.7 | 13.2 | | | 12.8 | | |
| | | 1.0 | 4.5 | | | 4.0 | | |
| | | 1.5 | 1.6 | | | 0.9 | | |

**Table 2.** Out-of-control ARL and SDRL of the 3-sigma $\overline{Y}$-chart for samples of size $n = 5$. For the estimation we consider $m = 30$ or $M_b = 500$ subgroups of size $n = 5$. The process mean changed from $\mu = \mu_0 = 0$ to $\mu = \delta$.

More precisely, Table 1 presents estimates of the most commonly used measures of performance of a control chart, the ARL and the SDRL, obtained for the $\overline{Y}$-charts under study, and assuming that the process is in-control. Table 2 presents the ARL and the SDRL of the $\overline{Y}$-charts with estimated and exact control limits for samples of size $n = 5$, when the process is out-of-control due to a shift in the mean value from $\mu = \mu_0 = 0$ to $\mu = \delta = 0.3, 0.5, 0.7, 1.0, 1.5$, and for $m = 30$ and $M_b = 500$ subgroups of size $n = 5$.

Table 3 presents the percentiles (P) 1th, 5th, 10th, 25th, 50th (MRL), 75th, 90th, 95th and 99th of the in-control RL distribution, the interquartile range (a robust measure of spread), IQR=P75th-P25th, and the Fisher skewness coefficient, $g$, defined by $g := \frac{m_3}{m_2^{3/2}}$, where $m_r$ denotes the $r$-th central moment of the sampling distribution of RL.

| Mean-chart with estimated CL's | | | | | | | | | | | | | |
|---|---|---|---|---|---|---|---|---|---|---|---|---|---|
| Estimates | # subgroups | | Percentiles | | | | | | | | | | |
| | $m$ | $M_b$ | $1th$ | $5th$ | $10th$ | $25th$ | $50th$ | $75th$ | $90th$ | $95th$ | $99th$ | IQR | $g$ |
| $\left(\overline{\overline{X}}, \overline{S}/c_4\right)$ | 20 | | 3 | 12 | 25 | 73 | 204 | 504 | 1078 | 1675 | 3967 | 431 | 9.65 |
| | | 100 | 3 | 12 | 24 | 69 | 185 | 452 | 956 | 1475 | 3277 | 383 | 8.45 |
| | | 500 | 3 | 12 | 25 | 69 | 186 | 450 | 922 | 1383 | 2987 | 381 | 8.73 |
| | | 1000 | 3 | 12 | 24 | 70 | 185 | 438 | 916 | 1360 | 2902 | 368 | 5.75 |
| | 30 | | 3 | 14 | 29 | 83 | 218 | 503 | 980 | 1441 | 2923 | 420 | 7.41 |
| | | 100 | 3 | 13 | 26 | 76 | 200 | 461 | 934 | 1393 | 2897 | 385 | 7.12 |
| | | 500 | 3 | 14 | 28 | 78 | 201 | 455 | 885 | 1287 | 2566 | 377 | 5.27 |
| | | 1000 | 3 | 14 | 28 | 79 | 207 | 466 | 907 | 1300 | 2562 | 387 | 4.56 |
| $\left(\overline{\overline{X}}, \overline{R}/d_2\right)$ | 20 | | 3 | 12 | 24 | 70 | 196 | 487 | 1050 | 1634 | 3810 | 417 | 6.67 |
| | | 100 | 2 | 11 | 22 | 63 | 174 | 429 | 914 | 1407 | 3114 | 366 | 9.03 |
| | | 500 | 3 | 12 | 24 | 68 | 181 | 429 | 884 | 1317 | 2748 | 361 | 5.29 |
| | | 1000 | 3 | 12 | 25 | 67 | 180 | 423 | 874 | 1283 | 2721 | 356 | 7.02 |
| | 30 | | 3 | 14 | 28 | 80 | 211 | 494 | 988 | 1461 | 3051 | 414 | 8.70 |
| | | 100 | 3 | 13 | 25 | 71 | 186 | 443 | 895 | 1312 | 2778 | 372 | 9.45 |
| | | 500 | 3 | 14 | 28 | 78 | 201 | 452 | 878 | 1247 | 2389 | 374 | 3.96 |
| | | 1000 | 3 | 14 | 28 | 79 | 204 | 455 | 860 | 1248 | 2332 | 376 | 4.53 |
| $\left(\overline{TMd}, \overline{TR}/c\right)$ | 20 | | 3 | 12 | 25 | 73 | 199 | 488 | 1050 | 1615 | 3751 | 415 | 9.16 |
| | | 100 | 2 | 11 | 22 | 63 | 171 | 416 | 900 | 1383 | 2977 | 353 | 7.82 |
| | | 500 | 3 | 12 | 23 | 67 | 180 | 430 | 882 | 1312 | 2844 | 363 | 8.11 |
| | | 1000 | 3 | 11 | 24 | 68 | 180 | 428 | 881 | 1321 | 2753 | 360 | 7.40 |
| | 30 | | 3 | 14 | 29 | 80 | 210 | 489 | 973 | 1456 | 2900 | 409 | 5.67 |
| | | 100 | 3 | 12 | 25 | 71 | 190 | 440 | 898 | 1333 | 2825 | 369 | 5.39 |
| | | 500 | 3 | 13 | 27 | 77 | 200 | 453 | 869 | 1261 | 2426 | 376 | 4.57 |
| | | 1000 | 3 | 14 | 28 | 77 | 202 | 459 | 870 | 1239 | 2419 | 382 | 4.97 |
| Mean-chart with exact CL's | | | | | | | | | | | | | |
| | | | 4 | 19 | 40 | 108 | 260 | 515 | 856 | 1110 | 1693 | 407 | 1.97 |

**Table 3.** Percentiles, interquartile range (IQR) and Fisher coefficient of asymmetry (g) of the in-control RL distribution of the 3-sigma $\overline{Y}$-charts for samples of size $n = 5$. For the estimation we consider $m = 20$ or $M_b = 100, 500, 1000$ subgroups of size $n = 5$.

Finally, to illustrate the in-control performance of the chart when we increase the sample size $n$, we present in Table 4 estimates for the in-control ARL and SDRL values of the Mean-chart implemented for samples of size $n = 10$.

| Mean-chart with | | ARL | | | SDRL | | |
|---|---|---|---|---|---|---|---|
| Estimated CL's # subgroups | | Estimates | | | Estimates | | |
| $m$ | $M_b$ | $(\overline{\overline{X}}, \overline{S}/c_4)$ | $(\overline{\overline{X}}, \overline{R}/d_2)$ | $(\overline{TMd}, \overline{TR}/c)$ | $(\overline{\overline{X}}, \overline{S}/c_4)$ | $(\overline{\overline{X}}, \overline{R}/d_2)$ | $(\overline{TMd}, \overline{TR}/c)$ |
| 20 | | 363 | 372 | 355 | 479 | 516 | 490 |
| | 100 | 348 | 333 | 328 | 499 | 477 | 448 |
| | 500 | 339 | 335 | 326 | 437 | 437 | 421 |
| | 1000 | 338 | 330 | 330 | 453 | 430 | 427 |
| 30 | | 364 | 367 | 355 | 449 | 460 | 433 |
| | 100 | 348 | 338 | 335 | 434 | 435 | 422 |
| | 500 | 345 | 340 | 339 | 424 | 413 | 404 |
| | 1000 | 357 | 341 | 339 | 444 | 413 | 409 |
| Exact CL's | | 371 | | | 371 | | |

**Table 4.** In-control ARL and SDRL of the 3-sigma $\overline{Y}$-chart for samples of size $n = 10$. For the estimation we consider $m = 20, 30$ or $M_b = 100, 500, 1000$ subgroups of size $n = 10$.

## 4 Some comments on the performance of the $\overline{Y}$-charts

As expected, for all the different combinations of the number of subgroups used in the estimation, $m$ or $M_b$, and all the estimates $(\hat{\mu}_0, \hat{\sigma}_0)$ here considered, the estimation of the nominal values have effect on the ARL and on the SDRL of the $\overline{Y}$-charts. However, the effect on the in-control and out-of-control RL behaviour becomes small when $m$ increases, and specially if we consider a large number $M_b$ of subgroups of size $n = 5, 10$ obtained by bootstrapping from the initial $m$ subgroups of the reference sample.

As $m$ and $M_b$ increases the ARL value of the chart with estimated control limits tends faster than the SDRL to the corresponding values obtained when the $\overline{Y}$-chart is implemented with exact CL's. For instance, if we consider $M_b = 500$ or 1000 subgroups $n = 5$ obtained by bootstrapping from the initial $m = 20, 30$ subgroups of the reference sample, we obtain an in-control ARL approximately equal to 370.4, although the SDRL value maintains yet larger than 370.4. Concerning the different estimates of the nominal values here considered, the results are qualitatively the same, at least when monitoring normal data.

For detecting small shifts in the process mean value, we also get some improvements in terms of performance if we consider, for instance, $M_b = 500$ subgroups of size $n = 5$ for the estimation of $(\mu_0, \sigma_0)$, by bootstrapping from the initial $m = 30$ subgroups of the reference sample.

The RL distribution although more right-skewed in all cases than a geometric distribution, its asymmetry decreases significantly as $m$ and $M_b$ increases.

Moreover, the lower percentiles of the RL distribution are almost equal for all combinations of $m$, $M_b$ and $(\hat{\mu}_0, \hat{\sigma}_0)$, but the same statement is not true for the upper percentiles. As $m$ and $M_b$ increases, the upper percentiles become closer to the corresponding percentiles of the RL distribution of the $\overline{Y}$-chart with exact CL's, implemented for samples of size $n = 5$.

As $n$ increases, the benefits of using the bootstrap methodology become irrelevant. We obtain SDRL values smaller, but the ARL values are smaller too, which is not desirable.

Finally, when it is not possible to consider a large reference sample or there is not available a modified chart parameter, $K$, that takes into consideration the variability introduced by the estimation of the nominal process values, the use of the bootstrap methodology should be explored because it can lead to some improvements in the performance of the chart.

## Aknowledgments

Research partially supported by National Funds through FCT - Fundação para a Ciência e a Tecnologia, project PEst-OE/MAT/UI0006/2014 (CEAUL).

## References

1. Balakrishnan, N. and Kocherlakota, S., "Effects of nonnormality on $\overline{X}$ charts: single assignable cause model", *Dankhya: The Indian Journal of Statistics*, 48(B), 439–444 (1986).
2. Castagliola, P. and Figueiredo, F., "The median chart with estimated parameters", *European J. Industrial Engineering*, 7(5), 594–614 (2013).
3. Chan, L. K., Hapuarachchi, K. P., and Macpherson, B. D., "Robustness of $\overline{X}$ and $R$ charts", *IEEE Transactions on Reliability*, 37(1), 117–123. (1988).
4. Champ, W. C. and Jones, A. L., "Design Phase I $\overline{X}$ charts with Small Sample Sizes", *Quality and Reliability Mathematical Engineering International*, 20, 497–510 (2004).
5. Chakraborti, S., "Run length, average run length and false alarm rate of Shewhart $\overline{X}$ chart: exact derivations by conditioning", *Communications in Statistics – Simulation and Computation*, 29(1), 61–81 (2000).
6. Chakraborti, S., "Parameter Estimation and Design Considerations in Prospective Applications of the $\overline{X}$ Chart", *Journal of Applied Statistics*, 33(4), 439–459 (2006).
7. Chakraborti, S., "Run Length Distribution and Percentiles: The Shewhart Chart With Unknown Parameters", *Quality Engineering*, 19, 119–127 (2007).
8. Chen, G., "The mean and standard deviation of the run length distribution of $\overline{X}$ charts when control limits are estimated", *Statistica Sinica*, 7(3), 789–798 (1997).
9. Cox, M. G. and Iguzquiza, E. P., "The total median and its uncertainity", in *Advanced Mathematical and Computational Tools in Metrology*, Ciarlini *et al.*, Eds, 106–117 (2001).
10. Davison, A. and Hinkley, D.V., *Bootstrap Methods and their Application*, Cambridge University Press (2006).
11. Dull, R.B. and Tegarden, D.P., "Using control charts to monitor financial reporting of public companies", *Int. J. of Accounting Information Systems*, 5, 109–127 (2007).

12. Efron, B., "Bootstrap methods: another look at the jackknife", *Ann. Statist.*, 7(1), 1–26 (1979).
13. Efron, B. and Tibshirani, R.J., *An Introduction to the Bootstrap*, Chapman and Hall (1993).
14. Figueiredo, F., "Robust estimators for the standard deviation based on a bootstrap sample", *Proc. 13th European Young Statisticians Meeting*, 53–62 (2003).
15. Figueiredo, F. and Gomes, M.I., "The total median is Statistical Quality Control", *Applied Stochastic Models in Business and Industry*, 20, 339–353 (2004).
16. Jensen, W. A., Jones-Farmer, L. A., Champ, C. H., and Woodall, W.H., "Effects of Parameter Estimation on Control Chart Properties: A Literature Review", *J. Quality Technology*, 38, 349–364 (2006).
17. MacCarthy, B.L. and Wasusri, T., "A review of non-standard applications of statistical process control (SPC) charts", *Int. J. of Quality and Reliability Management*, 19, 295–320 (2002).
18. Montgomery, D.C., *Introduction to Statistical Quality Control: a Modern Introduction*, 6th edition, John Wiley & Sons (2009).
19. Nedumaran, G. and Pignatiello, J.J., "On Estimating $\overline{X}$ Control Limits", *J. Quality Technology* 33(2), 206–212 (2001).
20. Quesenberry, D.C., "The Effect of Sample Size on Estimated Limits for $\overline{X}$ and $X$ Control Charts", *J. Quality Technology*, 25(4), 237–247 (1993).
21. Rocke, D.M., "Robust control charts", *Technometrics*, 31(2), 173–184 (1989).
22. Rocke, D.M., "$\overline{X}_Q$ and $R_Q$ charts: robust control charts", *The Statistician*, 41, 97–104 (1992).
23. Schoonhoven, M., Riaz, M., and Does, R.J.M.M., "Design and Analysis of Control Charts for Standard Deviation with Estimated Parameters", *J. Quality Technology*, 43(4), 307–333 (2011).
24. Schoonhoven, M., Nazir, H.Z., Riaz, M., and Does, R.J.M.M., "Robust Location Estimators for the $\overline{X}$ Control Chart", *J. Quality Technology*, 43(4), 363–379 (2011).
25. Schilling, E.G. and Nelson, P.R., "The Effect of Non-Normality on the Control Limits of the $\overline{X}$ Charts", *J. Quality Technology*, 8(4), 183–188 (1976).
26. Vardeman, S., Hamada, M.S., Burr, T., Morris, M., Wenderberger, J., Jobe, J.M., Moore, L., and Wu, H., "an Introduction to Statistical Issues and Methods in Metrology for Physical Science and Engineering", *J. Quality Technology*, 46(1), 33–62 (2014).
27. Woodall, W.H. and Montgomery, D.C., "Research Issues and Ideas in Statistical Process Control", *J. Quality Technology*, 31(4), 376–386 (1999).
28. Woodall, W.H. and Montgomery, D.C., "Some Current Directions in the Theory and Application of Statistical Process Control", *J. Quality Technology*, 46(1), 78–94 (2014).
29. Zhang, Y. and Castagliola, P., "Run Rules $\overline{X}$ Charts When Process Parameters Are Unknown", *Int. J. of Reliability, Quality and Safety Engineering*, 17(4), 381–399 (2010).

# Statistical design of an adaptive control chart for linear profile monitoring

**Maysa S. De Magalhães[1], Viviany L. Fernandes[2] and Francisco D. Moura Neto[3]**

[1]National School of Statistical Sciences, Brazilian Institute of Geography and Statistics (ENCE/IBGE), Rio de Janeiro, Brazil
Email: maysa.magalhaes@ibge.gov.br
[2,3]Polytechnic Institute, State University of Rio de Janeiro (IPRJ/UERJ), Nova Friburgo, RJ, Brazil
[2]Email: vivianylefer@hotmail.com
[3]Email: fmoura@iprj.uerj.br

**Abstract:** In some production processes the quality characteristics can be represented by profiles or linear functions. We propose an adaptive control chart to monitor the coefficient vector of a simple linear regression model, once fixed parameter control charts are slow in detecting small to moderate shifts in the process parameters, that is, the intercept and the slope. A study on the performance of the proposed control chart was done, considering the adjusted average time until a signal.
**Keywords:** Linear profile, Adaptive control chart, Markov chain

## 1 Introduction

In adaptive control charts, one or more design parameters vary in real time during the production process based on recent data obtained from the process. Authors who have been studying this subject have shown that these charts present superior performance when compared to a fixed parameter control chart. Approaches for the design of univariate adaptive control charts have been proposed by several authors, as for example, Reynolds *et al.* (1988), Amin and Miller (1993), Costa (1994, 1997), De Magalhães *et al.* (2002, 2009).

In some processes, however, the simultaneous control of two or more related quality characteristics is necessary, considering that, the design of multivariate fixed parameter and adaptive control charts have been studied by several authors, see for example, Aparisi (1996, 2001), Bersimis *et al.* (2007), Zhang

*Stochastic Modeling, Data Analysis and Statistical Applications* (*pp*. 515-528)
Lidia Filus - Teresa Oliveira - Christos H Skiadas (Eds)



and Shing (2008). Adaptive control schemes have shown better performance than fixed parameter control schemes in detecting small and moderate process shifts.

Nonetheless, some quality characteristics are best represented by a functional relationship between a response variable and one or more explanatory variables, that is, in this case, the quality characteristic is expressed by a function or profile (see, Kang and Albin, 2000; Kim *et al.*, 2003; Zhang and Albin, 2009; Mahmoud *et al.*, 2010; Moura Neto and De Magalhães, 2012). The monitoring of profiles is used to verify the stability of this relationship over time. When the profile does not suffer alteration, it is said that the process is under control. However, if any excessive variation occurs, it is said that the process is out of control, thus, requiring investigation procedures and remedial actions. Some applications of profile monitoring methods include lumber manufacturing (Staudhammer *et al.*, 2007) and calibration of instruments and machines (Stover and Brill, 1998; Kang and Albin, 2000).

Kang and Albin (2000) proposed a fixed parameter chi-square control chart to monitor the intercept and the slope of a linear profile represented by a simple linear regression model.

In this paper, we propose a model for the statistical design of a chi-square control chart with variable sample size and sampling intervals for the monitoring of linear profiles. The performance measure is obtained through a Markov chain approach. The performance of the variable sample size and sampling intervals chi-square chart (VSSI $\chi^2$ control chart) is compared to the fixed parameter chi-square chart (FP $\chi^2$ chart) proposed by Kang and Albin (2000) to monitor the intercept and the slope of a model. Numerical comparisons between these charts are made considering the semiconductor manufacturing process studied in the paper of Kang and Albin.

## 2. VSSI $\chi^2$ control chart

Based on the studies of Kang and Albin (2000) and Costa (1997), we propose the variable sample size and sampling intervals chi-square chart for monitoring a linear profile. As the chart considered in Kang and Albin, the proposed chart aims to monitor the intercept ($\beta_0$) and the slope coefficient ($\beta_1$) of a simple linear regression model.

It is considered a production process where the quality of the produced items is evaluated by the value of a measurable characteristic $Y$ which is a linear function of an independent variable $x$, that is,

$$Y = \beta_0 + \beta_1 x + \varepsilon$$

where $\beta_0$ and $\beta_1$ are parameters, $\varepsilon$'s are independent random variables normally distributed with mean zero and variance $\sigma^2$ (denoted by, $\varepsilon \sim N(\mu, \sigma^2)$). It is assumed, in matrix notation, that the parameters $\boldsymbol{\beta} = [\beta_0 \ \ \beta_1]^T$ and $\sigma^2$ of the model, when the process is under control, are

$$\sigma = \sigma_*$$

known, more specifically, $\boldsymbol{\beta} = \boldsymbol{\beta}_* = [\beta_*^0 \ \ \beta_*^1]^T$ and . Then, from the observations, the aim is to verify if the process remains under control, i.e., if the parameters have not changed. Changes or deviations from the parameter vector $\boldsymbol{\beta} = [\beta_0 \ \beta_1]^T$ are analyzed. When the process is out of control, the parameter vector is given by:

$$\tilde{\boldsymbol{\beta}} = [\beta_*^0 + \delta_0 \sigma_* \ \ \beta_*^1 + \delta_1 \sigma_*]^T$$

where $\boldsymbol{d} = [(\delta_0 \ \ \delta_1)$ represents the vector of the shifts, where $\delta_0$ and $\delta_1$ are, respectively, the magnitude of the shift in the intercept and the slope.

## *2.1 The statistic used in the monitoring of the process*

Consider that the profile $Y$ is measured in the values of the independent variable, $x = x_j$, $j = 1,..., n_k$, where $n_k = n_1$ or $n_k = n_2$, depending on the size of the sample that is being used; then, for each sample $i$ of size $n_k$ , $k=1, 2,$ the profile monitored is: $Y_1 i = \beta_1 i0 + \beta_1 i1 \, x_1 j + (_1 ij$ . For each sample $i$ composed by a set data $(x_1 \ y_{i1})$, $(x_2 \ y_{i2}), \ldots, (x_{nk} \ y_{ink})$ the least square estimators for parameters $\beta_0$ and $\beta_1$ are obtained and the estimator of the vector of parameters is denoted by $\hat{\boldsymbol{\beta}}_i = [\hat{\beta}_{i0}, \hat{\beta}_{i1}]$. The expressions of $\hat{\beta}_{i0}$ and $\hat{\beta}_{i1}$ are given by,

$$\hat{\beta}_{i0} = \bar{Y} - \hat{\beta}_{i1} \bar{X}$$

$$\hat{\beta}_{i1} = \frac{\sum_{j=1}^{nk}(x_j - \bar{x})(Y_{ij} - \bar{Y})}{\sum_{j=1}^{nk}(x_j - \bar{x})^2}, \qquad k = 1,2$$

For each sample $i$ taken from the process, it is assumed that $x_j$, $1 \leq j \leq n_k$, $k = 1, 2$, with $x_1 < x_2 < x_3 < \cdots < x_{n_k}$, are pre-set values for all samples taken.

The proposed control chart monitors the parameters $\beta$'s, to verify if the process is in control, that is, if the parameters $\beta_0$ and $\beta_1$ have not shifted. The statistic used in the control chart for monitoring the process is given by,

$$\chi_i^2 = \left[(\hat{\beta}_i - \beta_*)' \Sigma^{-1} (\hat{\beta}_i - \beta_*)\right]$$

where $\hat{\beta}_i = [\hat{\beta}_{i0}, \hat{\beta}_{i1}]$, the matrix $\Sigma$, the covariance-variance matrix of $\hat{\beta}_0$ and $\hat{\beta}_1$, and the vector $\beta_*$ are known.

When the process is in control, $\chi_i^2$ has chi-square distribution with two degrees of freedom and the upper control limit is equal to $\chi_{2,\alpha}^2$, that is, $UCL = \chi_{2,\alpha}^2$ where $\chi_{2,\alpha}^2$ is the $\alpha$ percentile point of the chi-square distribution. If $\chi_i^2 < \chi_{2,\alpha}^2$, it is assumed that the process is in control.

## *2.2 Surveillance policy*

The chi-square control chart with variable sample size and sampling intervals has, besides the upper control limit (*UCL*), a warning limit, $w$, such that $w < UCL$

. In contrast to the control chart used by Kang and Albin (2000), which has a fixed sample size ($n_0$) and sampling interval ($h_0$), the proposed control chart makes use of two different sample sizes, $n_1$ and $n_2$ such that $n_1 < n_0 < n_2$ and two different sampling intervals, $h_1$ and $h_2$ such that $h_2 < h_0 < h_1$.

A sample *i* of size $n_1$ or $n_2$ is taken randomly and estimates of $\hat{\beta}_i$, the parameter vector of the regression model, are obtained. Then, subsequently, the statistic $\chi_i^2$ is calculated and plotted in the VSSI $\chi^2$ control chart.

Regarding the sample size to be used, if $0 < \chi_{i-1}^2 < w$, the sample *i* will have size $n_1$ and should be taken after a long time interval, that is $h_1$, if $w < \chi_{i-1}^2 < UCL$, the sample *i* will have size $n_2$ and should be taken after a short time interval, that is $h_2$; finally, if $\chi_{i-1}^2 > UCL$, the process may be out of control. In this case, an investigation should be initiated to verify if there are indeed non-random causes acting in the process, so that corrective action can be undertaken. Otherwise, if an assignable cause is not found the process is considered in control and in this case the signal produced by the chart is a false alarm event.

The probability of a false alarm, that is, the probability of $\chi_i^2$ be greater than *UCL* given that the process is control is

$$\alpha = P(\chi_1^2 \geq UCL \mid \beta_1 \sim N(\beta_1, \Sigma))$$

.

## 3. Performance measure

As Costa (1997) to explicitly obtain all the expressions of the statistical model, the production process was represented by a Markov chain with five states:

State 1: if $\chi_i^2 \in [0, w]$ and the process is in control;

State 2: if $\chi_i^2 \in (w, UCL]$ and the process is in control;

State 3: if $\chi_i^2 \in [0, w]$ and the process is out of control;

State 4: if $\chi_i^2 \in (w, UCL]$ and the process is out of control;

State 5 (absorbing state): if $\chi_i^2 \in (UCL, \infty)$ .

It is necessary to obtain the transition probabilities to calculate the performance measure. The matrix of transition probabilities between the five states is given by

$$P = \begin{bmatrix} p_{11} & p_{12} & p_{13} & p_{14} & p_{15} \\ p_{21} & p_{22} & p_{23} & p_{24} & p_{25} \\ 0 & 0 & p_{33} & p_{34} & p_{35} \\ 0 & 0 & p_{43} & p_{44} & p_{45} \\ 0 & 0 & 0 & 0 & 1 \end{bmatrix}$$

where $p_{lm}$ denotes the transition probability to go from state l (previous state) to state m (present state).

The transition probabilities between the four transient states are given by

$$p_{11} = P\left[\chi_i^2 < w | \chi_i^2 < UCL\right] P\left[T > h_1\right] = \frac{P[\chi_i^2 < w]}{P[\chi_i^2 < UCL]} \cdot e^{-\lambda h_1}$$

$$p_{12} = P\left[w < \chi_i^2 < UCL | \chi_i^2 < UCL\right] P\left[T > h_1\right] = \frac{P[w < \chi_i^2 < UCL]}{P[\chi_i^2 < UCL]} \cdot e^{-\lambda h_1}$$

$$p_{21} = P[\chi_i^2 < w | \chi_i^2 < UCL] P[T > h_2] = \frac{P[\chi_i^2 < w]}{P[\chi_i^2 < UCL]} \cdot e^{-\lambda h_2}$$

$$p_{22} = P[w < \chi_i^2 < UCL | \chi_i^2 < UCL] P[T > h_2] = \frac{P[w < \chi_i^2 < UCL]}{P[\chi_i^2 < UCL]} \cdot e^{-\lambda h_2}$$

$$p_{13} = P[\chi_i^2 < w | \chi_i^2 < UCL]\ P[T < h_1] = \frac{P[\chi_i^2 < w]}{P[\chi_i^2 < UCL]} \cdot [1 - e^{-\lambda h_1}]$$

$$p_{14} = P[w < \chi_i^2 < UCL\ | \chi_i^2 < UCL]\ P[T < h_1] = \frac{P[w < \chi_i^2 < UCL]}{P[\chi_i^2 < UCL]} \cdot [1 - e^{-\lambda h_1}]$$

$$p_{23} = P[\chi_i^2 < w | \chi_i^2 < UCL]\ P[T < h_2] = \frac{P[\chi_i^2 < w]}{P[\chi_i^2 < UCL]} \cdot [1 - e^{-\lambda h_2}]$$

$$p_{24} = P[w < \chi_i^2 < UCL | \chi_i^2 < UCL]\ P[T < h_2] = \frac{P[w < \chi_i^2 < UCL]}{P[\chi_i^2 < UCL]} \cdot [1 - e^{-\lambda h_2}]$$

$$p_{33} = P\left[\chi_i^2 < \frac{w}{\gamma^2} \,\middle|\, \chi_i^2 \sim \chi_2^2(\tau_1))\right]$$

$$p_{34} = P\left[\frac{w}{\gamma^2} < \chi_i^2 < \frac{UCL}{\gamma^2} \,\middle|\, \chi_i^2 \sim \chi_2^2(\tau_1)\right]$$

$$p_{43} = P\left[\chi_i^2 < \frac{w}{\gamma^2} \,\middle|\, \chi_i^2 \sim \chi_2^2(\tau_2)\right]$$

$$p_{44} = P\left[\frac{w}{\gamma^2} < \chi_i^2 < \frac{UCL}{\gamma^2} \,\middle|\, \chi_i^2 \sim \chi_2^2(\tau_2)\right]$$

It is assumed that the process starts in control and sometime in the future it goes to out of control and, also, the time that the process remains in control is exponentially distributed with parameter $\lambda$.

The performance of the proposed chart, that is, the VSSI $\chi^2$ control chart, was compared to the FP $\chi^2$ control chart proposed by Kang and Albin (2000) for the monitoring of linear profiles. The performance measure utilized in this article is the adjusted average time to signal.

## *3.1 Adjusted average time to signal*

The adjusted average time to signal (*AATS*) is the expected time since the instant that the process goes to an out of control state until a signal, that is, until a sample generates a value of statistic $\chi_i^2$ above the *UCL*. When the process is out of control, it is expected that this situation be quickly detect, and then small values of *AATS* are desired. On the other hand, large values of *AATS* are expected when the process is in control. The *AATS* values depend on the magnitude of shift in the process parameters, that is, on the $\boldsymbol{d} = (\delta_0 \;\; \delta_1)$ $\gamma$.

vector as well as on

The expression for the adjusted average time to signal is given by:

$AATS = E(TC) - E(T)$, then $AATS = E(TC) - \frac{1}{\lambda}$

where $E(TC)$ represents the average time of the production cycle, that is, the average time since the beginning of the production process until a signal after an occurrence of a process shift and, $E(T)$ denotes the time the process remains in control.

The expression for the average time of the production cycle is given by:

$$E(TC) = \begin{bmatrix} P_1^{(0)} & P_2^{(0)} & P_3^{(0)} & P_4^{(0)} \end{bmatrix} \left( \begin{bmatrix} 1 & 0 & 0 & 0 \\ 0 & 1 & 0 & 0 \\ 0 & 0 & 1 & 0 \\ 0 & 0 & 0 & 1 \end{bmatrix} \begin{bmatrix} p_{11} & p_{12} & p_{13} & p_{14} \\ p_{21} & p_{22} & p_{23} & p_{24} \\ p_{31} & p_{32} & p_{33} & p_{34} \\ p_{41} & p_{42} & p_{43} & p_{44} \end{bmatrix} \right)^{-1} \begin{bmatrix} h_1 \\ h_2 \\ h_1 \\ h_2 \end{bmatrix}$$

where the transition probabilities are given above and $\begin{bmatrix} P_1^{(0)} & P_2^{(0)} & P_3^{(0)} & P_4^{(0)} \end{bmatrix}$ is the vector of initial probabilities with $P_1^{(0)} = P(\chi_i^2 < w | \chi_i^2 < UCL)$, $P_2^{(0)} = 1 - P_1^{(0)} = 1 - P(\chi_i^2 < w | \chi_i^2 < UCL)$, $P_3^{(0)} = 0$ and $P_4^{(0)} = 0$.

The expression for $E(TC)$ depends on the cumulative probability function of a central chi-square distribution with two degrees of freedom, and a non-central chi square distribution with two degrees of freedom with non-centrality parameter given by $\left[ \frac{1}{\gamma^2 (n]_k (\delta_0 + \delta_1 \bar{X})^2} + \delta_1^2 S_{xx} \right)$, $k = 1,2$

To compare the performance of the VSSI $X^2$ control chart and the FP $X^2$ control chart, we use the *AATS*, for a given value of the shift parameters. However, for the comparison to be fair, the same amount of resources/effort spent with inspections and false alarms, when the process is in control, should be imposed. This is done by the following constraints

$$n_1 P(\chi_i^2 < w | \chi_i^2 < UCL) + n_2 \left\{ 1 - P(\chi_i^2 < w | \chi_i^2 < UCL) \right\} = n_0$$

$$h_1 P(\chi_i^2 < w | \chi_i^2 < UCL) + h_2 \left\{ 1 - P(\chi_i^2 < w | \chi_i^2 < UCL) \right\} = h_0$$

## 4. Comparing charts

In this section, we compare the performance of the VSSI $\chi^2$ and the FP $\chi^2$ control charts for monitoring linear profiles relative to the detection speed of an out-of-control state considering several shifts magnitudes on the parameters.

For comparison purposes, the application of the developed statistical model for the VSSI $\chi^2$ control chart for monitoring linear profiles is shown by the numerical example of Kang and Albin (2000), which consists of a calibration application in a production process of semi-conductors, where several thousand inscriptions of chips need to be provided in a wafer. The critical device in this process is a mass flow controller (*MFC*). The pressure measure in the chamber is approximately a linear function of the mass flux through the *MFC*. In the example presented by Kang and Albin (2000), the chart employed is the FP $\chi^2$ control chart in which a single sample size $(n_0 = 4)$ is used. Moreover, based on the work of Costa (1997) and taking into account the following restrictions $n_1 < n_0 < n_2$, $h_2 < h_0 < h_1$, then the following design parameters were used: $n_0$=4, $h_0$=1, $\alpha_0$=0.005, for the FP $\chi^2$ chart; and $n_0$=4, $n_1$=2, $n_2$=12, $h_0$=1, $h_1$=1, 2, $h_2$=0.2, $\alpha_0$=0.005, for the VSSI $\chi^2$ chart. Again, based on the work of Costa (1997), we considered $\frac{1}{\lambda} = \frac{1}{0{,}0001}$.

As we are considering the example proposed by Kang and Albin (2000) and also as we are going to compare the chart proposed by them and our proposed chart, the shifts $\delta_0$ in $\beta_0^*$ varied from 0.2 to 2.0 in steps of 0.2, the shifts $\delta_1$ in $\beta_1^*$ assumed values from 0.025 to 0.250 in steps of 0.025.

Then, with the design parameters considered above, performance measures were calculated for the proposed chart. The results are presented in Tables 1 to 4.

Table 1 presents the values of the *AATS* for both charts with respect to the values of the shift parameter $\delta_0$. Table 2 and Fig.1 present the percentage gain of VSSI chart relative to FP chart as a function of intercept shifts.

**Table 1.** *AATSs* for both charts with intercept shifts.

| | 0.0 | 0.2 | 0.4 | 0.6 | 0.8 | 1.0 | 1.2 | 1.4 | 1.6 | 1.8 | 2.0 |
|---|---|---|---|---|---|---|---|---|---|---|---|
| $\chi^2$ Chart | $\delta_0$ | | | | | | | | | | |
| FP | 200.5 | 138.24 | 63.96 | 28.45 | 13.69 | 7.38 | 4.49 | 3.08 | 2.35 | 1.95 | 1.73 |
| VSSI | 200.5 | 129.43 | 40.38 | 10.46 | 4.31 | 2.93 | 2.43 | 2.16 | 1.98 | 1.86 | 1.78 |

**Table 2.** Percentage gain of VSSI chart relative to FP chart as a function of intercept shifts.

| | 0.0 | 0.2 | 0.4 | 0.6 | 0.8 | 1.0 | 1.2 | 1.4 | 1.6 | 1.8 | 2.0 |
|---|---|---|---|---|---|---|---|---|---|---|---|
| $\chi^2$ Chart | $\delta_0$ | | | | | | | | | | |
| VSSI | 0.00 | 0.06 | 0.37 | 0.63 | 0.69 | 0.60 | 0.46 | 0.30 | 0.16 | 0.05 | -0.03 |

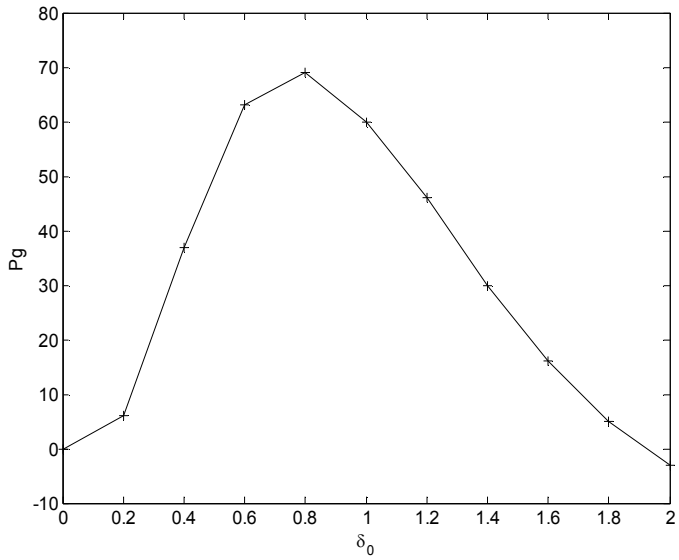


**Fig.1.** Percentage gain of VSSI chart with respect to FP chart as a function of intercept shifts.

As may be seen in Table 1, when the process is in control the *AATS* is equal to 200.5. It can be observed from this table that from small to moderate shifts in the intercept $(\delta_0 \leq 1.0)$, the VSSI $\chi^2$ chart is always quicker than the FP $\chi^2$ control chart, for the design parameters considered. Still the performance of the VSSI $\chi^2$ chart is superior to the FP $\chi^2$ control chart for shifts of magnitude $(\delta_0 \leq 1.8)$ for the design parameters considered. In contrast, in the presence of large shifts when $(\delta_0 = 2.0)$, the FP $\chi^2$ control chart is more efficient than the VSSI $\chi^2$ chart; although in this case, the average number of samples until a signal is below 2.0 for the VSSI $\chi^2$ chart.

From Table 2 and Fig.1, we can observe when $0.2 \leq \delta_0 \leq 0.8$, the percentage gain varies, approximately, from 6% to 69% and when $1.0 \leq \delta_0 \leq 1.8$, the percentage gain varies, approximately, from 60% to 5%, for the design parameters considered. When $\delta_0 = 2.0$, it is preferable to use the FP $\chi^2$ chart instead of the VSSI $\chi^2$ chart, in the case considered.

Table 3 presents the values of the *AATS* for both charts with respect to the values of the shift parameter $\delta_1$ . Table 4 and Fig.2 present the percentage gain of VSSI chart relative to FP chart as a function of slope shifts.

**Table 3.** *AATSs* for both charts with slope shifts.

| | 0.000 | 0.025 | 0.050 | 0.075 | 0.100 | 0.125 | 0.150 | 0.175 | 0.200 | 0.225 | 0.250 |
|---|---|---|---|---|---|---|---|---|---|---|---|
| $\chi^2$ Chart | $\delta_1$ | | | | | | | | | | |
| FP | 200.5 | 166.50 | 106.09 | 61.18 | 34.98 | 20.62 | 12.73 | 8.30 | 5.73 | 4.19 | 3.24 |
| VSSI | 200.5 | 162.35 | 87.70 | 35.39 | 13.49 | 6.29 | 3.98 | 3.12 | 2.70 | 2.43 | 2.25 |

**Table 4.** Percentage gain of VSSI chart relative to FP chart as a function of slope shifts.

| | 0.000 | 0.025 | 0.050 | 0.075 | 0.100 | 0.125 | 0.150 | 0.175 | 0.200 | 0.225 | 0.250 |
|---|---|---|---|---|---|---|---|---|---|---|---|
| $\chi^2$ Chart | $\delta_1$ | | | | | | | | | | |
| VSSI | 0.00 | 0.02 | 0.17 | 0.42 | 0.61 | 0.69 | 0.69 | 0.62 | 0.53 | 0.42 | 0.31 |

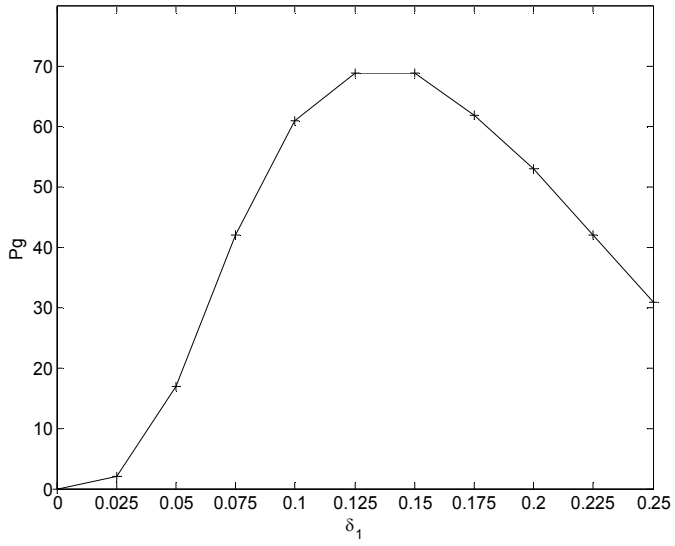


**Fig.2.** Percentage gain of VSSI chart with respect to FP chart as a function of slope shifts.

As may be seen in Table 3, when the process is in control the *AATS* is equal to 200.5. It can be observed from this table that for all considered shifts in the slope, the VSSI $\chi^2$ chart is always quicker than the FP $\chi^2$ control chart, for the design parameters considered.

From Table 4 and Fig.2, we can observe when $0.025 \leq \delta_1 \leq 0.150$, the percentage gain varies, approximately, from 2% to 69% and when $0.175 \leq \delta_0 \leq 0.250$, the percentage gain varies, approximately, from 62% to 31%, for the design parameters considered.

## 5. Conclusions

In this article, a model for the statistical design of a chi-square control chart with variable sample size and sampling interval for monitoring a linear profile was developed. This chart contemplates the monitoring of the intercept and the slope coefficient of a linear regression model. The proposed chart was developed based on the fixed parameter chi-square control chart existent in the literature for monitoring a linear profile employed by Kang & Albin (2000). Comparisons between the two charts considered the adjusted average time until a signal

(*AATS*). From a numerical example, the performance comparison between the two charts showed, in general, a better statistical performance for the VSSI chi-square chart.

## Acknowledgments

The authors acknowledge the partial financial support from the Brazilian Council for Scientific and Technological Development (CNPq), the State of Rio de Janeiro Research Foundation (FAPERJ), and the Brazilian Council for the Improvement of Higher Education (CAPES).

## References

1. R.W. Amin and R.W. Miller. A robustness study of $\overline{X}$ charts with variable sampling intervals. *Journal of Quality Technology*, **25**, 35-44, 1993.
2. F. Aparisi. Hotelling's $T^2$ control chart with adaptive sample sizes. *International Journal of Production Research*, **34**, 2835-2862, 1996.
3. F. Aparisi and C.L. Haro,. Hotelling's $T^2$ control chart with sampling intervals, *International Journal of Production Research*, **39**, 3127–3140, 2001.
4. Bersimis, S., Psarakis, S., and Panaretos, J., Multivariate statistical process control charts: an overview, Quality and Reliability Engineering International, **23**, 517–543, 2007.
5. Costa, A.F.B., $\overline{X}$ charts with variable sampling size, *Journal of Quality Technology*, **26**, 155-163, 1994.
6. Costa, A.F.B., $\overline{X}$ charts with variable sample size and sampling intervals, Journal of Quality Technology, **29**, 197–204, 1997.
7. De Magalhães, M.S., Costa, A.F.B., and Epprecht, E.K., Constrained optimization model for the design of an adaptive $\overline{X}$ chart, *International Journal of Production Research*, 40, 3199–3218, 2002.
8. De Magalhães, M. S., Costa, A.F.B., and Moura Neto, F.D., A hierarchy of adaptative $\overline{X}$ control charts, *International Journal of Production Economics*, **119**, 271-283, 2009.
9. Kang, L. and Albin, S.L., On-line monitoring when the process yields a linear profile, *Journal of Quality Technology*, **32**, 418-426, 2000.
10. Kim, K., Mahmoud, M., and Woodall, W.H., On the monitoring of linear profiles, *Journal of Quality Technology*, **35**, 317-328, 2003.

11. Mahmoud, M.A., Morgan, J.P., and Woodall, W.H., The monitoring of simple linear regression profiles with two observations per sample, *Journal of Applied Statistics*, **37**, 1249-1263, 2010.
12. Moura Neto, F.D. and De Magalhães, M.S., A laplacian spectral method in phase analysis of profiles, *Applied Stochastic Models in Business and Industry*, **28**, 251-263, 2012.
13. Reynolds Jr., M.R., Amin, R.W., Nachlas, J.C., $\bar{X}$ charts with variable sampling intervals, *Technometrics*, **30**, 181-192, 1988.
14. Staudhammer, C., Maness, T.C., and Kozac, R.A., Profile charts for monitoring lumber manufacturing using laser range sensor data, *Journal of Quality Technology*, **39**, 224-240, 2007.
15. Stover, F.S. and Brill, R.V., Statistical quality control applied to ion chromatography Calibrations, *Journal of Chromatography A*, **804**, 37-43, 1998.
16. Zhang, H. and Albin, S., Detecting outliers in complex profiles using a $\chi^2$ control chart method, ***IIE*** Transactions, **41**, 335-345, 2009.
17. Zhang, G. and Shing, I., Multivariate EWMA control charts using individual observations for process mean and variance monitoring and diagnosis, *International Journal of Production Research,* **46**, 6855-6881, 2008.

# Control charts for arbitrage-based trading

Angeliki Vyniou[1],Stelios Psarakis[1] and Kostas Triantafyllopoulos[2]
[1]Department of Statistics, Athens University of Economics & Business, Athens, Greece
[2]Department of Probability and Statistics, University of Sheffield, Sheffield, UK

**Abstract:** This paper concerns the role and contribution of SPC methods to pairs trading, a relative-value statistical arbitrage trading technique. Pairs trading and its numerous extensions have gained increased attention over the recent years and is a popular trading strategy among hedge funds and investments boutiques. The core idea of pairs trading is "buy low" and "short-sell high" and it is based on the assumption that the low-valued asset will gain value and the high-valued asset will lose value, so that the two assets are co-evolving or mean-reverting. Several authors have recently suggested that this mean-reversion may be appropriate only at some periods of time (in which profits may be realized) while in other periods of time mean-reversion is lost (resulting to significant losses, e.g. one could buy an asset which loses its value). In this paper we propose the use of appropriate SPC methods in order to detect mean-reversion, hence to identify tradable periods. The literature on pairs trading will be reviewed and examples will illustrate the need for a monitoring procedure. Finally, control charts for autocorrelated processes are proposed for the detection of mean-reversion.
**Keywords:** pairs-trading, control charts, SPC, autocorrelated processes, financial data, mean-reversion

## 1. Introduction

Pairs trading is a very common trading strategy among hedge funds and institutional investors because of the consistent, though usually modest, profitability. The strategy requires the choice of two assets whose prices are influenced by the same economic forces. The consequence of this is that the prices of these two assets actually co-move. The second step is to detect the time point that these prices diverge from their long term equilibrium so as to take action and short sell the overvalued share and buy the undervalued one. Profit is generated when the prices return to their long term equilibrium state. Several researchers propose methods and techniques for selecting the appropriate pairs of assets, identifying the spread magnitude that should trigger a trade, predict the next step of the process so as to proceed or not to opening a position.

More specifically, in order to apply a pairs trading strategy traders

*Stochastic Modeling, Data Analysis and Statistical Applications* (*pp*. 529-541)
Lidia Filus - Teresa Oliveira - Christos H Skiadas (Eds)


choose a pair of assets and decide on trading their spread. The spread of these assets could be defined as the difference of the prices of these assets or another linear combination of the two prices. The rationale behind profit generation is quite simple. When the price of one asset is low the trader buys this asset while simultaneously short-sell the other whose price is at that time high. Then it is said that the trader opens a position. Short-selling means that the trader lends an amount of shares and sells them. These shares though must be returned sometime in the future. To close the position the trader must sell the number of shares bought and buy the shares of the "short-sold" asset, in order to return them. Profits are generated when the price of the undervalued asset increases whereas the price of the overvalued asset decreases. For book length versions on pairs trading one can refer to Ehrman [1], Vidyamurthy [2] and Whistler [6].

There is a main assumption made for financial markets, which affects trading strategies, that is efficient market hypothesis (Fama [4]). This assumption is based on that information is considered to be instantly and equally distributed among all market participants. Therefore, it is argued that all relevant information is reflected and incorporated in current asset prices. A direct result of this assumption is that no excessive returns can be gained. Applying a pairs trading strategy, though, gives investors the opportunity to exploit temporary market inefficiencies, disturbances of the levels of asset prices that do not last long, and therefore, benefit from the excessive returns which then can be generated.

There are three main methods on pairs trading considered in the literature. The distance method proposed by Gatev *et al.* [5], according to which the pairs chosen are the ones that have the smallest sum of squared deviations. Although this method is cost efficient, it is based on the assumption that the price differences follow a standardized normal distribution while it is known that share prices usually follow a log-normal distribution.

The second is the correlation method discussed in Ehrman [2]. In his book he proposes to consider the correlation of a pair of shares as a factor affecting the selection of appropriate pairs to be traded. It is suggested that in cases when the correlation coefficient is greater than or equal to 0.7 then a pair of assets could be considered tradable. Moreover, it is recommended that the correlation coefficients be measured and monitored at several time intervals so as to detect any changes in the assets relation.

The third is cointegration method introduced in Engel and Granger [6] and Engel and Yoo [7]. According to this method two non-stationary price time series are said to be co-integrated when there exists at least one linear combination of them that is a stationary process see Figure 1. Moreover, the co-integrated pair is assumed to have a long-term equilibrium and a self adjustment mechanism that is triggered when deviations from the equilibrium state occur.

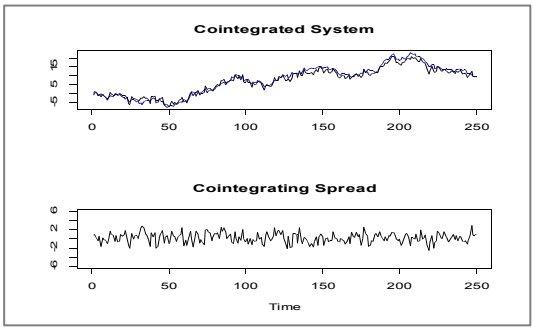


**Figure 1.** Cointegrated assets and their spread

Other approaches that can be found in the literature are those of stochastic modeling, copulas and artificial neural networks. Scholars also model the spread process either in the context of continuous (Ornstein-Ulenbeck processes) or discrete time. Several empirical studies have also been conducted to investigate the effectiveness of this trading strategy in different markets under various economic conditions.

As previously mentioned there are many studies published concerning pairs-trading. In this paper a review of some recently proposed methodologies will be presented as well as the potential of using Statistical Process Control methods in the pairs trading context. The studies that investigate the statistical properties of this trading strategy are to be presented in the next section. In Section 3 the potential of the use of Statistical Process Control techniques in the context of pairs-trading is to be investigated. In the last section the main conclusions of the study as well as some issues for further research are to be summarized.

## 2. Literature review – Pairs trading

Several researchers propose methods and techniques for selecting the appropriate pairs of assets, identify the spread magnitude that should trigger a trade, predict the next step of the process so as to proceed or not to opening or closing a position. As mentioned above, there are three main methods to approach a pairs trading strategy that are considered in the literature; the distance method Gatev [5], the correlation method Ehrman [1] and the co-integration mehtod Engel and Granger [6] and Engel and Yoo [7] see Figure 1. Other approaches that can be found in the literature are those of stochastic modeling, copulas and artificial neural networks. Scholars also model the spread process in the context of continuous time – Ornstein-Ulenbeck processes (Ulenbeck-Ornstein [8])– or discrete time. Several empirical studies have also been conducted to investigate the effectiveness of this trading strategy in

different markets under various economical conditions. In this talk a review of the several proposed methodologies will, first, be presented .

Reviewing pairs trading literature it is obvious that most scholars focus on improving the modeling of either spread or prices time series attempting to develop models that better reflect reality. Various models have been developed so far. Some can be found in the studies of Elliot *et al.* [9] who propose the use of a mean reverting Gaussian Markov chain model for the spread of pairs trading strategies. In another study, Dattasharma [10] introduce a general framework that can be used to predict the dependence between two stocks based on any user-defined criterion by applying the concepts of events and episodes. Triantafyllopoulos and Montana [11] propose a Bayesian state-space model for spread processes with time varying parameters. In this study the researchers also developed an on-line estimation algorithm that could be used to monitor data for mean reversion. Gatarek *et al.* [12] suggest a combination of Dirichlet process prior techniques with Bayesian estimation to estimate co-integrated models with non-normal disturbances. Triantafyllopoulos and Han [13] propose a methodology for detecting mean-reverted segments of data streams in algorithmic pairs trading using a state-space model for the spread and propose two new recursive least squares (RLS) algorithms with adaptive forgetting for predicting mean-reversion in real time. Tourin and Yan [14] in their study suggest the use of an optimal stochastic control model to address the problem of analyzing dynamic pairs trading strategies. In Fasen [15] the asymptotic properties of the least squares estimator for the model parameter of a multivariate Ornstein-Uhlenbeck model are investigated. Alrasheedi and Al-Ghamedi [16] apply a Vector Auto-Regressive model (VAR) for the simulation of the time series of two stocks and examine the influence of some of the model parameters on the total profits earned. Improving and developing models is indeed very important since more accurate predictions of assets future prices can then be obtained. Unlike other processes, financial processes are difficult to be predicted because of the nature of financial data and it is generally argued that the best prediction of a tomorrow's asset price is the price of the asset today. This explains the vast amount of studies published on modeling financial time series considering continuous or discrete time. There are also non-parametric approaches proposed for handling financial data, as well. An example is the study of Bogomolov [17] in which a novel non-parametric approach for pairs trading is proposed in which the only assumption to be made is that the statistical properties of the volatility of the spread process remain reasonably constant.

Gatev *et al.* [5] proposed the GGR model for applying a pairs trading strategy. The study leads to the conclusion that excessive returns are likely to be generated for market participants that have relatively low transaction costs and the ability to short sell securities. It is also observed that there is a latent risk factor that affects the profitability of pairs trading over time. Papadakis and Wysocki [18] examine whether accounting information events, such as earnings announcements and analysts' earnings forecasts, have an effect on the profitability of the pairs trading strategy proposed by Gatev *et al.* [5]. Broussard

and Vaihekoski [19] extended the work of Gatev *et al.[5]* through an empirical study showing that the aforementioned investment strategy is profitable even in markets with reduced liquidity. In the study of Wang and Mai [20] a comparison of GGR, Herlemont and FTBD pairs trading openning position strategies is conducted. The main conclusion obtained from this study is that after deducting the trading cost, the absolute income of the three strategies considered is significantly bigger than zero.

Portfolio optimization, i.e. the choice of which assets and the number of stocks from each asset are to be traded in order to attain maximum profits, is another issue considered in pairs trading literature. Perlin [21] suggests a multivariate version of pairs trading which can be used to create an artificial pair for a specific stock using the information associated to $m$ assets. Mudchanatongsuk et al. [22] propose a stochastic control approach to address pairs trading portfolio optimization. Chiu and Wong [23] investigate the continuous-time mean-variance portfolio selection problem considering co-integrated assets. Alsayedand and McGroarty [24] introduce a solution to the portfolio optimization problem when risky arbitrage trading is considered through the introduction of a nonlinear generalization of Ornstein-Uhlenbeck model which takes into consideration important risk factors.

Moreover, the trading costs are also taken into consideration in some studies. Transaction costs are those associated to opening or closing a position. In the study of Lin *et al.* [25] researchers propose the integration of loss limitation within the statistical modeling of pairs trading strategies. In several empirical studies transaction costs are also considered in order to assess the performance of the different methodologies. Trading costs can be significant and if not taken into consideration the returns of applying a pairs trading strategy could be minimized.

Various trading rules have also been proposed in order to perform successful pairs trading. In the study of Song and Zhang [26] pairs trading is investigated and a pairs trading rule is proposed which takes into account profit maximization or losses minimization. The approach of the researchers to address the problem considered is dynamic programming.

Some recent studies also consider the process's microstructure using intra-day data. Microstructure theory focuses on how specific trading mechanisms affect the price formation process. Zebedee and Kasch-Haroutounian [27] in their study examine the microstructure of the co-movement among the returns of stocks on an intra-day basis applying a combination of a traditional lead-lag model with a pseudo-error correction mechanism. Marshall *et al.* [28] investigate the microstructure of pairs trading on an intra-day basis. In other words, they examine the intra-day market characteristics that can be observed when arbitrage opportunities appear. Since pairs trading could be applied on an a daily basis and traders exploit daily market disturbances the examination of process' microstructure is indeed very

interesting.

A basic step in pairs trading is to be able to identify suitable pairs so that the pairs trading to be profitable. To this end, several researchers try to develop an optimal methodology for choosing the most suitable pairs. Gatev *et al.* [5] proposes choosing the pairs having the smallest sum of squared deviations for trading. Ehrman [1] suggests pairs to be chosen using the correlation coefficient. When this coefficient is greater than or equal to 0.7, the pair is tradable. Engle [6] introduce co-integration approach and proposed choosing pairs whose prices are co-integrated. In the study of Huck [29] the sensitivity of pairs trading strategies' returns on the length of the pairs formation period is investigated. Through an example it is shown that the choice of the formation period affects the returns of the strategy employed and after taking into consideration the data snooping bias this result does not change.

Various empirical studies have also been published. In Matteson *et al.* [30] researchers introduce a new methodology in identifying local stationarity of non-stationary processes. Through an empirical approach robust estimates of time varying windows of stationarity are "produced". Moreover, it is proven that using the adaptive window leads to higher returns and, in some cases, holding the positions open for a shorter period of time. Mai and Wang [31] published a limited study on the impact of the structure of the market on the returns of a pure statistical pairs trading. The researchers suggest that the annual rate of return of pairs trading can be improved by choosing the markets the traders are operating in.

Some different approaches have also been recently developed. Huck [29] proposes a methodology that can be used for pairs selection in a highly non-linear environment. The researcher combines forecasting techniques (Neural Networks) and multi-criteria decision making methods to select and trade pairs under pairs trading strategies. Artificial Neural Network models (ANN) are presented by Gomide and Milidiu [32] that are used to predict spread time series. Through obtaining spread predictions, times of the day when to perform a particular Pair Trading can be recommended. The use of copulas in development of pairs trading strategies is investigated in Liew and Wu [33] It is suggested that copulas approach is a good alternative to the traditional ones – distance approach and co-integration approach – since it is not necessary to assume the existence of correlation among the values of the assets to be traded and thus, argued to be realistic and robust.

## 3. Potential of the use of SPC tools

The main questions that arise considering pairs trading are summarized in the following: When is the optimal time to open and close a position? How many trades are optimal in a given time period? What is the optimal time for a position to be kept open? What is the optimal way to handle non-stationary spread processes? What is the optimal way to select pairs? All these questions

should be answered considering the ultimate goal of investors, i.e. maximum profitability, and the distinctive characteristics of financial time series.

Some of these questions could be addressed using Statistical Process Control techniques. Control charts signal when the process monitored is observed to be out of control. Thus, as long as we can model a process and we are able to estimate its long term parameters control charts can be constructed and used to aid traders identify tradable periods, in which they will have to take action, i.e. to open or close a position.

Moreover, control charts could be used to identify mean-reverting periods of a process that is locally mean-reverting (Figure 2). Mean reverting processes are those that are characterized by a long term equilibrium, they present a constant mean and variance in the long run. In case these processes are disturbed and deviate from their equilibrium they are expected to revert within a short time interval.

While this can be observed in some cases mean-reversion could be, as stated before, local, meaning that a series could be mean-reverting during some periods while in others could be non-stationary, non mean-reverting. In this case control charts could be constructed so as to signal when mean reversion is observed. In this case it is of great importance for practitioners to be able to identify mean reverting segments in non-mean reverting processes. This would actually mean that the possible pairs of stocks to be traded are not only the "obvious" ones. Practically a practitioner could arbitrary choose pairs of stocks and monitor their spread to detect periods where it is mean reverting. That would lead to more trading strategies since the pairs to be traded could be "uniquely" chosen by each trader without using any specific rule. That would actually mean higher returns for the traders. Unit root tests, Dickey – Fuller (Dickey and Fuller [34]), Phillips – Perron (Phillips and Perron [35]) KPSS (Kwiatkowski *et al.* [36]), can be employed to check whether a process is integrated of order one or stationary (mean-reverting).

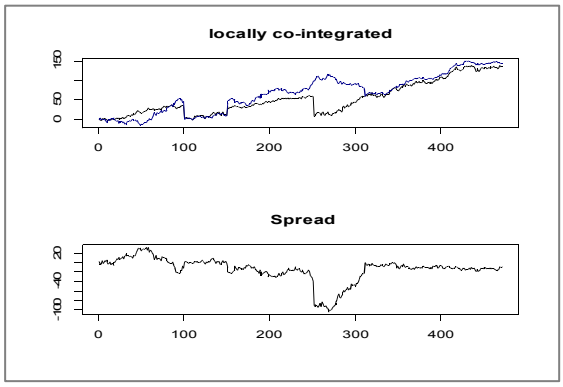


**Figure 2.** Locally co-integrated assets and their spread.

Several surveillance methodologies for detecting I(0) and I(1) segments of time series are developed in the studies of Steland [39], [40], [39] and [40] where he respectively proposes a control chart (stopping time) based on sequential Dickey-Fuller unit root test statistic to detect stationary segments of a time series, a control chart based on weighted Dickey-Fuller unit root test statistic to detect stationarity, a control chart for monitoring sequentially a time series with stopping times based on a sequential version of a kernel-weighted variance-ratio statistic and a sequential monitoring procedure that relies on KPSS unit root test statistic to detect whether the error terms in a polynomial regression model behave as a random walk or as a stationary process. In the study of Steland and Weidauer [41] the researchers investigated a monitoring procedure based on KPSS unit root test to address the problem of detecting sequentially stationary error terms in a multiple regression model, examining the case of co-integration as a special case, as well. The proposed monitoring procedures can be used for developing modifications that would be suitable for being used in the context of pairs trading. This issue is going to be examined further in an other study.

For all the above reasons, this study proposes the use of Statistical Process Control tools, i.e. control charts, as a means to enhance timely detection of potential market inefficiencies. Since mean reverting models are commonly used to describe the spread between the prices of two assets when a pairs trading investment strategy is applied, SPC techniques could be employed to identify tradable periods. The concept of co-integration is largely used in pairs trading literature to describe the relation between two financial variables. Co-integration refers to the co-movement of two time series, which actually means that the two processes considered have common stochastic trends. It has been proven that if the prices are "tied" together there will be a linear combination of them that will be stationary. This linear combination can be the spread of the two prices of interest. In order to estimate the long term mean and variance of the spread we have to estimate the parameters of this process. The unconditional expected value of the dependent variable, spread, is the estimated long-term mean and the unconditional variance is the long-term process variance.

In the context of SPC the long-run mean provides the center line of the control chart to be constructed and the variance assists in the construction of the respective control limits. Autocorrelated processes have been thoroughly investigated in the SPC literature. Several control charts have been proposed for monitoring stationary processes. A residuals control chart for the spread of two co-integrated processes is presented in Figure 3. The combined Shewhart – EWMA control chart of Lu and Reynolds [42] could also be employed to detect shifts of the disequilibrium factor. The rationale is quite simple considering that in pairs trading an appropriate control chart should timely detect step changes (shocks) as well as slow drifts of the process mean. This way short term disturbances would be detected and traders would act accordingly in order to make profitable investments. When the chart signals that would mean that the process is out-of-control which would lead the trader to decide upon opening or

closing a position. While opening a position can be achieved by using a control chart like the one mentioned before, the right time to close the position so as to maximize profits must then be determined. A lower one-sided CUSUM control chart for autocorrelated data could be used to determine this time point. This issue is usually tackled by using an impulse response function which gives detailed information about the effects of a possible shock over time (Alexander [43]). The combined Shewhart-EWMA and the lower one-sided CUSUM chart in the context of pairs trading are left to be investigated in a future study.

There are several tools used in the context of technical analysis, most of which are usually empirical. Traders use oscillators and indices to make decisions upon their trades. Bollinger Bands is such a technical analysis tool invented by John Bollinger. The construction of a chart using Bollinger Bands can be used to determine the time of opening and closing a position. Bollinger Bands are actually envelopes that surround the price bars plotted two standard deviations away from a simple moving average, which may or may not be displayed and they are defined as $(MA \pm K\sigma)$. The window for this moving average can vary but it is usually 20 and $K = 2\sigma$. In the case of the spread process a simple moving average of the spread process is used and the band surrounds this moving average. The time of opening a position is determined when the spread crosses the upper control limit while the position is closed when the process returns in the in-control area.

An example of the use of a simple residuals control chart and the respective Bollinger Bands are shown below in Figue 3. and Figure 4. The following charts were

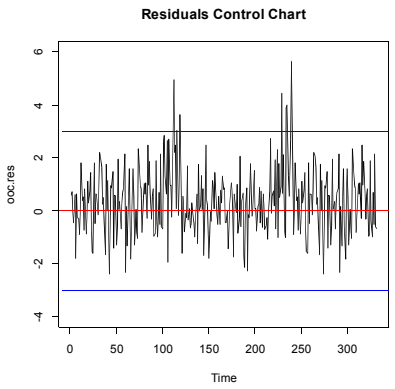


**Figure 3.** Residuals control chart for the spread of two co-integrated assets.

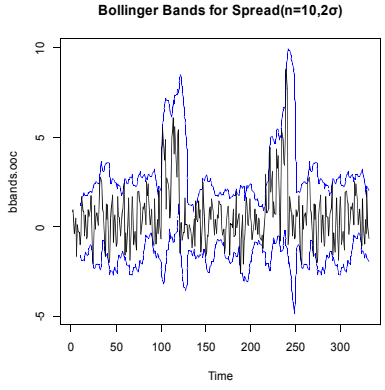


**Figure 4.** Bollinger Bands for the spread of the same two co-integrated assets.

constructed using a set of simulated data. The data were generated so as the co-integrating system of the two assets considered to present short term deviation from its long term equilibrium state. The two out-of-control segments can be easily observed. In the out-of-control segments both the mean and the variance of the spread process were different from the long term, true parameters. The residuals of the generated spread process are presented in Figure 3 in the residuals control chart. The Bollinger Bands for the respective spread process is presented in Figure 4.

Observing the two figures one can realize that the traditional residuals chart is able to detect the out of control segments while the technical analysis tool seems to be far less appropriate for this purpose. It can be seen that the upper limit of the Bollinger Bands chart is approached only in the second out-of-control period, whereas the first the out of control situation is not detected. In the trading context this actually can be interpreted as a missed opportunity of making profit.

## 4. Conclusions and Further Research

Since a symmetry of assumptions in Pairs-trading and Statistical Process Control literature is evident, one can straightforward conclude that SPC techniques can be effectively used in the pairs trading context. In the case of co-integrating assets, examined in this study, the use of the traditional residuals chart was proven to be more effective in identifying tradable periods than that of Bollinger Bands, the technical analysis tool which is usually used to trigger potential trades. Although this study is quite limited, it introduces a new area of research for the SPC scholars. The adjustment of SPC tools and theory to account for financial data and more specifically the use of these tools in the decision making process for traders employing relative-value statistical arbitrage trading techniques such as pairs-trading is a promising area of investigation.

The conclusions drawn from this study are to be substantiated further in a new study using real data, closing share prices. Furthermore, the use of all the control charts mentioned in the study (combined Shewhart-EWMA and lower CUSUM) are to be used in order to investigate the effectiveness of each under various circumstances. This investigation will also enable a comparison of the proposed charts, when used in the Pairs-trading context, that will eventually lead to the selection of the most appropriate charts to be used as trading decision making tools. Another issue to be investigated in the future is the use of control charts for detecting mean reverting segments of non-stationary processes.

## References

[1] D. S. Ehrman, *The handbook of pairs trading*. Wiley, New York, 2006.

[2] G. Vidyamurthy, *Pairs Trading: quantitative methods and analysis*, vol. 217. John Wiley & Sons, 2004.

[3] M. Whistler, *Trading Pairs: capturing profits and hedging risk with statistical*

*arbitrage strategies*, vol. 216. John Wiley & Sons, 2004.
[4] E. F. Fama, "Efficient capital markets: A review of theory and empirical work*," *J. Finance*, vol. 25, no. 2, pp. 383–417, 1970.
[5] E. Gatev, W. Goetzmann, and K. Rouwenhorst, "Pairs Trading: Performance of a Relative-Value Arbitrage Rule," *Rev. Financ. Stud.*, vol. 19, no. 3, pp. 797–827, Feb. 2006.
[6] R. F. Engle and C. W. J. Granger, "Co-Integration and Error Correction: Representation, Estimation, and Testing," *Econometrica*, vol. 55, no. 2, pp. 251–276, Mar. 1987.
[7] R. F. Engle and B. S. Yoo, "Forecasting and testing in co-integrated systems," *J. Econom.*, vol. 35, no. 1, pp. 143 – 159, 1987.
[8] G. E. Uhlenbeck and L. S. Ornstein, "On the Theory of the Brownian Motion," *Phys Rev*, vol. 36, no. 5, pp. 823–841, Sep. 1930.
[9] R. J. Elliott, J. Van Der Hoek *, and W. P. Malcolm, "Pairs trading," *Quant. Finance*, vol. 5, no. 3, pp. 271–276, Jun. 2005.
[10] A. Dattasharma, P. K. Tripathi, and S. Gangadharpalli, "Identifying stock similarity based on episode distances," in *Computer and Information Technology, 2008. ICCIT 2008. 11th International Conference on*, 2008, pp. 28–35.
[11] K. Triantafyllopoulos and G. Montana, "Dynamic modeling of mean-reverting spreads for statistical arbitrage," *Comput. Manag. Sci.*, vol. 8, no. 1–2, pp. 23–49, Apr. 2011.
[12] L. T. Gatarek, L. Hoogerheide, H. K. Van Dijk, and M. Verbeek, "A simulation-based Bayes' procedure for robust prediction of pairs trading strategies," *Tinbergen Inst. Discuss. Pap.*, pp. 09–061, 2011.
[13] K. Triantafyllopoulos and S. Han, "Detecting Mean-Reverted Patterns in Algorithmic Pairs Trading," in *Mathematical Methodologies in Pattern Recognition and Machine Learning*, Springer, 2013, pp. 127–147.
[14] A. Tourin and R. Yan, "Dynamic pairs trading using the stochastic control approach," *J. Econ. Dyn. Control*, vol. 37, no. 10, pp. 1972–1981, Oct. 2013.
[15] V. Fasen, "Statistical estimation of multivariate Ornstein–Uhlenbeck processes and applications to co-integration," *J. Econom.*, vol. 172, no. 2, pp. 325–337, Feb. 2013.
[16] M. A. Alrasheedi and A. A. Al-Ghamedi, "Some Quantitative Issues in Pairs Trading," *Res. J. Appl. Sci. Eng. Technol.*, vol. 5, no. 6, pp. 2264–2269, Feb. 2013.
[17] T. Bogomolov, "Pairs trading based on statistical variability of the spread process," *Quant. Finance*, vol. 13, no. 9, pp. 1411–1430, Sep. 2013.
[18] G. Papadakis and P. Wysocki, "Pairs trading and accounting information," *Boston Univ. MIT Work. Pap.*, 2007.
[19] J. P. Broussard and M. Vaihekoski, "Profitability of pairs trading strategy in an illiquid market with multiple share classes," *J. Int. Financ. Mark. Inst. Money*, vol. 22, no. 5, pp. 1188–1201, Dec. 2012.
[20] S. Wang and Y. Mai, "The GGR and Two Improved Pairs Trading Open Position Strategies," *Int. J. Adv. Inf. Sci. Serv. Sci.*, vol. 4, no. 7, pp. 326–334, Apr. 2012.
[21] M. Perlin, "M of a kind: A Multivariate Approach at Pairs Trading," 2007.

[22] S. Mudchanatongsuk, J. A. Primbs, and W. Wong, "Optimal pairs trading: A stochastic control approach," in *American Control Conference, 2008*, 2008, pp. 1035–1039.

[23] M. C. Chiu and H. Y. Wong, "Mean–variance portfolio selection of cointegrated assets," *J. Econ. Dyn. Control*, vol. 35, no. 8, pp. 1369–1385, Aug. 2011.

[24] H. Alsayed and F. McGroarty, "Optimal portfolio selection in nonlinear arbitrage spreads," *Eur. J. Finance*, vol. 19, no. 3, pp. 206–227, Mar. 2013.

[25] Y.-X. Lin, M. McCrae, and C. Gulati, "Loss protection in pairs trading through minimum profit bounds: A cointegration approach," *J. Appl. Math. Decis. Sci.*, vol. 2006, pp. 1–14, 2006.

[26] Q. Song and Q. Zhang, "An optimal pairs-trading rule," *Automatica*, vol. 49, no. 10, pp. 3007–3014, Oct. 2013.

[27] A. A. Zebedee and M. Kasch-Haroutounian, "A closer look at co-movements among stock returns," *J. Econ. Bus.*, vol. 61, no. 4, pp. 279–294, Jul. 2009.

[28] B. R. Marshall, N. H. Nguyen, and N. Visaltanachoti, "ETF arbitrage: Intraday evidence," *J. Bank. Finance*, vol. 37, no. 9, pp. 3486–3498, Sep. 2013.

[29] N. Huck, "Pairs trading and outranking: The multi-step-ahead forecasting case," *Eur. J. Oper. Res.*, vol. 207, no. 3, pp. 1702–1716, Dec. 2010.

[30] D. S. Matteson, N. A. James, W. B. Nicholson, and L. C. Segalini, "Locally stationary vector processes and adaptive multivariate modeling," in *Acoustics, Speech and Signal Processing (ICASSP), 2013 IEEE International Conference on*, 2013, pp. 8722–8726.

[31] Y. Mai and S. Wang, "Whether Stock Market Structure Will Influence the Outcome of Pure Statistical Pairs Trading?," 2011, pp. 291–294.

[32] P. Gomide and R. L. Milidiu, "Assessing Stock Market Time Series Predictors Quality through a Pairs Trading System," 2010, pp. 133–139.

[33] R. Q. Liew and Y. Wu, "Pairs trading: A copula approach," *J. Deriv. Hedge Funds*, vol. 19, no. 1, pp. 12–30, 2013.

[34] D. A. Dickey and W. A. Fuller, "Distribution of the Estimators for Autoregressive Time Series with a Unit Root," *J. Am. Stat. Assoc.*, vol. 74, no. 366a, pp. 427–431, 1979.

[35] P. C. B. Phillips and P. Perron, "Testing for a unit root in time series regression," *Biometrika*, vol. 75, no. 2, pp. 335–346, Jun. 1988.

[36] D. Kwiatkowski, P. C. Phillips, P. Schmidt, and Y. Shin, "Testing the null hypothesis of stationarity against the alternative of a unit root: How sure are we that economic time series have a unit root?," *J. Econom.*, vol. 54, no. 1, pp. 159–178, 1992.

[37] A. Steland, "On detection of unit roots generalizing the classic Dickey-Fuller approach," Technical Report/Universität Dortmund, SFB 475 Komplexitätsreduktion in Multivariaten Datenstrukturen, 2005.

[38] A. Steland, "Weighted Dickey–Fuller processes for detecting stationarity," *J. Stat. Plan. Inference*, vol. 137, no. 12, pp. 4011 – 4030, 2007.

[39] A. Steland, "MONITORING PROCEDURES TO DETECT UNIT ROOTS AND STATIONARITY," *Econom. Theory*, vol. null, no. 06, pp. 1108–1135, 2007.

[40] A. Steland, "Sequentially Updated Residuals and Detection of Stationary Errors in Polynomial Regression Models," *Seq. Anal.*, vol. 27, no. 3, pp. 304–329, Aug. 2008.

[41] A. Steland and S. Weidauer, "Detection of Stationary Errors in Multiple Regressions with Integrated Regressors and Cointegration," *Seq. Anal.*, vol. 32, no. 3, pp. 319–349, 2013.

[42] C. . Lu and R. M. Reynolds, "Control charts for monitoring the mean and variance of autocorrelated processes," *J. Qual. Technol.*, vol. 31, no. 3, pp. 259–274, 1999.

[43] C. Alexander, *Market risk analysis. quantitative methods in finance 2 2*. Chichester: Wiley, 2008.

## Author Index

# Stochastic Modeling, Data Analysis and Statistical Applications

This is the second book devoted to the 3rd Stochastic Modeling Techniques and Data Analysis (SMTDA) International Conference held in Lisbon, Portugal, June 11-14, 2014. Revised and expanded forms of papers from the conference presentations are included.

SMTDA main objective is to publish papers, both theoretical or practical, presenting new results having potential for solving real-life problems. Another important objective is to present new methods for solving these problems by analyzing the relevant data. Also, the use of recent advances in different fields is promoted such as for example, new optimization and statistical methods, data warehouse, data mining and knowledge systems, computing-aided decision supports and neural computing.

The first Chapter includes papers on Stochastic Modeling, First Passage Time and Copulas, whereas contributions on Statistics, Distributions, Bayesian Modeling are included in the second Chapter.

Papers on Model building and Modeling of particular cases are included in the third Chapter, and Data Analysis methods, techniques and applications are presented in the fourth Chapter.

Statistics in Health Sciences and Sports are presented in the fifth Chapter along with Statistical Modelling and Applications papers included in the sixth Chapter.

Chapter seven includes papers on Experimental Design and Related Topics, whereas, Information Theory and Risk Analysis topics are analyzed in Chapter eight.

Time Series, Signals, Networks papers along with works on Statistical Quality Control are included in Chapters nine and ten.

This book, like others in this SMTDA series is directed towards researchers and others in the fields of probability and statistics, data analysis and forecasting, demography and insurance, finance and management. It is a valuable tool for demographers, actuaries, mathematicians and statisticians, economists and policy makers.

**Lidia Filus, Teresa Oliveira , Christos H Skiadas,** *Editors*

**ISAST 2015**